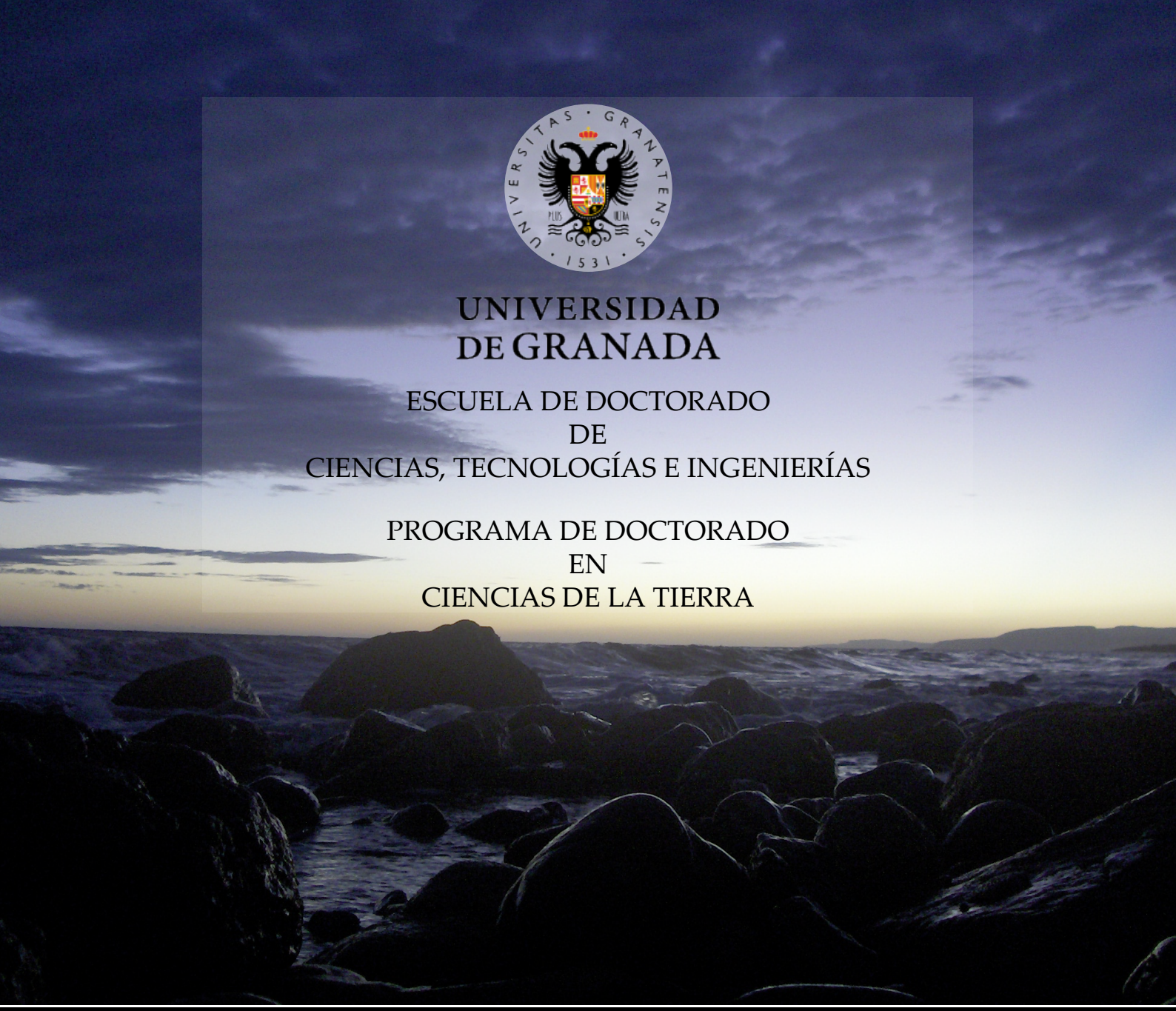

UNIVERSIDAD
DE GRANADA

ESCUELA DE DOCTORADO
DE
CIENCIAS, TECNOLOGÍAS E INGENIERÍAS

PROGRAMA DE DOCTORADO
EN
CIENCIAS DE LA TIERRA

DOCTORAL THESIS

Mineralogy, geochemistry and petrogenesis of a new jade deposit, Sierra del Convento Mélange, E. Cuba

DOCTORANDO/A:
D. JUAN CÁRDENAS PÁRRAGA

DIRECTORES:
DR. ANTONIO GARCÍA CASCO (Dpto Mineralogía y Petrología, UGR)
DR. GEORGE E. HARLOW (American Museum of Nat. History, NY)

Granada, enero de 2019

UNIVERSIDAD
DE GRANADA

ESCUELA DE DOCTORADO
DE CIENCIAS, TECNOLOGÍAS
E INGENIERÍAS

PROGRAMA DE DOCTORADO EN
CIENCIAS DE LA TIERRA

TESIS DOCTORAL

Mineralogy, geochemistry and petrogenesis of a new jade deposit, Sierra del Convento Mélange, E. Cuba

DOCTORANDO/A:

D. JUAN CÁRDENAS PÁRRAGA

DIRECTORES:

DR. ANTONIO GARCÍA CASCO (Dpto Mineralogía y Petrología, UGR)

DR. GEORGE E. HARLOW (American Museum of Nat. History, NY)

Granada, enero de 2019

Editor: Universidad de Granada. Tesis Doctorales
Autor: Juan Cárdenas Párraga
ISBN: 978-84-1306-223-5
URI: http://hdl.handle.net/10481/56036

"La tierra, por la magnificencia de sus horizontes, las frescuras de sus bosques y la pureza de sus fuentes, ha sido y continúa siendo la gran educadora y no ha cesado de llamar a las naciones a la armonía y a la conquista de la libertad"

Élisée Reclus (1830-1905)

Agradecimientos

La presentación de esta tesis es la consecución de un proceso largo, que ha sido muy condicionado por mis variantes estados de salud, los cuales seguiré acarreando el resto de mi vida. Por esto, me gustaría destacar y agradecer la empatía, comprensión y paciencia que han demostrado todas las personas que me han rodeado en el proceso de investigación. En este sentido, me gustaría recalcar mis agradecimientos sobre mis directores de Tesis, Antonio García Casco y George Eugene Harlow, y añadirlos al Departamento de Mineralogía y Petrología, a todos los profesores, investigadores y técnicos, a su director Nicolás Velilla Sánchez , y a su subdirector Juan Manuel Fernández Soler. Sin olvidar que de todos ellos he recibido siempre una ayuda incondicional para la elaboración de esta tesis.
Muchas gracias a Antonio García Casco y George Eugene Harlow por afrontar las correcciones más intensas en cada uno de los manuscritos publicados, gracias por vuestro apoyo y conocimientos prestados para poder estudiar una zona, geológicamente tan interesante como lo son las mélanges de subducción, sin estos, esta tesis nunca abría sido terminada. Gracias Antonio por dedicar tú escaso tiempo de forma tan incondicional en cada paso de esta investigación, y por el continuo aprendizaje que me has aportado durante estos años.
También me gustaría dar mis más sinceros agradecimientos a todo el que ha participado de una manera indirecta o directa en la elaboración de esta investigación. Agradezco vuestros comentarios, correcciones, la ayuda en los laboratorios y el apoyo diario que he recibido de vosotros. En este sentido, tengo que hacer especial mención a los compañeros de doctorado y despacho, de Granada y Barcelona: Idael Blanco Quintero, Lidia Butjosa Molines, Aitor Cambeses Torres, Juan Antonio Moreno Moreno, Concepción Lázaro Calisalvo, Cristina Villanova-de-Benavent, José Carlos Pomo, Manuel Jesús Román Alpiste, José Alberto Padrón Navarta, Eduardo Molina Piernas, Thaís Hyppolito, Patricia Ruano Roca, Pilar Navas-Parejo, Vinícius Tieppo Meira, Lisard Torro i Abat, Vanesa Nieto Moreno, Antonio Acosta Vigil, Libertad Cobos Porras, David Montes, Sandra Carrasquilla Ortiz y Alice Knaf ya que ha compartido conmigo cada tropiezo y ha sido mi primer recurso para afrontar los

problemas diarios. Junto con, Joaquin Proenza, Antonio Rodriguez Vega, Kenya Núñez Cambra, Jesús Montes Rueda, Rafael Torres Roldán, que han contribuido con numerosos aportes personales de diferente índole.
Mis agradecimientos a los técnicos del Centro de Instrumentación Científica (CIC) por su asesoramiento y ayuda en las abundantes horas pasadas en el CIC, en especial a Miguel Ángel Hidalgo Laguna, Isabel Guerra Tschuschke, Isabel Sánchez Almazo y Olga Cazalla Vázquez.
También estoy muy agradecido por las precisas dataciones de las rocas estudiadas gracias a Yamirka Rojas Agramonte, Fernando Bea Barredo, Pilar González Montero, y los comentarios posteriores para su interpretación.
Un agradecimiento especial por su apoyo personal a mi madre Elisa y mi hermano Andrés, y resto de mi familia y amigos que han compartido conmigo los buenos y los malos momentos, especialmente a Karen por su cariño y ayuda en la fase final de esta tesis.

Index

Abstract

The Sierra del Convento mélange (Eastern Cuba) represents a well preserved fragment of the Cretaceous oceanic subduction channel in the Caribbean realm, developed by the subduction of the Protocaribbean basin below the Caribbean Plate. The mélange is formed by a serpentinite matrix, which contains a variety of tectonic blocks metamorphosed to high pressure and low to high temperature, including blueschists, pelitic gneisses, anatectic tonalitic–trondhjemitic rocks, epidote-garnet plagioclase-lacking amphibolites and sepertinites. This mélange has unique characteristics by showing evidence of partial melting of the slab developed by subduction of very young oceanic plate. Recently, in situ jadeitite blocks have been discovered in the Sierra del Convento mélange surrounded by sheared serpentinitic rocks. The combination of hot subduction and occurrence of jadeitite generates an exceptional scenario to decipher the interaction at intermediate to high-temperature of fluids in the subduction channel and its boundary with the mantle wedge. This PhD thesis is focused on the study of jadeitite and related rocks with emphasis in their petrogenesis by fluid-rock interaction in a subductive context. In addition, the serpentinitic rocks associated with jadeitites have been included in the study in order to decipher the context of formation of jadeitites.

Serpentinite rocks preserve fertile protolith signatures that suggest low melting degrees of the peridotie protoliths. High concentration of immobile elements as Zr, Th, Nb, and the REE contents (from ~0.1 to ~2 CI-chondrite) point to early melt-rock interaction processes before serpentinization took place. Major- and trace-element compositions suggest an oceanic fracture-zone-transform-fault setting. A second, more

important, serpentinization stage is related to enrichment in U, Pb, Cs, Ba, and Sr due to the infiltration of slab-derived fluids. The local presence of anthophyllite and the replacements of lizardite by antigorite indicate a metamorphic evolution from cooling of peridotite/serpentinite at the oceanic context to mild heating and compression in a subduction setting. It is proposed that the serpentinites formed at an oceanic transform-fault setting that was the locus of subduction initiation of the Protocaribbean basin below the Caribbean plate during early Cretaceous times. Onset of subduction at the fracture zone allowed the preservation of abyssal transform-fault serpentinites at the upper plate, whereas limited downward drag during mature subduction placed the rocks in the subduction channel, where they tectonically mixed with the upward-migrating accreted block of the subducted Proto-Caribbean oceanic crust.

Petrographically, jadeitites have a huge variation producing various types of rocks, from end-members (quasi-monomineralic rocks) to a wide intermediate variation. There is a continuum from pure to impure jadeitite varieties rich in omphacite, epidote, white and dark micas, albite, chlorite and other minerals. Pure jadeitite varietie is essentially made of jadeite and omphacite (except rocks with >90 mode% of omphacite, which are named as omphacitite). Deep-green varieties rich in Cr of both jadeitite and omphacitite also occur. The term epidote-rich jadeitite is used for a variety of jadeite-omphacite rock that contains significant amount of epidote-(clino)zoisite (plus albite and chlorite), and mica-rich jadeitite is used for a variety of the latter group that contains significant amount of white mica (both, paragonite and phengite). Another group is made of albite-epidote rocks, which may contain relicts of jadeite and/or omphacite and bear low to moderate contents of chlorite and, occasionally, small amount of quartz. However, samples from this group that bear significant amount of chlorite and quartz have been grouped, respectively, in albite-epidote-chlorite and albite-epidote-quartz rocks. Due to mineral abundance, albite-epidote, albite-epidote-chlorite and albite-epidote-quartz rocks cannot be termed albitite. In addition, blackwalls have been grouped in chloritite and titanite-apatite-zircon-rich chloritite. Finally, actinolitite is also distinguished.

The jadeitites are characterized by very rare quartz inclusions and omphacite exsolutions/replacements in jadeite crystals, as well as clear replacements by, and void-infillings of, omphacite. Jadeitites present granoblastic massive jadeite, omphacite and epidote-(clino)zoisite with minor intergranular crystallization of accessory minerals. Minor minerals that may appear in the assemblages include epidote group minerals, biotite-phlogopite, albite, phengite, paragonite, pumpellyite, chlorite, sodic-calcic and sodic amphiboles, titanite, rutile, zircon and apatite. Oscillatory zoning in jadeite crystals and zircon ages suggest hydrothermal crystallization in veins formed in serpentinized peridotite, probably at the slab-mantle interface. The compositional gap between coexisting jadeite and omphacite indicates a temperature of jadeite formation higher than 500 ºC. Zircon $^{206}Pb/^{238}U$ ages of 107 to 113 Ma attest formation during the earliest stages of subduction in the region. These

formation ages and the isotopic, major and trace element whole-rock compositions of jadeitite and associated rocks suggest a genetic link between the jadeite-forming fluids and the fluids involved in the slightly earlier partial melting of amphibolites and associated crystallization of anatectic tonalite-trondhjemite melts.

Si-Al-Na-Mg-Ca-bearing fluids of variable composition deposited jadeitite in veins during episodic opening of the fractures at depth in the subduction environment, denoting a strong influence of fluid-ultramafic rock interaction. These geochemical composition of the studied samples indicate limited interaction/involvement of sediment-derived fluids. Two types of geochemical patterns for the different varieties of jadeitite are defined. On the one hand, pure jadeitites have depleted REE and HFSE patterns normalized to N-MORB, with Cr-rich compositions in some cases. On the other hand, epidote-rich jadeitites present relatively enriched Ba compositions respect to N-MORB, and REE patterns with similar compositions to N-MORB.

The interaction of jadeitite with fluid is divided according to the relative contribution of sediment-derived fluids evolved from the subducted slab. Ba-rich sedimentary fluids are denoted by: (1) K-bearing mineral species such as phlogopite-biotite and phengite, as well as paragonite, epidote group minerals (epidote-(clino)zoisite and allanite), (2) trace element patterns normalized to N-MORB showing enriched compositions mainly in LILE. In contrast, the interaction with Ba-poor sedimentary fluids is identified by: (1) low mica and epidote content and lower LILE concentrations and (2) higher REE and HFSE during crystallization of jadeite and omphacite and the intergranular crystallization of accessory minerals such as epidote-(clino)zoisite, allanite, rutile, and titanite at relatively high-T conditions.

A formation model, taking into account the geochemical and petrological characteristics of all types of studied rocks, is proposed that involves hydrofracturing of sheared serpentinite at the slab-mantle interface. The opening of fractures is accompanied by the crystallization of jadeitite veins, which leads the formation of the chloritic blackwall and omphacititic edges, with Cr-rich compositions in some cases. Subduction driven deformation generates late fractures and microfractures at the mineral-grain scale, increasing the permeability into the jadeitite veins. Therefore, the flow of external pervasive fluids was concentrated in the chloritic blackwall, which interact metasomatically with jadeitite veins producing albite-epidote (-chlorite) rocks and mica-rich jadeitite. A temporary development of these processes generate isolated blocks of albite-epidote (-chlorite) rocks, although a direct crystallization from a fluid in veins can not be ruled out for the formation of some of the samples of albite-epidote (-quartz) rocks.

From an archaeological point of view, former exploitation (probably of the beach deposits nearby the Sierra del Convento) by the pre-Columbian Taino inhabitants of Cuba is documented by a large number of jade artifacts (mostly, petaloid axes) found in eastern Cuba. This new occurrence of jadeitite in Cuba opens important perspectives for archaeological studies of pre-Columbian jade artifacts in the Caribbean region and their cultural and commercial trade.

Resumen

La mélange de la Sierra del Convento (Cuba Oriental) representa un fragmento bien conservado del canal de subducción oceánica del Cretácico en el ambiente Caribeño, desarrollado por la subducción de la cuenca oceánica protocaribeña bajo la placa del Caribe. La mélange está formada por una matriz serpentinítica, la cual contiene una variedad de bloques tectónicos metamorfizados a alta presión y de baja a alta temperatura, incluyendo esquistos azules, gneises pelíticos, rocas anatécticas trondhjemíticas y tonalíticas, anfibolitas de epidota y granate sin plagioclasa y serpentinitas. Esta mélange tiene características únicas por mostrar evidencias de fusión parcial de la lámina subducente gracias a la subducción de una placa oceánica muy joven. Recientemente, bloques *in situ* de jadeitita han sido descubiertos en la mélange de la Sierra del Convento rodeados por rocas serpentiníticas cizalladas. La combinación de subducción caliente y la aparición de jadeitita ofrece un escenario excepcional para descifrar la interacción de fluidos en el canal de subducción, y su límite con la cuña de manto. Esta tesis doctoral está focalizada en el estudio de la petrogénesis de jadeititas y rocas asociadas por interacción de fluido-roca en un contexto subductivo. Además, las rocas serpentiníticas asociadas a las jadeititas han sido incluidas en este estudio para descifrar el contexto de formación de las jadeititas.

Los bloques de serpentinita preservan signaturas de un protolito peridotítico fértil, lo que sugiere bajos grados de fusión del mismo. La alta concentración de elementos inmóviles como Zr, Th, Nb y los contenidos de REE (desde ~0.1 a ~2 CI-condrito) apuntan a procesos de interacción de fluido-roca tempranos antes de que la serpentinización tuviera lugar. Las composiciones de elementos traza y mayores

sugieren un escenario de falla transformante en una zona de fractura oceánica. Un segundo, y más importante, estadio de serpentinización está relacionado con enriquecimientos en U, Pb, Cs, Ba y Sr debido a la infiltración de fluidos derivados desde la lámina subducente. La presencia local de antofilita y los reemplazamientos de lizardita por antigorita indican una evolución metamórfica desde el enfriamiento de peridotitas/serpentinitas en un contexto oceánico a un calentamiento y compresión en un ambiente subductivo. Las serpentinitas fueron formadas en un ambiente oceánico de falla transformante que fue el foco del inicio de la subducción de la cuenca protocaribeña bajo la placa del Caribe durante el Cretácico temprano. El inicio de la subducción en una zona de fractura permite la preservación de serpentinitas abisales de falla transformante en la placa superior, mientras que el limitado arrastre hacia abajo durante la subducción madura colocó las rocas en el canal de subducción, donde se mezclaron tectónicamente con bloques acrecionados, siguiendo por una migración ascendentemente del conjunto hasta su exhumación.

Petrográficamente, las jadeititas tienen una gran variación produciendo varios tipos de rocas, desde rocas casi monominerálicas hasta una amplia gama de rocas con características intermedias. Hay un continuo desde las variedades de jadeititas puras e impuras ricas en onfacita, epidota, mica, albita, clorita, y otros minerales. La variedad jadeitita pura está esencialmente hecha de jadeita y onfacita (excepto rocas con >90% modal de onfacita, nombrada como onfacitita). También aparecen variedades verde oscuro ricas en Cr tanto de jadeitita como onfacitita. El término jadeitita rica en epidota es usado para una variedad de rocas de jadeita y onfacita que contienen contenidos significativos de epidota-(clino)zoisita (más albita y clorita), y una variedad del último grupo que contiene contenidos significantes de mica blanca (ambas, paragonita y fengita) se describe como jadeitita rica en mica. Otro grupo los conforman rocas de albita y epidota, el cual puede contener relictos de jadeita y/o onfacita y tener contenidos de bajos a moderados de clorita y, ocasionalmente, algo de cuarzo. Sin embargo, las muestras desde este grupo que tienen un contenido significativo de clorita y cuarzo han sido agrupadas, respectivamente, en rocas de albita, epidota y clorita y en rocas de albita, epidota y cuarzo. Debido a la abundancia modal de los distintos minerales, rocas de albita y epidota, rocas de albita, epidota y clorita y rocas de albita, epidota y cuarzo no pueden ser denominadas como albititas. Además, los hastiales melanocráticos (denominados blackwalls) han sido agrupados en cloritita y cloritita rica en titanita, apatito y zircón. Finalmente, son también distinguidas el grupo de actinolititas.

Las jadeititas se caracterizan por raras inclusiones de cuarzo y exoluciones/reemplazamientos de onfacita en los cristales de jadeita, así como reemplazamiento y relleno de espacios vacíos de onfacita. Presentan jadeita granoblástica masiva, onfacita y epidota-(clino)zoisita y, en cierta medida, cristalización intergranular de minerales accesorios. Minerales en menor proporción incluyen mineales del grupo de la epidota, biotita-flogopita, albita, fengita, paragonita, pumpellyita, anfíboles sodo-cálcicos y sódicos, titanita, rutilo, zircón, y apatito. La

zonación oscilatoria en cristales de jadeita y las edades del zircón sugieren cristalización hidrotermal en venas formadas en la peridotita serpentinizada, probablemente en la interfaz de la lámina subducente y el manto. La laguna composicional entre jadeíta y onfacita coexistentes indica una temperatura de formación para la jadeitita mayor que 500 ºC. Las edades de $^{206}Pb/^{238}U$ en zircón de 107 a 113 Ma atestiguan una formación durante los estadios tempranos de subducción en la región. Estas edades de formación y las composiciones isotópicas de elementos mayores y trazas de roca total de jadeititas y rocas asociadas sugieren una relación genética entre los fluidos formadores de jadeitita y los fluidos involucrados en la fusión parcial de anfibolitas y la cristalización de fundidos anatéticos tonalitico-trondhjemiticos ligeramente más antiguos.

Fluidos con Si, Al, Na, Mg and Ca de composición variable depositaron jadeititas en venas durante aberturas episódicas de las fracturas en profundidad en el ambiente de subducción, registrando una fuerte influencia de interacciones fluido-roca ultramáfica. La interacción con fluidos liberados por rocas de origen sedimentario no es importante para la formación de jadeitita. Se definen dos tipos de patrones geoquímicos para las diferentes variedades de jadeitita. Por un lado, la jadeitita pura tiene patrones normalizados al N-MORB empobrecidos en REE y HFSE, con composiciones ricas en Cr en algunos casos. Por otro lado, las jadeititas ricas en epidota presentan composiciones relativamente enriquecidas en Ba respecto al N-MORB, y patrones de REE con similar composición al N-MORB.

Las características mineralógicas y geoquímicas indican que la interacción jadeitita-fluido tuvo variable contribución sedimentaria en los fluidos involucrados liberados desde la lámina subducente. Fluidos sedimentarios ricos en Ba son caracterizados por: (1) especies minerales que contienen K como biotita flogopita y fengita, así como y paragonita y minerales del grupo de la epidota (epidota-(clino)zoisita y alanita), (2) patrones de elementos traza normalizados al N-MORB que muestran composiciones enriquecidas principalmente en LILE. En contraste, la interacción con fluidos sedimentarios pobres en Ba es definida por: (1) contenido bajo de mica y epidota y menores concentraciones en LILE, sugiriendo una contribución limitada de sedimentos, (2) adición de REE y HFSE durante la cristalización de jadeita y onfacita, y cristalización intergranular de minerales accesorios tales como epidota-(clino)zoisita, alanita, rutilo, y titanita a condiciones relativamente alta de T.

Teniendo en cuenta las características geoquímicas y petrológicas de las rocas estudiadas, se propone un modelo de formación que involucra hidrofracturación de serpentinitas cizallada en la interfaz de la lámina subducente y la cuña de manto. La apertura de fracturas es acompañada por la cristalización de jadeitita en venas, la cual dispara la formación de blackwall cloritíticos y bordes onfacíticos, con composiciones ricas en Cr en algunos casos. La deformación asociada al ambiente subductivo generó fracturas tardías y microfracturas a la escala de los granos minerales, incrementado la permeabilidad dentro de la vena de jadeitita. De esta forma, el flujo de fluidos pervasivos externos fue concentrado en el blackwall clorítico, el cual interactúa

metasomáticamente con las venas de jadeitita produciendo rocas de albita epidota (y clorita) y jadeitita rica en mica. El desarrollo temporal de estos procesos genera bloques de rocas de albita epidota (y clorita), aunque una cristalización directa desde un fluido en venas no puede ser descartada para la formación de algunas de las muestras de rocas con albita epidota (y cuarzo).

Desde un punto de vista arqueológico, el gran número de artefactos de jade (la mayoría, hachas petaloides) encontradas en Cuba Oriental apunta a la explotación (probablemente de los depósitos de las playas cercanas a la Sierra del Convento) por los habitantes Tainos precolombinos de Cuba y las Antillas Mayores. Este nuevo yacimiento de jadeitita en Cuba Oriental abre importantes perspectivas para estudios arqueológicos de artefactos de jade precolombinos en la región del Caribe y su dispersión cultural y comercial.

1 Introduction

1.1 Jade and Jadeitite

When the Spanish met with ancient civilizations that populated the actual territory of Mexico, they discovered that these native people used a solution of a green stone in water as a cure for internal medical problems. They called this green rock *piedra de yjada*, or colic stone (see Mottana, 2012). From these terminologies the term "Jade" was coined through a mistranslation into French (Buffon, 1749). Currently it is widely used in gemology and geology to include two fundamentally monomineralic rocks categorized as nephrite (amphibole jade) and jadeitite (pyroxene jade). The goal of this PhD Thesis is to elucidate the processes that led to the formation jadeitite in the Sierra del Convento mélange (eastern Cuba).

The synthesis of jadeite [$NaAlSi_2O_6$] and the experimental calibrations for the reactions albite = jadeite + quartz and nepheline + albite = jadeite were developed from 1953 to 1968 (see Roy and Tuttle, 1956; Robertson et al., 1957; Birch and LeComte, 1960, and Newton and Kennedy, 1968). During the sixties and onwards, the new models based on the plate tectonics theory offer a suitable context for the formation of jadeite in subduction zones, but concepts like subduction channel (Shreve and Cloos, 1986 and Cloos and Shreve, 1988a, b), that provide a mechanism for the exhumation of subducted high pressure rocks are necessary in order to explain jadeitite formation and exposure. Currently, jadeitite rocks described around the world occur associated with exhumed serpentinite-matrix mélanges from fossil subduction system (i.e., Tsujimori and Harlow 2012; Harlow et al., 2015).

In the Sierra del Convento serpentinite-matrix mélange (eastern Cuba) one of the later jadeitite deposit recognized in the World has been reported (García-Casco et al., 2009). In order to clarify the petrogenesis of the jadeitite jade deposit from the Sierra del Convento mélange, a variety of jadeitites and associated rocks have been studied in this PhD Thesis, including several types of albite-epidote rich rock, chloritite and serpentinite blocks crosscut by actinolitite veins. The serpentinites are addressed in a separate chapter, due to the complexity of the study of this type of rocks and their importance in the development of a geodynamic model of formation of these types of rock.

1.2 Where Jadeitites Form

Jadeitic pyroxene is a common rock forming mineral in exhumed mélange zones worldwide. However, jadeitites are spatially restricted to ca. 20 localities discovered to date around the world (Harlow et al., 2015). Due to the scarcity of jadeitite occurrences compared with the abundance of exhumed subduction channels, these deposits are exceptional natural systems through which to study the evolution of the subduction channel with particular emphasis in fluid-rock interactions. In recent years, new jadeitite localities have been documented in the Sierra del Convento mélange in Cuba (García-Casco et al., 2009), Sorkhan, Iran (Oberhänsli et al., 2007) and Río San Juan mélange, Dominican Republic (Schertl et al., 2007; Maresch et al., 2008).

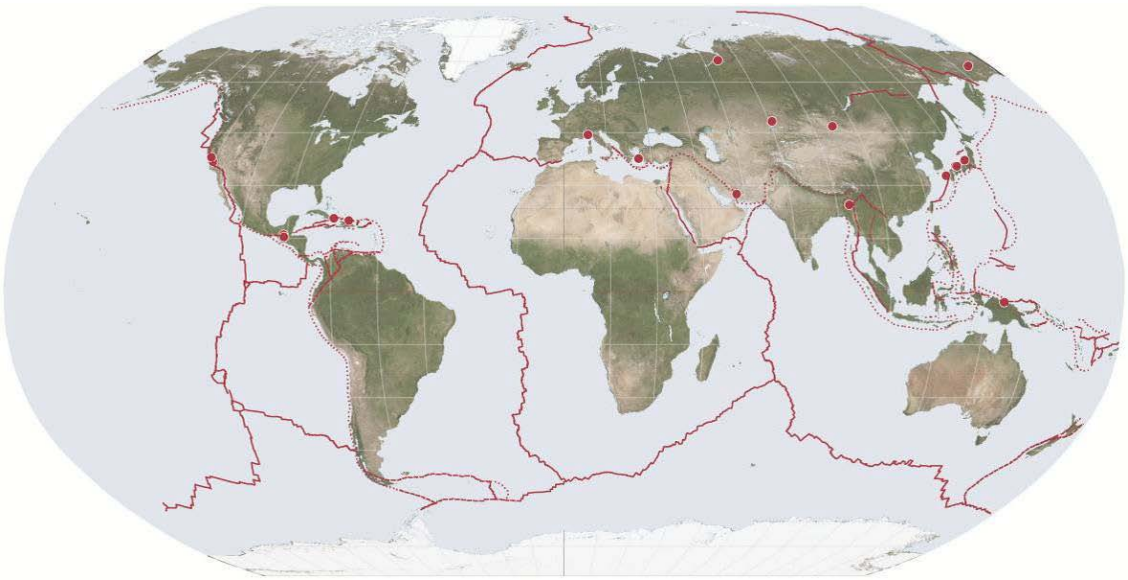

Figure 1.1. World map including the locations of jadeitite occurrences (red circles) and present day plate boundaries (continuous and dotted red lines). After of Harlow et al., (2015) and references therein.

The concept of subduction channels was first defined by Hsu (1971), Cloos (1982) and Cloos and Shreve (1988a, b). These authors defined them as complex rock assemblies developed in the interface between the subducting and the hanging wall plates in a convergent margin. Cloos and Shreve (1988a, b) developed the concept to model actual subduction environments (e.g., Japan, Mariana, Lesser Antilles, etc.). The

subduction channel model provides a mechanism for the exhumation of subducted high pressure rocks accreted as blocks to the overlying accretionary prism formed, mostly, by sediments. The subduction channel concept has been extended to much deeper near-sub-arc depths by means of thermal-mechanical (Figure 1.2; Gerya et al., 2002) and conceptual models (Figure 1.2; Guillot et al., 2000; 2001; 2009). In this context, the subduction channel is formed by serpentinites after hydration of the mantle wedge peridotite in the antigorite stability field (i.e., below ca. 650 °C). The fluids necessary for this serpentinization process are thought to be provided by prograde metamorphism of the subducted slab (oceanic plate, including its sedimentary cover). According to Iwamori (1998) the oceanic crust contains about 6 wt % water in chlorite, lawsonite and amphibole. This amount is reduced to less than 3 wt % at 50 km depth, providing the necessary free-water for the hydration of the mantle wedge and the exhumation of high pressure blocks in the mélanges. Also, the fluids play an important role within the subduction system because they influence the progress of the metamorphic reactions, magma generation in the mantle wedge and the generation of seismicity (double Benioff plane) due to the progress of dehydration reactions within the slab (Brudzinski et al., 2007). The exposed materials exhumed from the plate interface (i.e. mélange) contain information about processes taking place during long periods of time from ca. 100-150 km depth (Ernst, 1999).

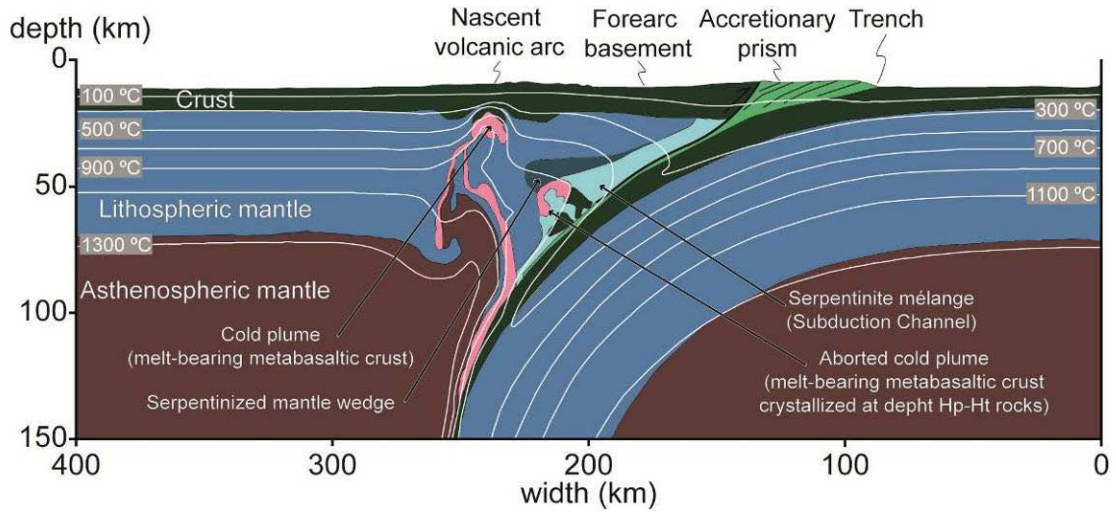

Figure 1.2. Thermo-mechanical model of oceanic subduction which includes the main components in subduction zones. This model is slightly modified from the results of numerical thermal-chemical experiments after of Blanco-Quintero et al. (2011b), representing an analogue scenario of hot subduction with partially melted subducted MOR basaltic amphibolites as in the Sierra del Convento and La Corea mélanges.

Jadeitites generally are found within serpentinite-matrix tectonic mélanges containing exotic blocks formed in high-pressure subduction environments. Two different possibilities of jadeite formation are described in the literature - (i) direct primary crystallization from a hydrous fluid (Garcia-Casco et al., 2009; Tsujimori and Harlow, 2012) or (ii) metasomatic replacement of mafic and/or felsic protoliths in the channel (e.g., Compagnoni et al., 2012; Shigeno et al., 2012). Both processes are

strontly tied to fluid-rock interactions within subduction zones. Hence, the study of jadeitite provides first-hand insights into fluid-rock interactions and the mechanism of fluid-flow and geochemical recycling in subduction zones. In particular, jadeitites provide information on major, trace element and isotopic signatures, fluid speciation, and salinities of subduction related fluids (Morishita et al., 2007; Sorensen et al., 2010).

1.3 Jadeitite deposit from Eastern Cuba

In the Sierra del Convento mélange, located in the Caribbean region of eastern Cuba (Figure 2.1, 2.3), tectonic blocks of jadeitite and associated high-pressure (15 kbar) high-temperature (700-750 °C) garnet amphibolites and trondhjemitic rocks within serpentinitic matrix are interpreted as having been formed during the subduction of Proto-Caribbean (i.e., Atlantic) lithosphere in the mid-Cretaceous time, probably the Aptian-Albian (Lázaro et al., 2009). The amphibolite blocks of La Corea mélange (eastern Cuba) followed counterclockwise P-T-t paths similar to those of the Sierra del Convento mélange, but jadeitite deposits have not been described to date (Blanco-Quintero et al., 2010). García-Casco et al., (2009) emphasized the high temperature (ca. 600 °C) of the formation of jadeitite in the Sierra del Convento, as compared to many worldwide occurrences of jadeitite, suggesting a genetic link with fluids released from the crystallization of anatectic tonalitic-trondhjemitic melts in the upper plate mantle. This hot subduction scenario and the occurrence of a well-preserved Cretaceous subduction channel in eastern Cuba (García-Casco et al., 2008b) differ from other jadeitite occurrences elsewhere in the world. The study of this jadeitite deposit from the aforementioned subduction mélange allows contributing to the knowledge of mass-transfer processes from the slab to mantle wedge, using jadeitite as a key rock for understanding these processes.

1.4 Aim and Structure of the thesis

This PhD Thesis is entitled “Mineralogy, geochemistry and petrogenesis of a new jade deposit, Sierra del Convento Mélange, E Cuba”. The manuscript is the result of a FPI grant to the author in the Department of Mineralogy and Petrology of the University of Granada, associated with the Spanish project CGL2009-12446 granted by Spanish Ministery of Science and Innovation to P.I. Antonio Garcia-Casco. The work has been supervised by Dr. Antonio García Casco (Department of Mineralogy and Petrology, University of Granada) and Dr. George E. Harlow (Department of Earth and Planetary Sciences, American Museum of Natural History, New York).

The main goal of this PhD thesis is the petrogenesis of the jade deposit in the Sierra del Convento Mélange. For this purpose, and to follow a systematic method during the study of jadeitite and related rocks, the following tasks were carried out: (i) description of jadeitite and associated rock occurrences in the field and their mineralogic, petrographic and geochemical (major, trace and isotope) compositions; (ii) description of the nature of the serpentinite matrix/blocks associated with jadeitite rocks; (iii)

determining the age of crystallization of jadeitite; and finally (iv) developing a petrogenetic model.

The PhD manuscript includes an abstract (in English and Spanish) and seven chapters, but it could be separated into (i) an introductory part, (ii) the main results and finally (iii) discussions and conclusions. The first part includes the chapters Introduction, Geological Setting and Analytical Techniques. The second part includes the field relationships between the main lithologies, petrography descriptions of the the broad variety of rocks included in the deposits (with variable jadeite + omphacite ± epidote ± chlorite ± albite ± white and dark micas) and surrounding serpentinite chloritite blackwalls and actinolitite veins. In the final part, a genetic model of the formations of the different rocks is discussed and incorporated into the existing model of evolution of the mélange.

2 Geological Setting

2.1 Regional setting

The Greater Antillean Arc formed by the convergence of the North American and the Farallon/Caribbean plates during the Lower Cretaceous to Tertiary (Burke 1988). After the Jurassic fragmentation of Pangea and the opening of the Proto-Caribbean oceanic basin, subduction of the latter underneath the Caribbean plate (of Pacific–Farallon plate-origin) created the Caribbean volcanic arc (Pindell et al., 2006; Pindell and Kennan, 2009; Boschman et al., 2014; and references therein). Subduction initiation has been dated at ca. 135 Ma in the leading northern edge of the Caribbean plate (Rojas-Agramonte et al., 2011, 2016; Lázaro et al., 2016; see also Torró et al., 2016, 2017, for subduction initiation basaltic magmatism in the Dominican Republic), likely in a transform-fault plate boundary termed the inter-American transform (Pindell et al., 2012; Boschman et al., 2014). This event does not appear to be related to the mid-late Cretaceous plume-induced subduction scenario proposed for the western and southern edges of the Caribbean plate (Gerya et al., 2015; Whattam and Stern, 2015). In the northern leading edge, the intraoceanic Caribbean arc system was tectonically emplaced by northward collision with the Maya block, the Caribeana terrane, and the Bahamas platform during the latest Cretaceous–Tertiary time (Iturralde-Vinent et al., 2008; García-Casco et al., 2008b; Van Hinsbergen et al., 2009; Solari et al., 2013). This collision event is recorded in obducted ophiolite bodies and serpentinite mélanges containing high-pressure blocks from Guatemala through Cuba to Hispaniola (Figure 2.1a).

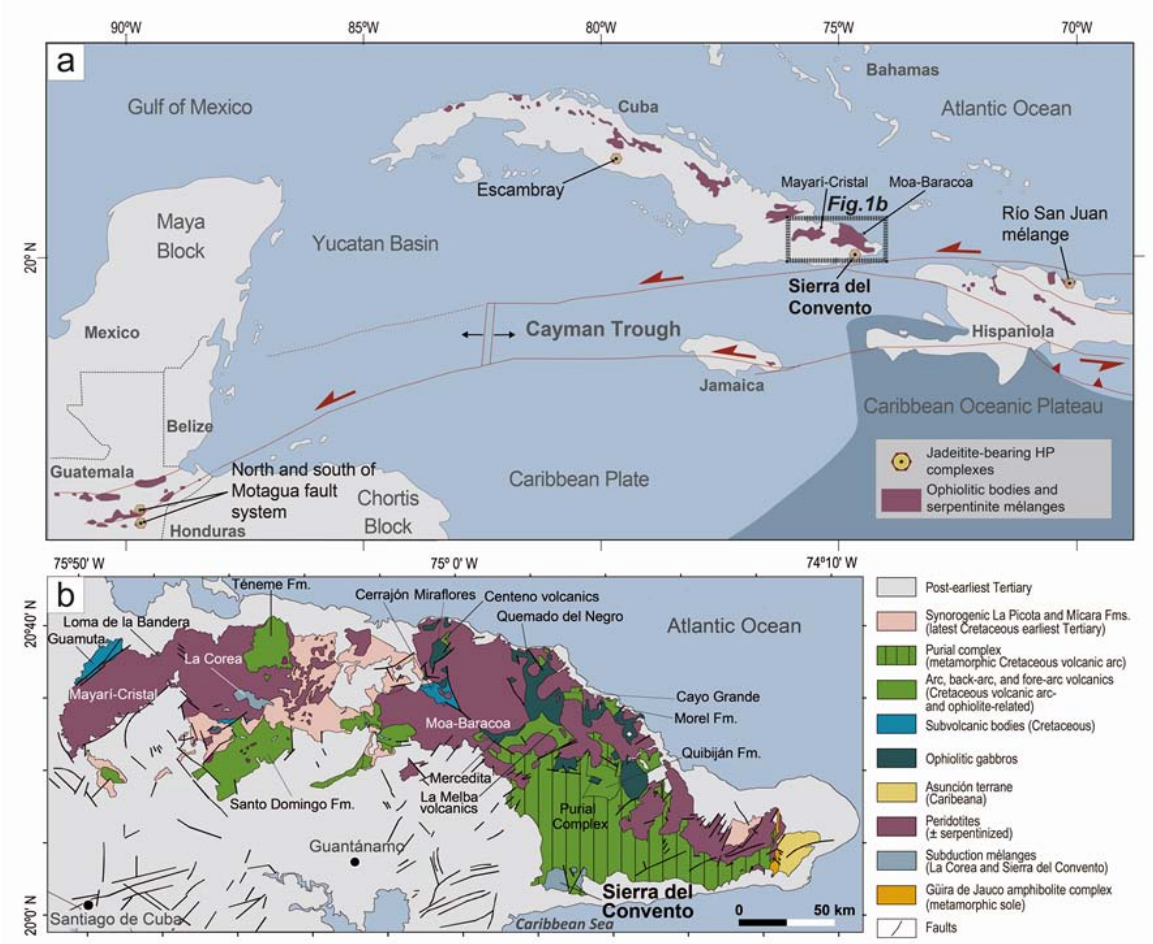

Figure 2.1. (a) Map of Greater Antilles with schematic indication of jadeitite-bearing HP complexes associated with ophiolite bodies and serpentinite mélanges (modified from Wadge et al., 1984). (b) Geological map of eastern Cuba showing the different geological units of the region, with indication of the location of the Sierra del Convento serpentinite mélange (modified from Pushcharovsky 1988).

2.2 Geology of eastern Cuba

In eastern Cuba, the orogenic belt includes oceanic units of Cretaceous volcanic arcs, ophiolites, and closely associated serpentinite-matrix subduction mélanges (Figure 2.1b). All these units constitute tectonic nappes with a general vergence towards the NE and accreted in the late Cretaceous–earliest Palaeocene (Cobiella et al., 1984; Núñez Cambra et al., 2004; Iturralde-Vinent et al., 2006a; figure 2.2). The ophiolite belt comprises two allochthonous massifs: the Mayarí–Cristal massif to the west, with a mantle section over 5 km thick, and the Moa–Baracoa massif to the east, with about 2.2 km of peridotite section (Proenza et al., 1999; Marchesi et al., 2006). Harzburgitic tectonites are dominant, with subordinate dunites, chromitite bodies, banded gabbros, and discordant microgabbro and pyroxenite, troctolite, wehrlite, and diabase bodies. Basaltic rocks with tholeiitic to boninitic signature and radiolarites tectonically underlie the mantle section (Kerr et al., 1999; Iturralde-Vinent et al., 2006b; Marchesi et al., 2006, 2007; Proenza et al., 2006). Dilek and Furnes (2011) have incorrectly classified the Cuban ophiolites as plume-related, as demonstrated by their supra-subduction geochemical signatures (e.g., Proenza et al., 1999, 2006; Gervilla et

al., 2005; Marchesi et al., 2006, 2007). Recently, Lázaro et al., (2013) and Lázaro et al., (2015) identified the Guira de Jauco amphibolite complex (650–665°C and 8.5–8.7 kbar) as the metamorphic sole of the Moa–Baracoa ophiolite sheet and related it to the inception of a new SW-dipping subduction of Late Cretaceous age (85 Ma) in the back-arc of the Cretaceous Caribbean arc. The ophiolitic massifs were tectonically emplaced over the tholeiitic to calc-alkaline Aptian–Campanian volcanic arc units during the late Campanian–Maastrichtian times (Iturralde-Vinent et al., 2006b and references therein) shortly after the volcanic-arc-related El Purial complex subducted to greenschist/blueschist facies conditions (Boiteau et al., 1972; Somin and Millán 1981; Cobiella et al., 1984) during the latest Cretaceous (75 ± 5 Ma; Iturralde-Vinent et al., 2006a). Zircon from an ophiolitic gabbroic body from Cayo Grande (Moa–Baracoa ophiolitic massif) yielded a $^{206}Pb/^{238}U$ age of ca. 124 Ma (Rojas-Agramonte et al., 2016). Similar early Cretaceous ages characterize low pressure serpentinite-matrix mélanges containing blocks of fore-arc metadiabase/metamicrogabbro whose basaltic protoliths formed at >123 Ma (Lázaro et al., 2016). The correlated Gaspar–Hernández serpentinite mélange in the Dominican Republic contains blocks of similar (meta)micrograbbro crystallized at 136 Ma from Mid-Ocean-Ridge Basalt (MORB) magmas formed in the proto-Caribbean oceanic lithosphere (Escuder-Viruete et al., 2011) or fore-arc basalts (Lázaro et al., 2016) formed during subduction initiation. These ages predate the ages of the exhumed products of subduction recorded in high-pressure subduction mélanges, as described below.

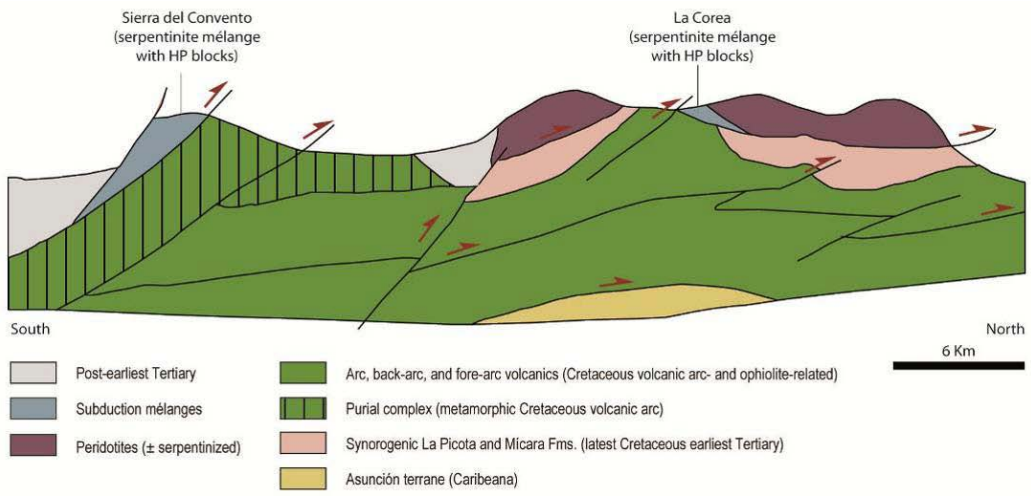

Figure 2.2. Schematic cross-section of eastern Cuba (S-N), showing the relations between La Corea and the Sierra del Convento mélanges and major geological complexes in the region (modified from Iturralde-Vinent, 1998).

2.3 High pressure mélanges

Two serpentinitic mélanges bearing high-P blocks, namely the Sierra del Convento and La Corea mélanges (Millán, 1996b; Figure 2.1b), record early to late stages of subduction of the Proto-Caribbean oceanic lithosphere below the Caribbean plate (García-Casco et al., 2008a; Blanco-Quintero et al., 2010, 2011d). These mélanges

share similar geological, petrological, and geochemical characteristics. The Sierra del Convento mélange occurs in between an upper body of partly hydrated ultramafic rocks lacking high-P tectonic blocks and above the metamorphosed Cretaceous volcanic arc Purial complex (Iturralde-Vinent, 1998; García-Casco et al., 2008a; figure 2.2). The distribution of field exposures of the mélange allows defining four sub-mélanges: El Palenque, Posango, Sabanalamar, and Macambo, to the north, east, west, and south, respectively, of the central hydrated ultramafic body (Figure 2.3). The La Corea mélange is completely surrounded by ultramafic rocks of the Mayarí–Cristal ophiolitic massif and its corresponding footwall rocks are not exposed. The tectonic relationships suggest that the mélange is overridden by the ophiolitic massif, and that both override the Cretaceous volcanic arc Santo Domingo unit (Figure 2.2).

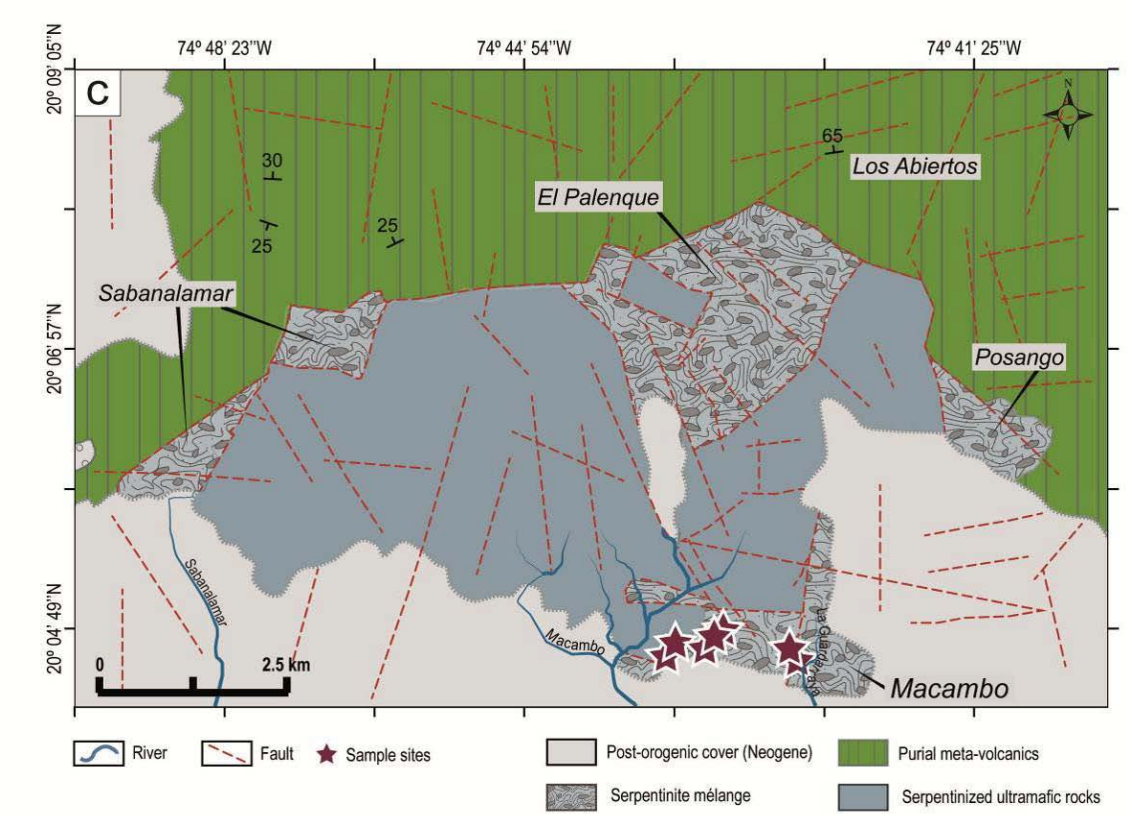

Figure 2.3. Geologic map of the Sierra del Convento mélange, showing the indication of sample sites and the location of the Posango, El Palenque, Sabanalamar, and Macambo sub-mélanges (after Kulachkov and Leyva 1990). See figure 2.1b for location.

Chaotic tectonic blocks of subducted material include MORB-derived garnet-epidote amphibolite and lower grade metavolcanic and metasedimentary blueschist and greenschist-facies rocks derived from abyssal and volcanic-arc-related settings (Millan, 1996b). In addition, serpentinites and serpentinitic blocks included in both mélanges have been interpreted as the footprint of the subduction initiation of the Proto-Caribbean basin below the Caribbean plate during early Cretaceous times (Cárdenas-Párraga et al., 2017). These serpentinites are derived from abyssal mantle

rocks affected by a small degree of melting and re-fertilization processes at an oceanic fracture zone, interacting with fluids in the subduction settings (Blanco-Quintero et al., 2011d; Cárdenas-Párraga et al., 2017; see Chapter 5). The association of serpentinite and high-P rocks in the eastern Cuba mélanges (fossil Cretaceous subduction channel) is consistent with the large-scale tectonic transport of blocks and matrix in the subduction channel (Blanco-Quintero et al., 2011a, d; Cárdenas-Párraga et al., 2017).

The earliest product of subduction is garnet-epidote amphibolite that reached supersolidus temperature at mantle depths (700– 50°C, 15 kbar, 50 km depth), as documented by anatectic leucocratic segregations and veins of trondhjemitic composition that crystallized at similar depths (García-Casco, 2007; Lázaro and García-Casco, 2008; Lázaro et al., 2011; Blanco-Quintero et al., 2011b, 2011c, 2011e). SHRIMP U–Pb ages of magmatic zircons from anatectic rocks range from 113 to 105 Ma (Lázaro et al., 2009; Blanco-Quintero et al., 2011e). Blocks of jadeitite occur at the Macambo region of the Sierra del Convento mélange (García-Casco et al., 2009; Cárdenas-Párraga et al., 2010, 2012). All these early subduction-related rocks show retrograde blueschist facies overprint, documenting counterclockwise P-T-t paths. The metamorphic/magmatic/hydrothermal evolution indicates the subduction of young hot oceanic lithosphere (close to a mid-ocean ridge) at ca. 120 Ma, accretion to the upper plate (near-isobaric cooling stage at 50 km depth dated at 115–105 Ma), and slow syn-subduction exhumation to ca. 25 km depth within the evolving serpentinitic channel until ca. 75 Ma (Lázaro et al., 2009; Blanco-Quintero et al., 2010, 2011a, 2011e), when subduction of the Purial volcanic arc complex accreted blocks of greenschist and blueschist to the mélange. At 70 Ma, arc-Caribeana terrane–Bahamas margin collision triggered exhumation to the surface, as documented by the Maastrichtian–Danian olistostromic synorogenic sediments of Micara and La Picota formations containing detrital ophiolitic material (Cobiella et al., 1984; Iturralde-Vinent et al., 2008).

3 Analytical Techniques

3.1 Major and trace element analysis

Fresh samples from all studied lithologies present in the area were selected for analyses of major and trace elements. Powdered whole-rock samples were obtained by grinding in a tungsten carbide mill. Major elements and Zr were analyzed with a PHILIPS Magix Pro (PW-2440) X-ray fluorescence (XRF) equipment (*Centro de Instrumentación Científica – CIC*, University of Granada). Measurements were carried out on glass beads prepared with 0.6 g of powdered sample diluted in 6 g of $Li_2B_4O_7$. Precision was better than ± 1.5–2% and ± 4% (relative) for concentrations of ≥10 wt. % and <10 wt. %, respectively.

Trace-element compositions were determined by Inductively-Coupled Plasma-Mass Spectrometry (ICP-MS) at CIC after HNO_3+HF digestion of 0.1 g of sample powder in a Teflon-lined vessel at ~180 °C and ~200 psi for 30 min, evaporation to dryness, and subsequent dissolution in 100 ml of 4 vol.% HNO_3. Blanks and international standards PMS, WSE, UBN, BEN, BR, and AGV (Govindaraju, 1994) were run as unknowns during analytical sessions. Precision was better than ±2% and ±5% for analyzed concentrations of 50 and 5 ppm, respectively.

Platinum-group element (PGE) concentrations were determined at the Genalysis Laboratory Services Pty. Ltd. at Maddington (Western Australia), following the method described by Chan and Finch (2001) using a ICP-MS isotopic dilution technique after nickel sulphide fire assay with detection limits of 1 ppb for Rh and 2 ppb for Os, Ir, Ru, Pt and Pd.

3.2 Scanning Electron Microscopy

Back-scattered electron (BSE) images were obtained using Variable Pressure Scanning Electron Microscopy (VPSEM) in a LEO 1430-VP and an Environmental Scanning Electron Microscope (ESEM) with a FEI mod. Quanta 400 (CIC, University of Granada) operated at 80–100 nA and 15–20 kV. The Cathodoluminescence (CL) images were acquired with a ChromaCLTM (Gatan) device attached to the ESEM operated at the same conditions as for BSE imaging. The CL colour images were constructed from a single scan, mixing live colour channels measured and integrated simultaneously. The signal inputs were controlled by DigiScanTM (Gatan).

To complement the volume of samples, a JEOL microscope model JSM 6490-LV from Universidad de Los Andes (Colombia) was used, working at an accelerating voltage of 20-30 kV, with a 3.0 nm spatial resolution. In all SEM equipment used, semi-quantitative mineral compositions were obtained by Energy-Dispersive X-ray spectroscopy (EDS), and elemental analyses were performed at 20 kV and 15 nA conditions.

3.3 Microprobe analyses

Chemical analysis of minerals in thin section was performed at CIC, University of Granada, using an electron microprobe CAMECA SX-100 operated at 15 kV and 15 nA with a beam size of 5 µm and with natural albite (Na), quartz (Si), diopside (Ca), vanadinite (Cl), sanidine (K), TiO_2 (Ti), $MnTiO_3$ (Mn), $BaSO_4$ (Ba), CaF_2 (F), Fe_2O_3 (Fe), and synthetic MgO (Mg), Al_2O_3 (Al), Cr_2O_3 (Cr), NiO (Ni) as calibration standards. The same instrument operated at 15 kV and 150 nA, with a focused beam, a step (pixel) size of 3 µm, and a counting time of 30 ms/pixel was used to obtain elemental (Si, Al, Ti, Fe, Mg, Mn, Ca, Ba, Na, and K) X-ray maps. The PAP scheme (Pouchou and Pichoir, 1984) was used to calculate the matrix correction coefficients. The X-ray maps were processed with software DWImager (Torres-Roldán and García-Casco, unpublished). The atomic concentrations of elements per formula unit are abbreviated as apfu and Mg# indicates atomic Mg/(Mg+Fe^{2+}) ratio. The Fe^{3+} content in clinopyroxene was calculated after normalization to 4 cations and 6 oxygens (Morimoto et al., 1988). Feldspar and epidote group compositions were normalized to 8 and 25 oxygens, respectively, and assume $Fe_{(total)}$ = Fe^{3+} and likewise for Mn. Dioctahedral (white) and trioctahedral (dark) micas were normalized to 22 oxygens, and chlorite was normalized to 28 oxygens, assuming Fe(total) = Fe^{2+}. Amphibole composition was normalized following the scheme of Leake et al. (1997) and Fe^{3+} was estimated after the method of Schumacher (in Leake et al. 1997). Pumpellyte formula was calculated to 24.5 oxygens and 16 cations. Software CSpace (Torres-Roldán et al., 2000) was used to calculate ternary phase diagrams. Mineral and end-members abbreviations are after Whitney and Evans (2010).

3.4 SHRIMP analytical procedure

Zircon was separated from approximately 1 kg of each sample and, crushed to a grain size of 250 µm using a jaw crusher and a roller mill. A low-magnetic heavy-mineral fraction was obtained using a Wilfley table and a Frantz magnetic separator. The final heavy mineral concentrates (mostly zircons) were obtained by panning with water and alcohol. Zircons for isotopic analysis were then hand-picked by means of optical inspection using a binocular microscope and mounted in epoxy resin together with chips of the Perth Consortium standard CZ3. The mount was ground and polished, and zircons were photographed in reflected and transmitted light as well as imaged via CL to enable selection of areas for analysis. The CL imaging was performed with a Hitachi SEM S-3000N equipped with a Gatan ChromaCL detector and a DigiSan II data recorder at the Beijing SHRIMP Center. Operating conditions were 9 kV, 99 nA. The mount was then cleaned and gold-coated. Isotopic analyses were performed on the Beijing SHRIMP II (sensitive high-resolution ion mass-spectrometer) using the instrumental characteristics described by De Laeter and Kennedy (1998). The analytical procedures are outlined in Compston et al., (1992), Claoue´-Long et al., (1995), Nelson (1997) and Williams (1998). Prior to each analysis, the surface of the analysis site was pre-cleaned by rastering of the primary beam for 2–3 min, to reduce or eliminate surface common Pb. Precise dating of young zircons by SHRIMP is best achieved by using $^{206}Pb/^{238}U$ ages (see Black et al., (2003) and Black and Jagodzinski (2003) for explanation). The reduced $^{206}Pb/^{238}U$ ratios and U contents were normalized to CZ3 ($^{206}Pb/^{238}U$ ¼ 0.09432, adopted age: 564 Ma, U ¼ 550 ppm). Pb/U ratios in the unknown samples were corrected using the ln(Pb/U)/ln(UO/U) relationship as measured on standard CZ3 and as outlined in Compston et al., (1984) and Nelson (1997). The 1s error in the ratio $^{206}Pb/^{238}U$ during analysis of all standard zircons was between 1.03 and 1.43 %. Primary beam current was between 4 and 4.5 nA, and a Köhler aperture of 100 mm diameter was used, giving a slightly elliptical spot size of about 30 mm. Mass resolution was about 5000, enabling clear separation of the ^{208}Pb-peak from the HfO peak. Sensitivity was about 30 cps/ppm Pb per nA. Analyses of samples and standards were alternated to allow assessment of Pb^+/U^+ discrimination and drift.

Raw data reduction and error assessment followed the method described by Nelson (1997). Common Pb corrections were applied using the ^{204}Pb-correction method and assuming the isotopic composition of Broken Hill, since common Pb is thought to be surface-related (Kinny, 1986).

3.5 Sr–Nd–Pb isotopes

Representative eleven whole rock samples were processed for Sr–Nd isotopic analyses at the CIC (University of Granada). Samples were digested in the same way as for ICP-MS and were analyzed by a Finnigan Mat 262 thermal ionization mass spectrometer (TIMS) after chromatographic separation by ion exchange resins. Isotopic data were normalized to $^{86}Sr/^{88}Sr=0.1194$ and $^{146}Nd/^{144}Nd=0.7219$. Procedural blanks were 0.6 and 0.09 ng for Sr and Nd, respectively. The external precision (2σ),

estimated by 10 replicate analyses of the WSE international standard (Govindaraju, 1994), was better than 0.003% for $^{87}Sr/^{86}Sr$ and 0.0015% for $^{143}Nd/^{144}Nd$. The long-term $^{87}Sr/^{86}Sr$ value of the NBS 987 international standard measured at the CIC is 0.710250±4 (n=106). Long-term measurements of the La Jolla Nd international standard in this lab yield $^{143}Nd/^{144}Nd$=0.511844±7 (n=49).

All the measured isotopic data have been corrected for radioactive decay from the inferred crystallization age at 113 Ma, according on SHRIMP analyses of zircons from chloritites, jadeitites, Ab-Ep rocks and trondhjemites samples of the Sierra del Convento mélange and La Corea mélanges (to see section 6.5).

3.6 Raman Spectroscopy

Representative serpentinite samples were selected for micro-Raman study and analyzed directly in polished thin sections with a HORIBA Jobin Yvon LabRam HR 800 dispersive spectrometer equipped with an Olympus BXFM optical microscope in the Serveis Científics i Tecnòlogics of Barcelona University (CCiT-UB). Raman spectra were obtained by applying a non polarized 532 nm laser, using a 50x objective (beam size around 2 µm), with 3 measurement repetitions for 60 seconds each. The instrument was calibrated by checking the position of the metallic Si band at ~520 cm-1. The micro-Raman spectra were processed using the LabSpec® software (JobinYvon). The final spectra were produced by subtracting the background fluorescence.

3.7 X-ray Diffraction

Samples analyzed by powder X-ray diffraction (PXRD) were milled and sieved for < 20 µm particle size, and prepared by manual pressing of the powders by means of a glass plate to get a flat surface in cylindrical standard sample holders of 16 millimeters in diameter and 2.5 millimeters in height. The diffractograms were obtained in a PANalytical X'Pert PRO MPD Alpha1 powder diffractometer in Bragg-Brentano θ/2θ geometry of 240 millimeters of radius, nickel filtered Cu Ka radiation (l = 1.5418 Å), and 45 kV – 40 mA, in the CCiT-UB. During analysis, the sample was spun at 2 revolutions per second. A variable divergence slit kept the area illuminated constant (10 mm) and a mask was used to limit the length of the beam (12 mm). Axial divergence Soller slits of 0.04 radians were used. Samples were scanned from 3 to 80° 2θ with step size of 0.017° and measuring time of 50 s per step, using a X'Celerator detector (active length = 2.122°). The software X'Pert Highscore® was used to substract the background of the patterns, to detect the peaks and to assign mineral phases and their corresponding dhkl to each peak. The data were treated by full profile Rietveld refinement for quantitative analyses of mineral phases using the software TOPAS V3.

3.8 LA-ICP-MS

Trace element LA-ICP-MS measurements of minerals were performed at the C.I.C. of Granada University using a 213-nm Mercantek Nd-YAG laser coupled to an Agilent

7500 ICP-MS with a shielded plasma torch. The ablation was carried out in a He atmosphere, using a laser beam fixed at 60 lm diameter. The spot was pre-ablated for 45 s using a laser repetition rate of 10 Hz and 40% output energy. Afterwards, the spot was ablated for 60 s at 10 Hz with laser output energy of 75%. To keep the laser focused during ablation, the sample stage was set to move 5 lm every 20 s. NIST-610 glass (ca. 450 ppb of each element) was employed as an external standard. In each analytical session of a single thin section, the NIST-610 glass was analyzed at the beginning and at the end, and also after every six spots to correct for drift. Silicon was used as internal standard. Data reduction was carried out using software written by F. Bea (freely available upon request) in STATA programming language (Statacorp 2005). The precision, calculated on five to seven replicates of the NIST-610 glass measured in every session, was in the range ±3 to ±7% for most elements. Further details on technical methods can be found in Bea et al. (2005).

4 Field Relations

4.1 Brief Introduction to Caribbean jadeitites

In addition to jadeitite from Cuba described in this PhD Thesis, jadeitite rocks have been documented to date in the Caribbean realm in two locations (Figure 2.1a). In the Motagua valley of Guatemala, this rock is present in two distinct serpentinite mélanges (North and South Motagua Mélanges) containing high-pressure, low-temperature (HP–LT) blocks including eclogite, garnet amphibole gneiss, and blueschist, documenting subduction-related complexes of Lower Cretaceous age juxtaposed across the Motagua fault (Harlow, 1994; Harlow et al., 2011; Brueckner et al., 2009; Flores et al., 2013).

In the northern Dominican Republic, jadeitite occurs as dispersed blocks as well as layers within lawsonite blueschist blocks in a serpentinite matrix interpreted as a diapir-like serpentinite mélange crosscutting Upper Cretaceous to Lower Ternary HP-LT mafic schist of the "Rio San Juan Complex" (Schertl et al., 2007, 2012; Krebs et al., 2008).

4.2 Jadeitite deposits from The Sierra del Convento mélange

Three types of deposits of jadeitite can be identified in the Macambo region: 1) in-situ deposits within the mélange, 2) detrital boulders in Late Miocene-Pliocene conglomerates of the Punta Imías Formation, and 3) recent deposits exposed in Macambo and Guardarraya rivers and their mouths (Cárdenas-Párraga et al., 2010).

The in-situ deposits within the mélange consist of isolated fine- to medium-grained jadeitite blocks of decimeter-to-meter in length (Figure 4.1 a, b). Jadeitite blocks occur closely associated with albite- and chlorite-rich rocks, and are spatially associated with tectonic blocks of trondhjemite, plagioclase-free epidote ± garnet amphibolite, pargasite amphibolitite, (clino)zoisitite, tremolite–actinolite schist, and glaucophane ± lawsonite schist.

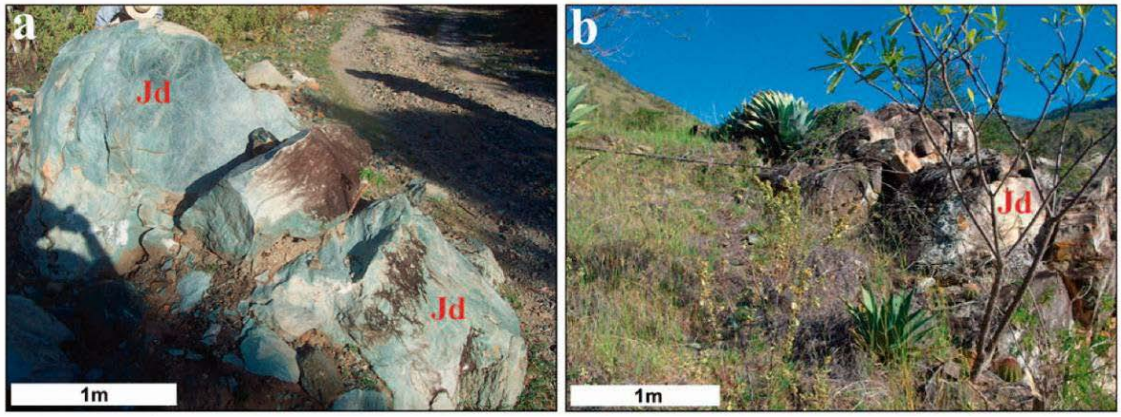

Figure 4.1. (a) and (b) In-situ outcrops of isolated jadeitite blocks within the mélange.

Most jadeitite samples have granoblastic texture, although local brecciation textures are common. Also, crosscutting veins and crusts around the jadeitite bodies are common.

The Late Miocene-Pliocene conglomerates of the Punta Imías Formation, with a total thickness of about 170 m (Cobiella et al., 1977), contain cm- to m- sized boulders of varied composition, including jadeitite, within a calcareous clay matrix (Figure 4.2). The types of jadeitite are similar to those observed in situ in the mélange.

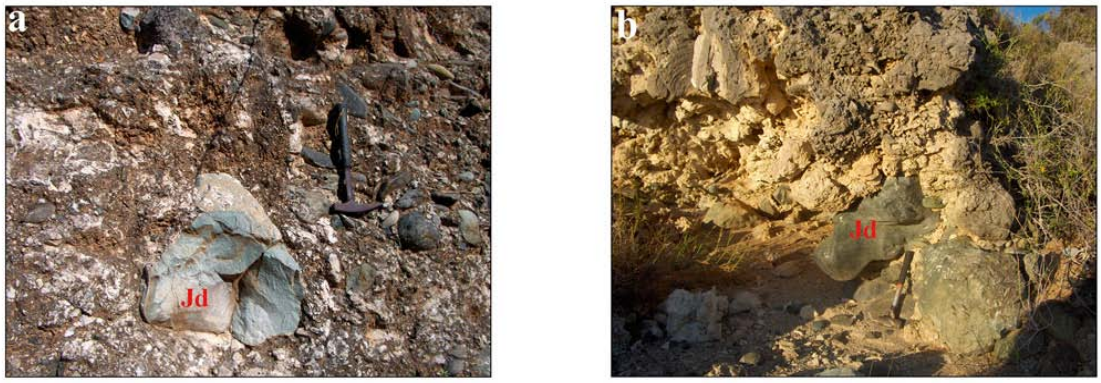

Figure 4.2. (a) and (b) Jadeitite detrital blocks (Jd) in the late Miocene-early Pliocene conglomerates of Punta Imías Formation.

The Recent beach deposits in the mouths of the Macambo and Guardarraya rivers extent along 750 and 650 m, respectively. The pebbles are millimeter- to centimeter-sized in the beach of the Macambo river, and centimeter- to decimeter- sized in the

beach of Guardarraya river. Both occurrences are composed of varied lithologies including jadeitite and all types of rocks found in the Sierra del Convento mélange, though serpentinite is dominant (Figure 4.3 a, b).

Figure 4.3. (a) Recent deposits on the beach of the Guardarraya River. (b) Recent deposits on the beach of the Macambo River. (c) Main variety of gem-quality jade

Taken together, samples of jadeitite from the three outcrops described above have heterogeneous textural and mineralogical composition, but the main variety of gem-quality jade is light green, homogeneous with granoblastic texture and fine- to-medium-grained, being formed by 95% pyroxene (jadeite ± omphacite), albite, biotite-phlogopite and epidote (ca. 5%) (Figure 4.3c).

4.3 Field Occurrence and Classification of Jadeitite and Associated Rocks.

Petrographic inspection of ca. 150 thin sections (see section 6.2 for details) shows a large variety of rocks, commonly gradual in character, that need to be systematically grouped for clarity of field, petrographic and geochemical descriptions. There is a continuum from pure to impure jadeitite varieties rich in omphacite, epidote, mica, albite, chlorite and other minerals. Pure jadeite is essentially made of jadeite and omphacite. There is a continuum between jadeitite and omphacitite. For this reason, we have included omphacite-rich samples within the pure jadeitite variety, even if omphacite may be higher in amount than jadeite in some samples, and we retain the term omphacitite for a fewer number of samples that are composed almost exclusively

of omphacite (>90 mode%). Also, we have distinguished deep-green varieties rich in Cr of both jadeitite and omphacitite. In contrast, we use the term epidote-rich jadeitite for a variety of jadeite-omphacite rock that contains a significant amount of epidote-(clino)zoisite (plus albite and chlorite), and mica-rich jadeitite for a variety of the latter group that contains a significant amount of white mica (both, paragonite and phengite, see below). Another group is made of albite-epidote rocks, which may contain relicts of jadeite and/or omphacite and bear low to moderate contents of chlorite and, occasionally, small amounts of quartz. However, samples from this group that bear significant amounts of chlorite and quartz have been grouped, respectively, in albite-epidote-chlorite and albite-epidote-quartz rocks. Due to mineral abundance, albite-epidote, albite-epidote-chlorite and albite-epidote-quartz rocks cannot be termed albitite. In addition, blackwalls have been grouped in chloritite and titanite-apatite-zircon-rich chloritite. Finally, actinolitite is also distinguished.

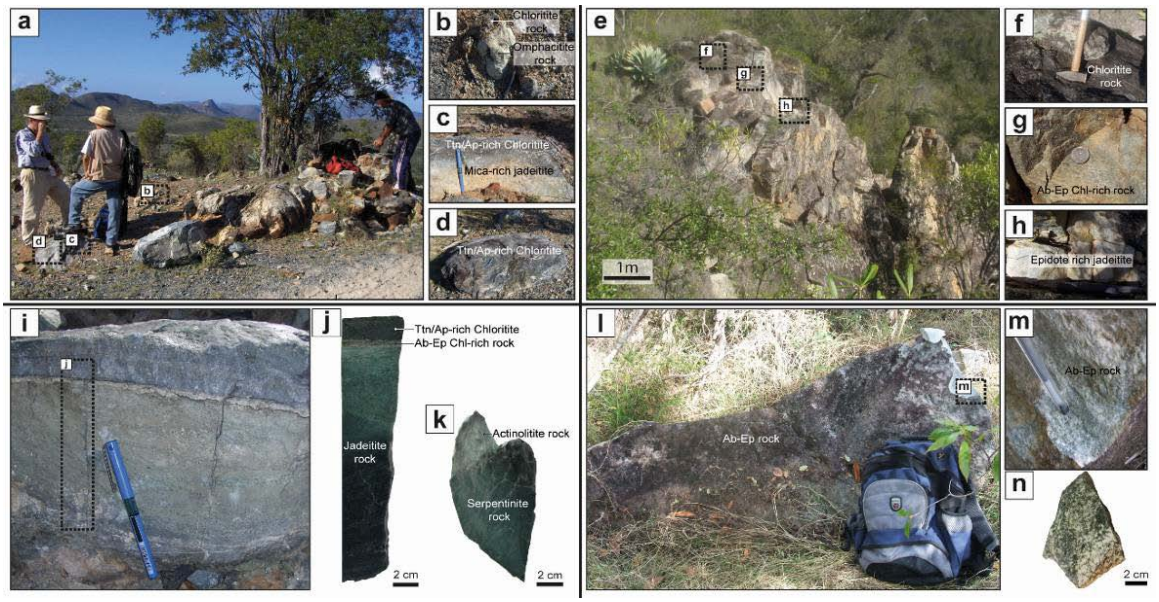

Figure 4.4. Field relations of representative blocks of jadeitite and associated rocks. (a) Fragmented block of jadeitite rimmed by chloritite surrounded by loose serpentinite and details of (b) the chloritite rim and adjacent omphacitite, (c) chloritite rim and adjacent mica-rich jadeitite and (d) chloritite. The apparent thickness of the jadeitite block and the chloritite rim are is ca. 5 m. and ca. 10 cm, respectively. (e) Heterogeneous block made of epidote-rich jadeitite and albite-epidote-chlorite rock rimmed by chloritite and details (f, g, and h). (i) and (j) Detail of jadeitite-chloritite contact in a small block. The location of (j) is indicated by a dotted box in (i). Note the occurrence of a layer of albite-epidote-chlorite at the contact and the increase of albite in adjacent jadeitite denoted by a lighter color. (k) Actinolitite vein within serpentinite taken adjacent to a block of jadeitite. (l) Fragment of albite-epidote block and details at the broken side (m and n).

All types of rocks listed above occur in tectonic blocks (in-situ) surrounded by sheared and foliated serpentinitic matrix (Cárdenas-Párraga et al., 2010; 2012; Figure 2.3). The distribution of blocks extends from the Macambo to the Guardarraya Rivers, spanning a distance of 2.5 km east-west (Figure 2.3). Blocks are of 0.5-6 meters in size (e.g., Figure 4.4a and e, respectively). When occurring in situ, the blocks are systematically

rimmed by blackwalls of chloritite (Figure 4.4a, b, c, d, e, f, I, j and 4.5k, l). Actinolitite is rare and

Figure 4.5. Photographs of representative jadeitite and associated rocks at the hand-sample scale: (a) Green to light-green fine-grained jadeitite (sample SCJ-12). (b) Light-green jadeitite bearing darker clots made of omphacite (sample 09-SC-31v). (c) Deep to light-green medium-grained epidote-rich jadeitite with a fine-grained black band of omphacitite. Note the oriented fabric and the light regions rich in epidote (sample MCB-4a). (d) Medium-grained mica-rich jadeitite crosscut by an albite vein (sample 09-SC-31u III). (e) Omphacitite and (f) Cr-rich omphacitite (samples 09-SC-9i and 09-SC-7b, respectively). (g) Medium- to coarse-grained albite-epidote rock and (h) albite-epidote-quartz rock (samples 09-SC-31a and MCB-3b, respectively). (i) Actinolitite and (j) deformed actinolitite (samples MCB-2a and MCB-3d,

respectively). (k) titanite-apatite-zircon rich chloritite and (l) Chloritite (samples 09-SC-27i and 09-SC-7g, respectively).

occurs as up to 10 cm wide veins/pods in serpentinite adjacent to chloritite blackwalls or surrounded by massive antigoritite (Figure 4.4k and 4.5i, j). Small blocks are generally made of jadeitite, though the grain size and the amount of omphacite generally increase towards the rim. Larger bocks are generally heterogeneous made of various rock types including all jadeitite varieties but, as in smaller blocks, omphacite generally dominates jadeite towards the rim. An oriented fabric is not uncommon (Figure 4.4j). The color of jadeitite varies from light to dark green, showing a fine to medium grain size (Figure 4.5). Dark-to-light green bands with varied jadeite/omphacite contents are common (Figure 4.5c). This group may also show dark clots of omphacite filling mm-sized voids (Figure 4.5b, see also Garcia-Casco et al., 2009 and Cárdenas-Párraga et al., 2012) and mm-sized nodular areas of chlorite-epidote and albite (Figure 4.5c). Omphacitite is generally fine-grained and occurs as dark green bands and diffuse regions that crosscut and overprint jadeitite close to the rims of the blocks (Figure 4.4b and 4.5e, f). Cr-rich varieties of jadeitite and omphacitite occur as small diffuse zones that clearly stand out by their green color (Figure 4.5f). They typically distribute close to the rim of the blocks. Locally, jadeitite may show significant amount of albite and chlorite towards the contact or distributed irregularly within the block (Figure 4.4g and j).

In complex blocks, epidote- and mica-rich jadeitites distribute irregularly but dominate towards the external parts of the block when pure jadeitite is abundant (Figure 4.4h and c, respectively). Epidote-rich jadeitite is heterogeneous at the outcrop scale, showing light- to dark-green color mottled with light white elongated clots of epidote (Figure 4.5c). Mica-rich jadeitite is fine grained and show varied color from light to dark green and black zones as a function of mica, albite, epidote and chlorite amount (Figure 4.5d). In these heterogeneous blocks whitish regions of albite-epidote and albite-epidote-chlorite rocks distribute irregularly (Figures 4.4l and m), but they also occur at the jadeitite-chloritite contact (Figure 4.4g and j). They show dark green to black patches of chlorite±epidote (Figures 4.4n and 4.5g and h). Blocks dominated by these rocks show irregular regions of epidote-rich jadeitite (Figure 4.4h). These relations clearly suggest an intimate genetic relation between all these types of rock.

4.4 Serpentinites

Serpentinites from the Sierra del Convento mélange show similar textural and field relations. Fourteen fresh serpentinite samples were selected from different outcrops at the Macambo sub-mélange (Figure 2.3 and 4.6a). The samples occur as plastically or brittly deformed bodies (massive to foliated fabrics; Figure 4.6b, c), surrounded by sheared serpentinite. At the hand-sample scale, they present green-coloured veins in a dark-green matrix, and inherited deformation from peridotite protoliths, which are locally defined by elongated (retrograde) Cr-bearing magnetite/ferrian chromite grains

(Figures 4.6c). Other primary minerals are lacking, and only bastite pseudomorphs after orthopyroxene are locally observed as irregular patches of green pseudomorphosed porphyroblasts/clasts (≤8 mm in size).

Blanco-Quintero et al., (2011d) identified two types of serpentinite of harzburgitic protolith in the La Corea mélange based on petrographic and major-element composition: i) large blocks of massive/sheared antigorite serpentinite interpreted as deep fragments of the channel developed after mantlewedge peridotite and ii) lizardite–antigorite serpentinite of abyssal origin accreted from the incoming plate at shallow depths. Both types occur intermixed at the outcrop scale and display massive to foliated textures in the field, with massive serpentinite blocks and other lithologies included as boudins in a strongly-sheared serpentinite matrix (Figure 4.6d; Blanco-Quintero et al., 2011d). The lizardite–antigorite type occurs as a foliated variety.

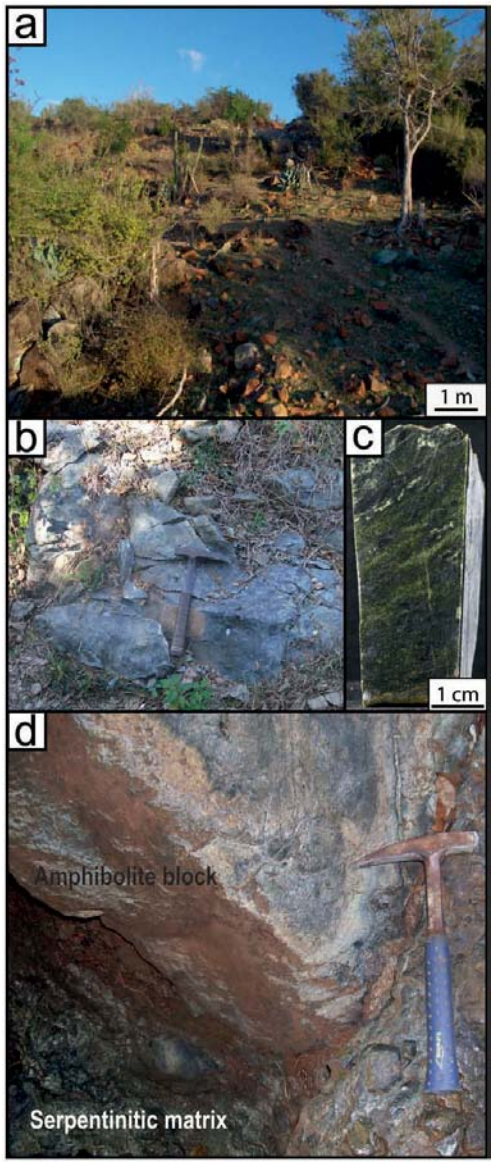

Figure 4.6. (a) Representative outcrop view of the Sierra del Convento mélange. (b) Representative outcrop close-up of a massive serpentinite block. (c) Sample MCB-2f showing a foliated fabric. (d) Contact zone between an amphibolite block within a serpentinite matrix from the La Corea mélange

5 Serpentinites

5.1 Introduction

The incorporation of up to 15-16 wt% H_2O into metaultramafic rocks during serpentinization of lithospheric mantle (e.g. Vils et al., 2008) controls much of the geochemical and geophysical characteristics of oceanic lithosphere (e.g. Harcker et al., 2003; Hattori and Guillot, 2007). This in turn affects the global geochemical cycle of lithosphere creation and consumption (Ulmer and Trommsdorff, 1995; Tatsumi, 2005). Serpentinized ultramafic rocks occur in a variety of geodynamic settings, including active plate margins, such as mid-ocean ridges, oceanic abyssal fracture zones and mantle zones above subducting plates, fore-arc and back-arc basins and passive continental margins (ocean-continent transition). The identification of the geodynamic setting of the ultramafic protolith of exhumed serpentinite bodies is, however, challenging (e.g. Deschamps et al., 2013; Martin et al., 2016).

At (or near) the seafloor, abyssal serpentinites occur at slow-spreading mid-ocean ridges and associated transform faults (Kerrick, 2002) as a result of exhumation of upper mantle peridotites which are hydrated after interaction with downwelling seawater (e.g. Cannat et al., 2010; Kodolányi et al., 2012) and/or by hot fluids (~350°C) released from ocean-ridge hydrothermal activity (e.g. Früh-Green et al., 2003). At transform faults serpentinization reaches great depths below the oceanic Moho (Peacock, 1990), creating zones of lithospheric weakness that may be favorable for subduction initiation (Müeller and Phillips, 1991; Stern, 2004; Gerya, 2011).

In the subduction scenario the infiltration of seawater into the subducting oceanic lithosphere at trenches, favored by normal faults developed during plate bending, causes serpentinization of the underlying oceanic lithospheric mantle (e.g. Ranero et al., 2003). Furthermore, tectonic extension in the fore-arc and the associated infiltration of seawater, as well as the release of fluids after dehydration of the subducted crust and mantle, are responsible for the serpentinization of the upper plate fore-arc mantle (Peacock, 1993; O'Hanley, 1996). Continued subduction during tens of millions years releases considerable amounts of fluid to the upper plate mantle as a result of the dehydration of subducted serpentinite, hydrated mafic crust, greenschist, blueschist, eclogite and sediments, promoting large-scale serpentinization of the mantle at the slab-mantle interface at moderate to low temperature (< 700 °C, <100 km depth) (Poli and Schmidt 2002; Stern 2002; Hacker, 2008; Schmidth and Poli 2013). The larger extent of serpentinization across-strike in the upper plate mantle occurs at shallow depths and low temperatures (<50 km; < 400 °C; Hyndman and Peacock, 2003; Savov et al., 2007), which is consistent with observed fore-arc serpentinite-mud volcanoes. Clasts of blueschist/greenschist rocks contained in serpentinite muds demonstrate that these diapiric structures are rooted to 20 km in the subducted oceanic crust (Maekawa et al., 1993; Yamamoto et al., 1995; Savov et al., 2005; Fryer, 2012). The roots of serpentinite diapirs may, however, be located at deeper depths within the upper-plate serpentinized mantle (Marschall and Schumacher, 2012), as proposed for fossil subduction complexes such as the Franciscan (North America; e.g. Ernst, 2016), Río San Juan (Dominican Republic; Krebs et al., 2008, 2011) and the Motagua (Guatemala; Tsujimori et al., 2006) mélanges that extracted blueschists and eclogites. This scenario is consistent with the development of a several-tens-of-km-long “soft” serpentinitic subduction channel in the slab-mantle interface that extends down to ca. 100 km depth (Guillot et al., 2001; Gerya et al., 2002). The extent of this slab-mantle interface depends on the spatial distribution of the maximum stability limit of antigorite (Ulmer and Trommsdorff, 1995; Wunder and Schreyer, 1997; Schmidt and Poli, 1998; Bromiley and Pawley, 2003). In the serpentinite channel, a low-viscosity/density mélange rises buoyantly along the subduction channel-mantle interface as a self-organized circulating system, and/or as sub-vertically diapirs through the mantle wedge to the crust of the upper plate (Guillot et al., 2015; Li et al., 2015).

As a result of this complex evolving scenario, serpentinites exhumed in suture zones worldwide cover different geodynamic settings including mid-ocean ridges, abyssal transform faults, forearcs, ocean–continent transitions (OCT) and passive margins (e.g. Zheng et al., 2005; Hattori and Guillot, 2007; Deschamps et al., 2013; Barnes et al., 2014; Guillot et al., 2015). Although the original lithologic associations can be partially preserved (e.g. in the western Alps, Zermatt-Saas, Monviso and Corsican ophiolites; Angiboust et al., 2009; 2012a; Beltrando et al., 2014), the primary contacts of serpentinites and associated HP rocks (i.e. the initial position with respect to the downgoing and upper plates) are generally missing. A more chaotic scenario emerges in exhumed subduction mélanges, varying in diversity among occurrences. While

tectonic-sedimentary processes at the forearc involving syn-subduction exhumation of serpentinite and HP slices/blocks, erosion, sedimentation and resubduction may explain mélanges with blocks of different PT conditions and age, serpentinite mélanges with blocks recording the same PT range and age are better explained by tectonic processes at the subduction channel (Wakabayashi, 2015).

As an example, serpentinites of varied origins occur in close spatial relationship together with tectonic blocks of subducted crust metamorphosed at various P-T conditions and ages in the northern boundary of the Caribbean plate (García-Casco et al., 2006; 2008a; Harlow et al., 2004; Hattori and Guillot, 2007; Tsujimori et al., 2006; Brueckner et al., 2009; Lázaro et al., 2009; Blanco-Quintero et al., 2010; Saumur et al., 2010; Krebs et al., 2008, 2011; Deschamps et al., 2011, 2012; Escuder-Viruete et al., 2011, 2013a, 2013b, 2013c). Except for rare cases (e.g., western Cuba; García-Casco et al., 2006), sedimentary matrix has not been described in these mélanges, suggesting tectonic origin in the subduction channel. Furthermore, they contain jadeitite blocks (also formed at various P-T conditions and ages) documenting fluid fluxes and fluid-rock interactions at the subduction environment (García-Casco et al., 2009; Cárdenas-Párraga et al., 2012; Schertl et al., 2012; Harlow, 1994; Harlow et al., 2011; Flores et al., 2013; Hertwig et al., 2016). Subduction initiation in the Caribbean has been explained by forced convergence at the so-called inter-American transform fault zone at about 135 Ma (Pindell et al., 2012; Boschman et al., 2014).

In this chapter, the published major element and platinum-group element (PGE) data of Blanco-Quintero et al., (2011d) are considered in addition to new trace-element data of these samples.

5.2 Petrography

All studied samples are strongly to completely-serpentinized peridotites, as supported by loss on ignition (L.O.I.) values higher than 10 wt% (Supplementary Table 2 and Blanco-Quintero et al., 2011d). Primary silicates and Cr-spinel are completely absent and only Cr-bearing magnetite and ferrian chromite are found as alteration products of the later. As in La Corea, most of the samples from the Sierra del Convento mélange show a general massive-to-fragmented mesh texture (Figure 5.1 and 5.2a). Samples 09-SC-3g and MCB-2f show a strong deformation fabric (Figures 4.6c and 5.2c). Antigorite is the main constituent in all samples (> 90%; Supplementary Table 1) forming pseudomorphic microtextures (mesh textures; figures 5.2a, b), millimetric blades that overprint the original peridotite texture (Figure 5.2b) and non-pseudomorphic massively-recrystallized microtextures characterized by interpenetrating needles (interlocking texture; Figure 5.2c, d). Bastite textures are frequent and made of elongated serpentine crystals parallel to the orientation of exfoliation planes/exolution lamellae of former orthopyroxene.

These petrographic observations were confirmed with micro-Raman and PXRD spectra obtained from Sierra del Convento samples which show very intense and sharp

bands at ~228, 371-374, ~680 and ~1043 cm-1, a weaker band at 456-459 cm-1 and a shoulder/peak at 636-637 cm-1 in the low wave-number spectral region (Figure 5.3a, b, c and d). According to Rinaudo et al., (2003), Groppo et al., (2006) and Schwartz et al., (2013), these typical bands of serpentine-group minerals are located at relatively low Raman shifts and are assigned to antigorite. In addition, in the high spectral region, two very intense bands at 3663-3670 and 3695-3699 cm-1 are observed (Figure 5.3a, b, c and d), which can be related to antigorite, according to Petriglieri et al., (2014). The calculated PXRD profiles of four representative samples are shown in the figure 5.3e, f, g and h. These samples consist mainly of antigorite (from 100% to 63.9%) associated with talc (up to 35.7% in the sample MCB-2f) or tremolite (4.93% in the sample 09-SC-31b), and minor chlorite (from 0.32% to 0.63%). Notably, brucite is absent in the samples, suggesting higher temperatures than in lizardite-brucite-bearing samples from La Corea mélange.

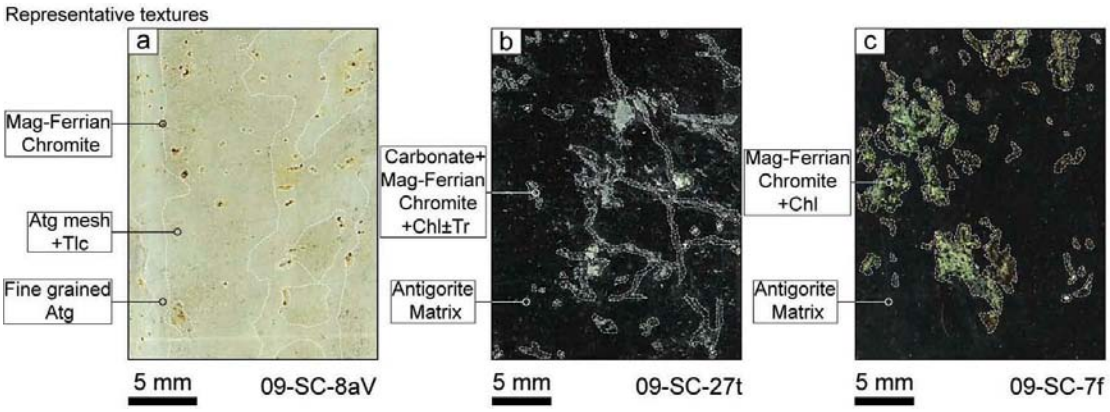

Figure 5.1. Scanned thin sections showing a summary of the different characteristic macroscopic textures of samples (a) 09-SC-8aV; (b) 09-SC-27t; and (c) 09-SC-7f.

Chlorite is present in all studied samples (Supplementary Table 1). It forms fine-grained idioblastic flakes (around 0.3 mm; Figures 5.2c and f) and xenoblastic felt-like aggregates (Figure 5.2e). Both types appear dispersed in the serpentine matrix and usually occur at the edge of mesh-texture bodies (Figure 5.2a). Chlorite systematically envelops ferrian chromite-magnetite that formed after complete replacement of disseminated primary Cr-spinel (Figure 5.2d). Chlorite is also locally interlocked with calcic amphibole (tremolite) grains (Figure 5.2e) in replacement textures after primary pyroxene(s). Talc is common in all sample types (Supplementary Table 1). It forms fine anhedral granules or dusty grains dispersed in the matrix, which are associated with chlorite and rare fine- to medium-grained subidioblastic tremolite (Figure 5.2a; Supplementary Table 1). Tremolite (Figure 5.2e) is locally included within carbonates. Anthophyllite occurs in one sample (09-SC-7k) as dispersed, anhedral granules overprinted by matrix antigorite and associated with magnetite and ferrian chromite after spinel; Figure5.2f). Fine-grained neoformed clinopyroxene occurs in sample 09-SC-09d (Figure 5.2e) associated with tremolite and in the cores of pseudomorphic-serpentine textures.

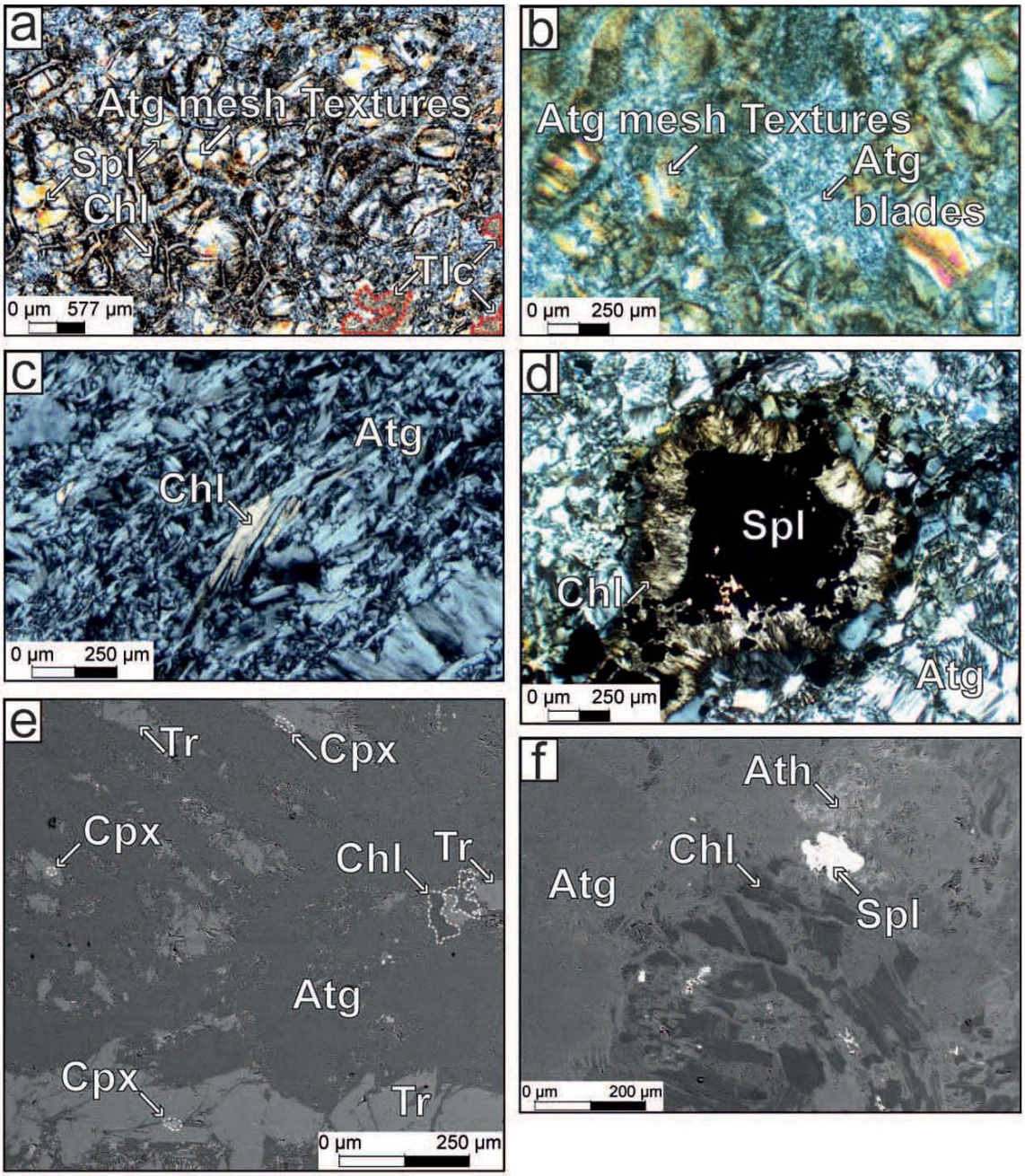

Figure 5.2. Cross-polarized light (a–d) and BSE images (e–f) showing serpentinite microtextures. (a) and (b) Mesh textures and blades of antigorite (Atg) in sample 09-SC-08aV (note some grains of altered spinel). (c) Interpenetrating (interlocking) needles in the antigoritic matrix, containing scattered chlorite (Chl) (sample 09-SC-3 g). (d) Chlorite rims around magnetite/ferrian chromite from alteration of spinel, all surrounded by the interlocking antigoritic matrix (sample 09-SC-31k). (e) Fine-grained clinopyroxene (Di) associated with tremolite (Tr) in sample 09-SC-9d. (f) Anhedral granules of relict anthophyllite (Ath) overprinted by the antigoritic matrix and associated with altered spinel (sample 09-SC-7k).

Antigorite serpentinite from La Corea mélange is characterized by nonpseudomorphic textures of interpenetrating needles of antigorite which is locally partially replaced by dolomite. Talc is variably abundant. Primary Cr-spinel grains are completely altered to ferrian chromite and magnetite generally surrounded by chlorite. On the other hand, antigorite-lizardite serpentinite from this mélange shows pseudomorphic features, such as the hourglass texture of lizardite and antigorite

replacing the orthopyroxene in bastite, fine-grained clinopyroxene, chlorite and magnetite and ferrian chromite that overgrew/replaced primary clinopyroxene porphyroblasts, and spinel. Veins of andradite garnet crosscut these rocks (see Blanco-Quintero et al., 2011d for additional petrographic information).

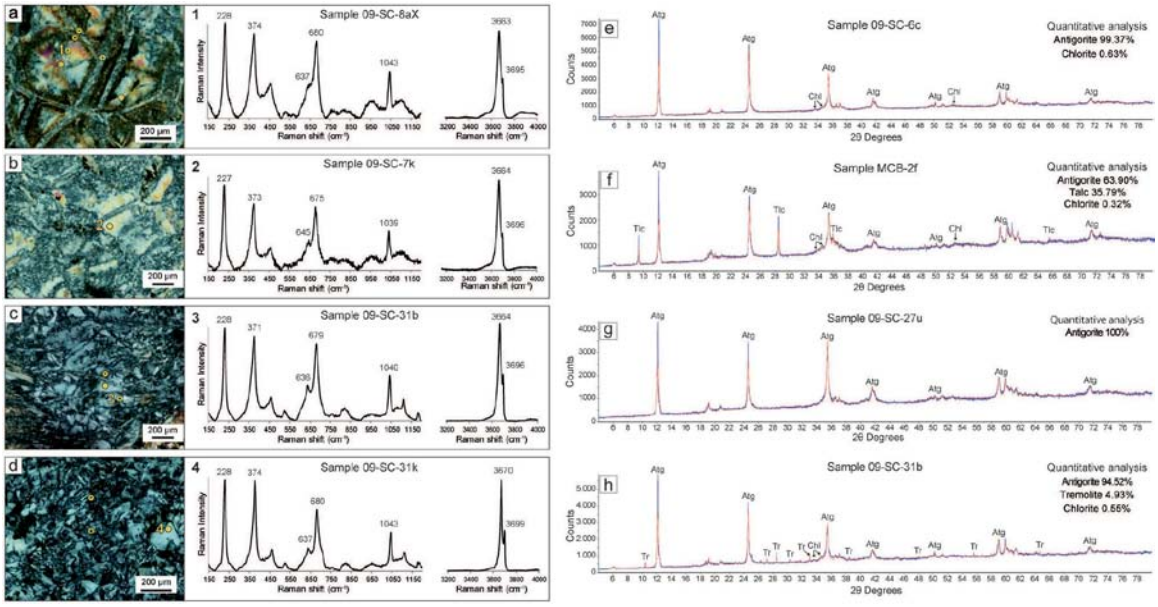

Figure 5.3. Representative micro-Raman spectra in the 150-1200 cm-1 and 3200-4000 cm-1 regions (central panel) and corresponding optical photomicrographs (left panel) indicating the analyzed spots (yellow circles) in samples (a) 09-SC-8aV; (b) 09-SC-7k; (c) 09-SC-31b; (d) 09-SC-31k. The numbered yellow circles indicate the location of the micro-Raman spectrum displayed. Peaks labelled in black are characteristic of antigorite. Representative PXRD results (right panel) for samples (e) 09-SC-6c; (f) MCB-2f; (g) 09-SC-27u and (h) 09-SC-31b with experimental (blue) and calculated (red) profiles.

5.3 Whole rock composition

5.3.1 Major-element geochemistry

The bulk composition of the analyzed samples from Sierra del Convento has LOI values from 9.69 wt% to 12.36 wt% (Supplementary Table 2). The contents of MgO and SiO_2 are variable, ranging from 36.59-42.93 wt% and 46.13-50.79 wt%, respectively (Supplementary Table 2, Figure 5.4a and c), as a likely consequence of mobilization during serpentinization (Snow and Dick, 1995; Niu 2004). The content of Al_2O_3 varies in the range 1.62-3.66 wt% (Figure 5.4). Narrower ranges are shown for FeO_{tot} (7.0 - 8.95 wt%, (Figure 7b), Mg# (100 x $Mg/[Mg+Fe^{2+}_{tot}]$, 88.48 - 91.55; Supplementary Table 2) and TiO_2 (0.02 - 0.17 wt%; Figure 5.4d). The CaO contents are generally low, but one sample reaches 1.10 wt% (09-SC-27t) as a likely consequence of limited carbonation, while typical values are around 0.5 wt% (Supplementary Table 2 and Figure 5.4e). These compositions are similar to the published values from La Corea mélange (Blanco-Quintero et al., 2011d).

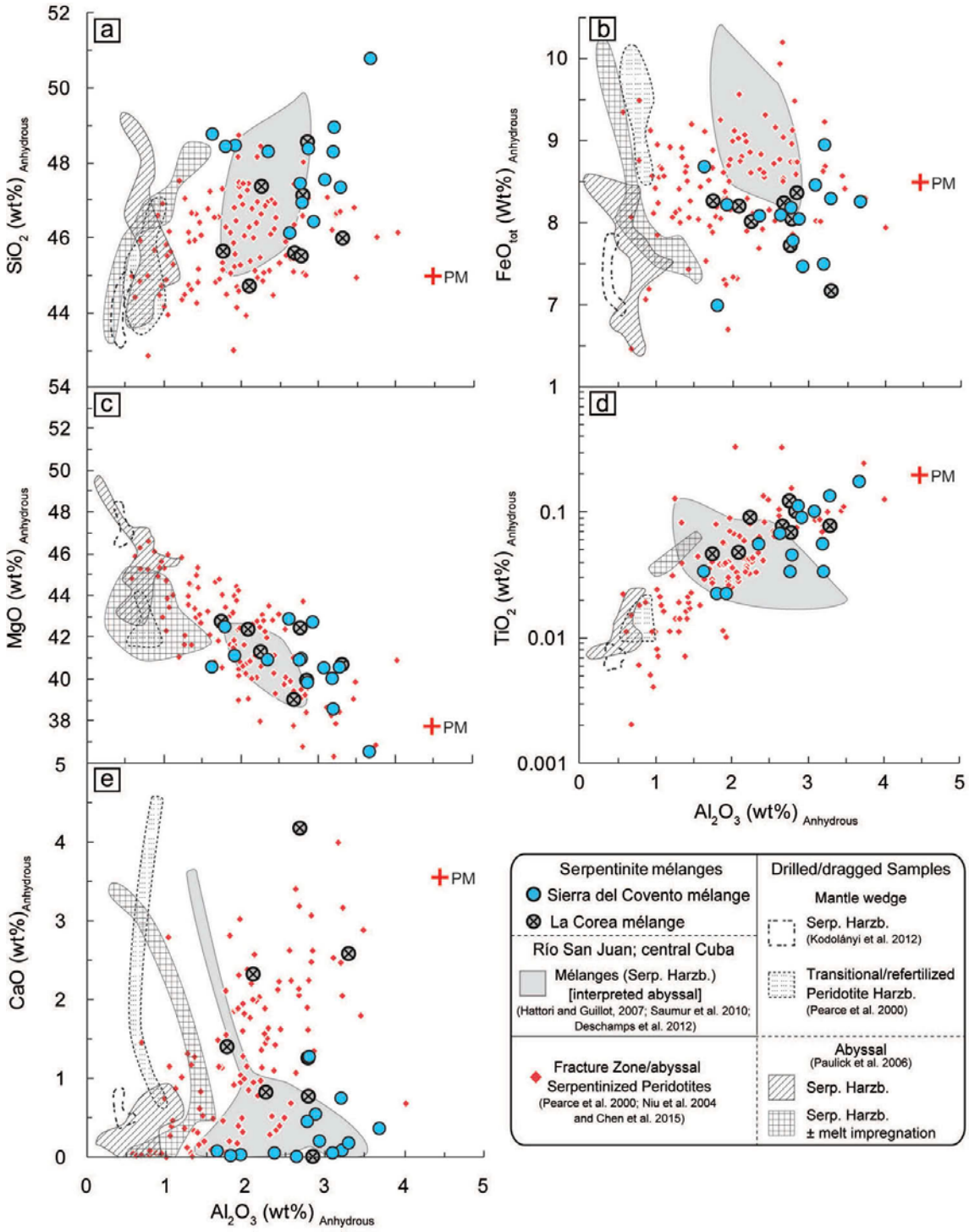

Figure 5.4. Major element diagrams displaying the composition of studied serpentinites (La Corea mélange from Blanco-Quintero et al., 2011d), with oxides recalculated to the anhydrous basis. (a) SiO_2 content (wt%); (b) FeO_{total} content (wt%); (c) MgO content (wt%); (d) TiO_2 content (wt%); and (e) CaO content (wt%); versus Al_2O_3 content (wt%). Silicate Earth (Primitive Mantle, PM) from McDonough and Sun (1995). Samples from different formation environments are plotted for comparison.

We have classified the samples in the Ol-Opx-Cpx ternary diagram calculated in oxy-equivalent or (gram-oxygen) units (Figure 5.5). This measure of mineral proportions was obtained from the molecular proportions of oxides in whole-rock samples using standard algebraic methods and has the advantage of being a measure of the volume

of solids in which oxygen is the only major anion (Brady and Stout 1980; Thompson 1982). We have performed the calculations and ternary projection using the software CSpace (Torres-Roldán et al., 2000) that makes use of the Singular Value Decomposition technique for solving linear equations (Fisher 1989, 1993). According to the fields defined by Le Maître et al., (2002), most samples of Sierra del Convento serpentinite show a harzburgitic protolith in this diagram, except samples MCB-2f and 09-SC-8aV, which have an apparent olivine orthopyroxenite composition. As expected, these two samples contain relatively high talc content, which may indicate a silica-metasomatic transformation of a former harzburgite. In contrast, the sample 09-SC-27t, with the highest calculated Cpx content, shows relatively abundant tremolite and carbonate, the latter suggesting metasomatic (carbonation) alteration. In this diagram the serpentinite samples from La Corea mélange of Blanco-Quintero et al., (2011d) plot as harzburgite and lherzolite compositions that overlap the field of the Sierra del Convento serpentinites, although a trend towards higher Ca is apparent. To a certain extent, this is the result of the presence of carbonates (dolomite).

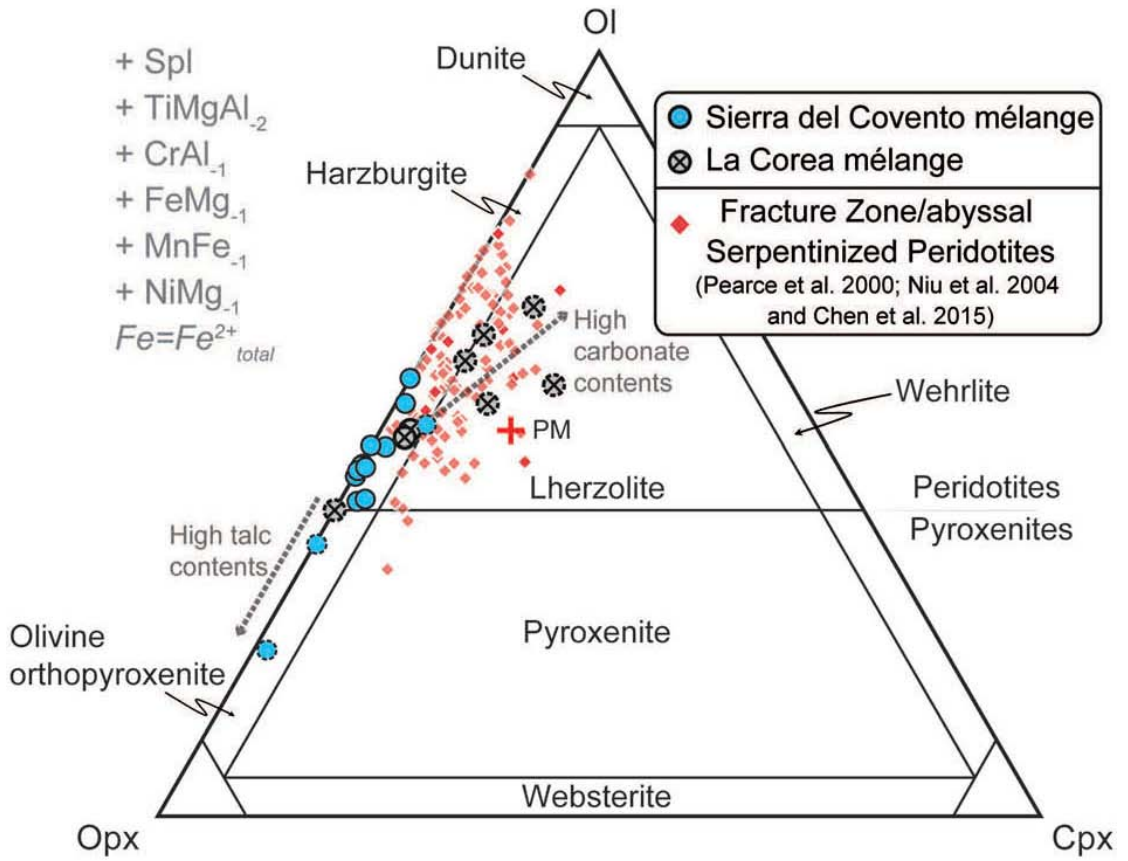

Figure 5.5. Ternary diagram showing oxi-equivalent molar proportions of olivine (Ol), orthopyroxene (Opx) and clinopyroxene (Cpx) within the ultramafic rocks classification scheme of Le Maître et al., (2002). Bulk rock major and trace element compositions (SiO_2, TiO_2, Al_2O_3, FeO_{total}, MnO, MgO, CaO, Cr_2O_3 and NiO) of La Corea (Blanco Quintero et al., 2011d) and Sierra del Convento serpentinite samples are mapped in the space defined by forsterite, enstatite, diopside and spinel (measured in oxy-equivalent units) and the exchange vectors $TiMgAl_{-2}$ (Ti-spinel), $FeMg_{-1}$, $MnFe_{-1}$, $CrAl_{-1}$ and $NiMg_{-1}$. This procedure allows approximating the volume proportions of olivine, ortho and clinopyroxene. Calculations were executed by means of the CSpace software (Torres-Roldán et al., 2000). Serpentinites and serpentinized peridotites from oceanic fracture zone/abyssal environments are plotted for comparison.

Figure 5.6 shows the relationships between the MgO/SiO2 and Al2O3/SiO2 ratios of the studied serpentinites from both eastern Cuba mélanges. All compositions are relatively consistent with an abyssal origin (values of Al2O3/SiO2 above 0.03 are considered typical of subducted abyssal harzburgitic serpentinite; Deschamps et al., 2013). Two samples plot within the field of the compositional evolution trend of melting residue ("terrestrial array" after Jagoutz et al., 1979, and Hart and Zindler, 1986), although most samples have depleted compositions with respect to the "terrestrial array".

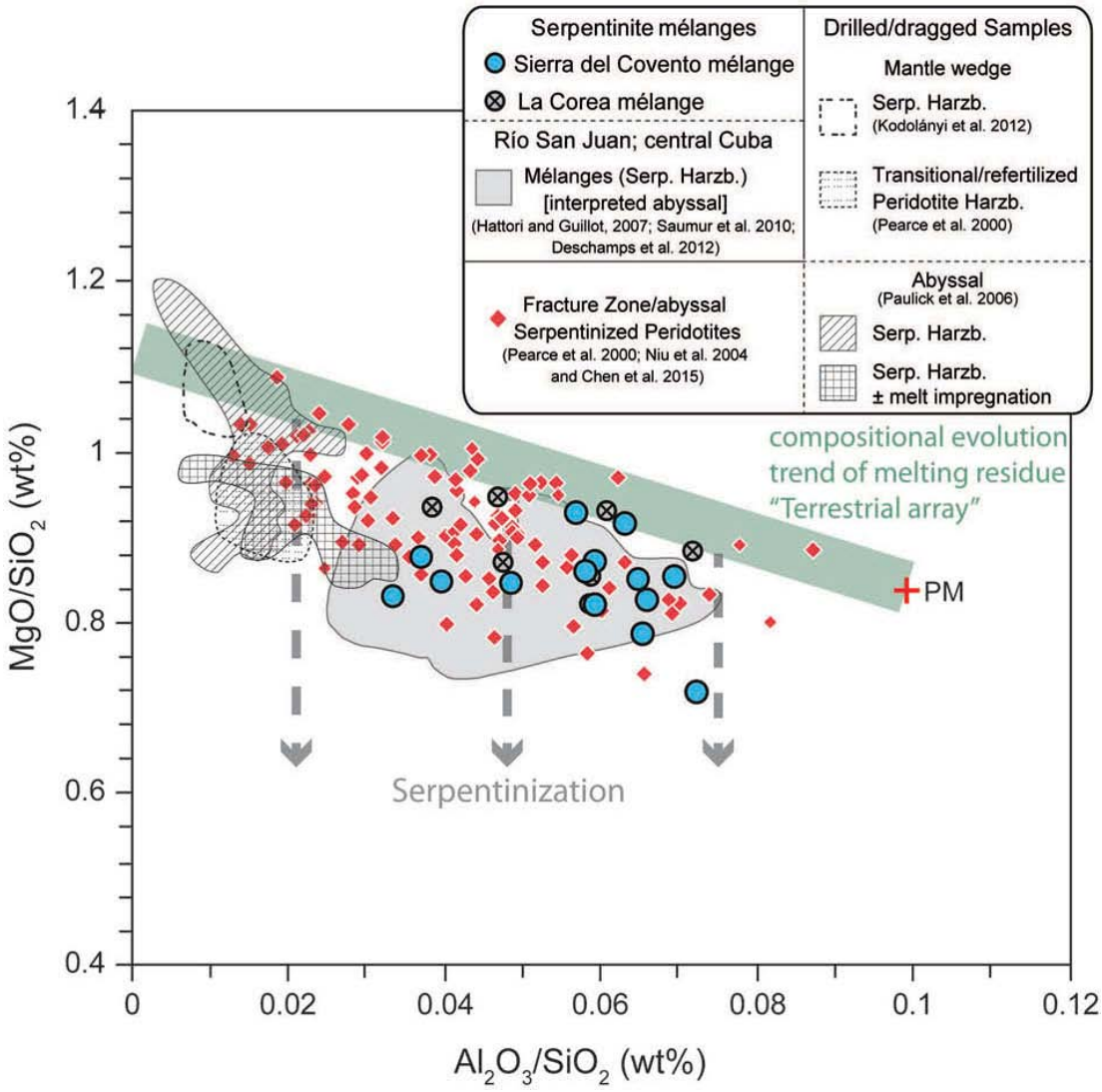

Figure 5.6. MgO/SiO_2 versus Al_2O_3/SiO_2 diagram of the studied serpentinite samples. The "terrestrial array" is after Jagoutz et al., (1979) and Hart and Zindler (1986) and primitive mantle (PM) is from McDonough and Sun (1995). Samples from different formation environments are plotted for comparison.

5.3.2 Trace-element geochemistry

The rare earth element (REE) contents of Sierra del Convento and La Corea serpentinites (Supplementary Tables 2 and 3) range from about 1 to 2 times CI-Chondrite (Figure 5.7a, b). The abundance of other trace elements is, in general,

depleted relative to estimates of the Primitive Mantle (PM), with exceptions in the Large Ion Lithophile Elements (LILE) (Figure 5.7c, d). The REE patterns vary from nearly flat with a mild negative Eu anomaly to slightly HREE-enriched (> CI-Chondrite) and LREE-depleted (Figure 5.7a). Primitive Mantle-normalized trace element patterns of serpentinites are characterized by similar or slightly enriched Cs, Ba, U, and Rb content and Th depletion (Figures 5.7c, d). In general, all samples show marked Hf and Sr depletion and Pb enrichment (Pb was not analyzed for La Corea mélange), though local prominent positive spike in Sr and a negative spike in Rb characterize some samples, suggesting mobilization of fluid-mobile trace elements during serpentinization.

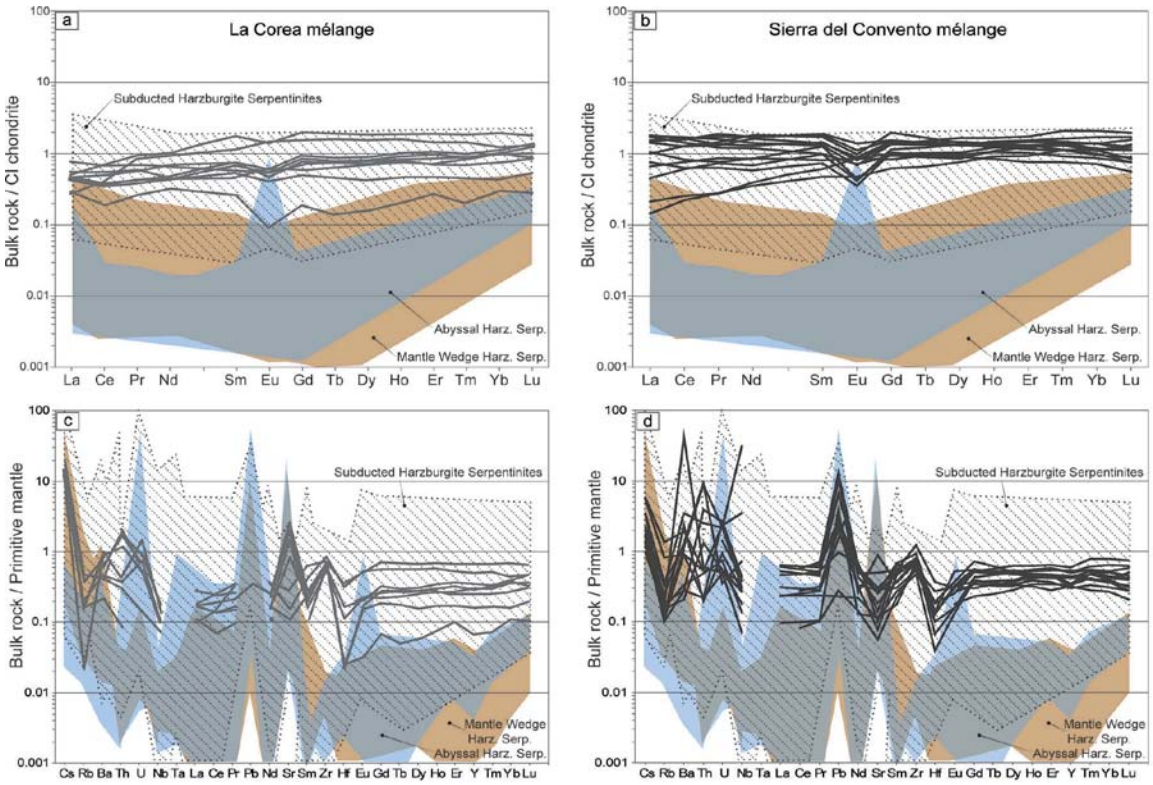

Figure 5.7. Trace element patterns normalized to CI-Chondrite (a and b) and to Silicate Earth/primitive mantle (c and d) (McDonough and Sun 1995) for La Corea (a and c) and Sierra del Convento mélanges (b and d). Subducted, abyssal, and mantle wedge harzburgite serpentinites data compiled by Deschamps et al., (2013; samples from exhumed interpreted bodies and drilled/dragged in oceanic basins) are plotted for comparison.

5.3.3 Platinum group elements composition

The total concentration of platinum group elements (PGE) in the Sierra del Convento serpentinite samples ranges from 18 ppb to 36 ppb (Supplementary Table 4). These low values are characterized by concentrations of Ir-type PGE (IPGE) from 10 ppb to 15 ppb (Os = 1-3 ppb, Ir = 3-4 ppb, Ru = 6-9 ppb) and concentrations of Pd-type PGE (PPGE) from 8 to 21 ppb (Rh = 1-2 ppb, Pt = 5-10 ppb, Pd = 2-9 ppb; Supplementary table 4). The samples have similar values to the Primitive Upper Mantle (PUM; Becker et al., 2006) for Ir, Ru, Pt and Pd, although one sample shows depletion in Pt and Pd and all samples show depletion in Os (Figure 5.8). Serpentinites from La

Corea mélange have similar concentrations of IPGE (Os, Ir, Ru) and PPGE (Rh, Pt, Pd), although they do not show a marked depletion in Os and Pd and have higher values of PPGE.

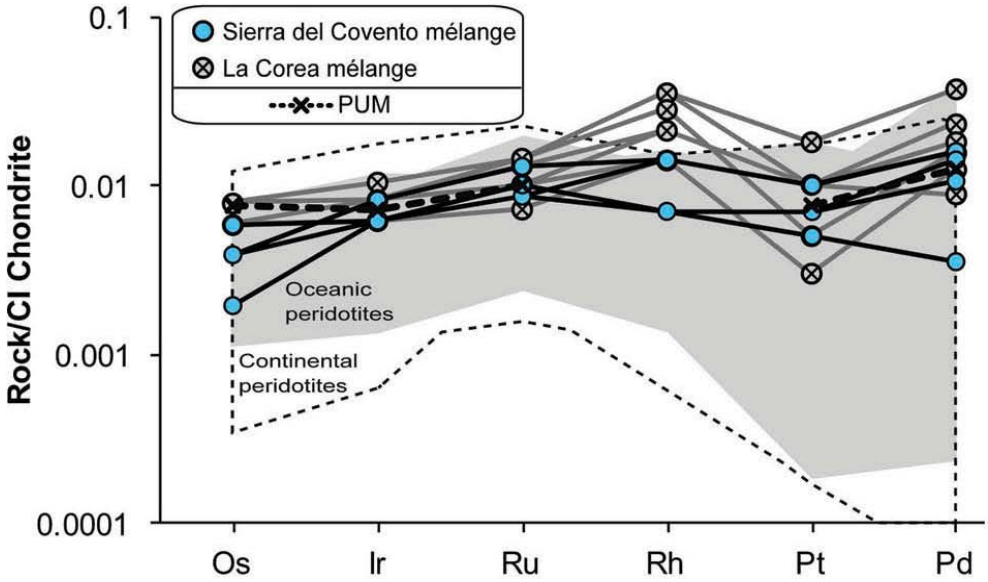

Figure 5.8. CI-Chondrite normalized PGE patterns of eastern Cuba mélanges. PGE of oceanic and continental peridotites compiled by Marchesi et al., (2013a) are plotted for comparison. Normalizing values are from Palme and Jones (2003). Primitive upper mantle (PUM) is from Becker et al., (2006).

5.4 Discussion

The mineral assemblages and textures characterized by antigorite±lizardite, chlorite, tremolite, diopside, talc and, importantly, anthophyllite, with antigorite replacements after lizardite, and the composition of analyzed samples point to a complex geodynamic history of serpentinite from both mélanges. In this section, we discuss the geochemical characteristics of studied samples and their P-T evolution, and propose a tectonic model within the framework of Cretaceous Caribbean tectonics which may be extended to other regions.

5.4.1 Environment of formation

Since extensive serpentinization is characteristic of studied mélanges, the mobility of elements during alteration/metamorphic processes may obscure protolith provenance (e.g. Niu 2004). Serpentinization is characterized by MgO loss, as illustrated by the trend of serpentinized peridotites from the fracture zone/abyssal (Figure 5.6). In a similar way, enrichment of SiO2 and/or CaO in several samples (Figures 5.1b, 5.4a, d and 5.6) may be related to serpentinization of oceanic peridotite by seawater (e.g. Marchesi et al., 2011). Indeed, the samples have PGE concentrations similar to Primitive Upper Mantle (PUM) denoting only local variations in the extent of residual character (Becker et al., 2006), except for Os, Pt and Pd in the Sierra del Convento mélange (Figure 5.8) which show depletions likely caused by limited mobility during serpentinization (Lorand et al., 2003; Pearson et al., 2004; Wang et al., 2008;

Lorand and Alard 2010; Luguet et al., 2003; Harvey et al., 2006; Liu et al., 2009; Marchesi et al., 2013a; Penniston-Dorland et al., 2014). Talc, found in some deformation textures (Figure 5.2a and figures 2b and c in Blanco-Quintero et al., 2011d), is present in the mineral assemblage of several antigorite and antigorite-lizardite serpentinites of both mélanges. The local presence of talc can be related to the variable degree of infiltration of metasomatic fluids. This type of alteration causes a mild negative Eu-anomaly, as shown by most analyzed samples (Figure 5.9; cf. Paulick et al., 2006; Boschi et al., 2006). We hence suggest that a secondary Eu anomaly caused by alteration in the oceanic environment is still preserved.

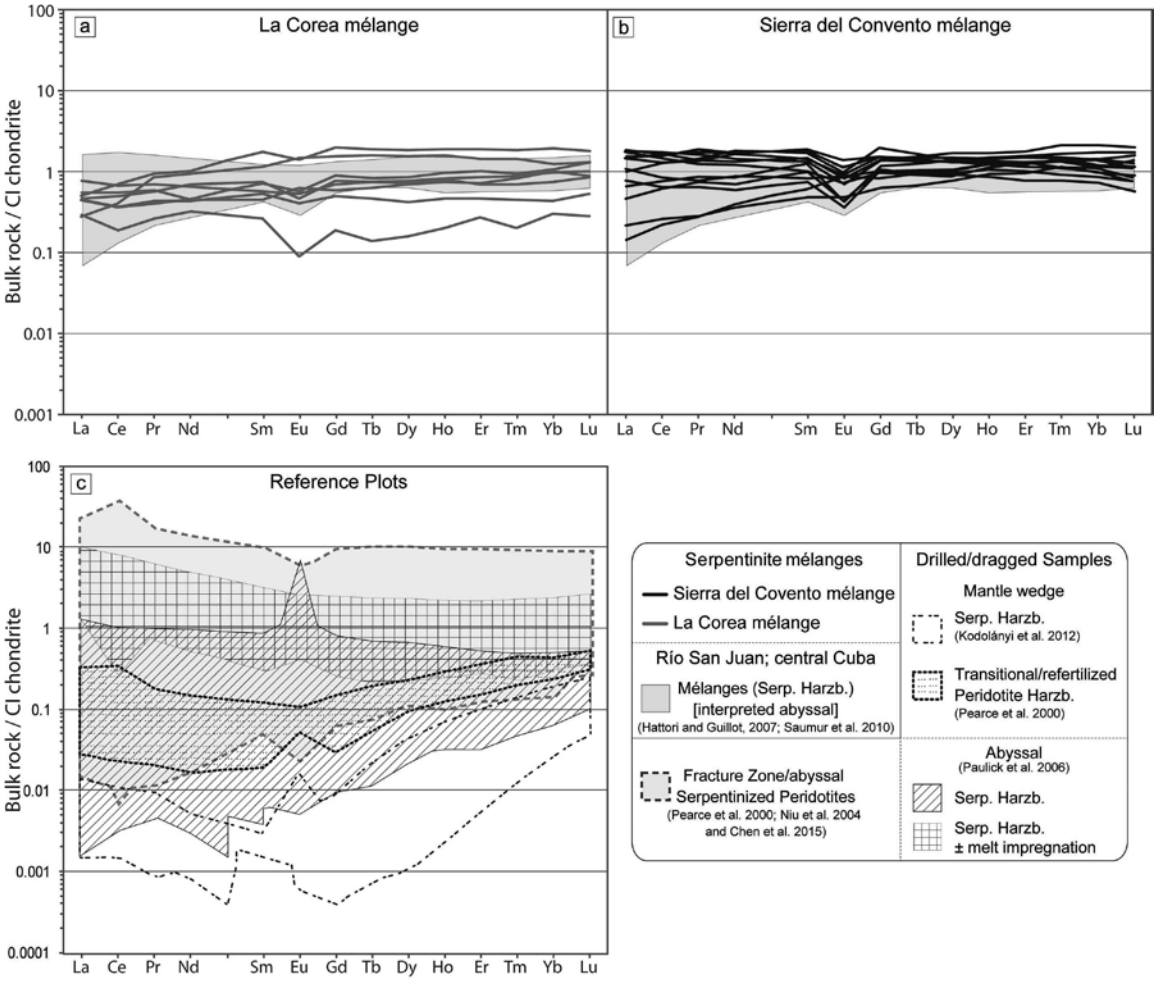

Figure 5.9: CI-Chondrite normalized comparison of samples from (a) La Corea mélange, (b) Macambo sub-mélange, and (c) drilled/dragged mantle wedge, abyssal and fracture zone/abyssal harzburgitic serpentinites/peridotites. In (a) and (b) the field of interpreted abyssal harzburgitic serpentinites from Rio San Juan (Dominican Republic) and central Cuba is plotted for comparison.

In spite of the effects of alteration, the abundance of major and trace elements suggests that serpentinite from both mélanges has similar geochemical signatures (Figures 5.4-5.9) and that all samples broadly conform to the compositional evolution trend of mantle melt residues (terrestrial array; Figure 5.6) with only a somewhat refractory Al_2O_3/SiO_2 signature (>0.03). Furthermore, major and trace element composition show no coincidence with drilled/dragged serpentinites/peridotites from

mantle wedges (Pearce et al., 2000; Kodolányi et al., 2012). Importantly also, they do not show coincidence with drilled/dragged abyssal serpentinites derived from harzburgite (Paulick et al., 2006), except where melt-related refertilization processes affected these rocks (Figures 5.4, 5.6 and 5.9; see below).

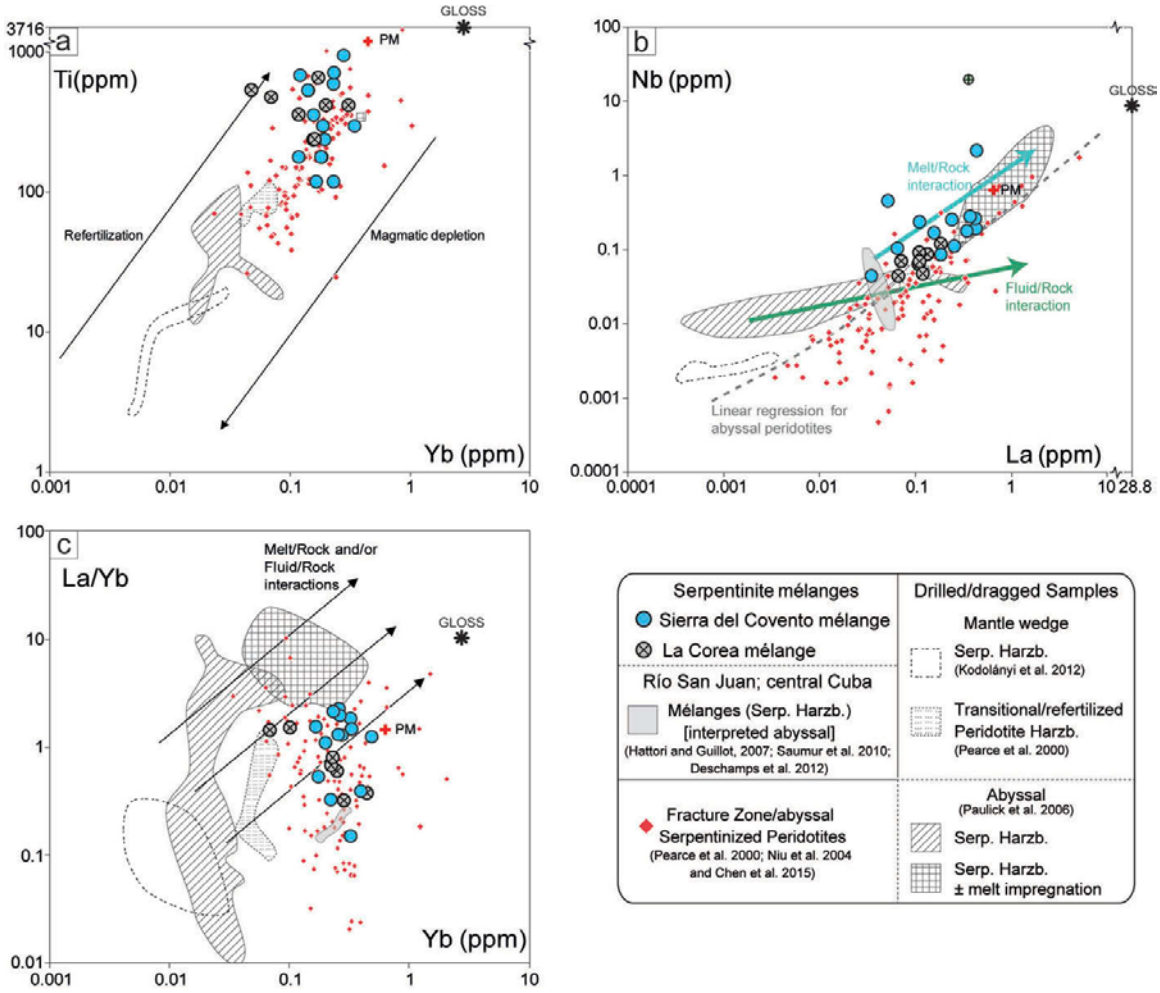

Figure 5.10. (a) Ti versus Yb, (b) Nb versus La and (c) La/Yb versus Yb diagrams for studied samples. Refertilization, magmatic depletion, fluid/rock and melt/rock interactions trends, are after Deschamps et al., (2013) and references therein. Linear regression for abyssal peridotites is shown by a dashed line (Paulick et al., 2006). PM is from McDonough and Sun (1995) and GLOSS after Plank and Langmuir (1998). Note rupture of the Ti and La scales in a and b, respectively.

Immobile trace elements must be used to gain additional insight. Titanium and La/Yb versus Yb relations (Figures 5.10a, c) confirm a less refractory composition (enrichment in Ti and Yb) than drilled/dragged harzburgitic abyssal and mantle wedge serpentinites/peridotites and are similar to compositions of fracture zone/abyssal serpentinized peridotites and drilled/dragged abyssal serpentinites with melt impregnation processes. In a similar way, the Nb versus La diagram (Figure 5.10b) shows a positive trend and a moderate fit to the linear regression for abyssal peridotites (Paulick et al., 2006). These characteristics may be related to refertilization controlled by melt/rock interaction processes. Mafic and differentiated melts percolating and reacting with mantle peridotite are identified as responsible for HFSE

and REE enrichment in samples drilled from transform settings (Niu 2004; Paulick et al., 2006). Higher REE, Zr, Th and Nb contents than abyssal and mantle wedge fields, as illustrated in figures 5.7c, d and 5.10b, would suggest melt impregnation processes that cannot be related to serpentinization due to their immobility in aqueous solutions (e.g. Paulick et al., 2006; Augustin et al., 2012). Thus, the enriched patterns displayed by the studied samples, with REE and IPGE concentrations close to 1 CI-Chondrite (Figures 5.7a, b and 5.9a, b) and PUM (Figure 5.8), respectively, and relatively high concentrations in HFSE can be interpreted as fracture zone/abyssal peridotites that experienced modest percentages of partial melting and likely refertilization processes (Pearce et al., 2000; Niu et al., 2004; Choi et al., 2008a; Chen et al., 2015).

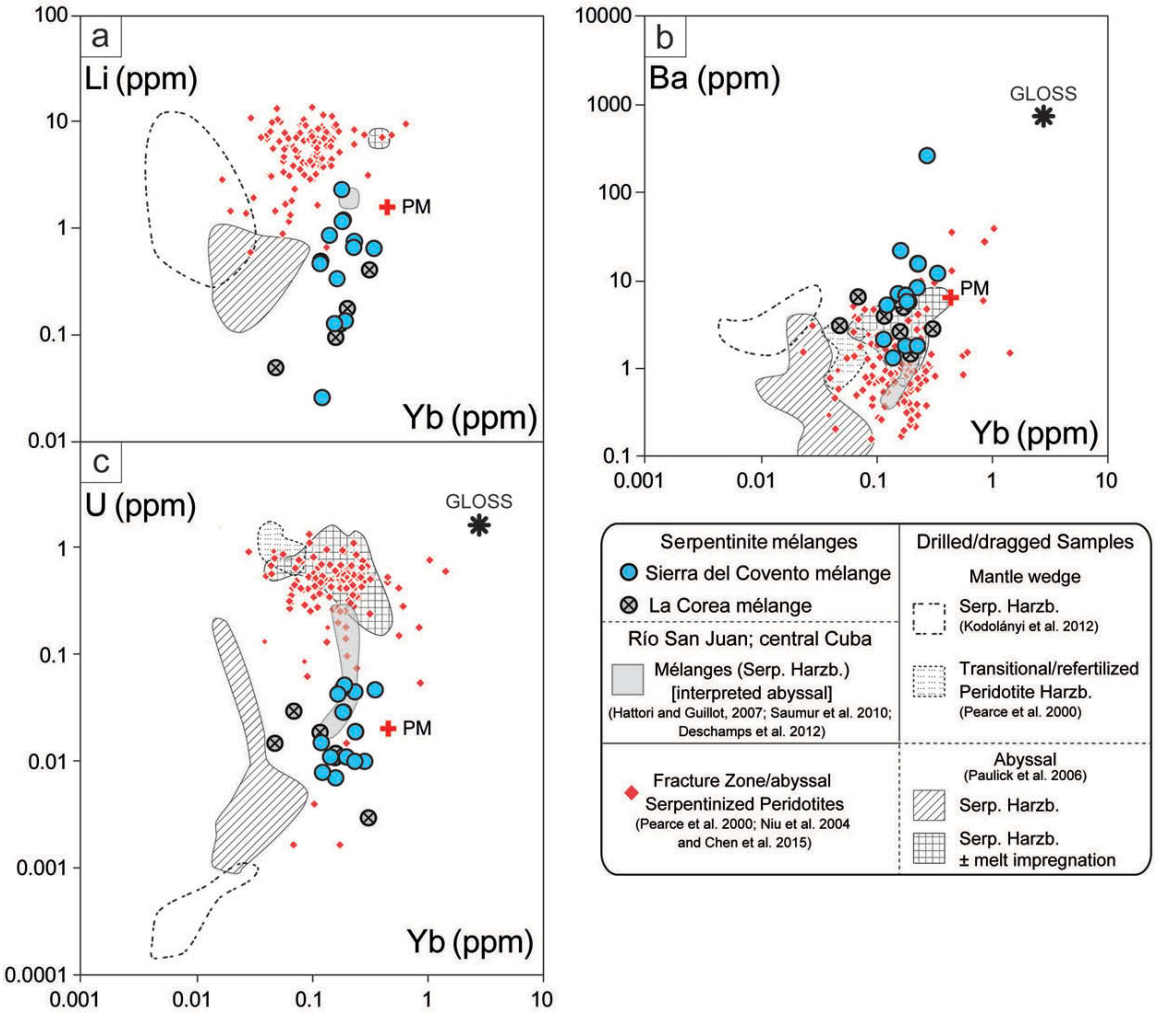

Figure 5.11. Fluid mobile element compositions of the studied serpentinites, (a) Li, (b) Ba and (c) U versus Yb content (ppm). PM is from McDonough and Sun (1995) and GLOSS after Plank and Langmuir (1998).

Enriched patterns of Cs, Rb and Ba with respect to drilled/dragged abyssal serpentinites, on the other hand, may be related to the influence of metasomatic fluids in the mantle wedge by slab-derived agents (Figures 5.7c, d; e.g. Bebout and Barton 2002; Hyndman and Peacock 2003; Scambelluri et al., 2004; Schmidt and Poli 1998). Eastern Cuba serpentinites are similar to serpentinites from the subduction

environment and show strong enrichment in Ba relative to serpentinized peridotites from fracture zones (Figure 5.11b), pointing to an influence of fluids evolved from subducted crust. Indeed, they also show depletion in U and Li (Figure 5.11a, c) relative to fracture-zone/abyssal serpentinized peridotite, pointing to effects of subduction-related fluids (e.g. Vils et al., 2011). Thus, despite their fracture zone/abyssal origin, serpentinites were hydrated in a subduction scenario where they experienced interactions with slab-derived fluids (cf., Choi et al., 2008a; Choi et al., 2008b; Deschamps et al., 2012).

5.4.2 Metamorphic evolution

A first seafloor serpentinization event is documented by the presence of low pressure mineral phases. Anthophyllite, present locally in the Sierra del Convento mélange (Supplementary Table 1; Figure 5.2f) is typical of metaultramafic rocks formed at relatively high temperatures 600-700 °C and relatively low pressures < 7 kbar (Figure 5.12). These conditions are incompatible with mature and warm subduction-related thermal gradients (Figure 5.12). Instead, they may be related to a hot subduction scenario related to subduction initiation of young oceanic lithosphere (as in the eastern Cuba mélanges) or to ocean-floor metamorphism characterized by high thermal gradients. The evidence from the associated tectonic blocks of MORB-derived amphibolite in the studied mélanges indicates a hot thermal gradient of ca. 15 °C/km related to subduction of young oceanic lithosphere (García-Casco et al., 2008a; Lázaro et al., 2009; Blanco-Quintero et al., 2010). This gradient is however incompatible with >31.2 °C/km expected for formation of anthophyllite at <7 kbar and ca. 675 °C. Still hotter gradients are expected for subduction initiation of very young oceanic lithosphere, as in Oman, where the associated metamorphic sole records up to 850 °C and 10-15 kbar (granulites of the Bani Hamid area, United Arab Emirates; Searle and Cox 2002) and a 18.3-27.5 °C/km gradient (3.3 g/cc density), still low compared to >31.2 °C/km. For this reason, alongside the lack of evidence of such a high thermal gradient in eastern Cuba mélanges, our preferred interpretation is that anthophyllite represents a relict of mid-ocean ridge metamorphism. Other minerals, like antigorite, talc, tremolite and diopside may have also formed upon cooling of the oceanic lithosphere down to 300-400 °C and further fluid infiltration (Figure 5.12). However, heating is documented by lizardite transformation to antigorite (Blanco-Quintero et al., 2011d; cf Schwartz et al., 2013). This prograde metamorphic event can hardly be related to the thermal evolution at a transform-zone environment characterized by cooling and must be related to subduction of serpentinite (Figure 5.12).

Tectonic blocks in Eastern Cuba serpentinite mélanges record subduction of oceanic and volcanic arc lithosphere. The earliest subducted metamorphic blocks are MORB-derived garnet-epidote amphibolite and are associated with partial melting-derived segregations and veins of trondhjemitic to tonalitic composition. They formed at high temperature and moderate pressure (700-750 °C, 15 kbar; Figure 5.12) as the result of subduction of a near-ridge lithosphere (García-Casco 2007; Lázaro and García-Casco 2008; Blanco-Quintero et al., 2011b, c, e; Lázaro et al., 2011). At similar depth (50 km)

but lower temperature (550-625 °C), jadeitite rocks were formed in the Sierra del Convento subduction channel (García-Casco et al., 2009; Cárdenas-Párraga et al., 2012; Figure 5.12). Metamorphic overprints bearing glaucophane and lawsonite document counter-clockwise P-T paths and progressive cooling of the channel during accretion (Figure 15). Subduction of the Purial volcanic arc complex during the latest Cretaceous (75-70 Ma) provided blocks of blueschist and greenschist to the mélanges, shortly before arc-terrane collision exhumed the ophiolitic units and associated mélanges (García-Casco et al., 2008b). In this context, before 75 Ma, lizardite-free antigorite serpentinites formed at an imprecise range of 10-14 kbar and 450-600 °C (Blanco-Quintero et al., 2011d; Figure 5.12). On the other hand, since lizardite is locally preserved and antigorite replaced lizardite in some samples, this material reached less than ca. 30 km depth during heating and compression in the channel (<10 kbar, ca. 400 °C; Figure. 5.12). This difference in P-T-path implies that high- and intermediate grade metamorphic blocks and antigorite serpentinite were brought back to the surface from depth and mixed with downgoing lizardite-bearing serpentinite at intermediate depth (Figure 5.13).

As a result of the plastic behavior of serpentinite, large-scale convective circulation is a process documented in subduction channels predicted by numerical models (Gerya et al., 2002 and Gorczyk et al., 2007). A natural example of large-scale convective circulation in mélanges was first presented by Blanco-Quintero et al., (2011a), who documented large P-T recurrences in garnet-bearing amphibolite blocks from La Corea mélange coupled with counterclockwise P-T paths documenting cooling and exhumation from ca. 50 km depth (García-Casco et al., 2008a; Lázaro et al., 2009 and Blanco-Quintero et al., 2011b, 2011e). Metasomatic rinds of actinolite- and chlorite-bearing rocks associated with amphibolite and jadeitite blocks document, in turn, a long-lasting history of fluid-rock interactions in the subduction channel (Cárdenas-Párraga et al., 2012; Blanco et al., 2011d). This evidence points to the large-scale tectonic transport of blocks and matrix in the subduction channel involving mixing of the deeper parts of the channel with shallower parts where large volumes of low-grade serpentinite form (Shervais et al., 2011; Shervais and Choi 2012), rather than exhumation, sedimentation and resubduction (Wakabayashi, 2012; 2015).

5.4.3 Tectonic model

In the model of Figure 5.13 a scenario of subduction and mixing in a subduction channel mélange is conceptualized within current models of plate tectonic evolution of the Caribbean region. Pindell et al., (2012) proposed that subduction nucleated at an inter-American transform fault system developed upon the detachment of North America from Gondwana related to Pangea break-up in the region. Boschman et al., (2014) discussed the plate-tectonic configuration of this fault and concluded that it separated Proto-Caribbean and Panthalassa (Farallon) lithospheres and that subduction of the former below the latter initiated along it during the early Cretaceous. Transform-fault is one possible general scenario for onset of subduction

(Stern 2004; Metcalf and Shervais 2008; Stern et al., 2012) that has been proposed in mélanges, such as the proto-Franciscan subduction zone (Shervais and Choi 2012).

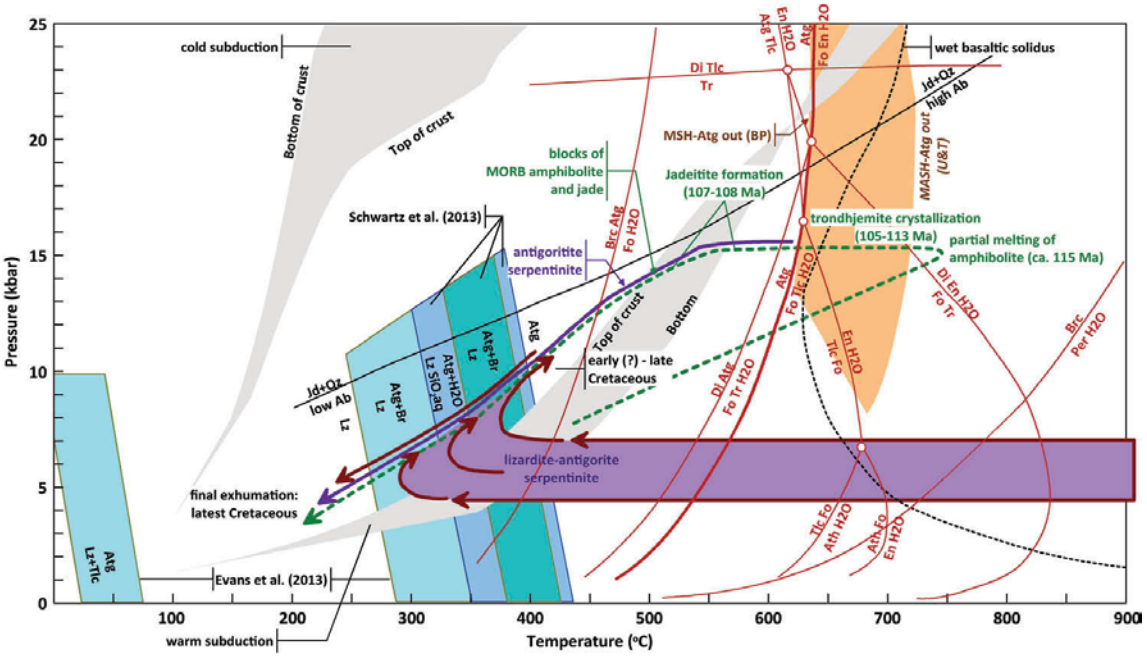

Figure 5.12. P-T diagram showing the metamorphic evolution of the serpentinite rocks of the Sierra del Convento and La Corea mélanges from the oceanic to the subduction environments. The red lines represent the reaction relationships in the CaO-MgO-SiO_2-H_2O system after Spear (1993) and Padrón-Navarta et al., (2012). The thick red reaction curves denote the calculated maximum stability of antigorite in the MgO-SiO_2-H_2O system. This reaction is almost coincident with the experimental stability limit of MSH-antigorite (denoted as "MSH-Atg out (BP)" in the figure, after Bromiley and Pawley 2003). Also shown is the experimental stability limit of Al-rich antigorite (denoted as "MASH-Atg out (UT)" after Ulmer and Tromsdorf 1995). The orange shaded region encompasses additional experimental stability limits of antigorite with variable Al after Bromiley and Pawley (2003), Wunder and Schreyer (1997) and Wunder et al., (2001). The phase relations between lizardite and antigorite (green and blue reaction bands) are from Evans et al., (2013) and Schwartz et al., (2013). For reference, the thermal gradients of the top (slab-mantle interface) and bottom of subducted oceanic crust in cold and warm subduction scenarios (Peacock and Wang 1999) and the wet basaltic solidus (Green 1982) are shown. The P-T paths of subducted MORB Grt-amphibolite blocks of the Sierra del Convento and La Corea mélanges followed counter-clockwise P-T paths, reaching peak conditions appropriate for partial melting at ca. 750 °C at 15 kbar (García-Casco et al., 2008a; Lázaro et al., 2009; Blanco-Quintero et al., 2010, 2011e). Note that related abyssal serpentinite from the downgoing plate subducted at this stage would have been transformed into metaharzburgite/meta-olivine orthopyroxenite, which are lacking in the mélanges. The timing and P-T conditions of jadeitite formation in the Sierra del Convento melange is after García-Casco et al., (2009) and Cardenas-Párraga et al., (2012). Retrograde hydration of peridotite down to ca. 300 °C in the context of a transform fault zone and ensuing down-drag of upper plate serpentinite (which experienced limited subduction down to ca. 30 km, up to 450 °C after onset of subduction) are indicated by deep-red arrows. Massive antigoritite formed at depths of ca. 15 kbar (Blanco-Quintero et al., 2011d). Exhumation of all types of blocks and serpentinite along the subduction channel allowed the formation of the melanges with low-T serpentinite at <10 kbar in a fore-arc setting before final collision-related exhumation during the latest Cretaceous (García-Casco et al., 2008b).

Our data and inferences support a transform-fault scenario for subduction initiation in the northern Caribbean during the early Cretaceous (Figures 5.13a, b). Serpentinitic masses formed along the inter-Americas transform contributed to the mechanical weak zone needed for subduction inception (Figures 5.13c, d; cf. Blanco-Quintero et

al., 2011b and references therein). In an ideal model with only one transform fault plate boundary (rather than a fault zone), once subduction initiated the fault-bounded Proto-Caribbean lithosphere rich in serpentinite was dragged down, while the Caribbean- (Farallon-) plate counterpart was trapped in the forearc region close to the trench at relatively shallow depth (Figure 5.12 and 5.13d; cf. Shervais and Choi 2012). In a more realistic wider fault boundary zone, fragments of subducted serpentinite accreted to the upper plate and contributed to the evolving serpentinitic channel. Upon development at 50 km depth (ca. 10 Ma after subduction initiation, Blanco-Quintero et al., 2011b), subducted oceanic crust (partially melted garnet amphibolites) accreted to the channel. Further development of the channel allowed the shallower part formed by lizardite-bearing serpentinite to be dragged down to <30 km depth, where it mixed with uprising deeper parts of the mélanges (Figures 5.12 and 5.13e).

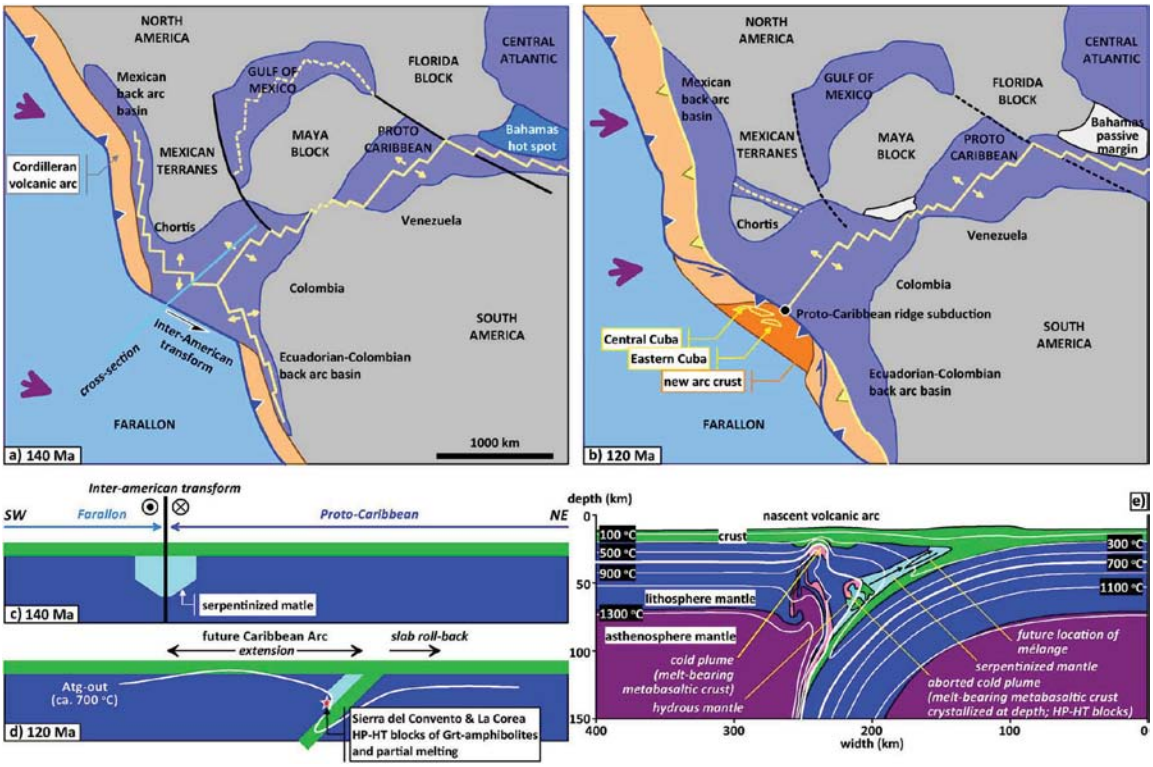

Figure 5.13. (a and b) Cretaceous geodynamic reconstruction of the Caribbean region after Pindell and Kennan (2009) and Pindell et al., (2012). Cretaceous spreading of the Proto-Caribbean oceanic basin separated North and South America. Subduction of the Proto-Caribbean below the abyssal Farallon lithosphere started in the early Cretaceous in the context of the inter-American transform. Ridge subduction formed partially melted metabasaltic crust of Sierra del Convento and La Corea mélanges. Location of cross-section is shown. (c and d) Schematic cross-sections (not to scale) showing early Cretaceous evolution from transform-fault zone to subduction. (e) Numerical thermal-chemical experiment of ocean-ocean subduction initiation of young oceanic lithosphere (age of 10 Ma; initial convergence rate of 4 cm/yr) appropriate for hot subduction and the development of aborted cold plumes (subducted melt-bearing metabasaltic crust crystallized at ca. 50 km depth -ca. 15 kbar- 10.9 Ma after onset of subduction) as an analogue of partially melted subducted MOR basaltic amphibolites of the Sierra del Convento and La Corea mélanges (after Blanco-Quintero et al., 2011b). Flow of matter is shown by black arrows. See text for details.

It is notable that similar fertile compositions as those of eastern Cuba mélanges characterize serpentinized harzburgites from Dominican Republic and central Cuba mélanges. These rocks are classified as abyssal by Hattori and Guillot (2007), Saumur et al., (2010) and Deschamps et al., (2012) but show similar flat patterns of normalized REE, a weak negative Eu-anomaly, and linearly increasing concentrations from LREE to HREE (Figure 5.9). Such coincidence strengthens the view of a transform fault environment for subduction initiation in the Caribbean.

The model presented here would indicate that fertile subducted serpentinite, as opposed to non-refertilized harzburgite serpentinites/peridotites from abyssal and mantle wedge environments as defined by Deschamps et al., (2013), may have formed in similar transform-fault environments. Geochemical enrichments in subducted serpentinite may be related to fluid-mediated processes in the subduction environment, but they may also simply reflect that subducted serpentinites are dominated by fracture zone lithologies. Indeed, it may be no coincidence that subducted serpentinite show similar REE, Th, Nb, Zr and Hf composition as fracture zone serpentinized peridotites (Pearce et al., 2000; Niu 2004; Chen et al., 2015; Figs.5.9 and 5.10). Hence, fertile subducted serpentinite can be considered the footprint of onset of subduction at transform fault zones, as identified in the Sierra del Convento and La Corea mélanges and in other subduction mélanges (e.g. Casey and Dewey 1984; Choi et al., 2008a and b; Shervais and Choi 2012).

6 Jadeitites and related rocks

6.1 Introduction

Commonly, jadeitite rocks are exposed as tectonic blocks within serpentinite-matrix mélanges, and associated with exotic blocks formed in high-pressure subduction environments and others lithologies (e.g., Tsujimori and Harlow, 2012; Harlow and Sorensen 2005; Harlow et al., 2007, 2015). Frequently, pure jadeitites are associated or in contact with more Ca-Mg-Fe-rich rocks (impure jadeitites), denoting a transition to rocks with higher contents of omphacite, epidote, chlorite and amphibole (Harlow et al., 2011). In this way, jadeitites are often found along with other monomineralic rocks as chloritites, omphacitites and albitites (e.g., Harlow 1994; Johnson and Harlow 1999; Sorensen et al., 2010).

The mineral association of the metamorphic rock denominated as jadeitite consists almost entirely of jadeite pyroxene (with a general chemical formula $NaAlSi_2O_6$). Frequently, jadeite suffers substitutions of Na and Al by Ca, Fe and Mg denoting the solid solution toward aegirine and omphacite. Omphacite usually appears as a phase and occurs as granular inclusions replacing and/or overgrowth the jadeite grains (e.g. Harlow et al., 2011; Cárdenas-Párraga et al., 2012). Other phases that can be found typically in jadeitite are albite, epidote, white mica and other minor minerals.

In most of the rocks classified as omphacitite the omphacitic pyroxene dominates over jadeitic, being common to find in the mineral association albite, Ca-amphibole, epidote, phengite and accessory mineral as titanite, apatite and zircon (e.g. Harlow et

al., 2016; Nishiyama et al., 2017). Albitite is a rock composed principally of albite, phases as white mica, epidote and other minor minerals can be present (e.g. Harlow 1994; Johnson and Harlow 1999; Harlow et al., 2016).

Fluids that are saturated in jadeite (Manning, 1998, 2004) have been classified by Tsujimori and Harlow, (2012) defining two types of processes for the formation of jadeitite rocks. P-type jadeitite is a product of fluid crystallization in cavity, crack, fracture and veins in metabasite and/or serpentinized mantle wedge, within and above the subduction channel respectively (e.g., García-Casco et al., 2009; Harlow et al., 2011; Schertl et al., 2012; Cárdenas-Párraga et al., 2012). R-type jadeitite is formed by fluids that cause metasomatic replacement of a pre-existing protolith, such as plagiogranite, in the serpentinitic subduction channel (Compagnoni et al., 2012; Shigeno et al., 2012). Both types of jadeitite forming fluids can be combined in some occurrences (e.g., Bröcker and Enders, 2001; Yui et al., 2010; Tsujimori and Harlow, 2012). To date, most published interpretations of jadeitite rocks are assigned to P-type (see review Harlow et al., 2015; Tsujimori and Harlow, 2012; Harlow et al., 2016). P-type jadeitite samples not show evidence of pseudomorphic replacement and/or minerals relics of a precursor protolith. Their interpretation is mainly based on petrographic characteristics as oscillatory zoning and fluid inclusion in jadeite crystals, along with trace element whole rock compositions characterized by enrichments in Ba, Pb and LILE, with trend toward high Li and Sr, and low Th/U for most samples (Harlow et al., 2016 and references therein). In contrast, R-type jadeitite partially preserves pseudomorphic microtextures of minerals prior to jadeite crystallization and mineral relics of a pre-existing protolith. The trace element whole rock data of metasomatic jadeitite (R-type) are characterized by nearly flat enriched REE patterns, with a negative Eu-anomaly or without it in some cases, these patterns mimic the kind of protolith interpreted by several authors (Bröcker and Enders, 2001; Compagnoni et al., 2012; Shigeno et al., 2012).

Therefore, the mineralogical and geochemical characteristics of jadeitites represent the mass transfer by fluids involved from a subduction channel to the mantle wedge, being a key rock type to understand the sources of the magmatic arc (e.g. Marschall and Schumacher 2012; Harlow et al., 2016).

6.2 Mineral assemblages and textures

6.2.1 Jadeitites and omphacitites

When not significantly retrogressed, the total amount of clinopyroxene in pure jadeitite variety is greater than ca. 80 % and the relative proportion of jadetite: omphacite ranges between 90:10 to 10:90,—with other constituents including (clino)zoisite-epidote, biotite, albite, phengite, titanite, rutile, zircon and apatite (Supplementary Table 5). At the scale of a hand specimen, these rocks have light to dark green colour. They show heterogeneous texture and mineralogy with grain size ranging 0.25-1.5 mm, and dark and light mm-sized nodular areas (Figure 4.5a, b), dark green bands and lighter green veins with diffuse limits crosscutting and overprinting

massive jadeitite (Figure 6.1f). The dominant microstructure is granoblastic (Figures 6.1a and 6.3a, b), with a subtle mineral preferred orientation in some samples, formed by idiomorphic blocky crystals of jadeite of 0.25-1 mm in size. Importantly, jadeite crystals contain quartz inclusions, suggesting relatively high temperature of jadeite crystallization in a changing chemical medium at relatively high pressure within the stability of jadite+quartz (Figure 6.1b), display oscillatory zoning in terms of Al, Na, Ca, Fe, Ti and Mg (Figure 6.2), and bear fine lamella of omphacite which we interpret as exsolution precipitates (Figures 6.1c, d).

Omphacite shows several textural positions, including grains in textural equilibrium with jadeite that suggesting simultaneous crystallization, but late crystallization in pods/voids and replacements after jadeite are abundant, denoting late omphacitization (Figures 6.1d and 6.3b, d).

Dark-coloured nodular areas are composed exclusively of omphacite or biotite ± epidote (Figure 6.1e). In contrast, light-coloured nodular zones consist of albite ± chlorite ± epidote. Both types of nodules occur as interstices within the jadeite-rich matrix and have a xenomorphic or faceted habit resembling negative crystals with a grain size similar to that of the blocky matrix jadeite. They appear to have crystallized late. There are dark green bands primarily consisting of omphacite, which occur as aggregates of xenomorphic fine to very fine grains intergrown with fine-grained jadeite. Lighter green veins consist of omphacite crystals (≤1 mm in size) with interstitial albite (Figure 6.1f).

Epidote occurs mostly as interstitial clusters (Figure 6.1h), associated with chlorite, and is characterized by idiomorphic to sub-idiomorphic habit with inclusions of albite and titanite. In two samples, botroidal aggregates of allanite–(Ce) occur interstitially with idiomorphic epidote and zircon (Figure 6.1h) and contain inclusions of chlorite and epidote. Rutile, titanite, zircon and apatite are minor constituents in jadeitite, dispersed in the matrix. Therefore, zircons with idiomorphic habit are a frequent accessory mineral, occupying interstitial positions as isolated grains and being also included in blocky jadeite and omphacite. They are generally large, with sizes above 100 µm long, with rare inclusions of jadeite, suggesting crystallization contemporaneous to jadeite formation. Biotite occurs at grain contacts associated with jadeite and omphacite and interstitially within the jadeite-rich matrix in a xenomorphic habit (Figure 6.1c, e). Retrograde grains of phengite, associated with albite, and dolomite occur in the interstituum (Figure 6.3b). Rutile is associated with apatite and shows xenomorphic habit. Apatite exhibits variable habit from xenomorphic to idiomorphic, is normally distributed as isolated grains, and contains small inclusions of albite and titanite (Figure 6.1g). Titanite is an abundant accessory mineral as small idiomorphic inclusions in jadeite, and with a xenomorphic habit in interstitial positions associated with apatite or isolated and variable size (Figure 6.3a, d). Thin films of albite at intergranular position within the clinopyroxene matrix denote late albitization (Figure 6.3c, d).

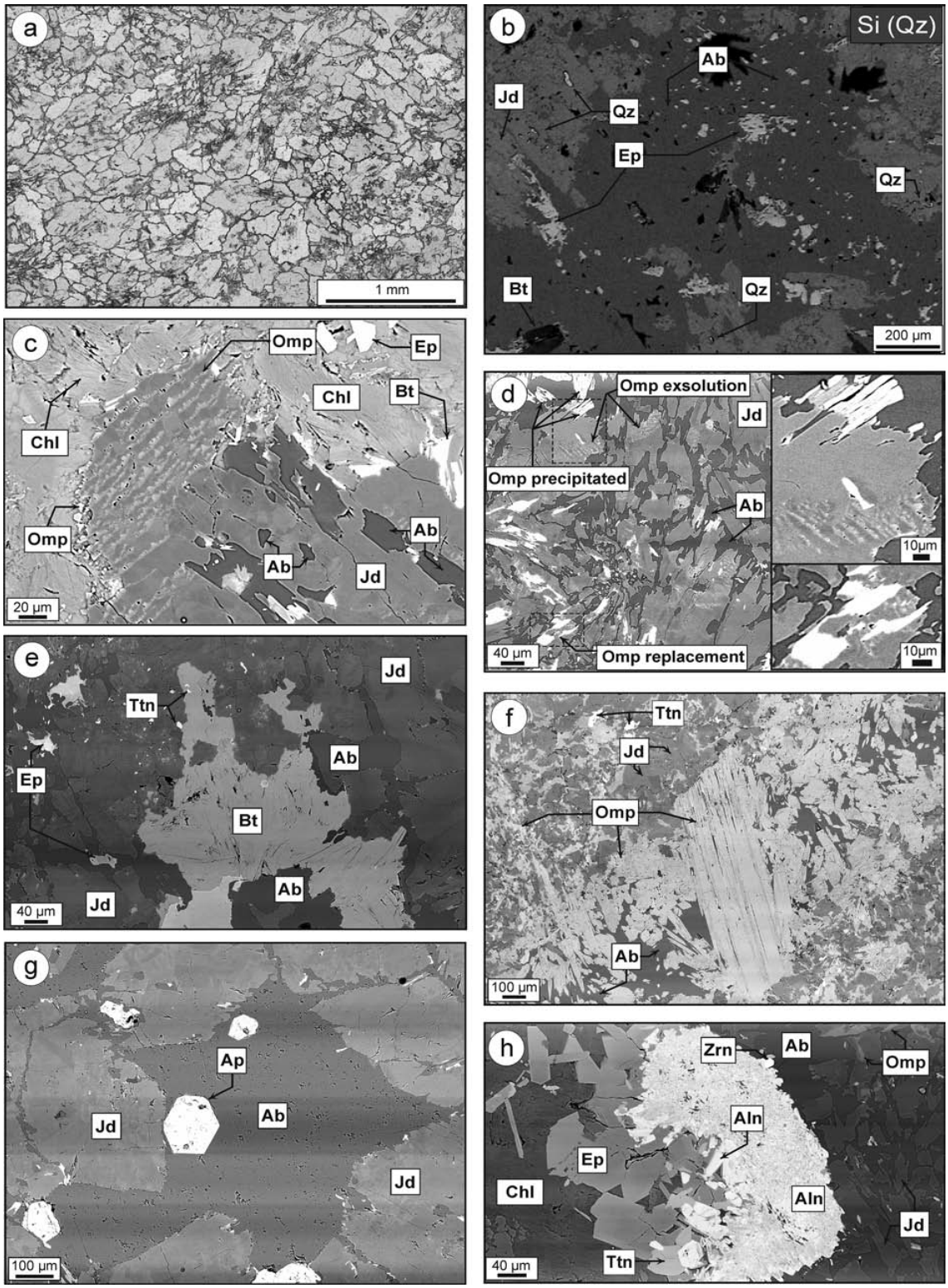

Figure 6.1. Microtextures and mineralogy of the pure jadeitite samples. (a) Optical image (plane-polarized view) showing general granoblastic texture composed of jadeite and albite along grain contacts. (b) X-ray image corresponding to Si in Qz inclusions into jadeite crystals. (c) BSE image showing omphacite exsolution lamellae. (d) BSE image with the types of omphacite found in different textural positions. Including extensions of the zones marked (e) BSE image of the dark nodular areas formed by biotite. (f) BSE image from a light green coloured vein composed of omphacite and interstitial albite crosscutting massive jadeite. (g) BSE image of apatite associated with albite surrounded by corroded jadeite. (h) BSE image of allanite in contact with epidote associated to chlorite at interstitial textural position.

Albite however is common in interstitial light-coloured nodular areas (Figure 6.3c), and frequently associated with chlorite, omphacite and (clino)zoisite-epidote interpreted as late products in the crystallization sequence (Figure 6.1f) Analcime is present in sample SC-MJ-10 with similar textural relationships to albite, suggesting growth during the latest stage of rock evolution. Significantly, albite is also found as inclusions within most major phases, and, particularly, is associated with quartz as inclusions within jadeite (Figure 6.1b).

The textural relationships indicate in pure jadeitites that jadeite, omphacite, epidote, (some) albite, allanite, apatite, zircon, titanite, and rutile formed during the early stages of rock formation, while biotite, chlorite, (most) albite, analcime, muscovite (phengite) and carbonates formed during the latest stages.

Epidote-rich jadeitite is characterized by abundant (>20-30 mode%) clinozoisite and epidote, both present in individual samples and forming subhedral to euhedral grains that may reach up to 1-2 mm in size (Figure 6.3e, f). Jadeite and omphacite (50-85 mode%) develop granoblastic texture with blocky crystals and omphacite also overprints jadeite (Figure 6-3e, g and h). White mica, chlorite, biotite, albite, allanite, apatite, titanite, rutile and carbonates may be present with similar textural position as in pure jadeitite (Figure 6.3f, g, h, i and j). Large and idiomorphic zircons crystals are frequently included in jadeite and omphacite as isolated grains (Figure 6.3i). These zircons were separated from one sample of this type of rock for U-Pb zircon dating (SC-09-27c, see section 6.5). Mica-rich jadeitite is characterized by abundant white mica (> 20-30 mole%) with decussate texture and similar mineralogical/textural relations as above but with rather heterogeneous modal abundance of other minerals (Figure 6.3k). The modal amount of clinopyroxenes ranges 45-75 % and the relative proportions of jadeite:omphacite is varied.

Omphacitite is a relatively fresh rock made essentially of omphacite showing only minor albitization (<5% albite). Relicts of jadeite are replaced by omphacite, suggesting a secondary origin. It may contain epidote, titanite, zircon, chlorite and phengite as accessory/secondary minerals (Figure 6.3l). Discrete dark green bands primarily consisting of omphacite within jadeitite occur as aggregates of xenomorphic fine to very fine grains intergrown with fine-grained jadeite. The chromium-rich variety contains chrome-omphacite in patches (identified in BSE images) that overprint jadeite (Figure 6.4a, b).

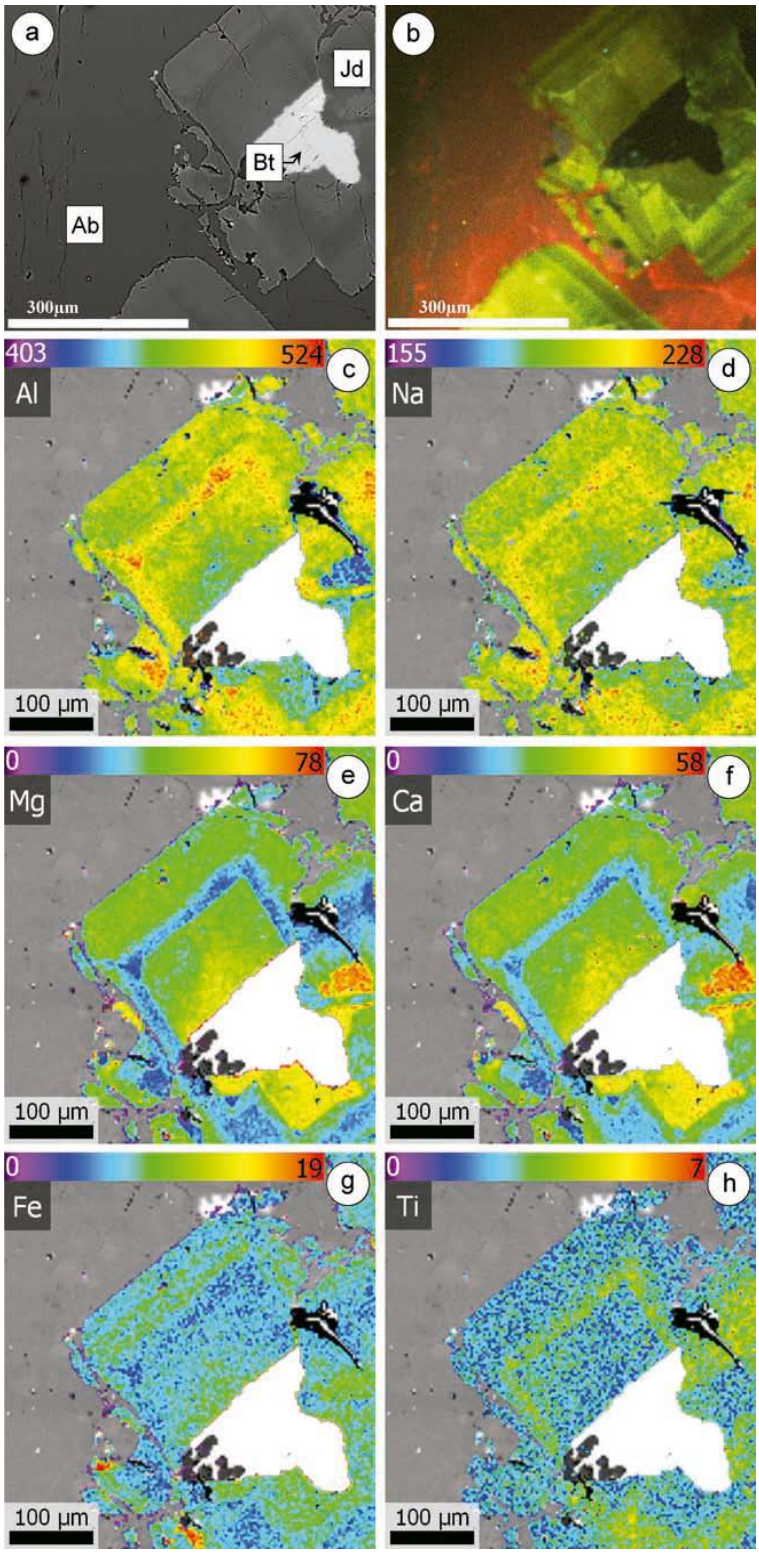

Figure 6.2. (a) BSE image of jadeite crystal displaying compositional oscillatory bands, biotite inclusion, all surrounded by albite. (b) CL image of the same area shown in (a). From (c) to (h) X-ray images of Al, Na, Mg, Ca, Fe and Ti, respectively, showing textures and zoning of jadeite in the same area. Other mineral phases, polish defects, and voids are masked out and the resulting images are overlain onto a gray-scale BSE image. Colour scale bar: counts/nA per second.

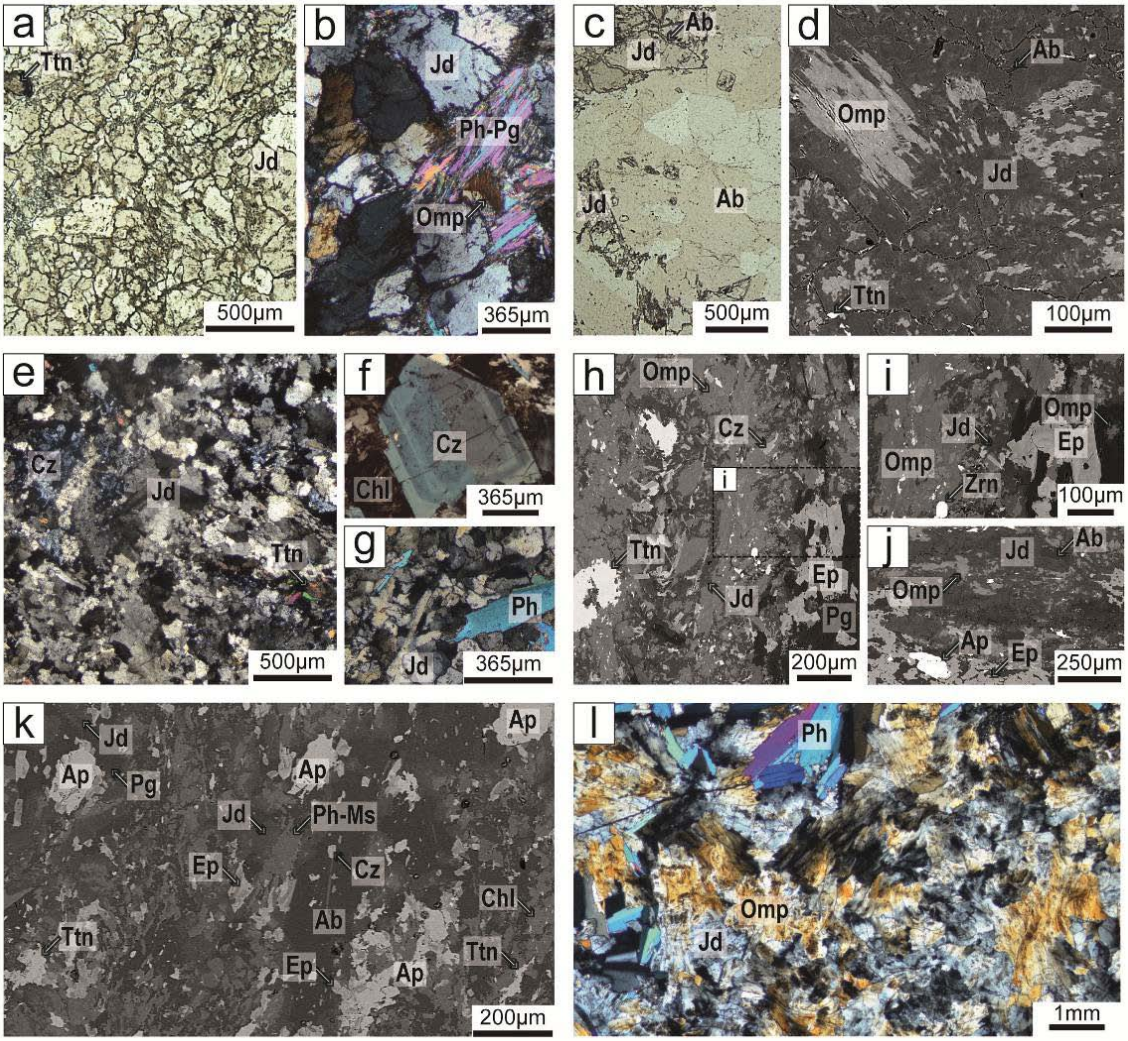

Figure 6.3. Representative photomicrographs and BSE images showing the textural and mineralogical characteristics of the studied rocks: (a) Pure jadeitite with granoblastic blocky crystals of jadeitite and accessory titanite: MCB-1f. (b) Detail of decussate texture of white micas (phengite and paragonite) associated with omphacite in pure jadeitite: MCB-1j. (c) and (d) Alteration of pure jadeitite by late crystallization of albite and omphacite, MCB-2d and 09-SC-8A III, respectively. (e) General texture of epidote-rich jadeitite with blocky crystals of jadeite and clinozoisite and titanite: CV-237f. (f) Detail from epidote-rich jadeitite showing zoned subhedral clinozoiste surrounded by chlorite and and (g) decussate texture of phengite in granoblastic jadeite matrix: 09-SC-27m and 09-SC-9g, respectively. (h) Example of alteration zone in epidote-rich jadeitite with clinozoisite/epidote, omphacite and paragonite and (i) close-up of this texture: MCB-1g. (j) Epidote-rich jadeitite showing the textural positions of albite and apatite: MCB-4a. (k) Representative texture and mineralogy of mica-rich jadeitite: 09-SC-31e. (l) Omphacitite with relicts of jadeite associated with omphacite and decussate phengite: 09-SC-9i.

6.2.2 Albite-epidote (-chlorite) (-quartz) rocks

Samples of albite-epidote rocks show a large petrographic variation. Albite and epidote are the most abundant minerals, summing up to more than 70 mode% though with variable relative amounts. Fine- to medium-grained anhedral albite generally occurs in intergranular position, while epidote-group minerals form clusters of typically euhedral/subhedral grains (Figure 6.4c, d). Chlorite is variably developed, forming also clusters of oriented to decussate grains. Quartz, on the other hand, is present in most samples, but it may occur only in small amount.

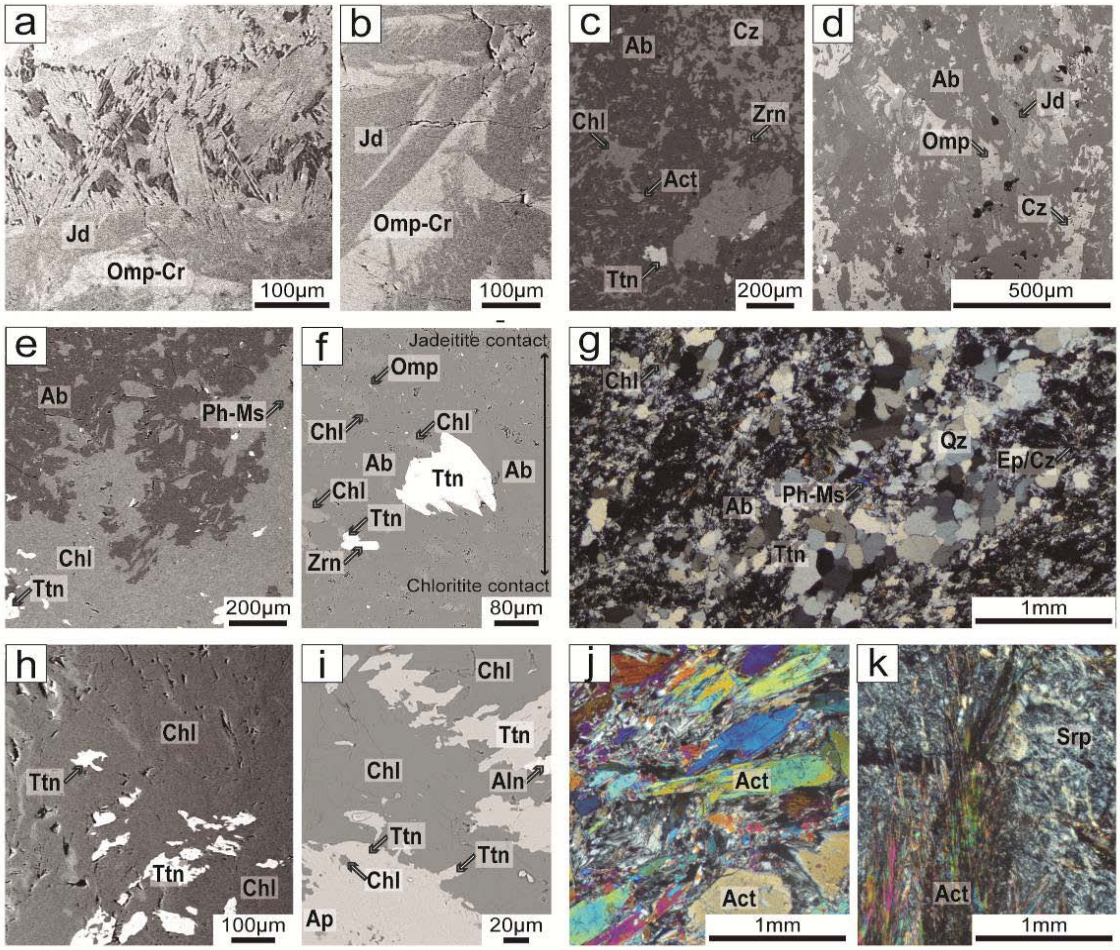

Figure 6.4. Representative photomicrographs and BSE images showing the textural and mineralogical characteristics of the studied rocks: a) and b) Cr-rich omphacitite formed mainly by chromium omphacite associated with jadeite: 09-SC-7b. c) Albite-epidote rock with an albititic matrix, abundant clinozoisite and minor chlorite, actinolite titanite and zircon: 09-SC-31a. d) Albite-epidote rock with similar textural characteristic of previous rocks, showing relict omphacite and jadeite crystals: 09-SC-9b. e) Sample of albite-epidote chlorite-rich rock mainly composed by the association of albite and chlorite, with abundant titanite and rare phengite-muscovite: 09-SC-27b. f) Fine band of albite-epidote chlorite-rich rock between jadeitite and chloritite: 09-SC-8a VII. g) Albite-epidote (-quartz) rock formed by a matrix of albite and quartz with clinozoisite/epidote, chlorite, titanite and phengite/muscovite: MCB-3b. h) Massive chloritite with titanite showing inclusions of chlorite: 09-SC-27a (chloritite group). i) Titanite-apatite-zircon rich chloritite with abundant titanite; note titanite growth over apatite and minor allanite: 09-SC-8a VIII j) Representative general texture of actinolitite: MCB-3d. k) Detail of contact between actinolitite vein and serpentinite rock: 09-SC-8b.

Accessory and occasional minerals include white mica (mostly phengite, but with occasional paragonite), hematite, apatite, titanite and zircon. They are mostly euhedral crystals included in albite and chlorite or dispersed in the matrix. Some samples contain subhedral fine grains of omphacite and/or jadeite within albite suggesting a relict nature (Figure 6.4d). In these samples, subhedral actinolite is present associated to albite, chlorite and epidote group minerals (Figure 6.4c), but we have not observed textural relations relating pyroxenes and actinolite.

The mineral assemblages and petrographic characteristics of albite-epidote-chlorite and albite-epidote-quartz rocks are similar those described above, but with significant

amount of chlorite (Figure 6.4e, f) and quartz (Figure 6.4g), respectively. In these groups of rock, chlorite rich regions show abundant titanite crystals (Figure 6.4e) while fine-grained quartz develops aggregates of granoblastic grains. In both cases the development of aggregates of chlorite and quartz, respectively, may be accompanied by mineralogical banding. Albite-epidote-chlorite rock samples, which normally occur towards the rims of the blocks close to the contacts with chlorite blackwalls, contain relicts of pyroxenes armored within albite grains (Figure 6.4f). Zircons were separated from one sample of this type of rock for U-Pb zircon dating (SC-09-27b, see section 6.5).

6.2.3 Chloritites and actinolitite

Massive chloritite from blackwalls is quasi-monomineralic. According to mineralogical proportions this type of rock is divided in chloritite (> 99 % chlorite) and titanite-apatite-zircon-rich chloritite (>85 % chlorite), though they are transitional. Subhedral to euhedral titanite, apatite and zircon and, locally, allanite, concentrate in clusters (Figure 6.4h, i). Titanite overgrows apatite and has variable size (50-150 µm) (Figure 6.4i). Zircons typically show well developed bipyramidal shape up to 200 µm in length. These zircons were separated from two samples of this type of rock for U-Pb zircon dating (SC-09-8aVIII and SC-09-27a, see section 6.5).

The actinolitite from veins/pods bear > 95 % amphibole. Prismatic crystals up to 1-2 mm size occur within fibrous aggregates arranged with variable orientation (Figures 6.4j) including radial growth from the vein walls (Figures 6.4k). Deformation in actinolite crystals is appreciable, suggesting shear deformation during or after mineral crystallization (Figure 6.4j). Antigorite and chlorite occur in apparent textural equilibrium with the actinolite and accessory apatite and titanite are dispersed in the actinolite matrix.

6.3 Mineral composition

6.3.1 Pyroxene

Representative analysis of jadeite and omphacite grains (e.g., Supplementary Table 9) from five samples of pure jadeitite are plotted in binary diagrams (figures 6.5) and classified on the Q-Jd-Aeg scheme (Figure 6.6). Quadrilateral (Q) pyroxene (wollastonite + clinoenstatite + clinoferrosilite components), jadeite and aegirine end-members were calculated following Morimoto et al., (1988).

Jadeite grains contain Jd component (Figure 6.6) from 75 to 97.6 mol%, while Q and Aeg components vary from 3.3 to 23.2, and from 0 to 3.3 mol %, respectively. The Aeg/(Q+Aeg) ratio ranges from 0 to 0.32. Omphacite grains contain Ae component of 0 -9.8 mol%, with Jd ranging from 37.4 to 62.5 mole %, and Q from 36.5 to 56.4 mol% (Figure 6.6). The highest value of the Aeg/(Q+Aeg) ratio is 0.20. Jadeite and omphacite solid solutions closely obey stoichiometry with the exchange $Ca(Mg,Fe)Na_{-1}Al_{-1}$ (Figure 6.5). As shown in this figure, the calculated Fe^{3+}, Fe^{2+} and total iron are low, such that

generally the solid solution compositions can be described along the jadeite-diopside join.

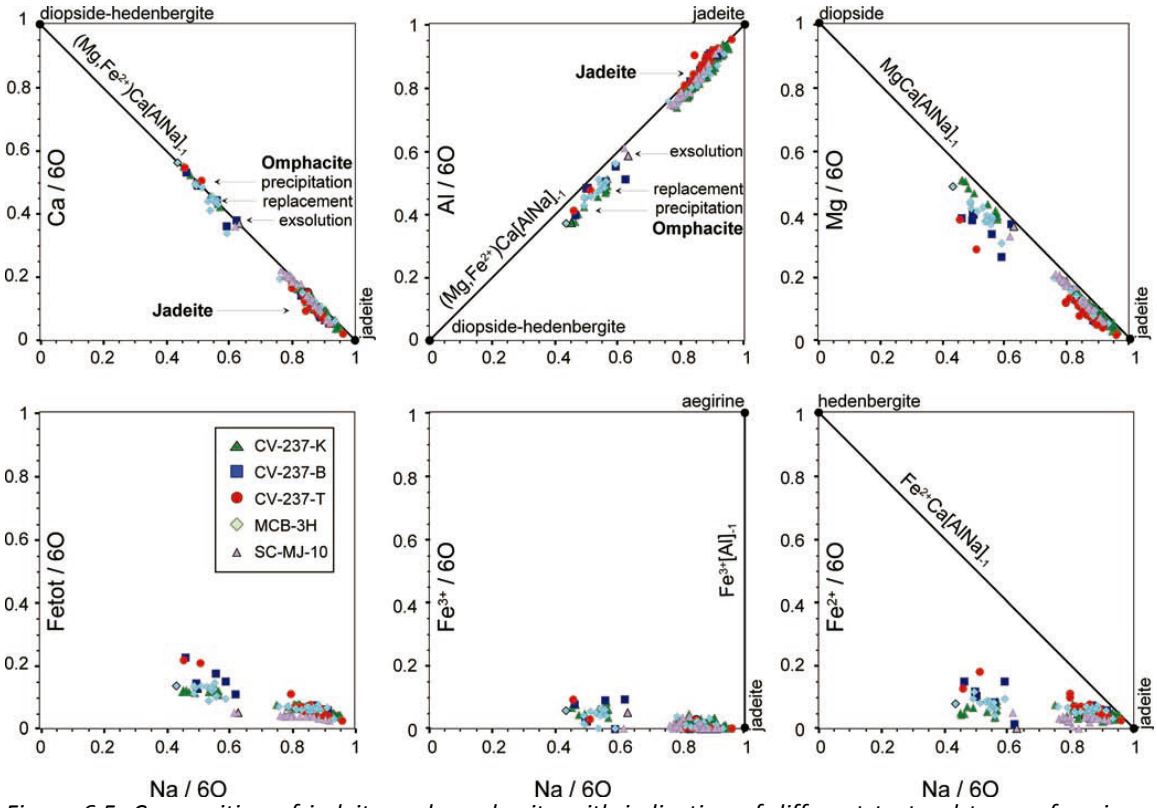

Figure 6.5. Composition of jadeite and omphacite with indication of different textural types of grains. Significant exchange vectors and endmembers are indicated.

Some of the investigated pure jadeitite show prismatic jadeite with oscillatory zoning similar to that described by García-Casco et al., (2009). Specifically, sample CV-237-T (Figure 6.2) has blocky jadeite crystals with cores poorer in jadeite component and several idiomorphic oscillatory bands in terms of Al, Na, Mg, Ca, Fe and Ti. Changes in Ca and Mg contents across the oscillations are inversely compensated by changes in Al, Na and Ti content. The variation of Fe is similar to that of Ca and Mg, but thin bands close to the rim of the crystals are slightly enriched in Fe but do not evidence Ca and Mg enrichment. These fine bands correspond to low signal in the CL image (Figure 6.2b, g).

The pyroxene from representative pure jadeitites indicates composition of jadeite and omphacite, with small immiscibility gap, suggesting high temperature during the pyroxenes formation. The compositional variations described above indicate a complex growth-replacement-growth history in a hydrothermal context characterized by fluid-filled in fractures and changing chemical environment.

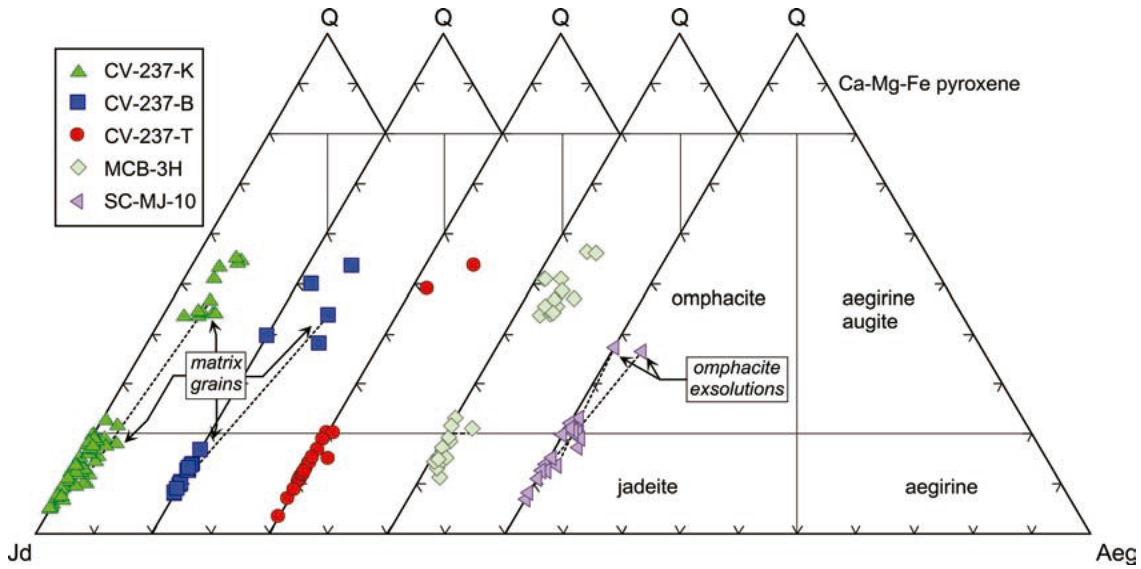

Figure 6.6. Pyroxene composition in the classification scheme of Morimoto et al., (1998). Dashed lines connect analyses of grains in contact.

The composition of pyroxene in all jadeitite groups and associated Ab-Ep rocks are shown in figures 6.6 and 6.7. These pyroxene compositions are quite varied, there being no systematic difference in composition between the different types of rock, except for omphacitites. Which also shows compositions with the lowest jadeite component (down to 29 mole%), and do not show jadeite. The continuity presented by all pyroxenes analyzed, with small or no immiscibility gap, also suggests, like in representative pure jadeitite, high temperature during the pyroxenes formation. On the other hand, agirine component reaches 21 mole%, with Aeg/(Q+Aeg) ratios up to ca. 0.5. Importantly, the composition of relict jadeite and omphacite in Ab-Ep rocks is comparable to pyroxene composition in other type of rocks, in particular, Ep-rich jadeitite.

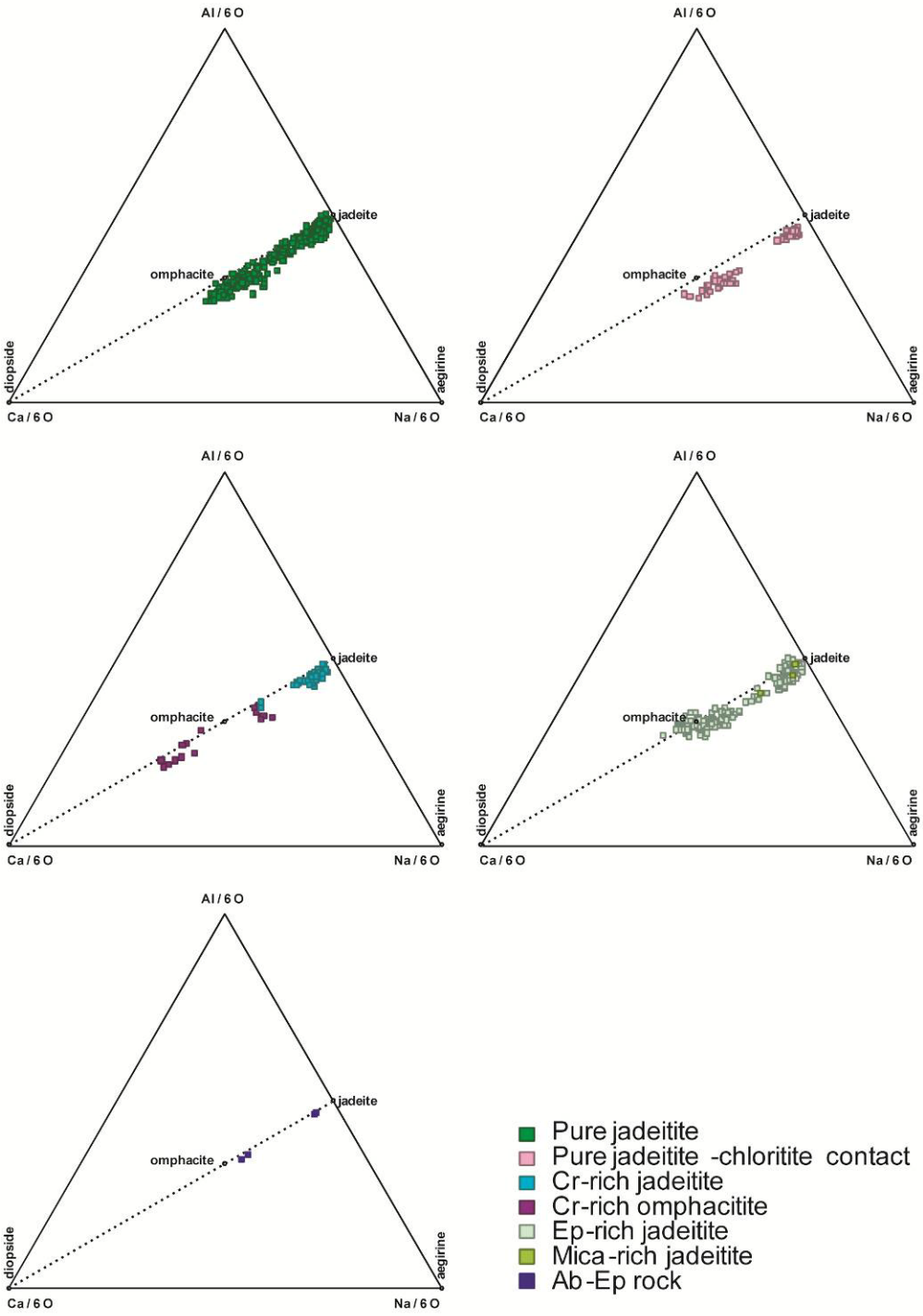

Figure 6.6. Composition of jadeite and omphacite in the Al-Ca-Na diagram (atomic proportions). Dashed lines connect the theoretical compositions of the solid solution between jadeite and diopside.

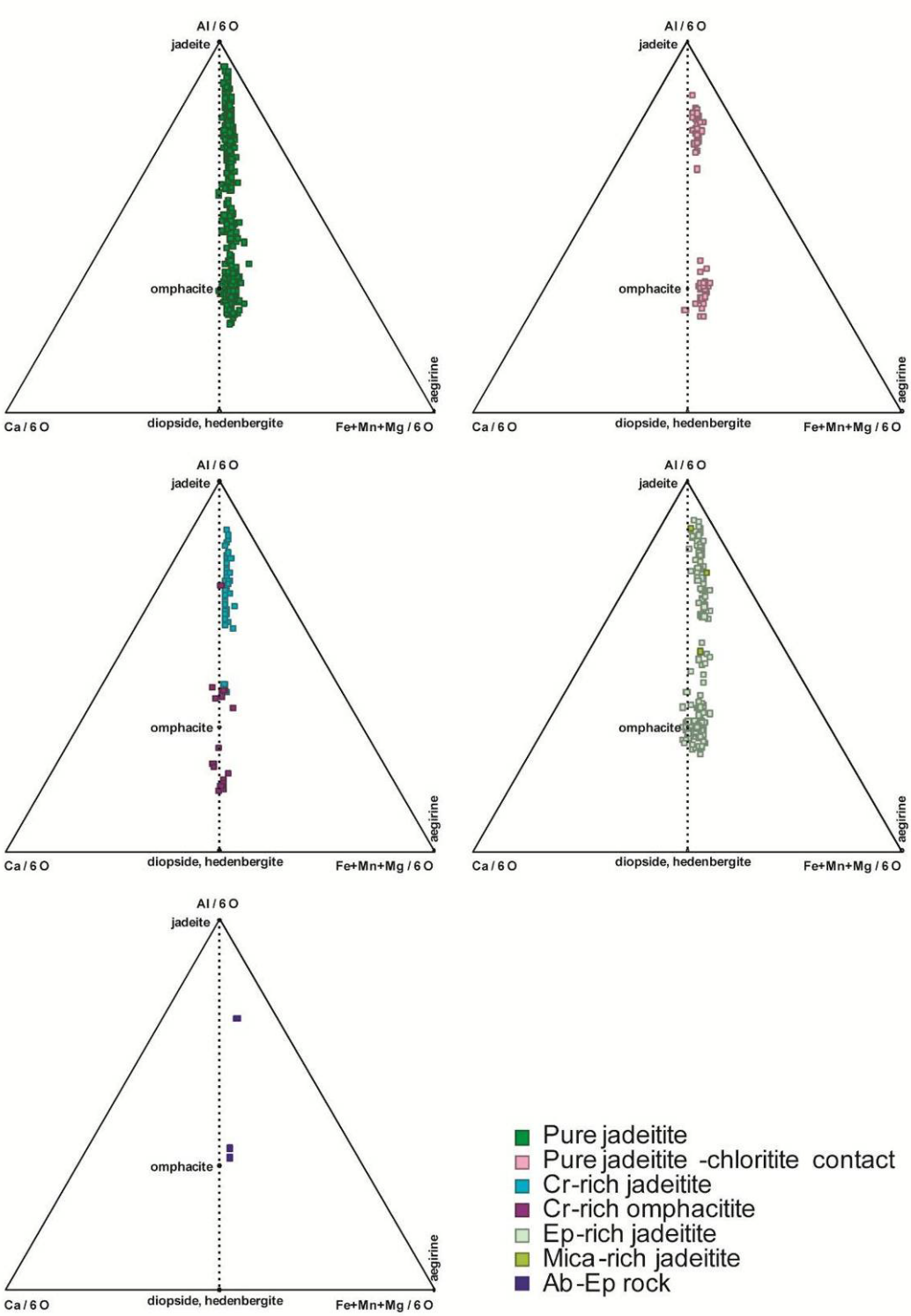

Figure 6.7. Composition of jadeite and omphacite in the Al-(Fe+Mn+Mg)-Ca diagram (atomic proportions). Scheme of Morimoto et al., (1988). Dashed lines connect the theoretical compositions of the solid solution between jadeite and diopside, hedembergite.

6.3.2 Plagioclase

In all group of rocks, plagioclase feldspar is virtually pure albite with X_{Ab} ranging from 0.94 to 1, (Supplementary Table 9). Albite in pure jadeitite can yield an orangey-pink CL luminescence (Figure 6.2b), which is unusual but may be related to purity. K-

feldspar (one sample) bears Xor= 0.75, Xab = 0.19. Analcime is pure (Ca up to 0.06 atoms per 6 oxygens + 1 H2O).

6.3.3 Epidote group

In all types of samples epidote group minerals includes clinozoisite and epidote, throughout the entire range (Figure 6.7). The highest pistacite (Xps = $Fe^{3+}/[(Al-2)+Fe^{3+}]$) content up to 0.89 occurs in epidote from pure jadeitites, though it can be as low as 0.04. In Ep-rich and Mica-rich jadeitites Xps ranges 0.00-0.59 and in albite-epidote and Ab-Ep Chl-rich rocks it ranges 0.01-0.65. Grains with high Al content are closely associated with jadeite and omphacite replacements after jadeite, while high Fe content are typically associated with albite and late omphacite precipitated in intergranular positions in the pure jadeitite (Supplementary Table 9)

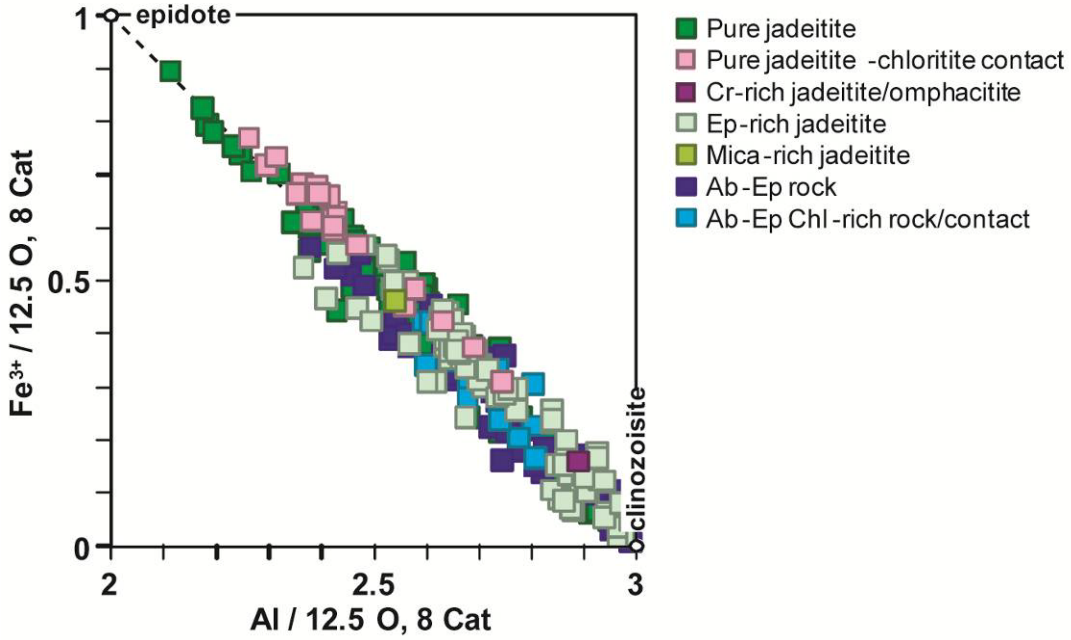

Figure 6.7. Compositions of epidote group minerals along the clinozoisite-epidote join.

6.3.4 White mica and Dark mica

Selected samples of pure jadeitite have white mica with phengitic composition (Figure 6.8a and (Supplementary Tables 5 and 9) with Si, Mg, Fe_{Total} and Na ranging 7 - 7.06, 0.88 - 0.89, 0.15-0.18, 0.06-0.07 apfu, respectively. Ba and Ti contents are low (≤ 0.02 apfu). In these samples, biotite grains cover a wide range of composition (Figure 6.8a, b). The K and Na contents vary from 1.41 to 1.88 apfu and 0.09 to 0.24 apfu, respectively. Si-contents vary from 5.17 to 5.54 apfu and Mg-contents ranges from 3.16 to 3.86 apfu. Mg#, assuming all Fe is ferrous, ranges from 0.64 to 0.76 apfu. The mica is classified as phlogopitic biotite following Deer et al., (1962) and Guidotti (1984) (Figure 6.8b). Biotite associated with jadeite shows high values of eastonite component whereas biotite in interstitial position has higher phlogopite component (Figure 6.8b). The compositional and textural variations of biotite may be explained by

variation of fluid composition filling the fractures during jadeite (+ phlogopite) crystallization and as compared to later infiltrations when omphacite and phlogopite are saturated.

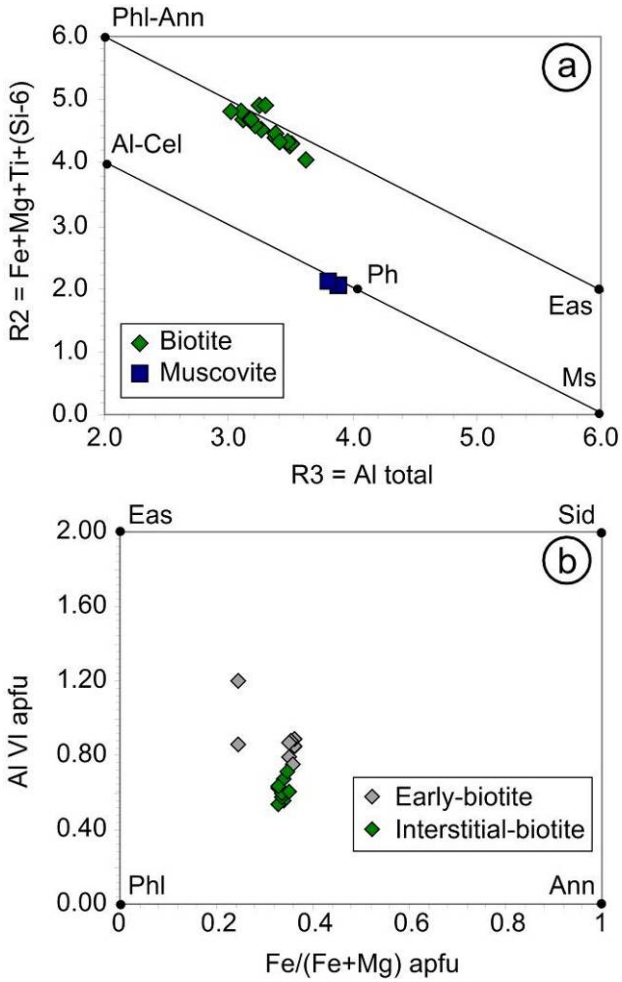

Figure 6.8. (a) Multi-cation diagram R2-R3 for micas with indication of dioctahedral and trioctahedral mica end-members. (b) Biotite compositions plotted in the ''ideal plane of the biotite'' (Deer et al., 1962; Guidotti, 1984).

The composition of white micas is varied in the different groups of jadeitites and Ab-Ep rocks (Figure 6.9). Potassic white mica is phengitic in composition with much of the compositional variation controlled by the Tschermak exchange and, to a lesser extent, the paragonite-muscovite exchange. The composition of phengite overlaps in all types of rock. For example, the amount of Si in pure jadeitite, Ep-rich jadeitite, Mica-rich jadeitite, Ab-Ep and Ab-Ep-Chl rocks ranges 6.8-7.1, 6.5-7.2, 6.8-7.0, 6.5-7.5 and 6.7-6.9 atoms pfu, respectively (Figure 6.9). Considering all samples as a whole, the amount of Na reaches 0.23 atoms pfu (in Ep-rich jadeitite). The composition of paragonite is more restricted, with up Ca contents up to 0.065 and 0.035 apfu in Ab-Ep rock and Ep-rich jadeitite, respectively (Figure 6.9). In the figure 6.10, dark mica is of biotite-phlogopite composition in pure jadeitites and Cr-rich jadeitites, which bear phlogopite with the highest Mg# (= 0.86). In Ep-rich rocks, dark mica is of biotite

composition very close to phlogopite, and preiswerkite (Na-Al dark mica) is present in one sample (MCB4a). In general, biotite-phlogopite from this type of rock has it has lower Mg# than in pure jadeitite and Cr-rich pure jadeitite (Figure 6.10). The Na contents in biotite-phlogopite from all types of rock significant, in the range 0.08-0.25 apfu (Supplementary Table 9).

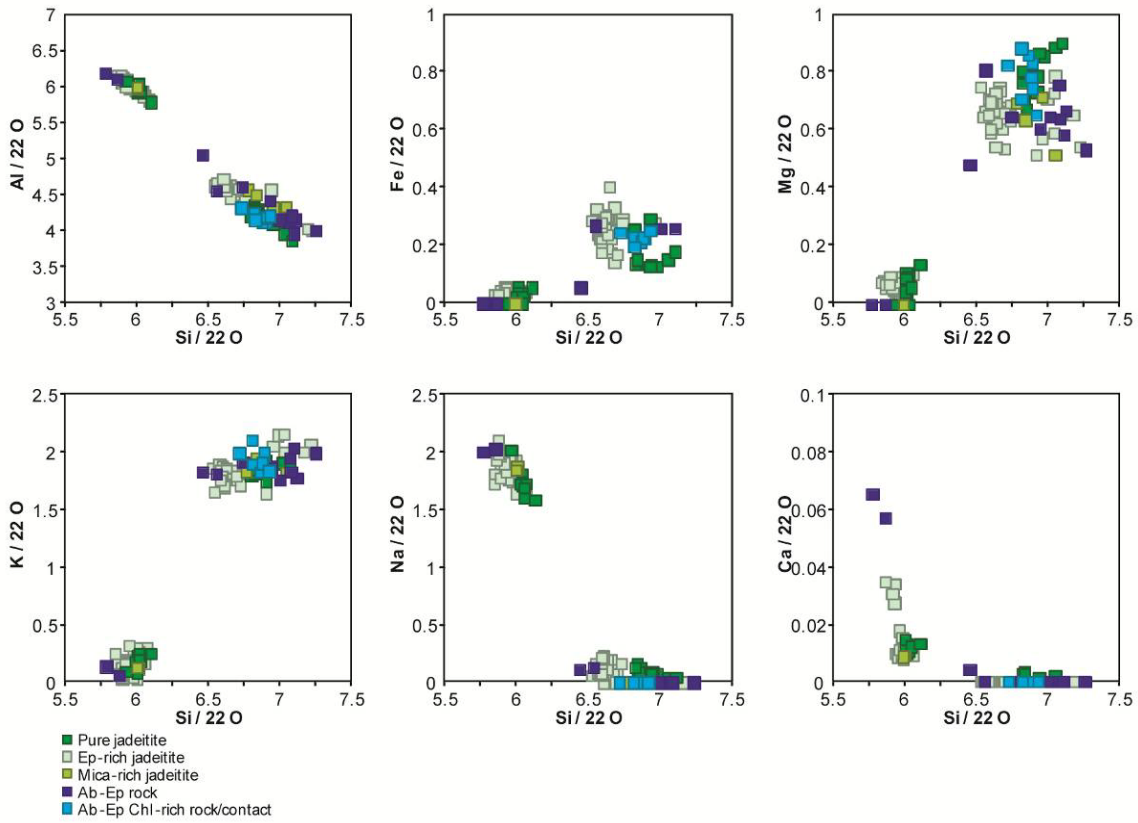

Figure 6.9. Composition of white micas (muscovite-phengite and paragonite).

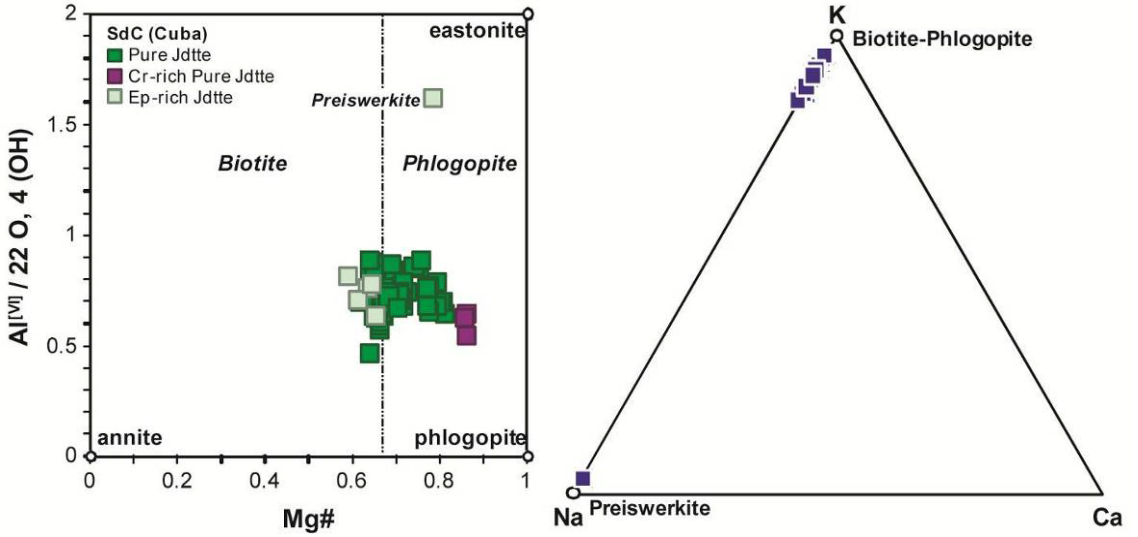

Figure 6.10. Composition of dark micas (K:Na:Ca in atomic proportions).

6.3.5 Chlorite and Pumpellyite

Chlorite shows a wide compositional range (Supplementary Table 9 and figure 6.11). Chlorite in jadeitites and Ab-Ep rocks is similar in composition and relatively poor in Mg# (0.55-0.80), while chlorite in jadeitite-chloritite, Cr-rich jadeitite/omphacitite and chloritites are more restricted in composition and richer in Mg (Mg# = 0.71-0.89; figure 6.11). Chlorite from chloritites is less aluminous (Al = 4.0-4.12 apfu) than chlorite from jadeitites and Ab-Ep rocks (Al = 4.22-5.35 apfu; figure 6.11). The heterogeneous compositions may result from changing fluid chemistry and conditions during growth and/or retrogression.

Pumpellyite approached the Al(Mg)-pumpellyite end-member (implying variable OH contents; figure 6.11).

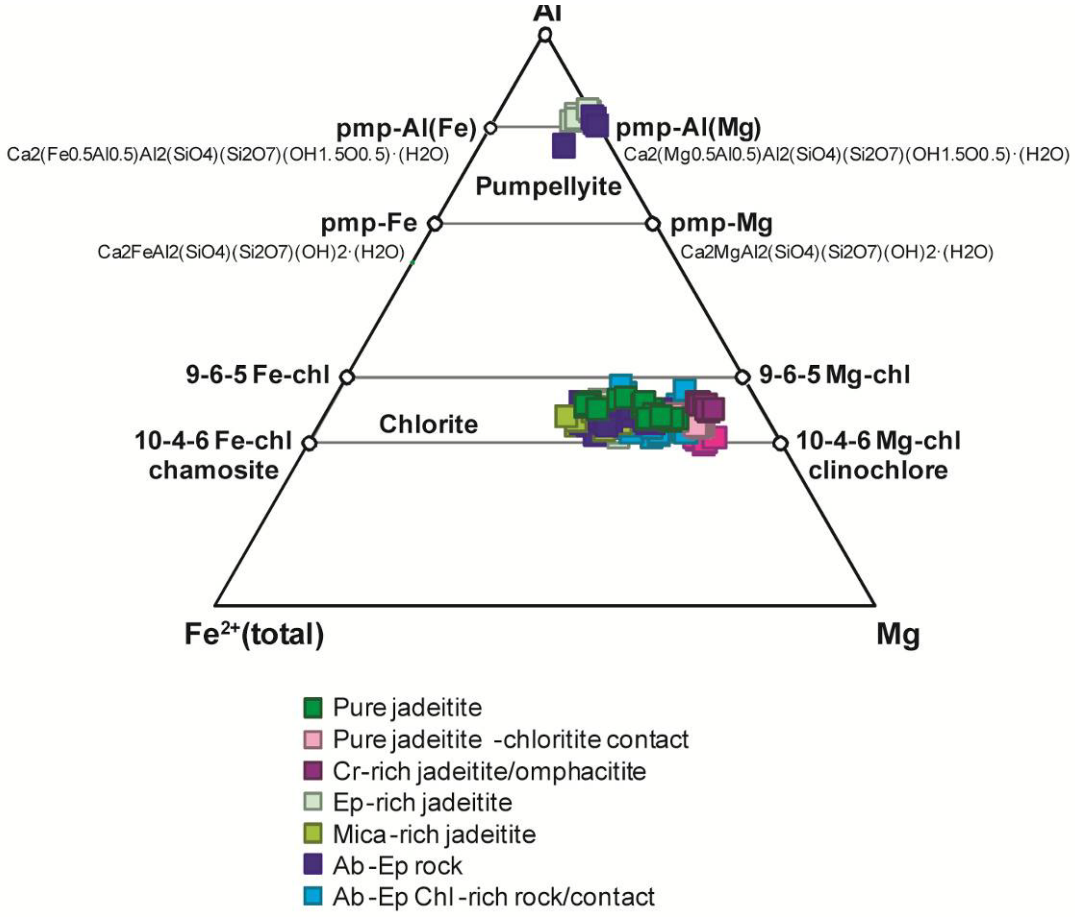

Figure 6.11. Composition of chlorite and pumpellyite (atomic proportions). The three numbers in the chlorite end-members refer to the number of Fe+Mg, Al and Si cations, respectively.

6.3.6 Amphibole

The composition of amphibole in pure jadeitite is sodic-calcic (magnesiokatophorite) and sodic (glaucophane; figure 6.12). In Ep-rich jadeitite amphibole is sodic-calcic (Mg-katophorite and taramite), while in Ab-Ep Chl-rich rocks (adjacent to block borders) it is sodic (glaucophane; figure 6.12).

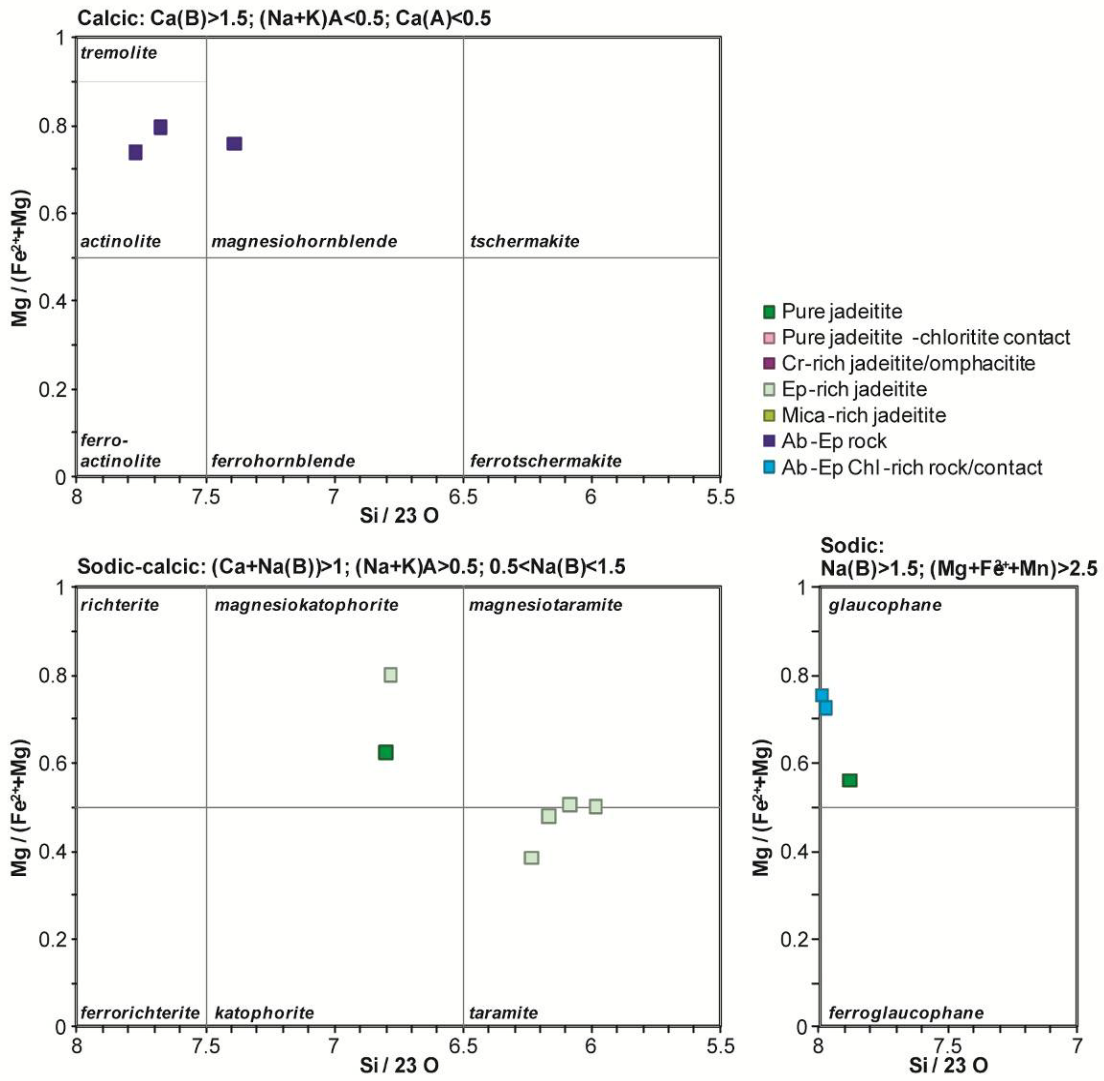

Figure 6.12. Composition of amphibole. Classification scheme after Leake et al. (1997).

6.3.7 Other minerals

Titanite is almost pure, with Al and Fe^{3+} up to 0.15 and 0.04 atoms per 5 oxygens. A representative analysis of titanite yielded has Si = 1.00 apfu, Ti = 0.957 apfu, Al = 0.05 apfu, and Ca = 1.01 apfu. Garnet (one sample of Ep-rich jadeitite) bears Xalm = 0.422-0.515, Xsps = 0.036-0.157, Xprp = 0.048-0.280 and Xgrs = 0.169-0.373.

6.4 Geochemistry

6.4.1 Major elements

Jadeitites and omphacitite

Bulk compositions of jadeitites and omphacitite mirror the dominant mineralogy of the different groups of rocks identified (Figure 6.13). Pure jadeitite are characterized by strong variations in SiO_2 (54.45-59.48 wt%), Al_2O_3 (15.56 to 23.22 wt%), FeO_{tot} (1.36-3.63 wt%), MgO (1.28-6.19 wt%), CaO (2.93-8.67 wt%) and Na_2O (7.82-12.24 wt%) (Figure 6.13), that reflects variations in jadeite/omphacite ratios in the samples.

However, these values reflect that jadeite dominates over omphacite in most of the samples. TiO_2 and P_2O_5 contents range from 0.18-0.97 wt% and 0.01-0.24 wt%, respectively, reflecting varying titanite/rutile and apatite contents, respectively. Compared to pure jadeitite, epidote-rich jadeitite is richer in CaO (4.15-11.88 wt%), FeO_{tot} (2.67-8.46 wt%), MgO (1.97-8.65 wt%), TiO_2 (0.30-2.18 wt%) and P_2O_5 (0.02-0.41 wt%) and poorer in SiO_2 (48.11-56.74 wt%) and Na_2O (4.35-9.16 wt%) (Figure 6.13), reflecting higher amounts of epidote, titanite, apatite and chlorite and lower amount of pyroxenes. However, even if Na_2O is lower, the amount of albite is generally greater than in pure jadeitite, reflecting transformation of jadeite to albite. Al_2O_3 content ranges between 13.36 and 23.86 wt%, rather similar to pure jadeitite, while K_2O content ranges 0.05-1.77 wt%, indicating variable abundance of phengite.

Compared to these two types of jadeitite, mica-rich jadeitite stands out due to its higher Al_2O_3 (20.07-31.28 wt%) and lower SiO_2, CaO and Na_2O (36.12-49.27 wt%, 1.20-4.46 wt% and 2.46-5.64 wt%, respectively; Figure 6.13), pointing to higher amounts of white mica and lower jadeite+omphacite contents. As expected, its K_2O content (0.28-2.28 wt%; Figure 6.13) is higher than pure jadeitite and epidote-rich jadeitite, but note that latter reach only slightly lower values of 0.01-1.24 wt% and 0.05-1.77 wt%, respectively, indicating that much of the white mica present is paragonite. Omphacitite has homogeneous composition, as expected after its definition here as a rock made almost exclusively of omphacite, with SiO_2 = 55.76-56.68 wt%, MgO = 7.17-7.33 wt%, P_2O_5 = 0.01 wt% and K_2O = 0.01-0.47 wt% (Figure 6.13). This group, however, show small variation in CaO (10.72-12.75 wt%), Al_2O_3 (11.73-13.75 wt%), FeO_{tot} (2.50-3.82 wt%), TiO_2 (0.15-0.90 wt%) and Na_2O (6.45-7.30 wt%), suggesting slight variation in omphacite composition between samples (Figure 6.13). The Cr-rich varieties of jadeitite and omphacitite have similar major element composition as pure jadeitite and omphacite (Figure 6.13), yielding Cr contents of 1153.75 ppm and from 977.58 to 1234.01 ppm, respectively, as opposed to Cr contents of 41.726-336.884 ppm and 98.37-480.808 ppm of the former, respectively (Figure 6.14b).

The relations between SiO_2 and Al_2O_3, CaO and Na_2O depicted in Figure 6.13 allow defining compositional trends. Among them, the trends pure jadeitite-omphacitite and pure jadeitite-epidote-rich jadeitite stand out clearly as two independent trends that suggest genetic relationships among these rock types.

Albite-epidote (-chlorite) (-quartz) rocks

Albite-epidote rock has SiO_2 contents ranging from 50.6 to 59.08 wt%, similar to pure jadeitite and epidote-rich jadeitite and much lower than trondhjemitic rocks of the Sierra del Convento and La Corea mélanges (Figure 6.13). In terms of all other elements the bulk composition of albite-epidote rock is similar to pure jadeitite and epidote-rich jadeitite, except for CaO (5.43-9.95 wt%) and Na_2O (4.52-6.79 wt%) which are slightly enriched and depleted, respectively in the former (even if their respective ranges overlap; Figures 6.13a, g). This allows defining a trend for albite-epidote rocks independent of the trends defined by jadeitites described above. This trend crosscut

the trend for pure jadeitite-omphacitite, but is almost parallel to the trend for pure jadeitite-epidote-rich jadeitite (Figures 6.13a, g). The composition of albite-epidote-

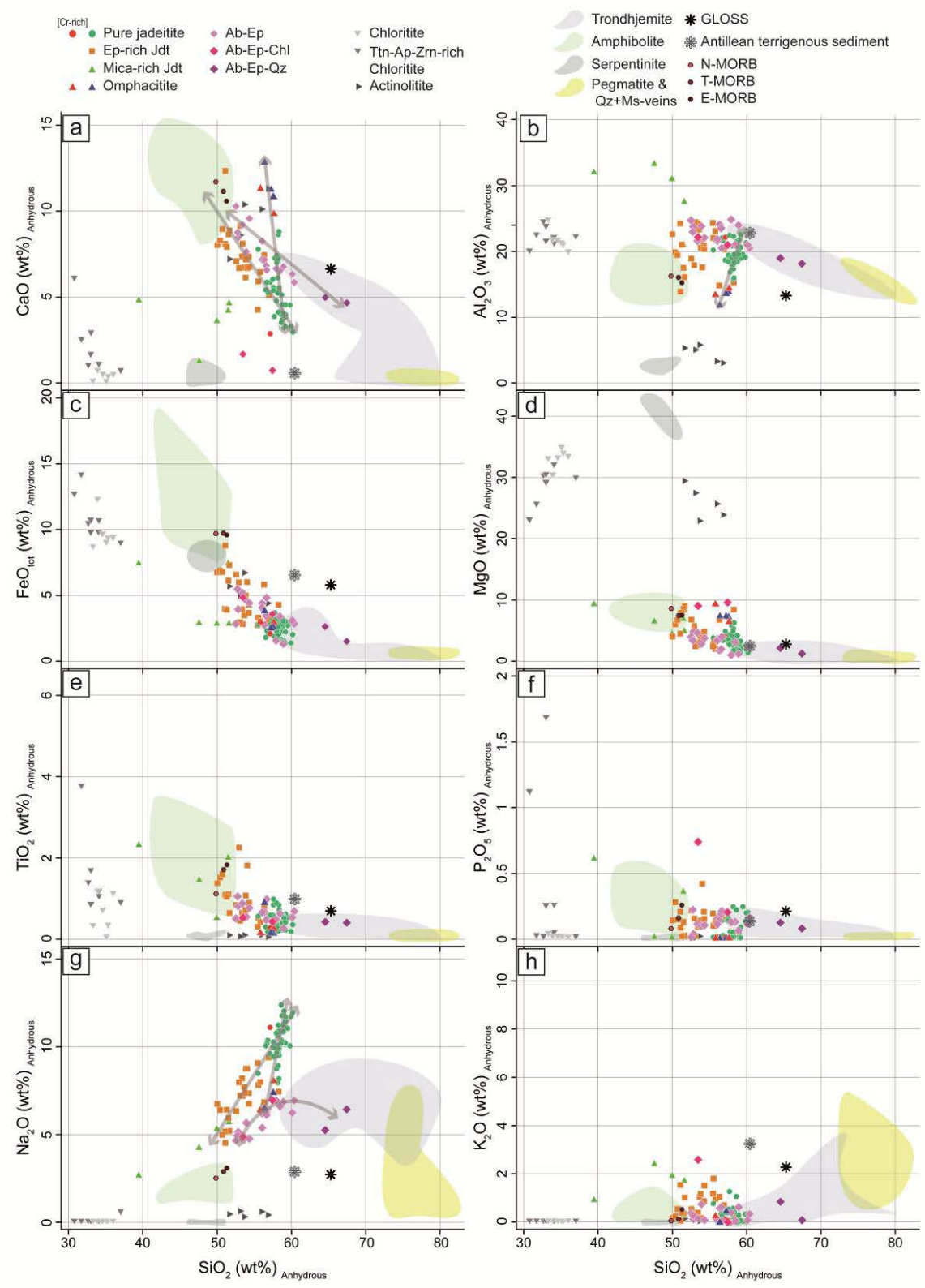

Figure 6.13. Binary diagrams of major oxides (CaO, Al_2O_3, FeO, MgO, TiO_2, P_2O_5, Na_2O and K_2O versus SiO_2) of the studied samples and published data of trondhjemites, amphibolites, serpentinites and pegmatite+Qz+Ms-veins from Sierra del Convento and La Corea mélanges (Lázaro and García Casco

2008; Lázaro et al., 2011; Blanco-Quintero et al., 2011c, Cárdenas-Párraga et al., 2017) for comparison. Also presented for comparison are the global subducted sediments (GLOSS) and Antillean terrigenous sediment from Plank and Langmuir, (1998), and N-MORB, T-MORB and E-MORB from Klein, (2003). The arrows indicate the main trends of groups of studied rocks. Major elements are presented on a volatile free basis.

chlorite rock, on the other hand, is similar to that of albite-epidote rocks in terms of most major elements, but this type of rock is not related to the albite-epidote rock trend for it has significantly lower CaO (0.69-1.58 wt%) and higher MgO (8.54-9.04 wt%). The two analyzed samples were taken close to the outer parts of two different jadeitite blocks, one being formed mostly by pure jadeitite (09-SC-8a; Figures 4.4i, j) and the other by epidote-rich jadeitite (09-SC-27b; Figures 4.4e, g). In the latter, the sample shows very high K_2O (2.44 wt%) and P_2O_5 (0.70 wt%) contents, much higher than albite-epidote rock and jadeitites (Figure 6.13). Finally, albite-epidote-quartz rock stands our clearly as a distinct type of rock rich in SiO_2 (63.21-66.47 wt%), like trondhjemitic rocks of the mélange. In terms of CaO and Al_2O_3, this type of rock is depleted, but it is similar in terms of all other major elements. It is however not clear whether this type of rock relates to the albite-epidote rock trend (Figure 6.13).

Chloritites and actinolitite

In terms of major elements, chloritites (including chloritite s.s. and titanite-apatite-zircon-rich chloritite) define a trend related to the modal abundance of titanite and apatite, with relatively constant Al_2O_3 (17.12-21.61 wt%), variable CaO (0.01-5.42 wt%), FeO (7.56-12.51 wt%), MgO (20.55-30.49 wt%), TiO_2 (0.02-5.82 wt%) and P_2O_5 (0.01-1.47 wt%) contents and negligible Na_2O and K_2O content as a result of the lack of jadeite and/or albite and K-micas, respectively. Actinolitite stand out clearly as a compositional cluster, as expected for its quasi-monomineralic nature (Figure 6.13). However, it is co-linear along with pure jadeitite and omphacite in terms of Al_2O_3, FeO, MgO, and Na_2O (Figure 6.13).

6.4.2 Minor elements

Jadeitites and omphacitite

Relative to primitive upper mantle (PUM), pure jadeitite shows moderate enrichment to slight depletion in REE (Figure 6.14a). While LREE are enriched, with La_n contents in the range 1.98-32.92 and slope downward from La to Sm with $(La/Sm)_n$ in the range 0.23-19.53, MREE to HREE are depleted to slightly enriched, with Lu_n in the range 0.38-34.32 and slope downward from Gd to Lu with $(Gd/Lu)_n$ in the range 0.50-3.82, although some samples show more attenuated slopes patterns with slight enrichments of Yb and Lu with respect to Er and Tm (Figure 6.14a). Most samples show a slight to moderate positive Eu anomaly with Eu_n/Eu^* in the range 2.12-7.63. Large ion lithophile elements (LILE) are highly variable, ranging from depleted to strongly enriched concentrations. Notably, K is relatively enriched in some samples while others show extreme depletion, with 0.13-17.15 times NMORB, while Ba ranges from 0.28 to 173.75 times NMORB (Figure 6.14b). This feature can hardly be related to a sediment-

derived fluid, but can be correlated with the chemical variability of trondhjemites of the mélange. Fluids evolved from crystallizing trondhjemitic magmas with variable K and Ba contents would explain this signature. Field strength elements (HFSE) show variable concentration, with Th, U, and Zr 0.08-29.39 times NMORB and Nb and Ti in the ranges 0.18-3 and 0.14-0.76 times NMORB, respectively. Sc is depleted in all samples reaching values between 0.02-0.32 times NMORB. Chromium and Ni are also depleted (ca. 0.1-1 times NMORB), except in the Cr-rich varieties (4.59 and 1.03 times NMORM of Cr and Ni, respectively). The Cr-rich jadeite sample is strongly depleted in REE, with slight concave-upwards (U-shaped) patterns from LREE to HREE but with positive Eu anomaly (Figure 6.14a). The composition of omphacitite is similar to pure jadeitite, including the positive Eu anomaly (0.22-3.42 times PUM, Figure 6.14a). The samples have similar slight concave-upwards REE patterns that some samples of pure jadeitite, from enriched LREE to enriched and, in one sample, depleted HREE. Omphacitite shows a high compositional variability in Cs, Rb, K, Ba and LREE, as well as slightly less variable compositions in Pb, Sr, HREE, Sc, Cr, Th, Zr, Hf, Ti and Nb (Figure 6.14b). The concentration of chromium in Cr-rich omphacitite is similar to that of Cr-rich pure jadeitite (ca. 5 times NMORB, Figure 6.14b).

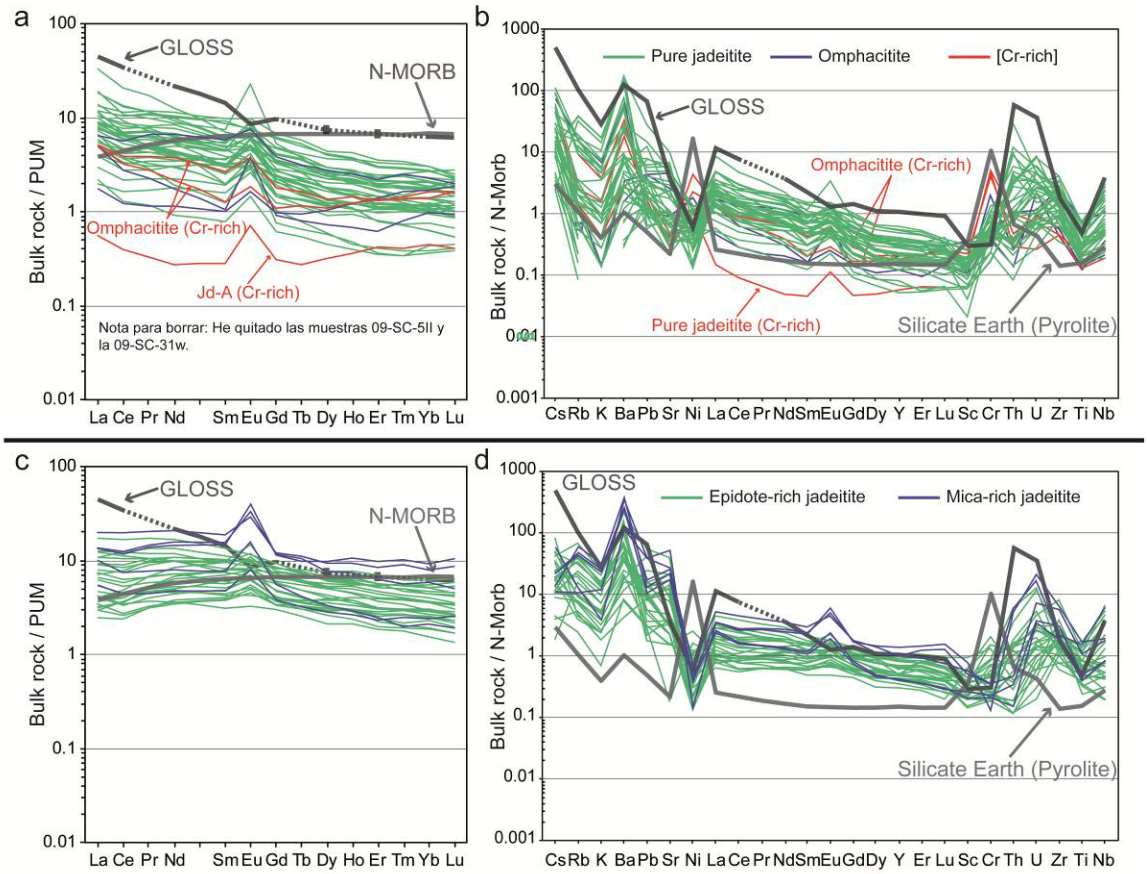

Figure 6.14. Rare earth element (REE) normalized to primitive upper mantle (PUM, McDonough and Sun, 1995) and trace-element "spidergram" normalized to N-MORB (Sun and McDonough, 1989, Ni, Cr and Sc from Klein, 2003) of studied rocks: a) and b) Jadeitite and omphacitite whole rock compositions. c) and d) Epidote-rich jadeitite and mica-rich jadeitite whole rocks compositions. Patterns for global N-MORB (Klein, 2003; Sun and McDonough, 1989) and subducting sediment (GLOSS: Plank and Langmuir, 1998)

and silicate earth (McDonough and Sun, 1995) are plotted for comparison. In spidergram the chemical elements are organized in increasing order of field strength (ionic charge/ionic radius) following to Harlow et al., 2016.

The composition of epidote-rich jadeitite in terms of REE is broadly similar to pure jadeitite but they differ in the shape of the PUM-normalized patterns (Figure 6.14c). Significantly, they show no or slight Eu anomaly and nearly flat or slightly concave-downwards shaped patterns (relatively depleted in LREE) with frequent weak slopes upwards from Ce to Sm that diverge from the negative slope of pure jadeitite patterns. A large number of samples bear MREE and HREE-enriched composition relative to pure jadeitite that fall within NMORB abundances, with nearly flat or with a sloping down patterns from Gd to Lu (Figure 6.14c). The minor and trace element abundances of epidote-rich jadeitite are also broadly similar to pure jadeitite, but they show ranges with higher lower limits in Rb, K, Ba, Pb, Sr, Sc, Ti and Nb (Figure 6.14d). While the ranges of Cr contents in epidote-rich and pure jadeitite are similar and the strong negative peak in NMORB-normalized Ni mirrors pure jadeitite, a negative anomaly in Sc is not appreciated. Such a decoupling is also observed in HFSE, with Th contents generally lower than pure jadeitite while both types of rock have similar U and Zr contents.

The REE patterns of mica-rich jadeitite are comparable to those of epidote-rich jadeitite though some samples are enriched and all show a positive Eu anomaly. LREE patterns are flat to slightly enriched, from 2 times the Lu content to 13 times Eu content with respect to PUM, with some samples enriched in La with respect to Ce, a marked positive Eu anomaly and the HREE patterns are nearly flats or with slope down from Gd to Lu (Figure 6.14c). In terms of N-MORB normalized patterns this group of rocks shows enrichment in Cs, Rb, K, Pb, Sr and especially Ba (with values around 500 times the N-MORB) (Figure 6.14d). The contents in K are large in most samples, similar to GLOSS contents, pointing to the abundance of muscovite-phengite, though the relative depletion in a couple of samples indicates the presence of paragonite.

Albite-epidote (-chlorite) (-quartz) rocks

Albite-epidote rocks present a mixture of the previously described patterns for jadeitites. They are enriched from 1 to 10.4 times with respect to PUM and their patterns show greater enrichment in LREE than in HREE (Figure 6.15a). Some samples have slight concave-downwards shaped patterns from LREE to HREE, while other present slight concave-upwards patterns. Many samples show a weak positive Eu anomaly or no anomaly that resemble epidote-rich jadeitite (Figure 6.15a). The N-MORB normalized spidergrams show similar patterns for minor and trace element abundance that epidote-rich jadeitite (Figures 6.14d and 6.15b). Their patters are enriched in Cs, Rb, K, Ba, Pb and Sr, although the high compositional variability of these elements reach depleted values of up to 0.1 for K in some samples (Figure 6.15b). Sc, Ti Ni and Cr are depleted relative to NMORB, while Th, U, Nb and Zr range from enriched to depleted, similar to jadeitites (Figure 6.15b). Albite-epidote-chlorite rocks and

Albite-epidote-quartz rocks are similar to albite-epidote rocks, though both groups have high variability in LILE, Th and U, with a high content in Ba (Figure 6.15b).

Chloritites and actinolitite

The composition of chloritite shows a large spread (Figures 6.15c, d). The generally show concave downward REE patterns, except one sample with concave upward pattern. The REE concentrations range from ca 0.01 to 10 times PUM, with positive, negative and no Eu anomaly, though they are depleted relative to NMORB (Figures 6.15c, d). Cs is enriched relative to NMORB, but all other LILE (Rb, K, Ba, Pb and Sr) and HFSE (Th, U, Zr, Ti, and Nb) are generally depleted. Marked peaks in Ni and Cr reach ca. 10 times NMORB (Figure 6.15d). Titanite-apatite-zircon-rich chloritite are enriched in REE relative to PUM and NMORB, except for some samples that show depletion in HREE (Figures 6.15c, d). The REE patterns slope down from LREE to HREE, and show marked to weak positive Eu anomaly. Similar to chloritite, this type of rock is generally depleted in LILE (except Cs), but they do not show marked peaks in Ni and Cr, which are close to NMORM abundance (Ni) or depleted (Cr), and HFSE are significantly enriched (except Ti in some samples).

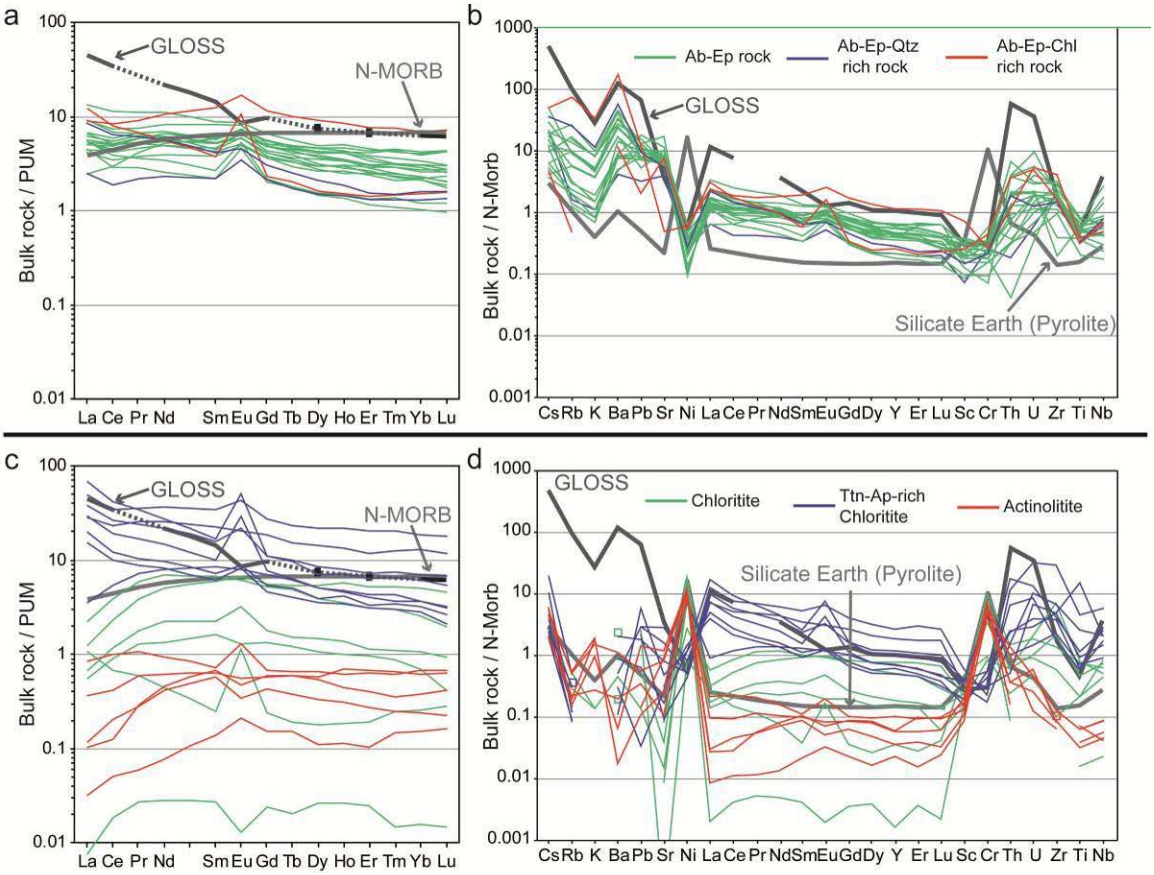

Figure 6.15. Rare earth element (REE) normalized to primitive upper mantle (PUM: McDonough and Sun, 1995) and trace-element "spidergram" normalized to N-MORB (Klein, 2003; Sun and McDonough, 1989) of studied rocks: a) and b) Albitites whole rocks compositions. c) and d) Chloritite and actinolitite whole rocks compositions. Comparison patterns and organization of chemical elements as in figure 6.14.

In terms of REE, actinolitite are depleted relative to PUM, but they diverge from chloritite in that the patterns are generally flat to concave downwards, with significant depletion in LREE in some samples. This type of rock may show positive, negative or no Eu anomaly (Figure 6.15c) and, similar to chloritite, they are generally depleted in LILE (except Cs) and HFSE and show clear peaks in Ni and Cr relative to NMORB.

6.4.3 Nd and Sr isotope systematic

Four pure jadeitite samples (CV237b, CV237k, CV237t, MCB-3h), four Ep-rich jadeitite samples (MCB-1d, MCB-1g, MCB-2c, 09-SC-27k), one mica-rich jadeitite sample (09-SC-7j) and two albite-epidote rocks samples (MCB-1e, 09-SC-31c) have been analyzed for Sr and Nd isotope geochemistry (Supplementary Table 7).

The measured $^{87}Sr/^{86}Sr$ ratio of pure jadeitite (range from 0.7034 to 0.7035), epidote jadeitite (0.7034-0.7035), albite-epidote rock (0.7349-0.7343) and mica-rich jadeitite (0.70344) are similar, though the latter is slightly higher (Supplementary Table 7). The $^{143}Nd/^{144}Nd$ ratio of analyzed samples is more diverse, ranging from 0.5127-0.5129 in epidote-jadeitite through 0.5127-0.5128 in albite-epidote rock, 0.5127-0.5128 in pure jadeitite to 0.5128 in mica-rich jadeitite (Figure 6.1; Supplementary Table 7).

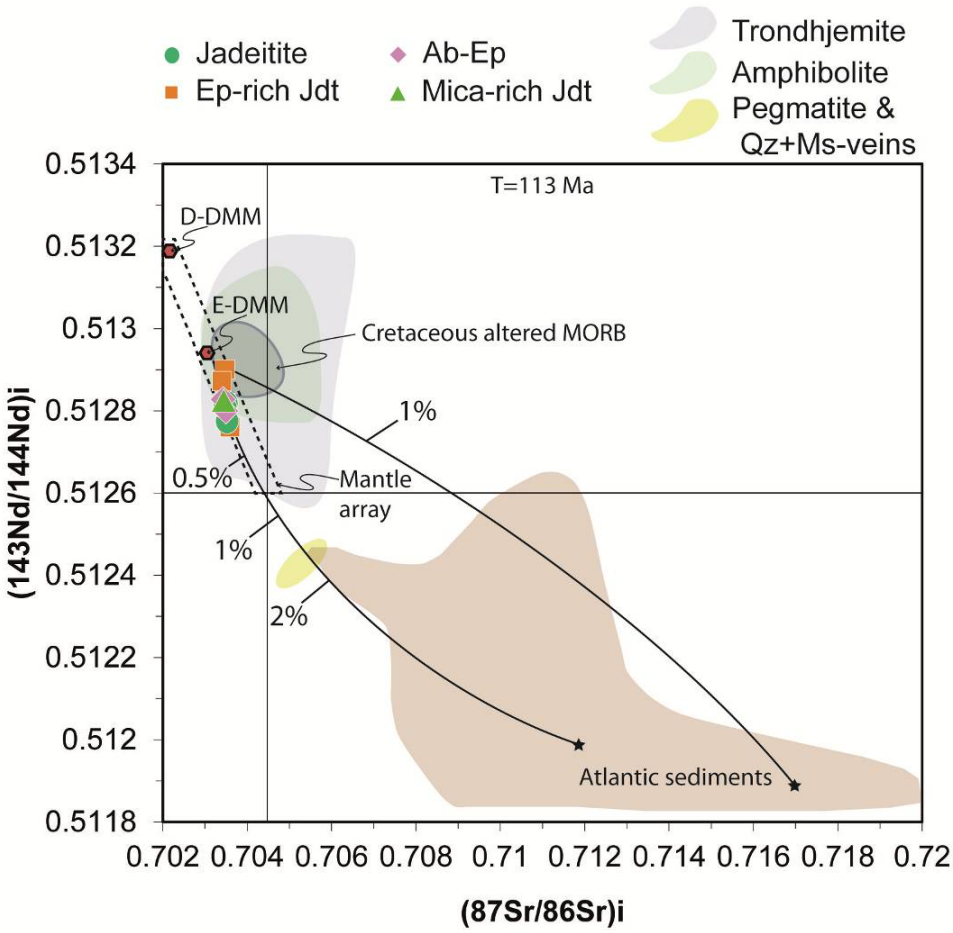

Figure 6.16. $^{87}Sr/^{86}Sr$ vs $^{143}Nd/^{144}Nd$ diagram of whole rock isotopic ratios of studied samples and published data of trondhjemites, amphibolites, and pegmatite+Qz+Ms-veins from Sierra del Convento

and La Corea mélanges (Lázaro and García Casco, 2008; Lázaro et al., 2011; Blanco-Quintero et al., 2011c) corrected to 113 Ma for comparison. Mixing lines and labels for fluid contributions are from Lázaro et al., (2011) and references therein. Age corrected isotopic ratios of data for depleted-depleted MORB mantle (D-DMM), and enriched DMM (E-DMM) are from Workman and Hart (2005). Field of Cretaceous altered Atlantic MORB is from Jahn et al., (1980) and field from Atlantic sediments are from Ben Othman et al. (1989) and Jolly et al. (2006). All fields are corrected to 113 Ma for comparison.

Initial isotopic ratios were recalculated at 113 Ma in Figure 6.16 (see section Zircon U-Pb geochronology). The corresponding isotopic systems show small differences in isotopic ratios, and all samples plot close to the mantle array, suggesting formation from a common isotopic reservoir with a prominent juvenile component. The relatively low Nd concentration in all types of rock is a further indication of a depleted source with a certain sediment-component imprint, as indicated by moderate enrichment in Sr (Figures 6.16). The studied samples compare well with the isotopic compositions of amphibolites and trondhjemites from the Sierra del Convento and La Corea mélanges, plotted for comparison in Figure 6.16. All jadeites and albite-epidote rocks show a similar trend defined by a mixing line between depleted trondhjemite and Atlantic sediments as calculated by Lázaro et al., (2011) and references therein. Remarkably, this mixing line intersects the isotopic compositions of pegmatite and Qz+Ms-veins, and suggests a sediment contribution of less than 0.5% (Figure 6.16).

6.5 Zircon U-Pb geochronology

Precise dating of zircons less than about 1000 M years old by ion-microprobe is best achieved by using $^{206}Pb/^{238}U$-ages (see Black and Jagodzinski, 2003, for explanation), because the proportions of these two isotopes have changed by easily measurable amounts over most of that time. The SHRIMP analytical data are presented in supplementary table 8.

Pure jadeitite sample CV-237-t consists mainly of jadeite with minor contents of omphacite and zircon as accessory minerals dispersed in the granoblastic matrix. The zircons are uniformly long-prismatic with slight rounding at their terminations. The CL images (Figure 6.17a) reveal well-developed oscillatory or sector zoning, and no older cores were seen in these grains. Six grains were analyzed on SHRIMP II and produced well-grouped concordant results (Figure 6.17 and Supplementary Table 8) with a mean $^{206}Pb/^{238}U$ age of 107.4±0.5 Ma (Figure 6.17b) which we interpret to reflect the time of zircon crystallization.

Sample CV-237-b (pure jadeitite) is composed of 80% pyroxene (mostly jadeite) with dark and light mm-sized nodular areas and zircons dispersed in the pyroxene matrix. The zircons are mostly euhedral with slight rounding at their terminations, and CL images show well developed oscillatory zoning. Six grains were analyzed and yielded concordant, well-grouped results (Supplementary Table 8) that define a mean $^{206P}b/^{238}U$ age of 107.8±1.1 Ma.

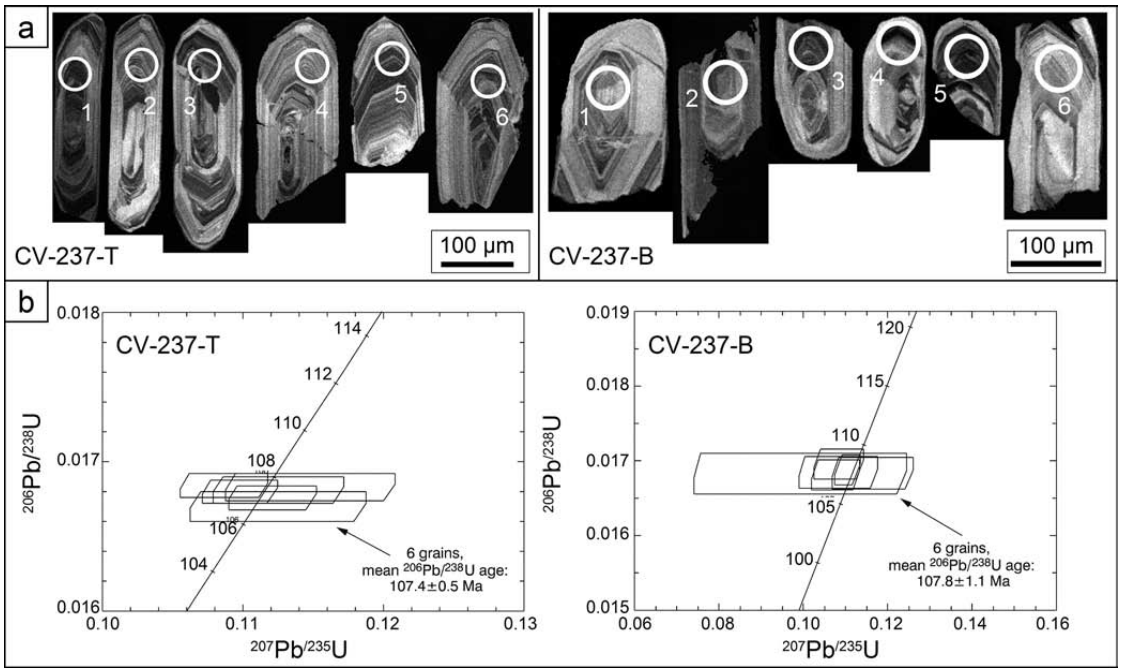

Figure 6.17. a) CL images and site location of each analysed zircon from jadeitite samples. b) SHRIMP II analysis represented in a Concordia diagrams for samples CV-237-T and CV-237-B. Standard errors in $^{207}Pb/^{235}U$, $^{206}Pb/^{238}U$ and $^{207}Pb/^{206}Pb$ for each analysis are shown as data boxes

The Th/U ratios for these zircons from pure jadeitite are relatively low (between 0.21 and 0.58 ppm, Supplementary Table 8), suggesting a hydrothermal origin for these grains (Tsujimori et al., 2005a) which probably precipitated and crystallized from a fluid evolved from crystallization of trondhjemitic fluid-saturated melt during 105-113 Ma (most ages of anatectic igneous rocks are slightly older 109-113 Ma; Figure 6.19). We suggest a sedimentary source from subducted oceanic crust to explain the high U and Th contents of analyzed zircons. Pegmatitic/hydrothermal segregations made of quartz, albitic plagioclase, paragonite, and epidote from residual melts saturated in H_2O and fluids were intruded and formed in the Sierra del Convento and La Corea mélanges (Lázaro and García-Casco, 2008; Blanco-Quintero et al., 2011c) at almost the same time of crystallization of the analyzed zircons, strenghthening the view of an hydrothermal origin of the dated zircons.

The dated ages of zircons from pure jadeitites (107-108 Ma) contrast with the ages of zircons from other types of rock. Samples 09-SC-27c and 09-SC-27d (both classified as Ep-rich jadeitite) are part of a single jadeitite block, and consist mainly of jadeite and omphacite, with clinozoisite, epidote, albite, and minor muscovite, paragonite, titanite and zircon contents. The zircon grains are mostly euhedral, in some cases with bipyramidal terminations, and their CL images show well developed oscillatory zoning without older cores. Six grains analyzed from sample 09-SC-27c yielded concordant results that define a mean $^{206P}b/^{238}U$ age of 113.9 ± 1.2 Ma (Fig. 6.17a, Supplementary Table 8). This age is very close to that defined by the mean $^{206P}b/^{238}U$ age of 112.1 ± 1.3 Ma in sample 09-SC-27d where seven grains were analyzed (Figure 6.18b).

In the same block, and with a position close to the edge, sample 09-SC-27b (Ab-Ep Chl-rich rock) has a mineralogy dominated by albite, epidote and abundant chlorite. Seventeen zircon grains with euhedral-subhedral morphologies and well-developed oscillatory zoning in CL images were analyzed and yielded concordant results (Supplementary Table 8) that define a mean $^{206P}b/^{238}U$ age of 113.1 ± 0.87 Ma (Figure 6.18c), indistinguishable of zircon ages of associated Ep-rich jadeitite. Because this rock formed after metasomatic alteration of Ep-jadeitite during retrogression, we consider this age as that of formation of the parental Ep-rich jadeitite.

The chloritite blackwall of the same block is represented by the sample 09-SC-27a. This sample is composed of 95% chlorite with minor amount of zircon and titanite. The zircons are mostly euhedral with slight rounding at their terminations, and CL images show well developed oscillatory zoning and no older cores were seen in these grains. Six grains were analyzed and yielded concordant results (Supplementary Table 8) that define a mean $^{206P}b/^{238}U$ age of 112.3 ± 1.5 Ma (Fig. 6.18d), also indistinguishable of zircon ages of associated rocks from the same block. This clearly indicates that chroritite blackwall formation took place during emplacement of jadeitite-forming fluids within peridotite/serpentinite and not at a later stage during the exhumation of the block.

Associated with pure jadeitite in a contact zone (Figure 4.4k), the Ttn-Ap-Zr-rich chloritite sample 09-SC-8aVIII represents a blackwall. This sample is composed of 90% chlorite with abundant (10%) zircon, apatite and titanite. The CL images of twenty zircon grains (Figure 6.18e) reveal the absence of old cores and a well-developed oscillatory or sector zoning. The results of analises (Supplementary Table 8) define a mean $^{206P}b/^{238}U$ age of 113.6 ± 1.1 Ma (Figure 6.18e), older than dated zircons from pure jadeitite samples and similar to ages of zircon from Ep-rich jadeitite and associated blackwall. Though the pure jadeitite related to this blackwall has not being dated, we consider it likely that it formed synchronously with its associated chloritite, given the close age relation of Ep-rich jadeitite and its associated blackwall described above. Hence, we conclude that formation of pure jadeitite may have spanned 107-114 Ma.

In all samples described above, zircons with idiomorphic habit are found as isolated grains occupying interstitial positions, and within jadeite and omphacite crystals. They are generally large, with sizes above 100 microns long, with rare inclusions of jadeite, suggesting crystallization by fluids contemporaneous to jadeite formation. The timing of formation of jadeitite and associated rocks and, hence, of fluid flow, storage, precipitation and reaction is 107-114 Ma, with individual bodies formed at variable age within this age interval (Figure 6.19).

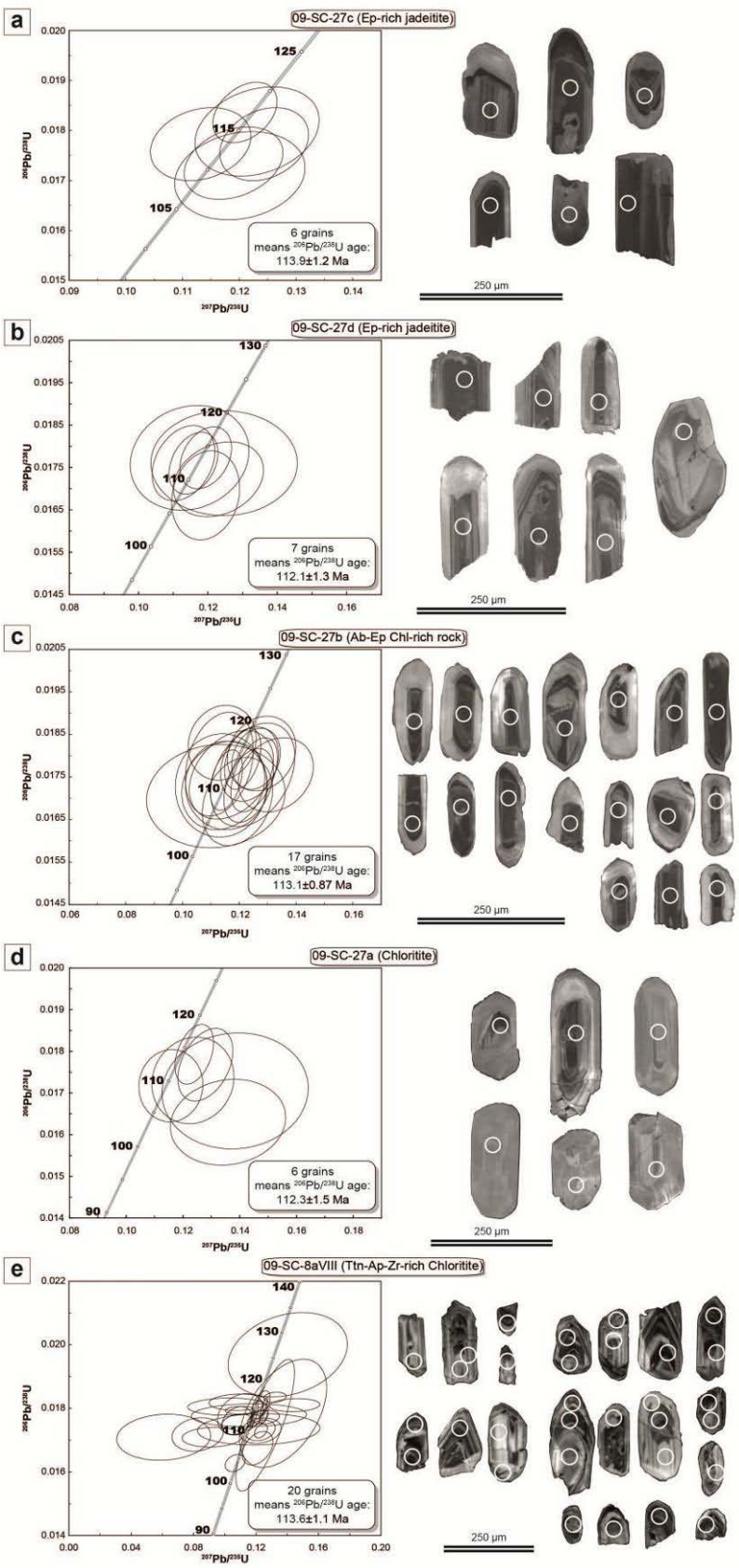

Figure 6.18. SHRIMP II analysis represented in concordia diagrams for the samples: a) 09-SC-27c epidote-rich jadeitite sample, b) 09-SC-27d epidote-rich jadeitite sample, c) 09-SC-27b Ab-Ep Chlorite-rich rock, d) 09-SC-27a chloritite, e) 09-SC-8aVIII Ttn-Ap-Zr-rich rock and CL images with site location of each analyzed zircon. Standard errors in $^{207}Pb/^{235}U$, $^{206}Pb/^{238}U$ and $^{207}Pb/^{206}Pb$ for each analysis are shown as data circles.

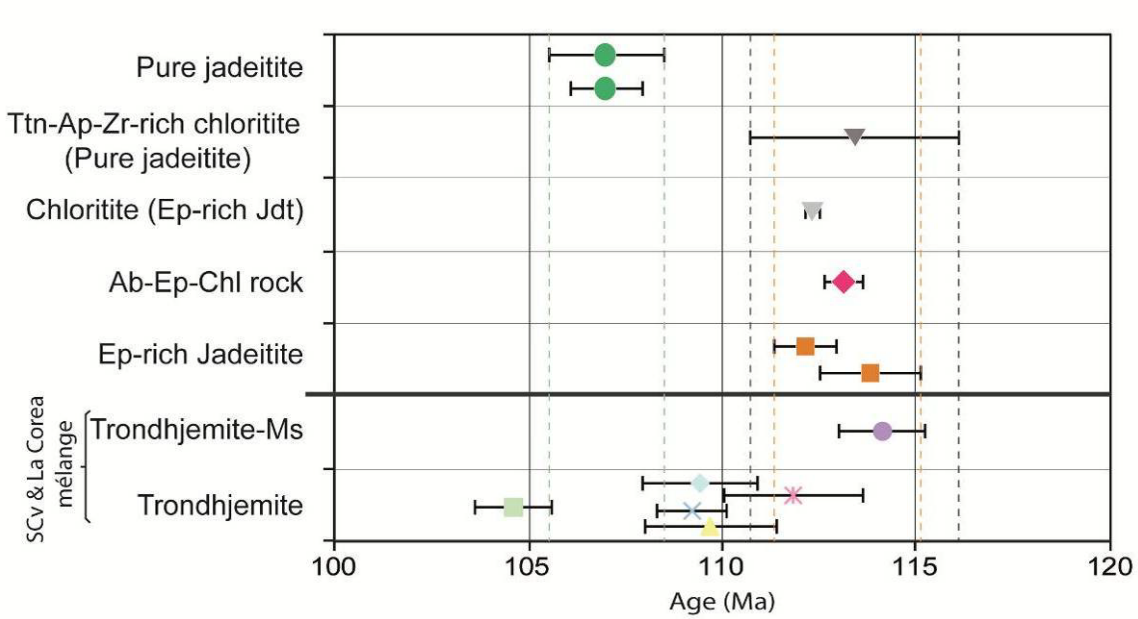

Figure 6.19. Time scale for the different lithologies studied, the error bars (black lines) were added. Trondhjemites from Sierra del Convento and La Corea mélanges were plotted for comparison (Blanco-Quintero et al., 2011e, Lázaro et al., 2009).

In this way, the data support a hypothesis in which the crystallization of jadeitites occurs during a short period of time, broadly coetaneous with crystallization of anatectic tonalite-trondhjemite melts in the Sierra del Convento and La Corea mélanges (Figure 6.19). The recurrent flow of fluids in the dated block of epidote-rich jadeitite can be constrained to a period of ca. 112-115 Ma, though it may have probably taken a much shorter time interval. Thus, if these ages are taken into account together with the ages of younger pure jadeitite and the age of the dated chloritite blackwall in contact with pure jadeitite, the formation of jadeitite and associated rocks in the Sierra del Convento mélange would cover a time period of less than 10 Ma (107-114 Ma; (Figure 6.19).

6.6 Petrogenesis and Discussion

The Cuban occurrence of jadeitite gets added to the list of rare occurrences of this rock type from high-pressure exhumed terranes reported worldwide. Harlow and Sorensen (2005) suggested a relationship between strike-slip plate boundaries and jadeitite exhumation to explain the scarcity of this rock type. However, the scarcity of jadeitite outcrops may also be due to restricted petrogenetic conditions and particular fluid-rock interactions in subduction zones.

The Cuban jadeitites are found as tectonic blocks within a serpentinite mélange but, as described above, textural and petrological relations indicate crystallization in fractures (García-Casco et al., 2009; Cárdenas-Párraga et al., 2012), as with other occurrences of this type of rock (Sorensen et al., 2006; Harlow et al., 2007; Sorensen et al., 2010). Therefore, jadeitite crystallization must be considered in the context of fluid

flow within a fractured peridotite/serpentinite, thus they are classified following Harlow et al., (2015) in P_S-type jadeitite.

6.6.1 Temperature and pressure of formation

Jadeitite worldwide has been interpreted as forming at relatively low temperatures (<500 °C). However, the composition of coexisting jadeite and omphacite in the studied rocks indicates minimum initial conditions of formation above 500 °C (Figure 6.20), unique among jadeitites. The composition of pyroxene is quite varied. Many analyses are within the forbidden region (solvii) at 500 °C, suggesting a) mixed analyses of jadeite-omphacite and omphacite-diopside (the latter only in omphacitite) intergrowths at the sub-microscopic level and/or b) high temperature of formation, eventually above the respective critical temperatures of the solvii (650-700 °C; Green et al., 2007; García-Casco et al., 2009).

There is no systematic difference in composition of pyroxenes between the different types of rock except for omphacitites, which, in addition to omphacite with composition within the jadeite-omphacite solvus, also show compositions with the lowest jadeite component (down to 29 mole%) within the omphacite-diposide solvus, and do not show jadeite.

On the other hand, agirine component reaches 21 mole%, with Aeg/(Q+Aeg) ratios up to ca. 0.5. Taking into account the shape of the theoretical phase relations diagrams proposed by Carpenter (1980) and Vinograd (2002) for different temperatures, the observed compositions should have formed at higher temperatures along the solvus between jadeite and omphacite. Although the solvus becomes narrower with increasing temperature and aegirine content (e.g., Tsujimori et al., 2005b; Green et al., 2007), the calculated amount of aegirine component in the studied pyroxenes does not justify crystallization≤ 500 ° C. Importantly, the composition of relict jadeite and omphacite in Ab-Ep rocks is comparable to pyroxene composition in other type of rocks, in particular, Ep-rich jadeitite.

For this study the NASH system was constructed using THERMOCLAC v. 3.33 and dataset 5.5 (Holland and Powell, 1998); all the minerals were treated as pure phase (Figure 6.21), although the Jd+Qz=Ab reaction was calculated for different activities of jadeite component in clinopyroxene (a_{jd} = 0.9-0.8-0.7) to account for variations in the composition of jadeite during formation. Quartz+albite inclusions within jadeite crystals indicate temperatures and pressures (slightly) above the Jd+Qz=Ab reaction. Using the P-T path of amphibolites and trondhjemites of the Sierra del Convento mélange (Lázaro et al., 2009), the intersections of the Jd+Qz=Ab in the NASH system occur at a temperature range of 550-625 °C at pressures around 15 kbar (Figure 6.21).

During a final event, omphacite poorer in Al-Na was formed from fluids largely modified after fluid-ultramafic rock interaction. These fluids that are not in equilibrium with previously precipitated blocky jadeite, triggering the replacement of jadeite by omphacite even in the interior of the grains (Figure 3d). Reaction of the fluid with jadeite triggered modification of the composition of the fluid until it reached

equilibrium with both jadeite and omphacite. At this point two pyroxenes coexisted in equilibrium as predicted by the solvus relations in the Jd-Di-Hd-Ae clinopyroxene system (e.g., Green et al., 2007), and Na-rich omphacite exsolutions within early jadeite were generated upon subsequent cooling (Figures 6.23 and 6.1c, d).

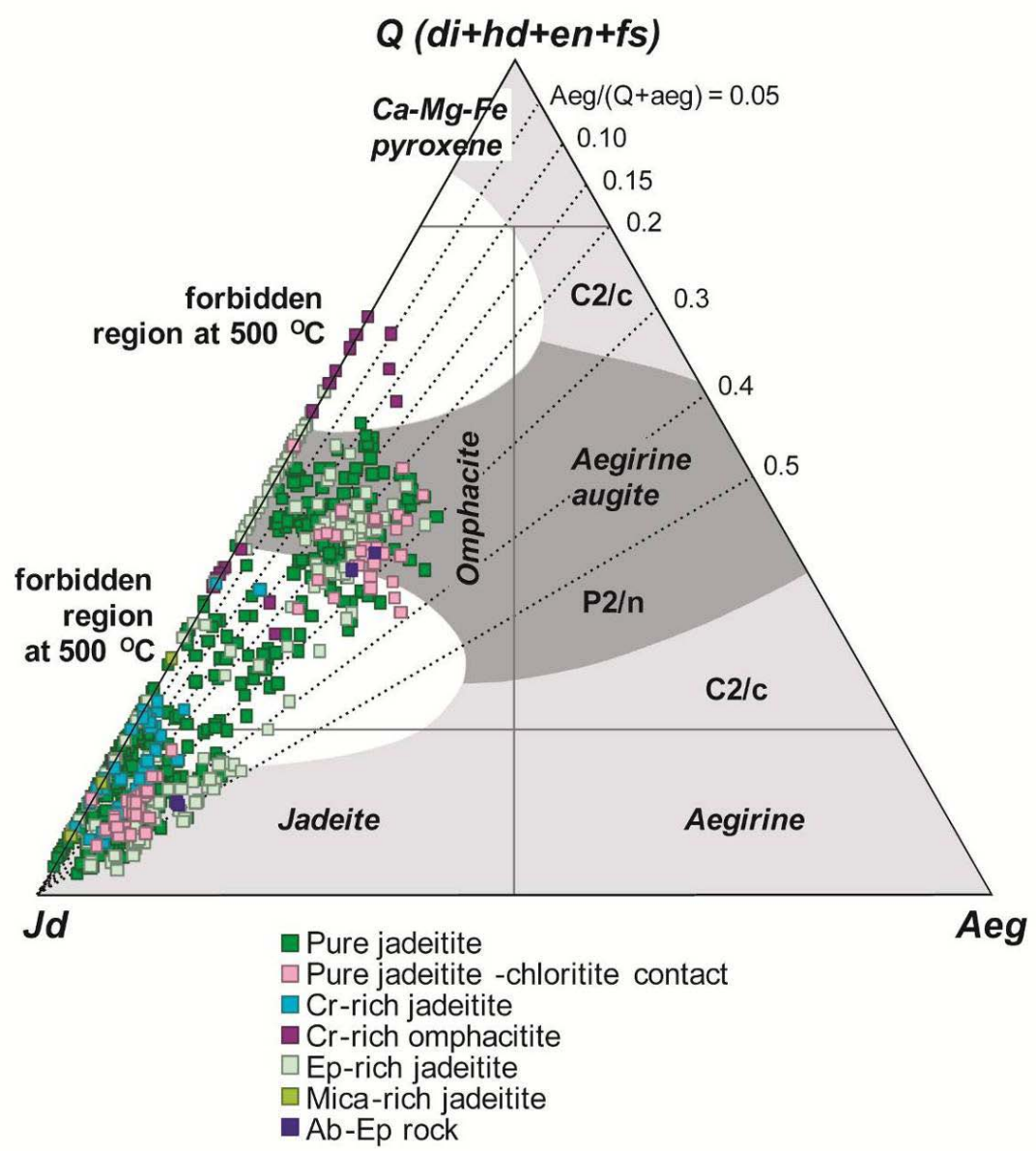

Figure 6.20. Composition of jadeite and omphacite in the Q-Jd-Aeg classification scheme of Morimoto et al. (1988; italic font) with indication of the phase relations of pyroxene calculated by Green et al. (2007) at 500 °C in the system jadeite-diopside-aegirine (regular font) for reference. Dashed lines indicate varying Aegirine/(Q + Aegirine) ratios.

The high temperature of jadeite formation is in agreement with thermodynamic calculations for sample CV-237-K presented by García-Casco et al., (2009), who indicated temperatures of ca. 600 °C. The interpreted exsolution of omphacite within jadeite, which is rare in other (low-T) jadeitites, also points to a high temperature of formation followed by cooling/annealing. Consequently, it appears that the Sierra del

Convento jadeitite constitutes the only high-temperature occurrence reported so far. On the other hand, albite growth during the late stages of rock evolution documents decreasing pressure and temperature (exhumation and cooling) in the albite stability field.

High temperature of jadeitite formation is indicated indirectly by the age of formation of jadeitite and associated rocks (107-114 Ma), coetaneous with the initial isobaric stage of post-peak cooling of garnet amphibolites and crystallization (i.e., decreasing temperature) of anatectic tronhjemitic melts and associated hydrothermal/pegmatititic fluids/melts at ca. 600-700 ºC (at 105-113 Ma; Lázaro et al., 2009; Blanco-Quintero et al., 2011e; Figures 6.19 and 6.21). The close age link between all these types of rock allows proposing a genetic link between the post-magmatic hydrothermal activity and jadeitite formation and associated fluid-rock interactions. In this context, the "sedimentary" imprint in the geochemistry of jadeitites and associated rocks may have developed as a result of infiltration of sediment-derived fluids during crystallization of trondhjemites and associated hydrothermal/pegmatitic rocks or directly as a result of the latter, for partial melting of amphibolite was triggered by the infiltration of fluids evolved from subducted juvenile hydrated crust/mantle and sediments (Lázaro et al., 2008, 2011; Blanco-Quintero et al., 2011c).

6.6.2 Composition of fluids involved in jadeitite formation

Sorensen et al. (2010) discussed the types of fluids involved in the jadeitite-peridotite/serpentinite-fluid system that have been proposed in the literature, including fluids that result from the serpentinization of peridotite (Harlow, 1994; Johnson and Harlow, 1999; Morishita et al., 2007; Yui et al., 2010), devolatilization of subducted sediments (Sorensen et al., 2006), devolatilization during blueschist to eclogite facies transition in subducted meta(altered)-MORB (Manning, 1998; Harlow and Sorensen, 2005; Sorensen et al., 2006) and "jadeititizing fluids"(from Russian literature, see Harlow et al., 2007). Other types of fluids that can be involved in the formation of jadeitite are supplied during the dehydration of subducted serpentinized oceanic mantle, as evidenced by subduction-zone magmas (Hattori and Guillot, 2003; Rüpke et al., 2002; Scambelluri et al., 2001, 2004; and Tenthorey and Hermann, 2004). Sorensen et al. (2006, 2010) and Morishita et al. (2007) have suggested that these different fluid components can be present in varying proportions during the formation of jadeitite. On the other hand, García-Casco et al., (2009) suggested the involvement of fluids generated after crystallization at the depth of hydrous tonalitic-trondhjemitic melts formed during fluid-fluxed partial melting of subducted-accreted oceanic crust, providing an explanation for the diversity in the chemical composition and oscillatory zoning in Cuban jadeite and for crystallization from chemically diversified fluids during recurrent episodes of infiltration.

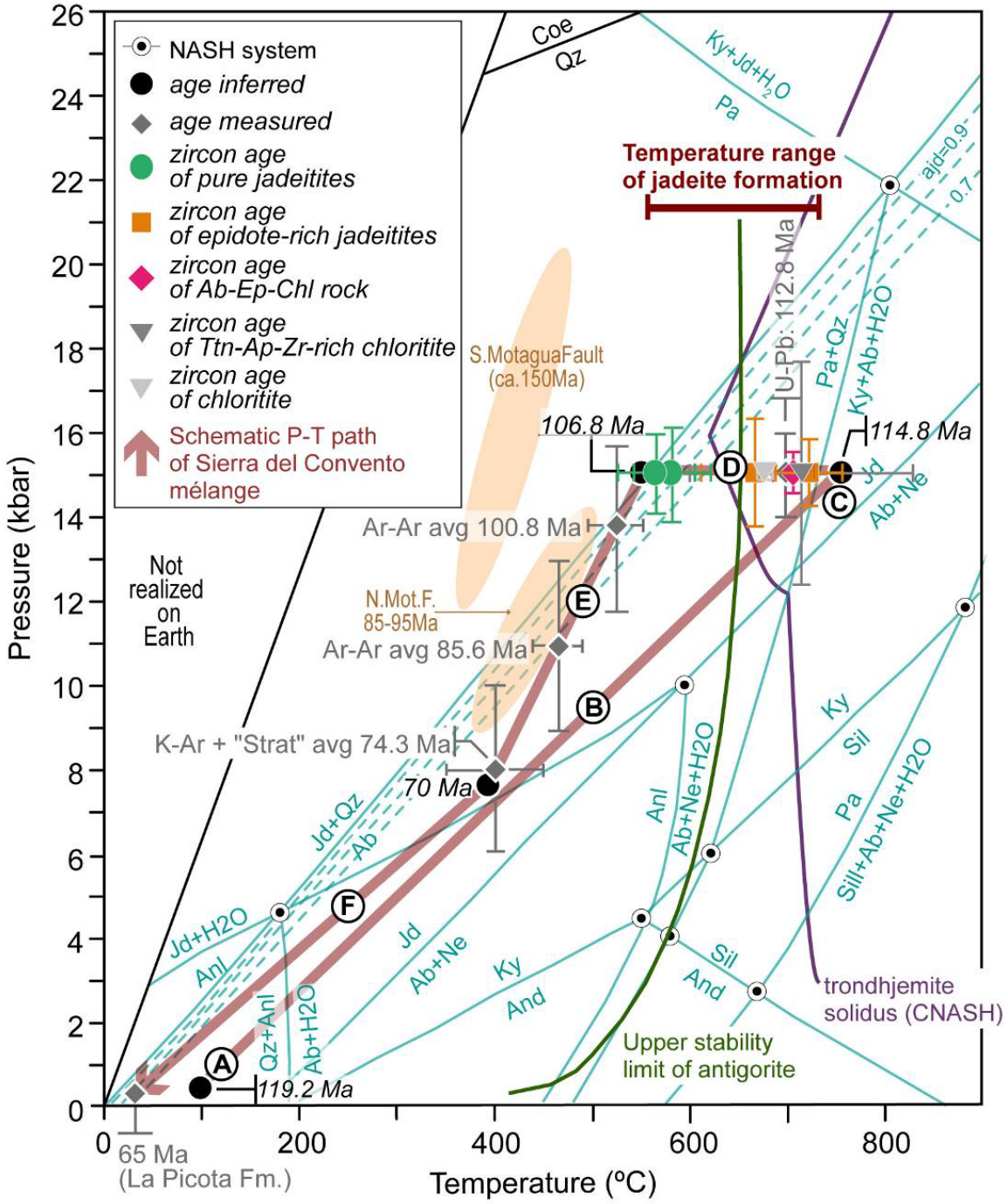

Figure 6.21. Geodynamic-petrologic model of the Sierra del Convento mélange (modified from Lázaro et al., 2009) with SHRIMP zircons ages plotted for pure jadeitite (107.4±0.5 Ma and 107.8±1.1 Ma), epidote-rich jadeitite (112.1±1.3 Ma and 113.9±1.2 Ma), Ab-Ep-Chl rock (113.1±0.87 Ma), Ttn-Ap-Zrn-rich chloritite (113.6±1.1 Ma) and chloritite (112.3±1.5 Ma). In this model geodynamic stages are noted as: A (onset of subduction), B (subduction, 45 °C kbar^{-1}, 150 °C Myr^{-1}, 11 km Myr^{-1}), C (accretion to the upper plate), D (cooling in the upper plate, 25 °C Myr^{-1}), E (syn-subduction exhumation, 21 °C kbar^{-1}, -4 °C Myr^{-1}, -0.7 km Myr^{-1}), F (syn-collision exhumation, 48 °C kbar^{-1}, -74 °C Myr^{-1}, -5 km Myr^{-1}). Inferred and measured ages after Lázaro et al., (2009) and references therein. Areas and ages of Guatemalan jadeitites according to Harlow et al., (2011). Thick curves represent the trondhjemite solidus (García-Casco, 2007) and the upper stability of antigorite (Wunder et al., 2001). Reactions in the NASH system (thin curves) calculated using THERMOCALC v.3.33. See text for explanation. The predicted location of P-T-age data of Ep-rich jadeitites, chloritite blackwalls and Ab-Ep Chl-rich rocks above the trondhjemite solidus suggest that the age of peak conditions by Lázaro et al (2009) is, in fact, slightly older (ca. 120-125 Ma).

The presence of zircon in the studied samples suggests, however, that the chemical characteristics of fluids that formed the Cuban jadeitite may be similar to those that formed Guatemalan and Dominican Republic jadeitite: reduced fluids with high pH capable of mobilizing Al, Na, Zr and Hf (Yui et al., 2010) and undersaturated with respect to quartz (Harlow, 1994; Schertl et al., 2007; Maresch et al., 2008; Hetwin 2014). A geochemical comparison between these deposits is offered below.

Genetic link with trondhjemitic liquids

The P-T-t data reported above can be related to the P-T-t evolution of blocks of amphibolites and associated anatectic trondhjemites of the Sierra del Convento presented by García-Casco et al. (2008b) and Lázaro et al., (2009). These authors proposed counterclockwise P-T paths for the formation and exhumation of the blocks in the mélange (Figure 6.21), which are related to hot subduction of young oceanic lithosphere between 120-115 Ma (prograde paths), accretion of MORB-derived amphibolite to the mantle wedge and wet-melting at ca. 15 kbar and 700-750 °C. This resulted in a plagioclase-lacking residual amphibolite and peraluminous tonalitic-trondhjemitic melts that segregated into veins and layers at ca. 115 Ma (peak conditions). Melting was triggered by the influx of slab-derived fluids (dehydration of subducting serpentinite, hydrated crust and sediments; as indicated by geochemical data provided by Lázaro and García-Casco, 2008; Blanco-Quintero et al., 2011c), at temperatures above the wet solidus of basaltic compositions. The accreted partially-melted blocks of amphibolite underwent a relatively fast near-isobaric cooling (750-550 °C) in the hosting mantle wedge between 115-107 Ma (Figure 6.21). Such cooling reflects refrigeration of the mantle wedge/channel upon continued subduction (Gerya et al., 2002). At this stage, serpentinite was not formed after hydration of upper plate peridotite because (a) the temperature (in the 750-650 °C range) is above the stability of antigorite (Ulmer and Tromsdorff, 1995; Wunder et al., 2001) and (b) any water released by the slab and fluxed to the upper plate at this stage was consumed by melting of accreted amphibolite and/or dissolution of water into trondhjemitic liquids (750- ca. 600 °C, i.e., until the wet-solidi of the implied systems were crossed). Hence, serpentinization of the upper plate peridotite triggered by infiltration of fluids started at ca. 640 °C. Part of the fluid may have been released by the downgoing slab, but a significant part of it was released by the crystallization of water-bearing trondhjemites melts, as documented by the presence of pegmatites and quartz-veins (Lázaro and García-Casco, 2008; Blanco-Quintero et al., 2011c). At 106.8 Ma (i.e., around 540 °C), the extent of serpentinization was large enough to allow ductile flow of serpentinite and the formation of a serpentinite-matrix mélange. Henceforth, the mélange (serpentinitic subduction channel and margin) started slow exhumation (107-70 Ma; Lázaro et al., 2009) until the arc-platform collision caused orogenic build-up and general exhumation in the region (70-65 Ma; García-Casco et al., 2008a).

The zircon $^{206}Pb/^{238}U$ ages from jadeitites, Ab-Ep-Chl-rich rock and chloritites (107-113 Ma (see section Zircon U-Pb geochronology) are considered to represent the main hydrothermal crystallization event of the jadeitite veins and associated chloritite

blackwalls. This age corresponds to the isobaric (15 kbar) cooling stage of the above scheme (Figure 6.21), fully in agreement with the high temperature of jadeitite formation inferred above and with the presence of quartz inclusions in jadeite (note that the Ab=Jd+Qz reaction intersects these conditions, and that the reaction itself is a band due to the effects of Ca, Mg, Fe and other elements not considered in the NASH system, Figure 6.21). Nd and Sr Isotopic compositions of the pure jadeitite, Ep-rich jadeitite, mica-rich jadeitite and Ab-Ep rocks overlap the mantle array as well as the fields of MORB-derived amphibolite and anatectic trondhjemite from the Sierra del Convento and La Corea mélanges (Figure 6.14). These compositions and the trend towards pegmatite and Qz+Ms-veins indicate a strong influence of fluids derived from trondhjemite crystallization with juvenile signature and a smaller contribution from fluids with sedimentary signature (< to 5%; Figure 6.14).

The previous observations are reinforced by the comparison between the trace element whole-rock compositions of the different varieties of amphibolite, trondhjemite and pegmatite & Qz+Ms-veins from eastern Cuba mélanges with the chemical compositions of studied rocks (Figures 6.22 and 6.21). In general, pure jadeitite and omphacitite have similar REE trends as trondhjemite and pegmatite & Qz+Ms-veins (Figure 6.22a, d), which were defined as having been formed by the differentiation of trondhjemitic melts and crystallization from a primary sediment-derived fluid, respectively (Lázaro and García Casco, 2008; Lázaro et al., 2011; Blanco-Quintero et al., 2011c). Only sample SC-MJ-10, classified as pure jadeitite (Cr-rich), shows a depleted composition in LREE with respect to pegmatite & Qz+Ms-veins, but similar to the compositions of trondhjemite. In this way, the REE variations of about an order of magnitude in pure jadeitite and one half-order of magnitude in omphacitites suggest a strong fluid-jadeitite interaction (Figure 6.22a). An alternative explanation for the observed strong variation range of REE patterns is a direct crystallization from fluids with compositions from REE depleted to REE enriched. In both cases, however, the fluids that formed pure jadeitite and omphacitite can be related to fluids differentiated from the crystallization of trondhjemitic and pegmatitic melts and a primary sediment-derived fluid. The REE variation of slightly less than an order of magnitude is also characteristic of epidote-rich jadeitite, mica-rich jadeitite and Ab-Ep rocks (Figure 6.22b, c). These three groups bear enriched compositions with respect to primitive upper mantle (PUM). Their REE trends show LREE similar to amphibolite, Ms-amphibolite and partially similar to Ms-trondhjemite, as well as HREE between Ms-amphibolite and enriched HREE compositions of Ms-trondhjemite (Figure 6.22b-e). These trends suggest that the fluids related to formation of these three groups share a similar process of differentiation after crystallization of Ms-trondhjemitic hydrous melt. Thus the sedimentary signatures of these different rocks are strongly influenced by a primary sediment-derived fluid (see GLOSS and Antillean terrigenous sediments trend in figure 6.22b, c).

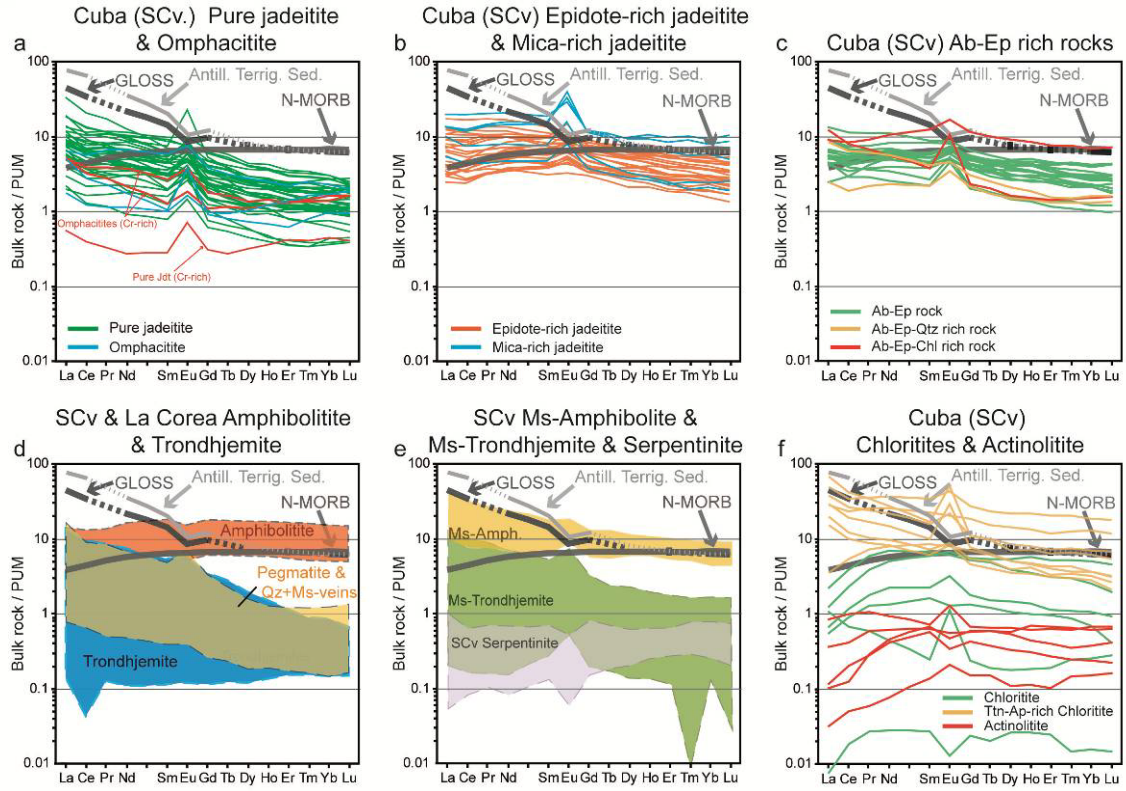

Figure 6.22. Rare earth element (REE) plots of studied rocks normalized to primitive upper mantle (PUM, McDonough and Sun, 1995). Published data of trondhjemites, amphibolites, serpentinites and pegmatite+Qz+Ms-veins from Sierra del Convento and La Corea mélanges are included for comparison (Lázaro and García Casco 2008; Lázaro et al., 2011; Blanco-Quintero et al., 2011c, Cárdenas-Párraga et al., 2017). Also are plotted for comparison GLOSS and Antilles terrigenous sediment (Plank and Langmuir, 1998). Elements sorted as in figure 6.14.

The REE patterns of chloritite blackwall are quite varied, from 0.1 to 100 times the concentration of PUM, showing a transition from the most depleted to the more enriched compositions (Figure 6.22f). These variable patterns are consistent with the classification in two groups made for chloritite (i.e. Ttn-Ap-rich chloritite and chloritite), and only the patterns of Ttn-Ap-rich chloritite show some similarity to compositions of Ms-amphibolite (Figure 6.22e, f). LREE patterns of Ttn-Ap-rich chloritite range from N-MORB to GLOSS and Antillean terrigenous sediments. However, HREE are enriched and depleted with respect to these reference types of rock, respectively (Figure 6.22f). The patterns of chloritite range from depleted with respect to PUM to values similar to N-MORB. The more depleted REE patterns show some coincidence with the patterns defined by actinolitite (Figure 6.22f), which are similar to subducted serpentinites from Sierra del Convento mélange (Figure 6.22e, f). Both types of chlorititic blackwall represent the metasomatized host peridotitic mantle/serpentinite where fluids forming jadeitite crystallized in veins. On the other hand, actinolites represent the products of crystallization of fluids derived, likely, from subducted serpentinites. In figure 6.22f three types of signature that are involved in the formation of jadeitites, Ab-Ep rocks, and in the fluid-jadeitite interaction processes are indentified. In this regard, chlorititic blackwall patterns show: (i) enriched compositions with respect to PUM influenced by GLOSS and Antillean terrigenous

sediments signatures, (ii) concave patterns, enriched by no more than an order of magnitude, with a N-MORB signature (fluids reacting with amphibolites and/or differentiated from trondhjemite melts) and (iii) depleted patterns with respect to PUM with signatures related to actinolitite and subducted serpentinites (Figure 6.22f).

The REE patterns normalized to N-MORB of all groups of studied rocks (Figure 6.23) allow similar conclusions as those exposed for the PUM-normalized diagrams of Figure 6.22. Nevertheless, trace-element plots as "spidergrams" show that enriched patterns in LILE, especially Ba for all jadeitite varieties and omphacitite, are significant, pointing to a sedimentary signature (Figure 6.23a, b). These samples show similar LILE contents as trondhjemite and Ms-trondhjemite and are depleted in Ba with respect to pegmatite & Qz+Ms-veins from Easter Cuba (Figure 6.23a-d). Only a group of samples of pure jadeitite and omphacitite shows depleted LILE compositions, with depleted Ba contents with respect to N-MORB (Figure 6.23a). The trends of LILE of the latter samples are not similar to the patterns of pegmatite & Qz+Ms-veins, trondhjemite and Ms-trondhjemite (Figure 6.23a, c and d). Their LILE patterns mimic the PUM trend and show similar depleted Ba contents as blackwall chloritite and actinolitite veins (Figure 6.23a, e). In contrast, enriched patterns of Ni and Cr in samples mainly classified as pure jadeitite and omphacitite cannot be related to trondhjemitic liquids, suggesting a subducted serpentinite related fluid (Figure 6.23a, f). The trace element patterns of chloritites blackwall discriminate two types of fluids, both relatively depleted in Ba and LILE with respect to N-MORB (Figure 6.23e). Ttn-Ap-rich chloritite patterns suggest a REE- HFSE-rich sedimentary source that can be related to Ba-poor fluids differentiated from crystallization of trondhjemitic and Ms-trondhjemitic melts (Figure 6.23c, d, e). The high variability of chloritite patterns are however enriched in Ni and Cr, denoting affinity with actinolitite and the interactions of Ba-poor fluids from a serpentinitic source (Figure 6.23e, f).

In summary, normalized REE and trace element "spidergrams" of studied samples indicate mixing of fluids derived from three sources: sediment (GLOSS), amphibolite/trondhjemite (MORB) and serpentinite (PUM). However, spidergrams also suggest that two types of sediment-derived fluid interacted with fluids differentiated from the crystallization of trondhjemitic-pegmatitic melts and fluids related from subducting serpentinites. A primary Ba-rich sediment-derived fluid defined by the patterns of pegmatite and Qz+Ms-veins, with REE trending towards GLOSS and not necessarily enriched in HFSE and, on the other hand, a Ba-poor fluid capable of generating REE- and HFSE-enriched patterns.

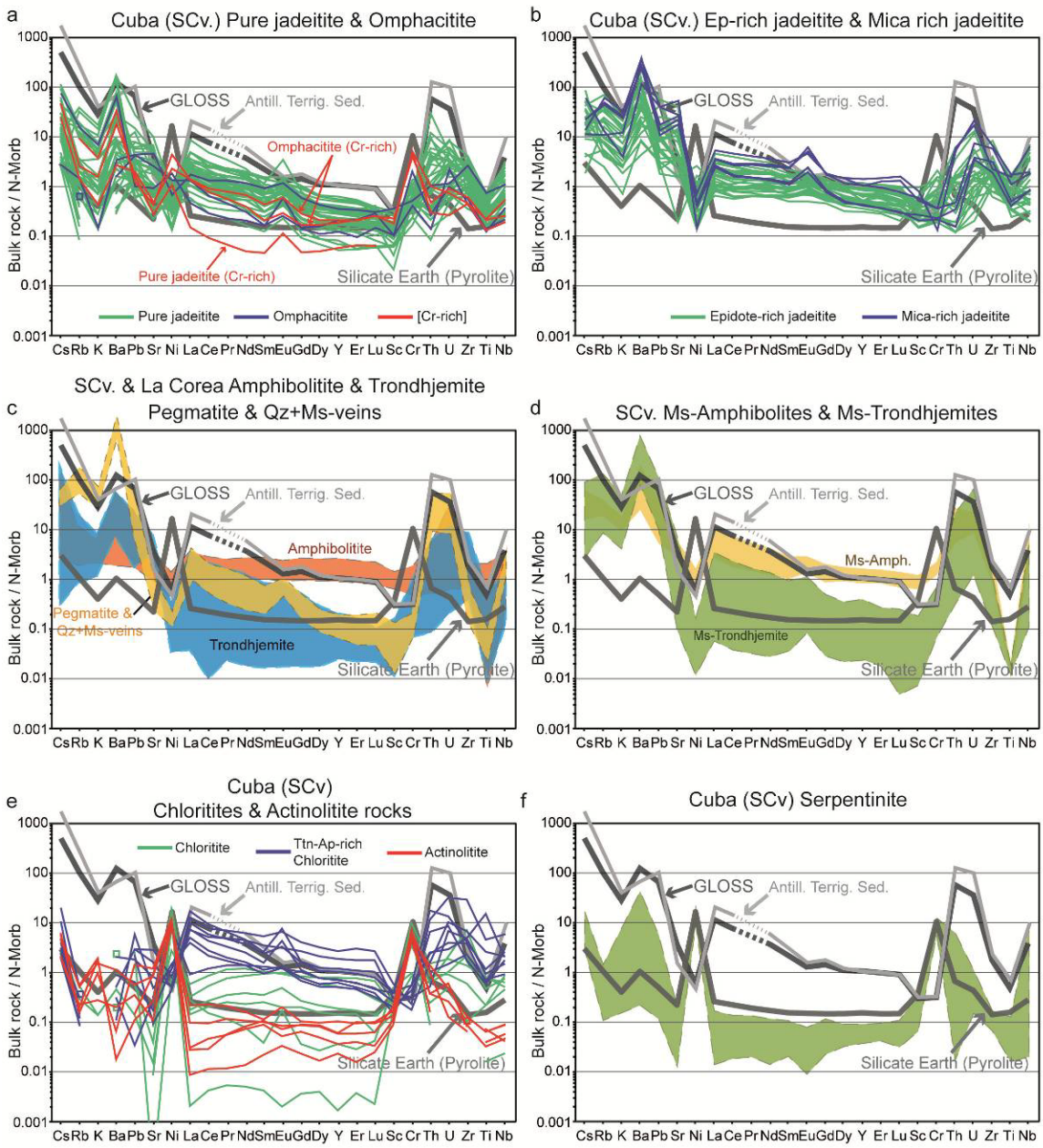

Figure 6.23. Spidergrams plot for (a) pure jadeitite and omphacitite, (b) Ep-rich jadeitite and mica-rich jadeitite, (c), (d) and (f) amphibolites, trondhjemite, pegmatite + Qz-Ms rocks and serpentinite from the La Corea and Sierra del Convento mélanges (Lázaro and García Casco 2008; Lázaro et al., 2011; Blanco-Quintero et al., 2011c, Cárdenas-Párraga et al., 2017), (e) chloritites and actinolitite normalized to N-MORB (Sun and McDonough, 1989, Ni, Cr and Sc from Klein, 2003). GLOSS, Antilles terrigenous sediment (Plank and Langmuir, 1998), and silicate earth (McDonough and Sun, 1995) are plotted for comparison. Organization of chemical elements as in figure 6.14

6.6.3 Fluid-Ultramafic rock and Fluid-Jadeitite Interaction

Pulses of fluids from cooling trondhjemitic melts would have been rich in SiO_2, Na_2O and Al_2O_3 and poor in FeO and MgO (thus not capable of forming jadeite-omphacite deposits upon precipitation). Reaction of these fluids with matrix peridotite/serpentinite produced chlorite-bearing rocks, which lowered the chemical potential of SiO_2 (which evolved towards subsaturation) and increased the amount of dissolved MgO and FeO (e.g. Sorensen et al., 2010), making possible the formation of

jadeite-omphacite veins. The whole rock major and trace element signatures that most closely reflect this fluid-ultramafic rock interaction can be related to those of jadeitites close to the contact (e.g. relict chromite in omphacitite, Harlow and Olds, 1987). Cr-rich pure jadeitite and omphacitite occurring as edges and latter Cr-rich veins indicate a strong fluid-ultramafic rock interaction in their formation. The depleted REE signatures of Cr-rich pure jadeitite and omphacitite with respect to N-MORB can be modified by later fluid-jadeitite interactions triggered by recurrent pulses of compositionally varied fluids (Figure 6.23a).

In a hot subduction scenario such as in the Sierra del Convento mélange pervasive fluid-rock interaction occurred in the subduction channe, asl indicated by metasomatic rocks such as zoisitite and talc-bearing rocks (e.g., Lázaro and García-Casco, 2008). Jadeitite veins surrounded by serpentinite/peridotite experienced the effects of focused fluid flow and fluid-ultramafic rock interaction at the blackwalls. The fluid-rock interaction during large fluid fluxes through a foliated serpentinitic matrix and relatively massive jadeitite is concentrated at the vein margins (e.g. Ague 2007). In these zones, foliated serpentinite host is metasomatically transformed into foliated chloritite blackwall. Microfractures by brittle deformation favor diffusive transport of some chemical elements that can be produced by intergranular fluids (e.g. Penniston-Dorland et al., 2010; Pogge von Strandmann et al., 2015). This process can also be important in jadeitite veins, where its permeability decreases within the crystallized vein. Recurrent deformation periods in the subduction channel favored the cataclastic processes in jadeitite veins, increasing their permeability by fractures and allowing the formation of new jadeitite and omphacitite veins. The deformation processes in jadeitite produce fluid-rock interactions that can drastically change their whole rock and trace element signatures.

The ternary diagram Cr-Ba-La(x10) has been used to discriminate the different signatures of fluid-jadeitite interaction (Figure 6.24). In this diagram, the Cr-rich samples, with signatures of strong fluid-ultramafic rock interaction, were used as a reference point to infer interactions with fluids with sedimentary signature. Fluids with a near-zero sedimentary component are represented by actinolitite and chloritite, close to the Cr appex. Only one sample of Ttn-Ap-rich chloritite plots at this apex of the diagram (Figure 6.24). The rest of Ttn-Ap-rich chloritite samples indicate a transition towards Ba-poor fluids enriched in La.

Fluids with two distinguishable sedimentary signatures, Ba-rich and Ba-poor/LREE-rich, were mixed with fluids differentiated from trondhjemite and pegmatite melts. These fluid-jadeitite interactions changed the signatures of jadeitites already formed by crystallization of minerals such as new jadeite-omphacite, epidote, apatite, rutile, allanite, zircon and titanite, evidencing REE mobility in intergranular fluids. Thus, pure jadeitite shows a group of samples with low Ba-rich fluids interaction, although many samples were affected to varied degree by Ba-rich fluids (Figure 6.24). Ep-rich jadeitite covers a broad field of mantle-sediment trends, but a large number of Ep-rich jadeitite and all samples of mica-rich jadeitite indicate strong influence of Ba-rich fluids (Figure

6.24). Ab-Ep rocks and omphacitites denote both trends with respect to Ba, but Ab-Ep rocks suffered a greater influence of Ba-rich fluids and metasomatic origin after jadeititic protoliths (Figure 6.24).

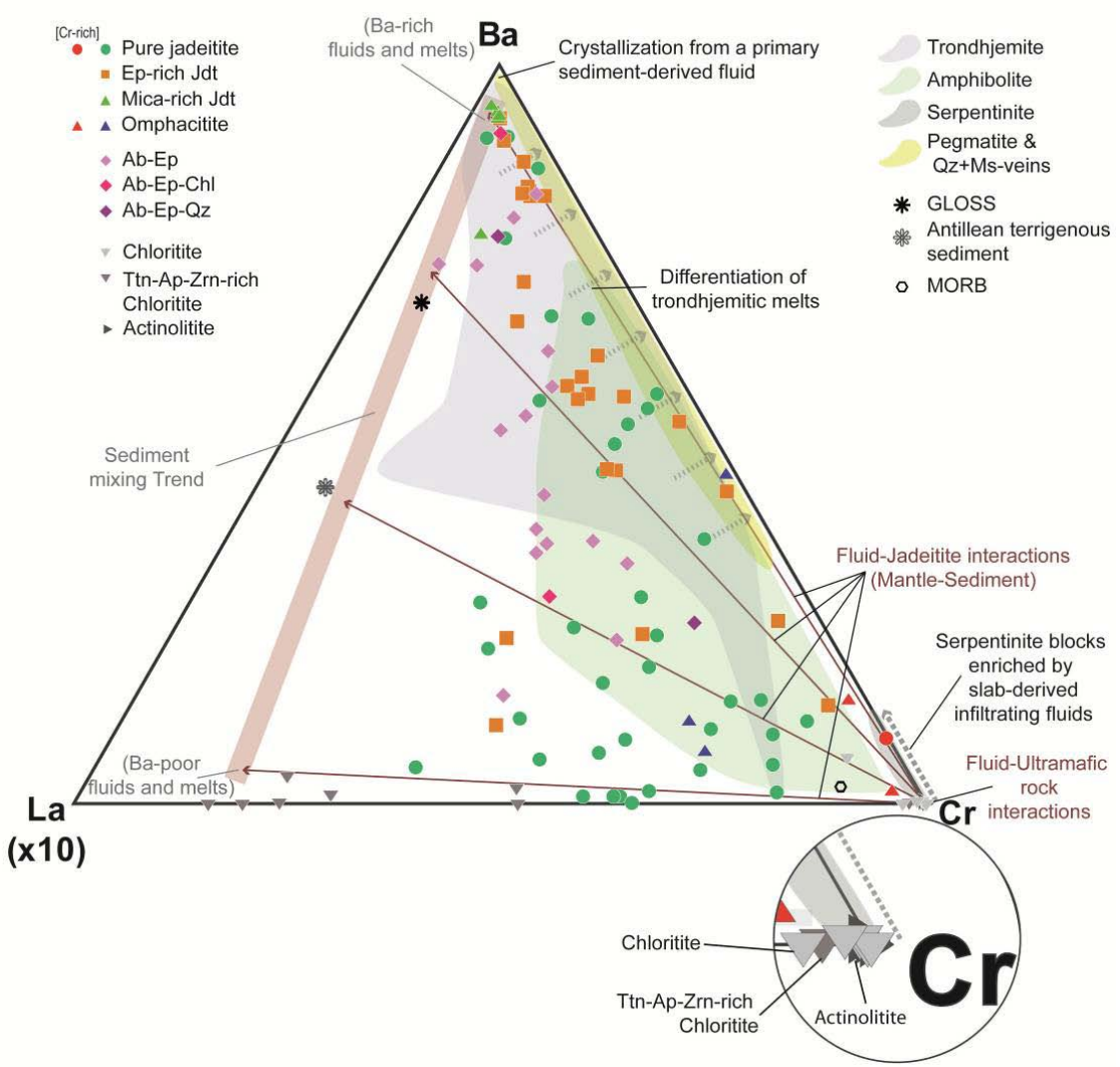

Figure 6.24. Cr-Ba-La$_{(x10)}$ ternary diagram of the studied samples, showing red arrows for different trends of fluid-jadeitite interactions, and a field for sediment mixing trend between Ba-poor fluids and Ba-rich fluids. Published data of trondhjemites, amphibolites, serpentinites and pegmatite+Qz+Ms-veins from Sierra del Convento and La Corea mélanges (Lázaro and García Casco 2008; Lázaro et al., 2011; Blanco-Quintero et al., 2011c, Cárdenas-Párraga et al., 2017) are also plotted for comparison. The gray and dashed arrows indicate the main processes defined by trondhjemites, amphibolites, serpentinites and pegmatite+Qz+Ms-veins from the Sierra del Convento and La Corea mélanges, including crystallization from a primary sediment-derived fluid. Also shown for comparison are the global subducting sediment (GLOSS) and Antillean terrigenous sediment from Plank and Langmuir (1998) and N-MORB from Sun and McDonough, (1989).

A detailed analysis by sample is necessary to compare and check the petrological characteristics with the defined geochemical tendencies and the mineralogy involved for each one.

Fluid-Jadeitite interaction

Pure jadeitite and mica-rich jadeitite

The different degrees of pure jadeitite interaction with Ba-poor and Ba-rich sedimentary fluids are represented by seven selected samples, MCB-3h, MCB-3f, CV-237b, SC-MJ-10, 08-SC-8a I, CV-237k, 09-SC-7l. Their whole-rock trace compositions have been highlighted in the Cr-Ba-$La_{(x10)}$ ternary diagram of Figures 6.25, 6.27 and 6.28, which also incude the corresponding trace element spidergrams normalized to N-MORB and textural images for each sample. Samples MCB-3h and MCB-3f represent compositions located at the end of the trend between PUM/N-MORB and Ba-poor sediment signature, denoting strong fluid-jadeitite interaction in the ternary diagram (Figure 6.25a, b). Both samples have characteristic trace element patterns enriched in LREE (specially La), Th, U and Zr, and slightly enriched in LILE, except Cs which is enriched by an order of magnitude with respect to N-MORB (Figure 6.25c). The petrographic characteristics of these samples include abundant intergranular crystallization of albite, which corrode jadeite crystals that frequently are appear replaced by omphacite (Figure 6.25a, b). Acicular omphacite crystals, epidote and, remarkably, a large amount of titanite and allanite crystallized in intergranular positions and voids (Figure 6.25a, b). In-situ LA-ICP-MS analyses were performed in sample MCB-3h in order to identify the minerals that host the trace element cargo described in the spidergrams (Figure 6.26). Normalized to N-MORB, all minerals are relatively enriched in Li and Cs, epidote and titanite are slightly enriched in Ba, but only allanite presents high Ba content (Figure 6.26). Allanite, titanite and zircon are enriched in REE, Th and U; notably allanite shows five orders of magnitude enrichment in La and Th with respect to N-MORB (Figure 6.26). Epidote and albite are slightly enriched in REE, Th and U, especially in Eu, and are depleted in Y with respect to N-MORB (Figure 6.26). Jadeite and omphacite show high variability of REE content, from enriched to depleted with respect to N-MORB, but Eu, Lu, Th and U are enriched in all analyses (Figure 6.26). Ni, Cr and Sc are depleted in all minerals, except in epidote and allanite compositions slightly enriched with respect to N-MORB (Figure 6.26).

These results suggest that the enrichment in REE, Th and U of pure jadeitite MCB-3h is due to a strong sediment-derived fluid-jadeitite interaction that triggered intergranular crystallization of allanite, titanite and zircon. A limited trend towards Ba-rich fluids in MCB-3h is justified by the contents of Ba of allanite and accessory black mica, not analyzed by LA-ICP-MS.

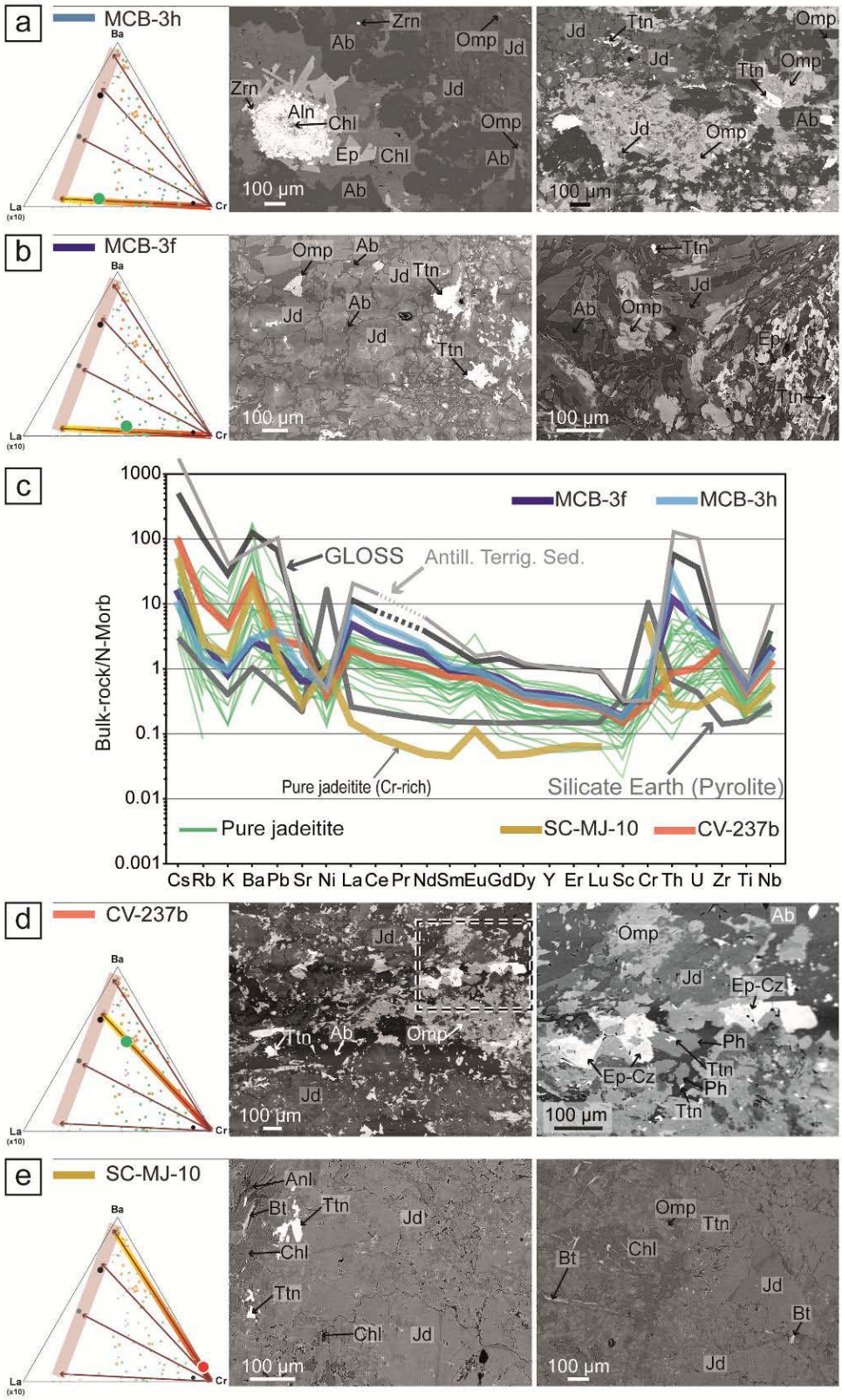

Figure 6.25. Selected samples of pure jadeitite (a) MCB-3h, (b) MCB-3f, (d) CV-237b and (e) SC-MJ-10 highlighted in the Cr-Ba-La$_{(x10)}$ ternary diagram, which includes a color degraded bar that indicates the intensity of the fluid-jadeitite interaction. Microtextural images were included to document the interactions between pure jadeitite and fluids (to see text for details). (c) Trace-element spidergram plots for pure jadeitite compositions normalized to N-MORB (Sun and McDonough, 1989, Ni, Cr and Sc from Klein, 2003), with selected samples highlighted. Reference rock patterns and order of chemical elements as in figure 6.14.

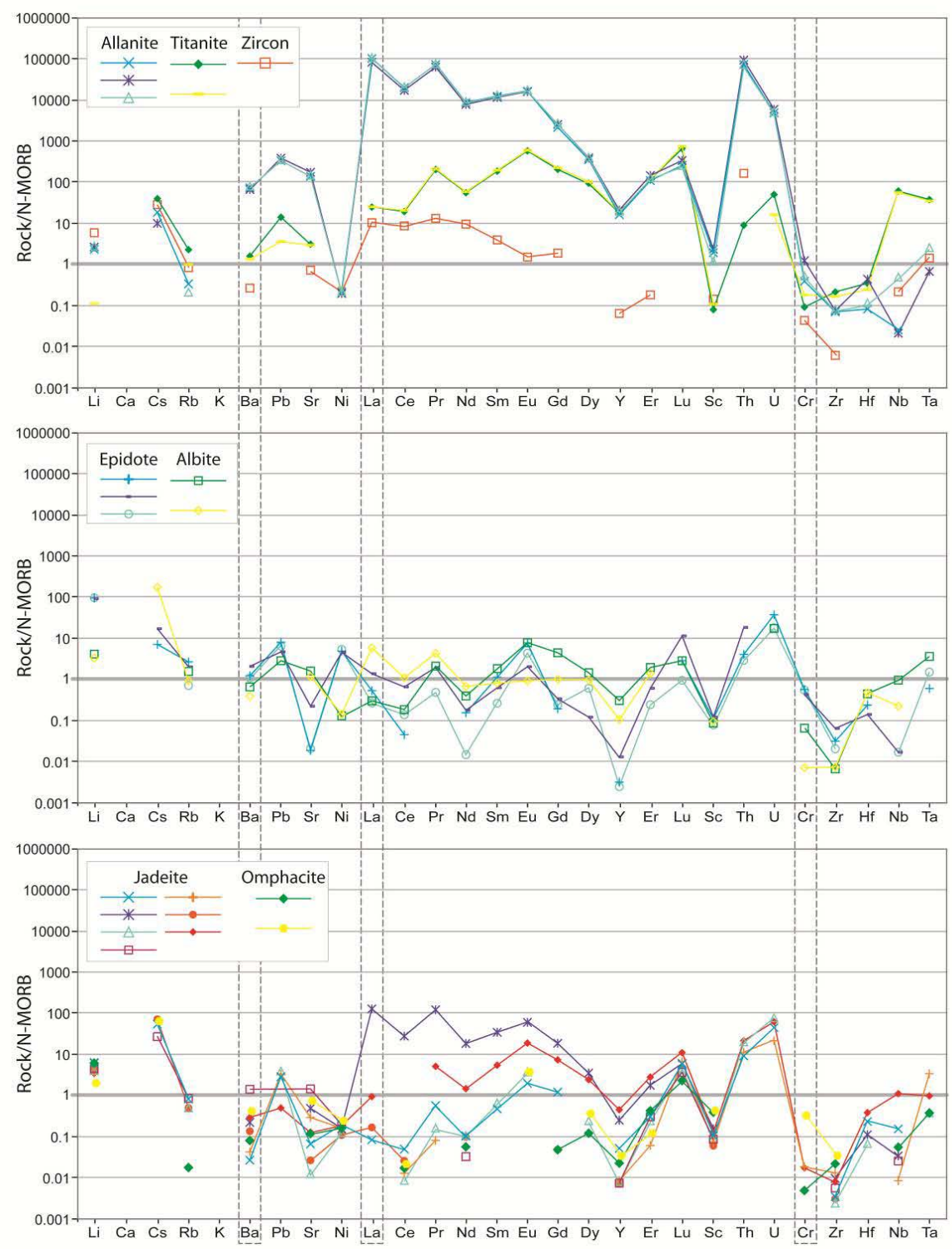

Figure 6.26. Trace element spidergrams for in situ LA-ICP-MS analyses of allanite, titanite, zircon, epidote, albite, jadeite and omphacite from pure jadeitite sample MCB-3h normalized to N-MORB (Sun and McDonough, 1989). Dashed rectangles indicate the key element used for ternary diagram of Cr-Ba-La$_{(x10)}$.

In contrast, the sample CV-237b indicates a moderate interaction with Ba-rich fluids. Its composition in the ternary diagram suggests a transition towards the richest compositions in Ba (Figure 6.26d). In the spidergrams this sample has LILE enriched compositions and is slightly depleted in REE and Th, U, except for slight enrichments in

La and Ce (Figure 6.26c). Petrographically this sample shows a strong crystallization of omphacite in voids, along with titanite, phengite and epidote. Albite occurs between jadeite grains and in voids (Figure 6.26d). The chemical signatures of this sample can be explained mainly by its content in titanite and the crystallization of phengite and epidote.

The jadeitite nodule SC-MJ-10 (part of a vein that crosscrut a jadeitite block) is classified as pure jadeitite with chromium-rich composition. The position in the ternary diagram is slightly above the Cr appex, indicating a limited contribution of Ba-rich fluids in the composition of this sample (Figure 6.26e). The corresponding spidergram show a pattern enriched in Cr and LILE (especially in Cs and Ba), in addition to depleted compositions in REE and HFSE with respect to N-MORB. Except for its LILE content, this sample has a trace element pattern close to aht of PUM (Figure 6.26c). In this sample jadeite crystals are massive, with minor omphacite replacement and intergranular analcime, titanite, biotite and chlorite (Figure 6.26e). The previously described characteristics suggest that these late veins record the REE content of pristine jadeititic fluids with minor fluid-jadeitite interaction.

Sample 09-SC-8a I is a pure jadeitite with moderate fluid-rock interaction, representing a transition to compositions more strongly influenced by Ba-poor fluids like samples MCB-3h and, MCB-3f (Figure 6.27a). The Cs, La, Ce Th, U and Zr contents of this sample are enriched by than an order of magnitude with respect to N-MORB, and the rest of the trace elements are depleted (Figure 6.27c). In this sample massive and zoned jadeite is corroded by Na-Si-rich fluids that triggered crystallization of albite omphacite and titanite in intergranular position (Figure 6.27a). Another transitional composition towards Ba-poor and LREE-rich fluids is represented in the ternary diagram by the sample CV-237k (Figure 6.27b). This sample mimics the trace element pattern of the sample 09-SC-8a I, but is slightly enriched in Ba with respect to N-MORB (Figure 6.27c). This sample has a preferred orientation of minerals, with omphacite-rich dark bands likely formed by fluid-rock interaction during deformation (Figure 6.27b). Omphacite-rich zones are developed by infiltration of albite rich fluids, crosscutting and replacing zoned jadeite crystals (Figure 6.27b).

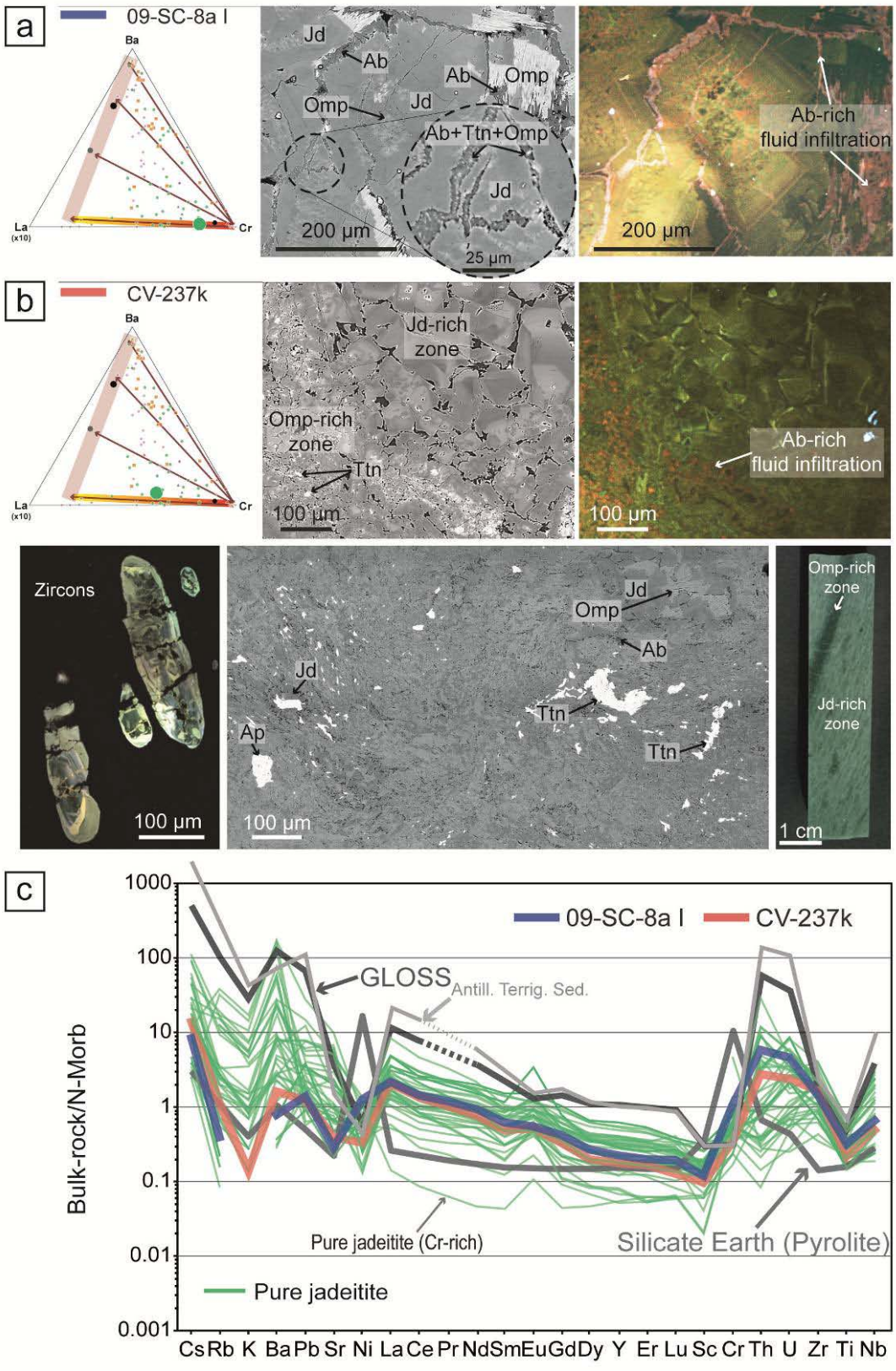

Figure 6.27. Selected samples of pure jadeitite (a) 09-SC-8a I and (b) CV-237k highlighted in the Cr-Ba-La$_{(x10)}$ ternary diagram, which includes a color degraded bar that indicates the intensity of the fluid-jadeitite interaction. (a) and (b) include SEM and CL images showing different degrees of fluid-jadeitite interaction. In (b) in-situ CL image of zoned zircons and a photograph of the sample on a hand scale were included. (c) Trace-element spidergram plots for pure jadeitite compositions normalized to N-MORB (Sun and McDonough, 1989, Ni, Cr and Sc from Klein, 2003), with selected samples highlighted. Reference rock patterns and order of chemical elements as in figure 6.14.

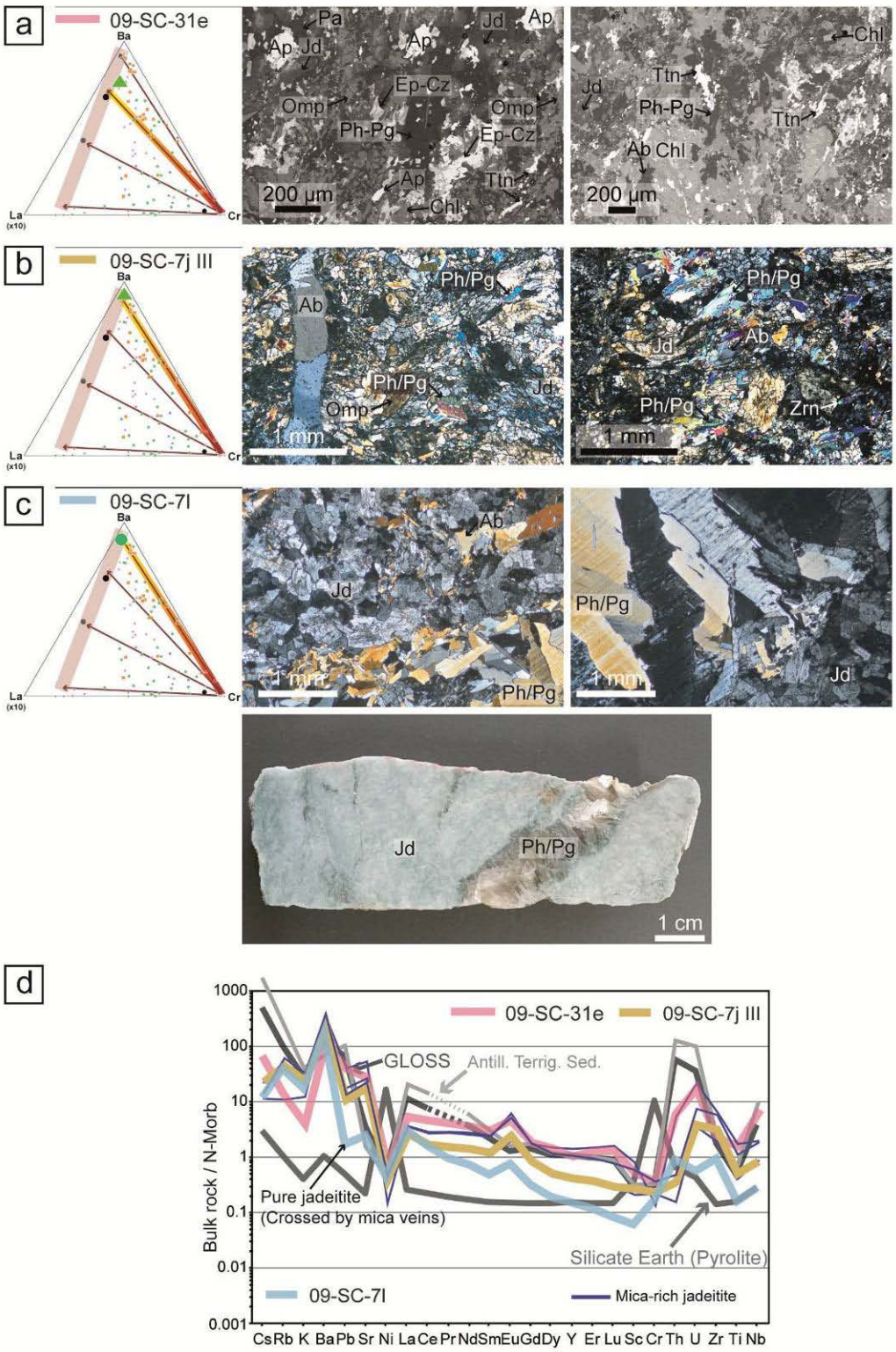

Figure 6.28. Selected samples of mica-rich jadeitite (a) 09-SC-31e, (b) 09-SC-7j III and pure jadeitite (c) 09-SC-7l highlighted in the Cr-Ba-La$_{(x10)}$ ternary diagram, which includes a color degraded bar that indicates the intensity of the fluid-jadeitite interaction. (a) and (b) include SEM and microscope images showing different degrees of fluid-jadeitite interaction. (c) microscope images of pure jadeitite crossed by mica veins, and a photograph of the hand scale sample. (d) Trace-element spidergram plots for mica-rich jadeitite and one sample of pure jadeitite compositions normalized to N-MORB (Sun and McDonough, 1989, Ni, Cr and Sc from Klein, 2003), with selected samples highlighted. Reference rock patterns and order of chemical elements as in figure 6.14.

Apatite, titanite and zircon are abundant accessory minerals crystallized in intergranular positions. In-situ CL images of zoned zircons show they were affected by deformation processes (Figure 6.27b).

Two samples of mica-rich jadeitites have been selected, 09-SC-31e and 09-SC-7j III, both representing a strong fluid-rock interaction with Ba-rich sedimentary fluids (Figure 6.28a, b). Sample 09-SC-31e represents the compositions more enriched in LREE from this group. This sample is also enriched in LILE and HFSE with respect to N-MORB (Figure 6.28d). The position in the ternary diagram indicates a strong component of Ba-rich fluid and a relatively less important LREE-rich fluid component during fluid-jadeitite interaction (Figure 6.28a). Petrographically this sample shows a strong replacement of jadeite by omphacite, associated with intense crystallization of apatite, titanite, epidote-clinozoisite, paragonite-phengite and chlorite (Figure 6.28a). Sample 09-SC-7j III has a composition strongly influenced by Ba-rich sedimentary fluids with a very low LREE-rich signature (Figure 6.28b). Thus, its trace element pattern normalized to N-MORB has enriched compositions in LILE, LREE, U and Zr, though less than enriched than sample 09-SC-31e, except for K and Rb (Figure 6.28d). The strong fluid-jadeitite interactions are indicated by albite veins, omphacite replacing jadeite and massive phengite-paragonite crystallization in intergranular position (Figure 6.28b).

On the other hand, one sample of pure jadeite 09-SC-7l represents the Ba-rich extreme in the trends of fluid-rock interaction of this group (Figure 6.28c). This sample has similar LILE content to previously described samples 09-SC-31e and 09-SC-7j III, but is depleted in REE and HFSE with respect to N-MORB, except for La and Ce (Figure 6.28d). In contrast to 09-SC-31e and 09-SC-7j III, sample 09-SC-7l is crosscut by phengite-paragonite veins, but micas in intergranular positions are scarce (Figure 6.28c; the whole-rock trace element analysis of this sample was performed excluding the crosscutting mica veins).

Epidote-rich jadeitite

Fluid-epidote-rich jadeitite interactions are represented by samples CV-237f, MCB-4a, MCB-1g and 09-SC-31j, as shown in figure 6.29. The composition of sample CV-237f plots close to the Cr apex of the ternary diagram, indicating a lower contribution of Ba-rich fluids of sedimentary signature (Figure 6.29a). In the spidergrams normalized to N-MORB this sample has enriched LILE compositions, except for K. In addition, it has an almost flat pattern from Ni to Cr and depleted HFSE with respect to N-MORB (Figure 6.29e). This trace element pattern suggests an N-MORB signature related to formation of trondhjemite by fluid-fluxed melting of amphibolite. Massive crystallization of jadeite and epidote/clinozoisite with accessory minerals such as mica, titanite and zircon also indicates a low fluid-epidote-rich jadeitite interaction (Figure 6.29a).

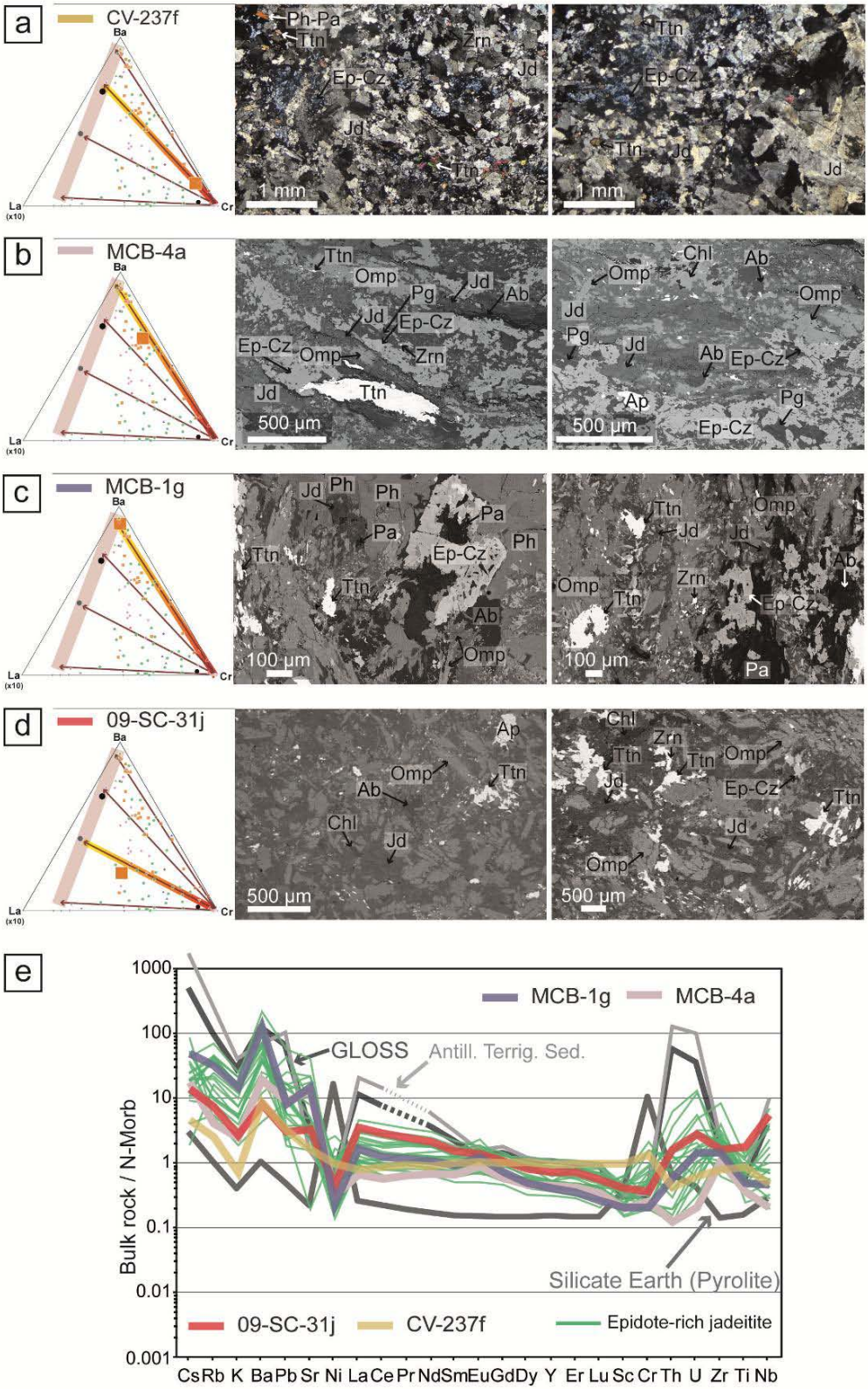

Figure 6.29. Selected samples of epidote-rich jadeitite (a) CV-237f, (b) MCB-4a, (c) MCB-1g and (d) 09-SC-31j highlighted in the Cr-Ba-La$_{(x10)}$ ternary diagram, which includes a color degraded bar that indicates the intensity of the fluid-jadeitite interaction. Microtextural images were included to document the interactions between epidote-rich jadeitite and fluids (to see text for details). (e) Trace-element spidergram plots for epidote-rich jadeitite compositions normalized to N-MORB (Sun and McDonough, 1989, Ni, Cr and Sc from Klein, 2003), with selected samples highlighted. Reference rock patterns and order of chemical elements as in figure 6.14.

Sample MCB-4a, on the other hand, plots in the ternary diagram in a transitional position within the trend towards greater interaction with Ba-rich sedimentary fluids (Figure 6.29b). This sample has LILE enriched composition and it is slightly depleted, by less than an order of magnitude, in Ni, REE, Cr and HFSE with respect to N-MORB, except for Eu and Zr (Figure 6.29e). Texturally, sample MCB-4a indicates this transitional composition by abundant omphacite replacing jadeite, as well as intergranular crystallization of epidote/clinozoisite, albite, paragonite, chlorite, titanite and apatite (Figure 6.29b). The greatest interaction between Ba-rich sedimentary fluids and epidote-rich jadeitite, relative to the trend described by the previous samples, is shown by sample MCB-1g (Figure 6.29c). The spidergram plot for this sample normalized to N-MORB shows enriched LILE compositions, with Ba over two orders of magnitude and slight enrichment in LREE, U and Zr, as well as depletion in HREE, Ni, Cr, Th, Ti and Nb (Figure 6.29e). Petrographically the high fluid-epidote-rich jadeitite interaction is indicated by abundant crystallization of phengite, paragonite epidote/clinozoisite, omphacite titanite and albite (Figure 6.29c).

In the ternary diagram, sample 09-SC-31j shows a composition that suggests intense interaction between epidote-rich jadeitite and relatively Ba-poor and LREE-rich sedimentary fluid(s) (Figure 6.29d). The trace element pattern is characterized by enriched LILE, LREE and HFSE and depleted HREE, Ni and Cr composition with respect to N-MORB (Figure 6.29e). This geochemical trend is texturally represented by abundant omphacite replacing jadeite and intergranular crystallization of abundant titanite, and minor albite, chlorite, epidote/clinozoisite, apatite and zircon (Figure 6.29d).

The different trends observed in the analyses performed for each group of jadeitite can be summarized as follow:

(1) Samples affected by a low interaction of sedimentary fluids with jadeitite show granoblastic massive jadeite, omphacite and epidote/clinozoisite with minor intergranular crystallization of accessory minerals. This mineralogy is associated with two types of geochemical patterns for different varieties of jadeitite. On the one hand, depleted REE, HFSE patterns normalized to N-MORB for pure jadeitite, with a strong mantle signature (Cr-rich) in some cases and, on the other hand, epidote-rich jadeitite relatively enriched in Ba with respect to N-MORB and REE patterns similar to N-MORB.

(2) Fluid-jadeitite interactions are divided according to the sedimentary contribution of fluids evolved from the subducting slab. Ba-rich sedimentary fluids are defined by the crystallization of K-bearing mineral species (phlogopite-biotite, phengite and, to a lesser extent, paragonite) and epidote group minerals (epidote/clinozoisite and allanite). Trace element patterns of samples showing interaction with Ba-rich fluid show enriched compositions mainly in LILE with respect to N-MORB. Ba-poor fluid-jadeitite interaction is characterized by low mica and epidote content and lower LILE compositions, suggesting a limited contribution from sediments. This interaction with Ba-poor sedimentary fluids is denoted by addition of REE and HFSE and crystallization

of jadeite and omphacite and intergranular accessory minerals such as epidote/clinozoisite, allanite, rutile, and titanite at relatively high-T conditions.

Fluid-Omphacitite interaction

Embrittlement and weakening of ultramafic material of the upper plate during serpentinization allow the formation of fractures that act as preferential pathways for fluids evolved in the subduction environment, including Al_2O_3-Na_2O-SiO_2-rich fluids that crystallize after reaction with the enclosing peridotite/serpentinite. The recurrent transport of these types of fluids reacting with jadeite in open veins is recorded by oscillatory zoning of jadeite blocky crystals and the formation of late veins of jadeite and omphacite (e.g., Harlow and Sorensen, 2005).

In the Sierra del Convento mélange, omphacitite occurs mainly at the edges of, and occasionally as veins within, jadeitite blocks. These omphacititic edges were sampled in contact with a chloritic blackwall in block 09-SC-7 (sample 09-SC-7h; Figure 4.4b). This position indicates that fluids involved in omphacitite formation have a significant ultramafic fluid signature and that omphacitite records fluid-ultramafic rock interactions. However, trace element signatures of omphacitite indicate later fluid-omphacitite interaction, as much as they show similar chemical trends described so far for jadeitites (Figure 6.30).

The compositions of the samples 09-SC-5(IV) and 09-SC-7b classified as Cr-rich omphacitite indicate low fluid-omphacitite interaction in the ternary diagrams (Figure 6.30a, b). Both samples are enriched in Ni, Cr and La, and depleted in HFSE and REE (except La) with respect to N-MORB and their HREE content trends to compositions defined by PUM (Figure 6.30e). Sample 09-SC-5(IV) has more depleted LILE contents than 09-SC-7b, with only K depleted with respect to N-MORB (Figure 6.30e). Conversely, sample 09-SC-7b has enriched LILE compositions, reaching a value of Ba enriched by about two orders of magnitude with respect to N-MORB (Figure 6.30e). Both samples are composed by massive Cr-rich omphacite (see SEM images of figure 6.4a, b), but they denote different sources of interacting fluids (Figure 6.30a, b). Sample 09-SC-5(IV), with a weak interaction with sedimentary Ba-poor and LREE-rich fluids show intergranular crystallization of albite and omphacite (Figure 6.30a). In contrast, sample 09-SC-7b, with a transitional composition influenced by Ba-rich sedimentary fluids, is composed of small veins of phengite and paragonite crystallized between omphacite grains (Figure 6.30b). The evolution in the previously described trend of omphacitite is indicated by the compositions of samples 09-SC-9i and 09-SC-7h in the ternary diagram (Figure 6.30c, d).

Ssample 09-SC-9i has a similar trace element pattern to that of sample 09-SC-7b, except for depleted LREE contents reaching PUM values (Figure 6.30e). Ba-rich fluids with sedimentary signatures are inferred by abundant crystallization of decussate phengite and paragonite surrounded by omphacite (Figure 6.30c).

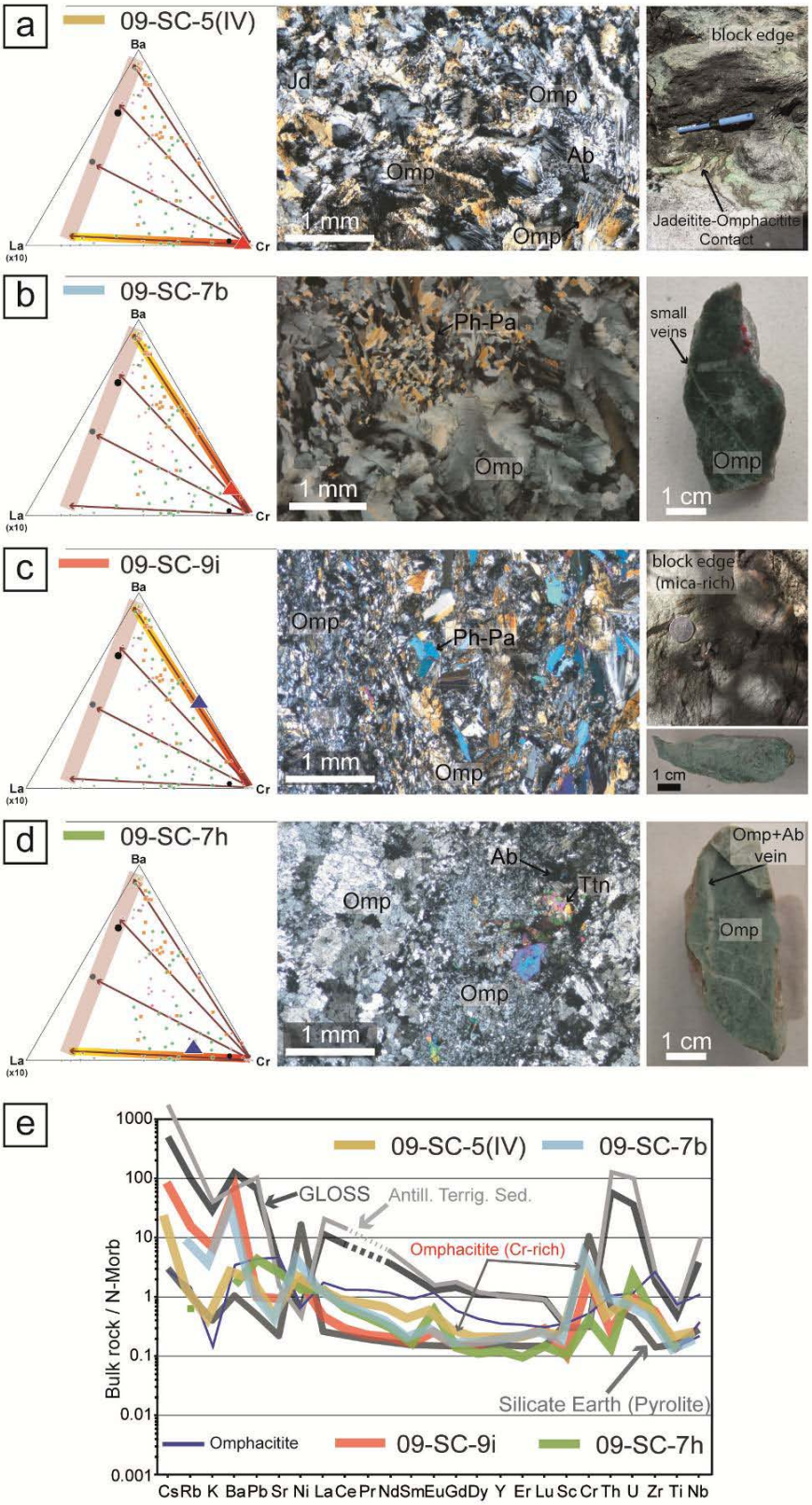

Figure 6.30. Selected samples of omphacitite (a) 09-SC-5(IV), (b) 09-SC-7b, (c) 09-SC-9i and (d) 09-SC-7h highlighted in the Cr-Ba-La$_{(x10)}$ ternary diagram, which includes a color degraded bar that indicates the intensity of the fluid-jadeitite interaction. Microscope and hand scale photographs of omphacitite were included to document the interactions between omphacitite and fluids (to see text for details). (e) Trace-element spidergram plots for omphacitite compositions normalized to N-MORB (Sun and McDonough, 1989, Ni, Cr and Sc from Klein, 2003), with selected samples highlighted. Reference rock patterns and order of chemical elements as in figure 6.14.

Sample 09-SC-7h shows stronger fluid-omphacitite interaction than 09-SC-5(IV), even if their trace element patterns are similar, as long as sample 09-SC-7h is enriched in Pb and U and slightly depleted in REE, Ni and Cr with respect to 09-SC-5(IV) (Figure 6.30d, e). Texturally, this sample is formed by massive omphacite crosscut by fine grained albite and omphacite veins with accessory minerals such as titanite (Figure 6.30d).

These geochemical, petrological and field observations indicate that omphacitites formed after fluids with an ultramafic signature that was modified by fluids with different sedimentary sources (Ba-rich and LREE-rich) similar to those that interacted with jadeitites. In all omphacitites, the whole-rock analyses were performed in selected zones, excluding distinguishable veins, but including small veins that could not be separated.

Fluid-Albite Rocks interaction

Four samples were selected to assess the interaction between fluids and albite-epidote and albite-epidote-chlorite rocks associated with the jadeitites from Sierra del Convento (see Chapter 4 and figure 6.31). Albite-epidote-quartz rocks were excluded from this analysis because this variety does not show significant geochemical differences relative to the rest of the rocks (Figure 6.31e). They are texturally characterized by the crystallization of small quartz veins with mica and, like albite-epidote rocks, represent insolated blocks close to, but no in contact with, jadeitite (see Figure 4.4i).

Two samples of Ab-Ep rock (MCB-1a and MCB1e) indicate interaction with sedimentary Ba-rich fluid in the ternary diagram (Figure 6.31a, b). Sample MCB 1a represents a transitional composition indicated by enriched LILE (especially Pb) and La contents and N-MORB concentrations for the rest LREE, and is depleted in HREE, Ni, Cr and HFSE except U and Zr with respect to N-MORB (Figure 6.31e). This sample is composed of a massive albitic matrix including heterogeneous aggregates of abundant crystals of epidote/clinozoisite and titanite, with occasional phengite and chlorite (Figure 6.31a). Sample MCB-1e shares petrographic and geochemical characteristics with the sample MCB-1a, but shows a more intense interaction with Ba-rich fluid (Figure 6.31b, e) is denoted by greater enrichments in LILE (except Pb), and enriched compositions in Zr with respect to sample MCB-1a (Figure 6.31e).

The Ab-Ep Chl-rich samples 09-SC-27b and 09-SC-8a VII are in contact with epidote-rich jadeitite and pure jadeitite respectively, occurring between jadeitite and the chloritite blackwall (Figure 4.4e, f, g, h, i and j). They represent the two trends described so far resulting from interaction with Ba-poor and Ba-rich fluids (Figure 6.31c, d). Sample 09-SC-27b plots close to the Ba appex in the ternary diagram, showing a composition richest in Rb, K and especially Ba in this group, with similar contents to GLOSS (Figure 6.31c, e).

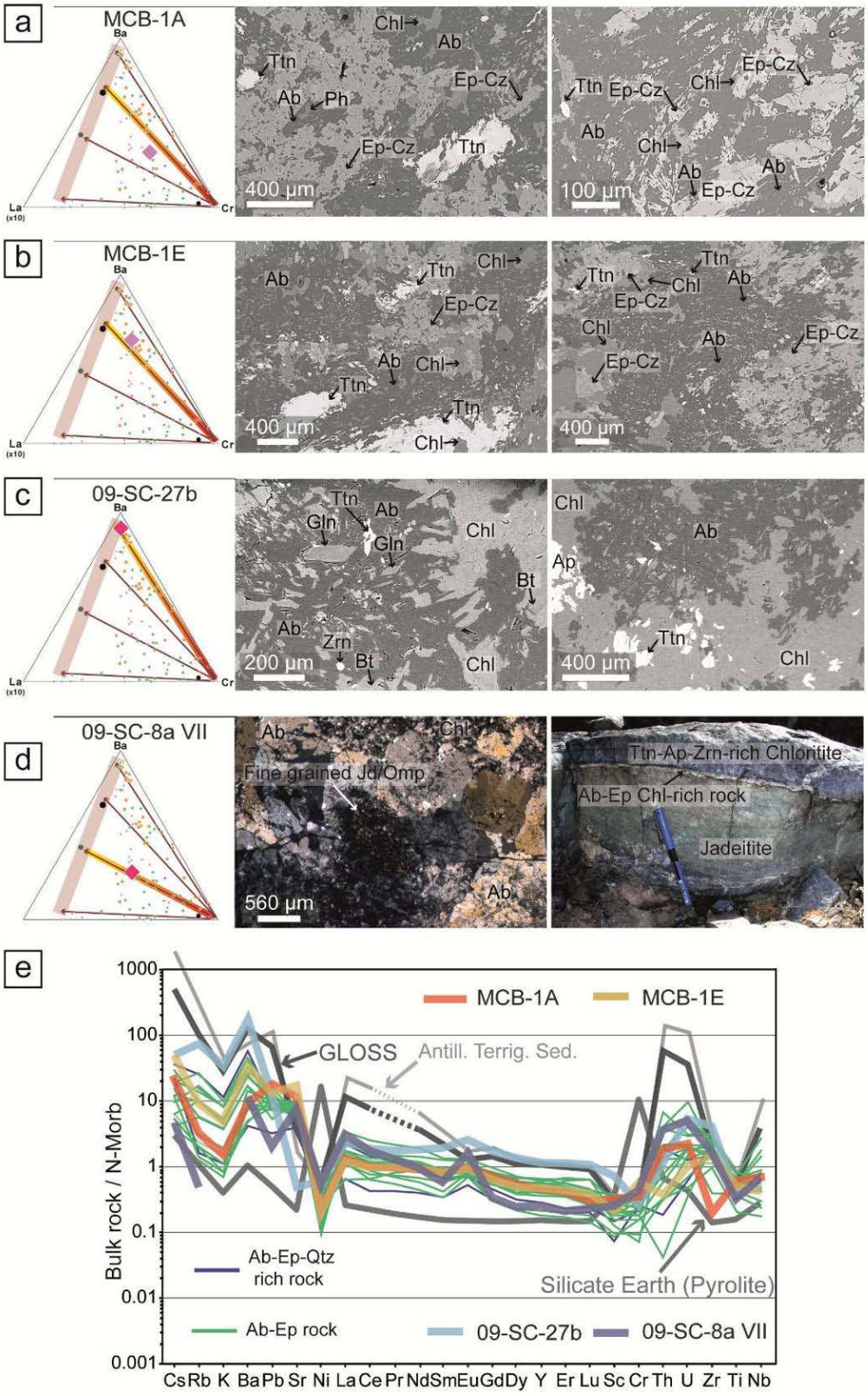

Figure 6.31. Selected samples of albite-epidote rocks (a) MCB-1a, (b) MCB-1e and (c) 09-SC-27b highlighted in the Cr-Ba-La$_{(x10)}$ ternary diagram, which includes a color degraded bar that indicates the intensity of the fluid-jadeitite interaction. Microtextural and field images were included to document the interactions between albite-epidote rich rocks and fluids (to see text for details). (d) Trace-element spidergram plots for albite-epidote rocks compositions normalized to N-MORB (Sun and McDonough, 1989, Ni, Cr and Sc from Klein, 2003), with selected samples highlighted. Reference rock patterns and order of chemical elements as in figure 6.14.

In this sample Sr, Ni, Sc, Cr, Ti and Nb are depleted with respect to N-MORB, while LREE, U and Zr are enriched and HREE and Th show similar values to N-MORB and GLOSS (Figure 6.31e). The textural characteristics of 09-SC-27b include abundant albite and chlorite, with titanite, glaucophane, zircon, apatite, biotite and phengite included (Figures 6.4e and 6.31c). Furthermore, the composition of sample 09-SC-8a VII indicates a lower interaction with Ba-rich fluids than 09-SC-27b in the ternary diagram (Figure 6.31d). The contents of Ba and Sr in sample 09-SC-8a VII are enriched by an order of magnitude with respect to N-MORB (Figure 6.31e). In the N-MORB normalized spidergram this sample is also characterized by enrichment in La, Ce and HFSE, except Ti and Nb, and by depleted HREE contents close to PUM (Figure 6.31e). The small band (1 cm of thickness; Figure 4.4j) of Ab-Ep Chl-rich rock that represents sample 09-SC-8a VII is formed by albite crystals which corrode the pure jadeitite zone, showing relictic fine-grained jadeite and omphacite (Figures 6.4f and 6.31d), and inclusions of titanite, apatite, zircon and chlorite (Figures 6.4f).

It is important to note that, in contrast to sample 09-SC-8a VII, sample 09-SC-27b represents a large band 10-20 cm in thickness (Figure 4.4g). Both Ab-Ep Chl-rich samples suggest replacement of jadeite by albite induced by the addition of externally-derived fluids that percolate through chloritic zone. Thus, the different thickness of each band may be related to the time of interaction with external fluids, suggesting that Ep-rich jadeitite in these studied blocks experienced greater interaction with fluids than pure jadeitite. The same replacement process, involving a jadeititic protolith, may be related to the formation of albite-epidote (-quartz) rocks, as indicated by the presence of relictic jadeite, omphacite and secondary actinolite-magnesiohornblende in some samples (Figures 6.4c, d; 6.7 and 6.12). Both groups occur as isolated blocks and are not in contact with jadeitite, so a direct crystallization, like P-type jadeitites, from fluids can not be ruled out for some samples.

Fluid-Chloritite interaction

At the interface of jadeitite blocks, the development of chloritite blackwalls represents the product of fluid-ultramafic rock interaction, a process that allow fixing of chemical components from hydrous fluids in host ultramafic rocks. This is a common process in subduction zones settings (Bebout and Barton, 2002; Marschall and Schumacher, 2012), where pervasive fluid-rick interaction is enhanced at the margins of blocks and fractures (Ague, 2007). Three samples of chloritite (09-SC-7g, 09-SC-7j-V and 09-SC-27i) were selected to characterize fluid-ultramafic rock interaction and its effects on jadeitite blocks (Figure 6.32).

The samples classified as chloritite show a geochemical signature clearly related to fluids rich in ultramafic components (i.e., enriched in Cr and Ni), producing compositions ranging from depleted harzburgite-like to PUM-like (Figure 6.32d). In the Cr-Ba-$La_{(x10)}$ ternary diagram the depleted compositions are plotted in the Cr apex, but some samples indicate interactions with fluids of sedimentary signature (Figures 6.24 and 6.32d). Sample 09-SC-7g, which plots in the Cr apex, is a massive chloritite occurring in contact with omphacitite (Figure 6.32a). Its trace element pattern is

depleted, reaching REE values of three orders of magnitude lower than N-MORB, except for Ni and Cr, with enriched compositions similar to PUM (Figure 6.32d). Sample 09-SC-7g, like other samples from the chloritite group, is a monomineralic rock, suggesting an entry of Cr and Ni into chlorite solid solution as ripidolite–brunsvigite variety (e.g. Randive et al., 2015), and/or other not-identified accessory minerals that may host these elements (Figure 6.32a, d).

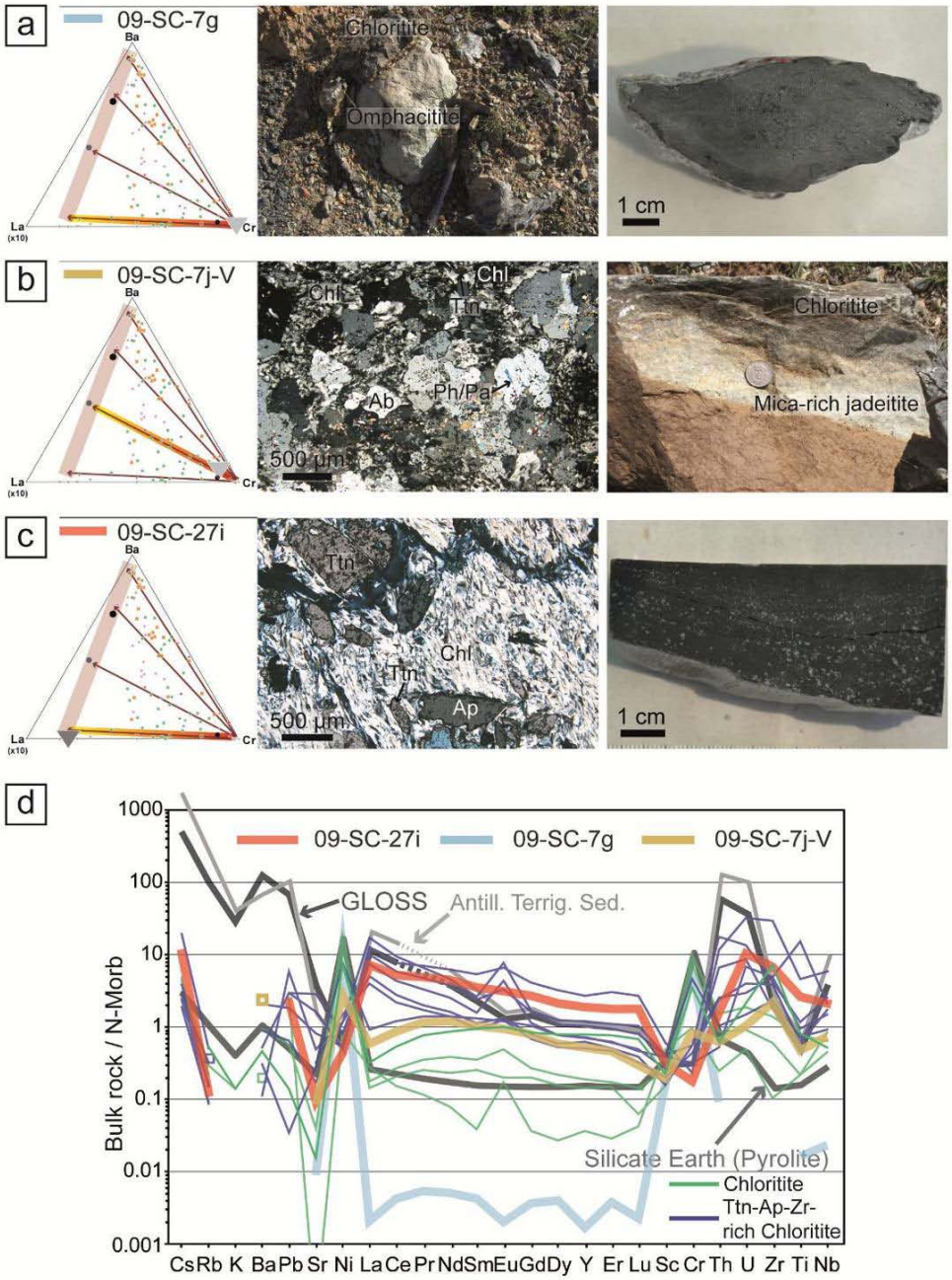

Figure 6.32. Selected samples of chloritite (a) 09-SC-7g, (b) 09-SC-7j-V and titanite-apatite-zircon-rich chloritite (c) 09-SC-27i highlighted in the Cr-Ba-La$_{(x10)}$ ternary diagram, which includes a color degraded bar that indicates the intensity of the fluid-chloritite interaction. Microscope, visu and field photographs are shown to document the interactions between chloritite blackwall and fluids (see text for details). (d) Trace-element spidergram plots for chloritite blackwall compositions normalized to N-MORB (Sun and McDonough, 1989, Ni, Cr and Sc from Klein, 2003), with selected samples highlighted. Reference rock patterns and order of chemical elements as in figure 6.14.

Sample 09-SC-7j-V indicates a slight influence of Ba-rich sedimentary fluids in the ternary diagram. It is a chloritite with a diffuse contact towards mica-rich jadeitite, with chlorite including titanite and surrounding phengite-paragonite grains within albite crystals (Figure 6.32b). The trace element pattern normalized to N-MORB of this sample is enriched in Ba, Ni and Zr, and depleted in Sr and HREE, with similar composition to N-MORB in terms of LREE, Cr, Th, U, Ti and Nb (Figure 6.32d). This sample and other samples of the chloritite group denote a chemical transition marked by the influence of fluids with sedimentary components (Figure 6.32d).

This chemical transition evolves towards the compositions defined by titanite-apatite-zircon-rich chloritite. For example, sample 09-SC-27i plots close to the $La_{(x10)}$ apex in the ternary diagram (Figure 6.32c), and the trace element pattern of this sample is enriched in Cs, Pb, REE and HFSE and depleted in Sr, Ni, Sc and Cr with respect to N-MORB (Figure 6.32d). Petrographically, sample 09-SC-27i is composed of massive chlorite including crystalline aggregates of titanite and/or apatite up to 1 millimeter in size (Figure 6.32c), as well as dispersed zircon crystals. The more depleted compositions in Ni and Cr of titanite-apatite-zircon-rich chloritite suggest that these elements were remobilized by pervasive fluids, and perhaps be be incorporated into adjacent jadeitite and omphacitite.

6.6.4 Formation model

As described, Cuban jadeitites are formed in a subduction context associated with other rocks typically formed in this context. They crystallized in veins within serpentinitite/peridotite (Figure 6.33), likely in the subduction channel. Fluids emanating from the various lithologies of the slab and fluxing towards the slab-mantle interface reache "hybrid" signatures after mixing with other primary fluids and fluids with modified composition after fluid-rock interaction (e.g., Bebout and Barton, 2002; King et al., 2006, 2007; Spandler et al., 2008 and Marschall and Schumacher 2012; figure 6.33). In the Sierra del Convento mélange, partial melting of amphibolites during a hot subduction event (ca. 113 Ma) at a high temperature (700-750 °C) and high pressure (15 kbar; García-Casco 2008a; Lázaro et al., 2009) was assisted by fluid flow towards amphibolite. The process produced pristine slab melts that did not react with the upper plate mantle, allowing the crystallization of rocks from trondhjemitic melts emplaced, mostly, in parent amphibolite (García-Casco 2008a; Lázaro et al., 2009; figure 6.33). The fluids that interacted in the partial melting processes have different sources, juvenile and sedimentary, as documented by the formation of Ms-amphibolite and Ms-trondhjemite and the subsequent crystallization of evolved pegmatite and Qz+Ms-veins after differentiation of trondhjemitic melts and crystallization from a primary sediment-derived fluid, respectively (Lázaro et al., 2011; Blanco-Quintero et al., 2011c). Therefore, these pegmatite-forming fluids generated by differentiation of trondhjemitic melts, and the fluids involved in the partial melting of amphibolites, have chemical compositions suitable for the formation of pure jadeitite and epidote rich jadeitite, respectively, as discussed previously in the section 6.6.3 (see also García-Casco et al., 2009; Cárdenas-Párraga et al., 2012).

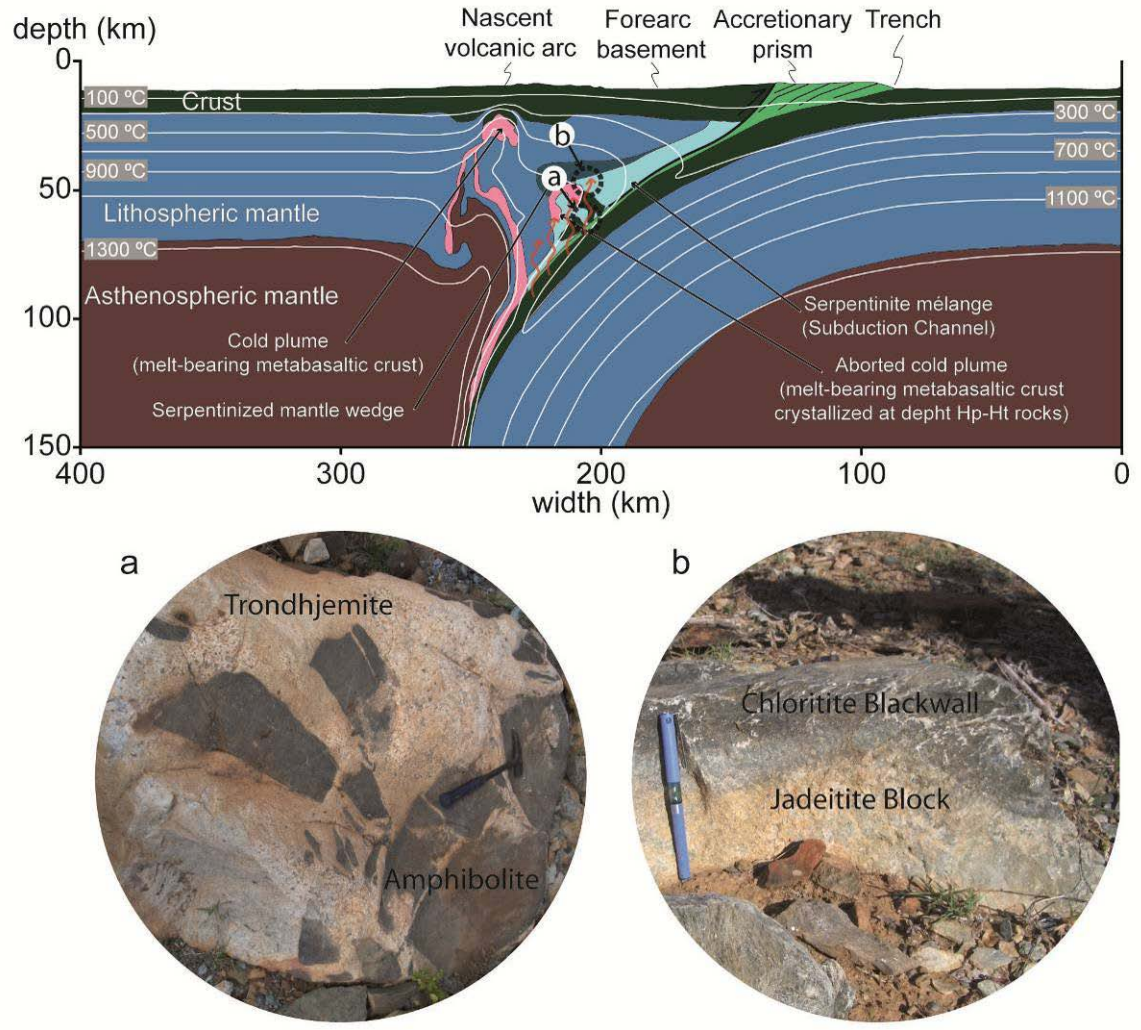

Figure 6.33. Thermo-mechanical model of oceanic subduction including the main components in the subduction zones. This model is modified from numerical thermal-chemical experiments of ocean–ocean subduction initiation of young oceanic lithosphere (age 10 million years; initial convergence rate 4 cm/year) after of Blanco-Quintero et al., (2011b). The model was drawn selecting an analogue scenario of hot subduction and the development of aborted cold plumes (subducted melt bearing metabasaltic crust crystallized at ca. 50 km depth – ca. 15 kbar – 10.9 million years after the onset of subduction), with partially melted subducted MOR basaltic amphibolites as in the Sierra del Convento and La Corea mélanges. The dotted circles indicate the formation context for: (a) amphibolite and trondhjemite and (b) jadeitite block and chloritite blackwall. The general fluid flow direction is shown by red arrows. See text for details.

In the Sierra del Convento mélange, the crystallization of jadeite-forming fluids in open fractures of serpentinite/peridotite is indicated by the presence of abundant chloritite blackwall, generally foliated, that surround jadeitite blocks, along with Cr-rich compositions in omphacitite and pure jadeitite that form at the edges of, and/or veins within, the blocks. Field relations indicate that jadeitite blocks are found only in association with the serpentinitic matrix of the mélange. They have never been observed in in fractures, veins or bodies within metabasites and throndhjemitc bodies. Thus, a crystallization of P_s-type jadeite-forming fluids at the subduction channel and/or the mantle wedge is suggested. These rocks are derived from abyssal mantle rocks formed at an oceanic fracture zone tha was emplaced at the mantle wedge and

latter dragged down (subduction erosion?) at the upper plate mantle-slab interface (Blanco-Quintero et al., 2011d; Cárdenas-Párraga et al., 2017). Thus, the context for jadeitite formation at this boundary may involve shear zones that create permeability regions after deformation and, hence, allow channelized fluid flow and strong fluid-rock interaction. This is inferred to occurr at the contact with massive ultramafic fragments from the mantle wedge affected by (micro)fractures, allowing latter strong fluid-rock interaction along grain boundaries by pervasive fluids fluxing the jadeitite blocks (see discussion of Konrad-Schmolke et al., 2011 and references therein).

A formation model is illustrated in figure 6.34a, including the formation of open fractures according to the presence of actinolitite veins that cut blocks of serpentinite/serpentinized peridotite (Figure 4.4k). These fractures are justified as follows: (1) brittle deformation in subduction environments has been described by Hermann et al., (2000), John et al., (2004), Healy et al., (2009), Angiboust et al., 2011, 2012, 2014 and Menant et al. (2018) based on field observations of brittle features in exhumed rocks from subducted slabs, (2) hydraulic fracturing is considered an important mechanism acting during hydrous metasomatism of mantle wedge xenoliths (Schneider and Eggler, 1986; Wilshire and Kirby, 1989; McInnes et al., 2001; Soustelle et al., 2010), (3) hydrofracturing processes have been described in high-pressure rocks (Toriumi and Hara, 1995; Pennacchioni, 1996; Cesare et al., 2001, Padrón-Navarta et al., 2010) and have been related to intermediate seismicity (Lund and Austrheim, 2003; Andersen et al., 2008; Angiboust and Agard, 2010), hydrofracturing is also a common process in ultra-high-pressure rocks (Vrijmoed et al., 2006, 2008; Malaspina et al., 2009), (4) brittle deformation and hydrofracturing have been studied by means of dehydration experiments and numerical models and have been related to seismicity in subduction zones (Miller et al., 2003; Tenthorey and Cox, 2003; Perrillat et al., 2005; Furukawa, 2009). Furthermore, this is in agreement with cataclasis processes identified in jadeitite sample CV-237-K (Figure 6.27b; García-Casco et al., 2009).

The formation model of figure 6.34a includes temporal indications labeled as t_0-t_1-t_2, which cover ages in the range between 114 Ma and 107 Ma and emphasize a complex evolution of processes of formation and metasomatic interactions. The formation processes for Cuban P-type jadeitite outlined in this figure can not be constrained with more temporal precision. This is due to the errors associated with zircon U-Pb geochronology coupled with the short time interval of dated zircons of the studied samples (around 7 Ma, figure 6.19). Taking this into account, a second evolutionary step in the model of the figure 6.34b involves crystallization of epidote-rich jadeitite in open veins, at about 113 Ma, when high temperature (around 700 ºC) is recorded in rocks accreted to the slab-mantle interface (Figure 6.21). In general, epidote-rich jadeitite samples have compositions strongly affected by interaction with fluids; samples with mild interaction with fluids are scarce and show N-MORB signatures (Figures 6.24 and 6.29). These signatures and the oldest ages suggest that the first crystallization of jadeitite in veins (Figure 6.34b) involved fluids characterized by a strong genetic relation to hydrous amphibolite (Figures 6.16; 6.19; 6.21; 6.23 and

6.29). Chloritite blackwall and/or omphacitite (Cr-rich) were also formed at this time (Figure 6.34b), in contact with serpentinite/peridotite and partially surrounding the epidote-rich jadeitite vein. The composition of these rocks denotes a strong fluid-ultramafic rock interaction (Figures 6.24; 6.30; 6.32). This interaction of fluids with ultramafic rocks occurs in a context of active serpentinization, where the breakdown of phases such as chromian spinel, pyroxene and olivine in peridotite releases Cr, Mg, Ca and Ni to fluids, as indicate the presence of omphacitite and Cr-omphacite (e.g. Harlow et al., 2015). The significant thickness of some of the chloritite blackwall sampled in the Sierra del Convento mélange suggests that epidote-rich jadeitite veins formed in a releatively high permeability scenario (Figure 4.4). The fluid flow is, however, concentrated at the margins of blocks (chloritite blackwall) where highly foliated and sheared serpentinite/peridotite develops (Ague, 2007). Subduction driven deformation induces the formation of new open fractures in serpentinite/peridotite and in the fracturing of the already formed epidote-rich jadeitite veins (Figure 6.34b). This process increases the permeability of epidote-rich jadeitite veins by microfractures and late veins, the latter with varied mineralogy (Figures 4.5c and 6.34b).

The fluid that interacts with the chloritite blackwalls pervasively migrated into the veins, which is mainly controlled by the development of microfractures a response to the internal strain distributed among and around mineral grains (Figure 6.34b). External and episodic pervasive fluid migration generates the modification of trace element patterns of vein rocks by interaction with fluids of sedimentary signature, as has been shown for all groups of jadeitite and associated rocks (Figures 6.16; 6.24; 6.25; 6.26; 6.27; 6.28; 6.29; 6.30 and 6.31). The process described so far also explains the formation of mica-rich jadeitite and Ab-Ep Chl-rich rock bands between chloritite and jadeitite (Figures 4.4e, g, i and j). These bands are characterized by albite crystals that corrode jadeitite, while larger patchtes of this rocks show relictic jadeite and omphacite that document a late metasomatic origin of these rocks (Figure 6.31d). The large thickness of a band of Ab-Ep Chl-rich rock sampled in contact with epidote-rich jadeitite (Figure 6.4e, g) denote the growth of this band after its exposure to pervasive fluid migration, which is dependent on the increase in permeability generated by deformation as previously described.

Mica-rich jadeitite shows strong mineralogical and geochemical evidences for interaction with Ba-rich sedimentary fluids (Figure 28a, b), suggesting a formation context related to the development of late veins (Figures 6.28a, b and 6.34b). Thus, in figure 6.34c, the temporal evolution of the epidote-rich jadeitite vein is characterized by an increase in the thickness of the Ab-Ep Chl-rich rock bands and the development of omphacitite and mica-rich jadeitite. Locally, where the vein is narrowest, Ab-Ep Chl-rich rock bands can form Ab-Ep rocks by metasomatic replacement of epidote-rich jadeititic protolith (Figure 6.34c). As noted above, the Ab-Ep rocks are characterized by the local preservation of jadeite and omphacite relicts (Figure 6.4c, d) with similar composition to piroxenes from jadeitites (Figures 6.5 and 6.7). This type of rock can be mechanically separated from Ep-rich jadeitite veins due to the development of new

fractures generated in a different stress scenario, which may produce the slicing and rotation of veins (Figure 6.34c). The new fractures are an appropriate context for the direct crystallization of Ab-Ep (-quartz) rocks from fluids saturated in albite.

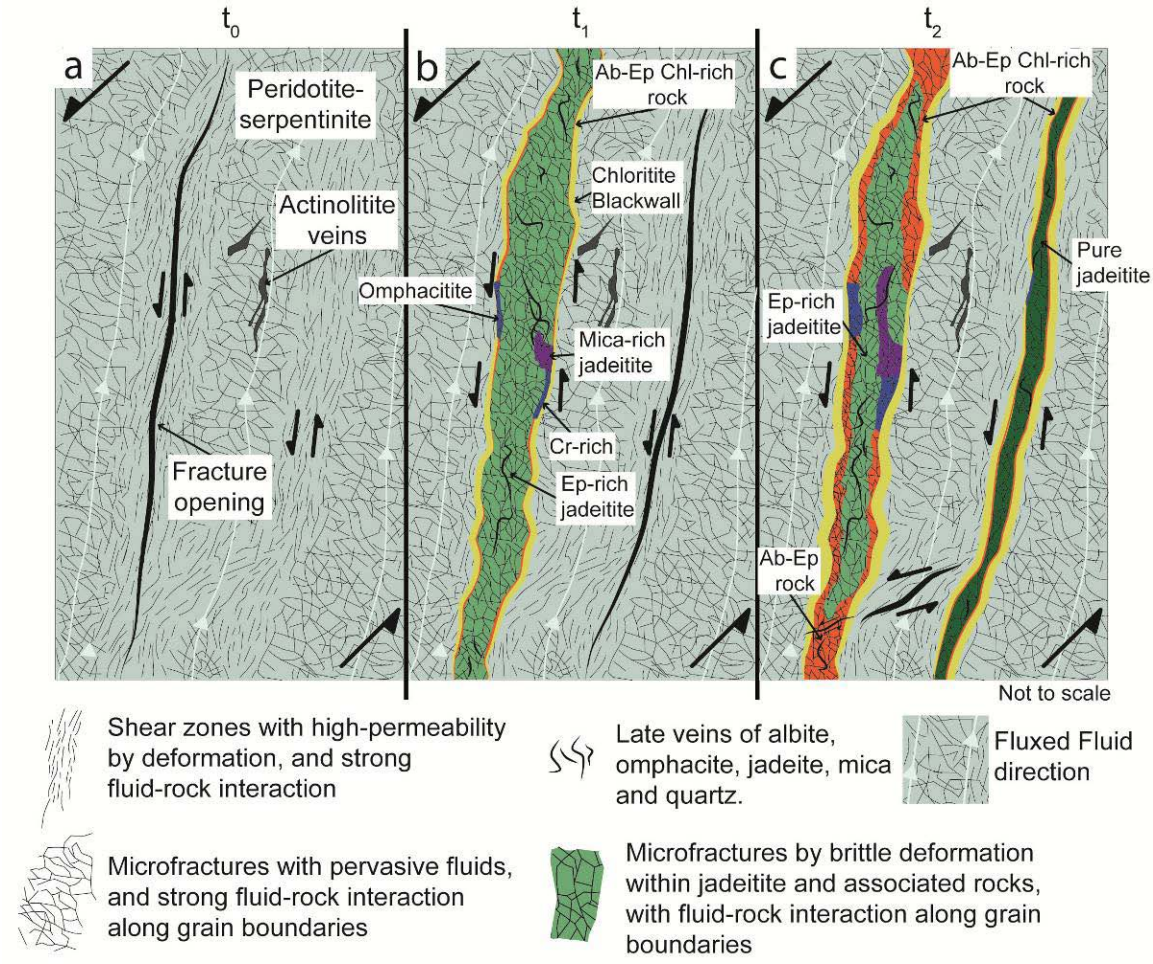

Figure 6.34. Schematic illustration of P-type jadeitite formation and its evolution with time: (a) Serpentinitic/peridotitic matrix with shear zones where a fracture is opening and formation of actinolitite veins (t_0). (b) Crystallization of Ep-rich jadeitite in venins and associated chloritite blackwall and omphacitites edges (locally Cr-rich). Ab-Ep Chl-rich rock may start formation at this stage. At time t_1, Ep-rich jadeitite undergoes brittle deformation and fluid-jadeitite interaction due to increased permeability. Also, new fractures open. (c) Enhanced fluid-Ep-rich jadeitite interaction by deformation and formation of late veins (> permeability), with generalized formation of Ab-Ep rock and mica rich jadeitite after the replacement of Ep-rich jadeitite. At t_2, crystallization of pure jadeitite occurs in fractures, increasing its permeability with time in a maner similar to Ep-rich jadeitite. Also at this time, Ab-Ep rocks are mechanically separated from veins by fractures; these fractures can also be filled by Ab-Ep rocks crystallized directly from albite-saturared fluids (produced after jadeitite-fluid interactions).

For a single block of epidote-rich jadeitite the hydrothermal zircon crystallization dates very similar ages for the formation chloritite blackwall that surround the block and, perhaps of associated Ab-Ep Chl-rich rock (around 113 Ma; Figure 6.18). This indicates that all previously described processes in epidote-rich jadeitite occurred in a short time span of about 1.5 Ma (Figure 6.18). With the limited geochronological data presented in this Thesis, and taking into account the age of 113.2 Ma of a chloritite

blackwall in contact with pure jadeitite, it is not possible to establish whether the crystallization of pure jadeitite was coetaneous with epidote-rich jadeitite, as described above in reference to the model of the figure 6.34. Hydrothermal zircon crystallization from pure jadeitites is dated in 107–108 Ma (Figure 6.17) and hence is represented in the model of figure 6.34c as a distinct late stage of evolution. The least altered compositions of pure jadeitite show depleted REE patterns with respect to N-MORB that correlate throndhjemitic rocks, suggesting that related fluids evolved from differentiation of trondhjemitic melts at temperatures below ca. 625 ºC (Figures 6.20 and 6.21). Fluid-pure jadeitite interaction took place by similar processes to those described for epidote-rich jadeitite (Figure 6.34c). Their interaction with sedimentary fluids is mainly characterized by addition of LREE, HFSE and LILE (Figures 6.25; 6.26; 6.27 and 6.28). Thus, jadeitite rocks were affected by episodic fluids infiltrations that incorporate REE to jadeite-omphacite pyroxenes and/or by intergranular crystallization of accessory mineral like titanite, allanite or apatite (Figures 6.25; 6.27 and 6.28).

In general, the similar SHRIMP $^{206}Pb/^{238}U$ ages of jadeitite (107-114 Ma) and slab-derived hydrous trondhjemitic magmatic rocks (SHRIMP U-Pb ages 105-113Ma; García-Casco 2008a; Lázaro et al., 2009) corroborate our model for the jadeitite formation after fluid-fluxed partial melting of amphibolite and trondhjemite crystallization (Figure 6.19). These data are hard to conciliate with a metasomatic replacement model for jadeitite formation (R-type, Tsujimori and Harlow, 2012) after igneous protholiths. In this model, a potential trondhjemite body crystallized within amphibolite would have been metasomatically transformed by fluids to produce the jadeitite, as proposed for other localities (Compagnoni et al., 2012; Shigeno et al., 2012). However, field relations of jadeitite in the Sierra del Convento mélange do not show a relationship between jadeitite and amphibolitite. In addition, it can be ruled out that the fluids generated after of the cristallization of trondhjemitic melts, in equilibrium with these rocks, can trigger metasomatic replacement reactions in parent trondhjemites.

The previously described processes of crystallization and alteration by fluids of jadeitite veins and related rocks clearly illustrate the mobility of elements in the subduction context. The observed mobility of elements in jadeitites and related rocks may be taken as a proxy of element mobility at higher temperature and pressure. The addition of elements such as La, Cr and Ba to jadeitite and related rocks, and the illustrated mobility of LILE, REE, HFSE, can be extrapolated, to some extent, to processes occurring at much deeper depths appropriate for the generation of arc magmas. In this regard, Castro et al. (2010) and Marschall and Schumacher (2012) have argued that devolatilization and partial melting of metasomatic mélange rocks in the mantle wedge have a strong influence in the geochemical signature of volcanic arc magmas. Perhaps, re-subduction and dehydration of these types of rock may also explain certain characteristics of arc magmas.

6.6.5 Comparison with other Caribbean Jadeitite occurrences

The final section of this thesis is dedicated to check whether processes involved in the Cuban jadeitite formation may have had an influence in other jadeitite occurrences in the Caribbean.

Figure 6.35 shows a comparison of the REE whole-rock compositions normalized to PUM of jadeitite and associated rocks from the Sierra del Convento (Eastern Cuba), Guatemala and Dominican Republic locations. All groups of studied jadeitite from Cuba (Figure 6.35a) show generally the same variability of REE patterns as in distinct settings on opposite sides of the Motagua fault in Guatemala (Figure 6.35b; Harlow et al., 2016) and the different groups defined in Dominican Republic (Figure 6.35c; Hertwig, 2014). In particular, some samples of Cuban mica-rich jadeitite show higher Eu contents than jadeitite from Guatemala and Dominican Republic, and jadeitite from North Motagua Mélange (NMM) shows a greater compositional variability in terms of REE that all jadeitites studied in the Caribbean area (Figure 6.35a, b, c). In fact, a large number of jadeitites studied here show REE composition similar to that of jadeitite from South Motagua Mélange (SMM) from Guatemala, as well as the jadeitite group from Dominican Republic (Figure 6.35a, b, c).

Omphacitite from Cuba has similar HREE contents to omphacitite from the two Guatemalan mélanges, and are depleted in some samples with respect to omphacitite from Dominican Republic (Figure 6.35d, e, f). The HREE contents are similar in Cuba and SMM from Guatemala, but are more depleted than in Dominican Republic omphacitite (Figure 6.35d, e, f).

An important difference with other jadeitite localities is the absence of a pure end-member albitite in Cuba (e.g. Harlow, 1994). The albite-epidote rich rocks from Sierra del Convento (Figure 6.35g) generally have higher REE content than Guatemala and Dominican Republic albitites, except for LREE contents in one albitite of SMM (Figure 6.35h, i). The more depleted compositions of this type of rock from Cuba is similar to the more enriched compositions from Guatemala and Dominican Republic albitites (Figure 6.35g, h, i).

The observations noted above for REE compositions can be completed using the spidergrams of figures 6.36 and 6.37. All groups of jadeitite from Cuba show similar trace element variations as Guatemalan jadeitited, although some chemical elements have different abundances (Figure 6.36a, c). For example, relative to Guatemalan jadeitites, Cuban jadeitites are characterized by: (1) depleted compositions in Rb, Ba and U in some samples of pure jadeitite and only U in some samples of Ep-rich jadeitite, (2) strong and slightly enriched compositions in Ti and Sc, respectively, in all Cuba jadeitites, (3) enriched compositions in Ni in Ep-rich jadeitite and Cr in pure and Ep-rich jadeitite, and (4) enriched compositions in Sr in mica-rich jadeitite and Nb-enriched compositions in Ep-Ab and mica-rich jadeitite (Figure 6.36a, c).

In contrast, comparison with Dominican Republic jadeitites shows that, generally, the variations of trace element compositions are similar, with Rb, Ba and Ni having the

same characteristics as those described with respect to Guatemala (Figure 6.36a, e). Additionally, Zr, Ti and Nb are enriched in all groups with respect to Dominican Republic (Figure 6.36a, e).

Omphacitite from Cuba has similar variations of chemical elements as Guatemalan omphacitite; only Ti is enriched in all Cuban jadeitites and some samples have slightly depleted U compositions with respect to Guatemalan jadeitites (Figure 6.36b, d). The comparison with Dominican Republic omphacitites shows that all Cuban omphacitites, except one sample, are depleted in LILE (Figure 6.36b, f). Ni and Cr are enriched in all omphacitites from Cuba, while HFSE have relatively similar concentrations that Dominican Republic omphacitites (Figure 6.36b, f).

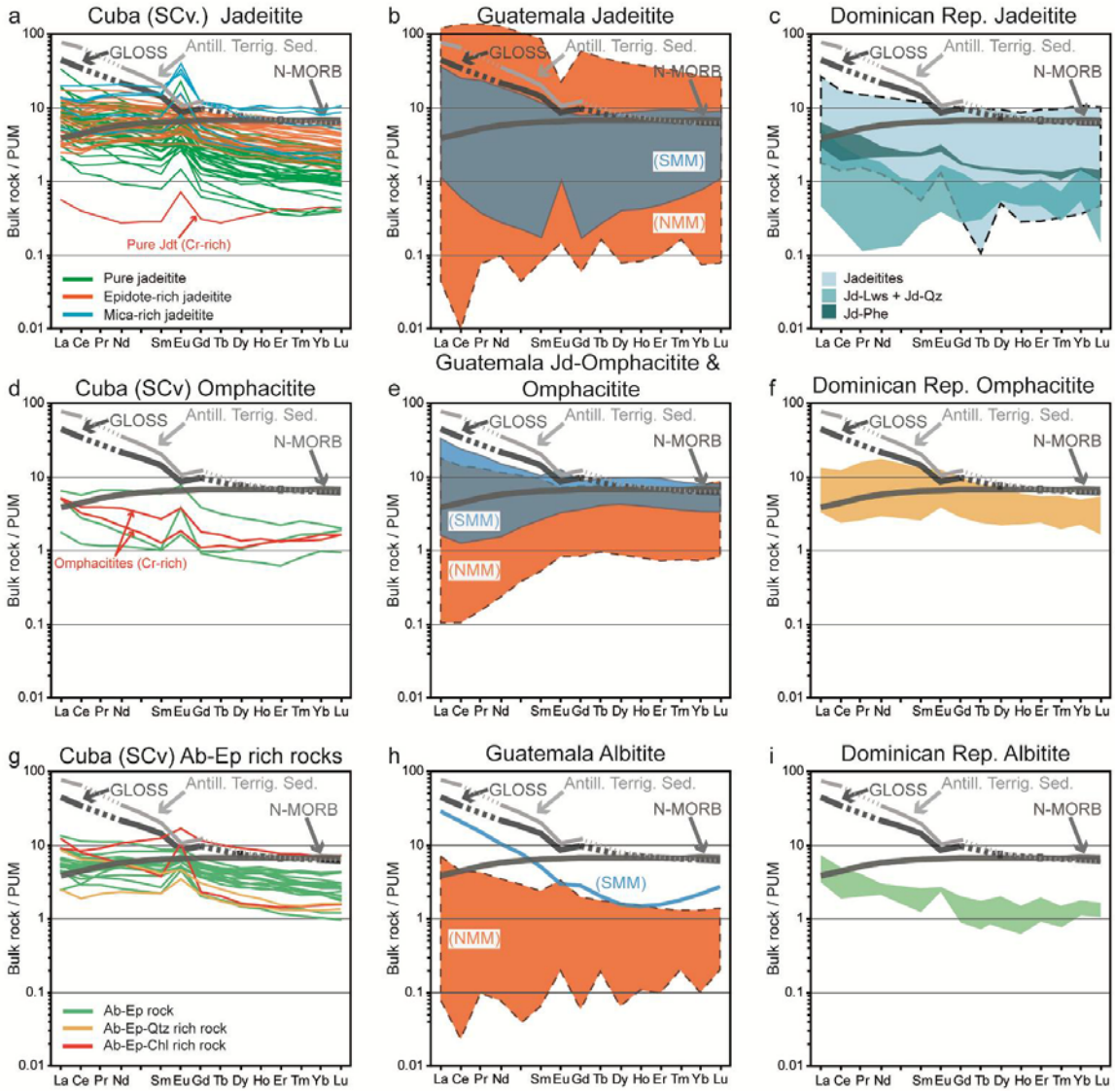

Figure 6.35. Rare earth element (REE) normalized to primitive upper mantle (PUM: McDonough and Sun, 1995) of studied rocks and Guatemala and Dominic Republic rock suites (Harlow et al., 2016 and Hetwin 2014). N-MORB (Sun and McDonough, 1989, Ni, Cr and Sc from Klein, 2003,), GLOSS and Antillean Terrigenous Sediment (Plank and Langmuir, 1998) are plotted for comparison.

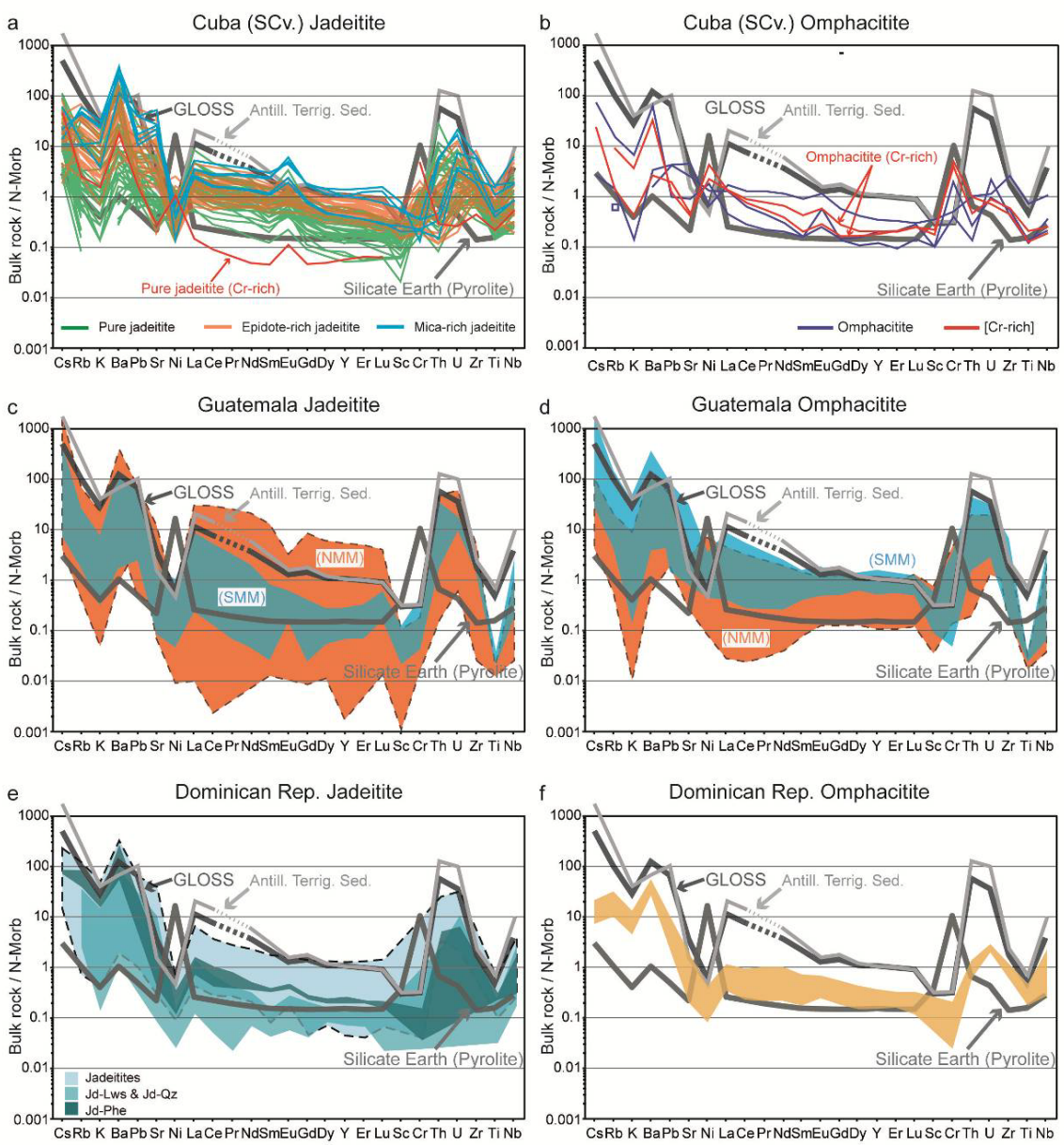

Figure 6.36. N-MORB normalized REE patterns for Cuban jadeitites and omphacitites and their equivalents in Motagua and Dominican Republic deposits. Patterns for global N-MORB (Klein, 2003; Sun and McDonough, 1989), subducting sediment (GLOSS and Antillean Terrigenous Sediment: Plank and Langmuir, 1998), silicate earth (McDonough and Sun, 1995) are plotted for comparison. Data from Guatemalan and Dominic Republic rocks were taken from Harlow et al., (2016) and Hertwig (2014).

In figure 6.37, spidergram patterns of Ab-Ep (-chlorite) (-quartz) rich rocks, and albitites from Guatemala and Dominican Republic are compared. With respect to Guatemala, Ab-Ep (-chlorite) (-quartz) rich rocks share similar patterns, but with more enriched compositions in Sc, Ni, Cr and Ti (Figure 6.37a, b). The Dominican Republic albitites have similar compositions to some trends defined by samples from Cuba, although albitites from Dominican Republic are depleted in Ni and Cr with respect to Cuban samples (Figure 6.37a, c).

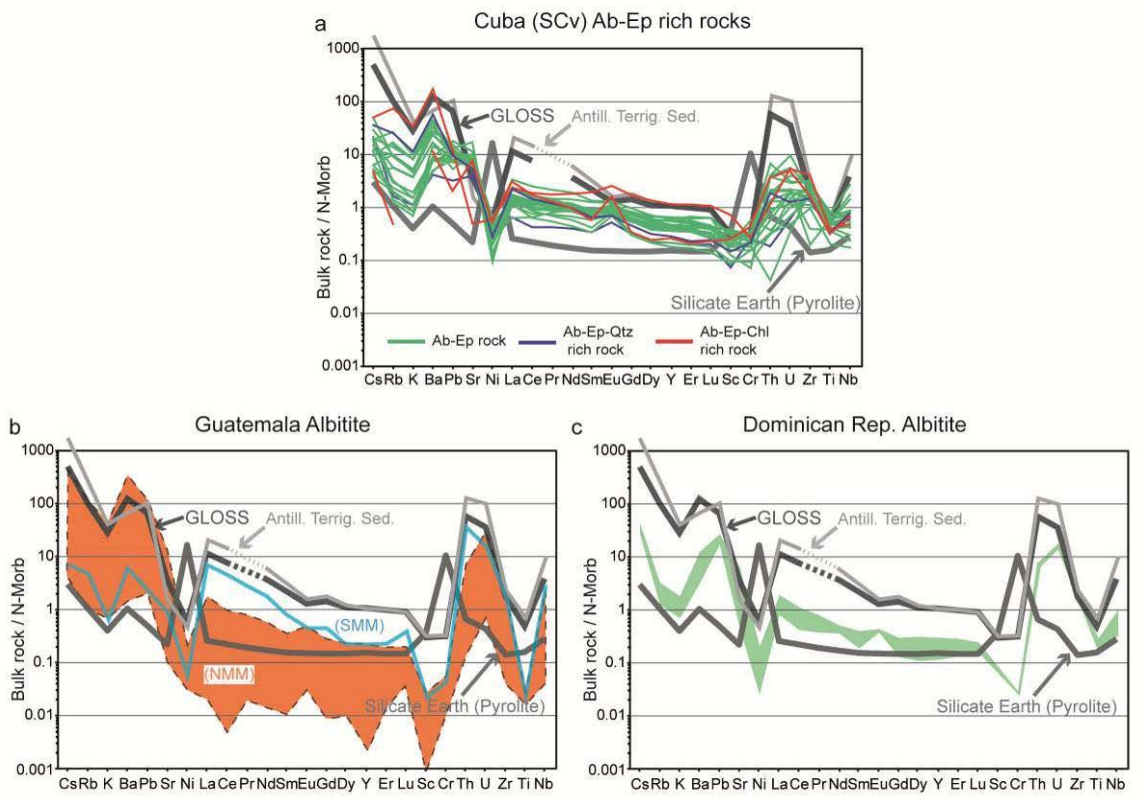

Figure 6.37. Spidergram plots for Cuban Ab-Ep (-chlorite) (-quartz) rich rocks and albitite from Guatemala and Dominican Republic (Harlow et al., 2016 and Hetwin 2014) whole rock compositions normalized to N-MORB (Klein, 2003; Sun and McDonough, 1989). Subducting sediment (GLOSS and Antillean Terrigenous Sediment: Plank and Langmuir, 1998) and silicate earth (McDonough and Sun, 1995) are plotted for comparison.

The comparisons offered above allow reaching the following conclusions:

a) Jadeitites from Guatemala and the Dominican Republic are characterized by a similar high compositional variability for some chemical elements, greater than two orders of magnitude in some cases, suggesting similar processes of late fluid-jadeitite interaction to those described for Cuban jadeitite. In this way, jadeitites from Guatemala with more depleted compositions with respect to N-MORB may be affected by Ba-rich and Ba-poor sedimentary fluids, increasing LILE, REE and HFSE (except Ti). A strong fluid-jadeitite interaction during relatively long periods of time could explain the low contents in Cr, Ni and Ti of Guatemalan jadeitites. Although these compositional differences also may be due to a mixture from different sources of fluid (sediment, altered oceanic crust and serpentinite), or an absence of evolved igneous fluid in Guatemala, as Harlow et al., (2016) pointed out in their comparison of Guatemalan and the Sierra del Convento rock suites.

b) Guatemalan omphacitite shows patterns from depleted to enriched compositions with respect to N-MORB. These patterns suggest similar fluid-omphacite interaction with sedimentary Ba-rich and Ba-poor fluids as in Cuban omphacite. In contrast, Dominican Republic omphacitite with

depleted patterns in Ni and Cr denotes the same Ba-rich fluid-omphacite interactions as those described in Cuban omphacitite.

c) The enriched REE compositions of Ab-Ep (-chlorite) (-quartz) rich rocks, as compared to Guatemalan and Dominican Republic albitite, can be related to the presence of other minerals, mainly epidote in Cuban samples, which are not true albitite rocks. Similar LILE and HFSE in albite rich rock of all deposits indicate fluid replacement of jadeititic protolith and/or fluid precipitated into open veins, like in P-type jadeitite.

In both Caribbean locations, a study using geochemical data and the petrographic characteristics of representative samples, such as the one made for this thesis, should be carried out in order to verify the interpretations presented here.

7 Conclusions

The Sierra del Convento subduction-related serpentinite-matrix mélange (eastern Cuba) host jadeitite bodies and associated rocks that document circulation of fluids and fluid-rock interactions in the subduction environment. Jadeitites formed due to precripitation of juvenile fluids in open fractures. These fluids evolved from hydrated metabasaltic rocks and related anatectic hydrous trondhjemtic melts. However, jadeitite-fluid and ultramafic rock-fluid interactions triggered by further fluid infiltration after rock formation largely modified initial rock compositions. The Sierra del Convento jadeitite deposit was likely exploited by the pre-Columbian Taino civilization for manufacturing of artifacts and, perhaps, for trade with other people from the Greater Antilles.

The serpentinite matrix of the Sierra del Convento (and La Corea) mélange derives from oceanic fertile peridotite with REE-enriched flat patterns and HFSE enrichment. The protoliths correspond to abyssal mantle rocks affected by small degree melting and possibly refertilization at an oceanic fracture zone. Serpentinization affected peridotite in this tectonic context as a consequence of infiltration of seawater, triggering formation of talc, tremolite, diopside, anthophyllite, and lizardite and remobilization of elements (SiO_2, CaO, Sr, Pb enrichment, and Mg, Os, Pt, Pd and Eu depletion). Subduction initiation along the transform-fault zone at ca. 135 Ma, identified as the inter-Americas transform zone, caused subduction of the Proto-Caribbean half-fault zone serpentinite (antigorite serpentinite) and capture of the Caribbean (Farallon) counterpart at the shallow upper plate close to the trench (lizardite-serpentinite). Upon establishment of mass-flow in the channel shortly after onset of subduction, subducted oceanic crust accreted and shallower serpentinite was dragged down to < 30 km depth where they mixed with the uprising deeper parts of the mélange. At the

cooler mature subduction stage, the influence of slab-derived infiltrating fluids caused enrichment in Pb, Cs, Ba and likely Sr. Other subduction mélanges bearing fertile serpentinite may record similar process and represent the footprint of subduction initiation at fracture zones.

Jadeitite and related rocks from Sierra del Convento show heterogeneous mineralogical compositions which allow to classify the rocks as pure jadeitite, epidote-rich jadeitite, mica-rich jadeitite, omphacitite and albite-epidote (-chlorite) (-quartz) rocks. Blackwalls are grouped in chloritite and titanite-apatite-zircon-rich chloritite. The Cuban jadeitites present textures and mineral compositions representative of jadeitite formed by hydrothermal processes high-temperature. Crystallization within fractures originated in the slab-mantle interface (peridotite/serpentinized peridotite), just above the subducting slab, from chemically diversified fluids during recurrent episodes of infiltration progressed together with the replacement of previously formed jadeite. The fluids precipitated jadeitite at high temperature (> 550 °C), suggesting a genetic link with hydrous trondhjemitic melts formed upon partial melting of subducted MORB amphibolite deep in the subduction channel, as indicated by the juvenile isotopic signature of all types of rock. The very local presence of quartz associated with jadeite indicates relatively high pressure of formation (15 kbar at 650 °C), in agreement with the conditions of partial melting of amphibolite (15 kbar, 700-750 °C) and of crystallization of trondhjemitic-tonalitic melts (15-13 kbar, ca. 650 °C). Zircon $^{206}Pb/^{238}U$ ages of 107 to 114 Ma attest for a short formation event synchronous with initial cooling of anatectic trondhjemitic melts in the mélange. This event is related to the isobaric cooling stage associated refrigeration of the subduction system shortly after onset of subduction, when leucocratic tonalitic-trondhjemitic melts derived after partial melting of amphibolite in the subduction environment crystallized. The studied samples with low late sedimentary fluid-jadeitite interaction show two types of geochemical patterns, pure jadeitites have depleted REE and HFSE patterns normalized to N-MORB, with Cr-rich compositions locally, and epidote-rich jadeitites show relatively enriched Ba compositions with respect to N-MORB, and REE patterns with similar compositions to N-MORB. Hence, Si-Al-Na-Mg-Ca-bearing fluids of variable composition evolved from both the crystallizing trondhjemitic magmas and hydrous metabasaltic rocks interacted with ultramafic rocks of the upper plate mantle and deposited jadeitite at high temperature, which denotes a strong influence of fluid-ultramafic rock interaction. Episodic opening of the fractures at depth in the subduction environment generates granoblastic massive jadeite, omphacite and epidote-(clino)zoisite with minor intergranular crystallization of accessory minerals.

Late interaction of jadeitite with fluids involved Ba-rich and Ba-poor sedimentary fluids. Ba-rich fluids are characterized by K-bearing mineral species as phlogopite-biotite, phengite and paragonite, as well as epidote group minerals (epidote-(clino)zoisite and allanite), and trace element patterns normalized to N-MORB that show enriched compositions mainly in LILE. In contrast, the interaction with Ba-poor sedimentary fluids is defined by low mica and epidote content and more depleted LILE compositions, suggesting a limited contribution from sediments and addition of REE and HFSE by crystallization of jadeite and omphacite and

intergranular crystallization of accessory minerals such as epidote-(clino)zoisite, allanite, rutile, and titanite at relatively high-T conditions.

A formation model involves hydrofracturing of sheared serpentinite at the slab-mantle interface. The crystallization of jadeitite veins, chloritic blackwalls and the omphacititic edges of blocks/bodies, with Cr-rich compositions locally, characterizes the main rock-forming event. However, subduction driven deformation increased permeability in the jadeitite veins by late fractures and microfractures at grain scale. An external pervasive fluids flow interacted metasomatically with jadeitite veins, being concentrated in the chloritic blackwalls. This metasomatic process explain the formation of albite-epidote (-chlorite) rocks and mica-rich jadeitite and the geochemical transformation of all types of rock. Albite-epidote (-quartz) rocks can be explained by a temporary evolution of these processes involving metasomatic replacement of earlier jadeitite, but a direct crystallization from a fluid, like P-type jadeitites, cannot be ruled out for the formation of some of these samples.

8 References

Ague, J.J. 2007. Models of permeability contrasts in subduction zone mélange: Implications for gradients in fluid fluxes, Syros and Tinos Islands, Greece. Chemical Geology 239, 217–227.

Andersen, T.B., Mair, K., Austrheim, H., Podladchikov, Y., Vrijmoed, J.C., 2008. Stress release in exhumed intermediate and deep earthquakes determined from ultramafic pseudotachylyte. Geology 36, 995–998.

Angiboust, S., Agard, P., Jolivet, L., Beyssac, O., 2009. The Zermatt-Saas ophiolite: the largest (60-km wide) and deepest (c. 70–80 km) continuous slice of oceanic lithosphere detached from a subduction zone?. Terra Nova 21(3), 171-180.

Angiboust, S., Agard, P. 2010. Initial water budget: The key to detaching large volumes of eclogitized oceanic crust along the subduction channel? Lithos 120, 453-474.

Angiboust, S., Agard, P., Raimbourg, H., Yamato, P., Huet, B. 2011, Subduction interface processes recorded by eclogite-facies shear zones (Monviso, W. Alps). Lithos 127(1-2), 222-238.

Angiboust, S., Langdon, R., Agard, P., Waters, D., Chopin, C., 2012a. Eclogitization of the Monviso ophiolite (W. Alps) and implications on subduction dynamics. Journal of Metamorphic Geology 30(1), 37-61.

Angiboust, S., Wolf, S., Burov, E., Agard, P., Yamato, P. 2012b. Effect of fluid circulation on subduction interface tectonic processes: Insights from thermo-mechanical numerical modelling. Earth and Planetary Science Letters 357-358, 238-248.

Angiboust, S., Pettke, T., De Hoog, J.C.M., Caron, B., Oncken, O., 2014. Channelized fluid flow and eclogite-facies metasomatism along the subduction shear zone. Journal of Petrology 55, 883-916.

Augustin, N., Paulick, H., Lackschewitz, K.S., Eisenhauer, A., Garbe-Schönberg, D., Kuhn, T., Botz, R., Schmidt, M., 2012. Alteration at the ultramafic-hosted Logatchev hydrothermal field: constraints from trace element and Sr–O isotope data. Geochemistry Geophysics Geosystems 13 (3).

Barnes, J. D., Beltrando, M., Lee, C. T. A., Cisneros, M., Loewy, S., Chin, E., 2014. Geochemistry of Alpine serpentinites from rifting to subduction: A view across paleogeographic domains and metamorphic grade. Chemical Geology 389, 29-47.

Bea, F., Fershtater, G.B., Montero, P., Smirnov, V.N., Molina, J.F., 2005. Deformation-driven differentiation of granitic magma: the Stepninsk pluton of the Uralides, Russia. Lithos 81, 209–233.

Bebout G.E., Barton, M.D., 2002. Tectonic and metasomatic mixing in a subduction zone mélange: insights into the geochemical evolution of the slab-mantle interface. Chemical Geology 187, 79–106.

Becker, H., Horan, M.F., Walker, R.J., Gao, S., Lorand, J.P., Rudnick, R.L., 2006. Highly siderophile element compositions of the Earth's primitive mantle. Geochimica et Cosmochimica Acta 70, 4528-4550.

Beltrando, M., Manatschal, G., Mohn, G., Dal Piaz, G. V., Brovarone, A. V., Masini, E., 2014. Recognizing remnants of magma-poor rifted margins in high-pressure orogenic belts: The Alpine case study. Earth-Science Reviews 131, 88-115.

Ben Othman, D., White, W.M., Patchett, J., 1989. The geochemistry of marine sediments, island arc magma genesis, and crust-mantle recycling. Earth and Planetary Science Letters 94, 1–21.

Birch F, LeComte P. 1960. Temperature-pressure plane for albite composition. Am. J. Sci. 258:209–17

Black, L.P., Kamo, S.L., Allen, C.M., 2003. TEMORA 1: a quality zircon standard for Phanerozoic U-Pb geochronology. Chemical Geology 200, 155–170.

Black L.P., Jagodzinski E.A., 2003. Importance of establishing sources of uncertainty for the derivation of reliable SHRIMP ages. Australian Journal of Earth Science 50, 503–512.

Blanco-Quintero, I.F., García-Casco, A., Rojas-Agramonte, Y., Rodríguez Vega, A., Lázaro, C., Iturralde-Vinent, M.A., 2010. Metamorphic evolution of subducted hot oceanic crust, La Corea mélange, Cuba. American Journal of Science 310, 889–915.

Blanco-Quintero, I. F., García-Casco, A., Gerya, T., 2011a. Tectonic blocks in serpentinite mélange (eastern Cuba) reveal large-scale convective flow of the subduction channel. Geology 39, 79-82.

Blanco-Quintero, I. F., Gerya, T. V., García-Casco, A., Castro, A., 2011b. Subduction of young oceanic plates: a numerical study with application to aborted thermal-chemical plumes. Geochemistry, Geophysics, Geosystems 12, Q10012.

Blanco-Quintero, I.F., Lázaro, C., García-Casco, A., Proenza, J., Rojas-Agramonte, Y., 2011c. Barium-rich fluids and melts in the subduction environment (La Corea and Sierra del Convento mélanges, eastern Cuba). Contributions to Mineralogy and Petrology 162, 395–413.

Blanco-Quintero, I.F., Proenza, J.A., García-Casco, A., Tauler, E., Galí, S., 2011d. Serpentinites and serpentinites within a fossil subduction channel: La Corea mélange, eastern Cuba. Geologica Acta 9(3-4), 389-405.

Blanco-Quintero, I.F., Rojas-Agramonte, Y., García-Casco, A., Kröner, A., Mertz, D.F., Lázaro, C., Blanco-Moreno, J., Renne, P.R., 2011e. Timing of subduction and exhumation in a subduction channel: Evidence from slab melts from La Corea mélange (eastern Cuba). Lithos 127, 86-100.

Boiteau, A., Michard, A., Saliot, P., 1972. Métamorphisme de haute pression dans le complexe ophiolitique du Purial (Oriente, Cuba): C.R. Acad: Sci., Série D, 274, 2137–2140.

Boschi, C., Früh-Green, G.L., Delacour, A., Karson, J.A, Kelley, D. S., 2006. Mass transfer and fluid flow during detachment faulting and development of an oceanic core complex, Atlantis Massif (MAR 30°N). Geochemistry Geophysics Geosystems 7 (1).

Boschman, L.M., van Hinsbergen, D.J.J., Torsvik, T.H., Spakman, W., Pindell, J.L., 2014. Kinematic reconstruction of the Caribbean region since the Early Jurassic. Earth-Science Reviews 138, 102-136.

Brady, J.B., Stout, J.H., 1980. Normalizations of thermodynamic properties and some implications for graphical and analytical problems in Petrology. American Journal of Science 280, 173-189.

Bröcker, M., Enders, M., 2001. Unusual bulk-rock compositions in eclogite-facies rocks from Syros and Tinos (Cyclades, Greece); implications for U–Pb zircon geochronology. Chemical Geology 175 (3–4), 581–603.

Bromiley, G.D., Pawley, A.R., 2003. The stability of antigorite in the systems MgO-SiO2-H2O (MSH) and MgO-Al2O3-SiO2-H2O (MASH): The effects of Al3+ substitution on high-pressure stability. American Mineralogist 88, 99-108.

Brudzinski, M.R., Thurber, C.H., Hacker, B.R., Engdahl, E.R., 2007. Global Prevalence of double Benioff zones. Science 316, 1472-1474.

Brueckner, H.K., Avé Lallemant, H.G., Sisson, V.B., Harlow, G.E., Hemming, S.R., Roden-Tice, M.K., Sorensen, S.S., Tsujimori, T., Francis, A.H., Gehrels, G.E., Blythe, A.E., 2009. Metamorphic reworking of a high-pressure-low temperature serpentinite-matrix mélange belt north of the Motagua fault, Guatemala: A revised record of Neocomian and Maastrichtian collisions. Earth and Planetary Science Letters 284, 228-235.

Buffon G-LL. 1749. Histoire Naturelle, G´en´erale et Particuli`ere, avec la Description du Cabinet du Roi. Paris: Imprim. R.

Burke, K., 1988. Tectonic evolution of the Caribbean. Annual Review of Earth and Planetary Sciences 16, 201–230.

Cannat, M., Fontaine, F., Escartin, J., 2010. Serpentinization and associated hydrogen and methane fluxes at slow spreading ridges, in Rona, P.A., Devey, C.W., Dyment, J., and Murton, B.J., eds., Diversity of hydrothermal systems on slow spreading ocean ridges: Washington, D. C., American Geophysical Union, p. 241&3x2013;264.

Castro, A., Gerya, T., García-Casco, A., Fernández, C., Diaz-Alvarado, J., Moreno-Ventas, I., Löw. I., 2010. Melting relations of MORB-sediment melanges in underplated mantle wedge plumes. Implications for the origin of cordilleran-type batholiths. Journal of Petrology, 51, 1267-1295.

Cárdenas-Párraga, J., García-Casco, A., Núñez-Cambra, K., Rodríguez-Vega, A., Blanco-Quintero, I.F., Harlow, G.E., Lázaro, C., 2010. Jadeitite jade occurrence from the Sierra del Convento mélange (Eastern Cuba). Boletín de la Sociedad Geológica Mexicana 62, 199–205.

Cárdenas-Párraga, J., García-Casco, A., Harlow, G.E., Blanco-Quintero, I.F., Rojas-Agramonte, Y., Kröner, A., 2012. Hydrothermal origin and age of jadeitites from Sierra del Convento Mélange (Eastern Cuba). European Journal of Mineralogy 24, 313-331.

Cárdenas-Párraga, J., García-Casco, A., Proenza, J. A., Harlow, G. E., Blanco-Quintero, I. F., Lázaro, C., Villanova-de-Benavent, C., Núñez-Cambra, K., 2017. Trace-element geochemistry of transform-fault serpentinite in high-pressure subduction mélanges (eastern Cuba): implications for subduction initiation. International Geology Review. 59, 16.

Carpenter, M.A., 1980. Mechanisms of exsolution in sodic pyroxenes. American Mineralogy 64, 102−108.

Casey, J.F., Dewey, J.F., 1984. Initiation of subduction zones along transform and accreting plate boundaries, triple-junction evolution, and forearc spreading centres: Implications for ophiolitic geology and obduction, in Gass, K.G., Lippard, S.J., and Shelton, A.W., eds., Ophiolites and Oceanic Lithosphere. Geological Society [London] Special Publication 13, 269–290.

Cesare, B., Poletti, E., Boiron, M.-C., Cathelineau, M., 2001. Alpine metamorphism and veining in the Zentralgneis Complex of the SW Tauern Window: a model of fluid– rock interactions based on fluid inclusions. Tectonophysics 336, 121–136.

Chan, T.K., Finch, I.J., 2001. Determination of platinum-group elements and gold by inductively coupled plasma mass spectrometry: in Australian Platinum Conference, Perth, Western Australia.

Chen, L., Chu, F. Y., Zhu, J. H., Dong, Y. H., Yu, X., Li, Z. G., Tang, L. M., 2015. Major and trace elements of abyssal peridotites: evidence for melt refertilization beneath the ultraslow-spreading Southwest Indian Ridge (53 E segment). International Geology Review 57(13), 1715-1734.

Choi, S.H., Shervais, J.W., Mukasa, S.B., 2008a. Supra-subduction and abyssal mantle peridotites of the Coast Range ophiolite, California. Contributions to Mineralogy and Petrology 155, 551–576.

Choi, S.H., Mukasa, S.B., Shervais, J.W., 2008b. Initiation of Franciscan subduction along a large-offset fracture zone: Evidence from mantle peridotites, Stonyford: California. Geology 36 (8), 595–598.

Claoué-Long, J.C., Compston, W., Roberts, J., Fanning, C.M., 1995. Two Carboniferous ages: a comparison of SHRIMP zircon dating with conventional zircon ages and 40Ar/39Ar analyses. Society of Sedimentary Geology Special Publication 54, 3–21.

Cloos, M., 1982. Flow mélanges: numerical modeling and geologic constraints on their origin in the Franciscan subduction complex, California. Geological Society of American Bulletin 93, 330–345.

Cloos, M., and Shreve, R.L., 1988a, Subduction-channel model of prism accretion, melange formation, sediment subduction, and subduction erosion at convergent plate margins: 1. Background and description: Pure and Applied Geophysics 128, 455–500.

Cloos, M., and Shreve, R.L., 1988b, Subduction-channel model of prism accretion, melange formation, sediment subduction, and subduction erosion at convergent plate margins: 2. Implications and discussion: Pure and Applied Geophysics 128, 501–545.

Cobiella, J. L., Campos, M., Boiteau, A., Quinta, F., 1977. Geología del flanco sur de la Sierra del Curial. Revista la Minería en Cuba 3, 54-62.

Cobiella, J., Quintas, F., Campos, M., Hernández, M., 1984. Geología de la Región Central y Suroriental de la Provincia de Guantánamo: Editorial Oriente, Santiago de Cuba, 125 p.

Compagnoni, R., Rolfo, F., Castelli, D., 2012. Jadeitite from the Monviso meta-ophiolite, western Alps: occurrence and genesis. European Journal of Mineralogy 24, 333–343.

Compston, W., Williams, I.S., Myer, C., 1984. U-Pb geochronology of zircons from Lunar Breccia 73217 using a sensitive high mass-resolution ion-microprobe. Journal of Geophysical Research 89 (Suppl.), B525-B534.

Compston, W., Williams, I.S., Kirschvink, J.L., 1992. Zircon U-Pb ages for the Early Cambrian time scale. Journal of the Geological Society of London 149, 171–184.

De Laeter, J.R. Kennedy, A.K., 1998. A double focusing mass spectrometer for geochronology. International Journal of Mass Spectromeetry 178, 43–50.

Deer, W.A., Howie, R.A., Zussman, J., 1962. Rock Forming Minerals. Vol 3. Sheet Silicates. John Wiley, New York, 270 p.

Deschamps, F., Guillot, S., Godard, M., Andreani, M., Hattori, K., 2011. Serpentinites act as sponges for fluid-mobile elements in abyssal and subduction zone environments. Terra Nova 23, 171-178.

Deschamps, F., Godard, M., Guillot, S., Chauvel, C., Andreani, M., Hattori, K., Wunder, B., France, L., 2012. Behavior of fluid-mobile elements in serpentines from abyssal to subduction environments: examples from Cuba and Dominican Republic. Chemical Geology 312–313, 93–117.

Deschamps, F., Godard, M., Guillot, S., Hattori, K., 2013. Geochemistry of subduction zone serpentinites: A review. Lithos 178, 96-127.

Dilek, Y., Furnes, H., 2011. Ophiolite génesis and global tectonics: Geochemical and tectonic fingerprinting of ancient oceanic lithosphere. Geological Society of America Bulletin 123, 387-411.

Ernst, W.G., 1999. Metamorphism, partial preservation, and exhumation of ultrahigh-pressure belts. Island Arc 8, 125-153.

Ernst. W.G., 2016. Franciscan mélanges: coherent blocks in a low-density, ductile matrix. International Geology Review 58, 626-642.

Escuder-Viruete J., Friedman R., Castillo-Carrión M., Jabites J., Pérez-Estaún A., 2011. Origin and significance of the ophiolitic high-P mélanges in the northern Caribbean convergent margin: insights from the geochemistry and large-scale structure of the Río San Juan metamorphic complex. Lithos 127, 483–504.

Escuder-Viruete J., Valverde-Vaquero P., Rojas-Agramonte Y., Jabites, J., Pérez-Estaún A., 2013a. From intra-oceanic subduction to arc accretion and arc–continent collision: insights from the structural evolution of the Río San Juan metamorphic complex, northern Hispaniola. Journal of Structural Geology 46, 34–56.

Escuder-Viruete J., Valverde-Vaquero P., Rojas-Agramonte Y., Gabites J., Castillo-Carrión M., Pérez-Estaún A., 2013b. Timing of deformational events in the Río San Juan complex: Implications for the tectonic controls on the exhumation of high-P rocks in the northern Caribbean subduction–accretionary prism. Lithos 177, 416–435.

Escuder-Viruete, J., Pérez-Estaún, A., 2013c. Contrasting exhumation P-T paths followed by high-P rocks in the northern Caribbean subduction-accretionary complex: Insights from the

structural geology, microtextures and equilibrium assemblage diagrams. Lithos 160-161, 117-144.

Evans, B.W., Hattori, K., Baronnet, A., 2013. Serpentinites: What, why, where?. Elements 9, 99-106.

Fisher, G.W., 1989. Matrix analysis of metamorphic mineral assemblages and reactions. Contributions to Mineralogy and Petrology 102, 69-77.

Fisher, G.W., 1993. An improved method for algebraic analysis of metamorphic mineral assemblages. American Mineralogist 78, 1257-1261.

Flores, K.E., Martens, U., Harlow, G.E., Brueckner, H.K., Pearson J.N., 2013. Jadeitite formed during subduction: In situ zircon geochronology constraints from two different tectonic events within the Guatemala Suture Zone. Earth and Planetary Science Letters 371–372, 67–81.

Früh-Green, G. L., Kelley, D. S., Bernasconi, S. M., Karson, J. A., Ludwig, K. A., Butterfield, D. A., Boschi, C., Proskurowski, G., 2003. 30,000 years of hydrothermal activity at the Lost City vent field. Science 301 (5632), 495-498.

Fryer, P., 2012. Serpentinite Mud Volcanism: Observations, Processes, and Implications. Annual Review of Marine Science 4, 345-373.

Furukawa, Y., 2009. Convergence of aqueous fluid at the corner of the mantle wedge: implications for a generation mechanism of deep low-frequency earthquakes. Tectonophysics 469, 85–92.

García-Casco, A., Torres-Roldán, R.L., Iturralde-Vinent, M.A., Millán, G., Núñez Cambra, K., Lázaro, C., Rodríguez Vega, A., 2006. High pressure metamorphism of ophiolites in Cuba. Geologica Acta 4(1-2), 63-88.

García-Casco, A., 2007. Magmatic paragonite in trondhjemites from the Sierra del Convento mélange, Cuba. American Mineralogy 92, 1232–1237.

García-Casco, A., Lázaro, C., Rojas-Agramonte, Y., Kröner, A., Torres Roldán, R.L., Núñez, K., Millán, G., Neubaurer, F., Blanco-Quintero, I.F., 2008a. Partial melting and counterclockwise P-T path of subducted oceanic crust (Sierra del Convento, E Cuba). Journal of Petrology 49, 129–161.

García-Casco, A., Iturralde-Vinent, M.A., Pindell, J., 2008b, Latest Cretaceous collision/accretion between the Caribbean Plate and Caribeana: origin of metamorphic terranes in the Greater Antilles. International Geology Review 50, 781–809.

García-Casco, A., Rodríguez Vega, A., Cárdenas Párraga, J., Iturralde-Vinent, M.A., Lázaro, C., Blanco Quintero, I., Rojas-Agramonte, Y., Kröner, A., Núñez Cambra, K., Millán, G., Torres-Roldán, R.L., Carrasquilla, S., 2009. A new jadeitite jade locality (Sierra del Convento, Cuba): First report and some petrological and archaeological implications. Contribution to Mineralogy and Petrology 158, 1-26.

Gervilla, F., Proenza, J.A., Frei, R., González-Jiménez, J.M., Garrido, C.J., Melgarejo, J.C., Meibom, A., Díaz-Martínez, R., Lavaut, W., 2005. Distribution of platinum-group elements and Os isotopes in chromite ores from Mayarí-Baracoa Ophiolitic Belt (eastern Cuba). Contributions to Mineralogy and Petrology 150, 589-607.

Gerya, T.V., Stoeckhert, B., Perchuk, A.L., 2002. Exhumation of high-pressure metamorphic rocks in a subduction channel-a numerical simulation. Tectonics 21, 6-1-6-19.

Gerya, T.V., 2011. Intra-oceanic Subduction Zones, in Brown, D., and Ryan, P.D., eds., Arc-Continent Collision. Frontiers in Earth Sciences 23-51. Springer-Verlag Berlin Heidelberg.

Gerya, T., Stern, R.J., Baes, M., Sobolev, S., Whattam, S., 2015. Plume-induced subduction initiation triggered plate tectonics on Earth. Nature 527, 221–225.

Gorczyk, W., Guillot, S., Gerya, T.V., Hattori, K., 2007. Asthenospheric upwelling, oceanic slab retreat and exhumation of UHP mantle rocks: Insights from Greater Antilles. Geophysical Research Letters 34, L211309.

Govindaraju, K., 1994. Compilation of working values and sample description for 383 geostandards. Geostandards and Geoanalytical Research 18, 1–158.

Green, T. H., 1982. Anatexis of mafic crust and high pressure crystallization of andesite, in Thorpe, R.S., ed., Andesites. Chichester, John Wiley, 465-487.

Green, E., Holland, T., Powell, R., 2007. An order-disorder model for omphacitic pyroxenes in the system jadeite-diopside-hedenbergite-acmite, with applications to eclogite rocks. American Mineralogist 92, 1181–1189.

Groppo, C., Rinaudo, C., Cairo, S., Gastaldi, D., Compagnoni, R., 2006. Micro-Raman spectroscopy for a quick and reliable identification of serpentine minerals from ultramafics. European Journal of Mineralogy 18, 319-329.

Guidotti, C.V., 1984. Micas in metamorphic rocks. Reviews in Mineralogy and Geochemistry 13 (1), 357-467.

Guillot, S., Hattori, K., Sigoyer de, J., 2000. Mantle wedge serpentinization and exhumation of eclogites: insights from eastern Ladakh, northwest Himalaya. Geology 28, 199-202.

Guillot, S., Hattori, K.H., De Sigoyer, J., Nägler, T., Auzende, A.-L., 2001. Evidence of hydration of the mantle wedge and its role in the exhumation of eclogites. Earth and Planetary Science Letters 193 (1-2), 115-127.

Guillot, S., Hattori, K., Agard, P., Schwartz, S., Vidal, O., 2009. Exhumation processes in oceanic and continental subduction contexts: a review. In: Lallemand, S., Funiciello, F., eds., Subduction Zone Dynamics, 175-204, doi 10.1007/978-3-540-87974-9, Springer-Verlag Berlin Heidelberg.

Guillot, S., Schwartz, S., Reynard, B., Agard, P., Prigent, C., 2015. Tectonic significance of serpentinites. Tectonophysics 646, 1-19.

Gyarmati, P., Méndez, I., Lay, M., 1997. Caracterización de las rocas del arco de islas Cretácico en la Zona Estructuro- Facial Nipe-Cristal-Baracoa, in Furrazola, G.F., and Nuñez-Cambra, K.E., eds., Estudios sobre Geología de Cuba. Ciudad de la Habana, Cuba, Instituto de Geología y Paleontología, 357–364.

Hacker, B.R., Abers, G.A., Peacock, S.M., 2003. Subduction factory 1. Theoretical mineralogy, densities, seismic wave speeds, and H2O contents. Journal of Geophysical Research Solid Earth 108(B1).

Hacker, B.R., 2008. H2O subduction beneath arcs. Geochemistry, Geophysics, Geosystems 9.

Harlow, G.E., Olds, E.P., 1987. Observations on terrestrial ureyite and ureyitic pyroxene. American Mineralogist 72, 126–136.

Harlow, G.E., 1994. Jadeitites, albitites and related rocks from the Motagua Fault Zone, Guatemala. Journal of Metamorphic Geology 12, 49–68.

Harlow, G.E., Hemming, S.R., Avé Lallemant, H.G., Sisson, V.B., Sorensen, S.S., 2004. Two HP/LT serpentine-matrix mélange belts, Motagua Fault Zone, Guatemala: a record of Aptian and Maastrichtian collisions. Geology 32 (1), 17–20.

Harlow, G.E., Sorensen, S.S., 2005. Jade (nephrite and jadeitite) and serpentinite: metasomatic connections. International Geology Review 47, 113–146.

Harlow, G.E., Sorensen, S.S., Sisson, V.B., 2007. Jade. In The Geology of Gem Deposits (ed., Lee A. Groat), Short Course Handbook Series 37, Mineralogical Association of Canada, Quebec, 207-254.

Harlow, G.E., Sisson, V.B., Sorensen, S.S., 2011. Jadeitite from Guatemala: new observations and distinctions among multiple occurrences. Geologica Acta 9 (3–4), 363–387.

Harlow, G.E., Tsujimori, T., Sorensen, S.S., 2015. Jadeitites and Plate Tectonics. Annual Review of Earth and Planetary Sciences 43, 105-138.

Harlow, G. E., Flores, K. E., Marschall, H. R., 2016. Fluid-mediated mass transfer from a paleosubduction channel to its mantle wedge: Evidence from jadeitite and related rocks from the Guatemala Suture Zone. Lithos, 258, 15-36.

Hart, S.R., Zindler, A., 1986. In search of a bulk-Earth composition. Chemical Geology 57 (3–4), 247–267.

Harvey, J., Gannoun, A., Burton, K.W., Rogers, N.W., Alard, O., Parkinson, I.J., 2006. Ancient melt extraction from the oceanic upper mantle revealed by Re-Os isotopes in abyssal peridotites from the Mid-Atlantic ridge. Earth and Planetary Science Letters 244, 606–621.

Hattori, K.H. Guillot, S., 2003. Volcanic fronts form as a consequence of serpentinite dehydration in the forearc mantle wedge. Geology 31, 525-528.

Hattori, K.H., Guillot, S., 2007. Geochemical character of serpentinites associated with high- to ultrahigh-pressure metamorphic rocks in the Alps, Cuba, and the Himalayas: Recycling of elements in subduction zones. Geochemistry, Geophysics, Geosystems 8, Q09010.

Healy, D., Reddy, S.M., Timms, N.E., Gray, E.M., Brovarone, A.V., 2009. Trench-parallel fast axes of seismic anisotropy due to fluid-filled cracks in subducting slabs. Earth and Planetary Science Letter 283, 75–86.

Hermann, J., Müntener, O., Scambelluri, M., 2000. The importance of serpentinites mylonites for subduction and exhumation of oceanic crust. Tectonophysics 327, 225–238.

Hertwig, A., 2014. Genesis of jadeitites and their country rocks Rio San Juan Complex Dominican Republic. PhD Thesis Dissertation, 207 pp. (+Appendix). Ruhr-Universität Bochum, Germany.

Hertwig, A., McClelland, W.C., Kitajima, K., Schertl, H.P., Maresch, W.V., Stanek, K., Valley, J.W., Sergeev, S.A., 2016. Inherited igneous zircons in jadeitite predate high-pressure metamorphism and jadeitite formation in the Jagua Clara serpentinite mélange of the Rio San Juan Complex (Dominican Republic). Contributions to Mineralogy and Petrology 171, 48.

Holland, T.J.B., Powell, R., 1998. An internally consistent thermodynamic data set for phases of petrological interest. Journal of Metamorphic Geology 16, 309–343.

Hsu, K.J., 1971. Franciscan mélange as a model for eugeosunclinal sedimentation and underthrusting tectonics. Journal of Geophysical Research 76, 1162 – 1170.

Hyndman, R. D. Peacock, S. M., 2003. Serpentinization of the forearc mantle. Earth and Planetary Science Letters 212, 417-432.

Iturralde-Vinent M.A., 1998. Sinopsis de la constitución Geológica de Cuba. Acta Geologica Hispanica 33, 9–56.

Iturralde-Vinent, M.A., Díaz-Otero, C., Rodríguez-Vega, A., Díaz Martínez, R., 2006a. Tectonic implications of paleontologic dating of Cretaceous-Danian sections of Eastern Cuba. Geologica Acta 4, 89–102.

Iturralde-Vinent, M.A., Lidiak, E.G., 2006b. Caribbean tectonic, magmatic, metamorphic and stratigraphic events. Implications for plate tectonics. Geologica Acta 4, 1-5.

Iturralde-Vinent, M.A., Diaz Otero, C., García-Casco, A., Van Hinsbergen, D.J.J., 2008. Paleogene foredeep basin deposits of North-Central Cuba: a record of arc-continent collision between the Caribbean and North American plate. International Geology Review 50, 863–884.

Iwamori, H., 1998. Transportation of H_2O and melting in subduction zones. Earth and Planetary Science Letters 160 (1-2), 65-80.

Jagoutz, E., Palme, H., Baddenhausen, H., Blum, K., Cendales, M., Dreibus, G., Spettel, B., Lorenz, V., Vanke, H., 1979. The abundance of major, minor and trace elements in the earth's mantle as derived from primitive ultramafic nodules. Geochimica et Cosmochimica Acta 11 (2), 2031–2050.

Jahn, B. M., Bernard-Griffiths, J., Charlot, R., Cornichet, J., & Vidal, F., 1980. Nd and Sr isotopic compositions and REE abundances of Cretaceous MORB (Holes 417D and 418A, Legs 51, 52 and 53). Earth and Planetary Science Letters, 48(1), 171-184.

John, T., Scherer, E.E., Haase, K., Schenk, V., 2004. Trace element fractionation during fluid-induced eclogitization in a subducting slab: trace element and Lu–Hf–Sm–Nd isotope systematics. Earth Planetary Science Letters 227, 441–456.

Johnson, C.A., Harlow, G.E., 1999. Guatemala jadeitites and albitites were formed by deuterium-rich serpentinizing fluids deep within a subduction-channel. Geology 27, 629-632.

Jolly, W.T., Lidiak, E.G., Dickin, A.P., 2006. Cretaceous to mid-Eocene pelagic sediment budget in Puerto Rico and the Virgin Islands (northeast Antilles Island arc). Geologica Acta 4 (1–2), 35–62.

Kerr, A.C., Iturralde-Vinent, M., Saunders, A.D., Babbs, T.L., Tarney, J., 1999. A new plate tectonic model of the Caribbean: Implications from a geochemical reconnaissance of Cuban Mesozoic volcanic rocks. Geological Society of America Bulletin 111, 1581–1599.

Kerrick, D., 2002. Serpentinite seduction. Science 298 (5597), 1344-1345.

King, R.L., Bebout, G.E., Moriguti, T., Nakamura, E., 2006. Elemental mixing systematics and Sr–Nd isotope geochemistry of mélange formation: obstacles to identification of fluid sources to arc volcanics. Earth and Planetary Science Letters 246, 288–304.

King, R., Bebout, G.E., Grove, M., Moriguti, T., Nakamura, E., 2007. Boron and lead isotope signatures of subduction-zone mélange formation: hybridization and fractionation along the slab–mantle interface beneath volcanic fronts. Chemical Geology 239, 305-322.

Kinny, P.D., 1986. 3820 Ma zircons from a tonalitic Amitsoq gneiss in the Godthab district of southern West Greenland. Earth Planetary Science Letters 79, 337-347.

Klein, E.M., 2003. Geochemistry of the igneous oceanic crust. In: Holland, H.D., Turekian, K.K. (Eds.), Treatise on Geochemistry The Crust 3. Elsevier, 443–463.

Kodolányi, J., Pettke, T., 2011. Loss of trace elements from serpentinites during fluidassisted transformation of chrysotile to antigorite — an example from Guatemala. Chemical Geology 284, 351–362.

Kodolányi, J., Pettke, T., Spandler, C., Kamber, B.S., Gméling, K., 2012. Geochemistry of ocean floor and fore-arc serpentinites: constraints on the ultramafic input to subduction zones. Journal of Petrology 53, 235–270.

Krebs, M., Maresch, W.V., Schertl, H.P., Münker, C., Baumann, A., Draper, G., Idleman, B., Trapp, E., 2008. The dynamics of intra-oceanic subduction zones: a direct comparison between fossil petrological evidence (Rio San Juan Complex, Dominican Republic) and numerical simulation. Lithos 103, 106–137.

Krebs, M., Schertl, H.-P., Maresch, W.V., Draper, G., 2011. Mass flow in serpentinite-hosted subduction channels: P–T–t path patterns of metamorphic blocks in the Rio San Juan mélange (Dominican Republic). Journal of Asian Earth Sciences 42, 569-595.

Kulachkov, L.V., Leyva, R.C., 1990. Informe sobre los resultados de los trabajos de reconocimiento geológico para cuarzo filoniano en la parte oriental de Cuba. Unpublished report of the Instituto Superior Minero-Metalúrgico de Moa.

Lázaro, C., García-Casco, A., 2008. Geochemical and Sr-Nd isotope signatures of pristine slab melts and their residues (Sierra del Convento mélange, eastern Cuba). Chemical Geology 255, 120-133.

Lázaro, C., García-Casco, A., Rojas-Agramonte, Y., Kröner, A., Neubauer, F., Iturralde-Vinent, M., 2009. Fifty-five-million-year history of oceanic subduction and exhumation at the northern edge of the Caribbean plate (Sierra del Convento mélange, Cuba). Journal of Metamorphic Geology 27, 19-40.

Lázaro, C., Blanco-Quintero, I.F., Marchesi, C., Bosch, D., Rojas-Agramonte, Y., García-Casco A., 2011. The imprint of subducion fluids on subducted MORB-derived melts (Sierra del Convento mélange, Cuba). Lithos 126, 341–354.

Lázaro, C., Blanco-Quintero, I.F., Rojas-Agramonte, Y., Proenza, J.A., Núñez-Cambra, K., García-Casco, A., 2013. First description of a metamorphic sole related to ophiolite obduction in the northern Caribbean: Geochemistry and petrology of the Güira de Jauco Amphibolite Complex (eastern Cuba) and tectonic implications. Lithos 179, 193–210.

Lázaro, C., García-Casco, A., Blanco-Quintero, I. F., Rojas-Agramonte, Y., Corsini, M., Proenza, J. A., 2015. Did the Turonian–Coniacian plume pulse trigger subduction initiation in the Northern Caribbean? Constraints from 40Ar/39Ar dating of the Moa-Baracoa metamorphic sole (eastern Cuba). International Geology Review 57, 919-942,

Lázaro, C., Blanco-Quintero, I. F., Proenza, J. A., Rojas-Agramonte, Y., Neubauer, F., Núñez-Cambra, K., García-Casco, A., 2016. Petrogenesis and 40Ar/39Ar dating of proto-forearc crust in the Early Cretaceous Caribbean arc: The La Tinta mélange (eastern Cuba) and its easterly correlation in Hispaniola. International Geology Review 58(8), 1020-1040.

Le Maître, R.W., Streckeisen, A., Zanettin, B., Le Bas, M.J., Bonin, B., Bateman, P., Bellieni, G., Dudeck, A., Efremova, S., Keller, J., Lameyre, J., Sabine, P.A., Schmid, R., Sorensen, H., Woolley, A.R., 2002. Igneous rocks. A Classification and Glossary of Terms: Recommendations of the International Union of Geological Sciences Subcommission on the Systematics of Igneous Rocks. Cambridge, 2nd Edition, Cambridge University Press, 252p.

Leake B.E., Woolley A.R., Birch W.D., Burke E.A.J., Ferraris G., Grice J.D., Hawthorne F.C., Kisch H.J., Krivovichev V.G., Schumacher J.C., Stephenson N.C.N., Whittaker E.J.W., 1997. Report.

Nomenclature of amphiboles: report of the subcommittee on amphiboles of the international mineralogical association commission on new minerals and mineral names. Mineralogical magazine, 61(2), 295-321.

Lee, C.-T.A., Brandon, A.D., Norman, M., 2003. Vanadium in peridotites as a proxy of Paleo-ƒO2 during partial melting: prospects, limitations and implications. Geochimica et Cosmochimica Acta 67, 3045–3064.

Li, Z.-X.A., Lee, C.-T.A., 2006. Geochemical investigation of serpentinized oceanic lithospheric mantle in the Feather River Ophiolite, California: implications for the recycling rate of water by subduction. Chemical Geology 235, 161–185.

Li, Z.H., Liu, M.Q., Gerya, T., 2015. Material transportation and fluid-melt activity in the subduction channel: Numerical modeling. Science China Earth Sciences 58 (8), 1251-1268.

Liu, C-Z., Snow, J.E., Brügmann, G., Hellebrand, E., Hofmann, A.W., 2009. Non-chondritic HSE budget in Earth's upper mantle evidenced by abyssal peridotites from Gakkel ridge (Arctic Ocean). Earth and Planetary Science Letters 283, 122–132.

Lorand, J-P., Alard, O., Luguet, A., Keays, R.R., 2003. Sulfur and selenium systematics of the subcontinental lithospheric mantle: inferences from the Massif Central xenolith suite (France). Geochimica et Cosmochimica Acta 67, 4137–4151.

Lorand, J-P., Alard, O., 2010. Determination of selenium and tellurium concentrations in Pyrenean peridotites (Ariege, France): new insight into S/Se/Te systematics of the upper in mantle samples. Chemical Geology 278, 120–130.

Luguet, A., Lorand, J-P., Seyler, M., 2003. Sulfide petrology and highly siderophile element geochemistry of abyssal peridotites: a coupled study of samples from the Kane Fracture Zone (45°W 23°20 N, MARK Area, Atlantic Ocean). Geochimica et Cosmochimica Acta 67, 1553–1570.

Lund, M.G., Austrheim, H., 2003. High-pressure metamorphism and deep-crustal seismicity: evidence from contemporaneous formation of pseudotachylytes and eclogite facies coronas. Tectonophysics 372, 59–83.

Maekawa, H., Shozui, M., Ishii, T., Fryer, P., Pearce, J.A., 1993. Blueschist metamorphism in an active subduction zone. Nature 364 (6437), 520-523.

Malaspina, N., Hermann, J., Scambelluri, M., 2009. Fluid/mineral interaction in UHP garnet peridotite. Lithos 107, 38–52.

Manning, C.E., 1998. Fluid composition at the blueschist-eclogite transition in the model system Na_2O-MgO-Al_2O_3-SiO_2-H_2O-HCl. Schweizerische Mineralogische und Petrographische Mitteilungen 78 (2), 225–242.

Manning, C.E., 2004. The chemistry of subduction-zone fluids. Earth and Planetary Science Letters 223, 1–16.

Marchesi, C., Garrido, C.J., Godard, M., Proenza, J.A., Gervilla, F., Blanco-Moreno, J., 2006. Petrogenesis of highly depleted peridotites and gabbroic rocks from the Mayarí-Baracoa Ophiolitic Belt (eastern Cuba). Contributions to Mineralogy and Petrology 151, 717–736.

Marchesi, C., Garrido, C.J., Bosch, D., Proenza, J.A., Gervilla, F., Monie, P., Rodriguez-Vega, A., 2007. Geochemistry of Cretaceous magmatism in eastern Cuba: Recycling of North American continental sediments and implications for subduction polarity in the Greater Antilles Paleo-arc. Journal of Petrology 48, 1813–1840.

Marchesi, C., Jolly, W.T., Lewis, J.F., Garrido, C.J., Fernandez, J.P., Lidiak, E.G., 2011. Petrogenesis of fertile mantle peridotites from the Monte del Estado massif (Southwest Puerto Rico): a preserved section of Proto-Caribbean lithospheric mantle?. Geologica Acta 9(3-4), 289-306.

Marchesi, C., Garrido, C. J., Harvey, J., González-Jiménez, J. M., Hidas, K., Lorand, J. P., Gervilla, F., 2013a. Platinum-group elements, S, Se and Cu in highly depleted abyssal peridotites from the Mid-Atlantic Ocean Ridge (ODP Hole 1274A): influence of hydrothermal and magmatic processes. Contributions to Mineralogy and Petrology 166(5), 1521-1538.

Marchesi, C., Garrido, C.J., Padrón-Navarta, J.A., López Sánchez-Vizcaíno, V., Gómez-Pugnaire, M.T., 2013b. Element mobility from seafloor serpentinization to highpressure dehydration of antigorite in subducted serpentinites: insights from the Cerro del Almirez ultramafic massif (southern Spain). Lithos 178, 128-142.

Maresch, W.V., Schertl, H. P., Krebs, M., Baese, M., Draper, G., 2008. Jadeitite from the Rio San Juan Complex, northern Dominican Republic. Abstracts and Program 18th Caribbean Geological Conference, 63-64.

Marschall, H. R., Schumacher, J. C., 2012. Arc magmas sourced from mélange diapirs in subduction zones. Nature Geoscience 5(12), 862-867.

Martin, C., Flores, K. E., Harlow, G. E., 2016. Boron isotopic discrimination for subduction-related serpentinites. Geology G38102-1.

McDonough, W.F., Sun, S.S., 1995. The composition of the Earth: Chemical Geology 120, 223–253.

McInnes, B.I.A., Gregoire, M., Binns, R.A., Herzig, P.M., Hannington, M.D., 2001. Hydrous metasomatism of oceanic sub-arc mantle, Lihir, Papua New Guinea: petrology and geochemistry of fluid-metasomatised mantle wedge xenoliths. Earth and Planetary Science Letters 188, 169–183.

Menant, A., Angiboust, S., Monié, P., Oncken, O., Guigner, J.-M. 2018. Brittle deformation during Alpine basal accretion and the origin of seismicity nests above the subduction interface. Earth and Planetary Science Letters 487, 84-93.

Metcalf, R.V., Shervais, J.W., 2008. Supra-subduction zone ophiolites: Is there really an ophiolite conundrum?, in Wright, J.E., and Shervais, J.W., eds., Ophiolites, Arcs, and Batholiths. Geological Society of America Special Paper 438, 191–222.

Millán, G., Somin, M., 1985. Nuevos aspectos sobre de la estratigrafía del macizo metamórfico de Escambray. Contribución al conocimiento geológico de las metamorfitas del Escambray y Curial. La Habana, Cuba, Instituto de Geología y Paleontología, Reportes de Investigación de la Academia de Ciencias de Cuba 2, 1-74.

Millán, G., 1996a. Metavulcanitas del Purial, in Iturralde-Vinent, M.A., ed., Cuban ophiolites and volcanic arcs: Miami, IGCP Project 364 Special Contribution 1, 218–221.

Millán, G., 1996b. Metamorfitas de la asociación ofiolítica de Cuba, in Iturralde-Vinent, M.A., ed., Ofiolitas y Arcos Volcánicos de Cuba: Miami, Florida, U.S.A. IGCP Project 364 Special Contribution 1, 131–146.

Miller, S.A., van der Zee, W., Olgaard, D.L., Connolly, J.A.D., 2003. A fluid-pressure feedback model of dehydration reactions: experiments, modelling, and application to subduction zones. Tectonophysics 370, 241–251.

Morimoto, N., Fabries, J., Ferguson, A.K., Ginzburg, I.V., Ross, M., Seifert, F.A., Zussman, J., Aoki, K., Gottardi, G., 1988. Nomenclature of pyroxenes. American Mineralogist 73, 1123–1133.

Morishita, T., Arai, S., Ishida, Y., 2007. Trace element compositions of jadeite (+omphacite) in jadeitites from the Itoigawa–Ohmi district, Japan: Implications for fluid processes in subduction zones. Island Arc 16, 40–56.

Mottana, A., 2012. Mineral novelties from America during Renaissance: the “stones” in Hernández’ and Sahag ´ un’s treatises (1576–1577). Rend. Lincei 23:165–86

Müeller, S., Phillips, R.J., 1991. On the initiation of subduction. Journal of Geophysical Research 96, 651–665.

Nelson, D.R., 1997. Compilation of SHRIMP U-Pb zircon geochronology data, 1996. Geological Survey of Western Australia, Record 1997/2, 189 p.

Newton MS, Kennedy GC. 1968. Jadeite, analcime, nepheline and albite at high temperatures and pressures.Am. J. Sci. 266:728–35

Nishiyama, T., Mori, Y., Shigeno, M., 2017. Jadeitites and associated metasomatic rocks from serpentinite mélanges in the Nishisonogi unit, Nagasaki Metamorphic Complex, western Kyushu, Japan: a review. Journal of Mineralogical and Petrological Sciences, 112(5), 197-216.

Niu, Y., 2004. Bulk-rock major and trace element compositions of abyssal peridotites: implications for mantle melting, melt extraction and post-melting processes beneath Mid-Ocean ridges. Journal of Petrology 45 (12), 2423–2458.

Nuñez Cambra, K.E., García-Casco, A., Iturralde-Vinent, M.A., Millán, G., 2004. Emplacement of the ophiolite complex in Eastern Cuba, in 32nd International Geological Congress, 22 C. Session G20.11 Caribbean Plate Tectonics: Florencia, Proceedings, CD-rom.

Oberhänsli, R., Bousquet, R., Moinzadeh, H,. Moazzen, M., Arvin, M., 2007. The field of stability of blue jadeite: a new occurrence of jadeitite at Sorkhan, Iran, as a case study. Canadian Mineralogist 45, 1501–1509.

O'Hanley, D.S., 1996. Serpentinites, records of tectonic and petrological history. Oxford Monographs on Geology and Geophysics no 34.

Padrón-Navarta, J.A., Tommasi, A., Garrido, C.J., Lopez Sanchez V., 2012. Plastic deformation and development of antigorite crystal preferred orientation in high-pressure serpentinites. Earth and Planetary Science Letters 349-350, 75-86.

Padrón-Navarta, J.A., Tommasi, A., Garrido, C.J., Sánchez-Vizcaíno, V.L., Gómez-Pugnaire, M.T., Jabaloy, A., Vauchez, A., 2010. Fluid transfer into the wedge controlled by high-pressure hydrofracturing in the cold top-slab mantle. Earth and Planetary Science Letters 297, 271–286.

Palme, H., Jones, A., 2003. Solar system abundances of the elements, in Davis, A.M., ed., Meteorites, Comets and Planets, Treatise Geochemistry 1: Elsevier, Oxford, 41–61.

Paulick, H., Bach, W., Godard, M., De Hoog, J.C.M., Suhr, G., Harvey, J., 2006. Geochemistry of abyssal peridotites (Mid-Atlantic Ridge, 15°20′N, ODP Leg 209): implications for fluid/rock interaction in slow spreading environments. Chemical Geology 234, 179–210.

Peacock, S.M., 1990. Fluid processes in subduction zones. Science 248, 329–337.

Peacock, S.M., 1993. Large-scale hydration of the lithosphere above subducting slabs. Chemical Geology 108, 49-59.

Peacock, S.M., and Wang, K., 1999. Seismic consequences of warm versus cool subduction zone metamorphism: examples from northeast and southwest Japan Science 286, 937-939.

Pearce, J.A., Barker, P.F., Edwards, S.J., Parkinson, I.J., Leat, P.T., 2000. Geochemistry and tectonic significance of peridotites from the South Sandwich arc-basin system, South Atlantic. Contributions to Mineralogy and Petrology 139, 36-53.

Pearson, D.G., Irvine, G.J., Ionov, D.A., Boyd, F.R., Dreibus, G.E., 2004. Re-Os isotope systematics and platinum group element fractionation during mantle melt extraction: a study of massif and xenolith peridotite suites. Chemical Geology 208, 29–59.

Pennacchioni, G., 1996. Progressive eclogitization under fluid-present conditions of pre-Alpine mafic granulites in the Austroalpine Mt Emilius Klippe (Italian Western Alps). Journal of Structural Geology 18, 549–561.

Penniston-Dorland, S.C., Sorensen, S.S., Ash, R.D., Khadke, S.V., 2010. Lithium isotopes as a tracer of fluids in a subduction zone melange: Franciscan complex, CA. Earth and Planetary Science Letters 292(1-2), 181-190.

Penniston-Dorland, S.C., Gorman, J.K., Bebout, G.E., Piccoli, P.M. Walker, R.J., 2014. Reaction rind formation in the Catalina Schist: Deciphering a history of mechanical mixing and metasomatic alteration. Chemical Geology 384, 47–61.

Perrillat, J.P., Daniel, I., Koga, K.T., Reynard, B., Cardon, H., Crichton, W.A. 2005. Kinetics of antigorite dehydration: a real-time X-ray diffraction study. Earth and Planetary Science Letters 236, 899–913.

Petriglieri, J.R., Bersani, D., Salvioli-Mariani, E., Mantovani, L., Tribaudino, M., Lottici, P.P., Laporte-Magoni, C., 2014. Polymorphs of serpentine identification by means of Raman spectroscopy: 11th GeoRaman Conference (Saint Louis, Missouri, USA; June 15-19), #5064.

Pindell, J.L., Kennan, L., Maresch, W.V., Stanek, K.P., Draper, G., Higgs, R., 2005. Plate-kinematics and crustal dynamics of circum-Caribbean arc-continent interactions: Tectonic controls on basin development in Proto-Caribbean margins. In: Avé Lallemant, H.G. & Sisson, V.B. (eds) Caribbean-South. American Plate Interactions, Venezuela. Geological Society of American Special Papers 394, 7-52.

Pindell, J.L., Kennan, L., Stanek, K.P., Maresch, W.V., Draper, G., 2006. Foundations of Gulf of Mexico and Caribbean evolution: eight controversies resolved. Geologica Acta 4, 303–341.

Pindell, J., and Kennan, L., 2009, Tectonic evolution of the Gulf of Mexico, Caribbean and northern South America in the mantle reference frame: An update, in James, K.H., Lorente, M.A., and Pindell, J.L., eds., The origin and evolution of the Caribbean plate: London, Geological Society, Special Publications, v. 328, p. 1–55.

Pindell, J.L., Maresch, W.V., Martens, U., Stanek, K.P., 2012. The greater antillean arc: Early Cretaceous origin and proposed relationship to Central American subduction mélanges: Implications for models of Caribbean evolution. International Geology Review 54, 131–143.

Plank, T., Langmuir, C. H., 1998. The chemical composition of subducting sediment and its consequences for the crust and mantle. Chemical geology 145(3), 325-394.

Plank, T. The Chemical Composition of Subducting Sediments in Treatise on Geochemistry (2nd, ed. Rudnick, R.L.) 607–629 (Elsevier, Oxford, 2014).

Pogge von Strandmann, P.A.E., Dohmen, R., Marschall, H.R., Schumacher, J.C., Elliott, T., 2015. Extreme magnesium isotope fractionation at outcrop scale records the mechanism and rate at which reaction fronts advance. Journal of Petrology 56, 33–58.

Poli, S., Schmidt, M.W., 2002. Petrology of subducted slabs. Annual Review of Earth and Planetary Sciences 30, 207-235.

Pouchou, L. J. Pichoir, F., 1984. New model quantitative x-ray microanalysis, 1. Application to the analysis of homogeneous samples, Rech. Aerosp., 3, 13-38.

Proenza, J., Gervilla, F., Melgarejo, J.C., Bodinier, J.L., 1999. Al- and Cr-rich chromitites from the Mayari-Baracoa ophiolitic belt (eastern Cuba); consequence of interaction between volatile-rich melts and peridotites in suprasubduction mantle. Economic Geology 94, 547–566.

Proenza, J.A., Díaz-Martínez, R., Iriondo, A., Marchesi, C., Melgarejo, J.C., Gervilla, F., Garrido, C.J., Rodríguez-Vega, A., Lozano-Santacruz, R., Blanco-Moreno, J.A., 2006. Primitive island-arc Cretaceous volcanic rocks in eastern Cuba: The Téneme Formation. Geologica Acta 4, 103–121.

Pushcharovsky, Y., ed., 1988, Mapa geológico de la República de Cuba escala 1:250 000. Havana, Cuba/Moscow, USSR: Academy of Sciences of Cuba and Academy of Sciences of USSR.

Randive, K. R., Korakoppa, M. M., Muley, S. V., Varade, A. M., Khandare, H. W., Lanjewar, S. G., Tiwari R.R., Aradhi, K. K., 2015. Paragenesis of Cr-rich muscovite and chlorite in green-mica quartzites of Saigaon–Palasgaon area, Western Bastar Craton, India. Journal of earth system science, 124(1), 213-225.

Ranero, C. R., Morgan, J. P., McIntosh, K., Reichert, C., 2003. Bending-related faulting and mantle serpentinization at the Middle America trench. Nature 425(6956), 367-373.

Rinaudo, C., Gastaldi, D., 2003. Characterization of chrysotile, antigorite and lizardite by FT-Raman spectroscopy. Canadian Mineralogist 41, 883-890.

Rojas-Agramonte, Y., Kröner, A., García-Casco, A., Iturralde-Vinent, M.A., Somin, M., Mattinson, J.M., Millán Trujillo, G., Sukar, K., Pérez Rodríguez, M., Wingate, M.T.D., 2011. Timing and evolution of Cretaceous island arc magmatism in Central Cuba: Implications for the history of arc systems in the Northwestern Caribbean. The Journal of Geology 119, 619-640.

Rojas-Agramonte, Y., García-Casco, A., Kemp, A., Kröner, A., Proenza J.A., Lázaro, C., Liu D., 2016. Recycling and transport of continental material through the mantle wedge above subduction zones: A Caribbean example. Earth and Planetary Science Letters 436, 93-107.

Robertson EC, Birch F, MacDonald GJF. 1957. Experimental determination of jadeite stability relations to 25,000 bars. Am. J. Sci. 255:115–37

Roy R, Tuttle OF. 1956. Investigations under hydrothermal conditions. Phys. Chem. Earth 1:138–80.

Rüpke, L.H., Morgan, J.P., Hort, M., Connolly, J.A.D., 2002. Are the regional variations in Central American arc lavas due to differing basaltic versus peridotitic slab sources of fluids?. Geology 30, 1035-1038.

Saumur, B.M., Hattori, K.H., and Guillot, S., 2010. Contrasting origins of serpentinites in a subduction complex, northern Dominican Republic. Geological Society of America Bulletin 122 292–304.

Savov I. P., Ryan J. G., D'antonio M., Kelley K., Mattie P., 2005. Geochemistry of serpentinized peridotites from the Mariana Forearc Conical Seamount, ODP Leg 125: Implications for the elemental recycling at subduction zones. Geochemistry Geophysics Geosystems 6, Q04J15.

Savov I. P., Ryan J. G., D'antonio M., Fryer P., 2007, Shallow slab fluid release across and along the Mariana arc-basin system: Insights from geochemistry of serpentinized peridotites from the Mariana fore arc: Journal of Geophysical Research, v. 112, B09205.

Scambelluri, M., Rampone, E., Piccardo, G.B., 2001. Fluid and element cycling in subducted serpentinite: A trace-element study of the Erro-Tobbio high-pressure ultramafites (Western Alps, NW Italy). Journal of Petrology 42, 55-67.

Scambelluri, M., Fiebig, J., Malaspina, N., Müntener, O., Pettke, T., 2004. Serpentinite subduction: implications for fluid processes and trace-element recycling. International Geology Review 46, 595–613.

Scambelluri, M., Müntener, O., Ottolini, L., Pettke, T.T., Vannucci, R., 2004. The fate of B, Cl and Li in the subducted oceanic mantle and in the antigorite-breakdown fluids. Earth and Planetary Science Letters 222, 217-234.

Schertl, H.P., Maresch, W.V., Krebs, M., Draper, G., 2007. The Rio San Juan serpentinite complex and its jadeitites (Dominican Republic). In: Martens U, García-Casco A (eds) High-pressure belts of Central Guatemala: the Motagua suture and the Chuacús Complex. IGCP 546 Special Contribution 1.

Schertl, H.-P., Maresch, W.V., Stanek, K.P., Hertwig, A., Krebs, M., Baese, R., Sergeev, S.S., 2012. New occurrences of jadeitite, jadeite quartzite and jadeite-lawsonite quartzite in the Dominican Republic, Hispaniola: Petrological and geochronological overview. European Journal of Mineralogy 24, 199-216.

Schmidt, M.W., Poli, S., 1998. Experimentally based water budgets for dehydrating slabs and consequences for arc magma generation. Earth and Planetary Science Letters 163, 361–379.

Schmidt, M.W., Poli, S., 2013. Devolatilization During Subduction, in Holland, H., and Turekian, K., "Treatise on Geochemistry" (Second Edition): Elsevier. Amsterdam, v. 4, p. 669-701.

Schneider, M.E., Eggler, D.H., 1986. Fluids in equilibrium with peridotite minerals: implications for mantle metasomatism. Geochimica et Cosmochimica Acta 50, 711–724.

Schwartz, S., Guillot, S., Reynard, B., Lafay, R., Debret, B., Nicollet, C., Lanari, P., Auzende, A. L., 2013. Pressure–temperature estimates of the lizardite/antigorite transition in high pressure serpentinites. Lithos 178, 197-210.

Searle, M.P., Cox, J., 2002. Subduction zone metamorphism during formation and emplacement of the Semail ophiolite in the Oman Mountains. Geological Magazine 139, 241–255.

Shervais, J.W., 2001. Birth, death, and resurrection: The life cycle of suprasubduction zone ophiolites. Geochemistry Geophysics Geosystems 2, GC000080.

Shervais, J.W., Choi, S.H., Sharp, W.D., Ross, J., Zoglman-Schuman, M., Mukasa, S.B., 2011. Serpentinite matrix mélange: Implications of mixed provenance for mélange formation, in Wakabayashi, J., and Dilek, Y., eds., Mélanges: Processes of Formation and Societal Significance. Geological Society of America Special Paper 480, 1–30.

Shervais, J. W., Choi, S. H., 2012. Subduction initiation along transform faults: The proto-Franciscan subduction zone. Lithosphere 4(6), 484-496.

Shreve, R. L., and M. Cloos, 1986. Dynamics of sediment subduction, melange formation, and prism accretion, Journal of Geophysical Research 91(B10), 10229–10245.

Shigeno, M., Mori, Y., Shimada, K., Nishiyama, T., 2012. Jadeitites with metasomatic zoning from the Nishisonogi metamorphic rocks, Western Japan: fluid–tectonic block interaction during exhumation. European Journal of Mineralogy 24, 289–311.

Solari, L.A., García-Casco, A., Martens, U., Lee, J.K.W., Ortega-Rivera, A., 2013. Late Cretaceous subduction of the continental basement of the Maya block (Rabinal Granite, central Guatemala): Tectonic implications for the geodynamic evolution of Central America. Bulletin of the Geological Society of America 125, 625-639.

Somin, M.L., Millán, G., 1981. Geology of the Metamorphic Complexes of Cuba: Moscow, Russia, Nauka, 219 p.

Sorensen, S., Harlow, G.E., Rumble, D.III., 2006. The origin of jadeitite forming subduction-zone fluids: CL-guided SIMS oxygen isotope and trace-element evidence. American Mineralogist 91, 979–996.

Sorensen, S.S., Sisson, V.B., Harlow, G.E., Avé Lallemant, H.G., 2010. Element residence and transport during subduction-zone metasomatism: evidence from a jadeitite-serpentinite contact, Guatemala. International Geology Review 52(9), 899-940.

Soustelle, V., Tommasi, A., Demouchy, S., Ionov, D., 2010. Deformation and fluid–rock interactions in the supra-subduction mantle: microstructures and water contents in peridotite xenoliths from the Avacha Volcano, Kamchatka. Journal of Petrology 51, 363–394.

Spandler, C.,Hermann, J., Faure, K., Mavrogenes, J.A., Arculus, R.J., 2008. The importance of talc and chlorite “hybrid” rocks for volatile recycling through subduction zones; evidence from the high-pressure subduction mélange of New Caledonia. Contributions to Mineralogy and Petrology 155, 181–198.

Spear, F.S., 1995. Metamorphic Phase Equilibria and Pressure-Temperature-Time Paths: Mineralogical Society of America, Washington, D.C. 2nd Print corrected edition, 799 p.

Stern, R.J., 2002. Subduction zones. Reviews of Geophysics 40, 1012. doi:10.1029/2001RG000108.

Stern, R.J., 2004. Subduction initiation: Spontaneous and induced. Earth and Planetary Science Letters 226, 275-292

Stern, R.J., Reagan, M., Ishizuka, O., Ohara, Y., Whattam, S., 2012. To understand subduction initiation, study forearc crust: To understand forearc crust, study ophiolites. Lithosphere 4, 469-483.

Sun, S. S., and McDonough, W., S., 1989. Chemical and isotopic systematics of oceanic basalts: implications for mantle composition and processes. Geological Society, London, Special Publications, 42(1), 313-345.

Tatsumi, Y., 2005. The subduction factory: how it operates in the evolving Earth. GSA Today 15 (7), 4–10.

Tenthorey, E., Cox, S.F., 2003. Reaction-enhanced permeability during serpentinites dehydration. Geology 31, 921–924.

Tenthorey, E., Hermann, J., 2004. Composition of fluids during serpentinite breakdown in subduction zones; evidence for limited boron mobility. Geology 32, 865-868.

Thompson, J.B. Jr., 1982. Composition space: An algebraic and geometric approach, in Ferry, J.M., ed., Characterization of metamorphism through mineral equilibria. Mineralogical Society of America, Reviews in Mineralogy 10, 1-31.

Toriumi, M., Hara, E., 1995. Crack geometries and deformation by the crack-seal mechanism in the Sambagawa metamorphic belt. Tectonophysics 245, 249–261.

Torres-Roldán, R.L., García-Casco, A., García-Sánchez, P.A., 2000. CSpace: An integrated workplace for the graphical and algebraic analysis of phase assemblages on 32-bit Wintel platforms. Computers and Geosciences 26, 779-793.

Torró, L., Garcia-Casco, A., Proenza, J. A., Blanco-Quintero, I. F., Gutiérrez-Alonso, G., Lewis, J. F., 2016. High-pressure greenschist to blueschist facies transition in the Maimón Formation (Dominican Republic) suggests mid-Cretaceous subduction of the Early Cretaceous Caribbean arc. Lithos 266, 309-331.

Torró, L., Proenza, J. A., Marchesi, C., Garcia-Casco, A., Lewis, J. F., 2017. Petrogenesis of meta-volcanic rocks from the Maimón Formation (Dominican Republic): Geochemical record of the nascent Greater Antilles paleo-arc. Lithos 278, 255-273.

Tsujimori T., Liou J.G., Wooden J., Miyamoto T., 2005a. U–Pb dating of large zircons in low-temperature jadeitite from the Osayama serpentinite mélange, SW Japan: insights into the timing of serpentinization. International Geology Review 47, 1048–1057.

Tsujimori, T., Liou, J.G., Coleman, R.G. 2005b. Coexisting retrograde jadeite and omphacite in a jadeite-bearing lawsonite eclogite from the Motagua Fault Zone, Guatemala. American Mineralogist 90, 836-842.

Tsujimori, T., Sisson, V. B., Liou, J. G., Harlow, G.E., Sorensen, S.S., 2006. Petrologic characterization of Guatemalan lawsonite eclogite: Eclogitization of subducted oceanic crust in a cold subduction zone. Geological Society of America Special Papers 403, 147-168.

Tsujimori, T., Harlow, G.E. 2012. Petrogenetic relationships between jadeitite and associated highpressure and low-temperature metamorphic rocks in worldwide jadeitite localities: a review. European Journal of Mineralogy 24, 371–390.

Ulmer, P., Trommsdorff, V., 1995. Serpentine stability to mantle depths and subduction-related magmatism. Science 268, 858-861.

Van Hinsbergen, D.J.J., Iturralde-Vinent, M.A., Van Geffen, P.W., García-Casco, A., Van Benthem, S., 2009. Structure of the accretionary prism, and the evolution of the Paleogene northern Caribbean subduction zone in the region of Camagüey, Cuba. Journal of Structural Geology 31, 1130-1144.

Vils, F., Pelletier, L., Kalt, A., Müntener, O., Ludwig,T., 2008. The lithium, boron and beryllium content of serpentinized peridotites from ODP Leg 209 (Sites 1272A and 1274A): implications for lithium and boron budgets of oceanic lithosphere. Geochimica et Cosmochimica Acta 72, 5475-5504.

Vils, F., Müntener, O., Kalt, A., Ludwig, T., 2011. Implications of the serpentine phase transition on the behaviour of beryllium and lithium–boron of subducted ultramafic rocks. Geochimica et Cosmochimica Acta 75, 1249-1271.

Vinograd, V.L., 2002. Thermodynamics of mixing and ordering in the diopside-jadeite system: I. A CVM model. Mineralogical Magazine 66, 513−536.

Vrijmoed, J.C., Van Roermund, H.L.M., Davis, G.R., 2006. Evidence for diamond-grade ultra-high pressure metamorphism and fluid interaction in the Svartberget Fe–Ti garnet peridotite–websterite body, Western Gneiss Region, Norway. Mineralogy and Petrology 88, 381–405.

Vrijmoed, J.C., Smith, D.C., Van Roermund, H.L.M., 2008. Raman confirmation of microdiamond in the Svartberget Fe–Ti type garnet peridotite, Western Gneiss Region, Western Norway. Terra Nova 20, 295–301.

Wadge, G., Draper, G., Lewis, J.F., 1984. Ophiolites of the northern Caribbean: A reappraisal of their roles in the evolution of the Caribbean plate boundary, in Gass, I.G., Lippard, S.J., and Shelton, A.W., eds., Ophiolites and 1335 Oceanic Lithosphere. Oxford, UK, Blackwell Scientific Publications 367–380.

Wakabayashi, J., 2012. Subducted sedimentary serpentinite mélanges: Record of multiple burial–exhumation cycles and subduction erosion. Tectonophysics 568, 230-247.

Wakabayashi, J., 2015. Anatomy of a subduction complex: Architecture of the Franciscan Complex, California, at multiple length and time scales. International Geology Review 57(5-8), 669-746.

Wang, J., Hattori, K.H., Stern, C., 2008. Metasomatic origin of garnet orthopyroxenites in the subcontinental lithospheric mantle underlying Pali Aike volcanic field, southern South America. Mineralogy and Petrology 94, 243–258.

Whattam, S.A., and Stern, R.J., 2015. Late Cretaceous plume-induced subduction initiation along the southern margin of the Caribbean and NW South America: The first documented example with implications for the onset of plate tectonics. Gondwana Research 27, 38–63.

Whitney, D.L., Evans, B.W., 2010. Abbreviations for names of rock-forming minerals. American Mineralogist 95, 185–187.

Williams, I.S., 1998. U–Th–Pb geochronology by ion microprobe. in McKibben, M. A., Shanks III, W. C., Ridley, W .I., editors, Applications of microanalytical techniques to understanding mineralizing processes. Reviews in Economic Geology 7, 1–35.

Wilshire, H.G., Kirby, S.H., 1989. Dikes, joints, and faults in the upper mantle. Tectonophysics 161, 23–31.

Workman, R. K., Hart, S. R., 2005. Major and trace element composition of the depleted MORB mantle (DMM). Earth and Planetary Science Letters, 231(1), 53-72.

Wunder, B., Schreyer, W., 1997. Antigorite: High-pressure stability in the system MgO-SiO2-H2O (MSH). Lithos 41, 213–227.

Wunder, B., Wirth, R., Gottschalk, M., 2001. Antigorite: Pressure and temperature dependence of polysomatism and water content. European Journal of Mineralogy 13, 485-495.

Yamamoto, K., Asahara, Y., Maekawa, H., and Sugitani, K., 1995, Origin of blueschist-facies clasts in the Mariana forearc, western Pacific: Geochemical Journal, v. 29, p. 259-275.

Yui, T.F., Kenshi, M., Tadashi, U., Ching-Ying, L., Uwe Martens, Chao-Ming, W., Tsai-Way, W., Liou, J.G., 2010. Genesis of Guatemala jadeitite and related fluid characteristics: Insight from zircon. Chem. Geol., 270, 45-55.

Zheng, Y. F., Zhou, J. B., Wu, Y. B., Xie, Z., 2005. Low-grade metamorphic rocks in the Dabie-Sulu orogenic belt: A passive-margin accretionary wedge deformed during continent subduction. International Geology Review 47(8), 851-871.

9 Supplementary Tables

Supplementary Table 1 Microtextural and mineral composition of samples from the Sierra del Convento and La Corea mélanges used in this study. For mineralogical details from La Corea mélange see Blanco-Quintero et al., (2011d).

Samples	Microtextures	Atg	Atg/Lz mixtures(*)	Chl	Tlc	Tr (Anth)	Di	Dol/Mst	Mag + Fe-Chromite	Brucite
09-SC-3g	Deformed	97%		X					X	
09-SC-3h	Mesh	96%		X					X	
09-SC-6a	Mesh	98%		X					X	
09-SC-6c	Mesh	97%		X	X				X	
09-SC-7f	Mesh	93%		X	X				5%	
09-SC-7k	Mesh+Bastite	95%		X	X	(X)		X	X	
09-SC-8aX	Mesh+Bastite	85%		X	10%				X	
09-SC-9d	Mesh+Bastite	96%		X		X	X		X	
09-SC-27t	Mesh	93%		X		X		5%	X	
09-SC-27u	Mesh	96%		X				X	X	
09-SC-31b	Mesh	95%		X		X			X	
09-SC-31k	Mesh deformed	96%		X					X	
09-SC-33b	Mesh	93%		X		X		5%	X	
MCB-2f	Mesh+Bastite	80%		X	10%	5%			X	
LC-G-4*	nonpseudomorphic textures	95%		X	X			X	X	
LC-M-17*	nonpseudomorphic textures	95%		X	X			X	X	
LC-55*	nonpseudomorphic textures	85%		X	10%			X	X	
LC-56*	nonpseudomorphic textures	95%		X	X			X	X	
LC-58*	nonpseudomorphic textures	96%		X	X			X	X	
LC-66*	Mesh+Bastite	50%	X	X					X	x
LC-88*	Mesh+Bastite	48%	16%	10%			18%		8%	
LC-97*	Mesh+Bastite	49%	X	X					X	x

x: present in the sample (4-1%)

(*) Data in Blanco-Quintero et al., 2011d

Supplementary Table 2. Major and trace element data from serpentinite samples from the Sierra del Convento mélange.

Sample	09-SC-3g	09-SC-3h	09-SC-6a	09-SC-6c	09-SC-7f	09-SC-7k	09-SC-8a X	09-SC-9d	09-SC-27t	09-SC-27u	09-SC-31b	09-SC-31k	09-SC-33b	MCB-2f
Major elements (wt%)														
SiO_2	41.34	42.52	42.3	42.54	42.26	41.36	42.79	42.32	40.39	41.54	42.38	40.17	40.27	45.5
TiO_2	0.09	0.03	0.02	0.05	0.02	0.12	0.03	0.1	0.04	0.03	0.05	0.06	0.08	0.16
Al_2O_3	2.67	1.41	1.67	2.06	1.56	2.86	2.79	2.5	2.39	2.41	2.79	2.28	2.52	3.28
FeO_{tot}	8.18	8.42	7.98	7.92	6.79	8.06	8.7	7.83	7.45	7.97	7.32	7.84	6.48	7.41
MnO	0.14	0.15	0.13	0.13	0.13	0.11	0.14	0.13	0.11	0.12	0.12	0.12	0.09	0.12
MgO	35.28	35.42	35.93	36.1	37.13	35.48	33.75	34.88	35.3	35.86	35.15	37.38	37.09	32.78
CaO	0.05	0.07	0.03	0.05	0.02	0.16	0.08	0.48	1.1	0.4	0.66	0.01	0.18	0.33
Na_2O	0	0	0	0	0	0	0	0	0	0	0	0	0	0
K_2O	0	0	0	0	0	0	0	0	0	0	0	0	0	0
P_2O_5	0.01	0.01	0.01	0.01	0.01	0.01	0.01	0.02	0.01	0.01	0.01	0.01	0	0.01
LOI	11.45	11.28	11.55	11.28	11.79	11.47	10.76	11.09	12.36	11.95	10.87	11.59	0.01	9.69
Total	99.21	99.31	99.62	100.14	99.71	99.63	99.04	99.34	99.15	100.29	99.35	99.46	99.28	100.1
Trace elements (ppm)														
Li	0.87	2.34	0.34	1.22	0.67	0.76	1.18	0.67	0.14	0.47	0.66	0.13	0.03	0
Rb	0.09	0.06	0.19	0.5	0.11	0.07	0.09	0.14	0.06	0.09	0.79	0.22	0.08	0.1
Cs	0.02	0.03	0.05	0.12	0.04	0.03	0.04	0.04	0.03	0.07	0.12	0.07	0.04	0.03
Be	0.03	0	0	0	0.16	0.31	0.01	0.18	0.07	0.01	0.1	0.01	0.23	0
Sr	1.57	2.04	2.85	5.12	1.14	6.06	3.71	4.99	5.65	2.21	9.78	2.3	6.39	17.28
Ba	1.36	1.86	22.51	5.93	1.84	15.99	6.98	8.56	5.92	2.2	12.42	7.31	5.46	270.59
Sc	8.99	2.83	5.57	7.32	7.36	12.99	7.68	10.02	10.91	7.37	16.78	14.34	12.7	10.73
V	53.85	32.47	34.22	41.18	39.84	65.41	64.1	62.59	50.8	51.09	72.13	66.66	59.65	58.93
Cr	1916.87	1921	2045.74	1932.17	2065.37	1944.34	2262.95	2292.48	1942.74	1656.37	2423.79	3126.14	2058.77	2072.54
Co	85.41	94.84	94.54	103.43	77.62	91.07	85.85	89.48	92.81	95.05	120.41	123.23	101.15	104.92
Ni	1580.2	1636.85	1866.93	1818.24	1640.3	1703.99	1534.56	1660.49	1764.18	1833.9	2084.92	2171	1812.71	1911.01
Cu	9.25	11.75	10.28	8.18	3.54	22.98	2.52	18.97	1.76	12.87	7.93	11.46	9.68	27.16
Zn	54.25	58.58	54.53	48.56	38.14	45.67	56.03	40.19	35.4	43.29	49.88	46.52	33.12	49.25
Ga	3.79	2.67	2.79	3.09	1.51	3.53	3.57	2.93	2.54	2.96	4.99	2.6	2.24	4.93
Y	1.3	1.94	1.89	1.83	1.51	2.36	1.43	2.11	1.8	1.36	2.53	1.42	1.03	2.17
Nb	0.18	0.26	20.35	0.29	0.05	0.19	0.27	0.2	0.12	0.09	2.24	0.47	0.1	0.25
Ta	0.09	0.09	1.21	0.16	0.08	0.07	0.13	0.14	0.07	0.1	0.39	0.26	0.14	0.09
Zr	8	6.3	5.9	9.6	6.2	8.4	7.8	7.1	5.5	4.9	12.6	7.2	6.7	7.2
Hf	0.02	0.05	0.04	0.04	0.08	0.04	0	0.05	0.04	0.01	0.1	0	0.05	0.03
Mo	1.35	1.13	1.35	2.66	1.69	1.31	0.72	1.94	1.2	2.2	0.68	1.55	1.64	1.16
Sn	0	0.03	0.11	0.35	0.04	0.05	0.15	0	0	0.26	0.57	0.38	0	0
Tl	0	0	0.02	0	0	0	0	0	0	0	0.01	0.01	0	0.02
Pb	0.31	0.15	0.41	1.92	0.04	1	1.69	0.36	0.41	0.03	1.49	0.56	0.33	0.42
U	0.01	0.05	0.04	0.05	0.01	0.02	0.03	0.05	0.01	0.02	0.05	0.01	0.01	0.01
Th	0.01	0.2	0.07	0.12	0	0	0.1	0.04	0.01	0.03	0.75	0.11	0	0.01
La	0.16	0.24	0.35	0.37	0.03	0.34	0.42	0.42	0.25	0.18	0.43	0.05	0.06	0.11

Sample	09-SC-3g	09-SC-3h	09-SC-6a	09-SC-6c	09-SC-7f	09-SC-7k	09-SC-8a X	09-SC-9d	09-SC-27t	09-SC-27u	09-SC-31b	09-SC-31k	09-SC-33b	MCB-2f
Ce	0.47	0.79	1.01	0.97	0.14	0.78	0.89	1.05	0.51	0.39	1.01	0.16	0.16	0.38
Pr	0.08	0.14	0.16	0.18	0.03	0.13	0.12	0.15	0.07	0.06	0.13	0.03	0.03	0.07
Nd	0.39	0.84	0.79	0.78	0.18	0.75	0.56	0.65	0.4	0.27	0.6	0.16	0.1	0.32
Sm	0.19	0.26	0.27	0.28	0.09	0.21	0.15	0.19	0.12	0.11	0.22	0.07	0.05	0.15
Eu	0.03	0.06	0.06	0.08	0.05	0.05	0.04	0.04	0.05	0.02	0.05	0.03	0.01	0.02
Gd	0.21	0.39	0.31	0.31	0.17	0.3	0.19	0.27	0.2	0.21	0.28	0.12	0.08	0.23
Tb	0.04	0.06	0.05	0.05	0.03	0.05	0.03	0.05	0.04	0.03	0.06	0.02	0.02	0.05
Dy	0.24	0.35	0.33	0.32	0.25	0.36	0.22	0.33	0.26	0.22	0.41	0.19	0.15	0.34
Ho	0.06	0.07	0.07	0.07	0.07	0.08	0.06	0.08	0.07	0.05	0.09	0.05	0.04	0.08
Er	0.16	0.21	0.19	0.2	0.21	0.24	0.2	0.25	0.19	0.12	0.28	0.15	0.12	0.25
Tm	0.02	0.03	0.03	0.03	0.03	0.04	0.03	0.04	0.04	0.02	0.05	0.03	0.02	0.04
Yb	0.14	0.18	0.16	0.19	0.23	0.23	0.18	0.23	0.19	0.12	0.34	0.16	0.12	0.28
Lu	0.02	0.02	0.02	0.03	0.03	0.03	0.03	0.04	0.03	0.01	0.05	0.02	0.01	0.04

Supplementary Table 3. Trace element data of La Corea mélange serpentinite samples (for major elements, see Blanco-Quintero et al., 2011d).

Sample	LC-M-17	LC-G-4	LC55	LC56	LC58	LC66	LC88	LC97
Li	0	0.5	0.1	0.05	0	0.13	0.18	0.42
Rb	0	0	0.09	0.12	0.01	0.23	0.1	0.28
Cs	0.02	0.21	0.26	0.31	0.27	0.3	0.3	0.41
Be	0	0.01	0.05	0.07	0.02	0.06	0.07	0.03
Sr	29.15	36.55	57.44	0	16.67	2.16	3.1	5.62
Ba	2.59	3.93	5.75	3.06	6.5	4.95	1.46	2.81
Sc	6.45	8.75	0	0	0	0	0	0
V	40.89	59.79	46.7	53.51	49.62	50.57	58.06	55.27
Cr	1810.87	2126.38	1997.79	2136.66	1732.34	1929.78	2130.44	2072.27
Co	88.75	97.7	93.59	74.98	83.84	93.66	85	93.87
Ni	1648.33	1869.08	1757.31	1349.06	1961.92	1785.51	1587.33	1678.94
Cu	11.66	23.44	13.55	10.23	7.98	7.62	11.27	7.64
Zn	28.77	48.84	30.17	41.3	37.26	33.52	37.71	60.62
Ga	1.56	2.4	2.01	2.94	1.85	2.2	2.15	1.91
Y	1.27	1.08	1.21	0.29	0.69	1.55	2.17	2.95
Nb	0.09	0.12	0.07	0.07	0.09	0.07	0.05	0.05
Ta	0.05	0.06	0.05	0.05	0.03	0.06	0.04	0.04
Zr	5.6	6.4	7.5	7	7	6.5	9.3	7.7
Hf	0.03	0	0.01	0.01	0.01	0.05	0.09	0.1
Mo	0.15	0.66	0.84	0.52	0.27	0.53	0.43	0.57
Sn	0	0	0.14	0.03	0.16	0.15	0.1	0.15
Tl	0	0.04	0.01	0	0	0.01	0	0
Pb	0	0	0.05	0	0	0	0	0
U	0.01	0.02	0.01	0.02	0.03	0	0	0
Th	0.01	0.02	0.02	0.02	0.01	0.03	0.01	0.02
La	0.13	0.18	0.11	0.07	0.11	0.11	0.07	0.12
Ce	0.34	0.41	0.31	0.11	0.23	0.22	0.25	0.42
Pr	0.05	0.07	0.05	0.02	0.04	0.04	0.08	0.09
Nd	0.21	0.29	0.32	0.15	0.2	0.21	0.42	0.46
Sm	0.07	0.08	0.11	0.04	0.08	0.11	0.17	0.26
Eu	0.04	0.03	0.03	0.01	0.02	0.03	0.08	0.08
Gd	0.12	0.14	0.15	0.04	0.1	0.18	0.31	0.39
Tb	0.02	0.03	0.03	0.01	0.02	0.03	0.06	0.07
Dy	0.17	0.18	0.19	0.04	0.1	0.21	0.38	0.45
Ho	0.04	0.04	0.05	0.01	0.03	0.05	0.09	0.1
Er	0.12	0.11	0.14	0.04	0.07	0.16	0.23	0.3
Tm	0.02	0.02	0.02	0.01	0.01	0.02	0.04	0.05
Yb	0.16	0.12	0.16	0.05	0.07	0.17	0.2	0.31
Lu	0.02	0.02	0.03	0.01	0.01	0.03	0.03	0.04

Supplementary Table 4. Platinum group elements content from representative serpentinite samples of the Sierra del Convento mélange (for La Corea mélange, see Blanco-Quintero et al., 2011d).

Sample	09-SC-9d	09-SC-7k	09-SC-31k	09-SC-27t	09-SC-8a
Os	2	3	3	1	2
Ir	3	3	3	3	4
Ru	6	6	7	6	9
Rh	1	2	1	1	2
Pt	7	10	7	5	10
Pd	8	9	6	2	9
Total	27	33	27	18	36
IPGE	11	12	13	10	15
PPGE	16	21	14	8	21
IPGE/PPGE	0.69	0.57	0.93	1.25	0.71
Ir/(Pt+Pd)	0.2	0.16	0.23	0.43	0.21

IPGE: Os+Ir+Ru. PPGE: Rh+Pt+Pd

Supplementary Table 5. Mineral composition of studied rocks

Sample	Rock classification	Px	Abundance of Px	Ep/Czo (Aln)	Ab	Chl	Ap	Ttn	Cal	Dol	Bt	Ph	Pg	Pmp	Zrn	Qz	Amp	Rt	Anl	Pmp	Grt	Opaque
09SC31l	Pure jadeitite	80	Jd>Omp		10			x			5				x							
09SC31m	Pure jadeitite	90	Jd>Omp		5			x							x							
09SC31v	Pure jadeitite	90	Omp>Jd	x	5			x			x				x							
09SC31w	Pure jadeitite	95	Omp>Jd		x	x	x	x							x							
09SC3b	Pure jadeitite	80	Jd>Omp	x	5	x						5	5		x							
09SC3d	Pure jadeitite	85	Jd=Omp			x		x				5	5		x							
09SC3e	Pure jadeitite	85	Jd=Omp	x	x			x				5	5		x							
09SC4a	Pure jadeitite	90	Jd=Omp	x	5			x				x	x		x							
09SC5 I	Pure jadeitite	95	Jd=Omp		x			x				x	x		x							
09SC5 II	Pure jadeitite	85	Jd>Omp		x			x				5	5		x	x						
09SC5 III	Pure jadeitite	55	Jd>Omp	5	15			x				5	5		x	x						
09SC5 V	Pure jadeitite	70	Jd>Omp	x	5			x				10	10		?							
09SC6d	Pure jadeitite	95	Jd>Omp	x	x			x							x							
09SC7c	Pure jadeitite	75	Jd>Omp	x	x			x	x			10	10		x							
09SC7l	Pure jadeitite	85	Jd>Omp		x			x				5	5		x							
09SC8a I	Pure jadeitite	95	Jd>Omp		x			x				x	x		x							
09SC8a II	Pure jadeitite	95	Jd>Omp		x			x				x	x		x							
09SC8a III	Pure jadeitite	95	Jd>Omp		x	x		x				x	x		x							
09SC8a IV	Pure jadeitite	95	Jd>Omp		x	x		x				x	x		x							
09SC8a V	Pure jadeitite	95	Jd>Omp	x(+Aln)	x	x		x				x	x		x							
09SC8a VI	Pure jadeitite	90	Jd>Omp	x(+Aln)	5	x		x				x	x		x							
09SC8c	Pure jadeitite	90	Jd>Omp		x			x			?	5			x							
09SC9a	Pure jadeitite	95	Kosm-Jd-Omp		x			x				x			x							
09SC9e	Pure jadeitite	95	Omp>Jd	x	x	x	?	x							x							
09SC9h	Pure jadeitite	90	Kosm-Omp-Jd		x			x				x			x							
CV237b	Pure jadeitite	80	Jd>Omp	x(+Aln)	x	x	x	x	x		x	x			x	x	x(Mkt)					
CV237k	Pure jadeitite	95	Jd>Omp	x	x		x	x			x				x							
CV237t	Pure jadeitite	90	Jd>Omp	x	5		x	x	x		x				x							
MCB1f	Pure jadeitite	90	Jd>Omp	x	5		x	x							x			x				
MCB1i	Pure jadeitite	75	Jd>Omp	5	10	x	x	x					5		x							
MCB1j	Pure jadeitite	75	Omp>Jd	x	x			x				10	10		x		x(Gln)					
MCB2d	Pure jadeitite	90	Jd>Omp	x	5		x	x							x			x				
MCB2e	Pure jadeitite	90	Jd>Omp		5							x	x		x							
MCB3f	Pure jadeitite	90	Jd>Omp	x(+Aln)	5	x		x							x			x				
MCB3h	Pure jadeitite	90	Jd=Omp	5(+Aln)	5			x			x				x							
SCJ1	Pure jadeitite	75	Jd>Omp		x			x				5	5		x							
SCJ12	Pure jadeitite	75	Jd>Omp		x		x	x				5	5		x							
SCJ2A	Pure jadeitite	75	Jd>Omp		x	x		x				5	5		x							
09SC27c	Ep-rich jadeitite	50	Jd>Omp	5	x			x				30	10		x							
09SC27d	Ep-rich jadeitite	50	Omp>Jd	10(+Aln)	x	x		x				35	-		x							
09SC27e	Ep-rich jadeitite	50	Jd>Omp	10				x				35			x							

Sample	Rock classification	Px	Abundance of Px	Ep/Czo (Aln)	Ab	Chl	Ap	Ttn	Cal	Dol	Bt	Ph	Pg	Pmp	Zrn	Qz	Amp	Rt	Anl	Pmp	Grt	Opaque
09SC27k	Ep-rich jadeitite	65	Jd>Omp	5	x			x			x	25			x							
09SC27m	Ep-rich jadeitite	50	Jd>Omp	20		x		x				25			x						x	x (Hem+Py)
09SC27n	Ep-rich jadeitite	40	Jd>Omp	25	x			x				30			x							
09SC27r	Ep-rich jadeitite	85	Omp>Jd	x	x			x				10			x							
09SC31f	Ep-rich jadeitite	55	Omp>Jd	x	x			x				40			x							
09SC31g	Ep-rich jadeitite	85	Omp>Jd	x	x	x	x	x			x	5	5		x							
09SC31h	Ep-rich jadeitite	95	Omp>Jd	x	x	x	x	x							x							
09SC31j	Ep-rich jadeitite	90	Omp>Jd	5	x	x	x	x							x							
09SC31q	Ep-rich jadeitite	85	Jd>Omp	x			x	x				10	10		x							
09SC31u II	Ep-rich jadeitite			15	50	25		5							x							x
09SC32b	Ep-rich jadeitite	90		x		x		x				5			x							
09SC33a	Ep-rich jadeitite	85	Omp>Jd		x			x				5	5		x							
09SC33d	Ep-rich jadeitite	85	Jd>Omp		x			x				5	5		x							
09SC7d	Ep-rich jadeitite	50	Jd>Omp	5	5	5	x	x				15	15		x			?				
09SC7i	Ep-rich jadeitite	60	Jd>Omp	5	x			x				15	15		x							
09SC9g	Ep-rich jadeitite	50	Jd>Omp	50		?		x				45			x							
CV237f	Ep-rich jadeitite	80	Jd>Omp	15	x		x	x				x	x		x							
MCB1d	Ep-rich jadeitite	60	Jd>Omp	5	5	x	x	x				10	20		x					x		
MCB1g	Ep-rich jadeitite	55	Jd>Omp	5	5		x	x				15	15		x							
MCB1h	Ep-rich jadeitite	85	Omp>Jd	x	x			x				5	5		x							
MCB2c	Ep-rich jadeitite	65	Jd>Omp	x	x		x	x					30		x							
MCB4a	Ep-rich jadeitite	65	Omp>Jd	15	15	x	x	x	x		x		10	x	x		x(Mkt & Mtm)			x		
09SC31e	Mica-rich jadeitite	40	Omp-Jd	5	25	x	5	x				10	10		x							
09SC31u III	Mica-rich jadeitite	65	Omp>Jd	5	10	5	x	x				5	5		x							x
09SC7j I	Mica-rich jadeitite	45	Jd>Omp	x				x				25	25		x							
09SC7j II	Mica-rich jadeitite	55	Jd>Omp	x	x	x		x				20	20		x	x						
09SC7j III	Mica-rich jadeitite	65	Jd>Omp	x	x	x		x				15	15		x							
09SC7a	Omphacitite	90	Omp>Jd	5	x			x							x							
09SC7h	Omphacitite	95	Jd>Omp	x	x			x							x							
09SC9i	Omphacitite	95	Omp>Jd					x				x			x							
09SC5 IV	Cr-rich Omphacitite	95	Omp>Jd												?							
09SC7b	Cr-rich Omphacitite	95	Omp>Jd		x	x		?							x							
SCMJ10	Cr-rich Pure jadeitite	95	Jd>Omp	x(+Aln)	x			x			x				x				x			
09SC27f	Ab-Ep rock		Jd>Omp	15	50	5		x	x		5	10	10		x		x(Act)					x (Hem+Py)
09SC27l	Ab-Ep rock			40	50	x	x	x	x			5			x							
09SC27q	Ab-Ep rock			5	90			x							?							
09SC31a	Ab-Ep rock			15	50	10	x	x							x		20(Mhb)					x (Hem)
09SC31c	Ab-Ep rock			35	55	5	x	x				x			x	-						
09SC31d	Ab-Ep rock			30	45	5		x				5	5		x	x	5(Act)					
09SC31n	Ab-Ep rock		-	35	55	x	x	x				x			x	x	x(Mhb)					
09SC31s	Ab-Ep rock	x		35	55	x	x	x				5			x	x	x?					x
09SC31t	Ab-Ep rock			25	65	5	x	x				x			x	x	x?					x
09SC8d	Ab-Ep rock			30	65	x		x	x			x			x	x						x

Sample	Rock classification	Px	Abundance of Px	Ep/Czo (Aln)	Ab	Chl	Ap	Ttn	Cal	Dol	Bt	Ph	Pg	Pmp	Zrn	Qz	Amp	Rt	Anl	Pmp	Grt	Opaque
09SC8e	Ab-Ep rock			30	50	5		x	x			x			x	10						
09SC9b	Ab-Ep rock	x	Jd=Omp	35	50			x				5			x	5						x
MCB1a	Ab-Ep rock			55	35	5		x				x			x							x
MCB1c	Ab-Ep rock			60	35	x		x				x			x							x
MCB1e	Ab-Ep rock			30	45	15	x	x		5		x	x		x		x(Mhb)					x
MCB3a	Ab-Ep rock			45	40	10	x	x				x	x		x		x?					x
09SC27b	Ab-Ep Chl-rich rock			15	45	5	x	x			x	30	-		x	-	x(Gln)	x				
09SC8a VII	Ab-Ep Chl-rich rock	X	Omp>Jd		90	5		x							x							
MCB3b	Ab-Ep Qtz-rich rock			30	55	x		x				x			x	10	x?					
MCB3c	Ab-Ep Qtz-rich rock			35	40	5		x				x	x		x	15						
09SC27a	Chloritite					95		x							x							
09SC27h	Chloritite					95		x							x							
09SC3a I	Chloritite					95		x							x							
09SC3f I	Chloritite					90		5							x							
09SC7g	Chloritite					95		x							x	?						
09SC7j V	Chloritite					95		x							x							
09SC27i	Ttn/Ap-rich Chloritite					85	x	10							x							
09SC31u I	Ttn/Ap-rich Chloritite					56	x	40							x							
09SC3a II	Ttn/Ap-rich Chloritite					95		x							x							
09SC3f II	Ttn/Ap-rich Chloritite					90	x	5							x							
09SC7e	Ttn/Ap-rich Chloritite					95	x	x							x							
09SC7j IV	Ttn/Ap-rich Chloritite					95	x	x							x							
09SC8a IX	Ttn/Ap-rich Chloritite			x(+Aln)		95	x	x							x							
09SC8a VIII	Ttn/Ap-rich Chloritite			x(+Aln)		95	x	x							x							
09SC27j	Actinolitite																95(Act)					
09SC31o	Actinolitite																100(Act)					
09SC31p	Actinolitite					x											90(Act)					
09SC8b I	Actinolitite																80(Act)					
MCB2a	Actinolitite																95(Act)					
MCB3d	Actinolitite																95(Act)					

Supplementary Table 6. Major and trace element data from jadeitites and related rocks from the Sierra del Convento mélange.

Sample	CV237b	CV237k	CV237t	MCB-1f	MCB-1i	MCB-1j	MCB-2d	MCB-2e
Group	Pure jadeitite	Pure jadeitite	Pure jadeitite	Pure jadeitite	Pure jadeitite	Pure jadeitite	Pure jadeitite	Pure jadeitite
SiO_2	58.950	57.950	59.480	57.620	55.400	55.410	58.990	58.700
TiO_2	0.540	0.270	0.350	0.330	0.500	0.290	0.530	0.220
Al_2O_3	18.840	20.510	20.520	17.760	21.520	23.220	19.400	20.450
FeO_{tot}	2.834	2.232	1.980	2.924	2.268	1.764	2.690	2.205
MnO	0.050	0.049	0.047	0.078	0.047	0.040	0.047	0.035
MgO	2.470	1.880	1.390	3.680	1.860	1.700	2.080	2.270
CaO	4.470	3.480	2.930	6.500	5.730	5.320	4.170	3.820
Na_2O	9.910	12.240	11.820	9.800	9.950	9.860	10.950	11.370
K_2O	0.330	0.010	0.110	0.010	0.250	0.340	0.030	0.070
P_2O_5	0.133	0.219	0.201	0.243	0.140	0.013	0.244	0.010
LOI	0.570	0.460	0.240	0.240	1.680	1.390	0.330	0.350
Total	98.527	98.840	98.828	99.511	99.597	99.543	99.761	99.745
Li	15.397	30.279	35.937	21.898	30.072	29.485	21.634	17.974
Rb	6.083	0.622	1.097	0.405	1.827	5.208	0.720	0.878
Cs	0.642	0.097	0.107	0.162	0.423	0.620	0.370	0.172
Be	0.401	0.520	0.322	0.560	0.495	0.837	0.226	0.095
Sr	208.977	35.113	89.815	53.191	608.306	523.099	101.978	58.575
Ba	147.765	9.999	14.200	7.555	51.996	131.604	27.692	19.164
Sc	6.679	4.189	3.014	6.261	5.945	3.729	5.550	2.606
V	67.618	45.551	37.984	52.385	49.379	36.047	46.674	35.509
Cr	74.635	85.211	57.877	122.406	98.072	106.458	92.733	138.771
Co	44.707	49.050	31.806	83.605	75.995	96.484	95.185	149.852
Ni	46.881	38.649	15.447	56.710	28.864	30.772	32.656	44.418
Cu	20.287	12.638	5.238	7.533	6.614	4.998	8.169	10.717
Zn	27.597	30.318	20.514	36.443	30.051	24.813	31.573	22.990
Ga	17.040	19.263	16.244	18.275	19.451	19.613	17.787	14.718
Y	8.112	4.860	4.956	6.387	8.871	6.078	8.730	1.451
Nb	2.842	1.142	1.225	1.376	1.280	1.177	1.012	0.601
Ta	0.405	0.484	0.325	0.673	0.611	0.815	0.673	1.061
Zr (XRF)	158.200	121.400	97.700	92.900	138.200	104.200	145.600	116.700
Hf	0.312	0.203	0.218	0.308	0.295	0.283	0.264	0.217
Mo	7.355	12.296	7.221	15.921	12.870	16.072	16.508	28.186
Sn	0.812	1.445	0.458	0.539	0.558	0.431	0.450	0.190
Tl	0.058	0.003	0.018	0.011	0.032	0.052	0.001	0.012
Pb	0.855	0.363	0.350	0.803	1.843	1.673	0.688	0.262
U	0.048	0.110	0.146	0.163	0.055	0.039	0.045	0.040
Th	0.102	0.327	0.482	0.407	0.047	0.047	0.130	0.043
La	4.902	5.096	5.194	4.136	3.624	3.310	5.094	1.431
Ce	10.833	10.173	10.146	7.632	7.615	6.206	9.711	2.153
Pr	1.642	1.338	1.304	1.112	1.200	0.971	1.478	0.299
Nd	7.562	5.611	5.304	4.816	6.329	4.464	6.620	1.155
Sm	2.026	1.279	1.223	1.316	1.783	1.240	1.810	0.322
Eu	0.751	0.522	0.462	0.517	0.991	0.907	0.756	0.228
Gd	1.951	1.220	1.115	1.302	1.914	1.347	1.761	0.333
Tb	0.303	0.167	0.175	0.208	0.287	0.197	0.272	0.054
Dy	1.635	0.886	0.921	1.219	1.618	1.112	1.527	0.308
Ho	0.308	0.183	0.185	0.252	0.335	0.230	0.323	0.060
Er	0.828	0.484	0.489	0.646	0.859	0.636	0.803	0.156
Tm	0.125	0.073	0.070	0.096	0.119	0.086	0.123	0.023
Yb	0.729	0.422	0.437	0.628	0.765	0.491	0.776	0.160
Lu	0.113	0.058	0.065	0.099	0.108	0.069	0.098	0.026

Supplementary Table 6 (continued). Major and trace element data from jadeitites and related rocks from the Sierra del Convento mélange.

Sample	MCB-3f	MCB-3h	09-SC-3b	09-SC-3d	09-SC-3e	09-SC-4a	09-SC-5-I	09-SC-5-II
Group	Pure jadeitite	Pure jadeitite	Pure jadeitite	Pure jadeitite	Pure jadeitite	Pure jadeitite	Pure jadeitite	Pure jadeitite
SiO_2	57.650	58.460	56.670	56.220	56.600	57.170	55.480	57.460
TiO_2	0.710	0.610	0.830	0.580	0.580	0.260	0.180	0.210
Al_2O_3	18.030	18.750	19.130	18.380	18.500	18.310	21.140	17.130
FeO_{tot}	3.401	2.996	3.446	2.753	3.041	2.277	2.133	2.582
MnO	0.078	0.068	0.072	0.079	0.073	0.065	0.056	0.065
MgO	3.610	3.230	2.830	4.770	3.300	4.850	3.300	4.420
CaO	5.470	4.490	5.470	5.780	5.950	6.950	5.140	7.140
Na_2O	9.770	10.070	9.290	9.440	9.850	7.820	10.120	9.570
K_2O	0.060	0.070	0.520	0.400	0.380	0.550	0.030	0.010
P_2O_5	0.009	0.009	0.157	0.009	0.137	0.017	0.025	0.014
LOI	0.380	0.430	0.590	0.700	0.280	0.990	1.220	0.310
Total	99.547	99.517	99.389	99.418	99.030	99.512	99.061	99.199
Li	29.595	31.917	24.439	26.260	18.590	38.598	33.405	62.573
Rb	1.596	0.808	8.701	7.022	6.949	10.900	0.395	6.844
Cs	0.103	0.068	0.000	0.000	0.000	0.311	0.073	3.890
Be	0.292	0.581	0.534	0.817	0.873	0.568	0.568	46.283
Sr	58.782	86.609	298.103	41.336	96.714	467.331	207.802	57.594
Ba	16.605	17.980	476.518	368.841	356.112	174.568	56.965	50.031
Sc	8.079	7.664	6.748	5.031	6.930	6.964	5.829	10.823
V	70.029	65.409	54.642	51.929	61.522	50.873	41.063	49.262
Cr	147.181	140.148	78.054	272.577	124.928	133.611	89.972	159.509
Co	93.152	88.649	76.116	67.356	65.155	66.696	104.707	111.752
Ni	71.769	61.696	46.084	141.933	62.229	135.173	66.651	121.418
Cu	8.466	7.391	32.724	19.837	126.436	6.596	4.399	18.170
Zn	40.073	35.482	31.955	21.263	27.110	18.741	14.209	53.741
Ga	18.383	17.032	13.269	13.118	14.451	14.054	13.371	23.431
Y	11.385	9.780	11.371	9.330	10.673	4.606	3.405	12.556
Nb	4.679	3.706	3.099	6.828	5.341	0.608	0.544	7.759
Ta	0.966	0.888	0.676	1.137	0.788	0.389	0.670	3.288
Zr (XRF)	170.700	163.400	297.000	210.900	203.400	46.000	60.700	61.800
Hf	0.332	0.309	0.360	0.445	0.407	0.339	0.196	8.787
Mo	16.004	17.321	11.414	12.584	13.190	8.666	17.265	48.100
Sn	0.813	0.717	0.999	0.845	1.009	0.919	0.433	11.189
Tl	0.019	0.005	0.049	0.053	0.052	0.177	0.003	4.404
Pb	0.550	1.155	1.201	0.324	0.326	4.416	0.929	11.817
U	0.262	0.217	0.143	0.209	0.127	0.027	0.013	4.628
Th	1.440	3.527	0.148	0.105	0.084	0.025	0.017	3.954
La	12.022	21.334	6.893	2.556	5.898	1.919	1.287	6.346
Ce	22.445	35.072	14.521	4.636	13.218	3.694	2.738	10.989
Pr	2.982	4.459	2.128	0.706	2.065	0.576	0.438	3.087
Nd	12.352	16.080	10.546	3.869	9.690	2.814	2.276	28.252
Sm	2.538	2.854	2.407	1.301	2.301	0.792	0.649	13.644
Eu	0.931	0.951	1.174	0.931	1.093	0.476	0.409	4.588
Gd	2.604	2.302	2.291	1.583	2.202	0.794	0.680	9.503
Tb	0.394	0.370	0.360	0.257	0.351	0.136	0.114	2.062
Dy	1.983	1.777	2.020	1.528	1.859	0.822	0.623	8.353
Ho	0.422	0.397	0.404	0.320	0.380	0.184	0.140	1.767
Er	1.023	0.958	1.075	0.865	0.963	0.578	0.358	8.252
Tm	0.165	0.141	0.167	0.138	0.142	0.091	0.051	1.375
Yb	0.938	0.898	1.027	0.826	0.939	0.542	0.338	9.913
Lu	0.120	0.118	0.148	0.133	0.129	0.086	0.046	2.317

Supplementary Table 6 (continued). Major and trace element data from jadeitites and related rocks from the Sierra del Convento mélange.

Sample	09-SC-5-III	09-SC-5-V	09-SC-6d	09-SC-7c	09-SC-7l	09-SC-8a I	09-SC-8a II	09-SC-8a III
Group	Pure jadeitite	Pure jadeitite	Pure jadeitite	Pure jadeitite	Pure jadeitite	Pure jadeitite	Pure jadeitite	Pure jadeitite
SiO_2	57.410	57.310	57.510	57.620	56.610	57.630	58.260	57.610
TiO_2	0.220	0.250	0.380	0.280	0.200	0.400	0.350	0.830
Al_2O_3	15.560	17.730	19.210	18.500	22.020	18.110	19.660	19.290
FeO_{tot}	2.753	2.609	1.773	1.989	1.854	3.221	2.636	3.158
MnO	0.072	0.065	0.046	0.056	0.044	0.072	0.060	0.065
MgO	5.180	4.250	3.790	4.070	2.610	4.090	2.830	3.010
CaO	8.500	6.910	6.060	6.350	3.800	4.480	3.890	4.040
Na_2O	8.790	9.540	9.970	9.400	9.760	10.080	11.140	10.750
K_2O	0.020	0.050	0.010	0.410	1.240	0.000	0.000	0.000
P_2O_5	0.009	0.012	0.120	0.010	0.013	0.014	0.010	0.017
LOI	0.220	0.310	0.420	0.450	0.960	0.650	0.340	0.260
Total	99.041	99.327	99.486	99.356	99.317	99.106	99.470	99.382
Li	29.370	30.206	27.704	33.848	31.010	23.348	26.782	29.438
Rb	0.305	0.811	0.383	8.424	21.229	0.223	0.091	0.048
Cs	0.078	0.094	0.000	0.146	0.080	0.058	0.032	0.017
Be	0.452	0.610	0.376	0.659	0.430	0.915	0.592	0.527
Sr	41.812	158.236	265.891	61.117	210.520	25.564	19.414	27.772
Ba	14.324	170.271	30.469	302.824	1045.936	4.935	2.316	1.807
Sc	5.961	6.715	8.724	5.097	2.605	5.221	5.101	10.945
V	48.876	42.603	63.366	41.911	28.348	45.355	39.771	58.201
Cr	219.197	151.098	156.440	127.361	41.726	268.093	163.216	117.088
Co	122.402	176.343	64.763	93.781	48.319	154.273	85.476	87.905
Ni	135.581	86.550	77.184	137.248	50.426	149.132	83.605	55.020
Cu	4.748	10.755	13.615	19.491	4.845	6.914	5.944	4.707
Zn	22.464	17.179	16.794	24.182	2.703	49.960	31.270	30.073
Ga	12.050	12.126	13.675	15.785	13.979	15.227	15.916	14.696
Y	4.851	4.874	5.862	3.872	4.090	6.274	5.075	15.067
Nb	0.607	0.745	1.263	0.678	0.634	1.510	1.092	4.088
Ta	0.750	1.104	0.536	0.623	0.392	1.007	0.593	0.850
Zr (XRF)	51.500	70.200	84.000	62.700	66.700	109.200	100.800	170.800
Hf	0.337	0.300	0.329	0.271	0.179	0.355	0.207	0.359
Mo	17.805	28.201	11.374	16.012	8.164	26.075	16.826	16.679
Sn	0.994	0.713	2.463	1.161	0.559	1.051	1.312	1.084
Tl	0.000	0.004	0.004	0.056	0.135	0.000	0.000	0.000
Pb	0.289	0.641	1.005	0.357	0.492	0.416	0.273	0.639
U	0.032	0.037	0.046	0.034	0.026	0.212	0.162	0.280
Th	0.048	0.042	0.038	0.045	0.106	0.706	1.066	0.430
La	4.202	5.888	3.580	3.144	7.467	5.483	9.045	7.809
Ce	7.898	11.444	7.084	5.582	11.531	10.831	15.789	17.821
Pr	1.242	1.807	1.113	0.773	1.223	1.577	1.833	2.874
Nd	5.489	8.471	5.190	3.819	5.284	6.903	6.704	13.400
Sm	1.249	2.172	1.475	0.806	1.231	1.596	1.252	3.625
Eu	0.797	1.374	0.798	0.477	0.744	0.553	0.494	1.192
Gd	1.224	1.887	1.349	0.786	1.141	1.545	1.303	3.260
Tb	0.192	0.264	0.192	0.130	0.155	0.224	0.189	0.500
Dy	0.915	1.203	1.127	0.787	0.840	1.230	0.898	2.843
Ho	0.181	0.215	0.217	0.159	0.163	0.247	0.186	0.574
Er	0.500	0.502	0.535	0.426	0.344	0.591	0.472	1.354
Tm	0.075	0.078	0.081	0.068	0.049	0.093	0.074	0.201
Yb	0.558	0.515	0.538	0.434	0.280	0.618	0.464	1.219
Lu	0.074	0.071	0.074	0.071	0.037	0.086	0.060	0.153

Supplementary Table 6 (continued). Major and trace element data from jadeitites and related rocks from the Sierra del Convento mélange.

Sample	09-SC-8a IV	09-SC-8a V	09-SC-8a VI	09-SC-8c	09-SC-9a	09-SC-9e	09-SC-9h	09-SC-31l
Group	Pure jadeitite	Pure jadeitite	Pure jadeitite	Pure jadeitite	Pure jadeitite	Pure jadeitite	Pure jadeitite	Pure jadeitite
SiO_2	57.300	56.730	58.710	56.770	57.730	57.450	57.090	58.280
TiO_2	0.880	0.970	0.420	0.410	0.230	0.200	0.340	0.570
Al_2O_3	18.900	18.200	19.230	16.540	21.110	15.760	16.980	19.300
FeO_{tot}	3.185	3.518	2.771	3.626	1.647	2.025	2.241	3.005
MnO	0.068	0.079	0.074	0.098	0.044	0.083	0.077	0.059
MgO	3.060	3.600	3.350	4.240	2.730	6.190	5.670	2.610
CaO	4.720	5.310	5.120	7.160	3.930	8.670	7.290	4.030
Na_2O	10.670	10.120	10.380	9.290	10.030	8.050	8.630	10.740
K_2O	0.000	0.000	0.000	0.060	1.040	0.020	0.070	0.280
P_2O_5	0.020	0.014	0.012	0.056	0.009	0.009	0.012	0.012
LOI	0.190	0.390	0.280	0.430	0.680	0.580	0.670	0.330
Total	99.348	99.323	100.656	99.084	99.363	99.262	99.319	99.551
Li	31.262	32.827	26.411	29.781	32.800	19.594	17.813	36.409
Rb	0.132	0.123	0.246	1.861	18.072	0.590	1.132	9.275
Cs	0.021	0.061	0.024	0.203	0.017	0.027	0.000	0.776
Be	0.572	0.589	0.698	0.674	0.169	0.504	0.360	0.509
Sr	32.406	42.832	75.374	162.090	61.766	176.625	84.179	91.301
Ba	1.941	4.527	23.803	40.564	885.486	0.000	51.819	61.241
Sc	11.331	13.586	7.027	6.447	2.854	7.771	14.348	8.281
V	62.790	63.969	39.488	39.547	25.293	64.575	61.359	70.153
Cr	136.874	187.437	164.976	336.884	58.520	232.756	102.033	111.678
Co	113.311	170.605	203.904	169.411	50.556	52.474	51.319	103.835
Ni	45.011	64.406	59.432	66.246	38.864	115.747	75.818	33.617
Cu	6.851	9.152	7.655	12.483	4.033	7.455	5.369	37.882
Zn	24.269	27.514	14.294	27.081	0.000	13.207	0.000	29.417
Ga	13.578	12.191	11.766	12.445	13.168	8.191	8.674	18.313
Y	15.512	17.259	5.251	9.958	1.897	8.010	9.960	8.406
Nb	6.213	5.495	1.857	1.653	0.433	0.554	2.171	2.862
Ta	1.185	1.469	1.376	1.215	0.350	0.299	0.651	0.830
Zr (XRF)	303.600	113.000	91.000	146.600	86.600	51.900	124.100	185.100
Hf	0.473	0.472	0.294	0.541	0.148	0.411	0.960	0.000
Mo	23.969	35.312	31.190	27.394	10.591	6.816	7.465	15.707
Sn	1.959	2.081	1.628	1.313	0.583	0.897	0.790	1.330
Tl	0.000	0.000	0.000	0.019	0.104	0.009	0.022	0.171
Pb	0.444	1.158	0.348	3.726	0.189	1.064	0.579	0.171
U	0.381	0.407	0.229	0.121	0.023	0.099	0.071	0.082
Th	0.348	0.381	0.204	0.199	0.010	0.103	0.539	1.147
La	7.860	8.866	4.752	5.774	3.764	12.220	6.413	11.962
Ce	17.814	19.573	8.867	12.015	6.318	18.593	11.131	22.201
Pr	2.749	3.051	1.205	1.840	0.840	2.512	1.595	2.917
Nd	12.657	14.346	4.863	8.125	3.773	11.101	7.206	11.699
Sm	3.786	4.008	1.033	1.963	0.819	3.019	1.890	2.445
Eu	1.179	1.522	0.573	0.957	0.441	3.491	1.445	0.769
Gd	3.411	3.732	1.062	1.844	0.569	2.916	1.898	1.925
Tb	0.538	0.590	0.150	0.302	0.079	0.383	0.301	0.307
Dy	2.778	2.988	0.855	1.604	0.398	1.653	1.794	1.720
Ho	0.555	0.651	0.186	0.381	0.068	0.298	0.355	0.353
Er	1.482	1.570	0.538	1.020	0.180	0.738	0.933	0.878
Tm	0.220	0.240	0.080	0.172	0.026	0.102	0.142	0.128
Yb	1.375	1.345	0.477	1.185	0.168	0.806	0.824	0.791
Lu	0.161	0.174	0.062	0.187	0.028	0.121	0.142	0.104

Supplementary Table 6 (continued). Major and trace element data from jadeitites and related rocks from the Sierra del Convento mélange.

Sample	09-SC-31m	09-SC-31v	09-SC-31w	SCJ-1	SCJ-2a	SCJ-12	SC-MJ-10	CV237f
Group	Pure jadeitite	Pure jadeitite	Pure jadeitite	Pure jadeitite	Pure jadeitite	Pure jadeitite	Cr-rich Pure Jdt	Ep-rich Jdt
SiO_2	58.330	58.360	59.140	57.430	57.340	54.450	56.000	49.190
TiO_2	0.520	0.410	0.190	0.200	0.280	0.550	0.270	1.050
Al_2O_3	21.510	22.240	21.020	21.970	20.570	19.830	21.700	13.360
FeO_{tot}	1.521	1.359	1.377	1.746	1.917	2.744	2.043	8.458
MnO	0.039	0.036	0.038	0.036	0.041	0.060	0.052	0.179
MgO	1.740	1.280	1.870	1.750	2.630	3.710	4.120	7.650
CaO	3.170	3.230	3.230	4.070	5.160	7.640	2.810	11.880
Na_2O	11.900	11.550	11.600	11.080	10.510	8.320	10.890	4.350
K_2O	0.070	0.050	0.020	0.090	0.120	0.760	0.110	0.050
P_2O_5	0.050	0.088	0.197	0.237	0.054	0.013	0.011	0.083
LOI	0.240	0.550	0.600	0.420	0.580	0.670	1.370	2.100
Total	99.259	99.304	99.435	99.223	99.415	99.053	99.603	96.250
Li	30.934	27.103	28.448	25.468	23.526	34.738	21.956	17.251
Rb	1.543	1.118	1.005	1.359	2.033	9.557	1.390	1.358
Cs	0.089	0.302	0.490	0.125	0.055	0.197	0.308	0.031
Be	0.347	0.608	4.570	0.335	0.479	0.651	0.282	0.523
Sr	67.984	557.139	91.305	464.653	435.109	905.492	24.117	138.276
Ba	45.658	16.186	25.607	48.856	144.858	1094.625	109.970	52.362
Sc	4.466	1.794	4.635	0.918	8.749	11.394	0.000	41.038
V	17.146	29.546	35.497	21.648	48.354	52.151	38.243	254.855
Cr	57.848	113.454	135.776	123.335	111.699	148.069	1153.750	325.027
Co	64.026	114.126	141.190	172.793	109.403	92.086	432.197	49.652
Ni	19.900	16.627	36.073	29.466	157.382	93.633	122.767	110.081
Cu	10.308	4.235	5.731	9.833	5.408	59.570	16.580	5.606
Zn	15.291	15.899	11.905	23.819	15.205	19.366	14.170	58.255
Ga	16.501	15.825	15.576	15.057	14.392	15.280	10.544	15.050
Y	4.644	3.320	4.052	2.252	7.690	13.487	1.563	25.470
Nb	6.451	6.994	1.136	1.045	1.055	2.647	1.188	1.075
Ta	0.991	1.196	1.352	1.325	0.805	0.798	2.275	0.178
Zr (XRF)	142.500	156.700	119.400	78.300	25.800	260.000	32.400	56.400
Hf	0.135	0.000	0.968	0.117	0.217	0.472	0.158	0.598
Mo	11.645	19.520	26.016	31.198	20.654	17.865	67.604	1.914
Sn	0.367	0.691	1.521	0.221	0.507	0.611	0.495	0.577
Tl	0.020	0.086	0.540	0.009	0.000	0.051	0.007	0.005
Pb	0.306	2.306	1.541	2.375	1.437	8.183	0.481	0.927
U	0.152	0.126	0.785	0.101	0.033	0.026	0.012	0.028
Th	0.589	0.122	0.626	0.092	0.030	0.035	0.034	0.049
La	6.512	5.802	2.287	4.347	2.631	3.152	0.359	1.926
Ce	10.694	9.738	4.171	6.270	5.465	6.941	0.661	6.146
Pr	1.300	1.233	0.830	0.732	0.886	1.256	0.085	1.189
Nd	5.146	4.871	5.740	2.438	4.408	6.886	0.347	6.253
Sm	0.817	1.066	2.393	0.514	1.488	2.231	0.116	2.523
Eu	0.559	0.649	0.808	0.505	0.711	1.246	0.111	1.016
Gd	0.799	0.849	2.517	0.416	1.467	2.667	0.167	3.604
Tb	0.118	0.133	0.336	0.065	0.232	0.415	0.027	0.671
Dy	0.671	0.772	2.101	0.391	1.376	2.506	0.217	4.500
Ho	0.150	0.183	0.455	0.072	0.301	0.533	0.054	1.008
Er	0.470	0.546	1.462	0.162	0.730	1.308	0.187	2.807
Tm	0.075	0.083	0.236	0.023	0.097	0.197	0.028	0.446
Yb	0.470	0.502	1.530	0.194	0.611	1.193	0.200	2.898
Lu	0.075	0.079	0.244	0.030	0.082	0.157	0.028	0.432

Supplementary Table 6 (continued). Major and trace element data from jadeitites and related rocks from the Sierra del Convento mélange.

Sample	MCB-1d	MCB-1g	MCB-1h	MCB-2c	MCB-4a	09-SC-7d	09-SC-7i	09-SC-9g
Group	Ep-rich Jdt	Ep-rich Jdt	Ep-rich Jdt	Ep-rich Jdt	Ep-rich Jdt	Ep-rich Jdt	Ep-rich Jdt	Ep-rich Jdt
SiO_2	52.260	52.460	49.820	52.180	51.780	49.090	50.630	52.740
TiO_2	0.630	0.600	0.620	0.500	0.440	1.050	0.810	0.780
Al_2O_3	22.820	22.820	15.510	23.710	23.860	23.320	18.200	20.290
FeO_{tot}	3.869	3.401	7.046	2.762	2.870	3.815	6.344	3.581
MnO	0.071	0.068	0.148	0.047	0.049	0.076	0.114	0.075
MgO	2.580	3.140	8.650	3.020	2.370	4.350	6.540	4.400
CaO	7.220	6.590	8.570	7.930	8.920	7.800	6.840	7.150
Na_2O	8.030	7.530	5.020	7.040	7.060	4.980	6.110	7.160
K_2O	0.350	1.020	0.980	0.390	0.170	1.480	0.520	0.840
P_2O_5	0.116	0.127	0.027	0.091	0.025	0.201	0.211	0.202
LOI	1.350	1.550	2.250	1.610	1.780	2.600	2.230	1.600
Total	99.727	99.685	99.425	99.588	99.644	99.187	99.255	99.217
Li	27.644	28.032	27.450	29.473	32.937	30.161	34.528	25.011
Rb	5.178	17.532	19.049	5.454	2.195	23.328	8.772	13.224
Cs	0.348	0.335	0.135	0.242	0.118	0.081	0.013	0.074
Be	0.762	0.737	0.282	0.183	0.183	1.521	0.791	0.633
Sr	1519.619	1294.850	137.719	1051.010	1143.643	3569.408	274.331	430.724
Ba	214.457	764.138	383.802	153.498	118.864	1319.822	228.944	235.492
Sc	9.138	8.622	26.984	8.909	8.427	15.405	17.052	10.287
V	75.355	65.445	177.544	70.518	61.296	89.703	123.786	60.866
Cr	144.812	48.921	504.952	45.754	61.352	52.776	209.752	124.493
Co	64.628	47.584	63.824	37.999	41.662	27.143	39.210	38.454
Ni	24.135	26.214	147.363	19.651	35.973	37.486	130.720	92.187
Cu	12.881	20.005	11.804	31.402	16.353	73.203	33.132	21.449
Zn	36.112	28.250	65.221	24.826	26.324	41.882	66.206	39.580
Ga	19.945	18.360	15.067	18.611	18.973	16.961	16.658	17.539
Y	13.121	11.079	13.755	9.768	12.189	23.242	14.444	14.353
Nb	0.973	1.032	0.965	1.770	0.457	1.589	3.864	4.975
Ta	0.500	0.337	0.454	0.348	0.305	0.173	0.328	0.495
Zr (XRF)	113.500	103.200	55.600	44.300	75.300	219.800	145.300	200.500
Hf	0.339	0.316	0.655	0.237	0.222	0.318	0.483	0.289
Mo	32.207	7.046	4.877	5.356	6.528	2.281	2.384	6.488
Sn	0.648	0.564	0.388	0.406	0.462	0.976	0.747	0.890
Tl	0.055	0.127	0.151	0.043	0.022	0.191	0.088	0.085
Pb	3.864	2.371	0.527	4.708	2.561	16.376	2.954	1.653
U	0.049	0.065	0.072	0.093	0.009	0.147	0.120	0.079
Th	0.045	0.067	0.079	0.166	0.014	0.161	0.190	0.124
La	3.078	4.016	2.063	3.601	1.608	5.208	7.014	5.808
Ce	7.235	8.942	6.241	7.301	4.071	12.578	17.673	14.080
Pr	1.285	1.499	1.150	1.207	0.803	2.310	2.686	2.455
Nd	6.799	7.510	6.114	5.799	4.785	12.294	12.637	12.383
Sm	2.135	2.299	1.764	1.793	1.657	3.958	3.106	3.335
Eu	0.963	1.222	0.663	0.800	0.862	1.872	1.047	1.260
Gd	2.308	2.578	2.150	2.033	2.068	4.179	3.118	3.218
Tb	0.356	0.402	0.360	0.305	0.325	0.694	0.489	0.479
Dy	2.222	2.124	2.434	1.785	2.040	4.161	2.871	2.713
Ho	0.464	0.425	0.507	0.355	0.443	0.878	0.564	0.540
Er	1.285	0.993	1.352	0.883	1.204	2.253	1.362	1.335
Tm	0.200	0.139	0.209	0.132	0.179	0.338	0.201	0.205
Yb	1.193	0.843	1.322	0.836	1.087	1.994	1.260	1.291
Lu	0.175	0.115	0.198	0.116	0.148	0.282	0.180	0.186

Supplementary Table 6 (continued). Major and trace element data from jadeitites and related rocks from the Sierra del Convento mélange.

Sample	09-SC-27c	09-SC-27d	09-SC-27e	09-SC-27k	09-SC-27m	09-SC-27n	09-SC-27r	09-SC-31f
Group	Ep-ric Jdt	Ep-ric Jdt	Ep-ric Jdt	Ep-ric Jdt	Ep-ric Jdt	Ep-ric Jdt	Ep-ric Jdt	Ep-ric Jdt
SiO_2	54.260	52.130	54.670	53.940	52.230	48.110	54.950	48.510
TiO_2	0.520	0.700	0.410	0.300	1.040	1.330	0.770	1.460
Al_2O_3	21.520	21.110	22.630	23.660	19.940	21.760	14.480	19.130
FeO_{tot}	3.230	4.742	3.005	2.672	4.841	6.506	5.687	6.641
MnO	0.069	0.094	0.061	0.058	0.080	0.102	0.101	0.115
MgO	2.800	3.730	1.970	2.330	3.130	3.860	6.580	5.800
CaO	5.790	5.940	6.330	4.150	6.980	7.730	7.270	7.970
Na_2O	7.640	7.150	7.840	8.830	8.480	6.490	6.690	6.160
K_2O	1.770	1.130	0.940	1.150	0.170	0.170	1.030	0.230
P_2O_5	0.099	0.136	0.141	0.189	0.094	0.136	0.016	0.269
LOI	1.310	1.740	1.200	1.920	1.820	2.390	1.070	2.280
Total	99.368	99.130	99.532	99.497	99.344	99.308	99.277	99.304
Li	32.712	31.067	25.976	38.615	34.515	53.595	25.988	40.555
Rb	37.810	22.576	18.935	21.333	2.938	2.457	24.407	4.244
Cs	0.290	0.097	0.126	0.166	0.028	0.563	0.170	0.131
Be	0.638	0.560	0.485	0.575	0.427	0.522	0.427	0.724
Sr	208.284	278.382	299.111	203.260	441.464	795.047	16.605	1873.023
Ba	607.273	421.823	303.201	376.087	97.755	106.317	433.967	73.968
Sc	8.951	12.931	6.159	6.699	11.752	15.306	14.440	17.524
V	63.263	81.668	45.754	58.816	100.155	126.064	102.188	142.523
Cr	66.740	67.809	46.447	52.809	57.929	62.109	380.760	180.072
Co	32.241	36.000	29.446	18.517	48.578	40.492	43.145	82.522
Ni	20.401	47.940	20.221	15.749	19.806	27.098	190.710	100.538
Cu	4.639	99.738	7.200	0.344	34.001	99.954	26.874	42.599
Zn	26.100	50.206	26.089	16.845	53.347	76.151	53.602	59.080
Ga	16.345	16.016	16.398	17.424	16.749	18.203	12.391	18.300
Y	13.244	22.876	11.655	11.340	17.997	30.073	14.438	22.987
Nb	1.239	0.647	0.441	0.726	1.226	1.572	1.282	15.143
Ta	0.281	0.176	0.187	0.194	0.349	0.239	0.254	1.438
Zr (XRF)	140.900	283.000	93.400	181.400	143.600	169.700	128.900	162.000
Hf	0.000	0.348	0.188	0.000	0.348	0.087	0.030	0.122
Mo	3.618	3.079	3.884	2.590	6.729	3.069	3.125	8.898
Sn	0.808	0.757	0.489	0.767	0.941	1.299	1.090	1.624
Tl	0.334	0.194	0.159	0.196	0.023	0.026	0.220	0.046
Pb	1.692	3.292	2.727	1.473	4.942	12.566	0.859	7.447
U	0.037	0.027	0.014	0.021	0.046	0.063	0.027	0.122
Th	0.018	0.014	0.014	0.022	0.022	0.056	0.148	0.092
La	2.628	2.405	1.960	2.242	2.113	2.625	2.566	7.065
Ce	5.731	6.702	4.425	4.599	6.055	8.252	6.759	20.493
Pr	1.042	1.371	0.814	0.832	1.334	1.754	1.319	3.492
Nd	5.588	8.621	4.407	4.500	8.086	10.549	7.509	17.170
Sm	1.997	3.218	1.548	1.579	2.861	3.941	2.292	4.610
Eu	0.997	1.227	0.704	0.763	1.232	1.581	0.975	1.565
Gd	2.223	4.068	1.858	1.860	3.334	4.530	2.204	4.603
Tb	0.379	0.698	0.306	0.328	0.554	0.792	0.368	0.725
Dy	2.543	4.267	1.943	2.092	3.442	5.269	2.652	4.290
Ho	0.568	0.891	0.452	0.455	0.691	1.166	0.603	0.942
Er	1.397	2.289	1.172	1.122	1.774	3.094	1.726	2.493
Tm	0.208	0.343	0.187	0.180	0.267	0.430	0.261	0.325
Yb	1.345	2.114	1.102	1.134	1.604	2.784	1.586	1.979
Lu	0.183	0.306	0.156	0.156	0.227	0.439	0.205	0.293

Supplementary Table 6 (continued). Major and trace element data from jadeitites and related rocks from the Sierra del Convento mélange.

Sample	09-SC-31g	09-SC-31h	09-SC-31j	09-SC-31q	09-SC-31ulI	09-SC-32b	09-SC-33a	09-SC-33d
Group	Ep-ric Jdt	Ep-ric Jdt	Ep-ric Jdt	Ep-ric Jdt	Ep-ric Jdt	Ep-ric Jdt	Ep-ric Jdt	Ep-ric Jdt
SiO_2	49.490	52.800	51.190	52.810	48.350	55.580	49.440	56.740
TiO_2	1.060	1.770	2.180	0.870	1.520	0.570	1.010	0.410
Al_2O_3	16.810	17.160	17.320	19.800	18.560	19.800	20.280	14.900
FeO_{tot}	5.876	5.867	5.786	4.175	6.461	3.095	3.761	4.175
MnO	0.125	0.103	0.094	0.091	0.106	0.066	0.080	0.089
MgO	8.200	4.360	5.570	4.710	6.380	3.450	7.590	8.190
CaO	8.320	6.530	6.460	6.570	8.550	4.980	7.640	5.270
Na_2O	5.710	8.560	7.720	6.580	4.760	9.160	6.190	7.260
K_2O	0.340	0.130	0.190	1.480	0.520	0.690	0.370	0.280
P_2O_5	0.127	0.410	0.151	0.148	0.142	0.148	0.020	0.034
LOI	2.290	0.970	1.720	1.680	3.060	1.240	2.710	1.430
Total	99.002	99.313	99.025	99.379	99.128	99.124	99.500	99.243
Li	37.252	37.647	33.060	31.178	19.764	36.016	32.657	22.401
Rb	7.268	2.730	3.972	25.234	10.852	11.906	5.509	4.457
Cs	0.328	0.222	0.095	0.081	0.129	0.129	0.074	0.061
Be	5.157	3.011	0.568	0.906	0.450	0.603	0.947	0.535
Sr	683.088	269.182	284.983	342.352	1870.525	335.517	936.057	138.140
Ba	245.683	26.391	49.511	828.754	232.285	996.030	287.130	134.143
Sc	19.563	16.034	17.399	16.480	19.508	9.729	27.364	25.173
V	131.472	135.532	132.904	106.833	131.672	66.088	177.252	97.884
Cr	218.244	110.594	87.716	115.938	124.003	174.219	71.587	384.601
Co	87.103	96.133	55.219	50.394	80.056	122.152	40.354	68.534
Ni	121.444	41.449	50.453	70.348	63.298	76.264	122.587	299.210
Cu	11.026	105.982	148.796	32.697	93.528	24.585	26.098	30.803
Zn	47.737	54.918	53.271	46.730	82.399	30.433	39.483	29.690
Ga	14.583	15.431	14.383	19.282	15.721	16.382	14.297	14.141
Y	14.133	16.720	19.199	18.391	23.965	11.418	17.826	8.323
Nb	8.864	10.630	12.242	2.258	7.503	3.062	1.796	1.089
Ta	1.305	1.181	0.958	0.395	0.922	0.978	0.307	0.403
Zr (XRF)	90.900	159.100	114.900	156.400	590.100	155.600	80.900	75.600
Hf	1.252	0.770	0.212	0.088	0.619	0.292	0.117	0.147
Mo	9.984	15.537	4.424	5.428	7.142	19.364	2.540	7.998
Sn	2.600	2.080	1.341	1.159	1.238	0.869	0.883	0.721
Tl	0.479	0.241	0.043	0.178	0.109	0.065	0.051	0.021
Pb	4.082	2.569	0.870	0.642	4.718	1.068	2.518	0.941
U	0.591	0.547	0.126	0.137	0.217	0.078	0.250	0.060
Th	0.727	0.421	0.189	0.163	0.165	0.034	0.219	0.138
La	8.063	11.211	8.389	6.087	4.609	4.278	4.833	2.716
Ce	18.649	28.536	20.502	14.997	13.117	9.941	10.553	5.752
Pr	2.661	4.367	3.094	2.664	2.520	1.734	1.695	0.938
Nd	12.301	21.173	14.852	13.811	13.582	9.004	8.993	4.527
Sm	4.015	5.479	3.905	4.188	4.180	2.456	3.058	1.261
Eu	2.306	1.800	1.361	1.524	1.461	1.086	1.686	0.501
Gd	3.495	5.058	3.767	4.008	4.584	2.621	3.668	1.634
Tb	0.596	0.739	0.616	0.608	0.757	0.419	0.582	0.253
Dy	3.877	4.103	3.614	3.538	4.588	2.214	3.411	1.429
Ho	0.832	0.860	0.795	0.751	0.990	0.445	0.665	0.316
Er	2.413	2.358	2.065	1.932	2.505	1.084	1.615	0.811
Tm	0.381	0.388	0.294	0.272	0.367	0.149	0.233	0.121
Yb	2.410	2.262	1.797	1.616	2.274	1.036	1.302	0.679
Lu	0.401	0.358	0.241	0.237	0.305	0.135	0.181	0.091

Supplementary Table 6 (continued). Major and trace element data from jadeitites and related rocks from the Sierra del Convento mélange.

Sample	09-SC-7j I	09-SC-7j II	09-SC-7j III	09-SC-31e	09-SC-31uIII	09-SC-7a	09-SC-7h	09-SC-9i
Group	Mica-rich Jdt	Mica-rich Jdt	Mica-rich Jdt	Mica-rich Jdt	Mica-rich Jdt	Omphacitite	Omphacitite	Omphacitite
SiO_2	47.410	49.270	44.560	48.980	36.120	55.760	56.680	56.220
TiO_2	0.500	0.620	1.370	1.920	2.130	0.900	0.150	0.170
Al_2O_3	29.510	26.380	31.280	20.070	29.380	11.730	13.750	13.420
FeO_{tot}	2.726	2.753	2.744	7.118	6.830	3.824	2.564	2.501
MnO	0.064	0.076	0.067	0.125	0.136	0.113	0.088	0.089
MgO	4.290	4.760	6.150	6.620	8.600	7.330	7.170	7.270
CaO	3.450	4.460	1.200	4.030	4.430	12.750	10.720	11.100
Na_2O	5.080	5.470	4.000	5.640	2.460	6.450	7.300	6.930
K_2O	1.840	1.660	2.280	0.280	0.860	0.010	0.000	0.470
P_2O_5	0.014	0.016	0.018	0.346	0.564	0.009	0.011	0.010
LOI	4.250	3.360	5.550	3.360	6.880	0.180	0.290	0.670
Total	99.438	99.132	99.525	99.281	99.150	99.482	99.009	99.129
Li	56.670	50.808	66.638	34.577	96.436	16.742	17.593	22.268
Rb	20.098	24.183	33.288	6.876	5.957	0.771	0.338	8.184
Cs	0.252	0.156	0.098	0.392	0.077	0.018	0.000	0.486
Be	2.519	2.551	3.151	4.846	2.315	0.456	0.555	0.428
Sr	1496.666	1569.349	1963.222	2391.767	4665.033	396.448	219.805	78.489
Ba	1620.146	1532.124	2371.375	717.111	2172.666	20.813	9.774	394.772
Sc	9.551	11.473	24.956	22.052	34.063	15.226	4.373	4.429
V	75.397	73.570	103.067	168.944	194.965	125.000	84.083	43.785
Cr	76.920	56.218	88.239	87.052	32.560	124.863	98.370	480.808
Co	117.333	44.680	36.786	44.360	28.651	44.637	56.630	60.890
Ni	53.155	45.834	52.873	82.088	16.851	77.336	151.848	209.984
Cu	7.749	2.537	4.181	27.144	73.989	9.706	7.653	6.697
Zn	22.612	21.775	32.027	58.475	69.472	30.017	13.754	16.530
Ga	14.058	14.524	14.330	15.442	15.448	4.794	6.593	10.103
Y	10.645	11.210	28.703	27.811	38.471	9.487	3.279	5.458
Nb	2.225	1.884	4.112	14.006	4.435	2.405	0.807	0.476
Ta	0.761	0.358	0.374	1.241	0.372	0.312	0.353	0.329
Zr (XRF)	135.700	224.600	416.000	160.200	470.200	187.000	30.700	40.700
Hf	0.000	0.369	0.487	1.174	0.197	0.897	0.263	0.468
Mo	11.963	6.479	4.943	3.742	1.307	4.752	7.049	7.529
Sn	1.386	1.648	2.766	2.909	1.590	0.906	0.525	0.928
Tl	0.250	0.188	0.239	0.566	0.131	0.014	0.000	0.058
Pb	3.998	3.160	3.940	11.555	11.635	1.255	1.226	0.290
U	0.146	0.175	0.339	0.779	0.986	0.052	0.100	0.044
Th	0.098	0.041	0.056	0.705	0.619	0.120	0.016	0.031
La	3.458	6.462	8.787	12.808	8.646	4.170	3.140	1.112
Ce	7.351	12.286	20.746	33.016	19.501	9.411	4.625	2.060
Pr	1.139	1.948	3.680	5.153	3.521	1.646	0.575	0.288
Nd	5.989	9.970	19.626	25.866	18.012	8.179	2.140	1.422
Sm	1.909	3.073	6.293	7.570	5.957	2.321	0.413	0.403
Eu	1.208	2.406	5.083	4.475	6.100	1.139	0.573	0.251
Gd	2.024	3.008	6.301	6.529	6.172	2.071	0.494	0.524
Tb	0.319	0.415	1.035	1.095	0.967	0.310	0.080	0.093
Dy	1.877	2.219	5.118	6.307	6.572	1.845	0.480	0.695
Ho	0.389	0.440	1.097	1.390	1.573	0.363	0.100	0.183
Er	1.022	1.068	2.748	3.691	4.265	0.958	0.272	0.596
Tm	0.169	0.136	0.382	0.613	0.691	0.166	0.055	0.112
Yb	1.060	0.939	2.568	3.492	4.056	0.997	0.423	0.733
Lu	0.173	0.129	0.339	0.582	0.703	0.133	0.064	0.126

Supplementary Table 6 (continued). Major and trace element data from jadeitites and related rocks from the Sierra del Convento mélange.

Sample	09-SC-5-IV	09-SC-7b	MCB-1a	MCB-1c	MCB-1e	MCB-3a	09-SC-8d	09-SC-8e
Group	Cr-rich Onfacitita	Cr-rich Onfacitita	Ab-Ep rock	Ab-Ep rock	Ab-Ep rock	Ab-Ep rock	Ab-Ep rock	Ab-Ep rock
SiO_2	56.860	54.800	50.600	57.640	50.810	51.490	57.060	54.290
TiO_2	0.260	0.160	0.780	0.260	0.490	0.850	0.610	0.640
Al_2O_3	14.280	13.220	22.800	23.470	23.930	20.820	20.500	20.880
FeO_{tot}	2.933	2.951	3.788	1.287	2.762	5.021	3.311	4.256
MnO	0.078	0.092	0.053	0.022	0.050	0.086	0.065	0.081
MgO	6.440	9.190	4.580	1.150	3.850	4.440	3.010	3.500
CaO	9.760	11.150	8.120	6.630	9.950	8.890	6.390	6.970
Na_2O	7.970	6.300	4.930	6.710	4.520	4.610	6.450	6.010
K_2O	0.030	0.260	0.110	0.610	0.370	0.140	0.050	0.060
P_2O_5	0.010	0.010	0.038	0.065	0.015	0.111	0.129	0.150
LOI	0.200	0.880	3.200	1.530	2.590	2.350	1.570	1.980
Total	99.148	99.342	99.421	99.517	99.645	99.367	99.514	99.291
Li	30.486	21.886	7.099	2.667	4.772	3.951	4.272	6.839
Rb	0.766	4.948	1.848	7.647	5.531	1.668	0.701	1.117
Cs	0.160	0.000	0.152	0.141	0.045	0.105	0.000	0.000
Be	0.495	1.209	0.087	0.284	0.012	0.429	0.094	0.271
Sr	41.804	37.008	1057.383	721.303	904.473	671.174	614.461	642.625
Ba	16.337	204.113	57.797	262.868	148.678	54.659	47.595	91.017
Sc	9.546	7.606	14.434	3.704	11.328	16.003	7.860	10.560
V	56.908	41.086	115.681	28.704	105.310	134.149	66.816	85.097
Cr	977.584	1234.012	86.401	39.561	60.703	66.413	45.782	44.924
Co	99.131	62.106	72.163	41.487	54.784	43.091	34.022	28.396
Ni	261.167	503.470	26.705	23.473	58.005	48.522	36.262	42.532
Cu	6.568	18.187	54.342	2.962	6.723	34.501	24.650	31.526
Zn	20.163	25.928	44.893	13.472	27.013	57.950	24.332	35.395
Ga	12.729	10.992	18.800	18.386	18.620	19.107	16.774	17.680
Y	5.644	5.005	12.883	5.115	12.216	15.977	11.079	13.349
Nb	0.575	0.427	1.619	0.406	1.128	2.076	0.969	1.024
Ta	0.594	0.302	0.562	0.341	0.444	0.279	0.211	0.172
Zr (XRF)	43.200	32.500	14.700	71.200	28.900	119.100	145.800	152.000
Hf	0.394	0.353	0.308	0.104	0.168	0.175	0.119	0.081
Mo	27.075	6.765	7.722	4.885	9.629	3.666	2.938	1.801
Sn	1.114	0.778	0.641	0.254	0.456	0.485	0.606	0.637
Tl	0.011	0.027	0.001	0.067	0.043	0.011	0.000	0.000
Pb	0.572	0.363	5.390	2.366	3.101	2.427	2.206	3.003
U	0.041	0.033	0.106	0.023	0.094	0.090	0.087	0.103
Th	0.055	0.116	0.227	0.039	0.090	0.166	0.070	0.257
La	3.333	3.249	3.333	2.917	3.329	3.266	3.498	4.446
Ce	6.547	5.553	7.359	4.819	6.904	8.157	8.320	10.025
Pr	0.996	0.710	1.271	0.729	1.159	1.485	1.386	1.706
Nd	4.724	2.769	6.722	3.198	6.155	8.258	7.013	8.725
Sm	1.103	0.523	2.147	0.891	1.881	2.355	2.146	2.308
Eu	0.582	0.286	0.978	0.701	1.007	1.135	0.922	1.113
Gd	1.003	0.596	2.637	1.094	2.355	3.001	2.272	2.645
Tb	0.163	0.116	0.425	0.175	0.381	0.453	0.349	0.410
Dy	0.917	0.745	2.468	0.978	2.119	2.744	2.029	2.615
Ho	0.217	0.187	0.507	0.202	0.417	0.611	0.450	0.533
Er	0.589	0.611	1.242	0.506	1.146	1.603	1.106	1.361
Tm	0.101	0.093	0.171	0.074	0.152	0.215	0.171	0.214
Yb	0.726	0.620	0.990	0.453	0.929	1.357	1.008	1.264
Lu	0.111	0.112	0.136	0.065	0.123	0.203	0.139	0.174

Supplementary Table 6 (continued). Major and trace element data from jadeitites and related rocks from the Sierra del Convento mélange.

Sample	09-SC-9b	09-SC-27f	09-SC-27l	09-SC-27q	09-SC-31a	09-SC-31c	09-SC-31d	09-SC-31n
Group	Ab-Ep rock	Ab-Ep rock	Ab-Ep rock	Ab-Ep rock	Ab-Ep rock	Ab-Ep rock	Ab-Ep rock	Ab-Ep rock
SiO_2	54.930	52.180	54.960	54.390	52.440	50.730	54.500	56.630
TiO_2	0.650	0.530	0.460	0.710	0.740	1.010	0.640	0.470
Al_2O_3	23.460	23.070	22.870	22.370	21.300	22.100	21.270	24.300
FeO_{tot}	2.690	4.454	3.347	2.546	4.256	5.273	3.959	1.539
MnO	0.054	0.087	0.081	0.052	0.077	0.096	0.074	0.035
MgO	1.700	2.730	1.900	3.530	3.660	3.270	3.280	0.980
CaO	6.990	7.400	6.630	7.390	9.250	8.440	8.030	6.510
Na_2O	6.230	5.480	6.070	5.810	4.600	4.770	5.230	6.790
K_2O	0.580	0.720	0.600	0.270	0.080	0.280	0.110	0.380
P_2O_5	0.144	0.096	0.186	0.317	0.103	0.214	0.109	0.126
LOI	1.670	2.170	1.950	1.500	2.270	2.570	1.850	1.490
Total	99.398	99.413	99.427	99.169	99.250	99.340	99.493	99.421
Li	19.948	16.108	4.886	4.225	4.287	6.129	3.258	11.258
Rb	9.431	14.822	8.797	3.187	1.129	3.233	1.322	5.557
Cs	0.068	0.133	0.000	0.029	0.026	0.125	0.044	0.086
Be	0.531	0.578	0.643	0.435	0.655	0.660	0.661	0.867
Sr	709.584	554.334	581.949	925.460	686.352	642.261	556.860	768.770
Ba	207.322	286.342	173.228	107.373	31.767	106.442	52.341	157.207
Sc	5.621	9.134	6.804	9.359	16.569	13.800	13.704	4.222
V	35.265	61.712	43.090	83.976	123.181	102.150	118.482	25.175
Cr	17.913	45.044	39.023	87.913	75.968	70.351	56.554	23.256
Co	28.018	24.011	25.674	44.138	52.718	114.921	34.571	31.367
Ni	11.145	31.263	16.403	75.254	56.834	24.089	41.781	13.791
Cu	43.543	18.248	8.326	25.713	14.501	28.969	2.255	7.616
Zn	29.180	45.515	34.901	24.702	49.742	52.791	42.360	19.380
Ga	20.489	17.679	16.241	15.288	20.918	19.615	19.180	18.891
Y	11.309	17.521	12.420	9.969	15.337	18.373	12.733	6.053
Nb	1.546	0.697	0.545	4.065	1.869	1.536	1.292	0.673
Ta	0.234	0.132	0.162	0.509	0.415	0.545	0.245	0.241
Zr (XRF)	235.400	154.500	119.900	217.200	95.800	208.600	82.000	196.400
Hf	0.139	0.181	0.145	0.160	0.000	0.000	0.000	0.115
Mo	2.838	1.759	2.229	4.325	4.356	13.463	2.219	3.832
Sn	0.656	0.538	0.400	0.659	1.038	1.119	0.873	0.302
Tl	0.129	0.158	0.069	0.026	0.008	0.044	0.009	0.050
Pb	3.364	3.865	4.647	1.583	2.390	2.355	2.173	2.782
U	0.139	0.017	0.033	0.145	0.096	0.192	0.054	0.071
Th	0.463	0.005	0.037	0.819	0.245	0.222	0.113	0.038
La	5.847	1.593	2.700	6.124	3.634	2.856	3.995	3.518
Ce	11.268	4.955	5.774	12.668	8.636	7.308	9.163	6.468
Pr	1.645	1.059	0.959	1.906	1.503	1.292	1.591	0.912
Nd	7.470	6.496	4.922	8.300	7.332	7.296	7.718	4.295
Sm	1.808	2.357	1.539	1.972	2.436	2.483	2.145	1.084
Eu	0.918	1.078	0.757	0.815	0.985	1.093	0.901	0.811
Gd	2.052	3.050	1.966	2.010	2.608	2.980	2.231	1.177
Tb	0.324	0.482	0.325	0.311	0.443	0.487	0.362	0.178
Dy	1.836	3.099	1.990	1.752	2.760	3.132	2.374	1.034
Ho	0.374	0.647	0.453	0.390	0.614	0.692	0.502	0.223
Er	1.097	1.680	1.266	1.032	1.480	1.886	1.320	0.579
Tm	0.159	0.246	0.197	0.159	0.209	0.305	0.197	0.093
Yb	0.972	1.492	1.200	0.915	1.345	1.856	1.136	0.530
Lu	0.155	0.207	0.184	0.125	0.186	0.292	0.174	0.081

Supplementary Table 6 (continued). Major and trace element data from jadeitites and related rocks from the Sierra del Convento mélange.

Sample	09-SC-31s	09-SC-31t	09-SC-33c	09-SC-8a VII	09-SC-27b	MCB-3b	MCB-3c	09 SC 3a I
Group	Ab-Ep rock	Ab-Ep rock	Ab-Ep rock	Ab-Ep-Chl-rich rock	Ab-Ep-Chl-rich rock	Ab-Ep-Qtz-rich rock	Ab-Ep-Qtz-rich rock	Cloritita
SiO_2	59.080	54.780	58.510	54.310	50.610	66.470	63.210	30.540
TiO_2	0.670	0.950	0.520	0.410	0.500	0.400	0.420	0.270
Al_2O_3	20.060	19.820	20.440	19.830	20.980	17.860	18.580	18.000
FeO_{tot}	2.789	4.670	3.014	3.392	4.580	1.476	2.582	8.008
MnO	0.055	0.084	0.063	0.100	0.096	0.034	0.049	0.170
MgO	2.180	3.840	2.320	9.040	8.540	1.220	2.090	29.180
CaO	5.730	6.360	6.180	0.690	1.580	4.610	4.870	0.260
Na_2O	6.790	5.910	6.080	6.580	4.630	6.340	5.150	0.000
K_2O	0.330	0.060	0.080	0.000	2.440	0.080	0.830	0.000
P_2O_5	0.163	0.207	0.111	0.193	0.700	0.080	0.122	0.010
LOI	1.350	2.100	1.580	4.390	4.310	1.060	1.510	11.690
Total	99.508	99.301	99.234	99.313	99.476	99.794	99.701	99.020
Li	3.324	2.727	1.407	23.103	36.905	1.212	2.844	25.196
Rb	5.642	0.793	1.130	0.270	41.620	0.906	14.220	0.122
Cs	0.204	0.080	0.037	0.033	0.350	0.151	0.252	0.021
Be	4.122	1.387	0.433	0.230	0.655	0.219	0.503	0.335
Sr	613.989	771.516	535.774	692.046	44.179	358.101	489.922	3.544
Ba	147.942	29.611	49.810	72.705	1089.250	26.250	361.576	5.967
Sc	8.055	12.838	8.570	11.192	31.764	3.220	6.522	6.673
V	55.399	100.624	65.812	38.795	68.681	26.058	48.232	60.736
Cr	75.854	87.299	54.918	108.525	67.033	65.241	53.674	1829.488
Co	50.570	38.608	59.674	108.716	61.767	47.751	35.139	90.909
Ni	30.386	55.428	28.891	63.468	71.936	29.650	33.191	1649.884
Cu	6.784	22.329	15.696	3.781	8.704	4.700	7.229	21.704
Zn	30.069	46.983	38.951	28.071	39.137	22.487	42.748	107.915
Ga	17.675	20.565	18.002	6.821	11.681	13.621	17.746	14.272
Y	10.954	16.801	10.049	7.185	32.218	6.027	7.984	3.934
Nb	3.328	6.173	1.015	1.566	1.130	1.422	1.797	1.041
Ta	0.726	0.596	0.414	0.709	0.330	0.409	0.301	0.161
Zr (XRF)	147.600	176.400	132.800	127.800	305.700	157.100	110.300	44.400
Hf	0.547	0.000	0.115	0.371	1.991	0.135	0.106	0.044
Mo	6.545	3.387	6.726	14.569	6.799	7.447	4.802	0.748
Sn	2.330	1.479	0.672	0.831	1.446	0.291	0.981	0.261
Tl	0.411	0.096	0.000	0.000	0.419	0.000	0.110	0.000
Pb	3.479	3.240	3.134	0.616	3.535	0.967	2.862	0.168
U	0.450	0.263	0.063	0.238	0.253	0.028	0.059	0.043
Th	0.482	0.476	0.158	0.427	0.137	0.022	0.225	0.104
La	5.835	8.585	4.233	7.862	5.878	1.622	5.556	0.357
Ce	12.325	18.951	8.616	13.286	14.094	3.186	10.894	1.536
Pr	1.912	2.817	1.313	1.723	2.318	0.560	1.577	0.328
Nd	10.263	13.873	6.105	7.052	13.308	2.923	7.157	1.663
Sm	3.335	3.554	1.717	1.543	5.063	0.903	1.701	0.664
Eu	1.243	1.330	0.785	1.639	2.608	0.536	0.714	0.202
Gd	2.787	3.552	1.983	1.264	6.326	1.178	1.683	0.737
Tb	0.466	0.552	0.289	0.204	0.998	0.172	0.253	0.122
Dy	2.861	3.289	1.764	1.102	6.200	1.019	1.438	0.715
Ho	0.623	0.746	0.391	0.227	1.274	0.218	0.282	0.149
Er	1.804	1.987	1.046	0.624	3.365	0.581	0.684	0.430
Tm	0.296	0.285	0.142	0.099	0.517	0.090	0.103	0.061
Yb	1.715	1.780	0.936	0.679	3.063	0.581	0.714	0.313
Lu	0.285	0.285	0.118	0.105	0.488	0.092	0.110	0.028

Supplementary Table 6 (continued). Major and trace element data from jadeitites and related rocks from the Sierra del Convento mélange.

Sample	09-SC-3fI	09-SC-7g	09-SC-7j V	09-SC-27a	09-SC-27h	09 SC 3a II	09-SC-3fII	09-SC-7e
Group	Cloritita	Cloritita	Cloritita	Cloritita	Cloritita	Ttn-Ap-Zr-rich Chlt	Ttn-Ap-Zr-rich Chlt	Ttn-Ap-Zr-rich Chlt
SiO_2	31.180	30.860	30.370	29.530	29.180	29.930	32.650	29.940
TiO_2	0.950	0.020	0.600	1.010	0.270	1.010	0.770	0.900
Al_2O_3	17.120	18.580	18.880	18.820	21.610	19.290	19.480	18.470
FeO_{tot}	8.044	7.873	8.413	10.636	7.558	8.539	7.846	9.304
MnO	0.171	0.131	0.155	0.170	0.200	0.201	0.193	0.146
MgO	28.770	30.490	28.950	26.290	28.810	27.940	26.210	27.980
CaO	0.360	0.010	0.380	0.570	0.030	0.890	0.570	0.880
Na_2O	0.000	0.000	0.000	0.000	0.000	0.000	0.470	0.000
K_2O	0.010	0.000	0.000	0.010	0.000	0.000	0.000	0.000
P_2O_5	0.007	0.010	0.012	0.011	0.029	0.035	0.009	0.220
LOI	11.690	11.690	11.610	10.970	11.600	11.510	10.730	10.980
Total	99.198	100.541	100.307	99.201	100.129	100.296	99.802	99.856
Li	24.736	4.611	8.895	19.912	70.705	48.940	45.671	6.269
Rb	0.163	0.070	0.071	0.294	0.084	0.048	0.051	0.205
Cs	0.030	0.000	0.000	0.000	0.033	0.021	0.013	0.000
Be	0.009	0.336	0.212	0.242	0.000	0.230	0.179	0.145
Sr	7.742	0.789	7.412	1.370	0.009	15.272	28.630	24.643
Ba	0.000	1.246	15.090	2.917	0.000	5.569	0.000	1.886
Sc	10.618	7.125	8.372	9.781	21.434	6.753	8.612	16.803
V	104.541	46.286	67.550	99.977	331.364	64.772	64.151	132.723
Cr	2499.450	1515.856	208.884	874.275	244.984	137.515	106.823	1155.111
Co	100.826	76.057	67.893	72.398	27.383	53.960	56.051	76.137
Ni	2204.913	1390.729	328.629	885.343	100.641	139.209	172.474	898.171
Cu	30.046	4.078	4.850	5.501	5.746	19.435	32.808	5.054
Zn	70.324	62.781	79.940	105.605	71.520	81.643	77.585	85.555
Ga	14.786	10.219	13.626	17.127	21.845	11.354	11.314	13.548
Y	5.174	0.046	14.313	21.764	1.014	17.112	14.141	19.662
Nb	1.487	0.054	1.721	1.189	1.944	4.941	6.523	2.100
Ta	0.209	0.029	0.152	0.078	0.091	0.338	0.554	0.169
Zr (XRF)	101.700	6.400	161.000	526.500	7.500	356.900	280.800	169.100
Hf	0.000	0.000	0.118	0.227	0.041	0.190	0.000	0.231
Mo	0.580	0.169	0.324	0.141	0.078	1.564	0.761	0.255
Sn	0.233	0.271	0.303	0.910	0.741	0.399	0.464	0.479
Tl	0.000	0.002	0.000	0.007	0.002	0.000	0.000	0.000
Pb	0.000	0.000	0.000	0.041	0.755	0.188	0.000	0.010
U	0.088	0.000	0.048	0.099	0.023	0.136	0.183	0.069
Th	0.181	0.011	0.074	0.074	0.029	0.298	0.281	0.123
La	0.443	0.005	1.470	0.801	0.695	12.678	9.807	2.281
Ce	1.973	0.031	6.421	3.930	1.130	20.523	16.472	9.003
Pr	0.456	0.007	1.509	1.004	0.153	2.644	2.246	1.848
Nd	2.803	0.036	8.619	6.240	0.563	11.866	10.155	9.954
Sm	0.906	0.011	2.700	2.436	0.100	2.925	2.449	3.404
Eu	0.494	0.002	0.946	1.029	0.173	1.340	1.249	1.206
Gd	0.986	0.013	2.879	3.049	0.131	2.905	2.468	3.741
Tb	0.151	0.002	0.481	0.540	0.019	0.501	0.393	0.604
Dy	0.983	0.018	2.625	3.609	0.122	2.640	2.346	3.418
Ho	0.204	0.004	0.534	0.843	0.028	0.628	0.514	0.702
Er	0.506	0.011	1.363	2.269	0.084	1.474	1.365	1.857
Tm	0.076	0.001	0.204	0.359	0.017	0.232	0.207	0.289
Yb	0.467	0.007	1.118	2.196	0.113	1.405	1.244	1.620
Lu	0.064	0.001	0.133	0.306	0.019	0.176	0.144	0.207

Supplementary Table 6 (continued). Major and trace element data from jadeitites and related rocks from the Sierra del Convento mélange.

Sample	09-SC-7j IV	09-SC-8a VIII	09-SC-8a IX	09-SC-27i	09-SC-31ul
Group	Ttn-Ap-Zr-rich Chlorititet	Ttn-Ap-Zr-rich Chlorititet	Ttn-Ap-Zr-rich Chlorititet	Ttn-Ap-Zr-rich Chloritite	Ttn-Ap-Zr-rich Chloritite
SiO_2	28.610	29.020	29.140	28.170	27.660
TiO_2	1.190	0.730	1.470	3.320	5.820
Al_2O_3	21.290	18.820	20.900	19.840	17.920
FeOtot	9.088	8.521	9.394	12.507	11.356
MnO	0.223	0.226	0.245	0.199	0.199
MgO	26.350	26.590	25.590	22.570	20.550
CaO	0.830	2.500	1.400	2.180	5.420
Na_2O	0.000	0.000	0.000	0.000	0.000
K_2O	0.000	0.000	0.000	0.000	0.000
P_2O_5	0.008	1.474	0.218	0.016	1.000
LOI	11.340	11.000	10.990	9.900	9.330
Total	99.941	99.830	100.393	100.095	100.519
Li	67.221	29.712	34.708	69.916	26.003
Rb	0.180	0.081	0.089	0.068	0.277
Cs	0.017	0.027	0.016	0.072	0.135
Be	0.127	0.269	0.072	0.028	1.955
Sr	72.313	252.045	43.036	8.449	142.536
Ba	12.883	3.277	0.714	0.000	0.000
Sc	17.404	11.531	17.912	13.415	25.917
V	76.715	49.128	100.537	117.217	132.405
Cr	78.594	79.567	136.421	44.165	58.214
Co	55.101	35.604	42.246	49.718	56.348
Ni	62.825	94.980	138.358	51.438	59.114
Cu	2.756	2.335	1.604	11.319	28.215
Zn	100.686	85.202	104.665	143.248	150.036
Ga	10.313	9.236	9.150	13.721	9.110
Y	28.520	20.159	32.854	52.452	75.504
Nb	3.424	4.000	5.944	4.946	13.445
Ta	0.304	0.533	0.463	0.198	0.807
Zr (XRF)	364.200	129.000	308.200	493.600	2173.700
Hf	0.259	0.174	0.067	0.664	1.080
Mo	2.598	1.541	0.401	0.416	1.678
Sn	0.756	0.960	1.809	2.522	2.959
Tl	0.001	0.000	0.003	0.000	0.252
Pb	0.540	0.881	1.763	0.650	0.870
U	0.320	0.398	0.641	0.481	1.494
Th	0.062	0.779	2.136	0.189	1.408
La	24.726	18.659	42.997	17.927	31.249
Ce	44.108	32.290	69.837	39.257	57.858
Pr	6.168	4.316	8.534	6.441	9.081
Nd	27.463	18.126	33.543	32.274	44.962
Sm	6.308	4.097	6.839	9.061	13.865
Eu	3.358	4.411	7.758	3.135	6.660
Gd	5.941	4.180	6.065	9.951	14.886
Tb	0.944	0.632	0.973	1.514	2.274
Dy	4.770	3.456	5.647	9.523	14.519
Ho	1.064	0.690	1.192	2.004	3.195
Er	2.794	1.772	3.191	5.206	8.808
Tm	0.448	0.250	0.503	0.845	1.361
Yb	2.738	1.635	3.092	5.705	8.224
Lu	0.360	0.220	0.461	0.796	1.217

Supplementary Table 6 (continued). Major and trace element data from jadeitites and related rocks from the Sierra del Convento mélange.

Sample	MCB-2a	MCB-3d	09-SC-8b I	09-SC-27j	09-SC-31o	09-SC-31p
Group	Actinolitite	Actinolitite	Actinolitite	Actinolitite	Actinolitite	Actinolitite
SiO_2	54.520	51.050	44.850	53.110	49.640	48.330
TiO_2	0.040	0.080	0.040	0.090	0.050	0.080
Al_2O_3	2.830	5.420	7.690	3.030	4.620	4.890
FeO_{tot}	4.175	6.335	5.021	3.842	4.580	5.282
MnO	0.112	0.190	0.104	0.093	0.100	0.118
MgO	22.740	21.640	27.080	24.170	25.520	27.370
CaO	10.790	9.830	5.900	9.540	7.990	6.700
Na_2O	0.360	0.260	0.000	0.540	0.560	0.400
K_2O	0.070	0.020	0.020	0.140	0.130	0.110
P_2O_5	0.008	0.017	0.010	0.008	0.008	0.008
LOI	3.410	3.800	7.740	4.290	5.330	6.280
Total	99.520	99.347	99.014	99.281	99.038	100.156
Li	2.841	3.338	0.695	0.615	0.453	0.750
Rb	0.087	0.126	0.101	0.305	0.111	0.284
Cs	0.042	0.014	0.034	0.032	0.014	0.038
Be	0.587	0.241	0.564	0.647	0.457	0.188
Sr	105.793	9.630	47.518	23.040	82.755	75.792
Ba	0.417	1.231	3.287	0.111	0.000	7.030
Sc	3.718	7.223	9.241	5.672	4.760	9.004
V	24.143	44.750	42.906	41.264	35.035	51.908
Cr	1074.203	1252.359	1764.241	1591.208	1841.354	1627.404
Co	72.620	63.334	67.809	71.259	78.183	82.774
Ni	1439.939	994.716	1312.471	1311.545	1403.494	1357.061
Cu	1.431	4.011	1.098	8.556	3.842	5.159
Zn	26.506	65.333	28.912	21.216	28.708	39.684
Ga	2.641	6.840	7.821	4.555	4.344	4.614
Y	0.646	2.845	1.261	1.669	1.019	1.616
Nb	0.107	0.207	0.104	0.097	0.130	0.197
Ta	0.116	0.123	0.118	0.103	0.122	0.155
Zr (XRF)	6.500	9.600	6.700	6.100	7.800	4.800
Hf	0.017	0.119	0.026	0.000	0.000	0.000
Mo	1.980	2.419	1.795	1.075	2.476	2.018
Sn	0.204	0.155	0.105	0.404	0.147	0.302
Tl	0.000	0.000	0.000	0.038	0.004	0.006
Pb	0.431	0.105	0.059	0.033	0.042	0.167
U	0.012	0.022	0.000	0.028	0.000	0.006
Th	0.044	0.167	0.005	0.045	0.020	0.121
La	0.021	0.548	0.095	0.068	0.076	0.239
Ce	0.084	1.678	0.294	0.213	0.339	0.697
Pr	0.015	0.273	0.081	0.075	0.071	0.150
Nd	0.097	1.181	0.411	0.581	0.519	0.774
Sm	0.056	0.296	0.174	0.277	0.234	0.259
Eu	0.033	0.199	0.042	0.072	0.053	0.085
Gd	0.084	0.372	0.198	0.328	0.231	0.314
Tb	0.015	0.065	0.032	0.058	0.037	0.059
Dy	0.075	0.435	0.204	0.387	0.222	0.364
Ho	0.017	0.093	0.041	0.103	0.047	0.067
Er	0.046	0.276	0.146	0.299	0.118	0.174
Tm	0.010	0.042	0.020	0.044	0.017	0.024
Yb	0.068	0.299	0.135	0.274	0.105	0.166
Lu	0.011	0.045	0.019	0.043	0.015	0.028

Supplementary Table 7. Rb/Sr and Sm/Nd isotope data of jadeitites and related rocks from the Sierra del Convento mélange.

Sample	*Rb(ppm)*	*Sr(ppm)*	*87Rb/86Sr*	*87Sr/86Sr*	*Error Sr/Sr*	*Sm(ppm)*	*Nd(ppm)*	*147Sm/144Nd*	*143Nd/144Nd*	*Error Nd/Nd*	*Age*	*87Sr/86Sr_t*	*Group*
MCB-3H	1.099	150.429	0.0211	0.703507	0.002	3.127	20.26312	0.0933	0.512879	0.002	113	0.70347312	Pure jadeitite
CV-237B	3.09	139.566	0.064	0.703566	0.003	1.37	5.389414	0.1537	0.512925	0.005	113	0.70346322	Pure jadeitite
CV-237K	0.647	45.694	0.041	0.703576	0.005	1.542	6.500264	0.1434	0.512924	0.005	113	0.70351016	Pure jadeitite
CV-237T	1.717	367.861	0.0135	0.703547	0.003	1.464	5.727759	0.1545	0.512889	0.004	113	0.70352532	Pure jadeitite
MCB-1D	5.398	2096.282	0.0074	0.703486	0.002	3.08	10.147	0.1835	0.513036	0.003	113	0.70347412	Ep-rich jadeitite
MCB-1G	17.326	1223.325	0.041	0.70347	0.003	2.722	8.946	0.184	0.513008	0.002	113	0.70340416	Ep-rich jadeitite
MCB-2C	7.93	1046.839	0.0219	0.703535	0.004	1.863	6.828	0.165	0.512941	0.0019	113	0.70349983	Ep-rich jadeitite
09SC-27K	4.51	115.76	0.113	0.703780	0.003	1.18	3.02	0.236	0.512935	0.002	113	0.70359918	Ep-rich jadeitite
09SC-7J	18.81	1108.88	0.049	0.703523	0.003	1.89	6.01	0.190	0.512966	0.003	113	0.70344415	Mica-rich jadeitite
MCB-1E	2.953	540.119	0.0158	0.70352	0.004	1.786	5.63	0.1918	0.512941	0.002	113	0.70349463	Ab-Ep rock
09SC-31C	2.47	607.20	0.012	0.703450	0.003	2.56	7.44	0.208	0.512981	0.002	113	0.70343105	Ab-Ep rock

Supplementary Table8. SHRIMP II analytical data and ages from spot analyses of zircons from analyzed samples

Sample No.	U (ppm)	Th (ppm)	Th/U	$^{207}Pb/^{206}Pb$	$^{206}Pb/^{238}U$	$^{207}Pb/^{235}U$	$^{206}Pb/^{238}U$ age± 1σ
CV-237-T (Pure jadeitite)							
CV-237-T-1	786	172	0.21	0.0495	0.0168	0.115	108 ± 1
CV-237-T-2	684	162	0.23	0.0474	0.0168	0.11	107 ± 1
CV-237-T-3	487	118	0.24	0.0488	0.0167	0.113	107 ± 1
CV-237-T-4	1304	495	0.37	0.0485	0.0168	0.112	107 ± 1
CV-237-T-5	1281	754	0.58	0.0468	0.0168	0.109	108 ± 1
CV-237-T-6	716	169	0.23	0.0485	0.0168	0.113	107 ± 1
CV-237-B (Pure jadeitite)							
CV-237-B-1	163	53	0.32	0.0428	0.0168	0.099	108 ± 2
CV-237-B-2	264	78	0.29	0.0502	0.0168	0.116	108 ± 1
CV-237-B-3	540	240	0.44	0.0464	0.017	0.1084	108 ± 1
CV-237-B-4	458	249	0.54	0.0465	0.0168	0.108	107 ± 1
CV-237-B-5	1214	627	0.51	0.0474	0.0169	0.11	108 ± 15
CV-237-B-6	329	104	0.31	0.0466	0.0168	0.108	108 ± 1
09-SC-27C (Epidote-rich jadeitite)							
09-SC-27C-1	56	13	0.22	0.0536	0.0171	0.1201	109 ± 4
09-SC-27C-2	96	29	0.30	0.0510	0.0173	0.1190	110 ± 3
09-SC-27C-3	97	15	0.15	0.0512	0.0180	0.1231	114 ± 4
09-SC-27C-4	151	53	0.35	0.0522	0.0177	0.1244	113 ± 3
09-SC-27C-5	210	32	0.15	0.0487	0.0184	0.1210	117 ± 3
09-SC-27C-6	62	27	0.44	0.0482	0.0177	0.1132	113 ± 3
09-SC-27D (Epidote-rich jadeitite)							
09-SC-27D-1	197	103	0.52	0.0487	0.0176	0.1158	112 ± 3
09-SC-27D-2	120	32	0.26	0.0481	0.0176	0.1129	112 ± 4
09-SC-27D-3	32	9	0.27	0.0564	0.0176	0.1247	112 ± 5
09-SC-27D-4	167	26	0.15	0.0534	0.0168	0.1194	108 ± 4
09-SC-27D-5	42	11	0.27	0.0488	0.0177	0.1147	113 ± 5
09-SC-27D-6	144	55	0.38	0.0499	0.0177	0.1194	113 ± 3
09-SC-27D-7	50	15	0.30	0.0538	0.0172	0.1230	110 ± 4
09-SC-27B (Ep-Ab Chl-rich rock)							
09-SC-27B-1	173	33	0.19	0.0497	0.0179	116	115 ± 3
09-SC-27B-2	82	18	0.22	0.0531	0.0181	122	115 ± 4
09-SC-27B-3	63	15	0.24	0.0501	0.0173	110	111 ± 4
09-SC-27B-4	100	27	0.27	0.0524	0.0169	114	108 ± 4
09-SC-27B-5	74	13	0.18	0.0472	0.0183	110	117 ± 4
09-SC-27B-6	140	26	0.19	0.0517	0.0178	118	114 ± 4
09-SC-27B-7	331	42	0.13	0.0489	0.0174	111	111 ± 3
09-SC-27B-8	61	20	0.33	0.0507	0.0173	109	111 ± 5
09-SC-27B-9	209	25	0.12	0.0521	0.0176	119	112 ± 5
09-SC-27B-10	121	17	0.14	0.0479	0.0178	109	114 ± 5
09-SC-27B-11	62	24	0.39	0.0565	0.0176	127	112 ± 4

09-SC-27B-12	125	14	0.11	0.0508	0.0173	111	111 ± 4
09-SC-27B-13	108	18	0.17	0.0499	0.0176	113	112 ± 4
09-SC-27B-14	40	9	0.23	0.0495	0.0170	108	109 ± 5
09-SC-27B-15	199	26	0.13	0.0527	0.0173	118	111 ± 4
09-SC-27B-16	203	39	0.19	0.0528	0.0176	120	112 ± 4
09-SC-27B-17	137	45	0.33	0.0526	0.0179	120	115 ± 3
09-SC-27A (Chloritite)							
09-SC-27A-1	153	19	0.12	0.0536	0.0177	122	113 ± 4
09-SC-27A-2	168	29	0.17	0.0512	0.0179	119	115 ± 3
09-SC-27A-3	76	21	0.27	0.0543	0.0173	118	111 ± 4
09-SC-27A-4	94	19	0.20	0.0511	0.0172	111	110 ± 4
09-SC-27A-5	26	7	0.26	0.0657	0.0163	129	104 ± 4
09-SC-27A-6	21	3	0.15	0.0685	0.0170	132	109 ± 6
09-SC-8A VII (Ttn-Ap-Zr-rich Chloritite)							
09-SC-8A VII-1.1	204	33	0.17	0.0531	0.0179	111	114 ± 1
09-SC-8A VII-10.1	502	105	0.21	0.0488	0.0177	105	112 ± 1
09-SC-8A VII-11.1	474	79	0.17	0.0503	0.0181	113	115 ± 2
09-SC-8A VII-11.2	602	237	0.40	0.0486	0.0177	114	113 ± 2
09-SC-8A VII-12.1	313	20	0.07	0.0475	0.0173	95	110 ± 1
09-SC-8A VII-13.1	542	113	0.21	0.0511	0.0177	114	113 ± 1
09-SC-8A VII-14.1	469	141	0.31	0.0468	0.0180	112	115 ± 1
09-SC-8A VII-15.1	324	103	0.33	0.0489	0.0175	111	112 ± 3
09-SC-8A VII-16.1	575	122	0.22	0.0475	0.0163	91	103 ± 1
09-SC-8A VII-17.1	554	104	0.19	0.0502	0.0179	115	114 ± 3
09-SC-8A VII-18.1	352	87	0.25	0.0524	0.0173	112	110 ± 1
09-SC-8A VII-18.2	662	129	0.20	0.0510	0.0173	112	110 ± 2
09-SC-8A VII-19.2	451	110	0.25	0.0486	0.0183	109	117 ± 1
09-SC-8A VII-19.3	161	30	0.19	0.0526	0.0173	110	110 ± 2
09-SC-8A VII-2.1	301	49	0.17	0.0493	0.0181	108	115 ± 2
09-SC-8A VII-2.2	304	56	0.19	0.0514	0.0178	110	113 ± 1
09-SC-8A VII-20.1	515	70	0.14	0.0499	0.0167	104	106 ± 3
09-SC-8A VII-20.2	790	167	0.22	0.0499	0.0176	115	112 ± 2
09-SC-8A VII-20.3	169	64	0.39	0.0516	0.0183	122	117 ± 1
09-SC-8A VII-20.4	230	71	0.32	0.0488	0.0176	108	112 ± 1
09-SC-8A VII-3.1	290	69	0.24	0.0484	0.0196	125	125 ± 7
09-SC-8A VII-5.1	400	40	0.10	0.0561	0.0178	95	111 ± 4
09-SC-8A VII-5.2	349	73	0.22	0.0489	0.0177	103	112 ± 9
09-SC-8A VII-6.1	395	89	0.23	0.0511	0.0179	120	115 ± 1
09-SC-8A VII-6.2	439	47	0.11	0.0494	0.0174	114	111 ± 11
09-SC-8A VII-7.1	626	146	0.24	0.0492	0.0181	111	115 ± 1
09-SC-8A VII-7.2	278	60	0.22	0.0529	0.0178	122	114 ± 2
09-SC-8A VII-8.1	1356	251	0.19	0.0500	0.0183	120	117 ± 1
09-SC-8A VII-9.1	340	68	0.21	0.0530	0.0174	112	111 ± 2

Supplementary Table 9. Mineral analyses normalized to the indicated number of O, Cl, F and H (sorted by mineral > type of rock > sample > Px type 1 > Px type 2). Note: due to space limitations, oxide wt% data are not presented.

Rock type	Sample	Phase	Point	serie	Px type	Px type	Jd mole%	Si	Ti	Al	Fe3+	Fe2+	Mn	Mg	Ca	Ba	Na	K	F	Cl	H	O
Ab-Ep Chl-rich rock	09SC27b	Amp	2205	SEM				8.05		1.83	0.00	1.05		2.26			1.68				2.00	24.00
Ab-Ep Chl-rich rock	09SC27b	Amp	2204	SEM				8.02		1.76	0.26	0.76		2.17			1.99				2.00	24.00
Ab-Ep Chl-rich rock	09SC27b	Amp	2214	SEM				7.99		1.71	0.17	0.90		2.37			1.90				2.00	24.00
Ab-Ep rock	09SC31a	Amp	2290	SEM				7.78		0.30	0.14	1.29		3.72	1.78						2.00	24.00
Ab-Ep rock	09SC31a	Amp	2260	SEM				8.07		0.53	0.00	1.14		3.00	1.94						2.00	24.00
Ab-Ep rock	09SC31a	Amp	2284	SEM				8.30			0.00	1.34		3.12	1.94						2.00	24.00
Ab-Ep rock	09SC31a	Amp	2287	SEM				8.05		0.25	0.00	1.37		3.33	1.83						2.00	24.00
Ab-Ep rock	09SC31a	Amp	2288	SEM				8.06		0.19	0.00	1.28		3.36	1.95						2.00	24.00
Ab-Ep rock	09SC31a	Amp	2292	SEM				8.03			0.00	1.45		3.55	1.94						2.00	24.00
Ab-Ep rock	09SC31a	Amp	2304	SEM				8.22			0.00	1.27		3.44	1.84						2.00	24.00
Ab-Ep rock	09SC31d	Amp	1697	SEM				7.85		0.34	0.00	1.28		3.69	1.82						2.00	24.00
Ab-Ep rock	09SC31d	Amp	1698	SEM				8.34			0.00	1.17		3.48	1.68						2.00	24.00
Ab-Ep rock	09SC31d	Amp	1699	SEM				8.04			0.00	1.36		3.62	1.94						2.00	24.00
Ab-Ep rock	09SC31d	Amp	1710	SEM				8.17			0.00	1.40		3.52	1.75						2.00	24.00
Ab-Ep rock	09SC31d	Amp	1712	SEM				8.35			0.00	1.03		3.46	1.81						2.00	24.00
Ab-Ep rock	09SC31d	Amp	1715	SEM				7.74		0.59	0.00	1.35		3.50	1.79						2.00	24.00
Ab-Ep rock	09SC31d	Amp	1731	SEM				8.36			0.00	1.31		3.35	1.62						2.00	24.00
Ab-Ep rock	09SC31d	Amp	1736	SEM				8.20			0.00	1.30		3.62	1.68						2.00	24.00
Ab-Ep rock	09SC31d	Amp	1747	SEM				8.01		0.33	0.00	1.07		3.50	1.92						2.00	24.00
Ab-Ep rock	09SC31d	Amp	1750	SEM				7.82		0.44	0.00	1.37		3.37	1.97						2.00	24.00
Ab-Ep rock	09SC31d	Amp	1761	SEM				7.87		0.30	0.00	1.42		3.47	1.91						2.00	24.00
Ab-Ep rock	MCB1e	Amp	3102	VPSEM				7.68	0.00	0.41	0.15	0.98	0.00	3.82	1.88		0.22	0.03			2.00	24.00
Ab-Ep rock	MCB1e	Amp	3096	VPSEM				7.40	0.00	0.94	0.16	1.09	0.00	3.45	1.72		0.57	0.00			2.00	24.00
Ep-rich jadeitite	09SC31g	Amp	1802	SEM				6.79		2.32	0.48	0.69		2.86	0.91		1.53				2.00	24.00
Ep-rich jadeitite	MCB4a	Amp	1493	VPSEM				6.79		2.97	0.00	1.77		1.27	1.26		1.31				2.00	24.00
Ep-rich jadeitite	MCB4a	Amp	1402	EPMA				6.09	0.04	2.92	0.52	1.66	0.02	1.74	1.29		1.67	0.04	0.06	0.00	1.94	23.94
Ep-rich jadeitite	MCB4a	Amp	1404	EPMA				5.99	0.01	3.17	0.56	1.61	0.03	1.65	1.27		1.66	0.04	0.05	0.00	1.94	23.94
Ep-rich jadeitite	MCB4a	Amp	1403	EPMA				6.17	0.03	2.97	0.35	1.79	0.02	1.69	1.28		1.63	0.05	0.06	0.00	1.94	23.94
Ep-rich jadeitite	MCB4a	Amp	1494	VPSEM				6.24		2.55	0.72	2.29		1.47	1.19		1.33				2.00	24.00
Pure jadeitite	CV237b	Amp	2522	VPSEM				7.83	0.00	2.09	0.00	1.41	0.00	1.57	0.14		2.15	0.00			2.00	24.00
Pure jadeitite	CV237b	Amp	2521	VPSEM				7.90	0.00	1.95	0.07	1.34	0.00	1.76	0.11		1.93	0.00			2.00	24.00
Pure jadeitite	CV237b	Amp	156	EPMA				6.81	0.00	2.48	0.03	1.37	0.02	2.30	1.24		1.37	0.00	0.04	0.00	1.96	23.96
Cr-rich Pure Jdt	SCMJ10	Anl	351	EPMA				2.03	0.00	1.01	0.00	0.00	0.00	0.00	0.00		0.79	0.04	0.01	0.01	1.99	6.99
Cr-rich Pure Jdt	SCMJ10	Anl	352	EPMA				2.00	0.00	1.02	0.00	0.00	0.00	0.00	0.00		0.92	0.01	0.00	0.00	2.00	7.00
Cr-rich Pure Jdt	SCMJ10	Anl	353	EPMA				2.00	0.00	1.03	0.00	0.00	0.00	0.00	0.00		0.88	0.03	0.00	0.00	2.00	7.00
Cr-rich Pure Jdt	SCMJ10	Anl	3631	VPSEM				1.99	0.00	1.01	0.00	0.00	0.00	0.00	0.00		0.97	0.02			2.00	7.00
Cr-rich Pure Jdt	SCMJ10	Anl	3643	VPSEM				1.97	0.00	1.02	0.00	0.00	0.00	0.00	0.01		1.03	0.00			2.00	7.00
Cr-rich Pure Jdt	SCMJ10	Anl	3646	VPSEM				1.98	0.00	1.04	0.00	0.00	0.00	0.00	0.00		0.97	0.00			2.00	7.00
Ep-rich jadeitite	09SC27d	Anl	1908	SEM				2.04		0.88					0.07		1.08				2.00	7.00
Ep-rich jadeitite	09SC31g	Anl	1808	SEM				2.11		0.92							0.82				2.00	7.00

Rock type	Sample	Phase	Point	serie	Px type	Px type	Jd mole%	Si	Ti	Al	Fe3+	Fe2+	Mn	Mg	Ca	Ba	Na	K	F	Cl	H	O
Ep-rich jadeitite	09SC31g	Anl	1810	SEM				2.02		0.95							1.07				2.00	7.00
Ep-rich jadeitite	MCB1d	Anl	1551	VPSEM				1.92		1.14					0.05		0.78	0.01			2.00	7.00
Ep-rich jadeitite	MCB1d	Anl	1552	VPSEM				1.96		1.07					0.04		0.84	0.01			2.00	7.00
Ep-rich jadeitite	MCB1d	Anl	1553	VPSEM				1.94		1.12					0.04		0.79	0.01			2.00	7.00
Ep-rich jadeitite	MCB1d	Anl	1667	VPSEM				1.99		1.13					0.03		0.58				2.00	7.00
Ep-rich jadeitite	MCB1d	Anl	1689	VPSEM				1.94		1.11					0.04		0.83	0.01			2.00	7.00
Ep-rich jadeitite	MCB2c	Anl	3405	VPSEM				1.90	0.00	1.21	0.00	0.01	0.00	0.04	0.00		0.63	0.02			2.00	7.00
Ep-rich jadeitite	MCB4a	Anl	1425	EPMA				1.96	0.00	1.09	0.00	0.00	0.00	0.00	0.01		0.88	0.01	0.00	0.00	2.00	7.00
Ep-rich jadeitite	MCB4a	Anl	1427	EPMA				1.95	0.00	1.10	0.00	0.00	0.00	0.00	0.00		0.88	0.01	0.00	0.00	2.00	7.00
Ep-rich jadeitite	MCB4a	Anl	1452	VPSEM				2.01		1.01							0.92				2.00	7.00
Ep-rich jadeitite	MCB4a	Anl	1486	VPSEM				2.07		1.00							0.73				2.00	7.00
Ep-rich jadeitite	MCB4a	Anl	1495	VPSEM				2.04		1.02							0.76				2.00	7.00
Ep-rich jadeitite	MCB4a	Anl	1501	VPSEM				2.07		1.03							0.64				2.00	7.00
Pure jadeitite	BCJ1	Anl	2500	VPSEM				1.95	0.01	1.00	0.00	0.01		0.02	0.03		1.05				2.00	7.00
Pure jadeitite	CV237K	Anl	2688	VPSEM				1.96	0.00	1.06	0.00	0.00	0.00	0.00	0.00		0.98	0.00			2.00	7.00
Pure jadeitite	CV237K	Anl	2690	VPSEM				1.97	0.00	1.05	0.00	0.00	0.00	0.00	0.01		0.94	0.01			2.00	7.00
Pure jadeitite	CV237K	Anl	2812	VPSEM				2.00	0.00	1.02	0.00	0.00	0.00	0.00	0.00		0.93	0.01			2.00	7.00
Pure jadeitite	CV237K	Anl	2840	VPSEM				1.99	0.00	1.06	0.00	0.00	0.00	0.00	0.00		0.85	0.01			2.00	7.00
Pure jadeitite	CV237K	Anl	2846	VPSEM				2.01	0.00	1.00	0.00	0.00	0.00	0.00	0.00		0.93	0.00			2.00	7.00
Pure jadeitite	CV237K	Anl	2848	VPSEM				2.01	0.00	1.05	0.00	0.00	0.00	0.00	0.00		0.82	0.01			2.00	7.00
Pure jadeitite	CV237t	Anl	2963	VPSEM				2.01	0.00	1.01	0.00	0.00	0.00	0.00	0.00		0.94	0.00			2.00	7.00
Pure jadeitite	MCB1f	Anl	3155	VPSEM				1.97	0.00	1.01	0.00	0.00	0.00	0.01	0.00		1.05	0.01	0.00	0.00	2.00	7.00
Pure jadeitite	MCB1f	Anl	3168	VPSEM				2.00	0.00	1.03	0.00	0.01	0.00	0.00	0.02		0.86	0.01	0.00	0.00	2.00	7.00
Pure jadeitite	MCB1f	Anl	3201	VPSEM				1.99	0.00	1.06	0.00	0.00	0.00	0.00	0.00		0.87	0.01	0.00	0.00	2.00	7.00
Pure jadeitite	MCB1f	Anl	3209	VPSEM				2.00	0.00	1.04	0.00	0.00	0.00	0.00	0.00		0.87	0.01	0.00	0.00	2.00	7.00
Pure jadeitite	MCB1j	Anl	1317	EPMA				1.98	0.00	1.07	0.00	0.00	0.00	0.00	0.00		0.87	0.01	0.00	0.01	1.99	6.99
Pure jadeitite	MCB1j	Anl	1370	EPMA				1.95	0.00	1.10	0.00	0.00	0.00	0.00	0.00		0.86	0.01	0.00	0.00	2.00	7.00
Ab-Ep Chl-rich rock	09SC27b	Ap	2164	SEM											4.61						1.00	13.00
Ab-Ep Chl-rich rock	09SC27b	Ap	2165	SEM											4.65						1.00	13.00
Ab-Ep Chl-rich rock	09SC27b	Ap	2172	SEM											4.59						1.00	13.00
Ab-Ep Chl-rich rock	09SC27b	Ap	2173	SEM											4.75						1.00	13.00
Ab-Ep rock	09SC31a	Ap	2271	SEM											4.52						1.00	13.00
Ab-Ep rock	09SC31a	Ap	2272	SEM											4.70						1.00	13.00
Ab-Ep rock	09SC31c	Ap	2339	SEM											4.54						1.00	13.00
Ab-Ep rock	09SC31n	Ap	1834	SEM											4.29						1.00	13.00
Ab-Ep rock	09SC31n	Ap	1837	SEM											4.68						1.00	13.00
Ab-Ep rock	09SC31n	Ap	1852	SEM											4.58						1.00	13.00
Ab-Ep rock	09SC31n	Ap	1853	SEM											4.94						1.00	13.00
Ab-Ep rock	09SC31n	Ap	1884	SEM											4.57						1.00	13.00
Ab-Ep rock	09SC31n	Ap	1885	SEM											4.85						1.00	13.00
Ab-Ep rock	MCB1e	Ap	56	EPMA				0.11	0.00	0.09	0.00	0.05	0.00	0.12	4.47		0.00	0.00	0.82	0.00	0.18	4.68
Ep-rich jadeitite	09SC31g	Ap	1791	SEM											4.37						1.00	13.00
Ep-rich jadeitite	09SC31g	Ap	1798	SEM											4.48						1.00	13.00
Ep-rich jadeitite	09SC31g	Ap	1806	SEM											5.01						1.00	13.00

Rock type	Sample	Phase	Point	serie	Px type	Px type	Jd mole%	Si	Ti	Al	Fe3+	Fe2+	Mn	Mg	Ca	Ba	Na	K	F	Cl	H	O
Ep-rich jadeitite	09SC31j	Ap	1932	SEM											4.62						1.00	13.00
Ep-rich Jadeitite	MCB1d	Ap	216	EPMA				0.00	0.00	0.00	0.00	0.00	0.00	0.01	4.98		0.00	0.00	0.47	0.00	0.53	5.03
Ep-rich jadeitite	MCB1d	Ap	1625	VPSEM				0.04							4.91						1.00	5.50
Ep-rich jadeitite	MCB1d	Ap	1626	VPSEM				0.05							4.91						1.00	5.50
Ep-rich jadeitite	MCB1g	Ap	3289	VPSEM				0.07	0.00	0.00	0.00	0.00	0.00	0.00	4.87		0.00	0.00			1.00	5.50
Ep-rich jadeitite	MCB2c	Ap	3394	VPSEM				0.05	0.00	0.00	0.00	0.00	0.00	0.00	4.90		0.00	0.00			1.00	5.50
Ep-rich jadeitite	MCB4a	Ap	1373	EPMA				0.00	0.00	0.00	0.00	0.01	0.00	0.01	4.96		0.00	0.00	0.44	0.01	0.55	5.05
Ep-rich jadeitite	MCB4a	Ap	1470	VPSEM											4.76						1.00	13.00
Mica-rich Jadeitite	09SC31e	Ap	1814	SEM											4.75						1.00	13.00
Mica-rich Jadeitite	09SC31e	Ap	1815	SEM											4.58						1.00	13.00
Mica-rich Jadeitite	09SC31e	Ap	1816	SEM											4.83						1.00	13.00
Mica-rich Jadeitite	09SC31e	Ap	1817	SEM											5.32						1.00	13.00
Mica-rich Jadeitite	09SC31e	Ap	1818	SEM											5.22						1.00	13.00
Mica-rich Jadeitite	09SC31e	Ap	2310	SEM											4.09						1.00	13.00
Mica-rich Jadeitite	09SC31e	Ap	2311	SEM											5.05						1.00	13.00
Mica-rich Jadeitite	09SC31e	Ap	2312	SEM											4.45						1.00	13.00
Pure jadeitite	CV237b	Ap	2643	VPSEM				0.06	0.00	0.00	0.00	0.00	0.00	0.00	4.89		0.00	0.00			1.00	5.50
Pure jadeitite	CV237b	Ap	2649	VPSEM				0.06	0.00	0.00	0.00	0.00	0.00	0.00	4.89		0.00	0.00			1.00	5.50
Pure jadeitite	CV237b	Ap	2654	VPSEM				0.07	0.00	0.00	0.00	0.00	0.00	0.00	4.86		0.00	0.00			1.00	5.50
Pure jadeitite	CV237b	Ap	2655	VPSEM				0.07	0.00	0.00	0.00	0.00	0.00	0.00	4.83		0.06	0.00			1.00	5.50
Pure jadeitite	CV237k	Ap	285	EPMA				0.01	0.00	0.00	0.00	0.00	0.00	0.01	4.98		0.00	0.00	0.29	0.00	0.71	5.21
Pure jadeitite	CV237k	Ap	286	EPMA				0.01	0.00	0.00	0.00	0.00	0.00	0.01	4.98		0.00	0.00	0.36	0.01	0.64	5.14
Pure jadeitite	CV237k	Ap	287	EPMA				0.00	0.00	0.00	0.00	0.00	0.00	0.00	4.98		0.00	0.00	0.27	0.00	0.73	5.23
Pure jadeitite	CV237k	Ap	288	EPMA				0.01	0.00	0.00	0.00	0.01	0.00	0.01	4.98		0.00	0.00	0.38	0.00	0.62	5.12
Pure jadeitite	CV237k	Ap	343	EPMA				0.00	0.00	0.00	0.00	0.00	0.00	0.01	4.98		0.00	0.00	0.26	0.00	0.74	5.24
Pure jadeitite	CV237K	Ap	2701	VPSEM				0.06	0.00	0.00	0.00	0.00	0.00	0.00	4.89		0.00	0.00			1.00	5.50
Pure jadeitite	CV237K	Ap	2702	VPSEM				0.07	0.00	0.00	0.00	0.00	0.00	0.00	4.86		0.00	0.00			1.00	5.50
Pure jadeitite	CV237K	Ap	2710	VPSEM				0.06	0.00	0.00	0.00	0.00	0.00	0.00	4.87		0.00	0.00			1.00	5.50
Pure jadeitite	CV237K	Ap	2779	VPSEM				0.06	0.00	0.00	0.00	0.00	0.00	0.00	4.88		0.00	0.00			1.00	5.50
Pure jadeitite	CV237K	Ap	2782	VPSEM				0.08	0.00	0.00	0.00	0.00	0.00	0.00	4.84		0.00	0.00			1.00	5.50
Pure jadeitite	CV237K	Ap	2822	VPSEM				0.04	0.00	0.00	0.00	0.00	0.00	0.00	4.92		0.00	0.00			1.00	5.50
Pure jadeitite	CV237K	Ap	2835	VPSEM				0.11	0.00	0.05	0.00	0.00	0.00	0.00	4.67		0.07	0.00			1.00	5.50
Pure jadeitite	CV237t	Ap	2887	VPSEM				0.06	0.00	0.00	0.00	0.00	0.00	0.00	4.89		0.00	0.00			1.00	5.50
Pure jadeitite	CV237t	Ap	2900	VPSEM				0.06	0.00	0.00	0.00	0.00	0.00	0.00	4.89		0.00	0.00			1.00	5.50
Pure jadeitite	CV237t	Ap	2903	VPSEM				0.04	0.00	0.00	0.00	0.02	0.00	0.00	4.89		0.00	0.01			1.00	5.50
Pure jadeitite	CV237t	Ap	2904	VPSEM				0.06	0.00	0.00	0.00	0.00	0.00	0.00	4.88		0.00	0.00			1.00	5.50
Pure jadeitite	CV237t	Ap	2905	VPSEM				0.06	0.00	0.00	0.00	0.00	0.00	0.00	4.87		0.00	0.00			1.00	5.50
Pure jadeitite	CV237t	Ap	2917	VPSEM				0.07	0.00	0.00	0.00	0.00	0.00	0.00	4.86		0.00	0.00			1.00	5.50
Pure jadeitite	CV237t	Ap	2922	VPSEM				0.08	0.00	0.00	0.00	0.00	0.00	0.00	4.85		0.00	0.00			1.00	5.50
Pure jadeitite	MCB1f	Ap	3145	VPSEM				0.00	0.00	0.00	0.00	0.00	0.00	0.00	4.91		0.00	0.00	0.97	0.00	0.03	12.03
Pure jadeitite	MCB1f	Ap	3146	VPSEM				0.00	0.00	0.00	0.00	0.00	0.00	0.00	4.84		0.00	0.00	0.87	0.00	0.13	12.13
Pure jadeitite	MCB1f	Ap	3194	VPSEM				0.00	0.00	0.00	0.00	0.00	0.00	0.00	4.84		0.00	0.00	0.00	0.00	1.00	13.00
Pure jadeitite	MCB1f	Ap	3213	VPSEM				0.00	0.00	0.00	0.00	0.00	0.00	0.00	4.87		0.00	0.00	1.18	0.03	-0.21	11.79
Pure jadeitite	MCB1j	Ap	1309	EPMA				0.00	0.00	0.00	0.00	0.00	0.00	0.01	4.97		0.00	0.00	0.43	0.00	0.57	5.07

Rock type	Sample	Phase	Point	serie	Px type	Px type	Jd mole%	Si	Ti	Al	Fe3+	Fe2+	Mn	Mg	Ca	Ba	Na	K	F	Cl	H	O
Pure jadeitite	MCB1j	Ap	1338	EPMA				0.00	0.00	0.00	0.00	0.00	0.00	0.01	4.98		0.00	0.00	0.43	0.00	0.57	5.07
Pure jadeitite	MCB2d	Ap	3232	VPSEM				0.00	0.00	0.00	0.00	0.00	0.00	0.00	4.81		0.00	0.00	1.43		-0.43	11.57
Pure jadeitite	MCB2d	Ap	3233	VPSEM				0.00	0.00	0.00	0.00	0.00	0.00	0.00	4.85		0.00	0.00	0.92		0.08	12.08
Pure jadeitite	MCB2d	Ap	3235	VPSEM				0.02	0.00	0.00	0.00	0.00	0.00	0.00	4.76		0.00	0.00	1.06		-0.06	11.94
Pure jadeitite	MCB2d	Ap	3236	VPSEM				0.02	0.00	0.00	0.00	0.00	0.00	0.00	4.85		0.00	0.00	0.66		0.34	12.34
Pure jadeitite	MCB2d	Ap	3255	VPSEM				0.00	0.00	0.00	0.00	0.00	0.00	0.00	4.83		0.00	0.00	0.81		0.19	12.19
Pure jadeitite	MCB3h	Ap	3503	VPSEM											4.81				1.14		-0.14	11.86
Pure jadeitite	MCB3h	Ap	3504	VPSEM											4.86				0.78		0.22	12.22
Pure jadeitite	MCB3h	Ap	3506	VPSEM											4.79				0.93		0.07	12.07
Pure jadeitite	MCB3h	Ap	3507	VPSEM											4.86				0.67		0.33	12.33
Pure Jdt/Ab-Ep rock/Chloritite	09SC8a3	Ap	2395	VPSEM											4.88				0.98		0.02	12.02
Pure Jdt/Ab-Ep rock/Chloritite	09SC8a3	Ap	2399	VPSEM											4.89				1.02		-0.02	11.98
Pure Jdt/Ab-Ep rock/Chloritite	09SC8a3	Ap	2404	VPSEM											4.93				0.74		0.26	12.26
Pure Jdt/Ab-Ep rock/Chloritite	09SC8a3	Ap	2410	VPSEM											4.92				0.91		0.09	12.09
Cr-rich Pure Jdt	SCMJ10	Bt	3621	VPSEM				5.40	0.00	3.23	0.00	0.77	0.00	4.63	0.00		0.23	1.68			4.00	24.00
Cr-rich Pure Jdt	SCMJ10	Bt	3624	VPSEM				5.44	0.00	3.18	0.00	0.77	0.00	4.62	0.00		0.22	1.70			4.00	24.00
Cr-rich Pure Jdt	SCMJ10	Bt	3642	VPSEM				5.51	0.00	3.02	0.00	0.77	0.00	4.71	0.00		0.24	1.70			4.00	24.00
Ep-rich jadeitite	09SC31g	Bt	1975	SEM				5.48		3.33	0.00	2.06		2.98			0.12	1.89			4.00	24.00
Ep-rich jadeitite	MCB4a	Bt	1376	EPMA				5.41	0.01	3.21	0.00	1.85	0.02	3.53	0.01		0.23	1.62	0.08	0.01	3.91	23.91
Ep-rich jadeitite	MCB4a	Bt	1378	EPMA				5.44	0.03	3.31	0.00	1.84	0.03	3.26	0.00		0.16	1.79	0.06	0.00	3.94	23.94
Ep-rich jadeitite	MCB4a	Bt	1380	EPMA				5.42	0.02	3.29	0.00	2.01	0.02	3.18	0.01		0.17	1.77	0.08	0.00	3.92	23.92
Ep-rich jadeitite	MCB4a	Bt	1381	EPMA				5.44	0.02	3.33	0.00	1.80	0.03	3.29	0.01		0.18	1.74	0.06	0.00	3.94	23.94
Ep-rich jadeitite	MCB4a	Bt	1395	EPMA				4.47	0.00	5.20	0.00	0.90	0.02	3.33	0.01		1.96	0.03	0.04	0.01	3.95	23.95
Pure jadeitite	CV237b	Bt	139	EPMA				5.48	0.01	3.20	0.00	1.77	0.01	3.43	0.01		0.14	1.83	0.06	0.00	3.93	23.93
Pure jadeitite	CV237b	Bt	141	EPMA				5.42	0.02	3.34	0.00	1.83	0.01	3.27	0.00		0.11	1.87	0.06	0.00	3.93	23.93
Pure jadeitite	CV237b	Bt	143	EPMA				5.42	0.02	3.30	0.00	1.79	0.01	3.37	0.00		0.12	1.86	0.07	0.00	3.93	23.93
Pure jadeitite	CV237b	Bt	145	EPMA				5.39	0.02	3.20	0.00	1.81	0.02	3.57	0.01		0.17	1.80	0.06	0.01	3.93	23.93
Pure jadeitite	CV237b	Bt	161	EPMA				5.42	0.02	3.22	0.00	1.75	0.02	3.57	0.00		0.18	1.76	0.08	0.00	3.92	23.92
Pure jadeitite	CV237b	Bt	2525	VPSEM				5.46	0.00	3.00	0.00	2.01	0.00	3.59	0.00		0.22	1.76			4.00	24.00
Pure jadeitite	CV237b	Bt	2544	VPSEM				5.35	0.00	3.35	0.00	2.01	0.00	3.29	0.00		0.17	1.78			4.00	24.00
Pure jadeitite	CV237b	Bt	2545	VPSEM				5.34	0.03	3.37	0.00	1.97	0.00	3.25	0.00		0.18	1.80			4.00	24.00
Pure jadeitite	CV237b	Bt	2663	VPSEM				5.35	0.00	3.35	0.00	1.95	0.00	3.34	0.00		0.20	1.77			4.00	24.00
Pure jadeitite	CV237K	Bt	2671	VPSEM				5.50	0.00	3.18	0.00	1.05	0.03	4.18	0.00		0.17	1.79			4.00	24.00
Pure jadeitite	CV237K	Bt	2673	VPSEM				5.54	0.00	3.15	0.00	1.02	0.03	4.15	0.00		0.20	1.78			4.00	24.00
Pure jadeitite	CV237K	Bt	2678	VPSEM				5.56	0.00	3.13	0.00	1.11	0.02	4.04	0.00		0.19	1.84			4.00	24.00
Pure jadeitite	CV237K	Bt	2679	VPSEM				5.53	0.00	3.11	0.00	1.00	0.03	4.28	0.00		0.18	1.77			4.00	24.00
Pure jadeitite	CV237K	Bt	2680	VPSEM				5.52	0.00	3.19	0.00	0.99	0.00	4.18	0.00		0.25	1.80			4.00	24.00
Pure jadeitite	CV237K	Bt	2685	VPSEM				5.58	0.00	3.13	0.00	1.03	0.00	4.15	0.00		0.16	1.78			4.00	24.00
Pure jadeitite	CV237K	Bt	2686	VPSEM				5.48	0.00	3.20	0.00	1.10	0.00	4.16	0.00		0.11	1.87			4.00	24.00
Pure jadeitite	CV237K	Bt	2692	VPSEM				5.40	0.00	3.41	0.00	1.04	0.00	4.02	0.00		0.18	1.85			4.00	24.00
Pure jadeitite	CV237K	Bt	2693	VPSEM				5.48	0.00	3.29	0.00	1.14	0.03	3.94	0.00		0.18	1.80			4.00	24.00
Pure jadeitite	CV237K	Bt	2695	VPSEM				5.51	0.00	3.25	0.00	1.15	0.04	3.89	0.00		0.18	1.86			4.00	24.00
Pure jadeitite	CV237t	Bt	64	EPMA				5.39	0.01	3.46	0.00	1.81	0.03	3.19	0.00		0.09	1.88	0.05	0.01	3.94	23.94
Pure jadeitite	CV237t	Bt	65	EPMA				5.32	0.01	3.57	0.00	1.79	0.03	3.16	0.00		0.11	1.88	0.07	0.01	3.93	23.93

Rock type	Sample	Phase	Point	serie	Px type	Px type	Jd mole%	Si	Ti	Al	Fe3+	Fe2+	Mn	Mg	Ca	Ba	Na	K	F	Cl	H	O
Pure jadeitite	CV237t	Bt	67	EPMA				5.30	0.01	3.58	0.00	1.76	0.03	3.24	0.00		0.11	1.86	0.08	0.01	3.91	23.91
Pure jadeitite	CV237t	Bt	68	EPMA				5.34	0.00	3.46	0.00	1.79	0.02	3.32	0.00		0.11	1.88	0.06	0.00	3.93	23.93
Pure jadeitite	CV237t	Bt	69	EPMA				5.31	0.01	3.56	0.00	1.75	0.02	3.25	0.00		0.12	1.85	0.05	0.01	3.94	23.94
Pure jadeitite	CV237t	Bt	103	EPMA				5.37	0.01	3.50	0.00	1.22	0.04	3.73	0.01		0.13	1.85	0.07	0.03	3.90	23.90
Pure jadeitite	CV237t	Bt	2854	VPSEM				5.46	0.00	3.21	0.00	1.18	0.03	4.06	0.00		0.16	1.84			4.00	24.00
Pure jadeitite	CV237t	Bt	2856	VPSEM				5.51	0.03	3.36	0.00	1.51	0.00	3.34	0.00		0.11	1.93			4.00	24.00
Pure jadeitite	CV237t	Bt	2857	VPSEM				5.33	0.00	3.44	0.00	1.46	0.03	3.66	0.00		0.18	1.87			4.00	24.00
Pure jadeitite	CV237t	Bt	2858	VPSEM				5.40	0.00	3.35	0.00	1.42	0.00	3.77	0.00		0.17	1.84			4.00	24.00
Pure jadeitite	CV237t	Bt	2868	VPSEM				5.42	0.04	3.27	0.00	1.18	0.04	4.00	0.00		0.11	1.80			4.00	24.00
Pure jadeitite	CV237t	Bt	2873	VPSEM				5.39	0.00	3.35	0.00	1.46	0.03	3.70	0.00		0.14	1.83			4.00	24.00
Pure jadeitite	CV237t	Bt	2885	VPSEM				5.31	0.00	3.48	0.00	1.46	0.04	3.69	0.00		0.13	1.82			4.00	24.00
Pure jadeitite	CV237t	Bt	2916	VPSEM				5.34	0.03	3.39	0.00	1.57	0.00	3.58	0.00		0.18	1.86			4.00	24.00
Pure jadeitite	CV237t	Bt	2931	VPSEM				5.45	0.00	3.23	0.00	1.48	0.00	3.77	0.00		0.18	1.82			4.00	24.00
Pure jadeitite	CV237t	Bt	2932	VPSEM				5.34	0.00	3.36	0.00	1.50	0.04	3.72	0.00		0.19	1.83			4.00	24.00
Pure jadeitite	CV237t	Bt	2933	VPSEM				5.38	0.00	3.37	0.00	1.51	0.04	3.66	0.00		0.11	1.85			4.00	24.00
Pure jadeitite	CV237t	Bt	2941	VPSEM				5.35	0.00	3.37	0.00	1.57	0.00	3.66	0.00		0.19	1.83			4.00	24.00
Pure jadeitite	CV237t	Bt	2950	VPSEM				5.46	0.00	3.27	0.00	1.51	0.00	3.68	0.00		0.13	1.83			4.00	24.00
Pure jadeitite	CV237t	Bt	2957	VPSEM				5.26	0.00	3.57	0.00	1.79	0.00	3.32	0.00		0.16	1.88			4.00	24.00
Pure jadeitite	CV237t	Bt	2958	VPSEM				5.24	0.00	3.66	0.00	1.81	0.04	3.22	0.00		0.09	1.83			4.00	24.00
Pure jadeitite	MCB1j	Bt	1339	EPMA				5.51	0.02	3.27	0.00	1.60	0.02	3.44	0.00		0.08	1.84	0.07	0.01	3.92	23.92
Pure jadeitite	MCB1j	Bt	1340	EPMA				5.36	0.01	3.48	0.00	1.57	0.02	3.47	0.00		0.15	1.79	0.03	0.00	3.97	23.97
Pure jadeitite	MCB1j	Bt	1341	EPMA				5.45	0.02	3.37	0.00	1.55	0.03	3.45	0.00		0.11	1.85	0.06	0.00	3.93	23.93
Pure jadeitite	MCB1j	Bt	1342	EPMA				5.45	0.02	3.33	0.00	1.60	0.02	3.47	0.01		0.10	1.85	0.07	0.01	3.93	23.93
Pure jadeitite	MCB1j	Bt	1343	EPMA				5.41	0.02	3.46	0.00	1.28	0.03	3.69	0.00		0.11	1.83	0.08	0.00	3.91	23.91
Pure jadeitite	MCB1j	Bt	1344	EPMA				5.39	0.01	3.45	0.00	1.55	0.03	3.47	0.00		0.13	1.81	0.06	0.00	3.94	23.94
Pure jadeitite	MCB2e	Bt	3281	VPSEM				5.56		3.31	0.00	1.20		3.76	0.00		0.15	1.72			4.00	24.00
Pure jadeitite	MCB2e	Bt	3283	VPSEM				5.39		3.32	0.00	1.70		3.58			0.15	1.77			4.00	24.00
Pure jadeitite	MCB3h	Bt	422	EPMA				5.43	0.01	3.18	0.00	1.81	0.02	3.57	0.00		0.24	1.69	0.08	0.01	3.91	23.91
Pure jadeitite	MCB3h	Bt	423	EPMA				5.37	0.02	3.26	0.00	1.88	0.02	3.45	0.00		0.20	1.79	0.06	0.01	3.93	23.93
Pure jadeitite	MCB3h	Bt	425	EPMA				5.55	0.03	3.09	0.00	1.72	0.02	3.51	0.01		0.14	1.74	0.04	0.00	3.96	23.96
Pure jadeitite	MCB3h	Bt	479	EPMA				5.49	0.03	3.13	0.00	1.84	0.03	3.46	0.00		0.16	1.74		0.00	4.00	24.00
Pure Jdt/Ab-Ep rock/Chloritite	09SC8a3	Bt	2440	VPSEM				5.27		3.44	0.00	1.24	0.02	4.07			0.13	1.79			4.00	24.00
Pure Jdt/Ab-Ep rock/Chloritite	09SC8a3	Bt	2443	VPSEM				5.30		3.43	0.00	1.23		4.06			0.14	1.81			4.00	24.00
Ab-Ep rock	MCB1e	Carb	2	EPMA				0.00	0.00	0.00	0.00	0.00	0.00	0.48	0.51		0.00	0.00	0.00	0.00	0.00	3.00
Ab-Ep rock	MCB1e	Carb	3	EPMA				0.00	0.00	0.00	0.00	0.00	0.00	0.47	0.53		0.00	0.00	0.00	0.00	0.00	3.00
Ab-Ep rock	MCB1e	Carb	6	EPMA				0.01	0.00	0.00	0.00	0.00	0.00	0.44	0.54		0.00	0.00	0.01	0.00	0.00	3.00
Ab-Ep rock	MCB1e	Carb	12	EPMA				0.00	0.00	0.00	0.00	0.00	0.00	0.48	0.52		0.00	0.00	0.00	0.00	0.00	3.00
Ab-Ep rock	MCB1e	Carb	29	EPMA				0.00	0.00	0.00	0.00	0.00	0.00	0.44	0.56		0.00	0.00	0.00	0.00	0.00	3.00
Ab-Ep rock	MCB1e	Carb	3095	VPSEM				0.00	0.00	0.00	0.00	0.00	0.00	0.48	0.52		0.00	0.00			0.00	3.00
Ab-Ep rock	MCB1e	Carb	3097	VPSEM				0.00	0.00	0.00	0.00	0.00	0.00	0.48	0.52		0.01	0.00			0.00	3.00
Ab-Ep rock	MCB1e	Carb	3100	VPSEM				0.00	0.00	0.00	0.00	0.00	0.00	0.48	0.52		0.00	0.00			0.00	3.00
Ab-Ep rock	MCB1e	Carb	3103	VPSEM				0.00	0.00	0.00	0.00	0.00	0.00	0.49	0.50		0.01	0.00			0.00	3.00
Ab-Ep rock/Chloritite	09SC31i	Carb	1987	SEM											1.00						0.00	3.00
Ab-Ep rock/Chloritite	09SC31i	Carb	1992	SEM											1.00						0.00	3.00

Rock type	Sample	Phase	Point	serie	Px type	Px type	Jd mole%	Si	Ti	Al	Fe3+	Fe2+	Mn	Mg	Ca	Ba	Na	K	F	Cl	H	O
Ab-Ep rock/Chloritite	09SC31i	Carb	1997	SEM											1.00						0.00	3.00
Ep-rich jadeitite	09SC27d	Carb	1922	SEM											1.00						0.00	3.00
Ep-rich jadeitite	MCB4a	Carb	1372	EPMA				0.00	0.00	0.00	0.00	0.00	0.00	0.00	0.99		0.00	0.00	0.01	0.00	0.00	2.99
Pure jadeitite	CV237b	Carb	2594	VPSEM				0.00	0.00	0.00	0.00	0.00	0.00	0.00	1.00		0.00	0.00			0.00	3.00
Pure jadeitite	CV237b	Carb	2610	VPSEM				0.00	0.00	0.00	0.00	0.00	0.00	0.00	1.00		0.00	0.00			0.00	3.00
Pure jadeitite	CV237b	Carb	2614	VPSEM				0.00	0.00	0.00	0.00	0.00	0.00	0.00	1.00		0.00	0.00			0.00	3.00
Pure jadeitite	CV237b	Carb	2615	VPSEM				0.00	0.00	0.00	0.00	0.00	0.00	0.00	1.00		0.00	0.00			0.00	3.00
Pure jadeitite	MCB1j	Carb	1337	EPMA				0.03	0.00	0.00	0.00	0.00	0.00	0.00	0.94		0.01	0.00	0.01	0.00	0.00	2.99
Ab-Ep Chl-rich rock	09SC27b	Chl	2168	SEM				5.92		4.32	0.00	1.96		7.73							16.00	36.00
Ab-Ep Chl-rich rock	09SC27b	Chl	2169	SEM				5.85		4.30	0.00	1.92		7.92							16.00	36.00
Ab-Ep Chl-rich rock	09SC27b	Chl	2171	SEM				5.87		4.47	0.00	2.47		7.08							16.00	36.00
Ab-Ep Chl-rich rock	09SC27b	Chl	2183	SEM				6.04		4.20	0.00	2.44		7.18							16.00	36.00
Ab-Ep Chl-rich rock	09SC27b	Chl	2209	SEM				5.64		4.33	0.40	2.56		7.08							16.00	36.00
Ab-Ep Chl-rich rock	09SC27b	Chl	2210	SEM				5.74		4.54	0.00	3.02		6.68							16.00	36.00
Ab-Ep Chl-rich rock	09SC27b	Chl	2219	SEM				5.78		4.61	0.00	2.77		6.76							16.00	36.00
Ab-Ep rock	09SC27f	Chl	2133	SEM				5.77		4.53	0.00	3.94		5.73							16.00	36.00
Ab-Ep rock	09SC27f	Chl	2138	SEM				6.06		4.33	0.00	3.47		5.91							16.00	36.00
Ab-Ep rock	09SC31a	Chl	2256	SEM				5.70		4.41	0.20	3.79		5.91							16.00	36.00
Ab-Ep rock	09SC31a	Chl	2257	SEM				5.68		4.55	0.09	4.05		5.63							16.00	36.00
Ab-Ep rock	09SC31a	Chl	2261	SEM				5.41		4.77	0.42	3.69		5.72							16.00	36.00
Ab-Ep rock	09SC31a	Chl	2266	SEM				6.16		4.34	0.00	3.48		5.69							16.00	36.00
Ab-Ep rock	09SC31a	Chl	2285	SEM				6.27		4.37	0.00	3.61		5.30							16.00	36.00
Ab-Ep rock	09SC31a	Chl	2286	SEM				6.02		4.45	0.00	3.50		5.78							16.00	36.00
Ab-Ep rock	09SC31a	Chl	2289	SEM				5.90		4.58	0.00	3.06		6.26							16.00	36.00
Ab-Ep rock	09SC31a	Chl	2291	SEM				6.07		4.16	0.00	3.78		5.84							16.00	36.00
Ab-Ep rock	09SC31a	Chl	2298	SEM				5.62		4.88	0.00	3.44		6.00							16.00	36.00
Ab-Ep rock	09SC31a	Chl	2300	SEM				5.96		4.53	0.00	3.51		5.79							16.00	36.00
Ab-Ep rock	09SC31a	Chl	2302	SEM				5.99		4.63	0.00	3.44		5.64							16.00	36.00
Ab-Ep rock	09SC31a	Chl	2305	SEM				6.36		4.25	0.00	3.31		5.59							16.00	36.00
Ab-Ep rock	09SC31c	Chl	2337	SEM				5.87		4.77	0.00	3.37		5.74							16.00	36.00
Ab-Ep rock	09SC31c	Chl	2341	SEM				5.98		4.53	0.00	3.42		5.82							16.00	36.00
Ab-Ep rock	09SC31c	Chl	2344	SEM				5.94		4.54	0.00	3.51		5.79							16.00	36.00
Ab-Ep rock	09SC31c	Chl	2345	SEM				5.99		4.66	0.00	3.18		5.86							16.00	36.00
Ab-Ep rock	09SC31c	Chl	2347	SEM				5.96		4.48	0.00	3.30		6.06							16.00	36.00
Ab-Ep rock	09SC31c	Chl	2349	SEM				6.01		4.44	0.00	3.43		5.90							16.00	36.00
Ab-Ep rock	09SC31c	Chl	2373	SEM				5.80		4.64	0.00	3.41		6.03							16.00	36.00
Ab-Ep rock	09SC31c	Chl	2374	SEM				6.13		4.67	0.00	2.95		5.79							16.00	36.00
Ab-Ep rock	09SC31c	Chl	2386	SEM				5.95		4.40	0.00	3.46		6.04							16.00	36.00
Ab-Ep rock	09SC31d	Chl	1691	SEM				5.68		5.04	0.00	2.98		6.12							16.00	36.00
Ab-Ep rock	09SC31d	Chl	1692	SEM				5.67		4.54	0.12	3.52		6.15							16.00	36.00
Ab-Ep rock	09SC31d	Chl	1714	SEM				5.71		4.76	0.00	3.22		6.23							16.00	36.00
Ab-Ep rock	09SC31d	Chl	1722	SEM				5.92		4.59	0.00	3.47		5.81							16.00	36.00
Ab-Ep rock	09SC31d	Chl	1728	SEM				6.13		4.64	0.00	3.34		5.44							16.00	36.00
Ab-Ep rock	09SC31d	Chl	1730	SEM				6.00		4.33	0.00	3.60		5.90							16.00	36.00

Rock type	Sample	Phase	Point	serie	Px type	Px type	Jd mole%	Si	Ti	Al	Fe3+	Fe2+	Mn	Mg	Ca	Ba	Na	K	F	Cl	H	O
Ab-Ep rock	09SC31d	Chl	1735	SEM				5.70		4.51	0.09	3.22		6.49							16.00	36.00
Ab-Ep rock	09SC31d	Chl	1744	SEM				5.81		4.77	0.00	3.67		5.55							16.00	36.00
Ab-Ep rock	09SC31d	Chl	1746	SEM				5.72		4.67	0.00	3.12		6.45							16.00	36.00
Ab-Ep rock	09SC31d	Chl	1749	SEM				5.83		4.42	0.00	3.48		6.23							16.00	36.00
Ab-Ep rock	09SC31d	Chl	1754	SEM				5.93		4.71	0.00	3.04		6.05							16.00	36.00
Ab-Ep rock	09SC31d	Chl	1759	SEM				5.81		4.48	0.00	3.46		6.20							16.00	36.00
Ab-Ep rock	09SC31n	Chl	1840	SEM				6.01		4.53	0.00	3.99		5.21							16.00	36.00
Ab-Ep rock	09SC31n	Chl	1841	SEM				5.87		4.94	0.00	3.72		5.12							16.00	36.00
Ab-Ep rock	09SC31n	Chl	1843	SEM				5.74		4.82	0.00	3.75		5.55							16.00	36.00
Ab-Ep rock	09SC31n	Chl	1880	SEM				5.66		4.86	0.00	3.90		5.48							16.00	36.00
Ab-Ep rock	09SC31n	Chl	1891	SEM				5.73		4.73	0.00	3.77		5.68							16.00	36.00
Ab-Ep rock	MCB1a	Chl	2969	VPSEM				5.53	0.00	4.66	0.29	2.56	0.00	6.97	0.00		0.00	0.00			16.00	36.00
Ab-Ep rock	MCB1a	Chl	2974	VPSEM				5.59	0.00	4.81	0.01	2.52	0.00	7.08	0.00		0.00	0.00			16.00	36.00
Ab-Ep rock	MCB1a	Chl	2976	VPSEM				5.62	0.00	4.77	0.00	2.56	0.07	6.98	0.00		0.00	0.00			16.00	36.00
Ab-Ep rock	MCB1a	Chl	2978	VPSEM				5.64	0.00	4.80	0.00	2.59	0.00	6.93	0.00		0.00	0.00			16.00	36.00
Ab-Ep rock	MCB1a	Chl	2984	VPSEM				5.56	0.00	4.77	0.10	2.75	0.00	6.82	0.00		0.00	0.00			16.00	36.00
Ab-Ep rock	MCB1a	Chl	2985	VPSEM				5.59	0.00	4.82	0.00	2.77	0.00	6.81	0.00		0.00	0.00			16.00	36.00
Ab-Ep rock	MCB1a	Chl	2986	VPSEM				5.59	0.00	4.91	0.00	2.60	0.05	6.81	0.00		0.00	0.00			16.00	36.00
Ab-Ep rock	MCB1a	Chl	2993	VPSEM				5.55	0.00	4.90	0.00	2.38	0.00	7.16	0.00		0.00	0.00			16.00	36.00
Ab-Ep rock	MCB1a	Chl	3007	VPSEM				5.55	0.00	4.99	0.00	2.55	0.00	6.88	0.00		0.00	0.00			16.00	36.00
Ab-Ep rock	MCB1a	Chl	3014	VPSEM				5.65	0.00	4.84	0.00	2.52	0.00	6.92	0.00		0.00	0.00			16.00	36.00
Ab-Ep rock	MCB1a	Chl	3017	VPSEM				5.71	0.00	4.77	0.00	2.75	0.00	6.68	0.00		0.00	0.00			16.00	36.00
Ab-Ep rock	MCB1a	Chl	3018	VPSEM				5.64	0.00	4.75	0.00	2.79	0.00	6.80	0.00		0.00	0.00			16.00	36.00
Ab-Ep rock	MCB1a	Chl	3022	VPSEM				5.61	0.00	4.81	0.00	2.67	0.05	6.85	0.00		0.00	0.00			16.00	36.00
Ab-Ep rock	MCB1a	Chl	3026	VPSEM				5.53	0.00	5.03	0.00	2.52	0.00	6.88	0.00		0.00	0.00			16.00	36.00
Ab-Ep rock	MCB1a	Chl	3028	VPSEM				5.53	0.00	4.89	0.05	2.60	0.05	6.88	0.00		0.00	0.00			16.00	36.00
Ab-Ep rock	MCB1a	Chl	3030	VPSEM				5.65	0.00	4.84	0.00	2.65	0.00	6.78	0.00		0.00	0.00			16.00	36.00
Ab-Ep rock	MCB1a	Chl	3031	VPSEM				5.64	0.00	4.86	0.00	2.45	0.06	6.92	0.00		0.00	0.00			16.00	36.00
Ab-Ep rock	MCB1a	Chl	3040	VPSEM				5.70	0.00	4.86	0.00	2.18	0.00	7.13	0.00		0.00	0.00			16.00	36.00
Ab-Ep rock	MCB1a	Chl	3047	VPSEM				5.56	0.00	4.78	0.09	2.85	0.06	6.65	0.00		0.00	0.00			16.00	36.00
Ab-Ep rock	MCB1a	Chl	3058	VPSEM				5.71	0.00	4.59	0.00	2.52	0.00	7.18	0.00		0.00	0.00			16.00	36.00
Ab-Ep rock	MCB1a	Chl	3070	VPSEM				5.56	0.00	5.01	0.00	2.75	0.00	6.60	0.00		0.00	0.00			16.00	36.00
Ab-Ep rock	MCB1a	Chl	3073	VPSEM				5.52	0.00	5.05	0.00	2.83	0.00	6.52	0.04		0.00	0.00			16.00	36.00
Ab-Ep rock	MCB1a	Chl	3077	VPSEM				5.53	0.00	4.96	0.00	2.87	0.00	6.64	0.00		0.00	0.00			16.00	36.00
Ab-Ep rock	MCB1a	Chl	3089	VPSEM				5.72	0.00	4.95	0.00	2.56	0.00	6.57	0.00		0.00	0.00			16.00	36.00
Ab-Ep rock	MCB1e	Chl	16	EPMA				5.72	0.00	4.68	0.00	2.82	0.04	6.65	0.03		0.01	0.01	0.05	0.01	15.93	35.93
Ab-Ep rock	MCB1e	Chl	23	EPMA				5.56	0.00	4.84	0.04	3.40	0.04	6.08	0.01		0.01	0.01	0.09	0.01	15.90	35.90
Ab-Ep rock	MCB1e	Chl	24	EPMA				5.77	0.01	4.60	0.00	2.97	0.03	6.52	0.02		0.01	0.02	0.06	0.01	15.93	35.93
Ab-Ep rock	MCB1e	Chl	25	EPMA				5.69	0.00	4.64	0.00	2.70	0.03	6.89	0.03		0.01	0.01	0.08	0.01	15.90	35.90
Ab-Ep rock	MCB1e	Chl	26	EPMA				5.76	0.00	4.70	0.00	2.68	0.03	6.67	0.04		0.02	0.02	0.05	0.01	15.95	35.95
Ab-Ep rock	MCB1e	Chl	27	EPMA				5.68	0.01	4.72	0.00	2.81	0.02	6.70	0.01		0.01	0.01	0.06	0.01	15.92	35.92
Ab-Ep rock	MCB1e	Chl	28	EPMA				5.81	0.00	4.59	0.00	2.68	0.04	6.74	0.03		0.01	0.02	0.08	0.01	15.91	35.91
Ab-Ep rock	MCB1e	Chl	32	EPMA				5.71	0.01	4.66	0.00	2.71	0.03	6.82	0.02		0.01	0.01	0.08	0.00	15.92	35.92
Ab-Ep rock	MCB1e	Chl	59	EPMA				5.70	0.00	4.71	0.00	2.60	0.03	6.86	0.02		0.01	0.01	0.06	0.00	15.93	35.93

Rock type	Sample	Phase	Point	serie	Px type	Px type	Jd mole%	Si	Ti	Al	Fe3+	Fe2+	Mn	Mg	Ca	Ba	Na	K	F	Cl	H	O
Ab-Ep rock	MCB1e	Chl	3106	VPSEM				5.79	0.00	4.57	0.00	2.63	0.05	6.89	0.00		0.00	0.00			16.00	36.00
Ab-Ep rock	MCB1e	Chl	3113	VPSEM				5.66	0.00	4.68	0.00	2.56	0.00	7.10	0.00		0.00	0.00			16.00	36.00
Ab-Ep rock	MCB1e	Chl	3114	VPSEM				5.71	0.00	4.60	0.00	2.66	0.00	7.02	0.00		0.00	0.00			16.00	36.00
Ab-Ep rock	MCB1e	Chl	3130	VPSEM				5.79	0.00	4.57	0.00	2.46	0.00	7.11	0.00		0.00	0.00			16.00	36.00
Ab-Ep rock	MCB1e	Chl	3136	VPSEM				5.71	0.00	4.73	0.00	2.56	0.00	6.91	0.00		0.00	0.00			16.00	36.00
Ab-Ep rock	MCB1e	Chl	3137	VPSEM				5.76	0.00	4.75	0.00	2.13	0.00	7.22	0.00		0.00	0.00			16.00	36.00
Ab-Ep rock	MCB1e	Chl	3142	VPSEM				5.66	0.00	4.72	0.00	2.51	0.04	7.04	0.00		0.00	0.00			16.00	36.00
Ab-Ep rock	MCB1e	Chl	3144	VPSEM				5.72	0.00	4.76	0.00	2.14	0.00	7.28	0.00		0.00	0.00			16.00	36.00
Ab-Ep rock/Chloritite	09SC31i	Chl	2005	SEM				5.43		4.39	0.75	2.64		6.79							16.00	36.00
Ab-Ep rock/Chloritite	09SC31i	Chl	2006	SEM				5.40		4.74	0.46	2.05		7.35							16.00	36.00
Ab-Ep rock/Chloritite	09SC31i	Chl	2010	SEM				5.10		4.75	1.05	2.00		7.10							16.00	36.00
Ab-Ep rock/Chloritite	09SC31i	Chl	2011	SEM				5.21		5.06	0.53	2.48		6.73							16.00	36.00
Ab-Ep rock/Chloritite	09SC31i	Chl	2012	SEM				5.40		4.70	0.49	2.13		7.27							16.00	36.00
Ab-Ep rock/Chloritite	09SC31i	Chl	2023	SEM				5.35		5.43	0.00	2.79		6.36							16.00	36.00
Ab-Ep rock/Chloritite	09SC31i	Chl	2024	SEM				5.73		4.46	0.08	3.28		6.45							16.00	36.00
Ab-Ep rock/Chloritite	09SC31i	Chl	2025	SEM				5.89		4.91	0.00	2.89		5.95							16.00	36.00
Ab-Ep rock/Chloritite	09SC31i	Chl	2026	SEM				5.32		5.13	0.23	1.74		7.58							16.00	36.00
Ab-Ep rock/Chloritite	09SC31i	Chl	2030	SEM				5.07		5.75	0.12	2.83		6.24							16.00	36.00
Ab-Ep rock/Chloritite	09SC31i	Chl	2031	SEM				5.83		4.39	0.00	3.49		6.26							16.00	36.00
Ab-Ep rock/Chloritite	09SC31i	Chl	2036	SEM				5.49		4.98	0.03	2.65		6.84							16.00	36.00
Ab-Ep rock/Chloritite	09SC31i	Chl	2037	SEM				5.70		4.09	0.51	2.64		7.06							16.00	36.00
Ab-Ep rock/Chloritite	09SC31i	Chl	2038	SEM				5.90		4.90	0.00	2.40		6.45							16.00	36.00
Ab-Ep rock/Chloritite	09SC31i	Chl	2041	SEM				5.51		4.96	0.02	3.06		6.46							16.00	36.00
Ab-Ep rock/Chloritite	09SC31i	Chl	2042	SEM				5.58		5.00	0.00	2.89		6.46							16.00	36.00
Ab-Ep rock/Chloritite	09SC31i	Chl	2043	SEM				4.80		5.36	1.05	1.40		7.40							16.00	36.00
Ab-Ep rock/Chloritite	09SC31i	Chl	2044	SEM				5.70		4.85	0.00	3.31		6.02							16.00	36.00
Ab-Ep rock/Chloritite	09SC31i	Chl	2048	SEM				5.48		4.85	0.19	2.87		6.61							16.00	36.00
Ab-Ep rock/Chloritite	09SC31i	Chl	2049	SEM				5.79		4.62	0.00	3.10		6.39							16.00	36.00
Ab-Ep rock/Chloritite	09SC31i	Chl	2050	SEM				5.29		4.71	0.70	2.62		6.67							16.00	36.00
Ab-Ep rock/Chloritite	09SC31i	Chl	2051	SEM				5.62		4.64	0.12	3.10		6.53							16.00	36.00
Ab-Ep rock/Chloritite	09SC31i	Chl	2053	SEM				5.82		4.73	0.00	2.98		6.29							16.00	36.00
Ab-Ep rock/Chloritite	09SC31i	Chl	2054	SEM				5.49		4.04	0.97	2.40		7.09							16.00	36.00
Ab-Ep rock/Chloritite	09SC31i	Chl	2055	SEM				5.89		4.27	0.00	3.07		6.74							16.00	36.00
Ab-Ep rock/Chloritite	09SC31i	Chl	2056	SEM				5.67		4.92	0.00	2.67		6.61							16.00	36.00
Ab-Ep rock/Chloritite	09SC31i	Chl	2057	SEM				5.76		4.54	0.00	2.91		6.76							16.00	36.00
Chloritite	09SC27a	Chl	2155	SEM				6.07		4.05	0.00	1.70		8.09							16.00	36.00
Chloritite	09SC27a	Chl	2156	SEM				6.04		4.09	0.00	1.72		8.07							16.00	36.00
Chloritite	09SC27a	Chl	2157	SEM				6.01		4.11	0.00	1.72		8.08							16.00	36.00
Chloritite	09SC27a	Chl	2158	SEM				6.00		3.97	0.04	1.66		8.34							16.00	36.00
Chloritite	09SC27a	Chl	2161	SEM				5.97		4.04	0.02	1.61		8.36							16.00	36.00
Chloritite	09SC27a	Chl	2163	SEM				5.82		4.12	0.24	1.33		8.49							16.00	36.00
Cr-rich Pure Jdt	SCMJ10	Chl	3622	VPSEM				5.56	0.00	5.04	0.07	1.26	0.06	7.80	0.00		0.00	0.22			16.00	36.00
Cr-rich Pure Jdt	SCMJ10	Chl	3625	VPSEM				5.42	0.00	5.13	0.03	1.28	0.00	8.14	0.00		0.00	0.00			16.00	36.00
Cr-rich Pure Jdt	SCMJ10	Chl	3627	VPSEM				5.62	0.00	4.85	0.00	1.19	0.05	8.24	0.00		0.00	0.00			16.00	36.00

Rock type	Sample	Phase	Point	serie	Px type	Px type	Jd mole%	Si	Ti	Al	Fe3+	Fe2+	Mn	Mg	Ca	Ba	Na	K	F	Cl	H	O
Cr-rich Pure Jdt	SCMJ10	Chl	3629	VPSEM				5.75	0.00	4.92	0.00	1.13	0.05	7.84	0.00		0.15	0.05			16.00	36.00
Cr-rich Pure Jdt	SCMJ10	Chl	3640	VPSEM				5.58	0.00	4.93	0.00	1.20	0.00	8.24	0.00		0.00	0.00			16.00	36.00
Cr-rich Pure Jdt	SCMJ10	Chl	3645	VPSEM				5.54	0.00	4.96	0.00	1.08	0.06	8.35	0.00		0.00	0.00			16.00	36.00
Ep-rich jadeitite	09SC27m	Chl	2081	SEM				5.75		4.81	0.00	3.42		5.88							16.00	36.00
Ep-rich jadeitite	09SC27m	Chl	2092	SEM				5.74		4.70	0.00	3.31		6.16							16.00	36.00
Ep-rich jadeitite	09SC27m	Chl	2125	SEM				5.83		4.49	0.00	3.23		6.37							16.00	36.00
Ep-rich jadeitite	09SC27m	Chl	2129	SEM				5.87		4.66	0.00	2.80		6.48							16.00	36.00
Ep-rich jadeitite	09SC31g	Chl	1785	SEM				5.51		4.80	0.17	2.86		6.65							16.00	36.00
Ep-rich jadeitite	09SC31g	Chl	1804	SEM				6.01		4.31	0.00	3.21		6.30							16.00	36.00
Ep-rich jadeitite	09SC31g	Chl	1813	SEM				5.71		4.74	0.00	3.15		6.32							16.00	36.00
Ep-rich jadeitite	09SC31g	Chl	1973	SEM				5.71		4.65	0.00	3.38		6.22							16.00	36.00
Ep-rich jadeitite	09SC31g	Chl	1979	SEM				5.51		4.68	0.30	3.24		6.27							16.00	36.00
Ep-rich jadeitite	09SC31j	Chl	1935	SEM				5.82		4.10	0.26	3.37		6.45							16.00	36.00
Ep-rich jadeitite	09SC31j	Chl	1949	SEM				5.43		4.50	0.63	3.33		6.11							16.00	36.00
Ep-rich jadeitite	09SC31j	Chl	1950	SEM				5.65		4.22	0.49	3.44		6.21							16.00	36.00
Ep-rich jadeitite	09SC31j	Chl	1956	SEM				5.49		4.71	0.31	3.51		5.98							16.00	36.00
Ep-rich jadeitite	09SC31j	Chl	1967	SEM				5.79		4.51	0.00	3.37		6.30							16.00	36.00
Ep-rich jadeitite	MCB4a	Chl	1394	EPMA				5.50	0.00	4.95	0.07	3.40	0.04	5.99	0.00		0.03	0.01	0.07	0.00	15.93	35.93
Ep-rich jadeitite	MCB4a	Chl	1396	EPMA				5.40	0.00	5.24	0.00	3.43	0.03	5.84	0.00		0.03	0.01	0.07	0.01	15.92	35.92
Ep-rich jadeitite	MCB4a	Chl	1397	EPMA				5.66	0.00	4.85	0.00	3.48	0.04	5.83	0.01		0.05	0.01	0.03	0.01	15.96	35.96
Ep-rich jadeitite	MCB4a	Chl	1398	EPMA				5.61	0.00	4.86	0.00	3.49	0.04	5.95	0.00		0.01	0.00	0.08	0.00	15.92	35.92
Ep-rich jadeitite	MCB4a	Chl	1399	EPMA				5.40	0.00	5.21	0.02	3.48	0.03	5.82	0.00		0.02	0.02	0.06	0.01	15.93	35.93
Ep-rich jadeitite	MCB4a	Chl	1464	VPSEM				5.73		4.84	0.00	2.97		6.31							16.00	36.00
Ep-rich jadeitite	MCB4a	Chl	1465	VPSEM				5.78		4.73	0.00	3.51		5.83							16.00	36.00
Mica-rich Jadeitite	09SC31e	Chl	1822	SEM				5.86		4.62	0.00	3.41		5.94							16.00	36.00
Mica-rich Jadeitite	09SC31e	Chl	1830	SEM				5.95		4.41	0.00	4.11		5.38							16.00	36.00
Mica-rich Jadeitite	09SC31e	Chl	1831	SEM				5.98		4.67	0.00	3.44		5.60							16.00	36.00
Mica-rich Jadeitite	09SC31e	Chl	2315	SEM				6.00		4.28	0.00	3.54		6.04							16.00	36.00
Mica-rich Jadeitite	09SC31e	Chl	2316	SEM				5.32		4.99	0.36	3.58		5.74							16.00	36.00
Mica-rich Jadeitite	09SC31e	Chl	2317	SEM				5.71		4.62	0.00	4.15		5.50							16.00	36.00
Mica-rich Jadeitite	09SC31e	Chl	2318	SEM				5.74		4.82	0.00	3.60		5.68							16.00	36.00
Mica-rich Jadeitite	09SC31e	Chl	2319	SEM				5.94		4.61	0.00	4.16		5.04							16.00	36.00
Mica-rich Jadeitite	09SC31e	Chl	2320	SEM				5.32		4.99	0.37	3.41		5.91							16.00	36.00
Mica-rich Jadeitite	09SC31e	Chl	2322	SEM				5.86		4.70	0.00	3.08		6.15							16.00	36.00
Mica-rich Jadeitite	09SC31e	Chl	2326	SEM				6.22		4.32	0.00	2.99		6.09							16.00	36.00
Pure jadeitite	CV237b	Chl	157	EPMA				5.58	0.00	4.95	0.00	3.65	0.03	5.73	0.01		0.01	0.01	0.06	0.00	15.94	35.94
Pure jadeitite	CV237b	Chl	158	EPMA				5.57	0.00	5.00	0.00	3.79	0.03	5.51	0.02		0.02	0.01	0.07	0.00	15.92	35.92
Pure jadeitite	CV237b	Chl	162	EPMA				5.64	0.01	4.88	0.00	3.62	0.04	5.72	0.01		0.01	0.02	0.04	0.01	15.95	35.95
Pure jadeitite	CV237b	Chl	2526	VPSEM				5.31	0.00	5.14	0.36	2.95	0.05	6.06	0.00		0.13	0.00			16.00	36.00
Pure jadeitite	CV237b	Chl	2541	VPSEM				5.44	0.00	5.11	0.00	3.74	0.07	5.63	0.00		0.00	0.00			16.00	36.00
Pure jadeitite	CV237b	Chl	2555	VPSEM				5.48	0.00	5.04	0.00	3.88	0.00	5.60	0.00		0.00	0.00			16.00	36.00
Pure jadeitite	CV237b	Chl	2557	VPSEM				5.52	0.00	5.06	0.09	3.62	0.00	5.53	0.00		0.19	0.00			16.00	36.00
Pure jadeitite	CV237b	Chl	2618	VPSEM				5.52	0.00	5.00	0.00	3.81	0.04	5.61	0.00		0.00	0.00			16.00	36.00
Pure jadeitite	CV237b	Chl	2620	VPSEM				5.59	0.00	4.99	0.02	3.68	0.00	5.52	0.00		0.20	0.00			16.00	36.00

Rock type	Sample	Phase	Point	serie	Px type	Px type	Jd mole%	Si	Ti	Al	Fe3+	Fe2+	Mn	Mg	Ca	Ba	Na	K	F	Cl	H	O
Pure jadeitite	CV237b	Chl	2628	VPSEM				5.51	0.00	5.10	0.00	3.74	0.00	5.52	0.00		0.12	0.00			16.00	36.00
Pure jadeitite	CV237b	Chl	2634	VPSEM				5.55	0.04	4.88	0.05	3.53	0.00	5.77	0.03		0.13	0.00			16.00	36.00
Pure jadeitite	MCB3h	Chl	402	EPMA				5.51	0.00	4.96	0.03	2.48	0.06	6.92	0.01		0.02	0.01	0.04	0.01	15.95	35.95
Pure jadeitite	MCB3h	Chl	413	EPMA				5.71	0.00	4.78	0.00	2.53	0.04	6.81	0.01		0.01	0.01	0.05	0.00	15.95	35.95
Pure jadeitite	MCB3h	Chl	414	EPMA				5.70	0.00	4.80	0.00	2.59	0.04	6.74	0.01		0.01	0.01	0.03	0.01	15.96	35.96
Pure jadeitite	MCB3h	Chl	415	EPMA				5.54	0.00	5.04	0.00	3.18	0.04	6.12	0.00		0.01	0.01	0.04	0.00	15.96	35.96
Pure jadeitite	MCB3h	Chl	416	EPMA				5.64	0.00	4.81	0.00	2.82	0.04	6.61	0.01		0.02	0.01	0.06	0.01	15.93	35.93
Pure jadeitite	MCB3h	Chl	418	EPMA				5.66	0.00	4.79	0.00	2.98	0.05	6.43	0.01		0.03	0.02	0.05	0.01	15.93	35.93
Pure jadeitite	MCB3h	Chl	420	EPMA				5.68	0.00	4.80	0.00	2.85	0.04	6.50	0.01		0.03	0.01	0.05	0.02	15.93	35.93
Pure jadeitite	MCB3h	Chl	421	EPMA				5.57	0.00	4.96	0.00	2.93	0.05	6.43	0.00		0.01	0.01	0.02	0.00	15.98	35.98
Pure jadeitite	MCB3h	Chl	445	EPMA				5.75	0.00	4.60	0.00	2.59	0.05	6.92	0.03		0.02	0.01	0.03	0.01	15.96	35.96
Pure jadeitite	MCB3h	Chl	480	EPMA				5.64	0.00	4.99	0.00	2.99	0.04	6.16	0.01		0.01	0.06		0.02	15.98	35.98
Pure jadeitite	MCB3h	Chl	3515	VPSEM				5.47		5.03	0.03	2.38		7.09							16.00	36.00
Pure jadeitite	MCB3h	Chl	3518	VPSEM				5.63		4.84	0.00	2.45		7.02							16.00	36.00
Pure jadeitite	MCB3h	Chl	3528	VPSEM				5.26		5.35	0.13	2.85		6.41							16.00	36.00
Pure jadeitite	MCB3h	Chl	3531	VPSEM				5.65		4.67	0.03	2.08		7.57							16.00	36.00
Pure jadeitite	MCB3h	Chl	3540	VPSEM				5.67		4.82	0.00	2.36		7.06							16.00	36.00
Pure jadeitite	MCB3h	Chl	3544	VPSEM				5.64		4.63	0.10	2.10		7.54							16.00	36.00
Pure jadeitite	MCB3h	Chl	3549	VPSEM				5.49		5.09	0.00	2.53		6.84							16.00	36.00
Pure jadeitite	MCB3h	Chl	3550	VPSEM				5.56		4.72	0.17	1.93		7.63							16.00	36.00
Pure jadeitite	MCB3h	Chl	3561	VPSEM				5.51		4.66	0.32	2.00		7.51							16.00	36.00
Pure jadeitite	MCB3h	Chl	3588	VPSEM				5.58		5.10	0.00	2.44		6.74							16.00	36.00
Pure jadeitite	MCB3h	Chl	3590	VPSEM				5.65		4.81	0.00	2.38		7.10							16.00	36.00
Pure jadeitite	MCB3h	Chl	3603	VPSEM				5.68		4.70	0.00	2.58		7.01							16.00	36.00
Pure jadeitite	MCB3h	Chl	3604	VPSEM				5.66		4.74	0.00	2.27		7.29							16.00	36.00
Pure Jdt/Ab-Ep rock/Chloritite	09SC8a3	Chl	2394	VPSEM				5.71		4.50	0.08	1.38	0.04	8.29							16.00	36.00
Pure Jdt/Ab-Ep rock/Chloritite	09SC8a3	Chl	2422	VPSEM				5.69		4.57	0.05	1.45		8.25							16.00	36.00
Pure Jdt/Ab-Ep rock/Chloritite	09SC8a3	Chl	2424	VPSEM				5.79		4.48	0.00	1.50	0.04	8.16							16.00	36.00
Pure Jdt/Ab-Ep rock/Chloritite	09SC8a3	Chl	2428	VPSEM				5.69		4.65	0.00	2.00	0.04	7.61							16.00	36.00
Pure Jdt/Ab-Ep rock/Chloritite	09SC8a3	Chl	2431	VPSEM				5.63		4.75	0.00	1.57	0.06	7.99							16.00	36.00
Pure Jdt/Ab-Ep rock/Chloritite	09SC8a3	Chl	2432	VPSEM				5.85		4.38	0.00	1.57		8.17							16.00	36.00
Pure Jdt/Ab-Ep rock/Chloritite	09SC8a3	Chl	2433	VPSEM				5.76		4.46	0.03	1.61	0.05	8.10							16.00	36.00
Pure Jdt/Ab-Ep rock/Chloritite	09SC8a3	Chl	2444	VPSEM				5.63		4.70	0.04	2.07	0.07	7.49							16.00	36.00
Pure Jdt/Ab-Ep rock/Chloritite	09SC8a3	Chl	2484	VPSEM				5.51		5.01	0.00	2.69	0.06	6.70							16.00	36.00
Pure Jdt/Chloritite	MCB3f	Chl	3456	VPSEM				5.69	0.00	4.64	0.00	1.93	0.04	7.69	0.00		0.00	0.00		0.00	16.00	36.00
Pure Jdt/Chloritite	MCB3f	Chl	3459	VPSEM				5.55	0.00	4.73	0.28	1.87	0.07	7.38	0.00		0.12	0.00		0.00	16.00	36.00
Pure Jdt/Chloritite	MCB3f	Chl	3460	VPSEM				5.56	0.00	4.80	0.09	1.97	0.04	7.55	0.00		0.00	0.00		0.00	16.00	36.00
Ab-Ep rock	09-SC-9b	Cpx	3655	SEM	PxNaCa	PxNaCa	47.64	1.84		0.61	0.17	0.00		0.36	0.46		0.64				0.00	6.00
Ab-Ep rock	09-SC-9b	Cpx	3656	SEM	PxNaCa	PxNaCa	44.01	1.84		0.58	0.20	0.00		0.36	0.49		0.61				0.00	6.00
Ab-Ep rock	09-SC-9b	Cpx	3654	SEM	PxNa	PxNa	79.78	1.86		0.93	0.11	0.00		0.11	0.12		0.95				0.00	6.00
Ab-Ep rock	09-SC-9b	Cpx	3657	SEM	PxNa	PxNa	79.87	1.85		0.94	0.11	0.00		0.12	0.11		0.96				0.00	6.00
Cr-rich Omphacitite	09SC7b	Cpx	2141	SEM	PxNaCa	PxNaCa	32.94	2.04		0.27	0.00	0.12		0.57	0.66		0.33				0.00	6.00
Cr-rich Omphacitite	09SC7b	Cpx	2143	SEM	PxNaCa	PxNaCa	31.56	2.00		0.31	0.06	0.06		0.56	0.64		0.37				0.00	6.00
Cr-rich Omphacitite	09SC7b	Cpx	2145	SEM	PxNaCa	PxNaCa	62.20	2.05		0.57	0.00	0.09		0.29	0.36		0.61				0.00	6.00

Rock type	Sample	Phase	Point	serie	Px type	Px type	Jd mole%	Si	Ti	Al	Fe3+	Fe2+	Mn	Mg	Ca	Ba	Na	K	F	Cl	H	O
Cr-rich Omphacitite	09SC7b	Cpx	2147	SEM	PxNaCa	PxNaCa	38.75	2.02		0.37	0.00	0.08		0.49	0.62		0.38				0.00	6.00
Cr-rich Omphacitite	09SC7b	Cpx	2148	SEM	PxNaCa	PxNaCa	34.49	2.03		0.29	0.00	0.12		0.55	0.65		0.35				0.00	6.00
Cr-rich Omphacitite	09SC7b	Cpx	2149	SEM	PxNaCa	PxNaCa	59.50	2.02		0.55	0.09	0.00		0.29	0.35		0.70				0.00	6.00
Cr-rich Omphacitite	09SC7b	Cpx	2150	SEM	PxNaCa	PxNaCa	42.20	2.02		0.43	0.00	0.07		0.48	0.56		0.41				0.00	6.00
Cr-rich Omphacitite	09SC7b	Cpx	2185	SEM	PxNaCa	PxNaCa	30.83	2.03		0.29	0.00	0.11		0.58	0.68		0.30				0.00	6.00
Cr-rich Omphacitite	09SC7b	Cpx	2186	SEM	PxNaCa	PxNaCa	60.69	2.04		0.57	0.00	0.08		0.31	0.38		0.60				0.00	6.00
Cr-rich Omphacitite	09SC7b	Cpx	2187	SEM	PxNaCa	PxNaCa	29.29	2.01		0.27	0.03	0.09		0.57	0.70		0.33				0.00	6.00
Cr-rich Omphacitite	09SC7b	Cpx	2190	SEM	PxNaCa	PxNaCa	61.56	2.03		0.58	0.00	0.08		0.31	0.37		0.61				0.00	6.00
Cr-rich Omphacitite	09SC7b	Cpx	2193	SEM	PxNaCa	PxNaCa	63.11	2.07		0.54	0.00	0.08		0.30	0.36		0.64				0.00	6.00
Cr-rich Omphacitite	09SC7b	Cpx	2194	SEM	PxNaCa	PxNaCa	58.12	2.02		0.54	0.07	0.00		0.31	0.40		0.67				0.00	6.00
Cr-rich Omphacitite	09SC7b	Cpx	2196	SEM	PxNaCa	PxNaCa	32.79	1.98		0.33	0.08	0.00		0.59	0.61		0.42				0.00	6.00
Cr-rich Omphacitite	09SC7b	Cpx	2197	SEM	PxNaCa	PxNaCa	37.32	2.03		0.36	0.00	0.10		0.49	0.63		0.36				0.00	6.00
Cr-rich Omphacitite	09SC7b	Cpx	2201	SEM	PxNaCa	PxNaCa	57.94	2.03		0.53	0.01	0.08		0.38	0.38		0.60				0.00	6.00
Cr-rich Omphacitite	09SC7b	Cpx	2202	SEM	PxNaCa	PxNaCa	62.22	2.04		0.58	0.00	0.07		0.27	0.39		0.61				0.00	6.00
Cr-rich Omphacitite	09SC7b	Cpx	2151	SEM	PxNa	PxNa	84.32	2.04		0.79	0.00	0.04		0.12	0.15		0.84				0.00	6.00
Cr-rich Pure Jdt	SCMJ10	Cpx	345	EPMA	PxNaCa	PxNaCa	58.39	2.00	0.00	0.58	0.05	0.00	0.00	0.36	0.37		0.63	0.00	0.01	0.00	0.00	6.00
Cr-rich Pure Jdt	SCMJ10	Cpx	346	EPMA	PxNaCa	PxNaCa	76.38	2.01	0.00	0.74	0.02	0.03	0.00	0.21	0.21		0.78	0.00	0.00	0.00	0.00	6.00
Cr-rich Pure Jdt	SCMJ10	Cpx	347	EPMA	PxNaCa	PxNaCa	62.57	2.01	0.00	0.61	0.00	0.05	0.00	0.33	0.36		0.62	0.01	0.01	0.00	0.00	6.00
Cr-rich Pure Jdt	SCMJ10	Cpx	348	EPMA	PxNaCa	PxNaCa	75.83	2.01	0.00	0.75	0.01	0.03	0.00	0.21	0.22		0.77	0.00	0.01	0.00	0.00	6.00
Cr-rich Pure Jdt	SCMJ10	Cpx	349	EPMA	PxNaCa	PxNaCa	77.46	2.00	0.00	0.77	0.02	0.02	0.00	0.18	0.20		0.80	0.00	0.00	0.00	0.00	6.00
Cr-rich Pure Jdt	SCMJ10	Cpx	354	EPMA	PxNaCa	PxNaCa	77.80	2.01	0.00	0.76	0.01	0.03	0.00	0.19	0.20		0.79	0.00	0.00	0.00	0.00	6.00
Cr-rich Pure Jdt	SCMJ10	Cpx	356	EPMA	PxNaCa	PxNaCa	77.91	2.01	0.00	0.76	0.01	0.03	0.00	0.19	0.21		0.79	0.00	0.01	0.00	0.00	6.00
Cr-rich Pure Jdt	SCMJ10	Cpx	357	EPMA	PxNaCa	PxNaCa	77.82	2.02	0.00	0.75	0.00	0.04	0.00	0.20	0.21		0.78	0.00	0.00	0.00	0.00	6.00
Cr-rich Pure Jdt	SCMJ10	Cpx	359	EPMA	PxNaCa	PxNaCa	77.84	2.01	0.00	0.77	0.02	0.02	0.00	0.19	0.20		0.80	0.00	0.01	0.00	0.00	6.00
Cr-rich Pure Jdt	SCMJ10	Cpx	360	EPMA	PxNaCa	PxNaCa	78.38	2.01	0.00	0.77	0.00	0.04	0.00	0.19	0.20		0.79	0.00	0.00	0.00	0.00	6.00
Cr-rich Pure Jdt	SCMJ10	Cpx	3636	VPSEM	PxNaCa	PxNaCa	73.52	2.00	0.00	0.74	0.04	0.00	0.00	0.24	0.21		0.78	0.00			0.00	6.00
Cr-rich Pure Jdt	SCMJ10	Cpx	350	EPMA	PxNa	PxNa	78.91	2.00	0.00	0.79	0.04	0.00	0.00	0.17	0.18		0.83	0.00	0.00	0.00	0.00	6.00
Cr-rich Pure Jdt	SCMJ10	Cpx	355	EPMA	PxNa	PxNa	77.56	2.00	0.00	0.77	0.03	0.01	0.00	0.18	0.19		0.81	0.00	0.00	0.00	0.00	6.00
Cr-rich Pure Jdt	SCMJ10	Cpx	358	EPMA	PxNa	PxNa	78.12	2.01	0.00	0.77	0.02	0.02	0.00	0.18	0.20		0.80	0.00	0.00	0.00	0.00	6.00
Cr-rich Pure Jdt	SCMJ10	Cpx	361	EPMA	PxNa	PxNa	85.99	2.01	0.00	0.84	0.00	0.04	0.00	0.12	0.12		0.86	0.00	0.00	0.00	0.00	6.00
Cr-rich Pure Jdt	SCMJ10	Cpx	362	EPMA	PxNa	PxNa	92.94	2.01	0.00	0.92	0.00	0.03	0.00	0.06	0.05		0.92	0.00	0.00	0.00	0.00	6.00
Cr-rich Pure Jdt	SCMJ10	Cpx	363	EPMA	PxNa	PxNa	84.34	2.01	0.00	0.83	0.02	0.02	0.00	0.12	0.13		0.87	0.00	0.00	0.00	0.00	6.00
Cr-rich Pure Jdt	SCMJ10	Cpx	364	EPMA	PxNa	PxNa	86.52	2.00	0.00	0.85	0.01	0.03	0.00	0.11	0.11		0.88	0.00	0.00	0.00	0.00	6.00
Cr-rich Pure Jdt	SCMJ10	Cpx	365	EPMA	PxNa	PxNa	80.25	2.01	0.00	0.79	0.00	0.04	0.00	0.17	0.18		0.80	0.00	0.00	0.00	0.00	6.00
Cr-rich Pure Jdt	SCMJ10	Cpx	366	EPMA	PxNa	PxNa	87.44	2.01	0.00	0.85	0.00	0.04	0.00	0.10	0.11		0.87	0.00	0.00	0.00	0.00	6.00
Cr-rich Pure Jdt	SCMJ10	Cpx	367	EPMA	PxNa	PxNa	88.85	2.01	0.00	0.87	0.00	0.03	0.00	0.10	0.10		0.89	0.00	0.00	0.00	0.00	6.00
Cr-rich Pure Jdt	SCMJ10	Cpx	368	EPMA	PxNa	PxNa	84.40	2.01	0.00	0.83	0.00	0.03	0.00	0.13	0.14		0.85	0.00	0.00	0.00	0.00	6.00
Cr-rich Pure Jdt	SCMJ10	Cpx	369	EPMA	PxNa	PxNa	91.88	2.01	0.00	0.91	0.00	0.03	0.00	0.07	0.06		0.91	0.00	0.00	0.00	0.00	6.00
Cr-rich Pure Jdt	SCMJ10	Cpx	3615	VPSEM	PxNa	PxNa	87.38	1.96	0.00	0.89	0.04	0.00	0.00	0.09	0.10		1.00	0.00			0.00	6.00
Cr-rich Pure Jdt	SCMJ10	Cpx	3616	VPSEM	PxNa	PxNa	89.49	1.96	0.00	0.92	0.03	0.00	0.00	0.08	0.08		0.98	0.00			0.00	6.00
Cr-rich Pure Jdt	SCMJ10	Cpx	3617	VPSEM	PxNa	PxNa	83.03	1.97	0.00	0.85	0.05	0.00	0.00	0.14	0.13		0.93	0.00			0.00	6.00
Cr-rich Pure Jdt	SCMJ10	Cpx	3619	VPSEM	PxNa	PxNa	81.57	1.97	0.00	0.84	0.05	0.00	0.00	0.14	0.15		0.90	0.00			0.00	6.00
Cr-rich Pure Jdt	SCMJ10	Cpx	3620	VPSEM	PxNa	PxNa	81.17	1.98	0.00	0.80	0.05	0.00	0.00	0.15	0.15		0.93	0.00			0.00	6.00
Cr-rich Pure Jdt	SCMJ10	Cpx	3623	VPSEM	PxNa	PxNa	86.26	1.97	0.00	0.88	0.03	0.00	0.00	0.11	0.11		0.94	0.00			0.00	6.00

Rock type	Sample	Phase	Point	serie	Px type	Px type	Jd mole%	Si	Ti	Al	Fe3+	Fe2+	Mn	Mg	Ca	Ba	Na	K	F	Cl	H	O
Cr-rich Pure Jdt	SCMJ10	Cpx	3626	VPSEM	PxNa	PxNa	90.01	1.95	0.00	0.93	0.04	0.00	0.00	0.07	0.07		1.02	0.00			0.00	6.00
Cr-rich Pure Jdt	SCMJ10	Cpx	3628	VPSEM	PxNa	PxNa	80.91	1.95	0.00	0.83	0.05	0.00	0.00	0.16	0.16		0.92	0.00			0.00	6.00
Cr-rich Pure Jdt	SCMJ10	Cpx	3630	VPSEM	PxNa	PxNa	89.13	1.96	0.00	0.92	0.04	0.00	0.00	0.08	0.08		0.99	0.00			0.00	6.00
Cr-rich Pure Jdt	SCMJ10	Cpx	3632	VPSEM	PxNa	PxNa	83.32	1.97	0.00	0.84	0.04	0.00	0.00	0.14	0.13		0.93	0.00			0.00	6.00
Cr-rich Pure Jdt	SCMJ10	Cpx	3633	VPSEM	PxNa	PxNa	91.18	1.96	0.00	0.94	0.02	0.00	0.00	0.08	0.06		1.00	0.00			0.00	6.00
Cr-rich Pure Jdt	SCMJ10	Cpx	3634	VPSEM	PxNa	PxNa	81.50	1.96	0.00	0.85	0.04	0.00	0.00	0.15	0.16		0.90	0.00			0.00	6.00
Cr-rich Pure Jdt	SCMJ10	Cpx	3637	VPSEM	PxNa	PxNa	80.54	1.95	0.00	0.83	0.04	0.00	0.00	0.17	0.17		0.90	0.00			0.00	6.00
Cr-rich Pure Jdt	SCMJ10	Cpx	3638	VPSEM	PxNa	PxNa	82.37	1.97	0.00	0.85	0.04	0.00	0.00	0.15	0.14		0.90	0.00			0.00	6.00
Cr-rich Pure Jdt	SCMJ10	Cpx	3648	VPSEM	PxNa	PxNa	86.78	1.97	0.00	0.89	0.04	0.00	0.00	0.11	0.09		0.94	0.00			0.00	6.00
Cr-rich Pure Jdt	SCMJ10	Cpx	3649	VPSEM	PxNa	PxNa	87.65	1.96	0.00	0.90	0.04	0.00	0.00	0.09	0.09		0.97	0.00			0.00	6.00
Cr-rich Pure Jdt	SCMJ10	Cpx	3650	VPSEM	PxNa	PxNa	77.13	1.96	0.00	0.79	0.07	0.00	0.00	0.17	0.17		0.89	0.00			0.00	6.00
Cr-rich Pure Jdt	SCMJ10	Cpx	3653	VPSEM	PxNa	PxNa	83.98	1.97	0.00	0.86	0.04	0.00	0.00	0.12	0.12		0.92	0.00			0.00	6.00
Ep-rich jadeitite	09SC27c	Cpx	2226	SEM	PxNaCa	PxNaCa	62.61	2.08		0.54	0.00	0.14		0.22	0.37		0.61				0.00	6.00
Ep-rich jadeitite	09SC27c	Cpx	2235	SEM	PxNaCa	PxNaCa	55.41	2.09		0.42	0.00	0.22		0.28	0.41		0.57				0.00	6.00
Ep-rich jadeitite	09SC27c	Cpx	2244	SEM	PxNaCa	PxNaCa	52.93	2.04		0.48	0.00	0.16		0.31	0.48		0.53				0.00	6.00
Ep-rich jadeitite	09SC27c	Cpx	2228	SEM	PxNa	PxNa	83.79	2.10		0.73	0.00	0.10		0.08	0.12		0.78				0.00	6.00
Ep-rich jadeitite	09SC27d	Cpx	1900	SEM	PxNaCa	PxNaCa	48.55	2.04		0.42	0.07	0.07		0.37	0.44		0.58				0.00	6.00
Ep-rich jadeitite	09SC27d	Cpx	1907	SEM	PxNaCa	PxNaCa	57.19	2.07		0.46	0.00	0.10		0.39	0.39		0.58				0.00	6.00
Ep-rich jadeitite	09SC27d	Cpx	1910	SEM	PxNaCa	PxNaCa	57.40	2.04		0.51	0.01	0.11		0.38	0.36		0.60				0.00	6.00
Ep-rich jadeitite	09SC27d	Cpx	1912	SEM	PxNaCa	PxNaCa	58.87	1.98		0.60	0.12	0.00		0.22	0.38		0.71				0.00	6.00
Ep-rich jadeitite	09SC27d	Cpx	1926	SEM	PxNaCa	PxNaCa	42.38	2.09		0.40	0.00	0.11		0.44	0.48		0.38				0.00	6.00
Ep-rich jadeitite	09SC27d	Cpx	1927	SEM	PxNaCa	PxNaCa	61.05	2.10		0.46	0.00	0.09		0.39	0.31		0.62				0.00	6.00
Ep-rich jadeitite	09SC27d	Cpx	1930	SEM	PxNaCa	PxNaCa	50.68	2.01		0.49	0.07	0.06		0.31	0.48		0.58				0.00	6.00
Ep-rich jadeitite	09SC27d	Cpx	1913	SEM	PxNa	PxNa	80.38	2.01		0.75	0.10	0.00		0.08	0.11		1.00				0.00	6.00
Ep-rich jadeitite	09SC27m	Cpx	2066	SEM	PxNaCa	PxNaCa	46.38	2.07		0.47	0.00	0.20		0.30	0.45		0.41				0.00	6.00
Ep-rich jadeitite	09SC27m	Cpx	2072	SEM	PxNaCa	PxNaCa	51.72	2.12		0.44	0.00	0.15		0.29	0.42		0.46				0.00	6.00
Ep-rich jadeitite	09SC27m	Cpx	2083	SEM	PxNaCa	PxNaCa	53.64	2.04		0.48	0.00	0.17		0.33	0.44		0.54				0.00	6.00
Ep-rich jadeitite	09SC27m	Cpx	2089	SEM	PxNaCa	PxNaCa	44.46	2.04		0.41	0.00	0.20		0.39	0.49		0.43				0.00	6.00
Ep-rich jadeitite	09SC27m	Cpx	2102	SEM	PxNaCa	PxNaCa	49.46	2.05		0.50	0.00	0.16		0.31	0.46		0.46				0.00	6.00
Ep-rich jadeitite	09SC27m	Cpx	2116	SEM	PxNaCa	PxNaCa	44.13	2.00		0.45	0.06	0.15		0.38	0.48		0.50				0.00	6.00
Ep-rich jadeitite	09SC27m	Cpx	2120	SEM	PxNaCa	PxNaCa	50.16	2.09		0.36	0.00	0.17		0.38	0.47		0.51				0.00	6.00
Ep-rich jadeitite	09SC27m	Cpx	2087	SEM	PxNa	PxNa	81.55	2.08		0.72	0.00	0.16		0.10	0.11		0.81				0.00	6.00
Ep-rich jadeitite	09SC27m	Cpx	2104	SEM	PxNa	PxNa	81.50	2.06		0.74	0.00	0.12		0.09	0.15		0.80				0.00	6.00
Ep-rich jadeitite	09SC27m	Cpx	2130	SEM	PxNa	PxNa	79.34	2.07		0.69	0.04	0.11		0.10	0.13		0.86				0.00	6.00
Ep-rich jadeitite	09SC31g	Cpx	1765	SEM	PxNaCa	PxNaCa	66.27	2.03		0.61	0.01	0.08		0.29	0.29		0.69				0.00	6.00
Ep-rich jadeitite	09SC31g	Cpx	1769	SEM	PxNaCa	PxNaCa	50.18	2.08		0.46	0.00	0.11		0.35	0.45		0.46				0.00	6.00
Ep-rich jadeitite	09SC31g	Cpx	1772	SEM	PxNaCa	PxNaCa	46.33	2.03		0.44	0.00	0.14		0.45	0.48		0.46				0.00	6.00
Ep-rich jadeitite	09SC31g	Cpx	1777	SEM	PxNaCa	PxNaCa	46.96	2.04		0.45	0.00	0.12		0.40	0.51		0.45				0.00	6.00
Ep-rich jadeitite	09SC31g	Cpx	1780	SEM	PxNaCa	PxNaCa	67.51	2.09		0.59	0.00	0.09		0.23	0.30		0.65				0.00	6.00
Ep-rich jadeitite	09SC31g	Cpx	1795	SEM	PxNaCa	PxNaCa	76.78	2.03		0.76	0.00	0.10		0.16	0.18		0.73				0.00	6.00
Ep-rich jadeitite	09SC31g	Cpx	1796	SEM	PxNaCa	PxNaCa	78.83	2.06		0.72	0.00	0.09		0.16	0.16		0.77				0.00	6.00
Ep-rich jadeitite	09SC31g	Cpx	1797	SEM	PxNaCa	PxNaCa	53.56	2.08		0.46	0.00	0.14		0.35	0.40		0.51				0.00	6.00
Ep-rich jadeitite	09SC31g	Cpx	1974	SEM	PxNaCa	PxNaCa	39.74	2.03		0.40	0.00	0.19		0.36	0.59		0.38				0.00	6.00
Ep-rich jadeitite	09SC31g	Cpx	1981	SEM	PxNaCa	PxNaCa	43.91	2.05		0.43	0.00	0.11		0.39	0.55		0.41				0.00	6.00

Rock type	Sample	Phase	Point	serie	Px type	Px type	Jd mole%	Si	Ti	Al	Fe3+	Fe2+	Mn	Mg	Ca	Ba	Na	K	F	Cl	H	O
Ep-rich jadeitite	09SC31g	Cpx	1982	SEM	PxNaCa	PxNaCa	45.11	2.05		0.42	0.00	0.12		0.43	0.51		0.43				0.00	6.00
Ep-rich jadeitite	09SC31j	Cpx	1933	SEM	PxNaCa	PxNaCa	46.62	2.08		0.47	0.00	0.18		0.27	0.48		0.41				0.00	6.00
Ep-rich jadeitite	09SC31j	Cpx	1936	SEM	PxNaCa	PxNaCa	69.38	2.07		0.64	0.00	0.15		0.20	0.23		0.65				0.00	6.00
Ep-rich jadeitite	09SC31j	Cpx	1938	SEM	PxNaCa	PxNaCa	51.08	2.08		0.44	0.00	0.20		0.29	0.46		0.49				0.00	6.00
Ep-rich jadeitite	09SC31j	Cpx	1947	SEM	PxNaCa	PxNaCa	47.62	2.06		0.43	0.00	0.17		0.32	0.51		0.46				0.00	6.00
Ep-rich jadeitite	09SC31j	Cpx	1955	SEM	PxNaCa	PxNaCa	48.56	2.06		0.44	0.00	0.16		0.30	0.53		0.47				0.00	6.00
Ep-rich jadeitite	09SC31j	Cpx	1960	SEM	PxNaCa	PxNaCa	45.12	2.09		0.41	0.00	0.15		0.33	0.51		0.41				0.00	6.00
Ep-rich jadeitite	09SC31j	Cpx	1962	SEM	PxNaCa	PxNaCa	54.37	2.05		0.49	0.00	0.19		0.27	0.44		0.53				0.00	6.00
Ep-rich jadeitite	09SC31j	Cpx	1969	SEM	PxNaCa	PxNaCa	49.80	2.05		0.45	0.00	0.21		0.28	0.48		0.48				0.00	6.00
Ep-rich jadeitite	09SC31j	Cpx	1970	SEM	PxNaCa	PxNaCa	79.15	2.10		0.71	0.00	0.09		0.14	0.15		0.72				0.00	6.00
Ep-rich jadeitite	09SC31j	Cpx	1934	SEM	PxNa	PxNa	83.62	2.07		0.75	0.00	0.11		0.10	0.10		0.81				0.00	6.00
Ep-rich Jadeitite	MCB1d	Cpx	206	EPMA	PxNaCa	PxNaCa	65.24	2.00	0.00	0.65	0.06	0.10	0.00	0.20	0.28		0.71	0.00	0.00	0.00	0.00	6.00
Ep-rich Jadeitite	MCB1d	Cpx	208	EPMA	PxNaCa	PxNaCa	47.20	1.98	0.00	0.50	0.09	0.11	0.00	0.32	0.44		0.55	0.00	0.01	0.00	0.00	6.00
Ep-rich Jadeitite	MCB1d	Cpx	212	EPMA	PxNaCa	PxNaCa	43.49	1.98	0.00	0.46	0.12	0.02	0.00	0.38	0.49		0.54	0.00	0.01	0.00	0.00	5.99
Ep-rich Jadeitite	MCB1d	Cpx	215	EPMA	PxNaCa	PxNaCa	67.24	2.00	0.00	0.67	0.06	0.12	0.00	0.16	0.24		0.74	0.00	0.01	0.00	0.00	6.00
Ep-rich Jadeitite	MCB1d	Cpx	234	EPMA	PxNaCa	PxNaCa	47.52	1.97	0.00	0.52	0.09	0.07	0.01	0.36	0.44		0.54	0.00	0.01	0.00	0.00	6.00
Ep-rich Jadeitite	MCB1d	Cpx	235	EPMA	PxNaCa	PxNaCa	44.44	1.98	0.00	0.47	0.10	0.13	0.00	0.31	0.46		0.54	0.00	0.01	0.00	0.00	6.00
Ep-rich jadeitite	MCB1d	Cpx	1562	VPSEM	PxNaCa	PxNaCa	43.98	1.96		0.49	0.13	0.04		0.35	0.47		0.55				0.00	6.00
Ep-rich jadeitite	MCB1d	Cpx	1564	VPSEM	PxNaCa	PxNaCa	45.98	1.96		0.52	0.12	0.03		0.34	0.47		0.56				0.00	6.00
Ep-rich jadeitite	MCB1d	Cpx	1579	VPSEM	PxNaCa	PxNaCa	41.26	1.95		0.48	0.16	0.00		0.37	0.50		0.54				0.00	6.00
Ep-rich jadeitite	MCB1d	Cpx	1581	VPSEM	PxNaCa	PxNaCa	55.83	1.95	0.01	0.61	0.16	0.01		0.23	0.32		0.68	0.02			0.00	6.00
Ep-rich jadeitite	MCB1d	Cpx	1584	VPSEM	PxNaCa	PxNaCa	50.92	1.97		0.56	0.10	0.03	0.01	0.33	0.41		0.59				0.00	6.00
Ep-rich jadeitite	MCB1d	Cpx	1585	VPSEM	PxNaCa	PxNaCa	36.83	1.95		0.43	0.17	0.00	0.01	0.41	0.55		0.50				0.00	6.00
Ep-rich jadeitite	MCB1d	Cpx	1586	VPSEM	PxNaCa	PxNaCa	43.13	1.93	0.03	0.48	0.15	0.03		0.34	0.49		0.56				0.00	6.00
Ep-rich jadeitite	MCB1d	Cpx	1587	VPSEM	PxNaCa	PxNaCa	45.80	1.96	0.01	0.50	0.11	0.06		0.34	0.47		0.55				0.00	6.00
Ep-rich jadeitite	MCB1d	Cpx	1590	VPSEM	PxNaCa	PxNaCa	63.22	1.98		0.66	0.10	0.07		0.21	0.27		0.72				0.00	6.00
Ep-rich jadeitite	MCB1d	Cpx	1594	VPSEM	PxNaCa	PxNaCa	46.08	1.96		0.51	0.15	0.03	0.01	0.32	0.44		0.58				0.00	6.00
Ep-rich jadeitite	MCB1d	Cpx	1623	VPSEM	PxNaCa	PxNaCa	46.31	1.98		0.50	0.10	0.05		0.36	0.47		0.55				0.00	6.00
Ep-rich jadeitite	MCB1d	Cpx	1642	VPSEM	PxNaCa	PxNaCa	44.94	1.97		0.50	0.14	0.03		0.34	0.47		0.56				0.00	6.00
Ep-rich jadeitite	MCB1d	Cpx	1650	VPSEM	PxNaCa	PxNaCa	46.06	1.97		0.51	0.10	0.07		0.36	0.46		0.54				0.00	6.00
Ep-rich jadeitite	MCB1d	Cpx	1652	VPSEM	PxNaCa	PxNaCa	42.55	1.95		0.48	0.16	0.00	0.01	0.37	0.48		0.55				0.00	6.00
Ep-rich jadeitite	MCB1d	Cpx	1680	VPSEM	PxNaCa	PxNaCa	41.37	1.97		0.46	0.12	0.10		0.36	0.50		0.51				0.00	6.00
Ep-rich jadeitite	MCB1d	Cpx	1687	VPSEM	PxNaCa	PxNaCa	43.06	1.96		0.49	0.12	0.06		0.37	0.49		0.52				0.00	6.00
Ep-rich Jadeitite	MCB1d	Cpx	210	EPMA	PxNa	PxNa	88.91	2.01	0.00	0.88	0.00	0.08	0.00	0.07	0.08		0.89	0.00	0.01	0.00	0.00	6.00
Ep-rich Jadeitite	MCB1d	Cpx	232	EPMA	PxNa	PxNa	89.39	2.01	0.00	0.88	0.00	0.07	0.00	0.06	0.07		0.89	0.00	0.00	0.00	0.00	6.00
Ep-rich Jadeitite	MCB1d	Cpx	240	EPMA	PxNa	PxNa	79.91	2.00	0.00	0.79	0.03	0.08	0.00	0.10	0.15		0.83	0.00	0.01	0.00	0.00	6.00
Ep-rich jadeitite	MCB1d	Cpx	1558	VPSEM	PxNa	PxNa	85.73	1.98		0.88	0.08	0.00		0.05	0.07		0.94				0.00	6.00
Ep-rich jadeitite	MCB1d	Cpx	1559	VPSEM	PxNa	PxNa	90.26	1.96		0.95	0.06	0.00		0.04	0.04		0.96				0.00	6.00
Ep-rich jadeitite	MCB1d	Cpx	1574	VPSEM	PxNa	PxNa	92.38	2.00		0.93	0.04	0.02		0.03	0.03		0.96				0.00	6.00
Ep-rich jadeitite	MCB1d	Cpx	1575	VPSEM	PxNa	PxNa	87.06	1.99		0.88	0.07	0.00		0.05	0.06		0.94				0.00	6.00
Ep-rich jadeitite	MCB1d	Cpx	1576	VPSEM	PxNa	PxNa	72.47	1.96		0.76	0.13	0.00		0.12	0.18		0.87				0.00	6.00
Ep-rich jadeitite	MCB1d	Cpx	1580	VPSEM	PxNa	PxNa	89.47	1.98		0.92	0.06	0.00		0.04	0.05		0.96				0.00	6.00
Ep-rich jadeitite	MCB1d	Cpx	1582	VPSEM	PxNa	PxNa	87.21	1.97		0.91	0.07	0.00		0.05	0.06		0.94				0.00	6.00
Ep-rich jadeitite	MCB1d	Cpx	1588	VPSEM	PxNa	PxNa	72.66	1.96		0.77	0.12	0.00		0.13	0.18		0.83				0.00	6.00

Rock type	Sample	Phase	Point	serie	Px type	Px type	Jd mole%	Si	Ti	Al	Fe3+	Fe2+	Mn	Mg	Ca	Ba	Na	K	F	Cl	H	O
Ep-rich jadeitite	MCB1d	Cpx	1589	VPSEM	PxNa	PxNa	71.61	1.95		0.77	0.14	0.00		0.13	0.17		0.85				0.00	6.00
Ep-rich jadeitite	MCB1d	Cpx	1592	VPSEM	PxNa	PxNa	79.96	1.97		0.83	0.10	0.00		0.09	0.11		0.90				0.00	6.00
Ep-rich jadeitite	MCB1d	Cpx	1595	VPSEM	PxNa	PxNa	87.52	1.97		0.91	0.08	0.00		0.04	0.05		0.97				0.00	6.00
Ep-rich jadeitite	MCB1d	Cpx	1596	VPSEM	PxNa	PxNa	77.62	1.98		0.80	0.12	0.00		0.09	0.13		0.88				0.00	6.00
Ep-rich jadeitite	MCB1d	Cpx	1602	VPSEM	PxNa	PxNa	86.68	1.97		0.90	0.07	0.00		0.06	0.07		0.93				0.00	6.00
Ep-rich jadeitite	MCB1d	Cpx	1608	VPSEM	PxNa	PxNa	74.35	2.00		0.75	0.09	0.05		0.11	0.17		0.83				0.00	6.00
Ep-rich jadeitite	MCB1d	Cpx	1609	VPSEM	PxNa	PxNa	75.86	1.96	0.01	0.79	0.12	0.00	0.01	0.11	0.15		0.88				0.00	6.00
Ep-rich jadeitite	MCB1d	Cpx	1611	VPSEM	PxNa	PxNa	75.11	1.95	0.01	0.81	0.12	0.00		0.11	0.15		0.85				0.00	6.00
Ep-rich jadeitite	MCB1d	Cpx	1612	VPSEM	PxNa	PxNa	86.17	1.98		0.88	0.08	0.00		0.06	0.07		0.96				0.00	6.00
Ep-rich jadeitite	MCB1d	Cpx	1622	VPSEM	PxNa	PxNa	78.62	1.98		0.81	0.09	0.02		0.09	0.13		0.87				0.00	6.00
Ep-rich jadeitite	MCB1d	Cpx	1634	VPSEM	PxNa	PxNa	71.26	1.96		0.75	0.15	0.00	0.01	0.13	0.17		0.85				0.00	6.00
Ep-rich jadeitite	MCB1d	Cpx	1646	VPSEM	PxNa	PxNa	82.81	1.97		0.87	0.08	0.01		0.08	0.10		0.89				0.00	6.00
Ep-rich jadeitite	MCB1d	Cpx	1649	VPSEM	PxNa	PxNa	76.95	1.97		0.81	0.10	0.03		0.11	0.13		0.85				0.00	6.00
Ep-rich jadeitite	MCB1d	Cpx	1657	VPSEM	PxNa	PxNa	77.78	1.98		0.81	0.12	0.00		0.08	0.13		0.88				0.00	6.00
Ep-rich jadeitite	MCB1d	Cpx	1662	VPSEM	PxNa	PxNa	90.22	1.99		0.91	0.07	0.00		0.02	0.04		0.99				0.00	6.00
Ep-rich jadeitite	MCB1d	Cpx	1668	VPSEM	PxNa	PxNa	73.18	1.98		0.76	0.12	0.02		0.11	0.17		0.84				0.00	6.00
Ep-rich jadeitite	MCB1d	Cpx	1678	VPSEM	PxNa	PxNa	65.87	1.96		0.70	0.15	0.00		0.16	0.23		0.79				0.00	6.00
Ep-rich jadeitite	MCB1d	Cpx	1684	VPSEM	PxNa	PxNa	79.92	1.97		0.83	0.11	0.00		0.07	0.11		0.91				0.00	6.00
Ep-rich jadeitite	MCB1g	Cpx	3293	VPSEM	PxNaCa	PxNaCa	50.22	1.95	0.00	0.56	0.18	0.00	0.00	0.29	0.38		0.65	0.00			0.00	6.00
Ep-rich jadeitite	MCB1g	Cpx	3294	VPSEM	PxNaCa	PxNaCa	62.06	1.94	0.00	0.68	0.16	0.00	0.00	0.19	0.28		0.78	0.00			0.00	6.00
Ep-rich jadeitite	MCB1g	Cpx	3317	VPSEM	PxNaCa	PxNaCa	51.11	1.95	0.00	0.57	0.18	0.00	0.00	0.28	0.38		0.67	0.00			0.00	6.00
Ep-rich jadeitite	MCB1g	Cpx	3320	VPSEM	PxNaCa	PxNaCa	48.43	1.96	0.00	0.51	0.14	0.00	0.00	0.37	0.42		0.65	0.00			0.00	6.00
Ep-rich jadeitite	MCB1g	Cpx	3329	VPSEM	PxNaCa	PxNaCa	47.63	1.94	0.01	0.53	0.14	0.00	0.00	0.36	0.42		0.61	0.00			0.00	6.00
Ep-rich jadeitite	MCB1g	Cpx	3333	VPSEM	PxNaCa	PxNaCa	44.23	1.95	0.00	0.49	0.16	0.00	0.00	0.38	0.44		0.59	0.00			0.00	6.00
Ep-rich jadeitite	MCB1g	Cpx	3334	VPSEM	PxNaCa	PxNaCa	46.19	1.97	0.00	0.50	0.11	0.05	0.00	0.37	0.45		0.55	0.00			0.00	6.00
Ep-rich jadeitite	MCB1g	Cpx	3341	VPSEM	PxNaCa	PxNaCa	45.29	1.97	0.00	0.49	0.12	0.00	0.00	0.41	0.46		0.56	0.00			0.00	6.00
Ep-rich jadeitite	MCB1g	Cpx	3343	VPSEM	PxNaCa	PxNaCa	46.71	1.95	0.00	0.52	0.14	0.00	0.00	0.36	0.45		0.59	0.00			0.00	6.00
Ep-rich jadeitite	MCB1g	Cpx	3344	VPSEM	PxNaCa	PxNaCa	48.65	1.96	0.00	0.54	0.14	0.00	0.00	0.35	0.41		0.61	0.00			0.00	6.00
Ep-rich jadeitite	MCB1g	Cpx	3348	VPSEM	PxNaCa	PxNaCa	43.98	1.96	0.00	0.48	0.16	0.00	0.00	0.39	0.45		0.58	0.00			0.00	6.00
Ep-rich jadeitite	MCB1g	Cpx	3359	VPSEM	PxNaCa	PxNaCa	44.62	1.97	0.00	0.48	0.15	0.00	0.00	0.37	0.45		0.59	0.00			0.00	6.00
Ep-rich jadeitite	MCB1g	Cpx	3360	VPSEM	PxNaCa	PxNaCa	39.21	1.96	0.00	0.43	0.15	0.00	0.00	0.43	0.51		0.53	0.00			0.00	6.00
Ep-rich jadeitite	MCB1g	Cpx	3364	VPSEM	PxNaCa	PxNaCa	37.18	1.94	0.00	0.43	0.21	0.00	0.01	0.38	0.50		0.55	0.00			0.00	6.00
Ep-rich jadeitite	MCB1g	Cpx	3304	VPSEM	PxNa	PxNa	82.42	1.97	0.00	0.83	0.07	0.00	0.00	0.12	0.11		0.96	0.00			0.00	6.00
Ep-rich jadeitite	MCB1g	Cpx	3310	VPSEM	PxNa	PxNa	92.65	1.97	0.00	0.95	0.04	0.00	0.00	0.03	0.04		1.01	0.00			0.00	6.00
Ep-rich jadeitite	MCB1g	Cpx	3318	VPSEM	PxNa	PxNa	74.62	1.96	0.00	0.77	0.12	0.00	0.00	0.13	0.16		0.90	0.00			0.00	6.00
Ep-rich jadeitite	MCB1g	Cpx	3321	VPSEM	PxNa	PxNa	75.20	1.95	0.01	0.77	0.13	0.00	0.00	0.12	0.15		0.94	0.00			0.00	6.00
Ep-rich jadeitite	MCB1g	Cpx	3340	VPSEM	PxNa	PxNa	89.58	1.96	0.00	0.92	0.06	0.00	0.00	0.05	0.05		1.01	0.00			0.00	6.00
Ep-rich jadeitite	MCB1g	Cpx	3347	VPSEM	PxNa	PxNa	83.20	1.97	0.00	0.86	0.08	0.00	0.00	0.08	0.10		0.95	0.00			0.00	6.00
Ep-rich jadeitite	MCB1g	Cpx	3354	VPSEM	PxNa	PxNa	86.86	1.96	0.00	0.89	0.05	0.00	0.00	0.09	0.09		0.99	0.00			0.00	6.00
Ep-rich jadeitite	MCB1g	Cpx	3363	VPSEM	PxNa	PxNa	74.94	1.96	0.00	0.78	0.12	0.00	0.00	0.13	0.16		0.90	0.00			0.00	6.00
Ep-rich jadeitite	MCB2c	Cpx	3370	VPSEM	PxNaCa	PxNaCa	51.25	1.97	0.00	0.55	0.11	0.00	0.00	0.37	0.40		0.61	0.00			0.00	6.00
Ep-rich jadeitite	MCB2c	Cpx	3371	VPSEM	PxNaCa	PxNaCa	42.46	1.97	0.00	0.46	0.14	0.00	0.00	0.42	0.48		0.55	0.00			0.00	6.00
Ep-rich jadeitite	MCB2c	Cpx	3378	VPSEM	PxNaCa	PxNaCa	45.14	1.95	0.00	0.51	0.15	0.00	0.00	0.38	0.45		0.57	0.00			0.00	6.00
Ep-rich jadeitite	MCB2c	Cpx	3380	VPSEM	PxNaCa	PxNaCa	49.67	1.94	0.00	0.55	0.13	0.00	0.00	0.37	0.41		0.63	0.00			0.00	6.00

Rock type	Sample	Phase	Point	serie	Px type	Px type	Jd mole%	Si	Ti	Al	Fe3+	Fe2+	Mn	Mg	Ca	Ba	Na	K	F	Cl	H	O
Ep-rich jadeitite	MCB2c	Cpx	3384	VPSEM	PxNaCa	PxNaCa	51.51	1.97	0.00	0.55	0.12	0.00	0.00	0.35	0.39		0.63	0.00			0.00	6.00
Ep-rich jadeitite	MCB2c	Cpx	3387	VPSEM	PxNaCa	PxNaCa	48.12	1.99	0.00	0.49	0.13	0.00	0.00	0.38	0.41		0.61	0.00			0.00	6.00
Ep-rich jadeitite	MCB2c	Cpx	3388	VPSEM	PxNaCa	PxNaCa	45.81	1.96	0.00	0.50	0.13	0.00	0.00	0.40	0.45		0.57	0.00			0.00	6.00
Ep-rich jadeitite	MCB2c	Cpx	3392	VPSEM	PxNaCa	PxNaCa	49.88	1.96	0.00	0.53	0.12	0.00	0.00	0.37	0.42		0.63	0.00			0.00	6.00
Ep-rich jadeitite	MCB2c	Cpx	3395	VPSEM	PxNaCa	PxNaCa	52.57	1.97	0.00	0.55	0.11	0.00	0.00	0.37	0.39		0.65	0.00			0.00	6.00
Ep-rich jadeitite	MCB2c	Cpx	3398	VPSEM	PxNaCa	PxNaCa	51.53	1.96	0.00	0.55	0.12	0.00	0.01	0.35	0.40		0.62	0.00			0.00	6.00
Ep-rich jadeitite	MCB2c	Cpx	3402	VPSEM	PxNaCa	PxNaCa	56.05	1.95	0.00	0.59	0.10	0.00	0.00	0.35	0.37		0.68	0.00			0.00	6.00
Ep-rich jadeitite	MCB2c	Cpx	3409	VPSEM	PxNaCa	PxNaCa	40.98	1.95	0.00	0.45	0.15	0.00	0.00	0.44	0.49		0.56	0.00			0.00	6.00
Ep-rich jadeitite	MCB2c	Cpx	3410	VPSEM	PxNaCa	PxNaCa	45.78	1.96	0.00	0.50	0.12	0.00	0.00	0.40	0.46		0.57	0.00			0.00	6.00
Ep-rich jadeitite	MCB2c	Cpx	3366	VPSEM	PxNa	PxNa	86.01	1.97	0.00	0.88	0.08	0.00	0.00	0.06	0.08		0.98	0.00			0.00	6.00
Ep-rich jadeitite	MCB2c	Cpx	3372	VPSEM	PxNa	PxNa	82.76	1.96	0.00	0.86	0.07	0.00	0.00	0.09	0.12		0.94	0.00			0.00	6.00
Ep-rich jadeitite	MCB2c	Cpx	3376	VPSEM	PxNa	PxNa	82.90	1.95	0.00	0.87	0.08	0.00	0.00	0.09	0.12		0.95	0.00			0.00	6.00
Ep-rich jadeitite	MCB2c	Cpx	3381	VPSEM	PxNa	PxNa	79.85	1.97	0.00	0.82	0.08	0.00	0.00	0.12	0.14		0.91	0.00			0.00	6.00
Ep-rich jadeitite	MCB2c	Cpx	3382	VPSEM	PxNa	PxNa	86.03	1.96	0.00	0.89	0.06	0.00	0.00	0.08	0.08		0.96	0.00			0.00	6.00
Ep-rich jadeitite	MCB2c	Cpx	3383	VPSEM	PxNa	PxNa	81.66	1.97	0.00	0.83	0.07	0.00	0.00	0.11	0.13		0.94	0.00			0.00	6.00
Ep-rich jadeitite	MCB2c	Cpx	3390	VPSEM	PxNa	PxNa	84.39	1.96	0.00	0.87	0.06	0.00	0.00	0.10	0.10		0.95	0.00			0.00	6.00
Ep-rich jadeitite	MCB2c	Cpx	3404	VPSEM	PxNa	PxNa	85.49	1.97	0.00	0.86	0.06	0.00	0.00	0.09	0.09		0.98	0.00			0.00	6.00
Ep-rich jadeitite	MCB2c	Cpx	3411	VPSEM	PxNa	PxNa	84.10	1.97	0.00	0.86	0.07	0.00	0.00	0.09	0.11		0.96	0.00			0.00	6.00
Ep-rich jadeitite	MCB4a	Cpx	1435	EPMA	PxNaCa	PxNaCa	41.81	1.99	0.00	0.44	0.05	0.10	0.01	0.43	0.54		0.46	0.00	0.01	0.00	0.00	5.99
Ep-rich jadeitite	MCB4a	Cpx	1437	EPMA	PxNaCa	PxNaCa	40.73	1.98	0.00	0.43	0.07	0.09	0.01	0.43	0.53		0.47	0.00	0.01	0.00	0.00	5.99
Ep-rich jadeitite	MCB4a	Cpx	1438	EPMA	PxNaCa	PxNaCa	47.17	1.99	0.00	0.49	0.06	0.10	0.00	0.35	0.48		0.53	0.00	0.02	0.00	0.00	5.99
Ep-rich jadeitite	MCB4a	Cpx	1439	EPMA	PxNaCa	PxNaCa	44.85	1.99	0.00	0.47	0.06	0.09	0.01	0.38	0.50		0.50	0.00	0.01	0.00	0.00	5.99
Ep-rich jadeitite	MCB4a	Cpx	1440	EPMA	PxNaCa	PxNaCa	49.75	1.99	0.00	0.50	0.04	0.10	0.01	0.37	0.46		0.53	0.00	0.01	0.00	0.00	6.00
Ep-rich jadeitite	MCB4a	Cpx	1445	VPSEM	PxNaCa	PxNaCa	45.70	2.08		0.44	0.00	0.15		0.35	0.48		0.41				0.00	6.00
Ep-rich jadeitite	MCB4a	Cpx	1449	VPSEM	PxNaCa	PxNaCa	50.15	2.07		0.47	0.00	0.18		0.28	0.46		0.46				0.00	6.00
Ep-rich jadeitite	MCB4a	Cpx	1453	VPSEM	PxNaCa	PxNaCa	46.84	2.08		0.45	0.00	0.19		0.30	0.48		0.42				0.00	6.00
Ep-rich jadeitite	MCB4a	Cpx	1460	VPSEM	PxNaCa	PxNaCa	48.03	2.07		0.46	0.00	0.13		0.34	0.48		0.44				0.00	6.00
Ep-rich jadeitite	MCB4a	Cpx	1475	VPSEM	PxNaCa	PxNaCa	43.66	2.09		0.43	0.00	0.15		0.35	0.50		0.38				0.00	6.00
Ep-rich jadeitite	MCB4a	Cpx	1478	VPSEM	PxNaCa	PxNaCa	45.22	2.10		0.43	0.00	0.13		0.32	0.50		0.39				0.00	6.00
Ep-rich jadeitite	MCB4a	Cpx	1481	VPSEM	PxNaCa	PxNaCa	45.04	2.09		0.42	0.00	0.16		0.32	0.50		0.40				0.00	6.00
Ep-rich jadeitite	MCB4a	Cpx	1482	VPSEM	PxNaCa	PxNaCa	55.93	2.07		0.52	0.00	0.16		0.24	0.42		0.52				0.00	6.00
Ep-rich jadeitite	MCB4a	Cpx	1487	VPSEM	PxNaCa	PxNaCa	57.19	2.07		0.52	0.00	0.22		0.23	0.36		0.54				0.00	6.00
Ep-rich jadeitite	MCB4a	Cpx	1489	VPSEM	PxNaCa	PxNaCa	56.30	2.06		0.53	0.00	0.14		0.27	0.40		0.52				0.00	6.00
Ep-rich jadeitite	MCB4a	Cpx	1499	VPSEM	PxNaCa	PxNaCa	50.55	2.08		0.48	0.00	0.16		0.29	0.45		0.46				0.00	6.00
Ep-rich jadeitite	MCB4a	Cpx	1429	EPMA	PxNa	PxNa	91.59	2.00	0.00	0.91	0.02	0.03	0.00	0.05	0.05		0.94	0.00	0.00	0.00	0.00	6.00
Ep-rich jadeitite	MCB4a	Cpx	1430	EPMA	PxNa	PxNa	90.12	2.00	0.00	0.89	0.03	0.03	0.00	0.05	0.06		0.93	0.00	0.00	0.00	0.00	6.00
Ep-rich jadeitite	MCB4a	Cpx	1431	EPMA	PxNa	PxNa	89.83	2.01	0.00	0.89	0.02	0.04	0.00	0.06	0.07		0.92	0.00	0.01	0.00	0.00	6.00
Ep-rich jadeitite	MCB4a	Cpx	1433	EPMA	PxNa	PxNa	83.40	2.00	0.00	0.83	0.03	0.05	0.00	0.09	0.12		0.87	0.00	0.00	0.00	0.00	6.00
Ep-rich jadeitite	MCB4a	Cpx	1434	EPMA	PxNa	PxNa	84.58	2.00	0.00	0.85	0.05	0.04	0.00	0.08	0.09		0.90	0.00	0.00	0.00	0.00	6.00
Ep-rich jadeitite	MCB4a	Cpx	1446	VPSEM	PxNa	PxNa	89.26	2.06		0.85	0.00	0.06		0.04	0.09		0.80				0.00	6.00
Ep-rich jadeitite	MCB4a	Cpx	1451	VPSEM	PxNa	PxNa	92.48	2.06		0.88	0.00	0.05		0.02	0.06		0.84				0.00	6.00
Ep-rich jadeitite	MCB4a	Cpx	1454	VPSEM	PxNa	PxNa	91.25	2.05		0.88	0.00	0.06		0.03	0.07		0.84				0.00	6.00
Ep-rich jadeitite	MCB4a	Cpx	1456	VPSEM	PxNa	PxNa	85.76	2.06		0.80	0.00	0.10		0.06	0.10		0.80				0.00	6.00
Ep-rich jadeitite	MCB4a	Cpx	1461	VPSEM	PxNa	PxNa	92.25	2.07		0.87	0.00	0.08		0.01	0.05		0.84				0.00	6.00

Rock type	Sample	Phase	Point	serie	Px type	Px type	Jd mole%	Si	Ti	Al	Fe3+	Fe2+	Mn	Mg	Ca	Ba	Na	K	F	Cl	H	O
Ep-rich jadeitite	MCB4a	Cpx	1473	VPSEM	PxNa	PxNa	85.49	2.08		0.80	0.00	0.08		0.06	0.12		0.77				0.00	6.00
Ep-rich jadeitite	MCB4a	Cpx	1476	VPSEM	PxNa	PxNa	87.56	2.07		0.83	0.00	0.08		0.05	0.09		0.80				0.00	6.00
Ep-rich jadeitite	MCB4a	Cpx	1500	VPSEM	PxNa	PxNa	91.15	2.05		0.88	0.00	0.06		0.03	0.07		0.82				0.00	6.00
Mica-rich Jadeitite	09SC31e	Cpx	1827	SEM	PxNaCa	PxNaCa	71.69	2.08		0.63	0.00	0.13		0.18	0.24		0.69				0.00	6.00
Mica-rich Jadeitite	09SC31e	Cpx	1825	SEM	PxNa	PxNa	86.56	2.12		0.74	0.00	0.08		0.09	0.08		0.80				0.00	6.00
Mica-rich Jadeitite	09SC31e	Cpx	1828	SEM	PxNa	PxNa	93.08	2.09		0.85	0.00	0.07			0.05		0.85				0.00	6.00
Pure jadeitite	BCJ1	Cpx	2490	VPSEM	PxNaCa	PxNaCa	44.44	1.96		0.50	0.15	0.00	0.01	0.38	0.45		0.57				0.00	6.00
Pure jadeitite	BCJ1	Cpx	2493	VPSEM	PxNaCa	PxNaCa	38.37	1.94		0.45	0.18	0.00	0.01	0.40	0.50		0.52				0.00	6.00
Pure jadeitite	BCJ1	Cpx	2498	VPSEM	PxNaCa	PxNaCa	37.58	1.95		0.43	0.18	0.00	0.02	0.39	0.52		0.52				0.00	6.00
Pure jadeitite	BCJ1	Cpx	2502	VPSEM	PxNaCa	PxNaCa	48.36	1.94	0.01	0.52	0.15	0.00		0.35	0.42		0.63				0.00	6.00
Pure jadeitite	BCJ1	Cpx	2506	VPSEM	PxNaCa	PxNaCa	48.60	1.94		0.54	0.15	0.00		0.35	0.41		0.63				0.00	6.00
Pure jadeitite	BCJ1	Cpx	2489	VPSEM	PxNa	PxNa	84.07	1.97		0.87	0.07	0.00		0.10	0.09		0.93				0.00	6.00
Pure jadeitite	BCJ1	Cpx	2494	VPSEM	PxNa	PxNa	77.78	1.95		0.81	0.08	0.00		0.14	0.15		0.91				0.00	6.00
Pure jadeitite	BCJ1	Cpx	2499	VPSEM	PxNa	PxNa	86.61	1.97		0.87	0.06	0.00		0.07	0.08		0.99				0.00	6.00
Pure jadeitite	BCJ1	Cpx	2503	VPSEM	PxNa	PxNa	72.76	1.93		0.78	0.11	0.00	0.01	0.14	0.21		0.88				0.00	6.00
Pure jadeitite	CV237b	Cpx	132	EPMA	PxNaCa	PxNaCa	64.45	2.00	0.00	0.64	0.03	0.07	0.00	0.26	0.32		0.67	0.00	0.01	0.01	0.00	5.99
Pure jadeitite	CV237b	Cpx	133	EPMA	PxNaCa	PxNaCa	68.43	2.01	0.00	0.68	0.00	0.10	0.00	0.24	0.28		0.68	0.00	0.01	0.00	0.00	6.00
Pure jadeitite	CV237b	Cpx	134	EPMA	PxNaCa	PxNaCa	47.60	1.99	0.01	0.48	0.03	0.10	0.01	0.40	0.49		0.50	0.00	0.01	0.00	0.00	5.99
Pure jadeitite	CV237b	Cpx	135	EPMA	PxNaCa	PxNaCa	38.93	2.00	0.00	0.39	0.08	0.15	0.01	0.39	0.53		0.46	0.00	0.01	0.00	0.00	6.00
Pure jadeitite	CV237b	Cpx	137	EPMA	PxNaCa	PxNaCa	47.73	2.00	0.00	0.48	0.02	0.12	0.01	0.38	0.49		0.50	0.00	0.01	0.00	0.00	6.00
Pure jadeitite	CV237b	Cpx	201	EPMA	PxNaCa	PxNaCa	52.26	2.01	0.00	0.51	0.10	0.02	0.00	0.37	0.38		0.62	0.00	0.01	0.00	0.00	6.00
Pure jadeitite	CV237b	Cpx	202	EPMA	PxNaCa	PxNaCa	47.97	1.98	0.00	0.50	0.09	0.09	0.00	0.34	0.44		0.56	0.00	0.01	0.00	0.00	6.00
Pure jadeitite	CV237b	Cpx	2537	VPSEM	PxNaCa	PxNaCa	42.27	1.97	0.00	0.46	0.14	0.05	0.01	0.35	0.48		0.54	0.00			0.00	6.00
Pure jadeitite	CV237b	Cpx	2547	VPSEM	PxNaCa	PxNaCa	36.78	1.96	0.00	0.42	0.15	0.08	0.00	0.37	0.54		0.49	0.00			0.00	6.00
Pure jadeitite	CV237b	Cpx	2548	VPSEM	PxNaCa	PxNaCa	75.32	2.02	0.00	0.73	0.00	0.11	0.00	0.17	0.21		0.74	0.00			0.00	6.00
Pure jadeitite	CV237b	Cpx	2549	VPSEM	PxNaCa	PxNaCa	42.25	1.96	0.00	0.48	0.11	0.04	0.01	0.39	0.51		0.51	0.00			0.00	6.00
Pure jadeitite	CV237b	Cpx	2562	VPSEM	PxNaCa	PxNaCa	44.39	1.95	0.00	0.51	0.13	0.01	0.00	0.36	0.49		0.55	0.00			0.00	6.00
Pure jadeitite	CV237b	Cpx	2564	VPSEM	PxNaCa	PxNaCa	42.35	1.97	0.00	0.47	0.12	0.04	0.00	0.38	0.49		0.53	0.00			0.00	6.00
Pure jadeitite	CV237b	Cpx	2573	VPSEM	PxNaCa	PxNaCa	45.44	1.97	0.00	0.49	0.14	0.01	0.00	0.36	0.45		0.57	0.00			0.00	6.00
Pure jadeitite	CV237b	Cpx	2576	VPSEM	PxNaCa	PxNaCa	58.19	2.02	0.00	0.56	0.00	0.16	0.00	0.28	0.38		0.57	0.01			0.00	6.00
Pure jadeitite	CV237b	Cpx	2580	VPSEM	PxNaCa	PxNaCa	45.79	1.96	0.00	0.50	0.15	0.03	0.00	0.33	0.44		0.58	0.00			0.00	6.00
Pure jadeitite	CV237b	Cpx	2586	VPSEM	PxNaCa	PxNaCa	47.50	1.97	0.00	0.53	0.07	0.12	0.00	0.31	0.47		0.53	0.01			0.00	6.00
Pure jadeitite	CV237b	Cpx	2587	VPSEM	PxNaCa	PxNaCa	52.61	2.00	0.00	0.53	0.07	0.09	0.00	0.29	0.42		0.60	0.00			0.00	6.00
Pure jadeitite	CV237b	Cpx	2589	VPSEM	PxNaCa	PxNaCa	43.97	1.96	0.00	0.48	0.14	0.00	0.00	0.36	0.50		0.56	0.00			0.00	6.00
Pure jadeitite	CV237b	Cpx	2597	VPSEM	PxNaCa	PxNaCa	45.49	1.98	0.00	0.49	0.08	0.07	0.00	0.35	0.50		0.53	0.00			0.00	6.00
Pure jadeitite	CV237b	Cpx	2602	VPSEM	PxNaCa	PxNaCa	47.71	1.97	0.00	0.52	0.14	0.05	0.00	0.31	0.42		0.59	0.00			0.00	6.00
Pure jadeitite	CV237b	Cpx	2612	VPSEM	PxNaCa	PxNaCa	42.84	1.98	0.00	0.45	0.11	0.10	0.00	0.34	0.48		0.53	0.00			0.00	6.00
Pure jadeitite	CV237b	Cpx	2616	VPSEM	PxNaCa	PxNaCa	46.31	1.95	0.00	0.53	0.13	0.05	0.00	0.33	0.42		0.56	0.02			0.00	6.00
Pure jadeitite	CV237b	Cpx	2626	VPSEM	PxNaCa	PxNaCa	47.36	2.02	0.00	0.44	0.01	0.20	0.00	0.35	0.48		0.49	0.00			0.00	6.00
Pure jadeitite	CV237b	Cpx	2645	VPSEM	PxNaCa	PxNaCa	42.77	1.98	0.00	0.45	0.08	0.06	0.01	0.41	0.52		0.49	0.00			0.00	6.00
Pure jadeitite	CV237b	Cpx	2650	VPSEM	PxNaCa	PxNaCa	36.22	1.97	0.00	0.40	0.16	0.07	0.00	0.36	0.54		0.49	0.00			0.00	6.00
Pure jadeitite	CV237b	Cpx	2661	VPSEM	PxNaCa	PxNaCa	48.12	1.97	0.00	0.52	0.12	0.06	0.00	0.31	0.43		0.58	0.00			0.00	6.00
Pure jadeitite	CV237b	Cpx	138	EPMA	PxNa	PxNa	89.66	2.01	0.00	0.89	0.00	0.06	0.00	0.07	0.08		0.88	0.00	0.01	0.00	0.00	6.00
Pure jadeitite	CV237b	Cpx	146	EPMA	PxNa	PxNa	85.85	2.00	0.00	0.85	0.00	0.07	0.00	0.10	0.11		0.86	0.00	0.00	0.00	0.00	6.00

Rock type	Sample	Phase	Point	serie	Px type	Px type	Jd mole%	Si	Ti	Al	Fe3+	Fe2+	Mn	Mg	Ca	Ba	Na	K	F	Cl	H	O
Pure jadeitite	CV237b	Cpx	147	EPMA	PxNa	PxNa	87.31	2.00	0.00	0.87	0.00	0.08	0.00	0.08	0.10		0.87	0.00	0.01	0.00	0.00	6.00
Pure jadeitite	CV237b	Cpx	149	EPMA	PxNa	PxNa	83.21	2.01	0.00	0.82	0.00	0.07	0.00	0.13	0.14		0.83	0.00	0.00	0.00	0.00	6.00
Pure jadeitite	CV237b	Cpx	150	EPMA	PxNa	PxNa	86.37	2.01	0.00	0.84	0.00	0.07	0.00	0.10	0.11		0.87	0.00	0.01	0.00	0.00	6.00
Pure jadeitite	CV237b	Cpx	152	EPMA	PxNa	PxNa	91.93	2.01	0.00	0.90	0.00	0.06	0.00	0.05	0.05		0.92	0.00	0.01	0.00	0.00	6.00
Pure jadeitite	CV237b	Cpx	189	EPMA	PxNa	PxNa	90.26	2.01	0.01	0.89	0.00	0.05	0.00	0.06	0.08		0.88	0.00	0.01	0.00	0.00	6.00
Pure jadeitite	CV237b	Cpx	190	EPMA	PxNa	PxNa	87.00	2.01	0.00	0.85	0.00	0.05	0.00	0.10	0.11		0.86	0.00	0.00	0.00	0.00	6.00
Pure jadeitite	CV237b	Cpx	191	EPMA	PxNa	PxNa	91.86	2.01	0.00	0.91	0.00	0.04	0.00	0.05	0.06		0.90	0.00	0.00	0.00	0.00	6.00
Pure jadeitite	CV237b	Cpx	192	EPMA	PxNa	PxNa	89.89	2.00	0.00	0.90	0.00	0.06	0.00	0.06	0.08		0.89	0.00	0.00	0.00	0.00	6.00
Pure jadeitite	CV237b	Cpx	193	EPMA	PxNa	PxNa	90.88	2.01	0.00	0.90	0.00	0.05	0.00	0.06	0.07		0.89	0.00	0.01	0.00	0.00	6.00
Pure jadeitite	CV237b	Cpx	194	EPMA	PxNa	PxNa	87.42	2.01	0.00	0.86	0.00	0.06	0.00	0.09	0.10		0.87	0.00	0.00	0.00	0.00	6.00
Pure jadeitite	CV237b	Cpx	195	EPMA	PxNa	PxNa	86.92	2.01	0.01	0.84	0.00	0.06	0.00	0.10	0.11		0.86	0.00	0.01	0.00	0.00	6.00
Pure jadeitite	CV237b	Cpx	2538	VPSEM	PxNa	PxNa	83.74	1.99	0.00	0.86	0.05	0.02	0.00	0.09	0.11		0.88	0.00			0.00	6.00
Pure jadeitite	CV237b	Cpx	2554	VPSEM	PxNa	PxNa	88.90	1.96	0.00	0.93	0.05	0.00	0.00	0.06	0.06		0.98	0.00			0.00	6.00
Pure jadeitite	CV237b	Cpx	2563	VPSEM	PxNa	PxNa	84.54	1.97	0.00	0.88	0.06	0.00	0.00	0.09	0.11		0.90	0.00			0.00	6.00
Pure jadeitite	CV237b	Cpx	2566	VPSEM	PxNa	PxNa	84.91	1.97	0.00	0.88	0.07	0.00	0.00	0.08	0.09		0.93	0.00			0.00	6.00
Pure jadeitite	CV237b	Cpx	2577	VPSEM	PxNa	PxNa	89.14	1.98	0.00	0.92	0.06	0.00	0.00	0.05	0.05		0.96	0.00			0.00	6.00
Pure jadeitite	CV237b	Cpx	2579	VPSEM	PxNa	PxNa	87.37	1.98	0.00	0.89	0.06	0.00	0.00	0.07	0.08		0.95	0.00			0.00	6.00
Pure jadeitite	CV237b	Cpx	2585	VPSEM	PxNa	PxNa	87.83	1.98	0.00	0.90	0.06	0.00	0.00	0.06	0.07		0.95	0.00			0.00	6.00
Pure jadeitite	CV237b	Cpx	2590	VPSEM	PxNa	PxNa	85.78	1.98	0.00	0.89	0.07	0.00	0.00	0.07	0.08		0.92	0.00			0.00	6.00
Pure jadeitite	CV237b	Cpx	2596	VPSEM	PxNa	PxNa	82.39	1.98	0.00	0.85	0.06	0.00	0.00	0.10	0.13		0.87	0.00			0.00	6.00
Pure jadeitite	CV237b	Cpx	2598	VPSEM	PxNa	PxNa	81.40	1.97	0.00	0.85	0.08	0.00	0.00	0.10	0.13		0.89	0.00			0.00	6.00
Pure jadeitite	CV237b	Cpx	2600	VPSEM	PxNa	PxNa	85.44	1.97	0.00	0.88	0.07	0.00	0.00	0.07	0.09		0.93	0.00			0.00	6.00
Pure jadeitite	CV237b	Cpx	2604	VPSEM	PxNa	PxNa	81.16	1.98	0.01	0.83	0.06	0.00	0.00	0.12	0.13		0.87	0.00			0.00	6.00
Pure jadeitite	CV237b	Cpx	2609	VPSEM	PxNa	PxNa	80.42	1.97	0.00	0.84	0.06	0.00	0.00	0.13	0.14		0.86	0.00			0.00	6.00
Pure jadeitite	CV237b	Cpx	2611	VPSEM	PxNa	PxNa	88.71	2.02	0.00	0.87	0.00	0.04	0.00	0.07	0.11		0.88	0.00			0.00	6.00
Pure jadeitite	CV237b	Cpx	2613	VPSEM	PxNa	PxNa	80.03	1.98	0.00	0.83	0.06	0.00	0.00	0.13	0.15		0.87	0.00			0.00	6.00
Pure jadeitite	CV237b	Cpx	2640	VPSEM	PxNa	PxNa	86.21	1.97	0.00	0.90	0.05	0.00	0.00	0.08	0.09		0.92	0.00			0.00	6.00
Pure jadeitite	CV237b	Cpx	2646	VPSEM	PxNa	PxNa	86.88	1.99	0.00	0.88	0.03	0.04	0.00	0.07	0.10		0.89	0.00			0.00	6.00
Pure jadeitite	CV237b	Cpx	2660	VPSEM	PxNa	PxNa	84.44	1.98	0.00	0.88	0.01	0.06	0.00	0.09	0.14		0.84	0.00			0.00	6.00
Pure jadeitite	CV237k	Cpx	256	EPMA	PxNaCa	PxNaCa	46.89	2.01	0.00	0.45	0.06	0.06	0.00	0.43	0.45		0.54	0.00	0.01	0.00	0.00	5.99
Pure jadeitite	CV237k	Cpx	263	EPMA	PxNaCa	PxNaCa	50.24	2.01	0.00	0.49	0.06	0.06	0.00	0.39	0.42		0.57	0.00	0.02	0.00	0.00	5.99
Pure jadeitite	CV237k	Cpx	270	EPMA	PxNaCa	PxNaCa	37.51	2.00	0.00	0.37	0.08	0.04	0.00	0.50	0.54		0.45	0.00	0.01	0.00	0.00	5.99
Pure jadeitite	CV237k	Cpx	271	EPMA	PxNaCa	PxNaCa	43.94	2.01	0.00	0.42	0.05	0.07	0.00	0.46	0.50		0.49	0.00	0.02	0.00	0.00	5.99
Pure jadeitite	CV237k	Cpx	272	EPMA	PxNaCa	PxNaCa	57.28	2.01	0.00	0.56	0.00	0.09	0.00	0.35	0.41		0.56	0.00	0.01	0.01	0.00	5.99
Pure jadeitite	CV237k	Cpx	273	EPMA	PxNaCa	PxNaCa	38.41	2.01	0.00	0.37	0.07	0.05	0.00	0.50	0.53		0.46	0.00	0.01	0.00	0.00	5.99
Pure jadeitite	CV237k	Cpx	274	EPMA	PxNaCa	PxNaCa	41.95	2.01	0.00	0.40	0.05	0.07	0.00	0.48	0.52		0.47	0.00	0.01	0.00	0.00	5.99
Pure jadeitite	CV237k	Cpx	275	EPMA	PxNaCa	PxNaCa	38.03	2.01	0.00	0.37	0.07	0.05	0.00	0.50	0.55		0.45	0.00	0.01	0.00	0.00	5.99
Pure jadeitite	CV237k	Cpx	276	EPMA	PxNaCa	PxNaCa	49.35	2.01	0.00	0.47	0.06	0.05	0.00	0.40	0.43		0.56	0.00	0.01	0.00	0.00	5.99
Pure jadeitite	CV237k	Cpx	277	EPMA	PxNaCa	PxNaCa	50.01	2.01	0.00	0.48	0.05	0.06	0.00	0.40	0.43		0.56	0.00	0.01	0.00	0.00	5.99
Pure jadeitite	CV237k	Cpx	278	EPMA	PxNaCa	PxNaCa	47.68	2.01	0.00	0.47	0.08	0.04	0.00	0.41	0.44		0.56	0.00	0.01	0.00	0.00	5.99
Pure jadeitite	CV237k	Cpx	279	EPMA	PxNaCa	PxNaCa	47.13	2.00	0.00	0.47	0.09	0.03	0.00	0.41	0.44		0.56	0.00	0.01	0.00	0.00	5.99
Pure jadeitite	CV237k	Cpx	324	EPMA	PxNaCa	PxNaCa	68.08	2.00	0.00	0.67	0.06	0.03	0.00	0.23	0.25		0.74	0.00	0.01	0.00	0.00	5.99
Pure jadeitite	CV237k	Cpx	325	EPMA	PxNaCa	PxNaCa	68.22	2.01	0.00	0.67	0.05	0.03	0.00	0.24	0.26		0.74	0.00	0.01	0.00	0.00	6.00
Pure jadeitite	CV237k	Cpx	329	EPMA	PxNaCa	PxNaCa	75.28	2.01	0.00	0.73	0.03	0.04	0.00	0.19	0.21		0.79	0.00	0.01	0.00	0.00	5.99

Rock type	Sample	Phase	Point	serie	Px type	Px type	Jd mole%	Si	Ti	Al	Fe3+	Fe2+	Mn	Mg	Ca	Ba	Na	K	F	Cl	H	O
Pure jadeitite	CV237k	Cpx	330	EPMA	PxNaCa	PxNaCa	76.63	2.01	0.00	0.74	0.01	0.07	0.00	0.19	0.20		0.78	0.00	0.01	0.00	0.00	5.99
Pure jadeitite	CV237k	Cpx	331	EPMA	PxNaCa	PxNaCa	52.89	2.01	0.00	0.51	0.03	0.07	0.00	0.38	0.42		0.57	0.00	0.01	0.00	0.00	5.99
Pure jadeitite	CV237k	Cpx	335	EPMA	PxNaCa	PxNaCa	66.70	2.01	0.00	0.65	0.05	0.09	0.00	0.21	0.27		0.72	0.00	0.01	0.00	0.00	5.99
Pure jadeitite	CV237k	Cpx	336	EPMA	PxNaCa	PxNaCa	65.97	2.01	0.00	0.64	0.06	0.09	0.00	0.21	0.27		0.72	0.00	0.02	0.00	0.00	5.99
Pure jadeitite	CV237k	Cpx	337	EPMA	PxNaCa	PxNaCa	63.18	1.99	0.00	0.65	0.12	0.01	0.00	0.23	0.25		0.74	0.01	0.01	0.00	0.00	5.99
Pure jadeitite	CV237k	Cpx	340	EPMA	PxNaCa	PxNaCa	60.87	2.00	0.00	0.60	0.06	0.05	0.00	0.29	0.33		0.67	0.00	0.02	0.00	0.00	5.99
Pure jadeitite	CV237k	Cpx	344	EPMA	PxNaCa	PxNaCa	63.54	2.00	0.00	0.63	0.08	0.03	0.00	0.25	0.29		0.71	0.00	0.01	0.00	0.00	5.99
Pure jadeitite	CV237K	Cpx	2672	VPSEM	PxNaCa	PxNaCa	48.50	1.97	0.00	0.53	0.13	0.00	0.00	0.36	0.41		0.60	0.00			0.00	6.00
Pure jadeitite	CV237K	Cpx	2674	VPSEM	PxNaCa	PxNaCa	49.22	1.98	0.00	0.52	0.12	0.00	0.00	0.37	0.42		0.60	0.00			0.00	6.00
Pure jadeitite	CV237K	Cpx	2700	VPSEM	PxNaCa	PxNaCa	54.86	1.97	0.01	0.58	0.11	0.04	0.00	0.28	0.36		0.64	0.00			0.00	6.00
Pure jadeitite	CV237K	Cpx	2706	VPSEM	PxNaCa	PxNaCa	61.04	1.95	0.00	0.67	0.10	0.00	0.00	0.25	0.34		0.71	0.00			0.00	6.00
Pure jadeitite	CV237K	Cpx	2707	VPSEM	PxNaCa	PxNaCa	42.68	1.97	0.00	0.47	0.13	0.00	0.00	0.40	0.50		0.54	0.00			0.00	6.00
Pure jadeitite	CV237K	Cpx	2708	VPSEM	PxNaCa	PxNaCa	61.69	1.94	0.02	0.65	0.11	0.00	0.01	0.23	0.34		0.73	0.00			0.00	6.00
Pure jadeitite	CV237K	Cpx	2712	VPSEM	PxNaCa	PxNaCa	60.51	1.98	0.00	0.64	0.11	0.05	0.00	0.21	0.31		0.70	0.00			0.00	6.00
Pure jadeitite	CV237K	Cpx	2719	VPSEM	PxNaCa	PxNaCa	43.83	1.96	0.00	0.49	0.09	0.04	0.00	0.40	0.50		0.51	0.00			0.00	6.00
Pure jadeitite	CV237K	Cpx	2721	VPSEM	PxNaCa	PxNaCa	66.42	1.99	0.00	0.68	0.10	0.04	0.00	0.18	0.25		0.76	0.00			0.00	6.00
Pure jadeitite	CV237K	Cpx	2730	VPSEM	PxNaCa	PxNaCa	50.04	1.97	0.00	0.52	0.11	0.00	0.00	0.37	0.43		0.61	0.00			0.00	6.00
Pure jadeitite	CV237K	Cpx	2731	VPSEM	PxNaCa	PxNaCa	41.98	1.97	0.00	0.44	0.11	0.00	0.00	0.46	0.51		0.54	0.00			0.00	6.00
Pure jadeitite	CV237K	Cpx	2734	VPSEM	PxNaCa	PxNaCa	45.79	1.99	0.00	0.47	0.11	0.02	0.00	0.40	0.45		0.56	0.00			0.00	6.00
Pure jadeitite	CV237K	Cpx	2735	VPSEM	PxNaCa	PxNaCa	47.78	1.96	0.00	0.53	0.17	0.04	0.00	0.28	0.39		0.62	0.00			0.00	6.00
Pure jadeitite	CV237K	Cpx	2738	VPSEM	PxNaCa	PxNaCa	65.57	2.01	0.00	0.63	0.02	0.09	0.00	0.27	0.28		0.68	0.00			0.00	6.00
Pure jadeitite	CV237K	Cpx	2740	VPSEM	PxNaCa	PxNaCa	64.70	1.99	0.00	0.66	0.04	0.07	0.00	0.25	0.30		0.69	0.00			0.00	6.00
Pure jadeitite	CV237K	Cpx	2743	VPSEM	PxNaCa	PxNaCa	58.30	1.97	0.00	0.62	0.11	0.03	0.00	0.28	0.31		0.68	0.00			0.00	6.00
Pure jadeitite	CV237K	Cpx	2745	VPSEM	PxNaCa	PxNaCa	54.61	1.97	0.00	0.58	0.13	0.01	0.00	0.28	0.36		0.66	0.00			0.00	6.00
Pure jadeitite	CV237K	Cpx	2748	VPSEM	PxNaCa	PxNaCa	70.42	1.92	0.04	0.74	0.09	0.00	0.00	0.17	0.27		0.83	0.00			0.00	6.00
Pure jadeitite	CV237K	Cpx	2753	VPSEM	PxNaCa	PxNaCa	64.08	1.96	0.01	0.68	0.10	0.00	0.00	0.22	0.31		0.73	0.00			0.00	6.00
Pure jadeitite	CV237K	Cpx	2757	VPSEM	PxNaCa	PxNaCa	62.47	1.97	0.01	0.65	0.11	0.02	0.00	0.23	0.28		0.72	0.00			0.00	6.00
Pure jadeitite	CV237K	Cpx	2761	VPSEM	PxNaCa	PxNaCa	56.84	1.96	0.00	0.61	0.13	0.00	0.00	0.28	0.34		0.69	0.00			0.00	6.00
Pure jadeitite	CV237K	Cpx	2767	VPSEM	PxNaCa	PxNaCa	48.58	1.97	0.00	0.53	0.10	0.02	0.01	0.36	0.45		0.57	0.00			0.00	6.00
Pure jadeitite	CV237K	Cpx	2768	VPSEM	PxNaCa	PxNaCa	61.93	1.95	0.01	0.66	0.10	0.00	0.00	0.25	0.33		0.72	0.00			0.00	6.00
Pure jadeitite	CV237K	Cpx	2769	VPSEM	PxNaCa	PxNaCa	59.72	2.00	0.00	0.60	0.05	0.08	0.00	0.27	0.36		0.64	0.00			0.00	6.00
Pure jadeitite	CV237K	Cpx	2770	VPSEM	PxNaCa	PxNaCa	69.09	1.98	0.00	0.72	0.03	0.06	0.00	0.24	0.26		0.71	0.00			0.00	6.00
Pure jadeitite	CV237K	Cpx	2780	VPSEM	PxNaCa	PxNaCa	71.05	1.95	0.01	0.76	0.09	0.00	0.00	0.17	0.24		0.79	0.00			0.00	6.00
Pure jadeitite	CV237K	Cpx	2781	VPSEM	PxNaCa	PxNaCa	63.97	1.99	0.00	0.65	0.06	0.05	0.01	0.23	0.31		0.69	0.00			0.00	6.00
Pure jadeitite	CV237K	Cpx	2784	VPSEM	PxNaCa	PxNaCa	72.42	2.00	0.00	0.73	0.00	0.09	0.00	0.21	0.25		0.72	0.00			0.00	6.00
Pure jadeitite	CV237K	Cpx	2785	VPSEM	PxNaCa	PxNaCa	62.83	1.98	0.01	0.65	0.10	0.04	0.00	0.21	0.29		0.72	0.00			0.00	6.00
Pure jadeitite	CV237K	Cpx	2787	VPSEM	PxNaCa	PxNaCa	61.62	1.99	0.00	0.63	0.05	0.10	0.00	0.27	0.30		0.66	0.00			0.00	6.00
Pure jadeitite	CV237K	Cpx	2788	VPSEM	PxNaCa	PxNaCa	64.38	1.97	0.00	0.69	0.11	0.00	0.00	0.23	0.28		0.73	0.00			0.00	6.00
Pure jadeitite	CV237K	Cpx	2789	VPSEM	PxNaCa	PxNaCa	48.94	1.96	0.01	0.53	0.12	0.02	0.00	0.35	0.43		0.59	0.00			0.00	6.00
Pure jadeitite	CV237K	Cpx	2790	VPSEM	PxNaCa	PxNaCa	66.00	1.97	0.00	0.69	0.09	0.00	0.00	0.22	0.29		0.76	0.00			0.00	6.00
Pure jadeitite	CV237K	Cpx	2791	VPSEM	PxNaCa	PxNaCa	62.20	1.95	0.01	0.66	0.13	0.00	0.00	0.21	0.30		0.75	0.00			0.00	6.00
Pure jadeitite	CV237K	Cpx	2793	VPSEM	PxNaCa	PxNaCa	67.31	1.98	0.00	0.70	0.12	0.00	0.00	0.18	0.25		0.78	0.00			0.00	6.00
Pure jadeitite	CV237K	Cpx	2794	VPSEM	PxNaCa	PxNaCa	74.56	1.99	0.00	0.76	0.04	0.05	0.00	0.20	0.18		0.78	0.00			0.00	6.00
Pure jadeitite	CV237K	Cpx	2816	VPSEM	PxNaCa	PxNaCa	43.82	1.96	0.00	0.47	0.11	0.00	0.00	0.44	0.49		0.54	0.00			0.00	6.00

Rock type	Sample	Phase	Point	serie	Px type	Px type	Jd mole%	Si	Ti	Al	Fe3+	Fe2+	Mn	Mg	Ca	Ba	Na	K	F	Cl	H	O
Pure jadeitite	CV237K	Cpx	2817	VPSEM	PxNaCa	PxNaCa	48.38	1.97	0.00	0.51	0.11	0.00	0.00	0.39	0.44		0.59	0.00			0.00	6.00
Pure jadeitite	CV237K	Cpx	2818	VPSEM	PxNaCa	PxNaCa	47.42	1.98	0.00	0.50	0.10	0.03	0.00	0.40	0.43		0.56	0.00			0.00	6.00
Pure jadeitite	CV237K	Cpx	2828	VPSEM	PxNaCa	PxNaCa	48.07	1.97	0.00	0.50	0.11	0.00	0.00	0.39	0.45		0.59	0.00			0.00	6.00
Pure jadeitite	CV237K	Cpx	2829	VPSEM	PxNaCa	PxNaCa	58.01	1.96	0.00	0.61	0.14	0.00	0.00	0.31	0.29		0.72	0.00			0.00	6.00
Pure jadeitite	CV237K	Cpx	2830	VPSEM	PxNaCa	PxNaCa	38.35	1.96	0.00	0.42	0.12	0.00	0.00	0.48	0.52		0.49	0.00			0.00	6.00
Pure jadeitite	CV237K	Cpx	2832	VPSEM	PxNaCa	PxNaCa	46.22	1.97	0.00	0.49	0.11	0.00	0.00	0.43	0.44		0.57	0.00			0.00	6.00
Pure jadeitite	CV237K	Cpx	2833	VPSEM	PxNaCa	PxNaCa	41.24	1.96	0.00	0.45	0.12	0.00	0.01	0.44	0.51		0.53	0.00			0.00	6.00
Pure jadeitite	CV237K	Cpx	2834	VPSEM	PxNaCa	PxNaCa	38.91	1.98	0.00	0.41	0.09	0.01	0.00	0.48	0.54		0.47	0.00			0.00	6.00
Pure jadeitite	CV237K	Cpx	2842	VPSEM	PxNaCa	PxNaCa	46.14	1.97	0.00	0.49	0.12	0.00	0.00	0.42	0.43		0.58	0.00			0.00	6.00
Pure jadeitite	CV237k	Cpx	245	EPMA	PxNa	PxNa	79.13	2.01	0.00	0.77	0.03	0.05	0.00	0.15	0.17		0.82	0.00	0.01	0.00	0.00	6.00
Pure jadeitite	CV237k	Cpx	246	EPMA	PxNa	PxNa	80.14	2.02	0.00	0.77	0.00	0.06	0.00	0.16	0.18		0.81	0.00	0.01	0.00	0.00	5.99
Pure jadeitite	CV237k	Cpx	247	EPMA	PxNa	PxNa	80.47	2.02	0.00	0.78	0.00	0.07	0.00	0.15	0.17		0.81	0.00	0.01	0.00	0.00	6.00
Pure jadeitite	CV237k	Cpx	248	EPMA	PxNa	PxNa	80.36	2.02	0.00	0.78	0.00	0.08	0.00	0.15	0.17		0.81	0.00	0.01	0.00	0.00	5.99
Pure jadeitite	CV237k	Cpx	249	EPMA	PxNa	PxNa	94.63	2.01	0.01	0.92	0.00	0.04	0.00	0.03	0.04		0.94	0.00	0.01	0.00	0.00	5.99
Pure jadeitite	CV237k	Cpx	250	EPMA	PxNa	PxNa	94.17	2.02	0.00	0.92	0.00	0.04	0.00	0.03	0.04		0.94	0.00	0.01	0.00	0.00	5.99
Pure jadeitite	CV237k	Cpx	251	EPMA	PxNa	PxNa	89.74	2.02	0.00	0.87	0.00	0.06	0.00	0.07	0.08		0.90	0.00	0.01	0.00	0.00	6.00
Pure jadeitite	CV237k	Cpx	252	EPMA	PxNa	PxNa	93.06	2.01	0.01	0.90	0.00	0.05	0.00	0.04	0.05		0.93	0.00	0.01	0.00	0.00	5.99
Pure jadeitite	CV237k	Cpx	253	EPMA	PxNa	PxNa	94.62	2.01	0.00	0.92	0.00	0.05	0.00	0.03	0.04		0.95	0.00	0.01	0.00	0.00	5.99
Pure jadeitite	CV237k	Cpx	254	EPMA	PxNa	PxNa	91.43	2.02	0.00	0.89	0.00	0.04	0.00	0.06	0.07		0.91	0.00	0.01	0.00	0.00	5.99
Pure jadeitite	CV237k	Cpx	255	EPMA	PxNa	PxNa	92.14	2.02	0.00	0.90	0.00	0.04	0.00	0.05	0.06		0.93	0.00	0.01	0.00	0.00	5.99
Pure jadeitite	CV237k	Cpx	257	EPMA	PxNa	PxNa	91.42	2.02	0.00	0.89	0.00	0.05	0.00	0.06	0.07		0.92	0.00	0.01	0.00	0.00	6.00
Pure jadeitite	CV237k	Cpx	258	EPMA	PxNa	PxNa	85.09	2.01	0.00	0.83	0.03	0.04	0.00	0.10	0.10		0.89	0.00	0.01	0.00	0.00	5.99
Pure jadeitite	CV237k	Cpx	259	EPMA	PxNa	PxNa	90.71	2.02	0.01	0.87	0.00	0.05	0.00	0.06	0.07		0.91	0.00	0.01	0.00	0.00	5.99
Pure jadeitite	CV237k	Cpx	260	EPMA	PxNa	PxNa	95.15	2.01	0.01	0.93	0.00	0.04	0.00	0.03	0.03		0.95	0.00	0.01	0.00	0.00	5.99
Pure jadeitite	CV237k	Cpx	261	EPMA	PxNa	PxNa	84.96	2.01	0.00	0.83	0.02	0.04	0.00	0.10	0.11		0.88	0.00	0.01	0.00	0.00	6.00
Pure jadeitite	CV237k	Cpx	262	EPMA	PxNa	PxNa	88.31	2.01	0.00	0.87	0.02	0.03	0.00	0.07	0.09		0.91	0.00	0.01	0.00	0.00	6.00
Pure jadeitite	CV237k	Cpx	264	EPMA	PxNa	PxNa	79.64	2.01	0.00	0.78	0.02	0.05	0.00	0.14	0.17		0.82	0.00	0.01	0.00	0.00	5.99
Pure jadeitite	CV237k	Cpx	265	EPMA	PxNa	PxNa	92.10	2.01	0.00	0.90	0.01	0.03	0.00	0.05	0.06		0.94	0.00	0.01	0.00	0.00	5.99
Pure jadeitite	CV237k	Cpx	266	EPMA	PxNa	PxNa	92.33	2.02	0.00	0.90	0.00	0.04	0.00	0.05	0.06		0.92	0.00	0.01	0.00	0.00	6.00
Pure jadeitite	CV237k	Cpx	267	EPMA	PxNa	PxNa	88.94	2.02	0.00	0.86	0.00	0.06	0.00	0.08	0.09		0.90	0.00	0.01	0.00	0.00	6.00
Pure jadeitite	CV237k	Cpx	268	EPMA	PxNa	PxNa	95.07	2.01	0.00	0.93	0.00	0.04	0.00	0.03	0.03		0.95	0.00	0.01	0.00	0.00	5.99
Pure jadeitite	CV237k	Cpx	269	EPMA	PxNa	PxNa	94.95	2.02	0.00	0.93	0.00	0.04	0.00	0.03	0.03		0.93	0.00	0.01	0.00	0.00	6.00
Pure jadeitite	CV237k	Cpx	283	EPMA	PxNa	PxNa	86.30	2.01	0.00	0.85	0.04	0.02	0.00	0.09	0.09		0.90	0.00	0.01	0.00	0.00	5.99
Pure jadeitite	CV237k	Cpx	284	EPMA	PxNa	PxNa	86.73	2.01	0.00	0.85	0.03	0.02	0.00	0.09	0.09		0.90	0.00	0.01	0.00	0.00	5.99
Pure jadeitite	CV237k	Cpx	289	EPMA	PxNa	PxNa	81.60	2.00	0.01	0.80	0.03	0.04	0.00	0.12	0.15		0.85	0.00	0.01	0.00	0.00	5.99
Pure jadeitite	CV237k	Cpx	290	EPMA	PxNa	PxNa	85.59	2.01	0.01	0.83	0.00	0.06	0.00	0.10	0.12		0.87	0.00	0.01	0.00	0.00	5.99
Pure jadeitite	CV237k	Cpx	291	EPMA	PxNa	PxNa	85.12	2.01	0.00	0.83	0.03	0.04	0.00	0.10	0.10		0.88	0.00	0.01	0.00	0.00	5.99
Pure jadeitite	CV237k	Cpx	292	EPMA	PxNa	PxNa	85.97	2.02	0.00	0.83	0.02	0.05	0.00	0.10	0.10		0.88	0.00	0.01	0.00	0.00	5.99
Pure jadeitite	CV237k	Cpx	293	EPMA	PxNa	PxNa	85.22	2.02	0.00	0.82	0.00	0.07	0.00	0.11	0.12		0.86	0.00	0.01	0.00	0.00	5.99
Pure jadeitite	CV237k	Cpx	294	EPMA	PxNa	PxNa	84.91	2.02	0.00	0.82	0.00	0.07	0.00	0.11	0.12		0.84	0.00	0.01	0.00	0.00	5.99
Pure jadeitite	CV237k	Cpx	295	EPMA	PxNa	PxNa	92.81	2.02	0.00	0.90	0.00	0.05	0.00	0.04	0.05		0.93	0.00	0.02	0.00	0.00	5.99
Pure jadeitite	CV237k	Cpx	296	EPMA	PxNa	PxNa	92.89	2.02	0.00	0.90	0.00	0.05	0.00	0.04	0.05		0.93	0.00	0.01	0.00	0.00	6.00
Pure jadeitite	CV237k	Cpx	297	EPMA	PxNa	PxNa	86.97	2.01	0.00	0.85	0.01	0.05	0.00	0.09	0.10		0.89	0.00	0.01	0.00	0.00	5.99
Pure jadeitite	CV237k	Cpx	298	EPMA	PxNa	PxNa	87.74	2.02	0.00	0.85	0.00	0.06	0.00	0.09	0.10		0.88	0.00	0.01	0.00	0.00	5.99

Rock type	Sample	Phase	Point	serie	Px type	Px type	Jd mole%	Si	Ti	Al	Fe3+	Fe2+	Mn	Mg	Ca	Ba	Na	K	F	Cl	H	O
Pure jadeitite	CV237k	Cpx	299	EPMA	PxNa	PxNa	90.40	2.02	0.00	0.87	0.00	0.05	0.00	0.07	0.08		0.91	0.00	0.01	0.00	0.00	6.00
Pure jadeitite	CV237k	Cpx	300	EPMA	PxNa	PxNa	90.46	2.02	0.00	0.88	0.00	0.05	0.00	0.07	0.08		0.91	0.00	0.01	0.00	0.00	5.99
Pure jadeitite	CV237k	Cpx	301	EPMA	PxNa	PxNa	83.25	2.02	0.00	0.81	0.01	0.06	0.00	0.12	0.14		0.85	0.00	0.01	0.00	0.00	5.99
Pure jadeitite	CV237k	Cpx	302	EPMA	PxNa	PxNa	79.19	2.01	0.00	0.77	0.03	0.05	0.00	0.15	0.17		0.82	0.00	0.01	0.00	0.00	6.00
Pure jadeitite	CV237k	Cpx	303	EPMA	PxNa	PxNa	82.65	2.01	0.00	0.81	0.03	0.03	0.00	0.12	0.14		0.86	0.00	0.01	0.00	0.00	5.99
Pure jadeitite	CV237k	Cpx	304	EPMA	PxNa	PxNa	82.86	2.02	0.00	0.80	0.01	0.05	0.00	0.12	0.14		0.84	0.00	0.01	0.00	0.00	5.99
Pure jadeitite	CV237k	Cpx	305	EPMA	PxNa	PxNa	81.66	2.01	0.00	0.80	0.02	0.05	0.00	0.13	0.15		0.84	0.00	0.01	0.00	0.00	5.99
Pure jadeitite	CV237k	Cpx	306	EPMA	PxNa	PxNa	82.06	2.01	0.00	0.79	0.01	0.06	0.00	0.13	0.15		0.84	0.00	0.01	0.00	0.00	5.99
Pure jadeitite	CV237k	Cpx	307	EPMA	PxNa	PxNa	82.35	2.02	0.00	0.80	0.00	0.07	0.00	0.13	0.16		0.82	0.00	0.01	0.00	0.00	5.99
Pure jadeitite	CV237k	Cpx	308	EPMA	PxNa	PxNa	88.26	2.01	0.01	0.86	0.02	0.04	0.00	0.07	0.08		0.91	0.00	0.01	0.00	0.00	5.99
Pure jadeitite	CV237k	Cpx	309	EPMA	PxNa	PxNa	89.46	2.02	0.01	0.86	0.00	0.06	0.00	0.07	0.08		0.90	0.00	0.01	0.00	0.00	5.99
Pure jadeitite	CV237k	Cpx	310	EPMA	PxNa	PxNa	80.73	2.01	0.01	0.78	0.01	0.06	0.00	0.13	0.17		0.82	0.00	0.01	0.00	0.00	5.99
Pure jadeitite	CV237k	Cpx	311	EPMA	PxNa	PxNa	81.37	2.01	0.01	0.78	0.00	0.07	0.00	0.14	0.17		0.82	0.00	0.01	0.00	0.00	5.99
Pure jadeitite	CV237k	Cpx	312	EPMA	PxNa	PxNa	91.00	2.01	0.01	0.88	0.00	0.05	0.00	0.06	0.07		0.91	0.00	0.05	0.00	0.00	5.97
Pure jadeitite	CV237k	Cpx	313	EPMA	PxNa	PxNa	85.28	2.01	0.00	0.83	0.02	0.04	0.00	0.10	0.11		0.87	0.00	0.01	0.00	0.00	5.99
Pure jadeitite	CV237k	Cpx	314	EPMA	PxNa	PxNa	86.08	2.02	0.00	0.83	0.00	0.06	0.00	0.10	0.11		0.87	0.00	0.01	0.00	0.00	5.99
Pure jadeitite	CV237k	Cpx	315	EPMA	PxNa	PxNa	92.24	2.01	0.01	0.90	0.00	0.05	0.00	0.05	0.06		0.92	0.00	0.01	0.00	0.00	5.99
Pure jadeitite	CV237k	Cpx	316	EPMA	PxNa	PxNa	91.81	2.01	0.01	0.90	0.01	0.04	0.00	0.05	0.06		0.93	0.00	0.02	0.00	0.00	5.99
Pure jadeitite	CV237k	Cpx	317	EPMA	PxNa	PxNa	77.27	2.00	0.00	0.76	0.05	0.03	0.00	0.15	0.17		0.82	0.00	0.01	0.00	0.00	5.99
Pure jadeitite	CV237k	Cpx	318	EPMA	PxNa	PxNa	78.81	2.01	0.00	0.77	0.02	0.06	0.00	0.15	0.17		0.81	0.00	0.02	0.00	0.00	5.99
Pure jadeitite	CV237k	Cpx	319	EPMA	PxNa	PxNa	79.21	2.01	0.00	0.77	0.03	0.04	0.00	0.15	0.17		0.83	0.00	0.01	0.00	0.00	5.99
Pure jadeitite	CV237k	Cpx	320	EPMA	PxNa	PxNa	80.10	2.01	0.00	0.78	0.01	0.06	0.00	0.15	0.17		0.82	0.00	0.01	0.00	0.00	5.99
Pure jadeitite	CV237k	Cpx	321	EPMA	PxNa	PxNa	80.70	2.02	0.00	0.77	0.00	0.07	0.00	0.15	0.17		0.82	0.00	0.01	0.00	0.00	5.99
Pure jadeitite	CV237k	Cpx	326	EPMA	PxNa	PxNa	81.71	2.02	0.00	0.80	0.00	0.07	0.00	0.13	0.16		0.81	0.00	0.01	0.00	0.00	5.99
Pure jadeitite	CV237k	Cpx	332	EPMA	PxNa	PxNa	87.34	2.02	0.00	0.85	0.00	0.05	0.00	0.09	0.10		0.88	0.00	0.02	0.00	0.00	5.99
Pure jadeitite	CV237k	Cpx	333	EPMA	PxNa	PxNa	87.02	2.01	0.00	0.85	0.01	0.05	0.00	0.09	0.11		0.88	0.00	0.01	0.00	0.00	5.99
Pure jadeitite	CV237k	Cpx	334	EPMA	PxNa	PxNa	88.96	2.00	0.01	0.88	0.00	0.06	0.00	0.06	0.10		0.89	0.00	0.02	0.00	0.00	5.99
Pure jadeitite	CV237k	Cpx	338	EPMA	PxNa	PxNa	81.69	2.02	0.00	0.79	0.01	0.06	0.00	0.14	0.15		0.83	0.00	0.01	0.00	0.00	5.99
Pure jadeitite	CV237k	Cpx	339	EPMA	PxNa	PxNa	86.28	2.02	0.00	0.83	0.00	0.07	0.00	0.10	0.11		0.87	0.00	0.01	0.00	0.00	6.00
Pure jadeitite	CV237k	Cpx	342	EPMA	PxNa	PxNa	88.93	2.01	0.00	0.87	0.00	0.06	0.00	0.07	0.08		0.89	0.00	0.01	0.00	0.00	5.99
Pure jadeitite	CV237K	Cpx	2666	VPSEM	PxNa	PxNa	88.38	1.99	0.00	0.90	0.04	0.00	0.00	0.07	0.07		0.92	0.00			0.00	6.00
Pure jadeitite	CV237K	Cpx	2667	VPSEM	PxNa	PxNa	84.56	1.97	0.00	0.87	0.06	0.00	0.00	0.08	0.10		0.92	0.00			0.00	6.00
Pure jadeitite	CV237K	Cpx	2668	VPSEM	PxNa	PxNa	86.27	1.98	0.00	0.89	0.05	0.00	0.00	0.07	0.09		0.91	0.00			0.00	6.00
Pure jadeitite	CV237K	Cpx	2669	VPSEM	PxNa	PxNa	84.40	1.98	0.00	0.88	0.06	0.00	0.00	0.09	0.10		0.89	0.00			0.00	6.00
Pure jadeitite	CV237K	Cpx	2670	VPSEM	PxNa	PxNa	81.98	1.97	0.00	0.84	0.08	0.00	0.00	0.10	0.11		0.92	0.00			0.00	6.00
Pure jadeitite	CV237K	Cpx	2676	VPSEM	PxNa	PxNa	72.71	1.98	0.00	0.76	0.11	0.00	0.00	0.14	0.19		0.83	0.00			0.00	6.00
Pure jadeitite	CV237K	Cpx	2677	VPSEM	PxNa	PxNa	87.74	1.97	0.01	0.90	0.05	0.00	0.00	0.06	0.08		0.94	0.00			0.00	6.00
Pure jadeitite	CV237K	Cpx	2682	VPSEM	PxNa	PxNa	88.22	1.97	0.00	0.92	0.05	0.00	0.00	0.06	0.07		0.94	0.00			0.00	6.00
Pure jadeitite	CV237K	Cpx	2683	VPSEM	PxNa	PxNa	79.50	1.98	0.00	0.82	0.08	0.00	0.00	0.13	0.14		0.87	0.00			0.00	6.00
Pure jadeitite	CV237K	Cpx	2684	VPSEM	PxNa	PxNa	77.40	1.98	0.00	0.80	0.07	0.00	0.00	0.15	0.17		0.84	0.00			0.00	6.00
Pure jadeitite	CV237K	Cpx	2687	VPSEM	PxNa	PxNa	91.31	1.97	0.00	0.95	0.04	0.00	0.00	0.05	0.05		0.96	0.00			0.00	6.00
Pure jadeitite	CV237K	Cpx	2689	VPSEM	PxNa	PxNa	87.51	1.97	0.00	0.90	0.04	0.00	0.00	0.08	0.08		0.93	0.00			0.00	6.00
Pure jadeitite	CV237K	Cpx	2691	VPSEM	PxNa	PxNa	86.88	1.98	0.00	0.89	0.05	0.00	0.00	0.07	0.09		0.93	0.00			0.00	6.00
Pure jadeitite	CV237K	Cpx	2697	VPSEM	PxNa	PxNa	92.41	1.98	0.00	0.95	0.04	0.00	0.00	0.03	0.05		0.96	0.00			0.00	6.00

Rock type	Sample	Phase	Point	serie	Px type	Px type	Jd mole%	Si	Ti	Al	Fe3+	Fe2+	Mn	Mg	Ca	Ba	Na	K	F	Cl	H	O
Pure jadeitite	CV237K	Cpx	2698	VPSEM	PxNa	PxNa	85.94	1.97	0.00	0.89	0.07	0.00	0.00	0.07	0.08		0.94	0.00			0.00	6.00
Pure jadeitite	CV237K	Cpx	2699	VPSEM	PxNa	PxNa	86.34	1.98	0.01	0.87	0.04	0.02	0.00	0.08	0.10		0.90	0.00			0.00	6.00
Pure jadeitite	CV237K	Cpx	2703	VPSEM	PxNa	PxNa	80.14	1.98	0.00	0.83	0.07	0.00	0.00	0.11	0.14		0.88	0.00			0.00	6.00
Pure jadeitite	CV237K	Cpx	2705	VPSEM	PxNa	PxNa	72.88	1.96	0.01	0.76	0.08	0.00	0.00	0.16	0.23		0.82	0.00			0.00	6.00
Pure jadeitite	CV237K	Cpx	2711	VPSEM	PxNa	PxNa	84.02	1.98	0.00	0.86	0.06	0.00	0.00	0.09	0.12		0.90	0.00			0.00	6.00
Pure jadeitite	CV237K	Cpx	2714	VPSEM	PxNa	PxNa	76.35	1.96	0.00	0.80	0.10	0.00	0.00	0.12	0.16		0.89	0.00			0.00	6.00
Pure jadeitite	CV237K	Cpx	2718	VPSEM	PxNa	PxNa	73.56	1.98	0.00	0.76	0.13	0.00	0.00	0.12	0.16		0.86	0.00			0.00	6.00
Pure jadeitite	CV237K	Cpx	2729	VPSEM	PxNa	PxNa	80.54	1.98	0.00	0.83	0.05	0.02	0.00	0.12	0.15		0.85	0.00			0.00	6.00
Pure jadeitite	CV237K	Cpx	2732	VPSEM	PxNa	PxNa	80.08	1.97	0.00	0.83	0.07	0.00	0.00	0.12	0.15		0.89	0.00			0.00	6.00
Pure jadeitite	CV237K	Cpx	2733	VPSEM	PxNa	PxNa	79.79	1.98	0.00	0.83	0.11	0.00	0.00	0.07	0.11		0.90	0.00			0.00	6.00
Pure jadeitite	CV237K	Cpx	2736	VPSEM	PxNa	PxNa	84.19	1.96	0.01	0.87	0.07	0.00	0.00	0.08	0.11		0.93	0.00			0.00	6.00
Pure jadeitite	CV237K	Cpx	2739	VPSEM	PxNa	PxNa	75.44	1.97	0.01	0.77	0.07	0.00	0.00	0.16	0.20		0.83	0.00			0.00	6.00
Pure jadeitite	CV237K	Cpx	2744	VPSEM	PxNa	PxNa	81.53	1.97	0.00	0.85	0.06	0.00	0.00	0.11	0.14		0.87	0.00			0.00	6.00
Pure jadeitite	CV237K	Cpx	2746	VPSEM	PxNa	PxNa	78.75	1.97	0.00	0.82	0.08	0.00	0.00	0.13	0.15		0.86	0.00			0.00	6.00
Pure jadeitite	CV237K	Cpx	2749	VPSEM	PxNa	PxNa	83.70	1.98	0.00	0.87	0.05	0.00	0.00	0.10	0.12		0.89	0.00			0.00	6.00
Pure jadeitite	CV237K	Cpx	2751	VPSEM	PxNa	PxNa	71.39	1.97	0.01	0.74	0.09	0.00	0.00	0.18	0.22		0.80	0.00			0.00	6.00
Pure jadeitite	CV237K	Cpx	2754	VPSEM	PxNa	PxNa	84.00	1.98	0.01	0.85	0.02	0.04	0.00	0.11	0.13		0.86	0.00			0.00	6.00
Pure jadeitite	CV237K	Cpx	2756	VPSEM	PxNa	PxNa	81.55	1.98	0.01	0.84	0.07	0.00	0.00	0.10	0.13		0.88	0.00			0.00	6.00
Pure jadeitite	CV237K	Cpx	2758	VPSEM	PxNa	PxNa	82.16	1.98	0.00	0.86	0.06	0.00	0.00	0.11	0.13		0.86	0.00			0.00	6.00
Pure jadeitite	CV237K	Cpx	2763	VPSEM	PxNa	PxNa	72.28	1.97	0.00	0.76	0.08	0.00	0.00	0.18	0.22		0.80	0.00			0.00	6.00
Pure jadeitite	CV237K	Cpx	2775	VPSEM	PxNa	PxNa	70.41	1.98	0.00	0.74	0.10	0.01	0.00	0.17	0.21		0.79	0.00			0.00	6.00
Pure jadeitite	CV237K	Cpx	2783	VPSEM	PxNa	PxNa	71.40	1.96	0.00	0.74	0.09	0.00	0.00	0.16	0.26		0.84	0.00			0.00	6.00
Pure jadeitite	CV237K	Cpx	2795	VPSEM	PxNa	PxNa	89.65	1.97	0.00	0.92	0.04	0.00	0.00	0.07	0.07		0.96	0.00			0.00	6.00
Pure jadeitite	CV237K	Cpx	2796	VPSEM	PxNa	PxNa	81.08	1.98	0.00	0.82	0.07	0.00	0.01	0.12	0.13		0.89	0.00			0.00	6.00
Pure jadeitite	CV237K	Cpx	2797	VPSEM	PxNa	PxNa	82.80	1.98	0.00	0.85	0.07	0.00	0.00	0.11	0.11		0.90	0.00			0.00	6.00
Pure jadeitite	CV237K	Cpx	2798	VPSEM	PxNa	PxNa	89.20	1.97	0.00	0.92	0.04	0.00	0.00	0.06	0.07		0.95	0.00			0.00	6.00
Pure jadeitite	CV237K	Cpx	2799	VPSEM	PxNa	PxNa	84.57	1.99	0.00	0.86	0.06	0.01	0.00	0.09	0.10		0.90	0.00			0.00	6.00
Pure jadeitite	CV237K	Cpx	2800	VPSEM	PxNa	PxNa	89.50	1.97	0.00	0.93	0.05	0.00	0.00	0.04	0.06		0.94	0.00			0.00	6.00
Pure jadeitite	CV237K	Cpx	2801	VPSEM	PxNa	PxNa	85.77	1.98	0.00	0.88	0.06	0.00	0.00	0.08	0.09		0.91	0.00			0.00	6.00
Pure jadeitite	CV237K	Cpx	2802	VPSEM	PxNa	PxNa	80.34	1.97	0.00	0.84	0.07	0.00	0.00	0.13	0.14		0.86	0.00			0.00	6.00
Pure jadeitite	CV237K	Cpx	2803	VPSEM	PxNa	PxNa	84.40	1.98	0.00	0.86	0.06	0.00	0.00	0.09	0.10		0.91	0.00			0.00	6.00
Pure jadeitite	CV237K	Cpx	2804	VPSEM	PxNa	PxNa	86.04	1.98	0.00	0.88	0.05	0.00	0.00	0.08	0.09		0.93	0.00			0.00	6.00
Pure jadeitite	CV237K	Cpx	2810	VPSEM	PxNa	PxNa	84.88	1.96	0.00	0.88	0.06	0.00	0.00	0.08	0.11		0.94	0.00			0.00	6.00
Pure jadeitite	CV237K	Cpx	2811	VPSEM	PxNa	PxNa	84.55	1.97	0.00	0.88	0.06	0.00	0.00	0.10	0.10		0.90	0.00			0.00	6.00
Pure jadeitite	CV237K	Cpx	2813	VPSEM	PxNa	PxNa	88.92	1.98	0.00	0.90	0.05	0.00	0.00	0.06	0.08		0.95	0.00			0.00	6.00
Pure jadeitite	CV237K	Cpx	2814	VPSEM	PxNa	PxNa	80.44	1.98	0.00	0.83	0.07	0.00	0.00	0.12	0.13		0.89	0.00			0.00	6.00
Pure jadeitite	CV237K	Cpx	2815	VPSEM	PxNa	PxNa	94.49	1.97	0.00	0.97	0.03	0.00	0.00	0.02	0.03		1.00	0.01			0.00	6.00
Pure jadeitite	CV237K	Cpx	2819	VPSEM	PxNa	PxNa	87.67	1.99	0.00	0.90	0.02	0.03	0.00	0.08	0.09		0.89	0.00			0.00	6.00
Pure jadeitite	CV237K	Cpx	2820	VPSEM	PxNa	PxNa	92.91	1.96	0.00	0.98	0.04	0.00	0.00	0.03	0.03		0.98	0.00			0.00	6.00
Pure jadeitite	CV237K	Cpx	2821	VPSEM	PxNa	PxNa	95.57	1.98	0.00	0.99	0.00	0.04	0.00	0.03	0.02		0.94	0.00			0.00	6.00
Pure jadeitite	CV237K	Cpx	2824	VPSEM	PxNa	PxNa	83.28	1.99	0.00	0.85	0.06	0.01	0.00	0.10	0.10		0.89	0.00			0.00	6.00
Pure jadeitite	CV237K	Cpx	2825	VPSEM	PxNa	PxNa	93.32	1.98	0.00	0.96	0.04	0.00	0.00	0.03	0.04		0.98	0.00			0.00	6.00
Pure jadeitite	CV237K	Cpx	2826	VPSEM	PxNa	PxNa	89.67	1.97	0.00	0.93	0.04	0.00	0.00	0.07	0.06		0.95	0.00			0.00	6.00
Pure jadeitite	CV237K	Cpx	2827	VPSEM	PxNa	PxNa	81.38	1.99	0.00	0.82	0.06	0.00	0.00	0.12	0.13		0.88	0.00			0.00	6.00

Rock type	Sample	Phase	Point	serie	Px type	Px type	Jd mole%	Si	Ti	Al	Fe3+	Fe2+	Mn	Mg	Ca	Ba	Na	K	F	Cl	H	O
Pure jadeitite	CV237K	Cpx	2837	VPSEM	PxNa	PxNa	93.73	2.00	0.01	0.95	0.00	0.03	0.00	0.04	0.05		0.89	0.00			0.00	6.00
Pure jadeitite	CV237K	Cpx	2838	VPSEM	PxNa	PxNa	85.39	1.98	0.01	0.87	0.05	0.01	0.00	0.08	0.10		0.90	0.00			0.00	6.00
Pure jadeitite	CV237K	Cpx	2839	VPSEM	PxNa	PxNa	86.93	1.97	0.00	0.89	0.05	0.00	0.00	0.08	0.09		0.95	0.00			0.00	6.00
Pure jadeitite	CV237K	Cpx	2841	VPSEM	PxNa	PxNa	92.44	1.99	0.00	0.94	0.04	0.00	0.00	0.03	0.04		0.97	0.00			0.00	6.00
Pure jadeitite	CV237K	Cpx	2844	VPSEM	PxNa	PxNa	82.87	1.99	0.00	0.84	0.07	0.00	0.00	0.09	0.11		0.90	0.00			0.00	6.00
Pure jadeitite	CV237K	Cpx	2845	VPSEM	PxNa	PxNa	89.13	1.99	0.00	0.91	0.05	0.00	0.00	0.05	0.06		0.95	0.00			0.00	6.00
Pure jadeitite	CV237K	Cpx	2847	VPSEM	PxNa	PxNa	93.68	1.96	0.00	0.96	0.03	0.00	0.00	0.04	0.03		1.01	0.01			0.00	6.00
Pure jadeitite	CV237t	Cpx	101	EPMA	PxNaCa	PxNaCa	38.16	1.98	0.00	0.41	0.09	0.13	0.01	0.38	0.55		0.46	0.00	0.01	0.00	0.00	5.99
Pure jadeitite	CV237t	Cpx	108	EPMA	PxNaCa	PxNaCa	79.99	2.01	0.00	0.78	0.00	0.11	0.00	0.12	0.17		0.80	0.00	0.01	0.00	0.00	6.00
Pure jadeitite	CV237t	Cpx	109	EPMA	PxNaCa	PxNaCa	78.72	2.00	0.00	0.78	0.01	0.10	0.00	0.12	0.18		0.80	0.00	0.01	0.00	0.00	5.99
Pure jadeitite	CV237t	Cpx	110	EPMA	PxNaCa	PxNaCa	48.33	1.98	0.03	0.47	0.03	0.18	0.01	0.29	0.51		0.51	0.01	0.02	0.01	0.00	5.99
Pure jadeitite	CV237t	Cpx	2879	VPSEM	PxNaCa	PxNaCa	45.13	1.97	0.00	0.49	0.15	0.04	0.00	0.34	0.43		0.59	0.00			0.00	6.00
Pure jadeitite	CV237t	Cpx	2881	VPSEM	PxNaCa	PxNaCa	51.64	1.98	0.00	0.54	0.18	0.04	0.00	0.28	0.31		0.68	0.00			0.00	6.00
Pure jadeitite	CV237t	Cpx	2893	VPSEM	PxNaCa	PxNaCa	39.65	1.96	0.00	0.44	0.11	0.07	0.01	0.38	0.53		0.49	0.00			0.00	6.00
Pure jadeitite	CV237t	Cpx	2966	VPSEM	PxNaCa	PxNaCa	39.91	1.97	0.00	0.42	0.23	0.00	0.01	0.35	0.43		0.62	0.00			0.00	6.00
Pure jadeitite	CV237t	Cpx	77	EPMA	PxNa	PxNa	82.47	2.00	0.00	0.82	0.02	0.04	0.00	0.11	0.16		0.85	0.00	0.01	0.00	0.00	6.00
Pure jadeitite	CV237t	Cpx	78	EPMA	PxNa	PxNa	89.33	2.00	0.00	0.89	0.00	0.05	0.00	0.08	0.09		0.88	0.00	0.01	0.00	0.00	6.00
Pure jadeitite	CV237t	Cpx	79	EPMA	PxNa	PxNa	89.79	2.01	0.00	0.88	0.00	0.06	0.00	0.06	0.08		0.89	0.00	0.00	0.00	0.00	6.00
Pure jadeitite	CV237t	Cpx	80	EPMA	PxNa	PxNa	89.80	2.01	0.00	0.89	0.00	0.05	0.00	0.07	0.08		0.88	0.00	0.00	0.00	0.00	6.00
Pure jadeitite	CV237t	Cpx	81	EPMA	PxNa	PxNa	89.75	2.01	0.00	0.89	0.00	0.05	0.00	0.07	0.08		0.89	0.00	0.00	0.00	0.00	6.00
Pure jadeitite	CV237t	Cpx	82	EPMA	PxNa	PxNa	87.55	2.01	0.00	0.86	0.00	0.06	0.00	0.08	0.10		0.86	0.00	0.01	0.00	0.00	6.00
Pure jadeitite	CV237t	Cpx	83	EPMA	PxNa	PxNa	91.26	2.00	0.00	0.91	0.00	0.05	0.00	0.05	0.07		0.89	0.00	0.00	0.00	0.00	6.00
Pure jadeitite	CV237t	Cpx	84	EPMA	PxNa	PxNa	93.12	2.02	0.00	0.92	0.00	0.04	0.00	0.04	0.05		0.91	0.00	0.00	0.00	0.00	6.00
Pure jadeitite	CV237t	Cpx	85	EPMA	PxNa	PxNa	88.65	2.01	0.00	0.88	0.00	0.05	0.00	0.08	0.10		0.88	0.00	0.01	0.00	0.00	5.99
Pure jadeitite	CV237t	Cpx	86	EPMA	PxNa	PxNa	88.85	2.01	0.00	0.88	0.00	0.05	0.00	0.07	0.09		0.87	0.00	0.01	0.00	0.00	6.00
Pure jadeitite	CV237t	Cpx	87	EPMA	PxNa	PxNa	89.63	2.01	0.00	0.89	0.00	0.05	0.00	0.07	0.08		0.89	0.00	0.00	0.00	0.00	6.00
Pure jadeitite	CV237t	Cpx	88	EPMA	PxNa	PxNa	89.27	2.01	0.00	0.88	0.00	0.05	0.00	0.08	0.09		0.88	0.00	0.00	0.00	0.00	6.00
Pure jadeitite	CV237t	Cpx	89	EPMA	PxNa	PxNa	89.18	2.01	0.00	0.88	0.00	0.05	0.00	0.07	0.09		0.88	0.00	0.01	0.00	0.00	6.00
Pure jadeitite	CV237t	Cpx	90	EPMA	PxNa	PxNa	88.38	2.01	0.00	0.87	0.00	0.05	0.00	0.08	0.10		0.87	0.00	0.01	0.00	0.00	6.00
Pure jadeitite	CV237t	Cpx	91	EPMA	PxNa	PxNa	87.81	2.01	0.00	0.86	0.00	0.06	0.00	0.08	0.10		0.88	0.00	0.00	0.01	0.00	5.99
Pure jadeitite	CV237t	Cpx	92	EPMA	PxNa	PxNa	87.68	2.01	0.00	0.87	0.00	0.06	0.00	0.09	0.10		0.87	0.00	0.00	0.00	0.00	6.00
Pure jadeitite	CV237t	Cpx	93	EPMA	PxNa	PxNa	88.31	2.01	0.00	0.87	0.00	0.06	0.00	0.08	0.09		0.88	0.00	0.00	0.00	0.00	6.00
Pure jadeitite	CV237t	Cpx	95	EPMA	PxNa	PxNa	87.53	2.01	0.00	0.86	0.00	0.06	0.00	0.09	0.10		0.86	0.00	0.01	0.00	0.00	6.00
Pure jadeitite	CV237t	Cpx	96	EPMA	PxNa	PxNa	91.22	2.01	0.00	0.90	0.00	0.04	0.00	0.06	0.07		0.90	0.00	0.00	0.00	0.00	6.00
Pure jadeitite	CV237t	Cpx	102	EPMA	PxNa	PxNa	87.41	1.97	0.00	0.90	0.04	0.00	0.00	0.08	0.09		0.95	0.00	0.01	0.00	0.00	5.99
Pure jadeitite	CV237t	Cpx	111	EPMA	PxNa	PxNa	81.24	2.00	0.00	0.81	0.00	0.07	0.00	0.14	0.17		0.81	0.00	0.01	0.00	0.00	6.00
Pure jadeitite	CV237t	Cpx	112	EPMA	PxNa	PxNa	86.10	2.01	0.00	0.85	0.00	0.08	0.00	0.09	0.11		0.86	0.00	0.01	0.00	0.00	6.00
Pure jadeitite	CV237t	Cpx	114	EPMA	PxNa	PxNa	91.20	2.01	0.01	0.90	0.00	0.05	0.00	0.05	0.07		0.89	0.00	0.00	0.00	0.00	6.00
Pure jadeitite	CV237t	Cpx	117	EPMA	PxNa	PxNa	96.64	2.02	0.00	0.95	0.00	0.03	0.00	0.02	0.02		0.96	0.00	0.00	0.00	0.00	6.00
Pure jadeitite	CV237t	Cpx	119	EPMA	PxNa	PxNa	87.04	2.01	0.00	0.85	0.00	0.05	0.00	0.09	0.11		0.86	0.00	0.00	0.00	0.00	6.00
Pure jadeitite	CV237t	Cpx	120	EPMA	PxNa	PxNa	83.17	2.01	0.00	0.82	0.00	0.07	0.00	0.12	0.15		0.83	0.00	0.00	0.00	0.00	6.00
Pure jadeitite	CV237t	Cpx	121	EPMA	PxNa	PxNa	85.87	2.01	0.00	0.84	0.00	0.07	0.00	0.09	0.12		0.85	0.00	0.00	0.00	0.00	6.00
Pure jadeitite	CV237t	Cpx	123	EPMA	PxNa	PxNa	84.76	2.01	0.00	0.84	0.00	0.06	0.00	0.11	0.13		0.83	0.00	0.00	0.00	0.00	6.00
Pure jadeitite	CV237t	Cpx	124	EPMA	PxNa	PxNa	87.65	2.01	0.00	0.86	0.00	0.06	0.00	0.08	0.10		0.87	0.00	0.00	0.00	0.00	6.00

Rock type	Sample	Phase	Point	serie	Px type	Px type	Jd mole%	Si	Ti	Al	Fe3+	Fe2+	Mn	Mg	Ca	Ba	Na	K	F	Cl	H	O
Pure jadeitite	CV237t	Cpx	2855	VPSEM	PxNa	PxNa	81.92	1.97	0.00	0.85	0.06	0.00	0.00	0.11	0.13		0.89	0.00			0.00	6.00
Pure jadeitite	CV237t	Cpx	2860	VPSEM	PxNa	PxNa	80.47	1.99	0.00	0.83	0.06	0.00	0.00	0.12	0.15		0.86	0.00			0.00	6.00
Pure jadeitite	CV237t	Cpx	2862	VPSEM	PxNa	PxNa	87.64	1.99	0.00	0.90	0.05	0.00	0.00	0.07	0.08		0.92	0.00			0.00	6.00
Pure jadeitite	CV237t	Cpx	2864	VPSEM	PxNa	PxNa	75.20	1.97	0.00	0.78	0.10	0.00	0.00	0.13	0.18		0.85	0.00			0.00	6.00
Pure jadeitite	CV237t	Cpx	2865	VPSEM	PxNa	PxNa	84.63	1.98	0.01	0.87	0.06	0.00	0.00	0.09	0.11		0.91	0.00			0.00	6.00
Pure jadeitite	CV237t	Cpx	2870	VPSEM	PxNa	PxNa	79.25	1.98	0.00	0.81	0.07	0.00	0.00	0.13	0.16		0.87	0.00			0.00	6.00
Pure jadeitite	CV237t	Cpx	2874	VPSEM	PxNa	PxNa	88.82	1.99	0.00	0.90	0.05	0.00	0.00	0.06	0.07		0.94	0.00			0.00	6.00
Pure jadeitite	CV237t	Cpx	2878	VPSEM	PxNa	PxNa	80.29	1.97	0.00	0.83	0.07	0.00	0.00	0.13	0.14		0.89	0.00			0.00	6.00
Pure jadeitite	CV237t	Cpx	2883	VPSEM	PxNa	PxNa	85.41	1.97	0.00	0.88	0.05	0.00	0.00	0.09	0.10		0.91	0.00			0.00	6.00
Pure jadeitite	CV237t	Cpx	2884	VPSEM	PxNa	PxNa	80.34	1.97	0.00	0.84	0.07	0.00	0.00	0.12	0.14		0.87	0.00			0.00	6.00
Pure jadeitite	CV237t	Cpx	2886	VPSEM	PxNa	PxNa	79.35	1.98	0.00	0.83	0.06	0.01	0.00	0.13	0.15		0.84	0.00			0.00	6.00
Pure jadeitite	CV237t	Cpx	2889	VPSEM	PxNa	PxNa	82.21	1.96	0.01	0.87	0.06	0.00	0.00	0.11	0.13		0.88	0.00			0.00	6.00
Pure jadeitite	CV237t	Cpx	2892	VPSEM	PxNa	PxNa	83.86	1.99	0.00	0.85	0.06	0.00	0.00	0.10	0.11		0.90	0.00			0.00	6.00
Pure jadeitite	CV237t	Cpx	2897	VPSEM	PxNa	PxNa	85.54	1.99	0.00	0.86	0.04	0.02	0.00	0.08	0.11		0.89	0.00			0.00	6.00
Pure jadeitite	CV237t	Cpx	2899	VPSEM	PxNa	PxNa	87.11	1.98	0.00	0.90	0.05	0.00	0.00	0.07	0.08		0.93	0.00			0.00	6.00
Pure jadeitite	CV237t	Cpx	2901	VPSEM	PxNa	PxNa	87.75	1.97	0.00	0.91	0.05	0.00	0.00	0.06	0.08		0.94	0.00			0.00	6.00
Pure jadeitite	CV237t	Cpx	2906	VPSEM	PxNa	PxNa	82.67	1.98	0.00	0.86	0.07	0.00	0.00	0.10	0.12		0.89	0.00			0.00	6.00
Pure jadeitite	CV237t	Cpx	2908	VPSEM	PxNa	PxNa	84.50	1.97	0.01	0.87	0.06	0.00	0.00	0.08	0.11		0.90	0.00			0.00	6.00
Pure jadeitite	CV237t	Cpx	2910	VPSEM	PxNa	PxNa	87.16	1.97	0.01	0.90	0.05	0.00	0.00	0.07	0.09		0.91	0.00			0.00	6.00
Pure jadeitite	CV237t	Cpx	2911	VPSEM	PxNa	PxNa	88.85	1.99	0.00	0.91	0.04	0.02	0.00	0.06	0.07		0.92	0.00			0.00	6.00
Pure jadeitite	CV237t	Cpx	2920	VPSEM	PxNa	PxNa	84.62	1.98	0.00	0.88	0.07	0.00	0.00	0.07	0.10		0.92	0.00			0.00	6.00
Pure jadeitite	CV237t	Cpx	2924	VPSEM	PxNa	PxNa	83.54	1.99	0.00	0.85	0.05	0.00	0.00	0.10	0.13		0.88	0.00			0.00	6.00
Pure jadeitite	CV237t	Cpx	2928	VPSEM	PxNa	PxNa	83.07	1.97	0.00	0.86	0.06	0.00	0.00	0.11	0.12		0.89	0.00			0.00	6.00
Pure jadeitite	CV237t	Cpx	2935	VPSEM	PxNa	PxNa	88.79	2.00	0.00	0.90	0.03	0.02	0.00	0.06	0.08		0.92	0.00			0.00	6.00
Pure jadeitite	CV237t	Cpx	2939	VPSEM	PxNa	PxNa	88.46	1.98	0.00	0.92	0.05	0.00	0.00	0.06	0.07		0.93	0.00			0.00	6.00
Pure jadeitite	CV237t	Cpx	2949	VPSEM	PxNa	PxNa	91.14	1.97	0.00	0.95	0.04	0.00	0.00	0.04	0.05		0.95	0.00			0.00	6.00
Pure jadeitite	CV237t	Cpx	2952	VPSEM	PxNa	PxNa	92.05	1.99	0.00	0.94	0.03	0.01	0.00	0.04	0.05		0.94	0.00			0.00	6.00
Pure jadeitite	CV237t	Cpx	2955	VPSEM	PxNa	PxNa	85.16	1.98	0.00	0.88	0.06	0.00	0.00	0.08	0.10		0.91	0.00			0.00	6.00
Pure jadeitite	CV237t	Cpx	2956	VPSEM	PxNa	PxNa	89.65	1.98	0.00	0.91	0.05	0.00	0.00	0.05	0.07		0.96	0.00			0.00	6.00
Pure jadeitite	CV237t	Cpx	2962	VPSEM	PxNa	PxNa	86.90	1.97	0.00	0.91	0.05	0.00	0.00	0.08	0.09		0.91	0.00			0.00	6.00
Pure jadeitite	MCB1f	Cpx	3151	VPSEM	PxNaCa	PxNaCa	48.15	1.97	0.00	0.50	0.09	0.00	0.00	0.44	0.45		0.58	0.00	0.00	0.00	0.00	6.00
Pure jadeitite	MCB1f	Cpx	3153	VPSEM	PxNaCa	PxNaCa	50.88	1.95	0.00	0.54	0.10	0.00	0.00	0.41	0.42		0.63	0.00	0.00	0.01	0.00	5.99
Pure jadeitite	MCB1f	Cpx	3158	VPSEM	PxNaCa	PxNaCa	45.77	1.95	0.00	0.50	0.13	0.00	0.01	0.39	0.47		0.59	0.00	0.00	0.00	0.00	6.00
Pure jadeitite	MCB1f	Cpx	3160	VPSEM	PxNaCa	PxNaCa	50.87	1.96	0.00	0.53	0.09	0.00	0.00	0.41	0.43		0.63	0.00	0.00	0.00	0.00	6.00
Pure jadeitite	MCB1f	Cpx	3163	VPSEM	PxNaCa	PxNaCa	49.17	1.96	0.00	0.52	0.09	0.00	0.01	0.42	0.45		0.58	0.00	0.00	0.00	0.00	6.00
Pure jadeitite	MCB1f	Cpx	3165	VPSEM	PxNaCa	PxNaCa	48.47	1.96	0.00	0.50	0.08	0.00	0.00	0.45	0.46		0.58	0.00	0.00	0.00	0.00	6.00
Pure jadeitite	MCB1f	Cpx	3170	VPSEM	PxNaCa	PxNaCa	42.88	1.96	0.00	0.47	0.13	0.00	0.01	0.41	0.48		0.54	0.00	0.00	0.00	0.00	6.00
Pure jadeitite	MCB1f	Cpx	3178	VPSEM	PxNaCa	PxNaCa	50.90	1.97	0.00	0.52	0.13	0.00	0.00	0.38	0.38		0.66	0.00	0.00	0.00	0.00	6.00
Pure jadeitite	MCB1f	Cpx	3179	VPSEM	PxNaCa	PxNaCa	42.09	1.97	0.00	0.43	0.08	0.00	0.01	0.49	0.53		0.52	0.00	0.00	0.00	0.00	6.00
Pure jadeitite	MCB1f	Cpx	3180	VPSEM	PxNaCa	PxNaCa	49.55	1.97	0.01	0.51	0.12	0.00	0.00	0.40	0.40		0.63	0.00	0.00	0.00	0.00	6.00
Pure jadeitite	MCB1f	Cpx	3181	VPSEM	PxNaCa	PxNaCa	50.72	1.98	0.00	0.49	0.13	0.00	0.00	0.37	0.40		0.68	0.00	0.00	0.00	0.00	6.00
Pure jadeitite	MCB1f	Cpx	3183	VPSEM	PxNaCa	PxNaCa	44.86	1.96	0.00	0.48	0.10	0.00	0.00	0.45	0.49		0.56	0.00	0.00	0.00	0.00	6.00
Pure jadeitite	MCB1f	Cpx	3185	VPSEM	PxNaCa	PxNaCa	50.99	1.95	0.00	0.55	0.13	0.00	0.01	0.34	0.40		0.64	0.00	0.00	0.00	0.00	6.00
Pure jadeitite	MCB1f	Cpx	3192	VPSEM	PxNaCa	PxNaCa	35.47	1.95	0.00	0.40	0.22	0.00	0.01	0.39	0.49		0.53	0.00	0.00	0.00	0.00	6.00

Rock type	Sample	Phase	Point	serie	Px type	Px type	Jd mole%	Si	Ti	Al	Fe3+	Fe2+	Mn	Mg	Ca	Ba	Na	K	F	Cl	H	O
Pure jadeitite	MCB1f	Cpx	3197	VPSEM	PxNaCa	PxNaCa	41.11	1.96	0.00	0.43	0.08	0.00	0.00	0.52	0.53		0.50	0.00	0.00	0.00	0.00	6.00
Pure jadeitite	MCB1f	Cpx	3198	VPSEM	PxNaCa	PxNaCa	48.52	1.96	0.00	0.50	0.07	0.00	0.00	0.47	0.46		0.58	0.00	0.00	0.00	0.00	6.00
Pure jadeitite	MCB1f	Cpx	3202	VPSEM	PxNaCa	PxNaCa	49.55	1.95	0.00	0.52	0.16	0.00	0.00	0.35	0.39		0.68	0.00	0.00	0.00	0.00	6.00
Pure jadeitite	MCB1f	Cpx	3203	VPSEM	PxNaCa	PxNaCa	43.36	1.94	0.00	0.49	0.16	0.00	0.01	0.39	0.46		0.58	0.00	0.00	0.00	0.00	6.00
Pure jadeitite	MCB1f	Cpx	3205	VPSEM	PxNaCa	PxNaCa	47.48	1.96	0.00	0.53	0.19	0.00	0.00	0.30	0.40		0.63	0.00	0.00	0.00	0.00	6.00
Pure jadeitite	MCB1f	Cpx	3211	VPSEM	PxNaCa	PxNaCa	46.54	1.96	0.00	0.49	0.20	0.00	0.00	0.33	0.39		0.67	0.00	0.00	0.00	0.00	6.00
Pure jadeitite	MCB1f	Cpx	3215	VPSEM	PxNaCa	PxNaCa	48.38	1.96	0.00	0.51	0.10	0.00	0.00	0.42	0.45		0.60	0.00	0.00	0.00	0.00	6.00
Pure jadeitite	MCB1f	Cpx	3221	VPSEM	PxNaCa	PxNaCa	52.78	1.95	0.00	0.54	0.08	0.00	0.00	0.43	0.42		0.65	0.00	0.00	0.00	0.00	6.00
Pure jadeitite	MCB1f	Cpx	3224	VPSEM	PxNaCa	PxNaCa	50.34	1.95	0.00	0.53	0.15	0.00	0.00	0.31	0.41		0.67	0.00	0.00	0.00	0.00	6.00
Pure jadeitite	MCB1f	Cpx	3152	VPSEM	PxNa	PxNa	86.94	1.95	0.00	0.90	0.05	0.00	0.00	0.09	0.09		0.98	0.00	0.00	0.00	0.00	6.00
Pure jadeitite	MCB1f	Cpx	3154	VPSEM	PxNa	PxNa	84.60	1.96	0.00	0.86	0.05	0.00	0.00	0.11	0.11		0.96	0.00	0.00	0.00	0.00	6.00
Pure jadeitite	MCB1f	Cpx	3159	VPSEM	PxNa	PxNa	85.97	1.96	0.00	0.88	0.06	0.00	0.00	0.09	0.09		0.97	0.00	0.00	0.00	0.00	6.00
Pure jadeitite	MCB1f	Cpx	3164	VPSEM	PxNa	PxNa	86.72	1.96	0.00	0.89	0.05	0.00	0.00	0.08	0.09		0.99	0.00	0.00	0.00	0.00	6.00
Pure jadeitite	MCB1f	Cpx	3166	VPSEM	PxNa	PxNa	83.38	1.97	0.00	0.85	0.07	0.00	0.00	0.10	0.11		0.95	0.00	0.00	0.00	0.00	6.00
Pure jadeitite	MCB1f	Cpx	3172	VPSEM	PxNa	PxNa	84.44	1.97	0.00	0.86	0.06	0.00	0.00	0.09	0.11		0.97	0.00	0.00	0.00	0.00	6.00
Pure jadeitite	MCB1f	Cpx	3173	VPSEM	PxNa	PxNa	79.92	1.95	0.00	0.83	0.09	0.00	0.00	0.11	0.13		0.93	0.00	0.00	0.00	0.00	6.00
Pure jadeitite	MCB1f	Cpx	3182	VPSEM	PxNa	PxNa	83.57	1.96	0.00	0.85	0.05	0.00	0.00	0.11	0.13		0.97	0.00	0.00	0.00	0.00	6.00
Pure jadeitite	MCB1f	Cpx	3184	VPSEM	PxNa	PxNa	84.21	1.96	0.00	0.87	0.05	0.00	0.00	0.11	0.11		0.94	0.00	0.00	0.00	0.00	6.00
Pure jadeitite	MCB1f	Cpx	3186	VPSEM	PxNa	PxNa	84.74	1.96	0.00	0.86	0.05	0.00	0.00	0.12	0.11		0.98	0.00	0.00	0.00	0.00	6.00
Pure jadeitite	MCB1f	Cpx	3193	VPSEM	PxNa	PxNa	86.91	1.95	0.00	0.90	0.05	0.00	0.00	0.08	0.10		0.98	0.00	0.00	0.00	0.00	6.00
Pure jadeitite	MCB1f	Cpx	3196	VPSEM	PxNa	PxNa	82.58	1.96	0.00	0.85	0.06	0.00	0.00	0.12	0.13		0.94	0.00	0.00	0.00	0.00	6.00
Pure jadeitite	MCB1f	Cpx	3204	VPSEM	PxNa	PxNa	84.17	1.94	0.00	0.88	0.05	0.00	0.00	0.12	0.11		0.95	0.00	0.00	0.00	0.00	6.00
Pure jadeitite	MCB1f	Cpx	3207	VPSEM	PxNa	PxNa	81.01	1.94	0.01	0.84	0.05	0.00	0.00	0.15	0.15		0.93	0.00	0.00	0.00	0.00	6.00
Pure jadeitite	MCB1f	Cpx	3208	VPSEM	PxNa	PxNa	86.72	1.96	0.00	0.89	0.04	0.00	0.00	0.10	0.10		0.97	0.01	0.00	0.00	0.00	6.00
Pure jadeitite	MCB1f	Cpx	3214	VPSEM	PxNa	PxNa	86.29	1.96	0.00	0.88	0.05	0.00	0.00	0.10	0.10		1.00	0.00	0.00	0.00	0.00	6.00
Pure jadeitite	MCB1f	Cpx	3220	VPSEM	PxNa	PxNa	86.34	1.95	0.00	0.89	0.04	0.00	0.00	0.10	0.10		0.99	0.00	0.00	0.00	0.00	6.00
Pure jadeitite	MCB1f	Cpx	3225	VPSEM	PxNa	PxNa	83.21	1.95	0.00	0.87	0.09	0.00	0.00	0.08	0.10		0.97	0.00	0.00	0.00	0.00	6.00
Pure jadeitite	MCB1j	Cpx	1319	EPMA	PxNaCa	PxNaCa	50.40	2.00	0.00	0.50	0.04	0.06	0.00	0.40	0.45		0.54	0.00	0.01	0.00	0.00	5.99
Pure jadeitite	MCB1j	Cpx	1320	EPMA	PxNaCa	PxNaCa	48.48	2.01	0.00	0.47	0.02	0.08	0.00	0.42	0.48		0.51	0.00	0.01	0.00	0.00	5.99
Pure jadeitite	MCB1j	Cpx	1321	EPMA	PxNaCa	PxNaCa	46.04	2.00	0.00	0.45	0.00	0.11	0.00	0.44	0.52		0.46	0.00	0.01	0.00	0.00	5.99
Pure jadeitite	MCB1j	Cpx	1322	EPMA	PxNaCa	PxNaCa	51.40	2.00	0.00	0.51	0.04	0.05	0.00	0.39	0.44		0.55	0.00	0.01	0.00	0.00	5.99
Pure jadeitite	MCB1j	Cpx	1323	EPMA	PxNaCa	PxNaCa	54.42	2.01	0.00	0.52	0.00	0.10	0.00	0.38	0.43		0.54	0.00	0.01	0.00	0.00	6.00
Pure jadeitite	MCB1j	Cpx	1310	EPMA	PxNa	PxNa	80.86	2.01	0.00	0.79	0.01	0.05	0.00	0.15	0.17		0.82	0.00	0.01	0.00	0.00	6.00
Pure jadeitite	MCB1j	Cpx	1311	EPMA	PxNa	PxNa	81.50	2.01	0.00	0.80	0.00	0.06	0.00	0.15	0.16		0.82	0.00	0.01	0.00	0.00	6.00
Pure jadeitite	MCB1j	Cpx	1312	EPMA	PxNa	PxNa	85.74	2.01	0.00	0.84	0.00	0.06	0.00	0.11	0.12		0.86	0.00	0.00	0.00	0.00	6.00
Pure jadeitite	MCB1j	Cpx	1313	EPMA	PxNa	PxNa	87.28	2.01	0.00	0.85	0.01	0.05	0.00	0.09	0.10		0.89	0.00	0.01	0.00	0.00	6.00
Pure jadeitite	MCB1j	Cpx	1314	EPMA	PxNa	PxNa	86.42	2.01	0.00	0.85	0.00	0.06	0.00	0.10	0.11		0.87	0.00	0.01	0.00	0.00	6.00
Pure jadeitite	MCB1j	Cpx	1316	EPMA	PxNa	PxNa	88.43	2.01	0.00	0.87	0.00	0.05	0.00	0.09	0.10		0.89	0.00	0.01	0.00	0.00	5.99
Pure jadeitite	MCB1j	Cpx	1365	EPMA	PxNa	PxNa	86.30	1.99	0.02	0.84	0.00	0.05	0.00	0.10	0.13		0.86	0.00	0.00	0.00	0.00	6.00
Pure jadeitite	MCB1j	Cpx	1367	EPMA	PxNa	PxNa	86.79	2.01	0.00	0.85	0.01	0.07	0.00	0.07	0.09		0.89	0.00	0.01	0.00	0.00	5.99
Pure jadeitite	MCB1j	Cpx	1371	EPMA	PxNa	PxNa	79.72	2.00	0.00	0.80	0.04	0.02	0.00	0.15	0.16		0.83	0.00	0.00	0.00	0.00	6.00
Pure jadeitite	MCB2d	Cpx	3229	VPSEM	PxNaCa	PxNaCa	39.98	1.95	0.00	0.45	0.17	0.00	0.00	0.42	0.47		0.55	0.00	0.00		0.00	6.00
Pure jadeitite	MCB2d	Cpx	3231	VPSEM	PxNaCa	PxNaCa	50.64	1.95	0.00	0.54	0.18	0.00	0.01	0.29	0.37		0.68	0.00	0.00		0.00	6.00
Pure jadeitite	MCB2d	Cpx	3239	VPSEM	PxNaCa	PxNaCa	45.87	1.95	0.00	0.50	0.15	0.00	0.00	0.38	0.44		0.60	0.00	0.00		0.00	6.00

Rock type	Sample	Phase	Point	serie	Px type	Px type	Jd mole%	Si	Ti	Al	Fe3+	Fe2+	Mn	Mg	Ca	Ba	Na	K	F	Cl	H	O
Pure jadeitite	MCB2d	Cpx	3241	VPSEM	PxNaCa	PxNaCa	35.54	1.95	0.00	0.41	0.19	0.00	0.00	0.42	0.53		0.52	0.00	0.00		0.00	6.00
Pure jadeitite	MCB2d	Cpx	3244	VPSEM	PxNaCa	PxNaCa	41.87	1.95	0.00	0.47	0.19	0.00	0.00	0.36	0.46		0.58	0.00	0.00		0.00	6.00
Pure jadeitite	MCB2d	Cpx	3246	VPSEM	PxNaCa	PxNaCa	42.57	1.95	0.00	0.48	0.15	0.00	0.00	0.40	0.46		0.55	0.00	0.00		0.00	6.00
Pure jadeitite	MCB2d	Cpx	3249	VPSEM	PxNaCa	PxNaCa	41.10	1.95	0.00	0.47	0.22	0.02	0.01	0.31	0.45		0.58	0.00	0.00		0.00	6.00
Pure jadeitite	MCB2d	Cpx	3263	VPSEM	PxNaCa	PxNaCa	46.80	1.96	0.00	0.51	0.14	0.00	0.00	0.37	0.43		0.60	0.00	0.00		0.00	6.00
Pure jadeitite	MCB2d	Cpx	3228	VPSEM	PxNa	PxNa	83.90	1.94	0.00	0.88	0.08	0.00	0.00	0.08	0.10		0.99	0.00	0.00		0.00	6.00
Pure jadeitite	MCB2d	Cpx	3242	VPSEM	PxNa	PxNa	84.87	1.95	0.00	0.88	0.06	0.00	0.00	0.09	0.11		0.99	0.00	0.00		0.00	6.00
Pure jadeitite	MCB2d	Cpx	3247	VPSEM	PxNa	PxNa	84.71	1.95	0.00	0.87	0.06	0.00	0.00	0.10	0.10		0.98	0.00	0.00		0.00	6.00
Pure jadeitite	MCB2d	Cpx	3252	VPSEM	PxNa	PxNa	83.00	1.96	0.00	0.85	0.06	0.00	0.00	0.11	0.12		0.95	0.00	0.00		0.00	6.00
Pure jadeitite	MCB2d	Cpx	3254	VPSEM	PxNa	PxNa	79.07	1.94	0.00	0.83	0.06	0.00	0.00	0.16	0.16		0.92	0.00	0.00		0.00	6.00
Pure jadeitite	MCB2d	Cpx	3256	VPSEM	PxNa	PxNa	88.53	1.95	0.00	0.92	0.05	0.00	0.00	0.07	0.07		1.01	0.00	0.00		0.00	6.00
Pure jadeitite	MCB3h	Cpx	370	EPMA	PxNaCa	PxNaCa	37.76	2.00	0.00	0.37	0.06	0.08	0.00	0.49	0.56		0.44	0.00	0.00	0.00	0.00	6.00
Pure jadeitite	MCB3h	Cpx	372	EPMA	PxNaCa	PxNaCa	52.00	2.01	0.00	0.50	0.04	0.06	0.00	0.39	0.43		0.56	0.00	0.00	0.00	0.00	6.00
Pure jadeitite	MCB3h	Cpx	375	EPMA	PxNaCa	PxNaCa	75.07	2.00	0.00	0.75	0.04	0.03	0.00	0.19	0.21		0.79	0.00	0.00	0.00	0.00	6.00
Pure jadeitite	MCB3h	Cpx	377	EPMA	PxNaCa	PxNaCa	50.24	2.00	0.00	0.50	0.06	0.04	0.00	0.39	0.44		0.56	0.00	0.00	0.00	0.00	6.00
Pure jadeitite	MCB3h	Cpx	378	EPMA	PxNaCa	PxNaCa	76.74	2.01	0.00	0.75	0.00	0.07	0.00	0.20	0.19		0.76	0.00	0.00	0.00	0.00	6.00
Pure jadeitite	MCB3h	Cpx	382	EPMA	PxNaCa	PxNaCa	70.71	2.00	0.00	0.70	0.04	0.03	0.00	0.22	0.25		0.75	0.00	0.01	0.00	0.00	6.00
Pure jadeitite	MCB3h	Cpx	419	EPMA	PxNaCa	PxNaCa	48.17	2.00	0.00	0.48	0.06	0.06	0.00	0.40	0.45		0.54	0.00	0.00	0.00	0.00	6.00
Pure jadeitite	MCB3h	Cpx	428	EPMA	PxNaCa	PxNaCa	47.84	2.02	0.00	0.45	0.01	0.12	0.00	0.42	0.49		0.49	0.00	0.01	0.00	0.00	6.00
Pure jadeitite	MCB3h	Cpx	430	EPMA	PxNaCa	PxNaCa	78.40	2.01	0.00	0.76	0.00	0.07	0.00	0.17	0.19		0.79	0.00	0.01	0.00	0.00	6.00
Pure jadeitite	MCB3h	Cpx	434	EPMA	PxNaCa	PxNaCa	44.88	2.01	0.00	0.43	0.04	0.10	0.00	0.43	0.50		0.49	0.00	0.01	0.00	0.00	6.00
Pure jadeitite	MCB3h	Cpx	438	EPMA	PxNaCa	PxNaCa	47.42	2.01	0.00	0.45	0.01	0.09	0.00	0.44	0.49		0.49	0.00	0.01	0.00	0.00	6.00
Pure jadeitite	MCB3h	Cpx	439	EPMA	PxNaCa	PxNaCa	48.10	2.01	0.00	0.47	0.05	0.08	0.00	0.42	0.44		0.53	0.00	0.00	0.00	0.00	6.00
Pure jadeitite	MCB3h	Cpx	443	EPMA	PxNaCa	PxNaCa	50.13	2.00	0.00	0.49	0.05	0.07	0.00	0.38	0.44		0.55	0.00	0.01	0.00	0.00	5.99
Pure jadeitite	MCB3h	Cpx	444	EPMA	PxNaCa	PxNaCa	50.19	2.00	0.00	0.49	0.04	0.09	0.00	0.38	0.45		0.55	0.00	0.01	0.00	0.00	5.99
Pure jadeitite	MCB3h	Cpx	447	EPMA	PxNaCa	PxNaCa	45.77	2.00	0.00	0.45	0.05	0.08	0.01	0.41	0.48		0.51	0.00	0.01	0.00	0.00	6.00
Pure jadeitite	MCB3h	Cpx	451	EPMA	PxNaCa	PxNaCa	49.51	2.00	0.00	0.48	0.06	0.08	0.00	0.37	0.44		0.56	0.00	0.01	0.00	0.00	6.00
Pure jadeitite	MCB3h	Cpx	453	EPMA	PxNaCa	PxNaCa	52.72	2.01	0.00	0.51	0.03	0.09	0.00	0.38	0.43		0.56	0.00		0.00	0.00	6.00
Pure jadeitite	MCB3h	Cpx	454	EPMA	PxNaCa	PxNaCa	47.05	2.01	0.00	0.46	0.03	0.10	0.00	0.41	0.49		0.51	0.00		0.00	0.00	6.00
Pure jadeitite	MCB3h	Cpx	456	EPMA	PxNaCa	PxNaCa	69.20	2.01	0.00	0.68	0.01	0.08	0.00	0.24	0.28		0.70	0.00		0.00	0.00	6.00
Pure jadeitite	MCB3h	Cpx	458	EPMA	PxNaCa	PxNaCa	71.71	2.01	0.00	0.70	0.00	0.09	0.00	0.23	0.25		0.72	0.00		0.00	0.00	6.00
Pure jadeitite	MCB3h	Cpx	462	EPMA	PxNaCa	PxNaCa	66.82	2.01	0.00	0.65	0.03	0.06	0.00	0.26	0.29		0.70	0.00		0.00	0.00	6.00
Pure jadeitite	MCB3h	Cpx	463	EPMA	PxNaCa	PxNaCa	64.90	2.02	0.00	0.62	0.00	0.09	0.00	0.29	0.32		0.65	0.00		0.00	0.00	6.00
Pure jadeitite	MCB3h	Cpx	464	EPMA	PxNaCa	PxNaCa	78.96	2.01	0.00	0.76	0.00	0.07	0.00	0.16	0.18		0.79	0.00		0.00	0.00	6.00
Pure jadeitite	MCB3h	Cpx	465	EPMA	PxNaCa	PxNaCa	58.21	2.01	0.00	0.56	0.02	0.08	0.00	0.33	0.38		0.61	0.00		0.00	0.00	6.00
Pure jadeitite	MCB3h	Cpx	466	EPMA	PxNaCa	PxNaCa	64.98	2.01	0.00	0.62	0.02	0.07	0.00	0.28	0.31		0.68	0.00		0.00	0.00	6.00
Pure jadeitite	MCB3h	Cpx	473	EPMA	PxNaCa	PxNaCa	79.52	2.02	0.00	0.77	0.00	0.07	0.00	0.16	0.18		0.80	0.00		0.00	0.00	6.00
Pure jadeitite	MCB3h	Cpx	476	EPMA	PxNaCa	PxNaCa	78.59	2.02	0.00	0.76	0.00	0.08	0.00	0.17	0.19		0.79	0.00		0.00	0.00	6.00
Pure jadeitite	MCB3h	Cpx	481	EPMA	PxNaCa	PxNaCa	52.62	2.01	0.00	0.50	0.03	0.08	0.00	0.39	0.43		0.56	0.00		0.00	0.00	6.00
Pure jadeitite	MCB3h	Cpx	482	EPMA	PxNaCa	PxNaCa	50.44	2.01	0.00	0.48	0.01	0.12	0.00	0.40	0.46		0.52	0.00		0.00	0.00	6.00
Pure jadeitite	MCB3h	Cpx	483	EPMA	PxNaCa	PxNaCa	50.62	2.01	0.00	0.48	0.02	0.10	0.00	0.39	0.46		0.53	0.00		0.00	0.00	6.00
Pure jadeitite	MCB3h	Cpx	485	EPMA	PxNaCa	PxNaCa	75.75	2.02	0.00	0.73	0.00	0.07	0.00	0.19	0.22		0.76	0.00		0.00	0.00	6.00
Pure jadeitite	MCB3h	Cpx	487	EPMA	PxNaCa	PxNaCa	52.02	2.01	0.00	0.50	0.03	0.09	0.00	0.38	0.44		0.55	0.00		0.00	0.00	6.00
Pure jadeitite	MCB3h	Cpx	488	EPMA	PxNaCa	PxNaCa	79.53	2.02	0.00	0.77	0.00	0.07	0.00	0.16	0.18		0.80	0.00		0.00	0.00	6.00

Rock type	Sample	Phase	Point	serie	Px type	Px type	Jd mole%	Si	Ti	Al	Fe3+	Fe2+	Mn	Mg	Ca	Ba	Na	K	F	Cl	H	O
Pure jadeitite	MCB3h	Cpx	493	EPMA	PxNaCa	PxNaCa	77.18	2.02	0.00	0.74	0.00	0.08	0.00	0.18	0.20		0.77	0.00		0.00	0.00	6.00
Pure jadeitite	MCB3h	Cpx	497	EPMA	PxNaCa	PxNaCa	78.09	2.02	0.00	0.75	0.00	0.08	0.00	0.17	0.19		0.78	0.00		0.01	0.00	6.00
Pure jadeitite	MCB3h	Cpx	499	EPMA	PxNaCa	PxNaCa	68.87	2.02	0.00	0.67	0.00	0.09	0.00	0.25	0.28		0.68	0.00		0.00	0.00	6.00
Pure jadeitite	MCB3h	Cpx	500	EPMA	PxNaCa	PxNaCa	65.22	2.02	0.00	0.62	0.00	0.09	0.00	0.29	0.32		0.66	0.00		0.00	0.00	6.00
Pure jadeitite	MCB3h	Cpx	502	EPMA	PxNaCa	PxNaCa	79.96	2.02	0.00	0.77	0.00	0.07	0.00	0.15	0.17		0.80	0.00		0.00	0.00	6.00
Pure jadeitite	MCB3h	Cpx	504	EPMA	PxNaCa	PxNaCa	78.98	2.02	0.00	0.76	0.00	0.07	0.00	0.16	0.18		0.79	0.00		0.00	0.00	6.00
Pure jadeitite	MCB3h	Cpx	507	EPMA	PxNaCa	PxNaCa	68.23	2.02	0.00	0.65	0.00	0.09	0.00	0.26	0.29		0.69	0.00		0.00	0.00	6.00
Pure jadeitite	MCB3h	Cpx	518	EPMA	PxNaCa	PxNaCa	75.83	2.02	0.00	0.73	0.00	0.08	0.00	0.19	0.21		0.75	0.00		0.00	0.00	6.00
Pure jadeitite	MCB3h	Cpx	3500	VPSEM	PxNaCa	PxNaCa	39.98	1.95		0.45	0.17	0.00		0.42	0.47		0.55				0.00	6.00
Pure jadeitite	MCB3h	Cpx	3502	VPSEM	PxNaCa	PxNaCa	50.57	1.96		0.54	0.18	0.00		0.29	0.37		0.68				0.00	6.00
Pure jadeitite	MCB3h	Cpx	3510	VPSEM	PxNaCa	PxNaCa	45.87	1.95		0.50	0.15	0.00		0.38	0.44		0.60				0.00	6.00
Pure jadeitite	MCB3h	Cpx	3521	VPSEM	PxNaCa	PxNaCa	36.75	1.95		0.41	0.18	0.00		0.44	0.52		0.53				0.00	6.00
Pure jadeitite	MCB3h	Cpx	3534	VPSEM	PxNaCa	PxNaCa	52.32	1.96		0.55	0.08	0.00		0.42	0.41		0.62				0.00	6.00
Pure jadeitite	MCB3h	Cpx	3536	VPSEM	PxNaCa	PxNaCa	74.24	1.93		0.78	0.06	0.00		0.23	0.21		0.87				0.00	6.00
Pure jadeitite	MCB3h	Cpx	3537	VPSEM	PxNaCa	PxNaCa	48.53	1.97		0.51	0.09	0.00		0.44	0.42		0.58				0.00	6.00
Pure jadeitite	MCB3h	Cpx	3538	VPSEM	PxNaCa	PxNaCa	53.92	1.96		0.57	0.08	0.00		0.39	0.39		0.63				0.00	6.00
Pure jadeitite	MCB3h	Cpx	3545	VPSEM	PxNaCa	PxNaCa	50.58	1.94		0.53	0.12	0.00		0.40	0.43		0.67				0.00	6.00
Pure jadeitite	MCB3h	Cpx	3552	VPSEM	PxNaCa	PxNaCa	49.19	1.92		0.53	0.10	0.00		0.46	0.45		0.63				0.00	6.00
Pure jadeitite	MCB3h	Cpx	3554	VPSEM	PxNaCa	PxNaCa	44.28	1.97		0.48	0.11	0.00		0.43	0.48		0.54				0.00	6.00
Pure jadeitite	MCB3h	Cpx	3563	VPSEM	PxNaCa	PxNaCa	44.63	1.96		0.48	0.11	0.00		0.45	0.47		0.55				0.00	6.00
Pure jadeitite	MCB3h	Cpx	3567	VPSEM	PxNaCa	PxNaCa	36.74	1.95		0.41	0.17	0.00		0.45	0.52		0.52				0.00	6.00
Pure jadeitite	MCB3h	Cpx	3570	VPSEM	PxNaCa	PxNaCa	37.57	1.95		0.43	0.17	0.00		0.45	0.49		0.52				0.00	6.00
Pure jadeitite	MCB3h	Cpx	3577	VPSEM	PxNaCa	PxNaCa	36.47	1.96		0.41	0.17	0.00		0.43	0.52		0.51				0.00	6.00
Pure jadeitite	MCB3h	Cpx	3581	VPSEM	PxNaCa	PxNaCa	48.54	1.96		0.51	0.12	0.00		0.40	0.44		0.62				0.00	6.00
Pure jadeitite	MCB3h	Cpx	3585	VPSEM	PxNaCa	PxNaCa	43.71	1.93		0.49	0.17	0.00		0.40	0.45		0.60				0.00	6.00
Pure jadeitite	MCB3h	Cpx	3587	VPSEM	PxNaCa	PxNaCa	42.85	1.96		0.46	0.11	0.00		0.49	0.47		0.54				0.00	6.00
Pure jadeitite	MCB3h	Cpx	3597	VPSEM	PxNaCa	PxNaCa	49.00	1.96		0.52	0.11	0.00		0.41	0.43		0.61				0.00	6.00
Pure jadeitite	MCB3h	Cpx	3605	VPSEM	PxNaCa	PxNaCa	45.03	1.96		0.48	0.14	0.00		0.39	0.46		0.59				0.00	6.00
Pure jadeitite	MCB3h	Cpx	3610	VPSEM	PxNaCa	PxNaCa	42.74	1.95		0.47	0.16	0.00	0.02	0.38	0.48		0.57				0.00	6.00
Pure jadeitite	MCB3h	Cpx	3614	VPSEM	PxNaCa	PxNaCa	43.67	1.95		0.49	0.15	0.00		0.39	0.46		0.57				0.00	6.00
Pure jadeitite	MCB3h	Cpx	374	EPMA	PxNa	PxNa	83.66	2.01	0.00	0.81	0.01	0.05	0.00	0.12	0.14		0.85	0.00	0.00	0.00	0.00	6.00
Pure jadeitite	MCB3h	Cpx	380	EPMA	PxNa	PxNa	85.47	2.01	0.00	0.84	0.03	0.02	0.00	0.10	0.11		0.89	0.00	0.01	0.00	0.00	6.00
Pure jadeitite	MCB3h	Cpx	381	EPMA	PxNa	PxNa	92.84	2.01	0.01	0.91	0.00	0.03	0.00	0.05	0.06		0.93	0.00	0.00	0.00	0.00	6.00
Pure jadeitite	MCB3h	Cpx	383	EPMA	PxNa	PxNa	80.00	2.01	0.00	0.78	0.01	0.05	0.00	0.16	0.17		0.82	0.00	0.00	0.00	0.00	6.00
Pure jadeitite	MCB3h	Cpx	384	EPMA	PxNa	PxNa	82.08	2.01	0.00	0.80	0.01	0.05	0.00	0.14	0.15		0.83	0.00	0.00	0.00	0.00	6.00
Pure jadeitite	MCB3h	Cpx	385	EPMA	PxNa	PxNa	85.00	2.01	0.00	0.84	0.02	0.04	0.00	0.11	0.12		0.87	0.00	0.00	0.00	0.00	6.00
Pure jadeitite	MCB3h	Cpx	386	EPMA	PxNa	PxNa	83.23	2.01	0.00	0.82	0.02	0.04	0.00	0.12	0.13		0.86	0.00	0.00	0.00	0.00	6.00
Pure jadeitite	MCB3h	Cpx	391	EPMA	PxNa	PxNa	82.42	2.01	0.00	0.80	0.02	0.04	0.00	0.13	0.14		0.85	0.00	0.00	0.00	0.00	6.00
Pure jadeitite	MCB3h	Cpx	392	EPMA	PxNa	PxNa	84.80	2.01	0.00	0.82	0.01	0.05	0.00	0.11	0.13		0.86	0.00	0.00	0.00	0.00	6.00
Pure jadeitite	MCB3h	Cpx	395	EPMA	PxNa	PxNa	83.84	2.01	0.00	0.82	0.01	0.05	0.00	0.12	0.13		0.86	0.00	0.00	0.00	0.00	6.00
Pure jadeitite	MCB3h	Cpx	396	EPMA	PxNa	PxNa	92.09	2.01	0.00	0.91	0.03	0.02	0.00	0.04	0.04		0.95	0.00	0.00	0.00	0.00	6.00
Pure jadeitite	MCB3h	Cpx	404	EPMA	PxNa	PxNa	84.19	2.01	0.00	0.82	0.01	0.04	0.00	0.12	0.14		0.86	0.00	0.00	0.00	0.00	6.00
Pure jadeitite	MCB3h	Cpx	429	EPMA	PxNa	PxNa	79.83	2.01	0.00	0.78	0.01	0.05	0.00	0.16	0.18		0.81	0.00	0.00	0.00	0.00	6.00
Pure jadeitite	MCB3h	Cpx	431	EPMA	PxNa	PxNa	86.52	2.01	0.00	0.84	0.01	0.06	0.00	0.09	0.11		0.88	0.00	0.01	0.00	0.00	6.00

Rock type	Sample	Phase	Point	serie	Px type	Px type	Jd mole%	Si	Ti	Al	Fe3+	Fe2+	Mn	Mg	Ca	Ba	Na	K	F	Cl	H	O
Pure jadeitite	MCB3h	Cpx	435	EPMA	PxNa	PxNa	88.47	2.02	0.00	0.86	0.00	0.06	0.00	0.08	0.09		0.89	0.00	0.01	0.00	0.00	6.00
Pure jadeitite	MCB3h	Cpx	436	EPMA	PxNa	PxNa	89.43	2.01	0.00	0.87	0.01	0.06	0.00	0.06	0.07		0.91	0.00	0.00	0.00	0.00	6.00
Pure jadeitite	MCB3h	Cpx	437	EPMA	PxNa	PxNa	84.79	2.01	0.00	0.83	0.00	0.06	0.00	0.11	0.12		0.86	0.00	0.00	0.00	0.00	6.00
Pure jadeitite	MCB3h	Cpx	440	EPMA	PxNa	PxNa	87.56	2.02	0.00	0.85	0.00	0.07	0.00	0.08	0.09		0.88	0.00	0.01	0.00	0.00	6.00
Pure jadeitite	MCB3h	Cpx	441	EPMA	PxNa	PxNa	84.39	2.01	0.00	0.82	0.00	0.07	0.00	0.11	0.13		0.85	0.00	0.01	0.00	0.00	6.00
Pure jadeitite	MCB3h	Cpx	449	EPMA	PxNa	PxNa	86.22	2.01	0.00	0.84	0.00	0.06	0.00	0.10	0.11		0.87	0.00	0.00	0.00	0.00	6.00
Pure jadeitite	MCB3h	Cpx	452	EPMA	PxNa	PxNa	87.33	2.02	0.00	0.84	0.00	0.06	0.00	0.09	0.10		0.88	0.00	0.00	0.00	0.00	6.00
Pure jadeitite	MCB3h	Cpx	455	EPMA	PxNa	PxNa	84.11	2.01	0.00	0.82	0.00	0.07	0.00	0.12	0.13		0.84	0.00		0.00	0.00	6.00
Pure jadeitite	MCB3h	Cpx	457	EPMA	PxNa	PxNa	87.09	2.01	0.00	0.85	0.00	0.06	0.00	0.10	0.10		0.87	0.00		0.00	0.00	6.00
Pure jadeitite	MCB3h	Cpx	459	EPMA	PxNa	PxNa	85.24	2.01	0.00	0.83	0.00	0.07	0.00	0.11	0.12		0.85	0.00		0.00	0.00	6.00
Pure jadeitite	MCB3h	Cpx	460	EPMA	PxNa	PxNa	85.50	2.01	0.00	0.83	0.00	0.06	0.00	0.11	0.12		0.86	0.00		0.00	0.00	6.00
Pure jadeitite	MCB3h	Cpx	461	EPMA	PxNa	PxNa	84.05	2.01	0.00	0.82	0.00	0.07	0.00	0.12	0.13		0.84	0.00		0.00	0.00	6.00
Pure jadeitite	MCB3h	Cpx	467	EPMA	PxNa	PxNa	86.85	2.02	0.00	0.84	0.00	0.06	0.00	0.10	0.10		0.86	0.00		0.00	0.00	6.00
Pure jadeitite	MCB3h	Cpx	468	EPMA	PxNa	PxNa	83.72	2.02	0.00	0.81	0.00	0.07	0.00	0.12	0.14		0.84	0.00		0.00	0.00	6.00
Pure jadeitite	MCB3h	Cpx	469	EPMA	PxNa	PxNa	82.37	2.02	0.00	0.80	0.00	0.07	0.00	0.14	0.14		0.82	0.00		0.00	0.00	6.00
Pure jadeitite	MCB3h	Cpx	470	EPMA	PxNa	PxNa	86.19	2.01	0.00	0.84	0.00	0.06	0.00	0.10	0.11		0.86	0.00		0.00	0.00	6.00
Pure jadeitite	MCB3h	Cpx	471	EPMA	PxNa	PxNa	83.88	2.01	0.00	0.82	0.00	0.07	0.00	0.12	0.14		0.84	0.00		0.00	0.00	6.00
Pure jadeitite	MCB3h	Cpx	472	EPMA	PxNa	PxNa	86.96	2.01	0.00	0.84	0.00	0.06	0.00	0.10	0.10		0.87	0.00		0.00	0.00	6.00
Pure jadeitite	MCB3h	Cpx	474	EPMA	PxNa	PxNa	81.44	2.01	0.00	0.79	0.00	0.07	0.00	0.14	0.16		0.81	0.00		0.00	0.00	6.00
Pure jadeitite	MCB3h	Cpx	475	EPMA	PxNa	PxNa	85.49	2.02	0.00	0.83	0.00	0.06	0.00	0.11	0.12		0.85	0.00		0.00	0.00	6.00
Pure jadeitite	MCB3h	Cpx	477	EPMA	PxNa	PxNa	86.17	2.01	0.00	0.84	0.00	0.06	0.00	0.10	0.11		0.86	0.00		0.00	0.00	6.00
Pure jadeitite	MCB3h	Cpx	484	EPMA	PxNa	PxNa	85.21	2.02	0.00	0.83	0.00	0.06	0.00	0.11	0.12		0.85	0.00		0.00	0.00	6.00
Pure jadeitite	MCB3h	Cpx	486	EPMA	PxNa	PxNa	85.45	2.02	0.00	0.83	0.00	0.06	0.00	0.11	0.12		0.85	0.00		0.00	0.00	6.00
Pure jadeitite	MCB3h	Cpx	489	EPMA	PxNa	PxNa	81.12	2.02	0.00	0.79	0.00	0.06	0.00	0.15	0.16		0.81	0.00		0.00	0.00	6.00
Pure jadeitite	MCB3h	Cpx	490	EPMA	PxNa	PxNa	84.06	2.02	0.00	0.82	0.00	0.06	0.00	0.12	0.13		0.84	0.00		0.00	0.00	6.00
Pure jadeitite	MCB3h	Cpx	491	EPMA	PxNa	PxNa	80.88	2.02	0.00	0.78	0.00	0.07	0.00	0.15	0.16		0.81	0.00		0.00	0.00	6.00
Pure jadeitite	MCB3h	Cpx	492	EPMA	PxNa	PxNa	84.15	2.02	0.00	0.81	0.00	0.07	0.00	0.12	0.13		0.84	0.00		0.00	0.00	6.00
Pure jadeitite	MCB3h	Cpx	494	EPMA	PxNa	PxNa	85.77	2.02	0.00	0.83	0.00	0.06	0.00	0.11	0.11		0.85	0.00		0.00	0.00	6.00
Pure jadeitite	MCB3h	Cpx	495	EPMA	PxNa	PxNa	85.38	2.02	0.00	0.83	0.00	0.06	0.00	0.11	0.12		0.85	0.00		0.00	0.00	6.00
Pure jadeitite	MCB3h	Cpx	496	EPMA	PxNa	PxNa	85.78	2.02	0.00	0.83	0.00	0.06	0.00	0.10	0.11		0.85	0.00		0.00	0.00	6.00
Pure jadeitite	MCB3h	Cpx	498	EPMA	PxNa	PxNa	84.14	2.02	0.00	0.82	0.00	0.07	0.00	0.12	0.13		0.84	0.00		0.00	0.00	6.00
Pure jadeitite	MCB3h	Cpx	501	EPMA	PxNa	PxNa	81.72	2.02	0.00	0.79	0.00	0.07	0.00	0.14	0.16		0.81	0.00		0.00	0.00	6.00
Pure jadeitite	MCB3h	Cpx	503	EPMA	PxNa	PxNa	85.58	2.02	0.01	0.83	0.00	0.06	0.00	0.11	0.12		0.85	0.00		0.00	0.00	6.00
Pure jadeitite	MCB3h	Cpx	505	EPMA	PxNa	PxNa	82.64	2.02	0.00	0.80	0.00	0.07	0.00	0.13	0.14		0.82	0.00		0.00	0.00	6.00
Pure jadeitite	MCB3h	Cpx	506	EPMA	PxNa	PxNa	82.00	2.02	0.00	0.79	0.00	0.08	0.00	0.15	0.13		0.82	0.00		0.00	0.00	6.00
Pure jadeitite	MCB3h	Cpx	508	EPMA	PxNa	PxNa	82.56	2.02	0.00	0.80	0.00	0.08	0.00	0.13	0.14		0.82	0.00		0.00	0.00	6.00
Pure jadeitite	MCB3h	Cpx	509	EPMA	PxNa	PxNa	82.17	2.02	0.00	0.79	0.00	0.07	0.00	0.13	0.15		0.82	0.00		0.00	0.00	6.00
Pure jadeitite	MCB3h	Cpx	510	EPMA	PxNa	PxNa	84.84	2.01	0.00	0.83	0.00	0.06	0.00	0.11	0.13		0.85	0.00		0.00	0.00	6.00
Pure jadeitite	MCB3h	Cpx	511	EPMA	PxNa	PxNa	84.51	2.01	0.00	0.82	0.00	0.06	0.00	0.12	0.13		0.84	0.00		0.00	0.00	6.00
Pure jadeitite	MCB3h	Cpx	512	EPMA	PxNa	PxNa	85.76	2.02	0.00	0.83	0.00	0.06	0.00	0.11	0.11		0.85	0.00		0.00	0.00	6.00
Pure jadeitite	MCB3h	Cpx	513	EPMA	PxNa	PxNa	83.50	2.02	0.00	0.81	0.00	0.07	0.00	0.12	0.13		0.83	0.00		0.00	0.00	6.00
Pure jadeitite	MCB3h	Cpx	514	EPMA	PxNa	PxNa	84.17	2.02	0.00	0.81	0.00	0.07	0.00	0.12	0.13		0.84	0.00		0.00	0.00	6.00
Pure jadeitite	MCB3h	Cpx	516	EPMA	PxNa	PxNa	84.38	2.01	0.00	0.82	0.00	0.06	0.00	0.12	0.13		0.85	0.00		0.00	0.00	6.00
Pure jadeitite	MCB3h	Cpx	517	EPMA	PxNa	PxNa	86.33	2.02	0.01	0.83	0.00	0.07	0.00	0.10	0.11		0.86	0.00		0.00	0.00	6.00

Rock type	Sample	Phase	Point	serie	Px type	Px type	Jd mole%	Si	Ti	Al	Fe3+	Fe2+	Mn	Mg	Ca	Ba	Na	K	F	Cl	H	O
Pure jadeitite	MCB3h	Cpx	519	EPMA	PxNa	PxNa	84.06	2.02	0.01	0.81	0.00	0.07	0.00	0.12	0.13		0.84	0.00		0.00	0.00	6.00
Pure jadeitite	MCB3h	Cpx	520	EPMA	PxNa	PxNa	92.50	2.02	0.00	0.91	0.00	0.05	0.00	0.05	0.05		0.90	0.00		0.00	0.00	6.00
Pure jadeitite	MCB3h	Cpx	3499	VPSEM	PxNa	PxNa	83.90	1.94		0.88	0.08	0.00		0.08	0.10		0.99				0.00	6.00
Pure jadeitite	MCB3h	Cpx	3525	VPSEM	PxNa	PxNa	84.88	1.97		0.86	0.05	0.00		0.11	0.10		0.96				0.00	6.00
Pure jadeitite	MCB3h	Cpx	3526	VPSEM	PxNa	PxNa	88.78	1.95		0.92	0.07	0.00		0.04	0.05		1.02				0.00	6.00
Pure jadeitite	MCB3h	Cpx	3530	VPSEM	PxNa	PxNa	86.27	1.93		0.92	0.07	0.00		0.07	0.09		1.00				0.00	6.00
Pure jadeitite	MCB3h	Cpx	3539	VPSEM	PxNa	PxNa	82.40	1.93		0.87	0.07	0.00		0.12	0.12		0.97				0.00	6.00
Pure jadeitite	MCB3h	Cpx	3543	VPSEM	PxNa	PxNa	85.43	1.95		0.88	0.04	0.00		0.11	0.13		0.97				0.00	6.00
Pure jadeitite	MCB3h	Cpx	3564	VPSEM	PxNa	PxNa	82.29	1.94		0.86	0.06	0.00		0.13	0.13		0.95				0.00	6.00
Pure jadeitite	MCB3h	Cpx	3573	VPSEM	PxNa	PxNa	83.42	1.97		0.86	0.05	0.00		0.12	0.12		0.91				0.00	6.00
Pure jadeitite	MCB3h	Cpx	3575	VPSEM	PxNa	PxNa	83.09	1.96		0.86	0.09	0.00		0.07	0.10		0.99				0.00	6.00
Pure jadeitite	MCB3h	Cpx	3576	VPSEM	PxNa	PxNa	86.86	1.96		0.90	0.06	0.00		0.08	0.09		0.99				0.00	6.00
Pure jadeitite	MCB3h	Cpx	3580	VPSEM	PxNa	PxNa	85.20	1.96		0.88	0.06	0.00		0.10	0.10		0.96				0.00	6.00
Pure jadeitite	MCB3h	Cpx	3586	VPSEM	PxNa	PxNa	82.72	1.97		0.84	0.06	0.00		0.10	0.14		0.95				0.00	6.00
Pure jadeitite	MCB3h	Cpx	3600	VPSEM	PxNa	PxNa	78.06	1.96		0.79	0.06	0.00		0.18	0.17		0.91				0.00	6.00
Pure jadeitite	MCB3h	Cpx	3602	VPSEM	PxNa	PxNa	84.72	1.94		0.90	0.06	0.00		0.10	0.11		0.95				0.00	6.00
Pure jadeitite	MCB3h	Cpx	3606	VPSEM	PxNa	PxNa	83.72	1.98		0.84	0.07	0.00		0.09	0.11		0.97				0.00	6.00
Pure jadeitite	MCB3h	Cpx	3613	VPSEM	PxNa	PxNa	80.69	1.95		0.84	0.07	0.00		0.14	0.13		0.93				0.00	6.00
Pure Jdt/Ab-Ep rock/Chloritite	09SC8a3	Cpx	2401	VPSEM	PxNaCa	PxNaCa	46.23	1.89	0.01	0.43	0.00	0.07		0.48	0.57		0.48				0.00	6.00
Pure Jdt/Ab-Ep rock/Chloritite	09SC8a3	Cpx	2430	VPSEM	PxNaCa	PxNaCa	42.31	1.96		0.46	0.14	0.00		0.43	0.47		0.56				0.00	6.00
Pure Jdt/Ab-Ep rock/Chloritite	09SC8a3	Cpx	2438	VPSEM	PxNaCa	PxNaCa	48.86	1.97		0.51	0.08	0.00		0.44	0.45		0.59				0.00	6.00
Pure Jdt/Ab-Ep rock/Chloritite	09SC8a3	Cpx	2442	VPSEM	PxNaCa	PxNaCa	45.19	1.97		0.48	0.10	0.00		0.48	0.44		0.55				0.00	6.00
Pure Jdt/Ab-Ep rock/Chloritite	09SC8a3	Cpx	2452	VPSEM	PxNaCa	PxNaCa	36.23	1.95		0.41	0.14	0.00	0.01	0.49	0.54		0.49				0.00	6.00
Pure Jdt/Ab-Ep rock/Chloritite	09SC8a3	Cpx	2455	VPSEM	PxNaCa	PxNaCa	44.76	1.95		0.50	0.15	0.00		0.39	0.43		0.58				0.00	6.00
Pure Jdt/Ab-Ep rock/Chloritite	09SC8a3	Cpx	2457	VPSEM	PxNaCa	PxNaCa	42.01	1.95		0.46	0.14	0.00		0.43	0.49		0.56				0.00	6.00
Pure Jdt/Ab-Ep rock/Chloritite	09SC8a3	Cpx	2459	VPSEM	PxNaCa	PxNaCa	46.82	1.95		0.50	0.15	0.00		0.38	0.42		0.62				0.00	6.00
Pure Jdt/Ab-Ep rock/Chloritite	09SC8a3	Cpx	2463	VPSEM	PxNaCa	PxNaCa	45.44	1.95		0.49	0.15	0.00		0.38	0.44		0.60				0.00	6.00
Pure Jdt/Ab-Ep rock/Chloritite	09SC8a3	Cpx	2467	VPSEM	PxNaCa	PxNaCa	39.44	1.94		0.45	0.17	0.00		0.40	0.51		0.54				0.00	6.00
Pure Jdt/Ab-Ep rock/Chloritite	09SC8a3	Cpx	2469	VPSEM	PxNaCa	PxNaCa	43.50	1.95		0.49	0.17	0.00		0.37	0.45		0.58				0.00	6.00
Pure Jdt/Ab-Ep rock/Chloritite	09SC8a3	Cpx	2473	VPSEM	PxNaCa	PxNaCa	51.71	1.96		0.54	0.11	0.00	0.01	0.37	0.40		0.64				0.00	6.00
Pure Jdt/Ab-Ep rock/Chloritite	09SC8a3	Cpx	2476	VPSEM	PxNaCa	PxNaCa	55.57	1.97		0.57	0.11	0.00	0.01	0.34	0.37		0.68				0.00	6.00
Pure Jdt/Ab-Ep rock/Chloritite	09SC8a3	Cpx	2485	VPSEM	PxNaCa	PxNaCa	42.03	1.96		0.46	0.14	0.00		0.42	0.48		0.55				0.00	6.00
Pure Jdt/Ab-Ep rock/Chloritite	09SC8a3	Cpx	2486	VPSEM	PxNaCa	PxNaCa	45.41	1.96		0.49	0.14	0.00	0.01	0.40	0.43		0.59				0.00	6.00
Pure Jdt/Ab-Ep rock/Chloritite	09SC8a3	Cpx	2435	VPSEM	PxNa	PxNa	90.91	1.97		0.93	0.03	0.00		0.06	0.07		0.99				0.00	6.00
Pure Jdt/Ab-Ep rock/Chloritite	09SC8a3	Cpx	2445	VPSEM	PxNa	PxNa	87.24	1.96	0.01	0.89	0.03	0.00		0.10	0.09		0.95				0.00	6.00
Pure Jdt/Ab-Ep rock/Chloritite	09SC8a3	Cpx	2446	VPSEM	PxNa	PxNa	82.29	1.97		0.84	0.05	0.00		0.13	0.13		0.91				0.00	6.00
Pure Jdt/Ab-Ep rock/Chloritite	09SC8a3	Cpx	2453	VPSEM	PxNa	PxNa	87.51	1.97		0.89	0.04	0.00		0.09	0.09		0.96				0.00	6.00
Pure Jdt/Ab-Ep rock/Chloritite	09SC8a3	Cpx	2456	VPSEM	PxNa	PxNa	84.07	1.97	0.01	0.85	0.06	0.00		0.11	0.11		0.94				0.00	6.00
Pure Jdt/Ab-Ep rock/Chloritite	09SC8a3	Cpx	2458	VPSEM	PxNa	PxNa	88.88	1.95	0.01	0.92	0.03	0.00		0.09	0.08		0.98				0.00	6.00
Pure Jdt/Ab-Ep rock/Chloritite	09SC8a3	Cpx	2460	VPSEM	PxNa	PxNa	85.09	1.96		0.88	0.05	0.00		0.11	0.11		0.95				0.00	6.00
Pure Jdt/Ab-Ep rock/Chloritite	09SC8a3	Cpx	2462	VPSEM	PxNa	PxNa	86.60	1.95	0.01	0.89	0.05	0.00		0.09	0.09		1.00				0.00	6.00
Pure Jdt/Ab-Ep rock/Chloritite	09SC8a3	Cpx	2468	VPSEM	PxNa	PxNa	85.54	1.96		0.87	0.05	0.00		0.11	0.10		0.96				0.00	6.00
Pure Jdt/Ab-Ep rock/Chloritite	09SC8a3	Cpx	2472	VPSEM	PxNa	PxNa	86.68	1.96		0.89	0.05	0.00		0.09	0.08		0.96				0.00	6.00
Pure Jdt/Ab-Ep rock/Chloritite	09SC8a3	Cpx	2475	VPSEM	PxNa	PxNa	83.70	1.97		0.85	0.05	0.00		0.12	0.12		0.93				0.00	6.00

Rock type	Sample	Phase	Point	serie	Px type	Px type	Jd mole%	Si	Ti	Al	Fe3+	Fe2+	Mn	Mg	Ca	Ba	Na	K	F	Cl	H	O
Pure Jdt/Ab-Ep rock/Chloritite	09SC8a3	Cpx	2477	VPSEM	PxNa	PxNa	84.92	1.97		0.87	0.04	0.00		0.11	0.12		0.91				0.00	6.00
Pure Jdt/Ab-Ep rock/Chloritite	09SC8a3	Cpx	2481	VPSEM	PxNa	PxNa	83.89	1.96		0.86	0.05	0.00		0.12	0.12		0.95				0.00	6.00
Pure Jdt/Ab-Ep rock/Chloritite	09SC8a3	Cpx	2482	VPSEM	PxNa	PxNa	83.08	1.96		0.85	0.05	0.00		0.12	0.13		0.93				0.00	6.00
Pure Jdt/Ab-Ep rock/Chloritite	09SC8a3	Cpx	2483	VPSEM	PxNa	PxNa	82.90	1.96		0.85	0.05	0.00		0.13	0.12		0.94				0.00	6.00
Pure Jdt/Chloritite	MCB3f	Cpx	3415	VPSEM	PxNaCa	PxNaCa	47.23	1.94	0.00	0.51	0.11	0.00	0.01	0.43	0.46		0.60	0.00		0.00	0.00	6.00
Pure Jdt/Chloritite	MCB3f	Cpx	3416	VPSEM	PxNaCa	PxNaCa	45.06	1.96	0.00	0.47	0.09	0.00	0.01	0.47	0.47		0.56	0.00		0.00	0.00	6.00
Pure Jdt/Chloritite	MCB3f	Cpx	3417	VPSEM	PxNaCa	PxNaCa	45.03	1.95	0.00	0.49	0.23	0.00	0.01	0.29	0.39		0.66	0.00		0.00	0.00	6.00
Pure Jdt/Chloritite	MCB3f	Cpx	3428	VPSEM	PxNaCa	PxNaCa	47.93	1.95	0.01	0.52	0.09	0.00	0.01	0.43	0.45		0.57	0.00		0.00	0.00	6.00
Pure Jdt/Chloritite	MCB3f	Cpx	3431	VPSEM	PxNaCa	PxNaCa	43.94	1.94	0.00	0.49	0.21	0.00	0.00	0.34	0.41		0.62	0.00		0.00	0.00	6.00
Pure Jdt/Chloritite	MCB3f	Cpx	3433	VPSEM	PxNaCa	PxNaCa	44.79	1.95	0.00	0.50	0.22	0.00	0.00	0.32	0.39		0.64	0.00		0.00	0.00	6.00
Pure Jdt/Chloritite	MCB3f	Cpx	3448	VPSEM	PxNaCa	PxNaCa	38.67	1.97	0.00	0.42	0.18	0.00	0.00	0.41	0.49		0.55	0.00		0.00	0.00	6.00
Pure Jdt/Chloritite	MCB3f	Cpx	3451	VPSEM	PxNaCa	PxNaCa	35.58	1.95	0.00	0.40	0.19	0.00	0.00	0.44	0.52		0.52	0.00		0.00	0.00	6.00
Pure Jdt/Chloritite	MCB3f	Cpx	3470	VPSEM	PxNaCa	PxNaCa	43.37	1.95	0.00	0.47	0.17	0.00	0.00	0.39	0.44		0.60	0.00		0.00	0.00	6.00
Pure Jdt/Chloritite	MCB3f	Cpx	3472	VPSEM	PxNaCa	PxNaCa	40.40	1.95	0.00	0.44	0.17	0.00	0.01	0.41	0.47		0.57	0.00		0.00	0.00	6.00
Pure Jdt/Chloritite	MCB3f	Cpx	3479	VPSEM	PxNaCa	PxNaCa	51.13	1.94	0.00	0.56	0.15	0.00	0.00	0.36	0.38		0.67	0.00		0.00	0.00	6.00
Pure Jdt/Chloritite	MCB3f	Cpx	3480	VPSEM	PxNaCa	PxNaCa	41.53	1.95	0.00	0.46	0.20	0.00	0.01	0.36	0.45		0.59	0.00		0.00	0.00	6.00
Pure Jdt/Chloritite	MCB3f	Cpx	3481	VPSEM	PxNaCa	PxNaCa	46.44	1.97	0.00	0.50	0.15	0.00	0.00	0.37	0.40		0.60	0.00		0.00	0.00	6.00
Pure Jdt/Chloritite	MCB3f	Cpx	3485	VPSEM	PxNaCa	PxNaCa	44.98	1.96	0.00	0.48	0.17	0.00	0.00	0.38	0.43		0.62	0.00		0.00	0.00	6.00
Pure Jdt/Chloritite	MCB3f	Cpx	3487	VPSEM	PxNaCa	PxNaCa	45.93	1.96	0.00	0.49	0.17	0.00	0.00	0.35	0.42		0.63	0.00		0.00	0.00	6.00
Pure Jdt/Chloritite	MCB3f	Cpx	3492	VPSEM	PxNaCa	PxNaCa	46.64	1.94	0.00	0.49	0.18	0.00	0.00	0.34	0.41		0.65	0.01		0.00	0.00	6.00
Pure Jdt/Chloritite	MCB3f	Cpx	3418	VPSEM	PxNa	PxNa	84.85	1.95	0.00	0.87	0.08	0.00	0.00	0.08	0.08		1.00	0.00		0.00	0.00	6.00
Pure Jdt/Chloritite	MCB3f	Cpx	3419	VPSEM	PxNa	PxNa	87.02	1.96	0.00	0.89	0.06	0.00	0.00	0.08	0.08		1.00	0.00		0.00	0.00	6.00
Pure Jdt/Chloritite	MCB3f	Cpx	3420	VPSEM	PxNa	PxNa	80.26	1.96	0.01	0.83	0.06	0.00	0.00	0.14	0.15		0.89	0.00		0.00	0.00	6.00
Pure Jdt/Chloritite	MCB3f	Cpx	3421	VPSEM	PxNa	PxNa	87.84	1.96	0.00	0.90	0.05	0.00	0.00	0.07	0.08		1.00	0.00		0.00	0.00	6.00
Pure Jdt/Chloritite	MCB3f	Cpx	3422	VPSEM	PxNa	PxNa	84.27	1.96	0.01	0.85	0.05	0.00	0.00	0.11	0.12		0.96	0.00		0.00	0.00	6.00
Pure Jdt/Chloritite	MCB3f	Cpx	3423	VPSEM	PxNa	PxNa	80.78	1.97	0.00	0.82	0.05	0.00	0.00	0.15	0.15		0.90	0.00		0.00	0.00	6.00
Pure Jdt/Chloritite	MCB3f	Cpx	3429	VPSEM	PxNa	PxNa	82.37	1.96	0.00	0.84	0.05	0.00	0.00	0.13	0.14		0.94	0.00		0.00	0.00	6.00
Pure Jdt/Chloritite	MCB3f	Cpx	3430	VPSEM	PxNa	PxNa	82.24	1.96	0.00	0.86	0.06	0.00	0.00	0.12	0.13		0.92	0.00		0.00	0.00	6.00
Pure Jdt/Chloritite	MCB3f	Cpx	3434	VPSEM	PxNa	PxNa	84.91	1.95	0.01	0.87	0.05	0.00	0.00	0.11	0.11		0.97	0.00		0.00	0.00	6.00
Pure Jdt/Chloritite	MCB3f	Cpx	3447	VPSEM	PxNa	PxNa	87.78	1.97	0.00	0.90	0.04	0.00	0.00	0.08	0.09		0.98	0.00		0.00	0.00	6.00
Pure Jdt/Chloritite	MCB3f	Cpx	3449	VPSEM	PxNa	PxNa	82.31	1.95	0.00	0.85	0.06	0.00	0.00	0.13	0.13		0.93	0.00		0.00	0.00	6.00
Pure Jdt/Chloritite	MCB3f	Cpx	3450	VPSEM	PxNa	PxNa	87.40	1.96	0.00	0.90	0.04	0.00	0.00	0.09	0.11		0.98	0.00		0.00	0.00	6.00
Pure Jdt/Chloritite	MCB3f	Cpx	3461	VPSEM	PxNa	PxNa	84.53	1.95	0.00	0.88	0.06	0.00	0.00	0.10	0.11		0.97	0.00		0.00	0.00	6.00
Pure Jdt/Chloritite	MCB3f	Cpx	3468	VPSEM	PxNa	PxNa	83.67	1.96	0.00	0.85	0.07	0.00	0.00	0.10	0.10		0.98	0.00		0.00	0.00	6.00
Pure Jdt/Chloritite	MCB3f	Cpx	3469	VPSEM	PxNa	PxNa	86.66	1.96	0.00	0.89	0.06	0.00	0.00	0.07	0.08		0.99	0.00		0.00	0.00	6.00
Pure Jdt/Chloritite	MCB3f	Cpx	3471	VPSEM	PxNa	PxNa	84.86	1.96	0.00	0.86	0.06	0.00	0.00	0.10	0.11		0.97	0.00		0.00	0.00	6.00
Pure Jdt/Chloritite	MCB3f	Cpx	3478	VPSEM	PxNa	PxNa	84.42	1.96	0.00	0.86	0.05	0.00	0.00	0.12	0.12		0.96	0.00		0.00	0.00	6.00
Pure Jdt/Chloritite	MCB3f	Cpx	3482	VPSEM	PxNa	PxNa	87.54	1.97	0.00	0.89	0.04	0.00	0.00	0.09	0.08		0.97	0.00		0.00	0.00	6.00
Pure Jdt/Chloritite	MCB3f	Cpx	3489	VPSEM	PxNa	PxNa	83.93	1.95	0.00	0.87	0.05	0.00	0.00	0.12	0.12		0.96	0.00		0.00	0.00	6.00
Pure Jdt/Chloritite	MCB3f	Cpx	3490	VPSEM	PxNa	PxNa	88.59	2.03	0.00	0.84	0.00	0.03	0.00	0.11	0.09		0.90	0.00		0.00	0.00	6.00
Pure Jdt/Chloritite	MCB3f	Cpx	3493	VPSEM	PxNa	PxNa	77.31	1.96	0.00	0.80	0.06	0.00	0.00	0.18	0.18		0.87	0.00		0.00	0.00	6.00
Ab-Ep rock	09SC27f	Ep	2132	SEM				3.08		2.47	0.55	0.00			1.81						1.00	13.00
Ab-Ep rock	09SC27f	Ep	2136	SEM				3.13		2.51	0.34	0.00			1.96						1.00	13.00
Ab-Ep rock	09SC27f	Ep	2137	SEM				3.08		2.54	0.43	0.00			1.89						1.00	13.00

Rock type	Sample	Phase	Point	serie	Px type	Px type	Jd mole%	Si	Ti	Al	Fe3+	Fe2+	Mn	Mg	Ca	Ba	Na	K	F	Cl	H	O
Ab-Ep rock	09SC31a	Ep	2255	SEM				3.00		2.90	0.09	0.00			2.01						1.00	13.00
Ab-Ep rock	09SC31a	Ep	2265	SEM				3.04		2.64	0.32	0.00			1.99						1.00	13.00
Ab-Ep rock	09SC31a	Ep	2268	SEM				2.99		2.76	0.26	0.00			1.99						1.00	13.00
Ab-Ep rock	09SC31a	Ep	2283	SEM				2.95		2.35	0.67	0.00			2.07						1.00	13.00
Ab-Ep rock	09SC31a	Ep	2293	SEM				3.11		2.37	0.50	0.00			1.97						1.00	13.00
Ab-Ep rock	09SC31a	Ep	2301	SEM				3.01		2.53	0.38	0.00			2.12						1.00	13.00
Ab-Ep rock	09SC31a	Ep	2303	SEM				3.03		2.75	0.21	0.00			2.01						1.00	13.00
Ab-Ep rock	09SC31c	Ep	2335	SEM				3.04		2.53	0.39	0.00			2.02						1.00	13.00
Ab-Ep rock	09SC31c	Ep	2338	SEM				3.12		2.55	0.31	0.00			1.97						1.00	13.00
Ab-Ep rock	09SC31c	Ep	2340	SEM				2.97		2.56	0.48	0.00			2.01						1.00	13.00
Ab-Ep rock	09SC31c	Ep	2346	SEM				3.12		2.48	0.41	0.00			1.92						1.00	13.00
Ab-Ep rock	09SC31c	Ep	2348	SEM				3.09		2.78	0.17	0.00			1.89						1.00	13.00
Ab-Ep rock	09SC31c	Ep	2352	SEM				3.14		2.77	0.07	0.00			1.95						1.00	13.00
Ab-Ep rock	09SC31c	Ep	2356	SEM				3.05		2.81	0.14	0.00			1.98						1.00	13.00
Ab-Ep rock	09SC31c	Ep	2358	SEM				3.09		2.74	0.15	0.00			1.97						1.00	13.00
Ab-Ep rock	09SC31c	Ep	2368	SEM				3.05		2.83	0.18	0.00			1.89						1.00	13.00
Ab-Ep rock	09SC31c	Ep	2379	SEM				3.17		2.46	0.47	0.00			1.78						1.00	13.00
Ab-Ep rock	09SC31c	Ep	2380	SEM				3.10		2.48	0.49	0.00			1.86						1.00	13.00
Ab-Ep rock	09SC31c	Ep	2381	SEM				3.19		2.43	0.52	0.00			1.70						1.00	13.00
Ab-Ep rock	09SC31c	Ep	2383	SEM				3.21		2.44	0.36	0.00			1.88						1.00	13.00
Ab-Ep rock	09SC31c	Ep	2385	SEM				3.02		2.56	0.40	0.00			2.03						1.00	13.00
Ab-Ep rock	09SC31d	Ep	1693	SEM				3.05		2.54	0.38	0.00			2.02						1.00	13.00
Ab-Ep rock	09SC31d	Ep	1702	SEM				3.07		2.82	0.13	0.00			1.94						1.00	13.00
Ab-Ep rock	09SC31d	Ep	1703	SEM				3.08		2.65	0.31	0.00			1.89						1.00	13.00
Ab-Ep rock	09SC31d	Ep	1719	SEM				3.04		3.00	0.01	0.00			1.90						1.00	13.00
Ab-Ep rock	09SC31d	Ep	1720	SEM				3.09		2.88	0.09	0.00			1.86						1.00	13.00
Ab-Ep rock	09SC31d	Ep	1725	SEM				3.07		2.93	0.08	0.00			1.85						1.00	13.00
Ab-Ep rock	09SC31d	Ep	1739	SEM				3.12		2.46	0.44	0.00			1.91						1.00	13.00
Ab-Ep rock	09SC31d	Ep	1741	SEM				3.08		2.38	0.56	0.00			1.93						1.00	13.00
Ab-Ep rock	09SC31d	Ep	1760	SEM				3.05		2.46	0.50	0.00			1.97						1.00	13.00
Ab-Ep rock	09SC31d	Ep	1763	SEM				3.08		2.72	0.22	0.00			1.93						1.00	13.00
Ab-Ep rock	09SC31n	Ep	1838	SEM				2.99		2.74	0.25	0.00			2.04						1.00	13.00
Ab-Ep rock	09SC31n	Ep	1845	SEM				3.10		2.58	0.28	0.00			2.00						1.00	13.00
Ab-Ep rock	09SC31n	Ep	1858	SEM				2.99		2.65	0.36	0.00			2.00						1.00	13.00
Ab-Ep rock	09SC31n	Ep	1859	SEM				3.01		2.79	0.21	0.00			1.98						1.00	13.00
Ab-Ep rock	09SC31n	Ep	1861	SEM				3.04		2.82	0.15	0.00			1.95						1.00	13.00
Ab-Ep rock	09SC31n	Ep	1867	SEM				3.02		2.54	0.46	0.00			1.96						1.00	13.00
Ab-Ep rock	09SC31n	Ep	1879	SEM				2.98		2.83	0.15	0.00			2.08						1.00	13.00
Ab-Ep rock	09SC31n	Ep	1881	SEM				3.01		2.69	0.31	0.00			2.00						1.00	13.00
Ab-Ep rock	09SC31n	Ep	1890	SEM				3.05		2.73	0.27	0.00			1.90						1.00	13.00
Ab-Ep rock	09SC31n	Ep	1893	SEM				3.03		2.63	0.36	0.00			1.96						1.00	13.00
Ab-Ep rock	09SC31n	Ep	1894	SEM				3.07		2.72	0.29	0.00			1.84						1.00	13.00
Ab-Ep rock	MCB1a	Ep	2970	VPSEM				2.97	0.00	2.98	0.06	0.00	0.00	0.00	2.00		0.00	0.00			1.00	13.00
Ab-Ep rock	MCB1a	Ep	2975	VPSEM				2.96	0.00	2.67	0.38	0.00	0.00	0.00	2.00		0.00	0.00			1.00	13.00

Rock type	Sample	Phase	Point	serie	Px type	Px type	Jd mole%	Si	Ti	Al	Fe3+	Fe2+	Mn	Mg	Ca	Ba	Na	K	F	Cl	H	O
Ab-Ep rock	MCB1a	Ep	2977	VPSEM				3.02	0.00	2.99	0.00	0.00	0.00	0.00	1.97		0.00	0.03			1.00	13.00
Ab-Ep rock	MCB1a	Ep	2979	VPSEM				2.92	0.00	3.05	0.05	0.00	0.00	0.00	2.01		0.00	0.00			1.00	13.00
Ab-Ep rock	MCB1a	Ep	2981	VPSEM				2.93	0.00	3.10	0.00	0.00	0.00	0.00	1.98		0.00	0.00			1.00	13.00
Ab-Ep rock	MCB1a	Ep	2983	VPSEM				2.96	0.00	2.97	0.09	0.00	0.00	0.00	2.01		0.00	0.00			1.00	13.00
Ab-Ep rock	MCB1a	Ep	2988	VPSEM				2.97	0.00	2.99	0.07	0.00	0.00	0.00	1.97		0.00	0.00			1.00	13.00
Ab-Ep rock	MCB1a	Ep	2989	VPSEM				2.96	0.00	3.01	0.05	0.00	0.00	0.00	2.00		0.00	0.00			1.00	13.00
Ab-Ep rock	MCB1a	Ep	2991	VPSEM				2.96	0.00	2.96	0.10	0.00	0.00	0.00	2.00		0.00	0.00			1.00	13.00
Ab-Ep rock	MCB1a	Ep	2995	VPSEM				2.98	0.00	2.99	0.05	0.00	0.00	0.00	1.98		0.00	0.00			1.00	13.00
Ab-Ep rock	MCB1a	Ep	2997	VPSEM				2.96	0.00	2.88	0.17	0.00	0.00	0.00	2.01		0.00	0.00			1.00	13.00
Ab-Ep rock	MCB1a	Ep	3001	VPSEM				2.95	0.00	3.04	0.03	0.00	0.00	0.00	1.99		0.00	0.00			1.00	13.00
Ab-Ep rock	MCB1a	Ep	3006	VPSEM				2.96	0.00	3.00	0.09	0.00	0.00	0.00	1.95		0.00	0.00			1.00	13.00
Ab-Ep rock	MCB1a	Ep	3008	VPSEM				2.94	0.00	3.02	0.08	0.00	0.00	0.00	1.97		0.00	0.00			1.00	13.00
Ab-Ep rock	MCB1a	Ep	3012	VPSEM				2.90	0.00	3.07	0.06	0.00	0.00	0.00	1.99		0.00	0.00			1.00	13.00
Ab-Ep rock	MCB1a	Ep	3015	VPSEM				2.99	0.00	2.99	0.05	0.00	0.00	0.00	1.97		0.00	0.00			1.00	13.00
Ab-Ep rock	MCB1a	Ep	3019	VPSEM				2.96	0.00	3.02	0.08	0.00	0.00	0.00	1.92		0.00	0.00			1.00	13.00
Ab-Ep rock	MCB1a	Ep	3025	VPSEM				2.95	0.00	3.01	0.08	0.00	0.00	0.00	1.96		0.00	0.01			1.00	13.00
Ab-Ep rock	MCB1a	Ep	3027	VPSEM				2.99	0.00	2.69	0.33	0.00	0.00	0.00	2.00		0.00	0.00			1.00	13.00
Ab-Ep rock	MCB1a	Ep	3029	VPSEM				2.99	0.00	3.01	0.04	0.00	0.00	0.00	1.95		0.00	0.00			1.00	13.00
Ab-Ep rock	MCB1a	Ep	3033	VPSEM				2.98	0.00	2.98	0.04	0.00	0.00	0.00	2.02		0.00	0.00			1.00	13.00
Ab-Ep rock	MCB1a	Ep	3034	VPSEM				2.98	0.00	2.99	0.04	0.00	0.00	0.00	1.99		0.00	0.00			1.00	13.00
Ab-Ep rock	MCB1a	Ep	3036	VPSEM				2.94	0.00	3.05	0.04	0.00	0.00	0.00	1.98		0.00	0.00			1.00	13.00
Ab-Ep rock	MCB1a	Ep	3041	VPSEM				2.98	0.00	3.00	0.03	0.00	0.00	0.00	1.98		0.00	0.00			1.00	13.00
Ab-Ep rock	MCB1a	Ep	3042	VPSEM				2.98	0.00	3.01	0.04	0.00	0.00	0.00	1.96		0.00	0.00			1.00	13.00
Ab-Ep rock	MCB1a	Ep	3045	VPSEM				2.93	0.00	3.03	0.05	0.00	0.00	0.00	2.01		0.00	0.00			1.00	13.00
Ab-Ep rock	MCB1a	Ep	3046	VPSEM				2.99	0.00	3.03	0.00	0.00	0.00	0.00	1.99		0.00	0.00			1.00	13.00
Ab-Ep rock	MCB1a	Ep	3052	VPSEM				2.93	0.00	3.05	0.03	0.00	0.00	0.00	2.01		0.00	0.00			1.00	13.00
Ab-Ep rock	MCB1a	Ep	3054	VPSEM				2.95	0.00	2.98	0.09	0.00	0.00	0.00	1.99		0.00	0.00			1.00	13.00
Ab-Ep rock	MCB1a	Ep	3059	VPSEM				2.94	0.00	3.03	0.05	0.00	0.03	0.00	1.96		0.00	0.00			1.00	13.00
Ab-Ep rock	MCB1a	Ep	3060	VPSEM				2.95	0.00	3.03	0.03	0.00	0.00	0.00	2.01		0.00	0.00			1.00	13.00
Ab-Ep rock	MCB1a	Ep	3063	VPSEM				2.95	0.02	2.99	0.06	0.00	0.00	0.00	1.98		0.00	0.00			1.00	13.00
Ab-Ep rock	MCB1a	Ep	3065	VPSEM				2.93	0.00	3.07	0.06	0.00	0.00	0.00	1.95		0.00	0.00			1.00	13.00
Ab-Ep rock	MCB1a	Ep	3067	VPSEM				2.95	0.00	3.00	0.08	0.00	0.00	0.00	1.99		0.00	0.00			1.00	13.00
Ab-Ep rock	MCB1a	Ep	3071	VPSEM				2.94	0.00	3.03	0.06	0.00	0.00	0.00	1.96		0.00	0.00			1.00	13.00
Ab-Ep rock	MCB1a	Ep	3074	VPSEM				2.98	0.00	2.89	0.14	0.00	0.00	0.00	2.01		0.00	0.00			1.00	13.00
Ab-Ep rock	MCB1a	Ep	3078	VPSEM				2.97	0.00	2.72	0.35	0.00	0.00	0.00	1.97		0.00	0.00			1.00	13.00
Ab-Ep rock	MCB1a	Ep	3081	VPSEM				2.95	0.00	2.84	0.23	0.00	0.00	0.00	2.01		0.00	0.00			1.00	13.00
Ab-Ep rock	MCB1a	Ep	3084	VPSEM				2.94	0.00	3.06	0.05	0.00	0.00	0.00	1.95		0.00	0.00			1.00	13.00
Ab-Ep rock	MCB1a	Ep	3088	VPSEM				2.95	0.00	2.99	0.08	0.00	0.00	0.00	2.00		0.00	0.00			1.00	13.00
Ab-Ep rock	MCB1a	Ep	3090	VPSEM				2.96	0.00	2.99	0.10	0.00	0.00	0.00	1.95		0.00	0.00			1.00	13.00
Ab-Ep rock	MCB1a	Ep	3092	VPSEM				2.94	0.00	2.95	0.14	0.00	0.00	0.00	1.99		0.00	0.00			1.00	13.00
Ab-Ep rock	MCB1e	Ep	34	EPMA				2.99	0.00	2.82	0.16	0.00	0.00	0.01	2.03		0.00	0.00	0.03	0.00	0.97	12.97
Ab-Ep rock	MCB1e	Ep	47	EPMA				2.95	0.00	2.90	0.14	0.00	0.00	0.01	2.02		0.00	0.00	0.02	0.00	0.98	12.98
Ab-Ep rock	MCB1e	Ep	48	EPMA				2.98	0.00	2.96	0.04	0.00	0.01	0.00	2.02		0.00	0.00	0.01	0.00	0.99	12.99
Ab-Ep rock	MCB1e	Ep	50	EPMA				3.00	0.00	2.95	0.02	0.00	0.00	0.00	2.03		0.00	0.00	0.02	0.00	0.98	12.98

Rock type	Sample	Phase	Point	serie	Px type	Px type	Jd mole%	Si	Ti	Al	Fe3+	Fe2+	Mn	Mg	Ca	Ba	Na	K	F	Cl	H	O
Ab-Ep rock	MCB1e	Ep	51	EPMA				3.00	0.00	2.95	0.03	0.00	0.00	0.00	2.02		0.01	0.00	0.01	0.00	0.99	12.99
Ab-Ep rock	MCB1e	Ep	52	EPMA				3.05	0.00	2.56	0.37	0.00	0.01	0.00	1.98		0.00	0.00	0.04	0.00	0.96	12.96
Ab-Ep rock	MCB1e	Ep	53	EPMA				2.98	0.00	2.94	0.05	0.00	0.00	0.00	2.04		0.00	0.00	0.03	0.00	0.97	12.97
Ab-Ep rock	MCB1e	Ep	3093	VPSEM				2.98	0.00	2.61	0.45	0.00	0.00	0.00	1.97		0.00	0.00			1.00	13.00
Ab-Ep rock	MCB1e	Ep	3094	VPSEM				3.00	0.00	2.56	0.48	0.00	0.00	0.00	1.94		0.00	0.00			1.00	13.00
Ab-Ep rock	MCB1e	Ep	3112	VPSEM				2.96	0.00	2.97	0.07	0.00	0.00	0.03	1.98		0.00	0.00			1.00	13.00
Ab-Ep rock	MCB1e	Ep	3116	VPSEM				2.96	0.00	2.98	0.09	0.00	0.00	0.00	1.99		0.00	0.00			1.00	13.00
Ab-Ep rock	MCB1e	Ep	3117	VPSEM				2.95	0.00	2.92	0.14	0.00	0.00	0.00	2.02		0.00	0.00			1.00	13.00
Ab-Ep rock	MCB1e	Ep	3119	VPSEM				2.95	0.02	2.63	0.43	0.00	0.00	0.00	1.97		0.00	0.00			1.00	13.00
Ab-Ep rock	MCB1e	Ep	3121	VPSEM				2.96	0.00	3.02	0.05	0.00	0.00	0.00	1.98		0.00	0.00			1.00	13.00
Ab-Ep rock	MCB1e	Ep	3122	VPSEM				2.97	0.00	2.96	0.10	0.00	0.00	0.00	1.98		0.00	0.00			1.00	13.00
Ab-Ep rock	MCB1e	Ep	3128	VPSEM				2.95	0.00	3.06	0.04	0.00	0.00	0.00	1.96		0.00	0.00			1.00	13.00
Ab-Ep rock	MCB1e	Ep	3132	VPSEM				2.98	0.00	3.00	0.06	0.00	0.00	0.00	1.96		0.00	0.00			1.00	13.00
Ab-Ep rock	MCB1e	Ep	3134	VPSEM				2.97	0.00	3.05	0.00	0.00	0.00	0.00	1.99		0.00	0.00			1.00	13.00
Ab-Ep rock	MCB1e	Ep	3138	VPSEM				2.97	0.00	3.03	0.02	0.00	0.00	0.00	1.98		0.00	0.00			1.00	13.00
Ab-Ep rock	MCB1e	Ep	3143	VPSEM				2.93	0.00	2.74	0.36	0.00	0.00	0.00	1.98		0.00	0.00			1.00	13.00
Ab-Ep rock/Chloritite	09SC31i	Ep	1986	SEM				3.11		2.50	0.35	0.00			2.00						1.00	13.00
Ab-Ep rock/Chloritite	09SC31i	Ep	1989	SEM				3.01		2.60	0.30	0.00			2.12						1.00	13.00
Ab-Ep rock/Chloritite	09SC31i	Ep	1995	SEM				2.89		2.73	0.33	0.00			2.14						1.00	13.00
Ab-Ep rock/Chloritite	09SC31i	Ep	1996	SEM				2.93		2.88	0.14	0.00			2.11						1.00	13.00
Ab-Ep rock/Chloritite	09SC31i	Ep	1998	SEM				3.04		2.80	0.16	0.00			1.98						1.00	13.00
Ab-Ep rock/Chloritite	09SC31i	Ep	2007	SEM				3.07		2.61	0.24	0.00			2.09						1.00	13.00
Ab-Ep rock/Chloritite	09SC31i	Ep	2008	SEM				2.97		2.76	0.28	0.00			2.00						1.00	13.00
Ab-Ep rock/Chloritite	09SC31i	Ep	2009	SEM				2.95		2.67	0.30	0.00			2.15						1.00	13.00
Ab-Ep rock/Chloritite	09SC31i	Ep	2016	SEM				2.93		2.80	0.22	0.00			2.11						1.00	13.00
Ab-Ep rock/Chloritite	09SC31i	Ep	2020	SEM				2.84		2.80	0.30	0.00			2.19						1.00	13.00
Ab-Ep rock/Chloritite	09SC31i	Ep	2021	SEM				3.07		2.77	0.20	0.00			1.92						1.00	13.00
Ab-Ep rock/Chloritite	09SC31i	Ep	2027	SEM				2.99		2.64	0.34	0.00			2.05						1.00	13.00
Ab-Ep rock/Chloritite	09SC31i	Ep	2028	SEM				3.05		2.73	0.23	0.00			1.96						1.00	13.00
Ab-Ep rock/Chloritite	09SC31i	Ep	2032	SEM				3.08		2.67	0.27	0.00			1.93						1.00	13.00
Ab-Ep rock/Chloritite	09SC31i	Ep	2034	SEM				3.00		2.60	0.41	0.00			1.97						1.00	13.00
Ab-Ep rock/Chloritite	09SC31i	Ep	2035	SEM				3.00		2.66	0.35	0.00			1.99						1.00	13.00
Ab-Ep rock/Chloritite	09SC31i	Ep	2047	SEM				3.08		2.54	0.28	0.00			2.13						1.00	13.00
Cr-rich Pure Jdt	SCMJ10	Ep	3651	VPSEM				2.99	0.00	2.89	0.15	0.00	0.00	0.00	1.96		0.00	0.00			1.00	13.00
Ep-rich jadeitite	09SC27c	Ep	2241	SEM				3.04		2.95	0.00	0.00			1.99						1.00	13.00
Ep-rich jadeitite	09SC27c	Ep	2247	SEM				3.09		2.41	0.46	0.00			2.01						1.00	13.00
Ep-rich jadeitite	09SC27m	Ep	2060	SEM				3.07		2.36	0.52	0.00			2.03						1.00	13.00
Ep-rich jadeitite	09SC27m	Ep	2078	SEM				3.04		2.54	0.49	0.00			1.86						1.00	13.00
Ep-rich jadeitite	09SC27m	Ep	2079	SEM				3.15		2.41	0.43	0.00			1.95						1.00	13.00
Ep-rich jadeitite	09SC27m	Ep	2086	SEM				3.01		2.66	0.39	0.00			1.91						1.00	13.00
Ep-rich jadeitite	09SC27m	Ep	2090	SEM				3.15		2.46	0.38	0.00			1.94						1.00	13.00
Ep-rich jadeitite	09SC27m	Ep	2093	SEM				2.97		2.52	0.54	0.00			1.98						1.00	13.00
Ep-rich jadeitite	09SC27m	Ep	2094	SEM				3.17		2.39	0.43	0.00			1.91						1.00	13.00
Ep-rich jadeitite	09SC27m	Ep	2100	SEM				3.05		2.46	0.45	0.00			2.04						1.00	13.00

Rock type	Sample	Phase	Point	serie	Px type	Px type	Jd mole%	Si	Ti	Al	Fe3+	Fe2+	Mn	Mg	Ca	Ba	Na	K	F	Cl	H	O
Ep-rich jadeitite	09SC27m	Ep	2101	SEM				3.01		2.43	0.55	0.00			2.01						1.00	13.00
Ep-rich jadeitite	09SC27m	Ep	2114	SEM				3.16		2.49	0.34	0.00			1.93						1.00	13.00
Ep-rich jadeitite	09SC27m	Ep	2118	SEM				3.03		2.49	0.42	0.00			2.07						1.00	13.00
Ep-rich jadeitite	09SC27m	Ep	2127	SEM				3.12		2.34	0.49	0.00			2.02						1.00	13.00
Ep-rich jadeitite	09SC31g	Ep	1779	SEM				3.14		2.60	0.31	0.00			1.85						1.00	13.00
Ep-rich jadeitite	09SC31g	Ep	1782	SEM				2.98		2.69	0.36	0.00			1.95						1.00	13.00
Ep-rich jadeitite	09SC31g	Ep	1793	SEM				3.00		2.67	0.40	0.00			1.91						1.00	13.00
Ep-rich jadeitite	09SC31g	Ep	1801	SEM				3.05		2.56	0.38	0.00			1.99						1.00	13.00
Ep-rich jadeitite	09SC31g	Ep	1972	SEM				3.15		2.50	0.34	0.00			1.94						1.00	13.00
Ep-rich Jadeitite	MCB1d	Ep	217	EPMA				3.00	0.00	2.98	0.04	0.00	0.00	0.00	1.96		0.00	0.00	0.02	0.00	0.97	12.97
Ep-rich Jadeitite	MCB1d	Ep	218	EPMA				3.00	0.00	2.90	0.11	0.00	0.00	0.01	1.97		0.01	0.00	0.01	0.00	0.99	12.99
Ep-rich Jadeitite	MCB1d	Ep	219	EPMA				3.02	0.00	2.91	0.11	0.00	0.00	0.00	1.94		0.00	0.00	0.02	0.00	0.98	12.98
Ep-rich Jadeitite	MCB1d	Ep	220	EPMA				2.99	0.00	2.94	0.07	0.00	0.00	0.00	2.00		0.00	0.00	0.01	0.00	0.99	12.99
Ep-rich Jadeitite	MCB1d	Ep	236	EPMA				2.97	0.01	2.64	0.35	0.00	0.01	0.01	2.04		0.00	0.00	0.04	0.00	0.96	12.96
Ep-rich jadeitite	MCB1d	Ep	1513	VPSEM				2.95		2.83	0.23	0.00			2.01						1.00	13.00
Ep-rich jadeitite	MCB1d	Ep	1514	VPSEM				2.98		3.00	0.04	0.00			1.98						1.00	13.00
Ep-rich jadeitite	MCB1d	Ep	1517	VPSEM				2.98		2.93	0.12	0.00			1.96						1.00	13.00
Ep-rich jadeitite	MCB1d	Ep	1518	VPSEM				3.00		2.52	0.53	0.00			1.91						1.00	13.00
Ep-rich jadeitite	MCB1d	Ep	1528	VPSEM				2.96	0.00	2.73	0.28	0.00	0.02		2.04						1.00	13.00
Ep-rich jadeitite	MCB1d	Ep	1529	VPSEM				2.96		3.00	0.00	0.00			2.08						1.00	13.00
Ep-rich jadeitite	MCB1d	Ep	1530	VPSEM				2.95		2.98	0.05	0.00			2.05						1.00	13.00
Ep-rich jadeitite	MCB1d	Ep	1531	VPSEM				2.94		2.86	0.19	0.00			2.04						1.00	13.00
Ep-rich jadeitite	MCB1d	Ep	1533	VPSEM				2.97		2.94	0.06	0.00			2.07						1.00	13.00
Ep-rich jadeitite	MCB1d	Ep	1534	VPSEM				2.93		3.04	0.02	0.00			2.07						1.00	13.00
Ep-rich jadeitite	MCB1d	Ep	1535	VPSEM				2.93		2.86	0.20	0.00			2.04						1.00	13.00
Ep-rich jadeitite	MCB1d	Ep	1536	VPSEM				3.00		2.62	0.43	0.00			1.92						1.00	13.00
Ep-rich jadeitite	MCB1d	Ep	1539	VPSEM				2.96	0.03	2.64	0.43	0.00			1.91						1.00	13.00
Ep-rich jadeitite	MCB1d	Ep	1541	VPSEM				2.97	0.02	2.62	0.42	0.00	0.02		1.94						1.00	13.00
Ep-rich jadeitite	MCB1d	Ep	1568	VPSEM				2.95		2.66	0.35	0.00			2.07						1.00	13.00
Ep-rich jadeitite	MCB1d	Ep	1569	VPSEM				2.96		2.68	0.35	0.00			2.02						1.00	13.00
Ep-rich jadeitite	MCB1d	Ep	1571	VPSEM				2.96		2.48	0.56	0.00			2.01						1.00	13.00
Ep-rich jadeitite	MCB1d	Ep	1572	VPSEM				2.96		2.67	0.34	0.00			2.05						1.00	13.00
Ep-rich jadeitite	MCB1d	Ep	1591	VPSEM				2.91		2.94	0.13	0.00			2.08						1.00	13.00
Ep-rich jadeitite	MCB1d	Ep	1598	VPSEM				2.93		2.68	0.34	0.00			2.11						1.00	13.00
Ep-rich jadeitite	MCB1d	Ep	1599	VPSEM				2.95		2.56	0.49	0.00			2.03						1.00	13.00
Ep-rich jadeitite	MCB1d	Ep	1601	VPSEM				2.97		2.87	0.14	0.00			2.05						1.00	13.00
Ep-rich jadeitite	MCB1d	Ep	1604	VPSEM				3.00		2.90	0.10	0.00			1.97		0.05				1.00	13.00
Ep-rich jadeitite	MCB1d	Ep	1605	VPSEM				2.96		2.89	0.13	0.00			2.05						1.00	13.00
Ep-rich jadeitite	MCB1d	Ep	1619	VPSEM				2.99		2.70	0.34	0.00			1.95						1.00	13.00
Ep-rich jadeitite	MCB1d	Ep	1620	VPSEM				2.95		2.53	0.48	0.00			2.09						1.00	13.00
Ep-rich jadeitite	MCB1d	Ep	1624	VPSEM				2.98		2.65	0.43	0.00			1.94						1.00	13.00
Ep-rich jadeitite	MCB1d	Ep	1627	VPSEM				2.96		2.63	0.37	0.00			2.08						1.00	13.00
Ep-rich jadeitite	MCB1d	Ep	1632	VPSEM				2.94		2.63	0.39	0.00			2.09						1.00	13.00
Ep-rich jadeitite	MCB1d	Ep	1635	VPSEM				2.95	0.02	2.64	0.36	0.00	0.02		2.05						1.00	13.00

Rock type	Sample	Phase	Point	serie	Px type	Px type	Jd mole%	Si	Ti	Al	Fe3+	Fe2+	Mn	Mg	Ca	Ba	Na	K	F	Cl	H	O
Ep-rich jadeitite	MCB1d	Ep	1636	VPSEM				2.98		2.86	0.15	0.00			2.00		0.04				1.00	13.00
Ep-rich jadeitite	MCB1d	Ep	1637	VPSEM				2.96		2.83	0.26	0.00			1.95						1.00	13.00
Ep-rich jadeitite	MCB1d	Ep	1640	VPSEM				2.95		3.00	0.05	0.00			2.02						1.00	13.00
Ep-rich jadeitite	MCB1d	Ep	1641	VPSEM				2.93		2.86	0.25	0.00			1.98						1.00	13.00
Ep-rich jadeitite	MCB1d	Ep	1643	VPSEM				2.95		2.66	0.36	0.00			2.06						1.00	13.00
Ep-rich jadeitite	MCB1d	Ep	1655	VPSEM				2.97	0.02	2.63	0.44	0.00			1.93						1.00	13.00
Ep-rich jadeitite	MCB1d	Ep	1656	VPSEM				2.93		2.92	0.13	0.00			2.07						1.00	13.00
Ep-rich jadeitite	MCB1d	Ep	1661	VPSEM				2.94		2.68	0.35	0.00			2.08						1.00	13.00
Ep-rich jadeitite	MCB1d	Ep	1663	VPSEM				2.95		2.65	0.37	0.00			2.06						1.00	13.00
Ep-rich jadeitite	MCB1d	Ep	1665	VPSEM				2.98		3.02	0.04	0.00			1.95						1.00	13.00
Ep-rich jadeitite	MCB1d	Ep	1669	VPSEM				2.94		2.70	0.34	0.00			2.07						1.00	13.00
Ep-rich jadeitite	MCB1d	Ep	1675	VPSEM				2.95		2.67	0.39	0.00			2.01						1.00	13.00
Ep-rich jadeitite	MCB1d	Ep	1677	VPSEM				2.96		2.83	0.24	0.00			1.97						1.00	13.00
Ep-rich jadeitite	MCB1d	Ep	1683	VPSEM				2.98		2.92	0.13	0.00			1.96			0.01			1.00	13.00
Ep-rich jadeitite	MCB1d	Ep	1688	VPSEM				2.97		2.67	0.34	0.00			2.04						1.00	13.00
Ep-rich jadeitite	MCB1g	Ep	3288	VPSEM				2.99	0.00	2.97	0.13	0.00	0.00	0.00	1.87		0.00	0.00			1.00	13.00
Ep-rich jadeitite	MCB1g	Ep	3298	VPSEM				2.99	0.00	3.06	0.02	0.00	0.00	0.00	1.91		0.00	0.00			1.00	13.00
Ep-rich jadeitite	MCB1g	Ep	3308	VPSEM				2.98	0.00	2.92	0.18	0.00	0.00	0.00	1.89		0.00	0.00			1.00	13.00
Ep-rich jadeitite	MCB1g	Ep	3313	VPSEM				2.97	0.00	2.96	0.14	0.00	0.00	0.00	1.91		0.00	0.00			1.00	13.00
Ep-rich jadeitite	MCB1g	Ep	3314	VPSEM				3.03	0.00	2.77	0.29	0.00	0.00	0.00	1.84		0.00	0.00			1.00	13.00
Ep-rich jadeitite	MCB1g	Ep	3322	VPSEM				3.01	0.00	2.74	0.28	0.00	0.00	0.05	1.90		0.00	0.00			1.00	13.00
Ep-rich jadeitite	MCB1g	Ep	3327	VPSEM				2.98	0.00	2.94	0.12	0.00	0.00	0.00	1.95		0.00	0.00			1.00	13.00
Ep-rich jadeitite	MCB1g	Ep	3332	VPSEM				3.00	0.00	2.96	0.15	0.00	0.00	0.00	1.82		0.00	0.00			1.00	13.00
Ep-rich jadeitite	MCB1g	Ep	3338	VPSEM				2.99	0.00	3.00	0.06	0.00	0.00	0.00	1.92		0.00	0.00			1.00	13.00
Ep-rich jadeitite	MCB1g	Ep	3342	VPSEM				2.94	0.00	2.66	0.36	0.00	0.00	0.00	2.04		0.08	0.02			1.00	13.00
Ep-rich jadeitite	MCB1g	Ep	3345	VPSEM				2.97	0.00	2.62	0.41	0.00	0.00	0.00	2.02		0.00	0.00			1.00	13.00
Ep-rich jadeitite	MCB1g	Ep	3349	VPSEM				2.97	0.00	2.96	0.08	0.00	0.00	0.00	1.99		0.00	0.00			1.00	13.00
Ep-rich jadeitite	MCB1g	Ep	3352	VPSEM				2.97	0.00	2.85	0.27	0.00	0.00	0.00	1.87		0.00	0.00			1.00	13.00
Ep-rich jadeitite	MCB1g	Ep	3357	VPSEM				2.95	0.00	2.92	0.17	0.00	0.00	0.00	1.97		0.00	0.00			1.00	13.00
Ep-rich jadeitite	MCB2c	Ep	3365	VPSEM				2.97	0.00	2.72	0.33	0.00	0.00	0.00	2.00		0.00	0.00			1.00	13.00
Ep-rich jadeitite	MCB2c	Ep	3373	VPSEM				2.99	0.00	2.65	0.36	0.00	0.00	0.00	1.99		0.00	0.00			1.00	13.00
Ep-rich jadeitite	MCB2c	Ep	3391	VPSEM				2.97	0.00	3.01	0.07	0.00	0.00	0.00	1.96		0.00	0.00			1.00	13.00
Ep-rich jadeitite	MCB2c	Ep	3393	VPSEM				2.99	0.00	2.75	0.29	0.00	0.00	0.00	1.95		0.00	0.00			1.00	13.00
Ep-rich jadeitite	MCB2c	Ep	3397	VPSEM				2.94	0.00	2.94	0.13	0.00	0.00	0.04	1.96		0.00	0.00			1.00	13.00
Ep-rich jadeitite	MCB2c	Ep	3403	VPSEM				2.98	0.00	3.03	0.00	0.00	0.00	0.00	1.99		0.00	0.00			1.00	13.00
Ep-rich jadeitite	MCB2c	Ep	3406	VPSEM				2.97	0.00	3.03	0.05	0.00	0.00	0.00	1.94		0.00	0.00			1.00	13.00
Ep-rich jadeitite	MCB2c	Ep	3408	VPSEM				2.96	0.00	2.90	0.13	0.00	0.00	0.00	2.00		0.09	0.00			1.00	13.00
Ep-rich jadeitite	MCB4a	Ep	1405	EPMA				2.98	0.01	2.71	0.30	0.00	0.00	0.01	2.00		0.00	0.00	0.02	0.00	0.98	12.98
Ep-rich jadeitite	MCB4a	Ep	1406	EPMA				2.99	0.01	2.71	0.30	0.00	0.00	0.01	1.99		0.00	0.00	0.03	0.00	0.97	12.97
Ep-rich jadeitite	MCB4a	Ep	1407	EPMA				2.99	0.01	2.77	0.25	0.00	0.00	0.01	1.95		0.01	0.00	0.03	0.00	0.97	12.97
Ep-rich jadeitite	MCB4a	Ep	1408	EPMA				2.98	0.01	2.70	0.31	0.00	0.00	0.01	2.00		0.01	0.00	0.03	0.00	0.97	12.97
Ep-rich jadeitite	MCB4a	Ep	1410	EPMA				2.99	0.00	2.88	0.14	0.00	0.00	0.01	1.98		0.01	0.00	0.03	0.00	0.97	12.97
Ep-rich jadeitite	MCB4a	Ep	1411	EPMA				2.99	0.00	2.88	0.14	0.00	0.00	0.01	1.97		0.01	0.00	0.04	0.00	0.96	12.96
Ep-rich jadeitite	MCB4a	Ep	1412	EPMA				2.99	0.00	2.87	0.15	0.00	0.00	0.01	1.96		0.01	0.00	0.03	0.00	0.97	12.97

Rock type	Sample	Phase	Point	serie	Px type	Px type	Jd mole%	Si	Ti	Al	Fe3+	Fe2+	Mn	Mg	Ca	Ba	Na	K	F	Cl	H	O
Ep-rich jadeitite	MCB4a	Ep	1413	EPMA				2.98	0.01	2.97	0.02	0.00	0.00	0.00	2.02		0.01	0.00	0.02	0.00	0.98	12.98
Ep-rich jadeitite	MCB4a	Ep	1414	EPMA				2.98	0.00	2.89	0.14	0.00	0.00	0.01	1.97		0.01	0.00	0.03	0.00	0.97	12.97
Ep-rich jadeitite	MCB4a	Ep	1415	EPMA				2.98	0.02	2.96	0.02	0.00	0.00	0.00	2.02		0.02	0.00	0.02	0.00	0.98	12.98
Ep-rich jadeitite	MCB4a	Ep	1417	EPMA				2.98	0.00	2.89	0.12	0.00	0.00	0.00	2.01		0.00	0.00	0.03	0.00	0.97	12.97
Ep-rich jadeitite	MCB4a	Ep	1418	EPMA				2.99	0.00	2.96	0.04	0.00	0.00	0.00	2.02		0.00	0.00	0.02	0.00	0.98	12.98
Ep-rich jadeitite	MCB4a	Ep	1419	EPMA				2.99	0.00	2.84	0.15	0.00	0.00	0.00	2.02		0.00	0.00	0.02	0.00	0.97	12.97
Ep-rich jadeitite	MCB4a	Ep	1444	VPSEM				3.12		2.61	0.31	0.00			1.88						1.00	13.00
Ep-rich jadeitite	MCB4a	Ep	1447	VPSEM				3.12		2.88	0.07	0.00			1.84						1.00	13.00
Ep-rich jadeitite	MCB4a	Ep	1455	VPSEM				3.11		2.85	0.09	0.00			1.87						1.00	13.00
Ep-rich jadeitite	MCB4a	Ep	1457	VPSEM				3.11		2.87	0.07	0.00			1.86						1.00	13.00
Ep-rich jadeitite	MCB4a	Ep	1468	VPSEM				3.11		2.83	0.11	0.00			1.88						1.00	13.00
Ep-rich jadeitite	MCB4a	Ep	1469	VPSEM				3.10		2.86	0.09	0.00			1.89						1.00	13.00
Ep-rich jadeitite	MCB4a	Ep	1492	VPSEM				3.12		2.67	0.24	0.00			1.89						1.00	13.00
Mica-rich Jadeitite	09SC31e	Ep	2334	SEM				3.03		2.54	0.47	0.00			1.94						1.00	13.00
Pure jadeitite	CV237b	Ep	125	EPMA				3.03	0.01	2.58	0.45	0.00	0.01	0.00	1.87		0.00	0.00	0.03	0.00	0.97	12.97
Pure jadeitite	CV237b	Ep	126	EPMA				3.00	0.01	2.38	0.60	0.00	0.00	0.00	2.00		0.01	0.00	0.03	0.00	0.97	12.97
Pure jadeitite	CV237b	Ep	140	EPMA				2.99	0.00	2.54	0.46	0.00	0.00	0.00	2.01		0.00	0.01	0.03	0.00	0.97	12.97
Pure jadeitite	CV237b	Ep	144	EPMA				2.98	0.00	2.48	0.53	0.00	0.01	0.00	2.00		0.00	0.00	0.03	0.00	0.97	12.97
Pure jadeitite	CV237b	Ep	155	EPMA				2.98	0.01	2.56	0.44	0.00	0.00	0.00	2.03		0.00	0.00	0.02	0.00	0.97	12.97
Pure jadeitite	CV237b	Ep	167	EPMA				3.00	0.01	2.61	0.39	0.00	0.00	0.00	1.99		0.00	0.00	0.02	0.00	0.98	12.98
Pure jadeitite	CV237b	Ep	169	EPMA				2.98	0.00	2.45	0.54	0.00	0.00	0.00	2.03		0.00	0.00	0.04	0.00	0.96	12.96
Pure jadeitite	CV237b	Ep	170	EPMA				2.96	0.00	2.61	0.40	0.00	0.00	0.00	2.05		0.00	0.00	0.03	0.00	0.97	12.97
Pure jadeitite	CV237b	Ep	172	EPMA				3.01	0.00	2.54	0.46	0.00	0.01	0.00	1.97		0.00	0.00	0.03	0.00	0.97	12.97
Pure jadeitite	CV237b	Ep	174	EPMA				2.98	0.01	2.61	0.38	0.00	0.00	0.00	2.03		0.00	0.00	0.02	0.00	0.98	12.98
Pure jadeitite	CV237b	Ep	176	EPMA				3.06	0.00	2.78	0.24	0.00	0.00	0.00	1.85		0.00	0.00	0.05	0.00	0.95	12.95
Pure jadeitite	CV237b	Ep	177	EPMA				3.02	0.00	2.70	0.32	0.00	0.00	0.00	1.91		0.00	0.00	0.02	0.00	0.98	12.98
Pure jadeitite	CV237b	Ep	178	EPMA				3.05	0.00	2.35	0.61	0.00	0.00	0.01	1.93		0.01	0.00	0.03	0.00	0.97	12.97
Pure jadeitite	CV237b	Ep	179	EPMA				3.01	0.00	2.68	0.37	0.00	0.00	0.01	1.87		0.01	0.01	0.06	0.00	0.93	12.93
Pure jadeitite	CV237b	Ep	180	EPMA				2.99	0.00	2.95	0.04	0.00	0.00	0.00	2.02		0.00	0.00	0.01	0.00	0.99	12.99
Pure jadeitite	CV237b	Ep	182	EPMA				3.00	0.00	2.87	0.12	0.00	0.00	0.00	2.00		0.00	0.00	0.02	0.00	0.98	12.98
Pure jadeitite	CV237b	Ep	183	EPMA				2.99	0.00	2.95	0.04	0.00	0.00	0.00	2.02		0.01	0.00	0.03	0.00	0.97	12.97
Pure jadeitite	CV237b	Ep	185	EPMA				2.99	0.02	2.91	0.05	0.00	0.00	0.01	2.03		0.00	0.00	0.02	0.00	0.97	12.97
Pure jadeitite	CV237b	Ep	2514	VPSEM				3.02	0.00	2.60	0.48	0.00	0.00	0.00	1.83		0.00	0.00			1.00	13.00
Pure jadeitite	CV237b	Ep	2515	VPSEM				2.91	0.02	2.44	0.62	0.00	0.00	0.00	2.05		0.00	0.00			1.00	13.00
Pure jadeitite	CV237b	Ep	2516	VPSEM				3.00	0.00	2.58	0.49	0.00	0.00	0.00	1.90		0.00	0.00			1.00	13.00
Pure jadeitite	CV237b	Ep	2517	VPSEM				2.99	0.00	2.66	0.45	0.00	0.00	0.00	1.85		0.00	0.00			1.00	13.00
Pure jadeitite	CV237b	Ep	2518	VPSEM				2.94	0.00	2.63	0.39	0.00	0.00	0.00	2.09		0.00	0.00			1.00	13.00
Pure jadeitite	CV237b	Ep	2520	VPSEM				3.08	0.00	2.44	0.54	0.00	0.00	0.00	1.85		0.00	0.00			1.00	13.00
Pure jadeitite	CV237b	Ep	2532	VPSEM				3.03	0.00	2.51	0.54	0.00	0.00	0.00	1.87		0.00	0.00			1.00	13.00
Pure jadeitite	CV237b	Ep	2539	VPSEM				2.97	0.00	2.58	0.43	0.00	0.00	0.00	2.04		0.00	0.00			1.00	13.00
Pure jadeitite	CV237b	Ep	2546	VPSEM				3.02	0.02	2.56	0.52	0.00	0.00	0.00	1.80		0.00	0.00			1.00	13.00
Pure jadeitite	CV237b	Ep	2550	VPSEM				3.01	0.00	2.58	0.49	0.00	0.00	0.00	1.87		0.00	0.00			1.00	13.00
Pure jadeitite	CV237b	Ep	2556	VPSEM				2.93	0.00	2.50	0.52	0.00	0.00	0.00	2.11		0.00	0.00			1.00	13.00
Pure jadeitite	CV237b	Ep	2559	VPSEM				2.97	0.04	2.56	0.47	0.00	0.00	0.00	1.94		0.00	0.00			1.00	13.00

Rock type	Sample	Phase	Point	serie	Px type	Px type	Jd mole%	Si	Ti	Al	Fe3+	Fe2+	Mn	Mg	Ca	Ba	Na	K	F	Cl	H	O
Pure jadeitite	CV237b	Ep	2565	VPSEM				2.96	0.00	2.60	0.46	0.00	0.01	0.00	1.97		0.00	0.00			1.00	13.00
Pure jadeitite	CV237b	Ep	2578	VPSEM				2.94	0.00	2.59	0.49	0.00	0.00	0.00	1.99		0.00	0.00			1.00	13.00
Pure jadeitite	CV237b	Ep	2581	VPSEM				2.99	0.00	2.57	0.47	0.00	0.00	0.00	1.96		0.00	0.00			1.00	13.00
Pure jadeitite	CV237b	Ep	2608	VPSEM				2.99	0.00	2.38	0.61	0.00	0.00	0.00	2.04		0.00	0.00			1.00	13.00
Pure jadeitite	CV237b	Ep	2619	VPSEM				2.94	0.00	2.39	0.64	0.00	0.00	0.00	2.08		0.00	0.00			1.00	13.00
Pure jadeitite	CV237b	Ep	2623	VPSEM				2.94	0.00	2.37	0.66	0.00	0.00	0.00	2.07		0.00	0.00			1.00	13.00
Pure jadeitite	CV237b	Ep	2625	VPSEM				2.96	0.00	2.32	0.71	0.00	0.00	0.00	2.05		0.00	0.00			1.00	13.00
Pure jadeitite	CV237b	Ep	2635	VPSEM				2.92	0.09	2.46	0.48	0.00	0.00	0.00	2.06		0.00	0.00			1.00	13.00
Pure jadeitite	CV237b	Ep	2636	VPSEM				3.01	0.03	2.53	0.48	0.00	0.00	0.00	1.92		0.00	0.00			1.00	13.00
Pure jadeitite	CV237b	Ep	2637	VPSEM				2.95	0.00	2.59	0.43	0.00	0.00	0.00	2.05		0.00	0.00			1.00	13.00
Pure jadeitite	CV237b	Ep	2638	VPSEM				3.03	0.05	2.38	0.56	0.00	0.00	0.05	1.87		0.06	0.00			1.00	13.00
Pure jadeitite	CV237b	Ep	2639	VPSEM				2.95	0.00	2.44	0.57	0.00	0.00	0.03	2.06		0.00	0.00			1.00	13.00
Pure jadeitite	CV237b	Ep	2664	VPSEM				2.94	0.00	2.96	0.07	0.00	0.00	0.00	2.05		0.00	0.00			1.00	13.00
Pure jadeitite	CV237b	Ep	2665	VPSEM				3.05	0.00	2.86	0.08	0.00	0.00	0.00	1.98		0.04	0.00			1.00	13.00
Pure jadeitite	CV237K	Ep	2675	VPSEM				2.96	0.02	2.27	0.71	0.00	0.00	0.00	2.08		0.00	0.00			1.00	13.00
Pure jadeitite	CV237K	Ep	2681	VPSEM				2.99	0.00	2.19	0.79	0.00	0.00	0.00	2.06		0.00	0.00			1.00	13.00
Pure jadeitite	CV237t	Ep	2849	VPSEM				2.99	0.00	2.38	0.60	0.00	0.00	0.00	2.05		0.00	0.00			1.00	13.00
Pure jadeitite	CV237t	Ep	2852	VPSEM				2.94	0.00	2.38	0.61	0.00	0.00	0.00	2.08		0.12	0.00			1.00	13.00
Pure jadeitite	CV237t	Ep	2853	VPSEM				2.94	0.00	2.46	0.58	0.00	0.00	0.00	2.06		0.00	0.00			1.00	13.00
Pure jadeitite	CV237t	Ep	2929	VPSEM				2.99	0.00	2.97	0.06	0.00	0.00	0.00	1.98		0.00	0.00			1.00	13.00
Pure jadeitite	CV237t	Ep	2930	VPSEM				2.97	0.00	2.59	0.44	0.00	0.00	0.00	2.02		0.00	0.00			1.00	13.00
Pure jadeitite	CV237t	Ep	2936	VPSEM				2.95	0.00	3.06	0.00	0.00	0.00	0.00	2.01		0.00	0.00			1.00	13.00
Pure jadeitite	CV237t	Ep	2937	VPSEM				2.99	0.00	2.71	0.42	0.00	0.00	0.00	1.83		0.00	0.00			1.00	13.00
Pure jadeitite	CV237t	Ep	2944	VPSEM				2.97	0.00	2.65	0.39	0.00	0.00	0.00	1.99		0.00	0.00			1.00	13.00
Pure jadeitite	CV237t	Ep	2947	VPSEM				3.00	0.00	2.60	0.38	0.00	0.00	0.00	2.01		0.04	0.00			1.00	13.00
Pure jadeitite	CV237t	Ep	2948	VPSEM				2.98	0.00	2.83	0.20	0.00	0.00	0.00	2.00		0.00	0.00			1.00	13.00
Pure jadeitite	MCB1f	Ep	3148	VPSEM				2.95	0.00	2.49	0.57	0.00	0.02	0.00	2.00		0.00	0.00	0.00	0.00	1.00	13.00
Pure jadeitite	MCB1f	Ep	3169	VPSEM				3.04	0.02	2.53	0.45	0.00	0.00	0.00	1.88		0.08	0.00	0.00	0.00	1.00	13.00
Pure jadeitite	MCB1f	Ep	3210	VPSEM				3.07	0.02	2.43	0.44	0.00	0.03	0.09	1.85		0.11	0.00	0.00	0.00	1.00	13.00
Pure jadeitite	MCB1f	Ep	3216	VPSEM				2.95	0.02	2.69	0.37	0.00	0.02	0.00	1.96		0.00	0.00	0.00	0.00	1.00	13.00
Pure jadeitite	MCB1f	Ep	3217	VPSEM				2.97	0.00	2.62	0.44	0.00	0.00	0.00	1.97		0.00	0.00	0.00	0.00	1.00	13.00
Pure jadeitite	MCB1f	Ep	3223	VPSEM				2.97	0.00	2.59	0.47	0.00	0.00	0.00	1.97		0.00	0.00	0.00	0.00	1.00	13.00
Pure jadeitite	MCB1f	Ep	3226	VPSEM				2.95	0.00	2.74	0.37	0.00	0.00	0.00	1.94		0.00	0.00	0.00	0.00	1.00	13.00
Pure jadeitite	MCB1j	Ep	1346	EPMA				3.00	0.01	2.93	0.06	0.00	0.00	0.00	2.01		0.00	0.00	0.03	0.00	0.97	12.97
Pure jadeitite	MCB1j	Ep	1348	EPMA				3.00	0.00	2.94	0.06	0.00	0.00	0.00	1.99		0.00	0.00	0.03	0.00	0.97	12.97
Pure jadeitite	MCB1j	Ep	1350	EPMA				2.99	0.00	2.97	0.04	0.00	0.00	0.00	2.00		0.00	0.00	0.03	0.00	0.97	12.97
Pure jadeitite	MCB1j	Ep	1351	EPMA				3.00	0.00	2.90	0.10	0.00	0.00	0.00	1.99		0.00	0.00	0.03	0.00	0.97	12.97
Pure jadeitite	MCB1j	Ep	1353	EPMA				2.99	0.01	2.82	0.18	0.00	0.00	0.01	1.97		0.01	0.00	0.02	0.00	0.98	12.98
Pure jadeitite	MCB1j	Ep	1355	EPMA				3.01	0.00	2.96	0.05	0.00	0.00	0.00	1.97		0.01	0.00	0.02	0.00	0.97	12.97
Pure jadeitite	MCB1j	Ep	1368	EPMA				3.00	0.03	2.74	0.21	0.00	0.00	0.01	2.00		0.01	0.00	0.03	0.00	0.97	12.97
Pure jadeitite	MCB2d	Ep	3234	VPSEM				2.95	0.00	2.72	0.35	0.00	0.00	0.00	1.98		0.00	0.00	0.00		1.00	13.00
Pure jadeitite	MCB2d	Ep	3257	VPSEM				2.98	0.00	2.70	0.43	0.00	0.00	0.00	1.83		0.00	0.00	0.00		1.00	13.00
Pure jadeitite	MCB2d	Ep	3261	VPSEM				2.99	0.00	2.64	0.41	0.00	0.00	0.00	1.92		0.05	0.00	0.00		1.00	13.00
Pure jadeitite	MCB2e	Ep	3269	VPSEM				3.12		2.68	0.24	0.00			1.88						1.00	13.00

Rock type	Sample	Phase	Point	serie	Px type	Px type	Jd mole%	Si	Ti	Al	Fe3+	Fe2+	Mn	Mg	Ca	Ba	Na	K	F	Cl	H	O
Pure jadeitite	MCB2e	Ep	3271	VPSEM				3.10		2.85	0.13	0.00			1.82						1.00	13.00
Pure jadeitite	MCB3h	Ep	408	EPMA				3.00	0.01	2.25	0.74	0.00	0.00	0.00	1.99		0.00	0.00	0.03	0.00	0.97	12.97
Pure jadeitite	MCB3h	Ep	409	EPMA				3.00	0.01	2.23	0.76	0.00	0.01	0.00	1.98		0.00	0.00	0.02	0.00	0.98	12.98
Pure jadeitite	MCB3h	Ep	410	EPMA				3.02	0.00	2.18	0.80	0.00	0.01	0.00	1.98		0.00	0.00	0.03	0.00	0.97	12.97
Pure jadeitite	MCB3h	Ep	412	EPMA				3.02	0.00	2.40	0.57	0.00	0.00	0.00	2.00		0.00	0.00	0.03	0.00	0.97	12.97
Pure jadeitite	MCB3h	Ep	3505	VPSEM				2.93		2.74	0.35	0.00			2.01						1.00	13.00
Pure jadeitite	MCB3h	Ep	3512	VPSEM				2.98		2.11	0.90	0.00			2.02						1.00	13.00
Pure jadeitite	MCB3h	Ep	3513	VPSEM				2.95		2.74	0.28	0.00			2.06						1.00	13.00
Pure jadeitite	MCB3h	Ep	3516	VPSEM				3.00		2.17	0.83	0.00			2.00						1.00	13.00
Pure jadeitite	MCB3h	Ep	3532	VPSEM				2.95		2.23	0.88	0.00			1.94						1.00	13.00
Pure jadeitite	MCB3h	Ep	3535	VPSEM				3.04		2.57	0.46	0.00			1.86						1.00	13.00
Pure jadeitite	MCB3h	Ep	3541	VPSEM				2.90		2.28	0.80	0.00			2.07						1.00	13.00
Pure jadeitite	MCB3h	Ep	3551	VPSEM				2.96		2.46	0.58	0.00			2.03						1.00	13.00
Pure jadeitite	MCB3h	Ep	3553	VPSEM				2.96		2.41	0.66	0.00			1.98						1.00	13.00
Pure jadeitite	MCB3h	Ep	3557	VPSEM				2.97		2.54	0.50	0.00			2.01						1.00	13.00
Pure jadeitite	MCB3h	Ep	3560	VPSEM				2.90		2.51	0.60	0.00			2.04						1.00	13.00
Pure jadeitite	MCB3h	Ep	3571	VPSEM				3.00		2.45	0.55	0.00			2.01						1.00	13.00
Pure jadeitite	MCB3h	Ep	3589	VPSEM				2.99		2.48	0.52	0.00			2.01						1.00	13.00
Pure jadeitite	MCB3h	Ep	3595	VPSEM				2.96		2.52	0.53	0.00			2.00						1.00	13.00
Pure jadeitite	MCB3h	Ep	3609	VPSEM				2.94		2.56	0.54	0.00			1.97						1.00	13.00
Pure Jdt/Ab-Ep rock/Chloritite	09SC8a3	Ep	2449	VPSEM				2.98		2.43	0.61	0.00			1.98						1.00	13.00
Pure Jdt/Ab-Ep rock/Chloritite	09SC8a3	Ep	2450	VPSEM				3.01		2.38	0.62	0.00			1.98						1.00	13.00
Pure Jdt/Chloritite	MCB3f	Ep	3432	VPSEM				2.99	0.00	2.56	0.46	0.00	0.00	0.00	1.96		0.07	0.00		0.00	1.00	13.00
Pure Jdt/Chloritite	MCB3f	Ep	3435	VPSEM				2.96	0.00	2.63	0.43	0.00	0.00	0.00	2.00		0.00	0.00		0.00	1.00	13.00
Pure Jdt/Chloritite	MCB3f	Ep	3436	VPSEM				3.09	0.00	2.47	0.58	0.00	0.00	0.06	1.70		0.00	0.00		0.00	1.00	13.00
Pure Jdt/Chloritite	MCB3f	Ep	3437	VPSEM				3.09	0.00	2.43	0.62	0.00	0.00	0.04	1.69		0.00	0.00		0.00	1.00	13.00
Pure Jdt/Chloritite	MCB3f	Ep	3438	VPSEM				3.10	0.00	2.36	0.69	0.00	0.00	0.05	1.66		0.00	0.00		0.00	1.00	13.00
Pure Jdt/Chloritite	MCB3f	Ep	3439	VPSEM				3.13	0.00	2.43	0.64	0.00	0.00	0.10	1.54		0.00	0.00		0.00	1.00	13.00
Pure Jdt/Chloritite	MCB3f	Ep	3440	VPSEM				3.14	0.00	2.43	0.63	0.00	0.00	0.07	1.56		0.00	0.00		0.00	1.00	13.00
Pure Jdt/Chloritite	MCB3f	Ep	3441	VPSEM				3.08	0.00	2.39	0.69	0.00	0.00	0.04	1.68		0.00	0.00		0.00	1.00	13.00
Pure Jdt/Chloritite	MCB3f	Ep	3442	VPSEM				2.98	0.00	2.43	0.60	0.00	0.00	0.00	1.99		0.00	0.00		0.00	1.00	13.00
Pure Jdt/Chloritite	MCB3f	Ep	3443	VPSEM				2.95	0.00	2.58	0.49	0.00	0.00	0.00	1.99		0.00	0.00		0.00	1.00	13.00
Pure Jdt/Chloritite	MCB3f	Ep	3445	VPSEM				2.97	0.00	2.26	0.78	0.00	0.00	0.00	1.99		0.00	0.00		0.00	1.00	13.00
Pure Jdt/Chloritite	MCB3f	Ep	3446	VPSEM				2.98	0.00	2.42	0.61	0.00	0.00	0.00	1.98		0.00	0.00		0.00	1.00	13.00
Pure Jdt/Chloritite	MCB3f	Ep	3458	VPSEM				3.00	0.00	2.30	0.73	0.00	0.00	0.00	1.96		0.00	0.00		0.00	1.00	13.00
Pure Jdt/Chloritite	MCB3f	Ep	3464	VPSEM				3.07	0.00	2.35	0.67	0.00	0.00	0.00	1.81		0.00	0.00		0.00	1.00	13.00
Pure Jdt/Chloritite	MCB3f	Ep	3465	VPSEM				3.13	0.00	2.31	0.74	0.00	0.00	0.00	1.65		0.00	0.00		0.02	0.98	12.98
Pure Jdt/Chloritite	MCB3f	Ep	3466	VPSEM				3.08	0.00	2.42	0.67	0.00	0.00	0.04	1.64		0.06	0.00		0.00	1.00	13.00
Pure Jdt/Chloritite	MCB3f	Ep	3467	VPSEM				3.13	0.00	2.39	0.67	0.00	0.00	0.05	1.57		0.06	0.00		0.00	1.00	13.00
Pure Jdt/Chloritite	MCB3f	Ep	3477	VPSEM				2.97	0.00	2.69	0.38	0.00	0.00	0.00	1.96		0.00	0.00		0.00	1.00	13.00
Pure Jdt/Chloritite	MCB3f	Ep	3495	VPSEM				2.96	0.00	2.74	0.31	0.00	0.01	0.00	1.98		0.00	0.00		0.00	1.00	13.00
Ep-rich jadeitite	09SC27m	Grt	2091	SEM				2.99		1.99	0.03	1.54	0.11	0.84	0.50						0.00	12.00
Ep-rich jadeitite	09SC27m	Grt	2108	SEM				3.01		2.00	0.00	1.26	0.47	0.14	1.12						0.00	12.00
Ab-Ep rock	09SC27f	Hem	2131	SEM							2.00	0.00									0.00	3.00

Rock type	Sample	Phase	Point	serie	Px type	Px type	Jd mole%	Si	Ti	Al	Fe3+	Fe2+	Mn	Mg	Ca	Ba	Na	K	F	Cl	H	O
Ab-Ep rock	09SC31a	Hem	2277	SEM							2.00	0.00									0.00	3.00
Ab-Ep rock	09SC31n	Hem	1847	SEM							2.00	0.00									0.00	3.00
Ep-rich jadeitite	09SC27m	Hem	2084	SEM					0.03		1.93	0.03									0.00	3.00
Ep-rich jadeitite	09SC27m	Hem	2085	SEM							2.00	0.00									0.00	3.00
Pure Jdt/Chloritite	MCB3f	Kfs	3484	VPSEM				2.99	0.00	0.99	0.00	0.02	0.00	0.00	0.06		0.19	0.73		0.00	0.00	8.00
Ab-Ep Chl-rich rock	09SC27b	Ms	2170	SEM				6.89		4.12	0.00	0.23		0.83				1.96			4.00	24.00
Ab-Ep Chl-rich rock	09SC27b	Ms	2176	SEM				6.81	0.07	4.24	0.00	0.23		0.70				1.89			4.00	24.00
Ab-Ep Chl-rich rock	09SC27b	Ms	2179	SEM				6.87	0.06	4.11	0.00	0.21		0.86				1.82			4.00	24.00
Ab-Ep Chl-rich rock	09SC27b	Ms	2180	SEM				6.89		4.17	0.00	0.22		0.75				2.00			4.00	24.00
Ab-Ep Chl-rich rock	09SC27b	Ms	2181	SEM				6.88		4.18	0.00	0.23		0.78				1.90			4.00	24.00
Ab-Ep Chl-rich rock	09SC27b	Ms	2208	SEM				6.72		4.33	0.00	0.25		0.82				1.99			4.00	24.00
Ab-Ep Chl-rich rock	09SC27b	Ms	2212	SEM				6.82		4.15	0.00	0.20		0.88				2.10			4.00	24.00
Ab-Ep Chl-rich rock	09SC27b	Ms	2220	SEM				6.93		4.22	0.00	0.25		0.66				1.83			4.00	24.00
Ab-Ep rock	09SC31c	Ms	2367	SEM				7.53		3.61				0.64				1.77			4.00	24.00
Ab-Ep rock	09SC31d	Ms	1700	SEM				7.06		4.11				0.75				1.94			4.00	24.00
Ab-Ep rock	09SC31d	Ms	1704	SEM				6.93		4.41				0.60				1.87			4.00	24.00
Ab-Ep rock	09SC31d	Ms	1705	SEM				6.74		4.61				0.65				1.91			4.00	24.00
Ab-Ep rock	09SC31d	Ms	1709	SEM				7.11		4.16				0.66				1.78			4.00	24.00
Ab-Ep rock	09SC31d	Ms	1758	SEM				7.07		4.20				0.64				1.82			4.00	24.00
Ab-Ep rock	09SC31n	Ms	1860	SEM				6.99		4.15	0.00	0.26		0.65				1.75			4.00	24.00
Ab-Ep rock	09SC31n	Ms	1882	SEM				7.24		3.99				0.53				1.99			4.00	24.00
Ab-Ep rock	09SC31n	Ms	1888	SEM				7.09		3.97	0.00	0.26		0.59				2.03			4.00	24.00
Ab-Ep rock	MCB1a	Ms	3061	VPSEM				6.56	0.00	4.56	0.00	0.27	0.00	0.80	0.00		0.14	1.81			4.00	24.00
Ab-Ep rock	MCB1e	Ms	33	EPMA				6.46	0.01	5.04	0.00	0.06	0.00	0.48	0.00		0.11	1.83	0.01	0.00	3.99	23.99
Ep-rich jadeitite	09SC27c	Ms	2224	SEM				7.21		4.01				0.54				2.06			4.00	24.00
Ep-rich jadeitite	09SC27c	Ms	2225	SEM				7.04		4.23				0.59				2.00			4.00	24.00
Ep-rich jadeitite	09SC27c	Ms	2227	SEM				6.98		4.17				0.71				2.15			4.00	24.00
Ep-rich jadeitite	09SC27c	Ms	2231	SEM				7.16		4.01				0.65				2.00			4.00	24.00
Ep-rich jadeitite	09SC27c	Ms	2242	SEM				6.96		4.14	0.00	0.28		0.57				2.05			4.00	24.00
Ep-rich jadeitite	09SC27c	Ms	2243	SEM				7.04		4.09				0.73				2.15			4.00	24.00
Ep-rich jadeitite	09SC27d	Ms	1896	SEM				6.91		4.56				0.51				1.64			4.00	24.00
Ep-rich jadeitite	09SC27d	Ms	1899	SEM				7.04		4.11				0.79				1.92			4.00	24.00
Ep-rich jadeitite	MCB1d	Ms	1509	VPSEM				6.70		4.54	0.00	0.30		0.54			0.10	1.82			4.00	24.00
Ep-rich jadeitite	MCB1d	Ms	1511	VPSEM				6.62		4.62	0.00	0.18		0.70			0.07	1.82			4.00	24.00
Ep-rich jadeitite	MCB1d	Ms	1523	VPSEM				6.63		4.62	0.00	0.30		0.54			0.15	1.78			4.00	24.00
Ep-rich jadeitite	MCB1d	Ms	1525	VPSEM				6.68		4.50	0.00	0.33		0.60			0.16	1.75			4.00	24.00
Ep-rich jadeitite	MCB1d	Ms	1526	VPSEM				6.66		4.56	0.00	0.18		0.75				1.83			4.00	24.00
Ep-rich jadeitite	MCB1d	Ms	1560	VPSEM				6.57		4.65	0.00	0.23		0.66	0.00		0.12	1.86			4.00	24.00
Ep-rich jadeitite	MCB1d	Ms	1561	VPSEM				6.61		4.63	0.00	0.20		0.65	0.00		0.11	1.85			4.00	24.00
Ep-rich jadeitite	MCB1d	Ms	1563	VPSEM				6.53		4.62	0.00	0.28		0.75	0.00		0.07	1.86			4.00	24.00
Ep-rich jadeitite	MCB1d	Ms	1565	VPSEM				6.57		4.66	0.00	0.22		0.65	0.00		0.09	1.89			4.00	24.00
Ep-rich jadeitite	MCB1d	Ms	1566	VPSEM				6.66		4.51	0.00	0.26		0.67	0.00		0.19	1.79			4.00	24.00
Ep-rich jadeitite	MCB1d	Ms	1567	VPSEM				6.66		4.50	0.00	0.25		0.68	0.00		0.20	1.81			4.00	24.00
Ep-rich jadeitite	MCB1d	Ms	1577	VPSEM				6.61		4.61	0.00	0.25		0.68				1.87			4.00	24.00

Rock type	Sample	Phase	Point	serie	Px type	Px type	Jd mole%	Si	Ti	Al	Fe3+	Fe2+	Mn	Mg	Ca	Ba	Na	K	F	Cl	H	O
Ep-rich jadeitite	MCB1d	Ms	1583	VPSEM				6.58		4.64	0.00	0.21		0.71			0.07	1.84			4.00	24.00
Ep-rich jadeitite	MCB1d	Ms	1593	VPSEM				6.66		4.55	0.00	0.22		0.66			0.11	1.82			4.00	24.00
Ep-rich jadeitite	MCB1d	Ms	1610	VPSEM				6.64		4.55	0.00	0.24		0.70			0.07	1.86			4.00	24.00
Ep-rich jadeitite	MCB1d	Ms	1617	VPSEM				6.67		4.54	0.00	0.14		0.73			0.08	1.84			4.00	24.00
Ep-rich jadeitite	MCB1d	Ms	1618	VPSEM				6.60		4.66	0.00	0.27		0.59			0.15	1.78			4.00	24.00
Ep-rich jadeitite	MCB1d	Ms	1629	VPSEM				6.64		4.45	0.00	0.40		0.62			0.19	1.85			4.00	24.00
Ep-rich jadeitite	MCB1d	Ms	1648	VPSEM				6.74		4.41	0.00	0.30		0.63			0.17	1.81			4.00	24.00
Ep-rich jadeitite	MCB1g	Ms	3287	VPSEM				6.61	0.00	4.55	0.00	0.30	0.00	0.70	0.00		0.20	1.69			4.00	24.00
Ep-rich jadeitite	MCB1g	Ms	3291	VPSEM				6.55	0.00	4.67	0.00	0.33	0.00	0.65	0.00		0.18	1.65			4.00	24.00
Ep-rich jadeitite	MCB1g	Ms	3296	VPSEM				6.63	0.00	4.59	0.00	0.19	0.00	0.73	0.00		0.12	1.76			4.00	24.00
Ep-rich jadeitite	MCB1g	Ms	3302	VPSEM				6.61	0.00	4.54	0.00	0.30	0.00	0.69	0.00		0.23	1.71			4.00	24.00
Ep-rich jadeitite	MCB1g	Ms	3305	VPSEM				6.59	0.00	4.65	0.00	0.19	0.00	0.70	0.00		0.13	1.78			4.00	24.00
Ep-rich jadeitite	MCB1g	Ms	3312	VPSEM				6.73	0.00	4.42	0.00	0.27	0.00	0.69	0.00		0.17	1.71			4.00	24.00
Ep-rich jadeitite	MCB1g	Ms	3355	VPSEM				6.59	0.00	4.62	0.00	0.28	0.00	0.60	0.00		0.21	1.78			4.00	24.00
Ep-rich jadeitite	MCB1g	Ms	3356	VPSEM				6.59	0.00	4.72	0.00	0.17	0.00	0.65	0.00		0.09	1.75			4.00	24.00
Ep-rich jadeitite	MCB1g	Ms	3358	VPSEM				6.70	0.00	4.59	0.00	0.17	0.00	0.66	0.00		0.00	1.79			4.00	24.00
Mica-rich Jadeitite	09SC31e	Ms	1824	SEM				6.77		4.56				0.69				1.84			4.00	24.00
Mica-rich Jadeitite	09SC31e	Ms	2325	SEM				6.83		4.48				0.63				1.94			4.00	24.00
Mica-rich Jadeitite	09SC31e	Ms	2328	SEM				6.95		4.31				0.71				1.86			4.00	24.00
Mica-rich Jadeitite	09SC31e	Ms	2330	SEM				7.04		4.34				0.51				1.82			4.00	24.00
Pure jadeitite	CV237b	Ms	186	EPMA				7.01	0.01	3.96	0.00	0.15	0.00	0.88	0.00		0.06	1.91	0.03	0.00	3.97	23.97
Pure jadeitite	CV237b	Ms	188	EPMA				7.06	0.01	3.87	0.00	0.18	0.00	0.89	0.00		0.06	1.90	0.04	0.00	3.96	23.96
Pure jadeitite	CV237b	Ms	2568	VPSEM				6.89	0.00	4.13	0.00	0.29	0.00	0.73	0.00		0.07	1.93			4.00	24.00
Pure jadeitite	CV237b	Ms	2570	VPSEM				6.79	0.03	4.22	0.00	0.25	0.00	0.80	0.00		0.14	1.85			4.00	24.00
Pure jadeitite	MCB1j	Ms	1356	EPMA				6.81	0.01	4.31	0.00	0.14	0.00	0.79	0.00		0.09	1.87	0.03	0.00	3.96	23.96
Pure jadeitite	MCB1j	Ms	1357	EPMA				6.94	0.01	4.10	0.00	0.13	0.00	0.85	0.00		0.08	1.87	0.00	0.00	4.00	24.00
Pure jadeitite	MCB1j	Ms	1358	EPMA				6.80	0.01	4.33	0.00	0.14	0.00	0.76	0.00		0.10	1.83	0.03	0.00	3.97	23.97
Pure jadeitite	MCB1j	Ms	1359	EPMA				6.80	0.01	4.32	0.00	0.20	0.00	0.71	0.00		0.18	1.79	0.04	0.01	3.95	23.95
Pure jadeitite	MCB1j	Ms	1360	EPMA				6.90	0.01	4.14	0.00	0.13	0.00	0.86	0.00		0.09	1.85	0.02	0.01	3.98	23.98
Pure jadeitite	MCB1j	Ms	1361	EPMA				6.82	0.01	4.31	0.00	0.22	0.00	0.67	0.00		0.14	1.81	0.03	0.00	3.97	23.97
Pure jadeitite	MCB1j	Ms	1362	EPMA				6.90	0.01	4.18	0.00	0.13	0.00	0.79	0.01		0.23	1.74	0.03	0.00	3.97	23.97
Pure jadeitite	MCB1j	Ms	1363	EPMA				6.81	0.01	4.29	0.00	0.15	0.00	0.80	0.00		0.09	1.86	0.04	0.00	3.96	23.96
Ab-Ep rock	MCB1e	Pa	3133	VPSEM				5.79	0.00	6.18	0.00	0.00	0.00	0.00	0.07		2.00	0.15			4.00	24.00
Ab-Ep rock	MCB1e	Pa	3139	VPSEM				5.88	0.00	6.10	0.00	0.00	0.00	0.00	0.06		2.03	0.06			4.00	24.00
Ep-rich Jadeitite	MCB1d	Pa	221	EPMA				6.06	0.00	5.88	0.00	0.03	0.00	0.06	0.01		1.75	0.17	0.00	0.00	4.00	24.00
Ep-rich Jadeitite	MCB1d	Pa	222	EPMA				5.96	0.00	6.01	0.00	0.04	0.00	0.03	0.01		1.86	0.10	0.00	0.00	4.00	24.00
Ep-rich Jadeitite	MCB1d	Pa	223	EPMA				6.02	0.00	5.92	0.00	0.04	0.00	0.05	0.01		1.78	0.16	0.00	0.00	4.00	24.00
Ep-rich Jadeitite	MCB1d	Pa	224	EPMA				6.03	0.00	5.92	0.00	0.03	0.00	0.04	0.01		1.80	0.13	0.02	0.01	3.97	23.97
Ep-rich Jadeitite	MCB1d	Pa	225	EPMA				5.99	0.00	5.99	0.00	0.03	0.00	0.02	0.01		1.88	0.07	0.00	0.00	3.99	23.99
Ep-rich Jadeitite	MCB1d	Pa	226	EPMA				5.97	0.00	6.01	0.00	0.02	0.00	0.02	0.01		1.89	0.07	0.01	0.01	3.99	23.99
Ep-rich Jadeitite	MCB1d	Pa	227	EPMA				5.98	0.00	5.97	0.00	0.03	0.00	0.04	0.02		1.83	0.15	0.00	0.00	4.00	24.00
Ep-rich Jadeitite	MCB1d	Pa	228	EPMA				6.00	0.00	5.98	0.00	0.03	0.00	0.02	0.01		1.84	0.09	0.00	0.00	3.99	23.99
Ep-rich Jadeitite	MCB1d	Pa	229	EPMA				6.01	0.00	5.93	0.00	0.04	0.00	0.05	0.02		1.85	0.12	0.00	0.01	3.99	23.99
Ep-rich Jadeitite	MCB1d	Pa	230	EPMA				5.99	0.00	5.97	0.00	0.04	0.00	0.04	0.01		1.85	0.10	0.00	0.01	3.99	23.99

Rock type	Sample	Phase	Point	serie	Px type	Px type	Jd mole%	Si	Ti	Al	Fe3+	Fe2+	Mn	Mg	Ca	Ba	Na	K	F	Cl	H	O
Ep-rich Jadeitite	MCB1d	Pa	231	EPMA				6.01	0.00	5.96	0.00	0.03	0.00	0.03	0.01		1.83	0.09	0.01	0.00	3.99	23.99
Ep-rich Jadeitite	MCB1d	Pa	239	EPMA				6.01	0.00	5.95	0.00	0.04	0.00	0.04	0.01		1.81	0.13	0.00	0.00	4.00	24.00
Ep-rich Jadeitite	MCB1d	Pa	243	EPMA				5.99	0.00	5.99	0.00	0.02	0.00	0.04	0.01		1.87	0.07	0.00	0.00	4.00	24.00
Ep-rich jadeitite	MCB1d	Pa	1502	VPSEM				5.99		5.96				0.08			1.86	0.13			4.00	24.00
Ep-rich jadeitite	MCB1d	Pa	1503	VPSEM				6.00		5.97				0.07			1.82	0.16			4.00	24.00
Ep-rich jadeitite	MCB1d	Pa	1504	VPSEM				5.93		6.07							2.02	0.05			4.00	24.00
Ep-rich jadeitite	MCB1d	Pa	1505	VPSEM				5.98		5.96				0.09			1.79	0.23			4.00	24.00
Ep-rich jadeitite	MCB1d	Pa	1506	VPSEM				6.01		5.97				0.09			1.75	0.12			4.00	24.00
Ep-rich jadeitite	MCB1d	Pa	1507	VPSEM				5.96		5.99	0.00	0.03		0.07			1.85	0.15			4.00	24.00
Ep-rich jadeitite	MCB1d	Pa	1508	VPSEM				6.03		5.94	0.00	0.03					1.87	0.13			4.00	24.00
Ep-rich jadeitite	MCB1d	Pa	1520	VPSEM				5.94		6.00	0.00	0.03		0.08			1.82	0.20			4.00	24.00
Ep-rich jadeitite	MCB1d	Pa	1524	VPSEM				5.95		6.03	0.00	0.03					1.90	0.12			4.00	24.00
Ep-rich jadeitite	MCB1d	Pa	1549	VPSEM				5.95		5.99	0.00	0.03		0.07	0.00		1.91	0.10			4.00	24.00
Ep-rich jadeitite	MCB1d	Pa	1550	VPSEM				5.90		6.12	0.00	0.04			0.00		1.91	0.04			4.00	24.00
Ep-rich jadeitite	MCB1d	Pa	1554	VPSEM				5.92		6.11							1.89	0.10			4.00	24.00
Ep-rich jadeitite	MCB1d	Pa	1555	VPSEM				5.98		5.95	0.00	0.04		0.06	0.00		1.88	0.14			4.00	24.00
Ep-rich jadeitite	MCB1d	Pa	1556	VPSEM				6.02		5.91	0.00	0.05		0.05	0.00		1.84	0.15			4.00	24.00
Ep-rich jadeitite	MCB1d	Pa	1557	VPSEM				5.97		5.98	0.00	0.03		0.07	0.00		1.81	0.16			4.00	24.00
Ep-rich jadeitite	MCB1d	Pa	1573	VPSEM				5.95		6.00	0.00	0.04		0.06			1.87	0.14			4.00	24.00
Ep-rich jadeitite	MCB1d	Pa	1597	VPSEM				5.92		6.07	0.00	0.03					1.93	0.11			4.00	24.00
Ep-rich jadeitite	MCB1d	Pa	1603	VPSEM				5.96		6.03	0.00	0.04					1.87	0.13			4.00	24.00
Ep-rich jadeitite	MCB1d	Pa	1607	VPSEM				5.95		6.05	0.00	0.03					1.89	0.10			4.00	24.00
Ep-rich jadeitite	MCB1d	Pa	1613	VPSEM				6.01		5.93	0.00	0.03		0.08			1.64	0.30			4.00	24.00
Ep-rich jadeitite	MCB1d	Pa	1614	VPSEM				5.94		6.00	0.00	0.04			0.03		1.98	0.09			4.00	24.00
Ep-rich jadeitite	MCB1d	Pa	1615	VPSEM				5.91		6.10	0.00	0.04					1.88	0.10			4.00	24.00
Ep-rich jadeitite	MCB1d	Pa	1616	VPSEM				5.98		6.02							1.97	0.06			4.00	24.00
Ep-rich jadeitite	MCB1d	Pa	1621	VPSEM				5.93		6.04	0.00	0.04		0.07			1.83	0.11			4.00	24.00
Ep-rich jadeitite	MCB1d	Pa	1630	VPSEM				5.87		6.10	0.00	0.03		0.08			1.81	0.15			4.00	24.00
Ep-rich jadeitite	MCB1d	Pa	1654	VPSEM				5.94		6.05				0.05	0.03		1.79	0.11			4.00	24.00
Ep-rich jadeitite	MCB1d	Pa	1659	VPSEM				5.95		6.00	0.00	0.04		0.07			1.79	0.19			4.00	24.00
Ep-rich jadeitite	MCB1d	Pa	1660	VPSEM				5.96		6.04				0.05			1.86	0.10			4.00	24.00
Ep-rich jadeitite	MCB1d	Pa	1666	VPSEM				5.89		6.08				0.06	0.03		1.95	0.07			4.00	24.00
Ep-rich jadeitite	MCB1d	Pa	1681	VPSEM				5.93		6.05	0.00	0.04					1.89	0.14			4.00	24.00
Ep-rich jadeitite	MCB1d	Pa	1685	VPSEM				5.98		5.95	0.00	0.04		0.09			1.85	0.14			4.00	24.00
Ep-rich jadeitite	MCB1d	Pa	1686	VPSEM				5.94		5.99	0.00	0.04		0.06	0.03		1.88	0.11			4.00	24.00
Ep-rich jadeitite	MCB1g	Pa	3286	VPSEM				5.96		5.96	0.00	0.04	0.00	0.07	0.00		1.88	0.17			4.00	24.00
Ep-rich jadeitite	MCB1g	Pa	3292	VPSEM				5.97	0.00	5.96	0.00	0.00	0.00	0.10	0.00		1.87	0.17			4.00	24.00
Ep-rich jadeitite	MCB1g	Pa	3297	VPSEM				5.90	0.00	6.10	0.00	0.00	0.00	0.00	0.00		1.99	0.10			4.00	24.00
Ep-rich jadeitite	MCB1g	Pa	3303	VPSEM				5.94	0.00	5.98	0.00	0.05	0.00	0.06	0.00		1.92	0.17			4.00	24.00
Ep-rich jadeitite	MCB1g	Pa	3307	VPSEM				5.92	0.00	6.08	0.00	0.00	0.00	0.00	0.00		1.95	0.12			4.00	24.00
Ep-rich jadeitite	MCB1g	Pa	3311	VPSEM				5.95	0.00	5.97	0.00	0.00	0.00	0.10	0.00		1.76	0.33			4.00	24.00
Ep-rich jadeitite	MCB1g	Pa	3316	VPSEM				5.86	0.00	6.14	0.00	0.00	0.00	0.07	0.00		1.73	0.26			4.00	24.00
Ep-rich jadeitite	MCB1g	Pa	3323	VPSEM				5.89	0.00	6.04	0.00	0.05	0.00	0.07	0.00		1.94	0.13			4.00	24.00
Ep-rich jadeitite	MCB1g	Pa	3326	VPSEM				5.96	0.00	5.99	0.00	0.03	0.00	0.00	0.00		1.93	0.18			4.00	24.00

Rock type	Sample	Phase	Point	serie	Px type	Px type	Jd mole%	Si	Ti	Al	Fe3+	Fe2+	Mn	Mg	Ca	Ba	Na	K	F	Cl	H	O
Ep-rich jadeitite	MCB1g	Pa	3339	VPSEM				5.92	0.00	6.07	0.00	0.04	0.00	0.00	0.00		1.98	0.07			4.00	24.00
Ep-rich jadeitite	MCB1g	Pa	3346	VPSEM				5.91	0.00	6.07	0.00	0.05	0.00	0.08	0.00		1.77	0.14			4.00	24.00
Ep-rich jadeitite	MCB1g	Pa	3361	VPSEM				5.90	0.00	6.12	0.00	0.00	0.00	0.00	0.00		1.98	0.06			4.00	24.00
Ep-rich jadeitite	MCB1g	Pa	3362	VPSEM				5.94	0.00	5.99	0.00	0.05	0.00	0.08	0.00		1.84	0.16			4.00	24.00
Ep-rich jadeitite	MCB2c	Pa	3385	VPSEM				5.92	0.00	5.99	0.00	0.04	0.00	0.10	0.00		1.91	0.16			4.00	24.00
Ep-rich jadeitite	MCB2c	Pa	3386	VPSEM				5.91	0.00	6.07	0.00	0.00	0.00	0.07	0.00		1.96	0.06			4.00	24.00
Ep-rich jadeitite	MCB2c	Pa	3389	VPSEM				5.88	0.00	6.15	0.00	0.00	0.00	0.00	0.00		1.93	0.08			4.00	24.00
Ep-rich jadeitite	MCB2c	Pa	3399	VPSEM				5.89	0.00	6.08	0.00	0.00	0.00	0.00	0.00		2.11	0.07			4.00	24.00
Ep-rich jadeitite	MCB2c	Pa	3401	VPSEM				5.89	0.00	6.11	0.00	0.03	0.00	0.00	0.00		1.98	0.08			4.00	24.00
Ep-rich jadeitite	MCB4a	Pa	1382	EPMA				5.98	0.00	5.96	0.00	0.03	0.00	0.06	0.01		1.80	0.17	0.04	0.00	3.96	23.96
Ep-rich jadeitite	MCB4a	Pa	1383	EPMA				6.08	0.00	5.81	0.00	0.04	0.00	0.11	0.01		1.62	0.31	0.02	0.00	3.98	23.98
Ep-rich jadeitite	MCB4a	Pa	1384	EPMA				6.01	0.00	5.94	0.00	0.02	0.00	0.04	0.01		1.93	0.04	0.00	0.00	4.00	24.00
Ep-rich jadeitite	MCB4a	Pa	1385	EPMA				5.97	0.00	5.98	0.00	0.03	0.00	0.07	0.01		1.79	0.17	0.03	0.00	3.97	23.97
Ep-rich jadeitite	MCB4a	Pa	1388	EPMA				6.00	0.00	5.94	0.00	0.03	0.00	0.09	0.01		1.80	0.15	0.01	0.00	3.99	23.99
Ep-rich jadeitite	MCB4a	Pa	1389	EPMA				5.99	0.00	5.96	0.00	0.02	0.00	0.07	0.01		1.79	0.17	0.01	0.01	3.99	23.99
Ep-rich jadeitite	MCB4a	Pa	1390	EPMA				5.98	0.00	5.94	0.00	0.04	0.00	0.08	0.01		1.74	0.24	0.00	0.01	3.99	23.99
Ep-rich jadeitite	MCB4a	Pa	1391	EPMA				6.03	0.00	5.87	0.00	0.04	0.00	0.10	0.01		1.69	0.28	0.02	0.00	3.98	23.98
Ep-rich jadeitite	MCB4a	Pa	1392	EPMA				6.01	0.00	5.91	0.00	0.04	0.00	0.07	0.01		1.75	0.23	0.01	0.00	3.99	23.99
Ep-rich jadeitite	MCB4a	Pa	1393	EPMA				6.01	0.00	5.94	0.00	0.03	0.00	0.06	0.01		1.73	0.21	0.00	0.01	3.99	23.99
Mica-rich Jadeitite	09SC31e	Pa	1821	SEM				6.02		5.97					0.01		1.87	0.13			4.00	24.00
Mica-rich Jadeitite	09SC31e	Pa	1829	SEM				6.01		5.98					0.01		1.85	0.13			4.00	24.00
Pure jadeitite	MCB1j	Pa	1329	EPMA				6.00	0.00	5.90	0.00	0.06	0.00	0.11	0.01		1.77	0.18	0.02	0.00	3.97	23.97
Pure jadeitite	MCB1j	Pa	1330	EPMA				6.01	0.00	5.91	0.00	0.04	0.00	0.09	0.01		1.71	0.23	0.02	0.00	3.98	23.98
Pure jadeitite	MCB1j	Pa	1331	EPMA				6.02	0.00	5.91	0.00	0.03	0.00	0.10	0.01		1.64	0.26	0.03	0.00	3.96	23.96
Pure jadeitite	MCB1j	Pa	1332	EPMA				6.01	0.00	5.99	0.00	0.01	0.00	0.03	0.01		1.80	0.09	0.01	0.00	3.98	23.98
Pure jadeitite	MCB1j	Pa	1333	EPMA				6.00	0.00	5.94	0.00	0.03	0.00	0.09	0.01		1.73	0.16	0.03	0.00	3.97	23.97
Pure jadeitite	MCB1j	Pa	1334	EPMA				5.99	0.00	5.98	0.00	0.02	0.00	0.05	0.01		1.72	0.18	0.02	0.00	3.98	23.98
Pure jadeitite	MCB1j	Pa	1335	EPMA				6.03	0.00	5.93	0.00	0.02	0.00	0.06	0.01		1.71	0.20	0.02	0.00	3.98	23.98
Pure jadeitite	MCB1j	Pa	1336	EPMA				6.09	0.00	5.79	0.00	0.06	0.00	0.14	0.01		1.58	0.26	0.01	0.00	3.99	23.99
Pure jadeitite	MCB2e	Pa	3279	VPSEM				6.02		6.03							1.69	0.15			4.00	24.00
Pure jadeitite	MCB2e	Pa	3280	VPSEM				6.02		6.04							1.60	0.20			4.00	24.00
Pure jadeitite	MCB3h	Pa	3522	VPSEM				5.92		6.07							2.01	0.11			4.00	24.00
Ab-Ep Chl-rich rock	09SC27b	Pl	2166	SEM				3.05		0.99							0.85				0.00	8.00
Ab-Ep Chl-rich rock	09SC27b	Pl	2167	SEM				3.05		0.94							0.97				0.00	8.00
Ab-Ep Chl-rich rock	09SC27b	Pl	2178	SEM				3.04		0.96							0.97				0.00	8.00
Ab-Ep Chl-rich rock	09SC27b	Pl	2182	SEM				3.05		0.94							0.97				0.00	8.00
Ab-Ep Chl-rich rock	09SC27b	Pl	2184	SEM				3.05		0.95							0.92				0.00	8.00
Ab-Ep Chl-rich rock	09SC27b	Pl	2211	SEM				3.03		1.01							0.85				0.00	8.00
Ab-Ep Chl-rich rock	09SC27b	Pl	2221	SEM				3.03		1.00							0.91				0.00	8.00
Ab-Ep rock	09SC27f	Pl	2134	SEM				3.08		0.94							0.86				0.00	8.00
Ab-Ep rock	09SC27f	Pl	2139	SEM				3.03		0.99							0.92				0.00	8.00
Ab-Ep rock	09SC31a	Pl	2258	SEM				3.04		0.98							0.91				0.00	8.00
Ab-Ep rock	09SC31a	Pl	2259	SEM				3.05		0.95							0.93				0.00	8.00
Ab-Ep rock	09SC31a	Pl	2267	SEM				3.05		0.95							0.94				0.00	8.00

Rock type	Sample	Phase	Point	serie	Px type	Px type	Jd mole%	Si	Ti	Al	Fe3+	Fe2+	Mn	Mg	Ca	Ba	Na	K	F	Cl	H	O
Ab-Ep rock	09SC31a	Pl	2274	SEM				3.08		0.93							0.91				0.00	8.00
Ab-Ep rock	09SC31a	Pl	2299	SEM				3.09		0.92							0.90				0.00	8.00
Ab-Ep rock	09SC31c	Pl	2336	SEM				3.04		0.97							0.93				0.00	8.00
Ab-Ep rock	09SC31c	Pl	2350	SEM				3.05		0.94							0.96				0.00	8.00
Ab-Ep rock	09SC31c	Pl	2351	SEM				3.02		0.97							1.01				0.00	8.00
Ab-Ep rock	09SC31c	Pl	2355	SEM				3.03		0.97							0.95				0.00	8.00
Ab-Ep rock	09SC31c	Pl	2357	SEM				3.05		0.96							0.92				0.00	8.00
Ab-Ep rock	09SC31c	Pl	2369	SEM				3.01		1.01							0.94				0.00	8.00
Ab-Ep rock	09SC31c	Pl	2371	SEM				3.03		0.95							1.02				0.00	8.00
Ab-Ep rock	09SC31c	Pl	2372	SEM				3.10		0.90							0.92				0.00	8.00
Ab-Ep rock	09SC31c	Pl	2378	SEM				3.12		0.90							0.82				0.00	8.00
Ab-Ep rock	09SC31c	Pl	2382	SEM				3.10		0.94							0.79				0.00	8.00
Ab-Ep rock	09SC31c	Pl	2387	SEM				3.00		1.04							0.89				0.00	8.00
Ab-Ep rock	09SC31d	Pl	1694	SEM				3.05		0.94							0.99				0.00	8.00
Ab-Ep rock	09SC31d	Pl	1701	SEM				3.04		0.94							1.03				0.00	8.00
Ab-Ep rock	09SC31d	Pl	1708	SEM				3.04		0.96							0.97				0.00	8.00
Ab-Ep rock	09SC31d	Pl	1734	SEM				3.03		0.97							0.99				0.00	8.00
Ab-Ep rock	09SC31d	Pl	1737	SEM				3.02		0.99							0.93				0.00	8.00
Ab-Ep rock	09SC31d	Pl	1745	SEM				3.02		0.98							0.97				0.00	8.00
Ab-Ep rock	09SC31d	Pl	1751	SEM				3.02		0.96							1.04				0.00	8.00
Ab-Ep rock	09SC31d	Pl	1752	SEM				3.05		0.96							0.92				0.00	8.00
Ab-Ep rock	09SC31d	Pl	1753	SEM				3.04		0.98							0.88				0.00	8.00
Ab-Ep rock	09SC31d	Pl	1757	SEM				3.01		0.98							1.00				0.00	8.00
Ab-Ep rock	09SC31n	Pl	1839	SEM				3.04		0.99							0.88				0.00	8.00
Ab-Ep rock	09SC31n	Pl	1846	SEM				3.01		1.02							0.89				0.00	8.00
Ab-Ep rock	09SC31n	Pl	1857	SEM				3.16		0.87							0.75				0.00	8.00
Ab-Ep rock	09SC31n	Pl	1862	SEM				3.19		0.76							0.95				0.00	8.00
Ab-Ep rock	09SC31n	Pl	1865	SEM				3.10		0.92							0.84				0.00	8.00
Ab-Ep rock	09SC31n	Pl	1878	SEM				3.09		0.95							0.79				0.00	8.00
Ab-Ep rock	09SC31n	Pl	1889	SEM				3.08		0.92							0.92				0.00	8.00
Ab-Ep rock	09SC31n	Pl	1892	SEM				3.12		0.89							0.83				0.00	8.00
Ab-Ep rock	09SC31n	Pl	1895	SEM				3.15		0.86							0.84				0.00	8.00
Ab-Ep rock	MCB1a	Pl	2968	VPSEM				2.94	0.00	1.04	0.00	0.00	0.00	0.00	0.01		1.09	0.00			0.00	8.00
Ab-Ep rock	MCB1a	Pl	2971	VPSEM				2.93	0.00	1.07	0.00	0.00	0.00	0.00	0.03		1.02	0.00			0.00	8.00
Ab-Ep rock	MCB1a	Pl	2973	VPSEM				2.94	0.00	1.03	0.01	0.00	0.00	0.00	0.01		1.08	0.00			0.00	8.00
Ab-Ep rock	MCB1a	Pl	2982	VPSEM				2.94	0.00	1.06	0.00	0.00	0.00	0.00	0.01		1.04	0.00			0.00	8.00
Ab-Ep rock	MCB1a	Pl	2992	VPSEM				2.95	0.00	1.04	0.00	0.00	0.00	0.00	0.00		1.08	0.00			0.00	8.00
Ab-Ep rock	MCB1a	Pl	2994	VPSEM				2.95	0.00	1.03	0.00	0.00	0.00	0.00	0.01		1.08	0.00			0.00	8.00
Ab-Ep rock	MCB1a	Pl	2996	VPSEM				2.94	0.00	1.05	0.00	0.00	0.00	0.00	0.01		1.07	0.00			0.00	8.00
Ab-Ep rock	MCB1a	Pl	3000	VPSEM				2.96	0.00	1.04	0.00	0.00	0.00	0.00	0.00		1.06	0.00			0.00	8.00
Ab-Ep rock	MCB1a	Pl	3002	VPSEM				2.95	0.00	1.04	0.00	0.00	0.00	0.00	0.00		1.09	0.00			0.00	8.00
Ab-Ep rock	MCB1a	Pl	3003	VPSEM				2.96	0.00	1.03	0.00	0.00	0.00	0.00	0.00		1.07	0.00			0.00	8.00
Ab-Ep rock	MCB1a	Pl	3004	VPSEM				2.94	0.00	1.05	0.00	0.00	0.00	0.00	0.03		1.03	0.00			0.00	8.00
Ab-Ep rock	MCB1a	Pl	3005	VPSEM				2.90	0.00	1.08	0.00	0.00	0.00	0.00	0.06		1.01	0.00			0.00	8.00

Rock type	Sample	Phase	Point	serie	Px type	Px type	Jd mole%	Si	Ti	Al	Fe3+	Fe2+	Mn	Mg	Ca	Ba	Na	K	F	Cl	H	O
Ab-Ep rock	MCB1a	Pl	3009	VPSEM				2.93	0.00	1.05	0.00	0.00	0.00	0.00	0.03		1.06	0.00			0.00	8.00
Ab-Ep rock	MCB1a	Pl	3011	VPSEM				2.90	0.01	1.07	0.01	0.00	0.00	0.00	0.04		1.04	0.00			0.00	8.00
Ab-Ep rock	MCB1a	Pl	3013	VPSEM				2.93	0.00	1.06	0.00	0.00	0.00	0.00	0.03		1.04	0.00			0.00	8.00
Ab-Ep rock	MCB1a	Pl	3016	VPSEM				2.95	0.00	1.04	0.01	0.00	0.00	0.00	0.00		1.06	0.00			0.00	8.00
Ab-Ep rock	MCB1a	Pl	3032	VPSEM				2.97	0.00	1.02	0.00	0.00	0.00	0.00	0.00		1.06	0.00			0.00	8.00
Ab-Ep rock	MCB1a	Pl	3035	VPSEM				2.96	0.00	1.02	0.00	0.00	0.00	0.00	0.00		1.08	0.00			0.00	8.00
Ab-Ep rock	MCB1a	Pl	3038	VPSEM				2.93	0.00	1.07	0.00	0.00	0.00	0.00	0.02		1.05	0.00			0.00	8.00
Ab-Ep rock	MCB1a	Pl	3043	VPSEM				2.96	0.00	1.03	0.00	0.00	0.00	0.00	0.00		1.09	0.00			0.00	8.00
Ab-Ep rock	MCB1a	Pl	3048	VPSEM				2.95	0.00	1.04	0.00	0.00	0.00	0.00	0.00		1.07	0.00			0.00	8.00
Ab-Ep rock	MCB1a	Pl	3051	VPSEM				2.93	0.00	1.05	0.00	0.00	0.00	0.00	0.01		1.11	0.00			0.00	8.00
Ab-Ep rock	MCB1a	Pl	3053	VPSEM				2.93	0.00	1.06	0.00	0.00	0.00	0.00	0.01		1.05	0.00			0.00	8.00
Ab-Ep rock	MCB1a	Pl	3062	VPSEM				2.93	0.00	1.06	0.00	0.00	0.00	0.00	0.00		1.11	0.00			0.00	8.00
Ab-Ep rock	MCB1a	Pl	3064	VPSEM				2.93	0.00	1.06	0.00	0.00	0.00	0.00	0.02		1.06	0.00			0.00	8.00
Ab-Ep rock	MCB1a	Pl	3072	VPSEM				2.94	0.00	1.05	0.00	0.00	0.00	0.00	0.01		1.05	0.00			0.00	8.00
Ab-Ep rock	MCB1a	Pl	3076	VPSEM				2.92	0.00	1.08	0.00	0.00	0.00	0.00	0.03		1.00	0.02			0.00	8.00
Ab-Ep rock	MCB1a	Pl	3083	VPSEM				2.94	0.00	1.06	0.00	0.00	0.00	0.00	0.03		1.03	0.00			0.00	8.00
Ab-Ep rock	MCB1a	Pl	3091	VPSEM				2.95	0.00	1.04	0.00	0.00	0.00	0.00	0.01		1.06	0.00			0.00	8.00
Ab-Ep rock	MCB1e	Pl	7	EPMA				3.00	0.00	1.00	0.00	0.00	0.00	0.00	0.00		0.99	0.00	0.00	0.00	0.00	8.00
Ab-Ep rock	MCB1e	Pl	8	EPMA				2.99	0.01	1.00	0.00	0.00	0.00	0.00	0.01		1.00	0.00	0.00	0.00	0.00	8.00
Ab-Ep rock	MCB1e	Pl	9	EPMA				2.99	0.00	1.00	0.01	0.00	0.00	0.00	0.01		1.01	0.00	0.01	0.00	0.00	8.00
Ab-Ep rock	MCB1e	Pl	11	EPMA				2.99	0.00	1.00	0.01	0.00	0.00	0.01	0.01		0.99	0.00	0.00	0.00	0.00	8.00
Ab-Ep rock	MCB1e	Pl	31	EPMA				3.00	0.00	1.00	0.00	0.00	0.00	0.00	0.00		0.99	0.00	0.00	0.00	0.00	8.00
Ab-Ep rock	MCB1e	Pl	35	EPMA				3.00	0.00	1.01	0.00	0.00	0.00	0.00	0.01		0.98	0.00	0.00	0.00	0.00	8.00
Ab-Ep rock	MCB1e	Pl	36	EPMA				3.00	0.00	1.01	0.00	0.00	0.00	0.00	0.01		0.98	0.00	0.00	0.00	0.00	8.00
Ab-Ep rock	MCB1e	Pl	38	EPMA				2.99	0.00	1.01	0.00	0.00	0.00	0.00	0.00		0.99	0.00	0.00	0.00	0.00	8.00
Ab-Ep rock	MCB1e	Pl	39	EPMA				3.00	0.00	1.00	0.00	0.00	0.00	0.00	0.00		0.98	0.00	0.00	0.00	0.00	8.00
Ab-Ep rock	MCB1e	Pl	40	EPMA				2.99	0.00	1.01	0.00	0.00	0.00	0.00	0.00		0.99	0.00	0.01	0.00	0.00	8.00
Ab-Ep rock	MCB1e	Pl	42	EPMA				2.99	0.00	1.01	0.00	0.00	0.00	0.00	0.00		1.00	0.00	0.00	0.00	0.00	8.00
Ab-Ep rock	MCB1e	Pl	43	EPMA				3.00	0.00	1.00	0.00	0.00	0.00	0.00	0.01		0.99	0.00	0.01	0.00	0.00	7.99
Ab-Ep rock/Chloritite	09SC31i	Pl	1985	SEM				3.04		1.00							0.84				0.00	8.00
Ab-Ep rock/Chloritite	09SC31i	Pl	1990	SEM				3.02		1.06							0.75				0.00	8.00
Ab-Ep rock/Chloritite	09SC31i	Pl	1993	SEM				3.00		1.04							0.87				0.00	8.00
Ab-Ep rock/Chloritite	09SC31i	Pl	2003	SEM				3.07		0.93					0.05		0.84				0.00	8.00
Ab-Ep rock/Chloritite	09SC31i	Pl	2013	SEM				3.03		1.01							0.84				0.00	8.00
Ab-Ep rock/Chloritite	09SC31i	Pl	2019	SEM				3.05		1.00							0.77				0.00	8.00
Ab-Ep rock/Chloritite	09SC31i	Pl	2040	SEM				3.01		1.03							0.89				0.00	8.00
Ab-Ep rock/Chloritite	09SC31i	Pl	2052	SEM				3.03		1.02							0.83				0.00	8.00
Ep-rich jadeitite	09SC27c	Pl	2245	SEM				3.07		0.93							0.91				0.00	8.00
Ep-rich jadeitite	09SC27c	Pl	2248	SEM				2.99		0.99							1.07				0.00	8.00
Ep-rich jadeitite	09SC27m	Pl	2115	SEM				3.06		0.95							0.89				0.00	8.00
Ep-rich jadeitite	09SC31g	Pl	1778	SEM				3.05		0.95							0.94				0.00	8.00
Ep-rich jadeitite	09SC31g	Pl	1783	SEM				3.05		0.93							1.02				0.00	8.00
Ep-rich jadeitite	09SC31g	Pl	1789	SEM				3.04		0.97							0.95				0.00	8.00
Ep-rich jadeitite	09SC31g	Pl	1794	SEM				3.06		0.93							0.97				0.00	8.00

Rock type	Sample	Phase	Point	serie	Px type	Px type	Jd mole%	Si	Ti	Al	Fe3+	Fe2+	Mn	Mg	Ca	Ba	Na	K	F	Cl	H	O
Ep-rich jadeitite	09SC31g	Pl	1805	SEM				2.93		1.07							1.07				0.00	8.00
Ep-rich jadeitite	09SC31g	Pl	1978	SEM				3.02		0.98							0.97				0.00	8.00
Ep-rich jadeitite	09SC31j	Pl	1937	SEM				3.13		0.88							0.87				0.00	8.00
Ep-rich jadeitite	09SC31j	Pl	1961	SEM				2.97		1.03							1.03				0.00	8.00
Ep-rich Jadeitite	MCB1d	Pl	241	EPMA				3.00	0.00	1.00	0.00	0.00	0.00	0.00	0.01		0.99	0.00	0.00	0.00	0.00	8.00
Ep-rich jadeitite	MCB1d	Pl	1633	VPSEM				2.99		1.02	0.00	0.01					0.98				0.00	8.00
Ep-rich jadeitite	MCB1d	Pl	1638	VPSEM				2.93		1.06					0.01		1.06	0.01			0.00	8.00
Ep-rich jadeitite	MCB1d	Pl	1639	VPSEM				2.97		1.04							0.99				0.00	8.00
Ep-rich jadeitite	MCB1d	Pl	1664	VPSEM				2.97		1.03							1.03				0.00	8.00
Ep-rich jadeitite	MCB1d	Pl	1676	VPSEM				2.97		1.03							1.03				0.00	8.00
Ep-rich jadeitite	MCB1d	Pl	1690	VPSEM				2.98		1.02							1.02				0.00	8.00
Ep-rich jadeitite	MCB1g	Pl	3295	VPSEM				2.96	0.00	1.04	0.00	0.00	0.00	0.00	0.00		1.04	0.00			0.00	8.00
Ep-rich jadeitite	MCB2c	Pl	3367	VPSEM				2.95	0.00	1.03	0.00	0.00	0.00	0.00	0.01		1.10	0.00			0.00	8.00
Ep-rich jadeitite	MCB2c	Pl	3377	VPSEM				2.95	0.00	1.04	0.00	0.00	0.00	0.00	0.00		1.09	0.00			0.00	8.00
Ep-rich jadeitite	MCB4a	Pl	1426	EPMA				2.98	0.00	1.01	0.00	0.00	0.00	0.00	0.01		1.00	0.00	0.01	0.00	0.00	8.00
Ep-rich jadeitite	MCB4a	Pl	1442	EPMA				2.99	0.00	1.01	0.00	0.00	0.00	0.00	0.01		0.97	0.00	0.01	0.00	0.00	8.00
Ep-rich jadeitite	MCB4a	Pl	1459	VPSEM				3.04		0.98							0.89				0.00	8.00
Ep-rich jadeitite	MCB4a	Pl	1474	VPSEM				3.02		1.01							0.90				0.00	8.00
Ep-rich jadeitite	MCB4a	Pl	1479	VPSEM				3.03		1.00							0.87				0.00	8.00
Ep-rich jadeitite	MCB4a	Pl	1485	VPSEM				3.03		1.00							0.87				0.00	8.00
Ep-rich jadeitite	MCB4a	Pl	1488	VPSEM				3.02		1.01							0.87				0.00	8.00
Pure jadeitite	CV237b	Pl	181	EPMA				2.98	0.01	0.99	0.00	0.00	0.00	0.00	0.03		0.98	0.00	0.01	0.00	0.00	8.00
Pure jadeitite	CV237b	Pl	196	EPMA				3.00	0.00	0.98	0.00	0.00	0.00	0.00	0.00		1.04	0.00	0.00	0.00	0.00	8.00
Pure jadeitite	CV237b	Pl	197	EPMA				2.98	0.00	1.00	0.00	0.00	0.00	0.00	0.00		1.09	0.00	0.00	0.00	0.00	8.00
Pure jadeitite	CV237b	Pl	204	EPMA				2.99	0.00	1.01	0.00	0.00	0.00	0.00	0.00		1.02	0.00	0.01	0.00	0.00	8.00
Pure jadeitite	CV237b	Pl	2507	VPSEM				2.98	0.00	1.03	0.00	0.00	0.00	0.00	0.00		0.99	0.00			0.00	8.00
Pure jadeitite	CV237b	Pl	2508	VPSEM				2.97	0.00	1.05	0.00	0.00	0.00	0.00	0.00		0.98	0.00			0.00	8.00
Pure jadeitite	CV237b	Pl	2509	VPSEM				2.98	0.00	1.03	0.00	0.00	0.00	0.00	0.00		1.01	0.00			0.00	8.00
Pure jadeitite	CV237b	Pl	2510	VPSEM				2.98	0.00	1.01	0.00	0.00	0.00	0.00	0.00		1.02	0.00			0.00	8.00
Pure jadeitite	CV237b	Pl	2552	VPSEM				2.98	0.00	1.01	0.00	0.00	0.00	0.00	0.01		1.01	0.00			0.00	8.00
Pure jadeitite	CV237b	Pl	2558	VPSEM				2.98	0.00	1.02	0.00	0.00	0.00	0.00	0.00		1.01	0.00			0.00	8.00
Pure jadeitite	CV237b	Pl	2572	VPSEM				2.98	0.00	1.02	0.00	0.00	0.00	0.00	0.01		1.00	0.00			0.00	8.00
Pure jadeitite	CV237b	Pl	2575	VPSEM				2.98	0.00	1.03	0.00	0.00	0.00	0.00	0.01		0.98	0.00			0.00	8.00
Pure jadeitite	CV237b	Pl	2583	VPSEM				2.96	0.00	1.04	0.00	0.00	0.00	0.00	0.01		1.01	0.00			0.00	8.00
Pure jadeitite	CV237b	Pl	2591	VPSEM				2.97	0.00	1.02	0.00	0.00	0.00	0.00	0.00		1.03	0.00			0.00	8.00
Pure jadeitite	CV237b	Pl	2593	VPSEM				2.97	0.00	1.02	0.01	0.00	0.00	0.00	0.00		1.01	0.00			0.00	8.00
Pure jadeitite	CV237b	Pl	2595	VPSEM				2.97	0.00	1.03	0.00	0.00	0.00	0.00	0.03		1.00	0.00			0.00	8.00
Pure jadeitite	CV237b	Pl	2601	VPSEM				2.98	0.00	1.03	0.00	0.00	0.00	0.00	0.00		1.00	0.00			0.00	8.00
Pure jadeitite	CV237b	Pl	2605	VPSEM				2.97	0.00	1.04	0.00	0.00	0.00	0.00	0.01		1.01	0.00			0.00	8.00
Pure jadeitite	CV237b	Pl	2606	VPSEM				2.97	0.00	1.04	0.00	0.00	0.00	0.00	0.00		1.02	0.00			0.00	8.00
Pure jadeitite	CV237b	Pl	2617	VPSEM				2.97	0.00	1.03	0.00	0.00	0.00	0.00	0.00		1.03	0.00			0.00	8.00
Pure jadeitite	CV237b	Pl	2622	VPSEM				2.98	0.00	1.03	0.00	0.00	0.00	0.00	0.00		1.00	0.00			0.00	8.00
Pure jadeitite	CV237b	Pl	2630	VPSEM				2.97	0.00	1.03	0.00	0.00	0.00	0.00	0.00		1.02	0.00			0.00	8.00
Pure jadeitite	CV237b	Pl	2632	VPSEM				2.97	0.00	1.03	0.00	0.00	0.00	0.00	0.00		1.02	0.00			0.00	8.00

Rock type	Sample	Phase	Point	serie	Px type	Px type	Jd mole%	Si	Ti	Al	Fe3+	Fe2+	Mn	Mg	Ca	Ba	Na	K	F	Cl	H	O
Pure jadeitite	CV237b	Pl	2641	VPSEM				2.96	0.00	1.04	0.00	0.00	0.00	0.00	0.00		1.01	0.00			0.00	8.00
Pure jadeitite	CV237b	Pl	2647	VPSEM				2.94	0.00	1.06	0.00	0.00	0.00	0.00	0.02		1.00	0.00			0.00	8.00
Pure jadeitite	CV237b	Pl	2662	VPSEM				2.98	0.00	1.02	0.00	0.00	0.00	0.00	0.00		1.02	0.00			0.00	8.00
Pure jadeitite	CV237k	Pl	280	EPMA				2.95	0.00	1.05	0.00	0.01	0.00	0.00	0.05		0.92	0.00	0.02	0.00	0.00	7.99
Pure jadeitite	CV237k	Pl	281	EPMA				2.95	0.00	1.05	0.00	0.00	0.00	0.00	0.05		0.94	0.00	0.01	0.00	0.00	8.00
Pure jadeitite	CV237K	Pl	2823	VPSEM				2.97	0.00	1.03	0.00	0.00	0.00	0.00	0.02		1.00	0.00			0.00	8.00
Pure jadeitite	CV237K	Pl	2831	VPSEM				2.94	0.00	1.07	0.00	0.00	0.00	0.00	0.05		0.95	0.00			0.00	8.00
Pure jadeitite	CV237K	Pl	2843	VPSEM				2.96	0.00	1.04	0.00	0.00	0.00	0.00	0.05		0.96	0.00			0.00	8.00
Pure jadeitite	CV237t	Pl	70	EPMA				3.00	0.00	1.00	0.00	0.00	0.00	0.00	0.00		0.98	0.00	0.00	0.00	0.00	8.00
Pure jadeitite	CV237t	Pl	71	EPMA				3.00	0.00	1.00	0.00	0.00	0.00	0.00	0.00		0.99	0.00	0.00	0.00	0.00	8.00
Pure jadeitite	CV237t	Pl	72	EPMA				3.00	0.00	1.00	0.00	0.00	0.00	0.00	0.00		0.98	0.00	0.00	0.00	0.00	8.00
Pure jadeitite	CV237t	Pl	73	EPMA				2.98	0.00	1.02	0.00	0.00	0.00	0.00	0.02		0.97	0.00	0.00	0.00	0.00	8.00
Pure jadeitite	CV237t	Pl	76	EPMA				2.98	0.00	1.02	0.00	0.00	0.00	0.00	0.01		0.98	0.00	0.00	0.00	0.00	8.00
Pure jadeitite	CV237t	Pl	97	EPMA				2.95	0.00	1.01	0.00	0.00	0.00	0.00	0.00		1.16	0.00	0.01	0.00	0.00	8.00
Pure jadeitite	CV237t	Pl	98	EPMA				2.94	0.00	1.02	0.00	0.00	0.00	0.00	0.00		1.14	0.00	0.00	0.00	0.00	8.00
Pure jadeitite	CV237t	Pl	99	EPMA				2.96	0.00	1.03	0.00	0.00	0.00	0.00	0.01		1.04	0.00	0.01	0.00	0.00	7.99
Pure jadeitite	CV237t	Pl	100	EPMA				3.00	0.00	1.00	0.00	0.00	0.00	0.00	0.00		0.99	0.00	0.00	0.00	0.00	8.00
Pure jadeitite	CV237t	Pl	113	EPMA				3.00	0.00	1.00	0.00	0.00	0.00	0.00	0.00		0.99	0.00	0.00	0.00	0.00	8.00
Pure jadeitite	CV237t	Pl	115	EPMA				3.00	0.00	1.00	0.00	0.00	0.00	0.00	0.00		0.99	0.00	0.00	0.00	0.00	8.00
Pure jadeitite	CV237t	Pl	116	EPMA				3.00	0.00	1.00	0.00	0.00	0.00	0.00	0.00		0.99	0.00	0.00	0.00	0.00	8.00
Pure jadeitite	CV237t	Pl	118	EPMA				3.00	0.00	1.00	0.00	0.00	0.00	0.00	0.00		0.99	0.00	0.01	0.00	0.00	8.00
Pure jadeitite	CV237t	Pl	122	EPMA				3.00	0.00	1.00	0.00	0.01	0.00	0.00	0.00		0.98	0.00	0.01	0.00	0.00	8.00
Pure jadeitite	CV237t	Pl	2850	VPSEM				2.98	0.00	1.02	0.00	0.00	0.00	0.00	0.01		1.01	0.00			0.00	8.00
Pure jadeitite	CV237t	Pl	2861	VPSEM				2.98	0.00	1.04	0.00	0.00	0.00	0.00	0.00		0.95	0.00			0.00	8.00
Pure jadeitite	CV237t	Pl	2863	VPSEM				2.98	0.00	1.02	0.00	0.00	0.00	0.00	0.01		1.00	0.00			0.00	8.00
Pure jadeitite	CV237t	Pl	2869	VPSEM				2.97	0.00	1.02	0.01	0.00	0.00	0.00	0.00		1.01	0.00			0.00	8.00
Pure jadeitite	CV237t	Pl	2871	VPSEM				2.97	0.00	1.06	0.00	0.00	0.00	0.00	0.01		0.95	0.00			0.00	8.00
Pure jadeitite	CV237t	Pl	2872	VPSEM				2.97	0.00	1.02	0.00	0.00	0.00	0.00	0.01		1.04	0.00			0.00	8.00
Pure jadeitite	CV237t	Pl	2888	VPSEM				2.97	0.00	1.04	0.00	0.00	0.00	0.00	0.00		1.01	0.00			0.00	8.00
Pure jadeitite	CV237t	Pl	2902	VPSEM				2.97	0.00	1.03	0.00	0.00	0.00	0.00	0.01		1.01	0.00			0.00	8.00
Pure jadeitite	CV237t	Pl	2918	VPSEM				2.97	0.00	1.03	0.00	0.00	0.00	0.00	0.00		1.02	0.00			0.00	8.00
Pure jadeitite	CV237t	Pl	2921	VPSEM				2.98	0.00	1.03	0.00	0.00	0.00	0.00	0.00		1.00	0.00			0.00	8.00
Pure jadeitite	CV237t	Pl	2923	VPSEM				2.98	0.00	1.02	0.00	0.00	0.00	0.00	0.00		1.03	0.00			0.00	8.00
Pure jadeitite	CV237t	Pl	2927	VPSEM				2.97	0.00	1.04	0.00	0.00	0.00	0.00	0.00		1.00	0.00			0.00	8.00
Pure jadeitite	CV237t	Pl	2934	VPSEM				2.98	0.00	1.03	0.00	0.00	0.00	0.00	0.00		1.00	0.00			0.00	8.00
Pure jadeitite	CV237t	Pl	2940	VPSEM				2.98	0.00	1.03	0.00	0.00	0.00	0.00	0.00		1.01	0.00			0.00	8.00
Pure jadeitite	CV237t	Pl	2946	VPSEM				2.96	0.00	1.04	0.00	0.00	0.00	0.00	0.01		1.04	0.00			0.00	8.00
Pure jadeitite	CV237t	Pl	2951	VPSEM				2.97	0.00	1.03	0.00	0.00	0.00	0.00	0.00		1.04	0.00			0.00	8.00
Pure jadeitite	CV237t	Pl	2953	VPSEM				2.97	0.00	1.03	0.00	0.00	0.00	0.00	0.00		1.03	0.00			0.00	8.00
Pure jadeitite	CV237t	Pl	2954	VPSEM				2.98	0.00	1.02	0.00	0.00	0.00	0.00	0.00		1.01	0.00			0.00	8.00
Pure jadeitite	CV237t	Pl	2964	VPSEM				2.96	0.00	1.05	0.00	0.00	0.00	0.00	0.03		0.98	0.00			0.00	8.00
Pure jadeitite	CV237t	Pl	2967	VPSEM				2.97	0.00	1.04	0.00	0.00	0.00	0.00	0.00		1.00	0.00			0.00	8.00
Pure jadeitite	MCB1f	Pl	3156	VPSEM				2.94	0.00	1.04	0.00	0.00	0.00	0.00	0.00		1.09	0.00	0.00	0.01	0.00	8.00
Pure jadeitite	MCB1f	Pl	3157	VPSEM				2.96	0.00	1.02	0.00	0.00	0.00	0.00	0.00		1.11	0.00	0.00	0.00	0.00	8.00

Rock type	Sample	Phase	Point	serie	Px type	Px type	Jd mole%	Si	Ti	Al	Fe3+	Fe2+	Mn	Mg	Ca	Ba	Na	K	F	Cl	H	O
Pure jadeitite	MCB1f	Pl	3167	VPSEM				2.95	0.00	1.04	0.00	0.00	0.00	0.00	0.01		1.07	0.00	0.00	0.00	0.00	8.00
Pure jadeitite	MCB1f	Pl	3171	VPSEM				2.92	0.00	1.06	0.00	0.00	0.00	0.00	0.04		1.05	0.00	0.00	0.00	0.00	8.00
Pure jadeitite	MCB1f	Pl	3174	VPSEM				2.95	0.00	1.03	0.00	0.00	0.00	0.00	0.00		1.08	0.00	0.00	0.00	0.00	8.00
Pure jadeitite	MCB1f	Pl	3175	VPSEM				2.94	0.00	1.05	0.00	0.00	0.00	0.00	0.00		1.09	0.00	0.00	0.00	0.00	8.00
Pure jadeitite	MCB1f	Pl	3176	VPSEM				2.94	0.00	1.04	0.00	0.00	0.00	0.00	0.00		1.11	0.00	0.00	0.00	0.00	8.00
Pure jadeitite	MCB1f	Pl	3177	VPSEM				2.95	0.00	1.03	0.00	0.00	0.00	0.00	0.00		1.09	0.00	0.00	0.00	0.00	8.00
Pure jadeitite	MCB1f	Pl	3187	VPSEM				2.95	0.00	1.04	0.00	0.00	0.00	0.00	0.00		1.10	0.00	0.00	0.00	0.00	8.00
Pure jadeitite	MCB1f	Pl	3199	VPSEM				2.95	0.00	1.04	0.00	0.00	0.00	0.00	0.00		1.08	0.00	0.00	0.00	0.00	8.00
Pure jadeitite	MCB1f	Pl	3206	VPSEM				2.92	0.00	1.07	0.00	0.00	0.00	0.00	0.04		1.06	0.00	0.00	0.00	0.00	8.00
Pure jadeitite	MCB1f	Pl	3222	VPSEM				2.91	0.00	1.07	0.00	0.00	0.00	0.00	0.04		1.06	0.00	0.00	0.00	0.00	8.00
Pure jadeitite	MCB1j	Pl	1324	EPMA				2.98	0.00	1.02	0.00	0.00	0.00	0.00	0.02		0.99	0.00	0.00	0.00	0.00	8.00
Pure jadeitite	MCB1j	Pl	1325	EPMA				2.99	0.00	1.01	0.00	0.00	0.00	0.00	0.01		0.98	0.00	0.00	0.00	0.00	8.00
Pure jadeitite	MCB1j	Pl	1326	EPMA				2.99	0.00	1.01	0.00	0.00	0.00	0.00	0.00		1.00	0.00	0.00	0.00	0.00	8.00
Pure jadeitite	MCB1j	Pl	1327	EPMA				3.00	0.00	1.00	0.00	0.00	0.00	0.00	0.00		0.99	0.00	0.01	0.00	0.00	8.00
Pure jadeitite	MCB1j	Pl	1328	EPMA				2.99	0.00	1.01	0.00	0.00	0.00	0.00	0.00		0.99	0.00	0.01	0.00	0.00	8.00
Pure jadeitite	MCB1j	Pl	1369	EPMA				2.99	0.00	1.01	0.00	0.00	0.00	0.00	0.00		1.00	0.00	0.01	0.00	0.00	8.00
Pure jadeitite	MCB2d	Pl	3230	VPSEM				2.95	0.00	1.04	0.00	0.00	0.00	0.00	0.00		1.11	0.00	0.00		0.00	8.00
Pure jadeitite	MCB2d	Pl	3240	VPSEM				2.94	0.00	1.04	0.00	0.00	0.00	0.00	0.00		1.10	0.00	0.00		0.00	8.00
Pure jadeitite	MCB2d	Pl	3243	VPSEM				2.94	0.00	1.04	0.00	0.00	0.00	0.00	0.00		1.09	0.00	0.00		0.00	8.00
Pure jadeitite	MCB2d	Pl	3245	VPSEM				2.94	0.00	1.05	0.00	0.00	0.00	0.00	0.00		1.08	0.00	0.00		0.00	8.00
Pure jadeitite	MCB2d	Pl	3258	VPSEM				2.95	0.00	1.04	0.00	0.00	0.00	0.00	0.00		1.08	0.00	0.00		0.00	8.00
Pure jadeitite	MCB2d	Pl	3259	VPSEM				2.93	0.00	1.05	0.00	0.00	0.00	0.00	0.02		1.07	0.00	0.00		0.00	8.00
Pure jadeitite	MCB2d	Pl	3260	VPSEM				2.95	0.00	1.05	0.00	0.00	0.00	0.00	0.00		1.05	0.00	0.00		0.00	8.00
Pure jadeitite	MCB2d	Pl	3262	VPSEM				2.94	0.00	0.99	0.00	0.00	0.00	0.00	0.03		0.99	0.00	0.00		0.00	8.00
Pure jadeitite	MCB2e	Pl	3272	VPSEM				2.99		1.02							0.99				0.00	8.00
Pure jadeitite	MCB2e	Pl	3282	VPSEM				3.00		1.02					0.03		0.87				0.00	8.00
Pure jadeitite	MCB3h	Pl	371	EPMA				2.99	0.00	1.00	0.00	0.00	0.00	0.00	0.00		1.01	0.00	0.00	0.00	0.00	8.00
Pure jadeitite	MCB3h	Pl	387	EPMA				3.00	0.00	1.00	0.00	0.00	0.00	0.00	0.00		1.00	0.00	0.00	0.00	0.00	8.00
Pure jadeitite	MCB3h	Pl	390	EPMA				2.97	0.00	1.02	0.01	0.00	0.00	0.02	0.01		1.00	0.00	0.00	0.00	0.00	8.00
Pure jadeitite	MCB3h	Pl	394	EPMA				2.98	0.00	1.02	0.01	0.00	0.00	0.01	0.01		0.99	0.00	0.00	0.00	0.00	8.00
Pure jadeitite	MCB3h	Pl	399	EPMA				2.97	0.00	1.02	0.01	0.00	0.00	0.01	0.02		1.00	0.00	0.00	0.00	0.00	8.00
Pure jadeitite	MCB3h	Pl	400	EPMA				2.98	0.00	1.02	0.00	0.00	0.00	0.00	0.00		1.00	0.00	0.00	0.00	0.00	8.00
Pure jadeitite	MCB3h	Pl	403	EPMA				2.98	0.00	1.02	0.00	0.00	0.00	0.00	0.00		1.01	0.00	0.00	0.00	0.00	8.00
Pure jadeitite	MCB3h	Pl	426	EPMA				3.00	0.00	0.99	0.00	0.00	0.00	0.00	0.00		1.00	0.00	0.00	0.00	0.00	8.00
Pure jadeitite	MCB3h	Pl	427	EPMA				3.00	0.00	0.99	0.00	0.00	0.00	0.00	0.00		1.00	0.00	0.00	0.00	0.00	8.00
Pure jadeitite	MCB3h	Pl	432	EPMA				3.00	0.00	1.00	0.00	0.00	0.00	0.00	0.00		0.99	0.00	0.01	0.00	0.00	8.00
Pure jadeitite	MCB3h	Pl	433	EPMA				3.00	0.00	1.00	0.00	0.00	0.00	0.00	0.00		1.00	0.00	0.00	0.00	0.00	8.00
Pure jadeitite	MCB3h	Pl	446	EPMA				3.00	0.00	0.99	0.00	0.00	0.00	0.00	0.00		1.00	0.00	0.00	0.00	0.00	8.00
Pure jadeitite	MCB3h	Pl	448	EPMA				3.00	0.00	0.99	0.00	0.00	0.00	0.00	0.00		0.99	0.00	0.00	0.00	0.00	8.00
Pure jadeitite	MCB3h	Pl	450	EPMA				2.99	0.00	1.01	0.00	0.00	0.00	0.00	0.00		1.00	0.00	0.00	0.00	0.00	8.00
Pure jadeitite	MCB3h	Pl	515	EPMA				2.99	0.00	1.00	0.00	0.01	0.00	0.00	0.01		0.98	0.00		0.00	0.00	8.00
Pure jadeitite	MCB3h	Pl	3501	VPSEM				2.95		1.04							1.10				0.00	8.00
Pure jadeitite	MCB3h	Pl	3511	VPSEM				2.94		1.04							1.10				0.00	8.00
Pure jadeitite	MCB3h	Pl	3519	VPSEM				2.94		1.06							1.09				0.00	8.00

Rock type	Sample	Phase	Point	serie	Px type	Px type	Jd mole%	Si	Ti	Al	Fe3+	Fe2+	Mn	Mg	Ca	Ba	Na	K	F	Cl	H	O
Pure jadeitite	MCB3h	Pl	3520	VPSEM				2.95		1.05							1.07				0.00	8.00
Pure jadeitite	MCB3h	Pl	3524	VPSEM				2.95		1.03							1.11				0.00	8.00
Pure jadeitite	MCB3h	Pl	3527	VPSEM				2.94		1.04							1.09				0.00	8.00
Pure jadeitite	MCB3h	Pl	3529	VPSEM				2.94		1.04							1.14				0.00	8.00
Pure jadeitite	MCB3h	Pl	3542	VPSEM				2.95		1.03							1.10				0.00	8.00
Pure jadeitite	MCB3h	Pl	3562	VPSEM				2.97		1.01							1.08				0.00	8.00
Pure jadeitite	MCB3h	Pl	3565	VPSEM				2.93		1.06							1.10				0.00	8.00
Pure jadeitite	MCB3h	Pl	3569	VPSEM				2.97		1.02							1.05				0.00	8.00
Pure jadeitite	MCB3h	Pl	3578	VPSEM				2.96		1.03							1.07				0.00	8.00
Pure jadeitite	MCB3h	Pl	3584	VPSEM				2.98		1.02							1.01				0.00	8.00
Pure jadeitite	MCB3h	Pl	3591	VPSEM				2.95		1.04							1.09				0.00	8.00
Pure jadeitite	MCB3h	Pl	3592	VPSEM				2.94		1.05							1.09				0.00	8.00
Pure jadeitite	MCB3h	Pl	3593	VPSEM				2.96		1.04							1.05				0.00	8.00
Pure jadeitite	MCB3h	Pl	3598	VPSEM				2.96		1.01							1.10				0.00	8.00
Pure jadeitite	MCB3h	Pl	3607	VPSEM				2.97		1.02							1.04				0.00	8.00
Pure Jdt/Ab-Ep rock/Chloritite	09SC8a3	Pl	2429	VPSEM				2.95		1.04							1.06				0.00	8.00
Pure Jdt/Ab-Ep rock/Chloritite	09SC8a3	Pl	2434	VPSEM				2.92		1.08					0.02		1.05				0.00	8.00
Pure Jdt/Ab-Ep rock/Chloritite	09SC8a3	Pl	2437	VPSEM				2.98		1.02					0.01		1.01				0.00	8.00
Pure Jdt/Ab-Ep rock/Chloritite	09SC8a3	Pl	2479	VPSEM				2.95		1.04					0.01		1.07				0.00	8.00
Pure Jdt/Ab-Ep rock/Chloritite	09SC8a3	Pl	2480	VPSEM				2.95		1.04					0.01		1.05				0.00	8.00
Pure Jdt/Chloritite	MCB3f	Pl	3424	VPSEM				2.96	0.00	1.03	0.00	0.00	0.00	0.00	0.00		1.09	0.00		0.00	0.00	8.00
Pure Jdt/Chloritite	MCB3f	Pl	3425	VPSEM				2.95	0.00	1.04	0.00	0.00	0.00	0.00	0.01		1.06	0.00		0.00	0.00	8.00
Pure Jdt/Chloritite	MCB3f	Pl	3426	VPSEM				2.93	0.00	1.06	0.00	0.00	0.00	0.00	0.00		1.08	0.00		0.00	0.00	8.00
Pure Jdt/Chloritite	MCB3f	Pl	3427	VPSEM				2.94	0.00	1.04	0.00	0.00	0.00	0.00	0.01		1.09	0.00		0.00	0.00	8.00
Pure Jdt/Chloritite	MCB3f	Pl	3452	VPSEM				2.94	0.00	1.04	0.00	0.00	0.00	0.00	0.00		1.10	0.00		0.00	0.00	8.00
Pure Jdt/Chloritite	MCB3f	Pl	3453	VPSEM				2.96	0.00	1.03	0.00	0.00	0.00	0.00	0.00		1.08	0.00		0.00	0.00	8.00
Pure Jdt/Chloritite	MCB3f	Pl	3454	VPSEM				2.96	0.00	1.02	0.00	0.00	0.00	0.00	0.00		1.10	0.00		0.00	0.00	8.00
Pure Jdt/Chloritite	MCB3f	Pl	3473	VPSEM				2.94	0.00	1.07	0.00	0.00	0.00	0.00	0.01		1.04	0.00		0.00	0.00	8.00
Pure Jdt/Chloritite	MCB3f	Pl	3474	VPSEM				2.93	0.00	1.06	0.00	0.00	0.00	0.00	0.01		1.08	0.00		0.00	0.00	8.00
Pure Jdt/Chloritite	MCB3f	Pl	3475	VPSEM				2.95	0.00	1.04	0.00	0.00	0.00	0.00	0.00		1.10	0.00		0.00	0.00	8.00
Pure Jdt/Chloritite	MCB3f	Pl	3483	VPSEM				2.93	0.00	1.06	0.00	0.00	0.00	0.00	0.00		1.11	0.00		0.00	0.00	8.00
Pure Jdt/Chloritite	MCB3f	Pl	3486	VPSEM				2.93	0.00	1.05	0.01	0.00	0.00	0.00	0.01		1.06	0.00		0.00	0.00	8.00
Pure Jdt/Chloritite	MCB3f	Pl	3494	VPSEM				2.93	0.00	1.03	0.01	0.00	0.00	0.02	0.03		1.06	0.00		0.00	0.00	8.00
Ab-Ep rock	09SC31n	Pmp	1842	SEM				3.06		2.35	0.00	0.20		0.37	1.97						3.63	14.00
Ab-Ep rock	MCB1a	Pmp	3021	VPSEM				3.00	0.00	2.46	0.01	0.12	0.02	0.45	1.94		0.00	0.00			3.54	14.00
Ab-Ep rock	MCB1a	Pmp	3024	VPSEM				2.98	0.00	2.47	0.04	0.11	0.02	0.43	1.95		0.00	0.00			3.53	14.00
Ab-Ep rock	MCB1a	Pmp	3050	VPSEM				2.94	0.00	2.57	0.10	0.00	0.00	0.43	1.93		0.06	0.00			3.44	14.00
Ab-Ep rock	MCB1a	Pmp	3086	VPSEM				3.07	0.00	2.47	0.00	0.20	0.00	0.28	1.86		0.08	0.00			3.52	14.00
Ab-Ep rock	MCB1a	Pmp	3087	VPSEM				2.96	0.00	2.52	0.09	0.03	0.00	0.43	1.98		0.00	0.00			3.48	14.00
Ab-Ep rock	MCB1e	Pmp	44	EPMA				2.99	0.01	2.46	0.04	0.08	0.01	0.41	1.99		0.02	0.00	0.04	0.00	3.50	13.96
Ab-Ep rock	MCB1e	Pmp	45	EPMA				2.99	0.00	2.46	0.05	0.05	0.01	0.43	1.99		0.03	0.00	0.04	0.00	3.50	13.96
Ab-Ep rock	MCB1e	Pmp	3135	VPSEM				2.98	0.00	2.52	0.04	0.09	0.02	0.43	1.93		0.00	0.00			3.48	14.00
Ab-Ep rock	MCB1e	Pmp	3141	VPSEM				2.97	0.00	2.46	0.06	0.08	0.00	0.46	1.97		0.00	0.00			3.54	14.00
Ep-rich jadeitite	MCB1d	Pmp	1510	VPSEM				2.97		2.50	0.11	0.00		0.39	1.99		0.05				3.50	14.00

Rock type	Sample	Phase	Point	serie	Px type	Px type	Jd mole%	Si	Ti	Al	Fe3+	Fe2+	Mn	Mg	Ca	Ba	Na	K	F	Cl	H	O
Ep-rich jadeitite	MCB1d	Pmp	1512	VPSEM				2.95		2.54	0.09	0.00		0.40	1.97		0.08				3.47	14.00
Ep-rich jadeitite	MCB1d	Pmp	1515	VPSEM				2.98		2.48	0.10	0.00		0.39	1.99		0.06				3.52	14.00
Ep-rich jadeitite	MCB1d	Pmp	1516	VPSEM				2.96		2.51	0.12	0.00		0.37	1.98		0.06				3.49	14.00
Ep-rich jadeitite	MCB1d	Pmp	1522	VPSEM				2.96		2.52	0.14	0.00		0.37	1.96		0.06				3.49	14.00
Ep-rich jadeitite	MCB4a	Pmp	1422	EPMA				3.01	0.00	2.49	0.04	0.11	0.00	0.34	1.93		0.07	0.00	0.05	0.00	3.46	13.95
Ep-rich jadeitite	MCB4a	Pmp	1423	EPMA				2.99	0.01	2.51	0.08	0.07	0.00	0.34	1.95		0.06	0.00	0.03	0.00	3.46	13.97
Ep-rich jadeitite	MCB4a	Pmp	1424	EPMA				2.99	0.01	2.50	0.06	0.08	0.00	0.35	1.94		0.06	0.00	0.03	0.00	3.47	13.97
Ab-Ep rock	09SC27F	Py	2222	SEM							0.00	100.00									0.00	100.00
Ep-rich jadeitite	09SC27m	Py	2058	SEM							0.00	100.00									0.00	100.00
Ab-Ep Chl-rich rock	09SC27b	Ttn	2174	SEM				0.85	1.22						0.86						0.00	5.00
Ab-Ep Chl-rich rock	09SC27b	Ttn	2215	SEM				0.99	0.95	0.07					1.01						0.00	5.00
Ab-Ep Chl-rich rock	09SC27b	Ttn	2216	SEM																	0.00	0.00
Ab-Ep Chl-rich rock	09SC27b	Ttn	2217	SEM																	0.00	0.00
Ab-Ep Chl-rich rock	09SC27b	Ttn	2218	SEM																	0.00	0.00
Ab-Ep rock	09SC31a	Ttn	2251	SEM				1.00	0.99						1.02						0.00	5.00
Ab-Ep rock	09SC31a	Ttn	2253	SEM				1.10	0.90						1.00						0.00	5.00
Ab-Ep rock	09SC31a	Ttn	2254	SEM				1.26	0.82						0.84						0.00	5.00
Ab-Ep rock	09SC31a	Ttn	2262	SEM				0.98	0.99						1.05						0.00	5.00
Ab-Ep rock	09SC31a	Ttn	2263	SEM				1.13	0.80						1.13						0.00	5.00
Ab-Ep rock	09SC31a	Ttn	2269	SEM				1.02	1.00						0.95						0.00	5.00
Ab-Ep rock	09SC31a	Ttn	2270	SEM				1.09	0.95						0.92						0.00	5.00
Ab-Ep rock	09SC31a	Ttn	2278	SEM				1.18	0.85						0.94						0.00	5.00
Ab-Ep rock	09SC31a	Ttn	2279	SEM				1.20	0.81						0.99						0.00	5.00
Ab-Ep rock	09SC31a	Ttn	2280	SEM				1.08	1.01						0.83						0.00	5.00
Ab-Ep rock	09SC31a	Ttn	2281	SEM				1.00	1.02						0.96						0.00	5.00
Ab-Ep rock	09SC31a	Ttn	2282	SEM				1.12	0.89						0.97						0.00	5.00
Ab-Ep rock	09SC31a	Ttn	2294	SEM				1.12	0.97						0.81						0.00	5.00
Ab-Ep rock	09SC31a	Ttn	2295	SEM				1.03	0.94						1.06						0.00	5.00
Ab-Ep rock	09SC31a	Ttn	2296	SEM				1.09	0.90						1.00						0.00	5.00
Ab-Ep rock	09SC31c	Ttn	2343	SEM				1.04	0.93	0.06					0.97						0.00	5.00
Ab-Ep rock	09SC31c	Ttn	2353	SEM				1.04	0.93	0.05					1.00						0.00	5.00
Ab-Ep rock	09SC31c	Ttn	2375	SEM				1.12	0.89						0.99						0.00	5.00
Ab-Ep rock	09SC31c	Ttn	2376	SEM				1.06	0.93						1.03						0.00	5.00
Ab-Ep rock	09SC31c	Ttn	2377	SEM				1.07	0.90						1.05						0.00	5.00
Ab-Ep rock	09SC31c	Ttn	2384	SEM				1.10	0.91						0.98						0.00	5.00
Ab-Ep rock	09SC31c	Ttn	2388	SEM				1.12	0.87						1.03						0.00	5.00
Ab-Ep rock	09SC31d	Ttn	1695	SEM				1.03	0.98						0.98						0.00	5.00
Ab-Ep rock	09SC31d	Ttn	1696	SEM				1.05	0.96						0.98						0.00	5.00
Ab-Ep rock	09SC31d	Ttn	1711	SEM				1.07	0.95						0.96						0.00	5.00
Ab-Ep rock	09SC31d	Ttn	1713	SEM				1.08	0.92						1.01						0.00	5.00
Ab-Ep rock	09SC31d	Ttn	1729	SEM				1.01	0.93	0.05					1.04						0.00	5.00
Ab-Ep rock	09SC31d	Ttn	1732	SEM				1.02	0.97						1.03						0.00	5.00
Ab-Ep rock	09SC31d	Ttn	1740	SEM				1.08	0.91						1.02						0.00	5.00
Ab-Ep rock	09SC31d	Ttn	1748	SEM				1.03	0.94						1.05						0.00	5.00

Rock type	Sample	Phase	Point	serie	Px type	Px type	Jd mole%	Si	Ti	Al	Fe3+	Fe2+	Mn	Mg	Ca	Ba	Na	K	F	Cl	H	O
Ab-Ep rock	09SC31d	Ttn	1755	SEM				1.07	0.92						1.02						0.00	5.00
Ab-Ep rock	09SC31d	Ttn	1756	SEM				1.06	0.88						1.12						0.00	5.00
Ab-Ep rock	09SC31d	Ttn	1762	SEM				1.03	0.92	0.07					1.01						0.00	5.00
Ab-Ep rock	09SC31n	Ttn	1835	SEM				1.06	0.97						0.94						0.00	5.00
Ab-Ep rock	09SC31n	Ttn	1836	SEM				1.05	0.93						1.04						0.00	5.00
Ab-Ep rock	09SC31n	Ttn	1848	SEM				0.99	1.02						0.99						0.00	5.00
Ab-Ep rock	09SC31n	Ttn	1854	SEM				0.87	1.20						0.86						0.00	5.00
Ab-Ep rock	09SC31n	Ttn	1874	SEM				0.97	1.01						1.04						0.00	5.00
Ab-Ep rock	09SC31n	Ttn	1875	SEM				1.04	0.99						0.94						0.00	5.00
Ab-Ep rock	09SC31n	Ttn	1877	SEM				0.89	1.07						1.07						0.00	5.00
Ab-Ep rock	09SC31n	Ttn	1886	SEM				0.99	1.09						0.84						0.00	5.00
Ab-Ep rock	09SC31n	Ttn	1887	SEM				1.02	0.96						1.04						0.00	5.00
Ab-Ep rock	MCB1a	Ttn	2980	VPSEM				1.00	0.92	0.08	0.00	0.00	0.00	0.00	1.03		0.00	0.00			0.00	5.00
Ab-Ep rock	MCB1a	Ttn	2999	VPSEM				1.05	0.91	0.09	0.00	0.00	0.00	0.00	0.93		0.05	0.00			0.00	5.00
Ab-Ep rock	MCB1a	Ttn	3049	VPSEM				0.99	0.96	0.05	0.00	0.00	0.00	0.00	1.02		0.00	0.00			0.00	5.00
Ab-Ep rock	MCB1a	Ttn	3055	VPSEM				1.00	0.96	0.04	0.00	0.00	0.00	0.00	1.02		0.00	0.00			0.00	5.00
Ab-Ep rock	MCB1a	Ttn	3056	VPSEM				1.01	0.95	0.05	0.00	0.00	0.00	0.00	1.01		0.00	0.00			0.00	5.00
Ab-Ep rock	MCB1a	Ttn	3066	VPSEM				0.99	0.96	0.05	0.00	0.00	0.00	0.00	1.03		0.00	0.00			0.00	5.00
Ab-Ep rock	MCB1a	Ttn	3068	VPSEM				0.99	0.95	0.07	0.01	0.00	0.00	0.00	1.00		0.00	0.00			0.00	5.00
Ab-Ep rock	MCB1e	Ttn	54	EPMA				1.00	0.95	0.05	0.01	0.00	0.00	0.01	1.01		0.00	0.00	0.03	0.00	0.00	4.99
Ab-Ep rock	MCB1e	Ttn	55	EPMA				1.00	0.95	0.06	0.00	0.00	0.00	0.00	1.01		0.00	0.00	0.03	0.00	0.00	4.98
Ab-Ep rock	MCB1e	Ttn	57	EPMA				1.00	0.95	0.05	0.00	0.00	0.00	0.00	1.02		0.00	0.00	0.03	0.00	0.00	4.99
Ab-Ep rock	MCB1e	Ttn	3099	VPSEM				0.99	0.97	0.04	0.00	0.00	0.00	0.00	1.03		0.00	0.00			0.00	5.00
Ab-Ep rock	MCB1e	Ttn	3101	VPSEM				1.00	0.94	0.07	0.01	0.00	0.00	0.00	0.99		0.00	0.00			0.00	5.00
Ab-Ep rock	MCB1e	Ttn	3104	VPSEM				1.02	0.90	0.09	0.00	0.00	0.01	0.00	1.01		0.00	0.00			0.00	5.00
Ab-Ep rock	MCB1e	Ttn	3105	VPSEM				0.99	0.95	0.06	0.00	0.00	0.00	0.00	1.02		0.00	0.00			0.00	5.00
Ab-Ep rock	MCB1e	Ttn	3107	VPSEM				0.99	0.96	0.05	0.00	0.00	0.00	0.00	1.03		0.00	0.00			0.00	5.00
Ab-Ep rock	MCB1e	Ttn	3108	VPSEM				0.99	0.96	0.05	0.00	0.00	0.00	0.00	1.01		0.00	0.00			0.00	5.00
Ab-Ep rock	MCB1e	Ttn	3109	VPSEM				0.99	0.97	0.04	0.00	0.00	0.00	0.00	1.01		0.00	0.00			0.00	5.00
Ab-Ep rock	MCB1e	Ttn	3111	VPSEM				1.02	0.93	0.05	0.00	0.00	0.00	0.00	1.02		0.00	0.00			0.00	5.00
Ab-Ep rock	MCB1e	Ttn	3126	VPSEM				1.00	0.95	0.05	0.00	0.00	0.00	0.00	1.01		0.00	0.00			0.00	5.00
Ab-Ep rock	MCB1e	Ttn	3140	VPSEM				1.02	0.93	0.08	0.00	0.00	0.00	0.00	0.97		0.03	0.00			0.00	5.00
Ab-Ep rock/Chloritite	09SC31i	Ttn	2014	SEM				1.07	0.93						1.00						0.00	5.00
Ab-Ep rock/Chloritite	09SC31i	Ttn	2029	SEM				0.99	0.91	0.10					1.04						0.00	5.00
Chloritite	09SC27a	Ttn	2153	SEM				1.18	0.85						0.95						0.00	5.00
Chloritite	09SC27a	Ttn	2154	SEM				1.11	0.89						0.99						0.00	5.00
Chloritite	09SC27a	Ttn	2159	SEM				1.02	1.00						0.96						0.00	5.00
Chloritite	09SC27a	Ttn	2160	SEM				1.08	0.90	0.06					0.97						0.00	5.00
Cr-rich Pure Jdt	SCMJ10	Ttn	3639	VPSEM				1.01	0.93	0.07	0.00	0.00	0.00	0.00	1.02		0.00	0.00			0.00	5.00
Cr-rich Pure Jdt	SCMJ10	Ttn	3641	VPSEM				1.02	0.94	0.06	0.00	0.00	0.00	0.00	1.00		0.00	0.00			0.00	5.00
Cr-rich Pure Jdt	SCMJ10	Ttn	3652	VPSEM				1.02	0.94	0.05	0.00	0.00	0.00	0.00	1.01		0.00	0.00			0.00	5.00
Ep-rich jadeitite	09SC27c	Ttn	2233	SEM				1.06	0.91						1.05						0.00	5.00
Ep-rich jadeitite	09SC27c	Ttn	2239	SEM				1.12	0.87						1.01						0.00	5.00
Ep-rich jadeitite	09SC27c	Ttn	2240	SEM				1.06	0.89						1.10						0.00	5.00

Rock type	Sample	Phase	Point	serie	Px type	Px type	Jd mole%	Si	Ti	Al	Fe3+	Fe2+	Mn	Mg	Ca	Ba	Na	K	F	Cl	H	O
Ep-rich jadeitite	09SC27d	Ttn	1914	SEM				1.11	0.91						0.96						0.00	5.00
Ep-rich jadeitite	09SC27d	Ttn	1921	SEM				1.10	0.97						0.86						0.00	5.00
Ep-rich jadeitite	09SC27d	Ttn	1924	SEM				1.08	1.00						0.85						0.00	5.00
Ep-rich jadeitite	09SC27d	Ttn	1931	SEM				1.10	0.89						1.02						0.00	5.00
Ep-rich jadeitite	09SC27m	Ttn	2067	SEM				0.96	1.02						1.05						0.00	5.00
Ep-rich jadeitite	09SC27m	Ttn	2070	SEM				1.03	0.97						0.99						0.00	5.00
Ep-rich jadeitite	09SC27m	Ttn	2074	SEM				1.03	0.91	0.08					1.00						0.00	5.00
Ep-rich jadeitite	09SC27m	Ttn	2076	SEM				1.05	0.94						1.01						0.00	5.00
Ep-rich jadeitite	09SC27m	Ttn	2088	SEM				1.05	0.95						1.00						0.00	5.00
Ep-rich jadeitite	09SC27m	Ttn	2106	SEM				1.03	0.93	0.06					0.99						0.00	5.00
Ep-rich jadeitite	09SC27m	Ttn	2110	SEM				1.07	0.92						1.02						0.00	5.00
Ep-rich jadeitite	09SC27m	Ttn	2111	SEM				1.00	0.94						1.12						0.00	5.00
Ep-rich jadeitite	09SC27m	Ttn	2112	SEM				1.06	0.97						0.93						0.00	5.00
Ep-rich jadeitite	09SC27m	Ttn	2113	SEM				1.04	0.96						1.01						0.00	5.00
Ep-rich jadeitite	09SC27m	Ttn	2123	SEM				1.02	0.96						1.04						0.00	5.00
Ep-rich jadeitite	09SC27m	Ttn	2128	SEM				1.01	0.93	0.08					1.00						0.00	5.00
Ep-rich jadeitite	09SC31g	Ttn	1770	SEM				1.02	0.94	0.06					1.00						0.00	5.00
Ep-rich jadeitite	09SC31g	Ttn	1774	SEM				1.03	0.95						1.05						0.00	5.00
Ep-rich jadeitite	09SC31g	Ttn	1775	SEM				0.95	1.03						1.03						0.00	5.00
Ep-rich jadeitite	09SC31g	Ttn	1776	SEM				0.93	1.00						1.14						0.00	5.00
Ep-rich jadeitite	09SC31g	Ttn	1784	SEM				1.05	0.95						1.00						0.00	5.00
Ep-rich jadeitite	09SC31g	Ttn	1792	SEM				1.06	0.96						0.97						0.00	5.00
Ep-rich jadeitite	09SC31g	Ttn	1799	SEM				1.01	1.02						0.94						0.00	5.00
Ep-rich jadeitite	09SC31g	Ttn	1800	SEM				1.04	1.04						0.84						0.00	5.00
Ep-rich jadeitite	09SC31g	Ttn	1807	SEM				0.98	1.04						0.96						0.00	5.00
Ep-rich jadeitite	09SC31g	Ttn	1976	SEM				1.04	0.99						0.95						0.00	5.00
Ep-rich jadeitite	09SC31g	Ttn	1977	SEM				1.02	0.97						1.02						0.00	5.00
Ep-rich jadeitite	09SC31g	Ttn	1983	SEM				1.08	0.91						1.02						0.00	5.00
Ep-rich jadeitite	09SC31j	Ttn	1939	SEM				1.01	0.95						1.07						0.00	5.00
Ep-rich jadeitite	09SC31j	Ttn	1941	SEM				1.00	0.93						1.13						0.00	5.00
Ep-rich jadeitite	09SC31j	Ttn	1942	SEM				0.97	0.96						1.13						0.00	5.00
Ep-rich jadeitite	09SC31j	Ttn	1944	SEM				1.04	0.93						1.05						0.00	5.00
Ep-rich jadeitite	09SC31j	Ttn	1951	SEM				1.06	0.96						0.96						0.00	5.00
Ep-rich jadeitite	09SC31j	Ttn	1952	SEM				1.04	0.92						1.07						0.00	5.00
Ep-rich jadeitite	09SC31j	Ttn	1953	SEM				0.99	0.95						1.13						0.00	5.00
Ep-rich jadeitite	09SC31j	Ttn	1963	SEM				1.01	0.92						1.15						0.00	5.00
Ep-rich jadeitite	09SC31j	Ttn	1964	SEM				1.04	0.92						1.09						0.00	5.00
Ep-rich jadeitite	09SC31j	Ttn	1966	SEM				0.87	1.11						1.03						0.00	5.00
Ep-rich Jadeitite	MCB1d	Ttn	211	EPMA				0.99	0.97	0.04	0.01	0.00	0.00	0.00	1.02		0.00	0.00	0.02	0.00	0.00	4.99
Ep-rich Jadeitite	MCB1d	Ttn	213	EPMA				0.99	0.96	0.04	0.00	0.00	0.00	0.00	1.02		0.00	0.00	0.02	0.00	0.00	4.99
Ep-rich Jadeitite	MCB1d	Ttn	244	EPMA				0.98	0.97	0.04	0.00	0.00	0.00	0.00	1.03		0.00	0.00	0.03	0.00	0.00	4.99
Ep-rich jadeitite	MCB1d	Ttn	1606	VPSEM				0.98	0.97	0.05					1.04						0.00	5.00
Ep-rich jadeitite	MCB1d	Ttn	1651	VPSEM				0.99	0.95	0.08					1.01						0.00	5.00
Ep-rich jadeitite	MCB1d	Ttn	1671	VPSEM				0.98	0.97	0.05					1.02						0.00	5.00

Rock type	Sample	Phase	Point	serie	Px type	Px type	Jd mole%	Si	Ti	Al	Fe3+	Fe2+	Mn	Mg	Ca	Ba	Na	K	F	Cl	H	O
Ep-rich jadeitite	MCB1g	Ttn	3299	VPSEM				1.00	0.96	0.04	0.00	0.00	0.00	0.00	1.01		0.00	0.00			0.00	5.00
Ep-rich jadeitite	MCB1g	Ttn	3300	VPSEM				1.01	0.96	0.04	0.00	0.00	0.00	0.00	1.01		0.00	0.00			0.00	5.00
Ep-rich jadeitite	MCB1g	Ttn	3301	VPSEM				0.99	0.97	0.03	0.00	0.00	0.00	0.00	1.03		0.00	0.00			0.00	5.00
Ep-rich jadeitite	MCB1g	Ttn	3325	VPSEM				1.01	0.96	0.04	0.00	0.00	0.00	0.00	1.00		0.00	0.00			0.00	5.00
Ep-rich jadeitite	MCB1g	Ttn	3328	VPSEM				1.02	0.94	0.05	0.00	0.00	0.00	0.00	1.00		0.00	0.00			0.00	5.00
Ep-rich jadeitite	MCB1g	Ttn	3330	VPSEM				1.02	0.93	0.07	0.00	0.00	0.00	0.00	0.96		0.05	0.00			0.00	5.00
Ep-rich jadeitite	MCB1g	Ttn	3336	VPSEM				1.01	0.94	0.06	0.01	0.00	0.00	0.00	0.99		0.00	0.00			0.00	5.00
Ep-rich jadeitite	MCB1g	Ttn	3350	VPSEM				1.00	0.96	0.05	0.00	0.00	0.00	0.00	1.01		0.00	0.00			0.00	5.00
Ep-rich jadeitite	MCB2c	Ttn	3368	VPSEM				1.01	0.95	0.05	0.00	0.00	0.00	0.00	1.01		0.00	0.00			0.00	5.00
Ep-rich jadeitite	MCB2c	Ttn	3375	VPSEM				0.99	0.96	0.05	0.00	0.00	0.00	0.00	1.01		0.00	0.00			0.00	5.00
Ep-rich jadeitite	MCB2c	Ttn	3379	VPSEM				1.01	0.95	0.05	0.00	0.00	0.00	0.00	1.01		0.00	0.00			0.00	5.00
Ep-rich jadeitite	MCB2c	Ttn	3400	VPSEM				1.00	0.97	0.04	0.00	0.00	0.00	0.00	1.00		0.00	0.00			0.00	5.00
Ep-rich jadeitite	MCB4a	Ttn	1374	EPMA				0.99	0.97	0.04	0.01	0.00	0.00	0.00	1.01		0.00	0.00	0.02	0.00	0.00	4.99
Ep-rich jadeitite	MCB4a	Ttn	1375	EPMA				0.99	0.97	0.04	0.01	0.00	0.00	0.00	1.01		0.00	0.00	0.03	0.00	0.00	4.99
Ep-rich jadeitite	MCB4a	Ttn	1443	VPSEM				1.06	0.91	0.07					0.95						0.00	5.00
Ep-rich jadeitite	MCB4a	Ttn	1450	VPSEM				1.08	0.90	0.07					0.94						0.00	5.00
Ep-rich jadeitite	MCB4a	Ttn	1466	VPSEM				1.06	0.89	0.08					0.96						0.00	5.00
Ep-rich jadeitite	MCB4a	Ttn	1483	VPSEM				1.11	0.85	0.11					0.89		0.05				0.00	5.00
Ep-rich jadeitite	MCB4a	Ttn	1484	VPSEM				1.07	0.90	0.09					0.92						0.00	5.00
Mica-rich Jadeitite	09SC31e	Ttn	1819	SEM				0.96	1.04						1.00						0.00	5.00
Mica-rich Jadeitite	09SC31e	Ttn	1820	SEM				0.93	1.05						1.04						0.00	5.00
Mica-rich Jadeitite	09SC31e	Ttn	1826	SEM				1.03	0.98						0.98						0.00	5.00
Mica-rich Jadeitite	09SC31e	Ttn	2309	SEM				1.03	0.99						0.95						0.00	5.00
Mica-rich Jadeitite	09SC31e	Ttn	2313	SEM				0.98	1.02						1.00						0.00	5.00
Mica-rich Jadeitite	09SC31e	Ttn	2331	SEM				1.03	0.94						1.06						0.00	5.00
Mica-rich Jadeitite	09SC31e	Ttn	2333	SEM				1.03	0.95						1.03						0.00	5.00
Pure jadeitite	BCJ1	Ttn	2487	VPSEM				1.01	0.94	0.05					1.01						0.00	5.00
Pure jadeitite	BCJ1	Ttn	2492	VPSEM				1.00	0.94	0.07					1.02						0.00	5.00
Pure jadeitite	BCJ1	Ttn	2495	VPSEM				1.01	0.93	0.06	0.02	0.00			1.01						0.00	5.00
Pure jadeitite	BCJ1	Ttn	2496	VPSEM				1.00	0.95	0.06					1.00						0.00	5.00
Pure jadeitite	BCJ1	Ttn	2497	VPSEM				1.01	0.92	0.07	0.01	0.00			1.00						0.00	5.00
Pure jadeitite	BCJ1	Ttn	2501	VPSEM				1.09	0.85	0.11	0.02	0.00			0.91		0.05				0.00	5.00
Pure jadeitite	BCJ1	Ttn	2504	VPSEM				1.11	0.79	0.12	0.02	0.00		0.02	0.91		0.07				0.00	5.00
Pure jadeitite	BCJ1	Ttn	2505	VPSEM				1.00	0.94	0.06	0.01	0.00			1.00						0.00	5.00
Pure jadeitite	CV237b	Ttn	2519	VPSEM				0.99	0.95	0.07	0.01	0.00	0.00	0.00	1.02		0.00	0.00			0.00	5.00
Pure jadeitite	CV237b	Ttn	2523	VPSEM				0.98	0.95	0.08	0.01	0.00	0.00	0.00	1.02		0.00	0.00			0.00	5.00
Pure jadeitite	CV237b	Ttn	2524	VPSEM				0.99	0.96	0.06	0.00	0.00	0.00	0.00	1.02		0.00	0.00			0.00	5.00
Pure jadeitite	CV237b	Ttn	2527	VPSEM				0.98	0.94	0.08	0.01	0.00	0.00	0.00	1.02		0.00	0.00			0.00	5.00
Pure jadeitite	CV237b	Ttn	2535	VPSEM				0.98	0.97	0.05	0.00	0.00	0.00	0.00	1.03		0.00	0.00			0.00	5.00
Pure jadeitite	CV237b	Ttn	2536	VPSEM				1.02	0.93	0.06	0.01	0.00	0.00	0.00	1.00		0.00	0.00			0.00	5.00
Pure jadeitite	CV237b	Ttn	2542	VPSEM				0.98	0.95	0.08	0.01	0.00	0.00	0.00	1.01		0.00	0.01			0.00	5.00
Pure jadeitite	CV237b	Ttn	2551	VPSEM				0.96	0.93	0.10	0.02	0.00	0.00	0.05	0.99		0.00	0.00			0.00	5.00
Pure jadeitite	CV237b	Ttn	2560	VPSEM				0.98	0.97	0.05	0.00	0.00	0.00	0.00	1.02		0.00	0.00			0.00	5.00
Pure jadeitite	CV237b	Ttn	2567	VPSEM				0.97	0.95	0.08	0.01	0.00	0.00	0.00	1.03		0.00	0.00			0.00	5.00

Rock type	Sample	Phase	Point	serie	Px type	Px type	Jd mole%	Si	Ti	Al	Fe3+	Fe2+	Mn	Mg	Ca	Ba	Na	K	F	Cl	H	O
Pure jadeitite	CV237b	Ttn	2569	VPSEM				1.02	0.88	0.14	0.01	0.00	0.00	0.02	0.93		0.00	0.04			0.00	5.00
Pure jadeitite	CV237b	Ttn	2571	VPSEM				1.02	0.93	0.08	0.00	0.00	0.00	0.00	0.95		0.03	0.01			0.00	5.00
Pure jadeitite	CV237b	Ttn	2574	VPSEM				1.08	0.86	0.11	0.01	0.00	0.00	0.00	0.92		0.04	0.00			0.00	5.00
Pure jadeitite	CV237b	Ttn	2582	VPSEM				0.98	0.85	0.19	0.04	0.00	0.00	0.00	0.99		0.00	0.00			0.00	5.00
Pure jadeitite	CV237b	Ttn	2592	VPSEM				0.98	0.97	0.05	0.00	0.00	0.00	0.00	1.03		0.00	0.00			0.00	5.00
Pure jadeitite	CV237b	Ttn	2603	VPSEM				0.98	0.96	0.05	0.00	0.00	0.00	0.00	1.03		0.00	0.00			0.00	5.00
Pure jadeitite	CV237b	Ttn	2607	VPSEM				0.98	0.97	0.04	0.00	0.00	0.00	0.00	1.03		0.00	0.00			0.00	5.00
Pure jadeitite	CV237b	Ttn	2624	VPSEM				0.97	0.97	0.04	0.01	0.00	0.00	0.00	1.03		0.00	0.00			0.00	5.00
Pure jadeitite	CV237b	Ttn	2631	VPSEM				0.99	0.92	0.08	0.03	0.00	0.00	0.03	0.98		0.02	0.00			0.00	5.00
Pure jadeitite	CV237b	Ttn	2644	VPSEM				0.99	0.94	0.08	0.00	0.00	0.00	0.00	1.03		0.00	0.00			0.00	5.00
Pure jadeitite	CV237b	Ttn	2656	VPSEM				0.98	0.97	0.05	0.00	0.00	0.00	0.00	1.03		0.00	0.00			0.00	5.00
Pure jadeitite	CV237b	Ttn	2657	VPSEM				0.98	0.97	0.05	0.00	0.00	0.00	0.00	1.02		0.00	0.00			0.00	5.00
Pure jadeitite	CV237b	Ttn	2658	VPSEM				0.98	0.98	0.05	0.00	0.00	0.00	0.00	1.02		0.00	0.00			0.00	5.00
Pure jadeitite	CV237b	Ttn	2659	VPSEM				0.99	0.95	0.06	0.01	0.00	0.00	0.00	1.01		0.00	0.00			0.00	5.00
Pure jadeitite	CV237K	Ttn	2704	VPSEM				0.98	0.96	0.05	0.00	0.00	0.00	0.00	1.03		0.00	0.00			0.00	5.00
Pure jadeitite	CV237K	Ttn	2716	VPSEM				1.04	0.86	0.13	0.01	0.00	0.00	0.02	0.91		0.09	0.00			0.00	5.00
Pure jadeitite	CV237K	Ttn	2717	VPSEM				1.07	0.84	0.13	0.02	0.00	0.00	0.03	0.90		0.08	0.00			0.00	5.00
Pure jadeitite	CV237K	Ttn	2720	VPSEM				0.98	0.98	0.05	0.00	0.00	0.00	0.00	1.03		0.00	0.00			0.00	5.00
Pure jadeitite	CV237K	Ttn	2722	VPSEM				0.98	0.97	0.06	0.01	0.00	0.00	0.00	1.01		0.00	0.00			0.00	5.00
Pure jadeitite	CV237K	Ttn	2723	VPSEM				0.98	0.96	0.06	0.00	0.00	0.00	0.00	1.02		0.00	0.00			0.00	5.00
Pure jadeitite	CV237K	Ttn	2724	VPSEM				0.96	0.97	0.06	0.01	0.00	0.00	0.00	1.03		0.00	0.00			0.00	5.00
Pure jadeitite	CV237K	Ttn	2726	VPSEM				1.10	0.83	0.12	0.02	0.00	0.00	0.02	0.91		0.03	0.00			0.00	5.00
Pure jadeitite	CV237K	Ttn	2727	VPSEM				1.01	0.94	0.07	0.01	0.00	0.00	0.00	0.99		0.02	0.00			0.00	5.00
Pure jadeitite	CV237K	Ttn	2741	VPSEM				1.00	0.95	0.06	0.00	0.00	0.00	0.00	1.01		0.00	0.00			0.00	5.00
Pure jadeitite	CV237K	Ttn	2752	VPSEM				0.99	0.98	0.04	0.00	0.00	0.00	0.00	1.00		0.00	0.00			0.00	5.00
Pure jadeitite	CV237K	Ttn	2762	VPSEM				0.99	0.96	0.06	0.00	0.00	0.00	0.00	1.00		0.02	0.00			0.00	5.00
Pure jadeitite	CV237K	Ttn	2764	VPSEM				1.02	0.92	0.08	0.01	0.00	0.00	0.00	0.98		0.03	0.00			0.00	5.00
Pure jadeitite	CV237K	Ttn	2765	VPSEM				0.98	0.97	0.05	0.00	0.00	0.00	0.00	1.02		0.00	0.00			0.00	5.00
Pure jadeitite	CV237K	Ttn	2774	VPSEM				0.98	0.98	0.04	0.00	0.00	0.00	0.00	1.01		0.00	0.00			0.00	5.00
Pure jadeitite	CV237K	Ttn	2776	VPSEM				0.98	0.98	0.05	0.00	0.00	0.00	0.00	1.01		0.00	0.00			0.00	5.00
Pure jadeitite	CV237K	Ttn	2786	VPSEM				0.99	0.96	0.06	0.00	0.00	0.00	0.00	1.01		0.00	0.00			0.00	5.00
Pure jadeitite	CV237t	Ttn	104	EPMA				1.00	0.96	0.05	0.00	0.00	0.00	0.00	1.01		0.00	0.00	0.01	0.00	0.00	4.99
Pure jadeitite	CV237t	Ttn	2907	VPSEM				1.00	0.94	0.08	0.00	0.00	0.00	0.00	0.98		0.03	0.00			0.00	5.00
Pure jadeitite	CV237t	Ttn	2909	VPSEM				1.04	0.88	0.12	0.01	0.00	0.00	0.00	0.94		0.06	0.00			0.00	5.00
Pure jadeitite	CV237t	Ttn	2912	VPSEM				1.06	0.87	0.12	0.01	0.00	0.00	0.00	0.91		0.07	0.00			0.00	5.00
Pure jadeitite	CV237t	Ttn	2915	VPSEM				0.97	0.99	0.05	0.00	0.00	0.00	0.00	1.02		0.00	0.00			0.00	5.00
Pure jadeitite	CV237t	Ttn	2925	VPSEM				0.99	0.97	0.04	0.00	0.00	0.00	0.00	1.02		0.00	0.00			0.00	5.00
Pure jadeitite	CV237t	Ttn	2926	VPSEM				0.97	0.97	0.05	0.00	0.00	0.00	0.00	1.03		0.00	0.00			0.00	5.00
Pure jadeitite	CV237t	Ttn	2938	VPSEM				0.99	0.94	0.09	0.00	0.00	0.00	0.00	1.00		0.02	0.00			0.00	5.00
Pure jadeitite	CV237t	Ttn	2942	VPSEM				1.01	0.90	0.12	0.00	0.00	0.00	0.00	1.01		0.00	0.00			0.00	5.00
Pure jadeitite	CV237t	Ttn	2943	VPSEM				1.02	0.85	0.13	0.03	0.00	0.00	0.05	0.93		0.00	0.04			0.00	5.00
Pure jadeitite	CV237t	Ttn	2945	VPSEM				0.99	0.97	0.05	0.00	0.00	0.00	0.00	1.01		0.00	0.00			0.00	5.00
Pure jadeitite	MCB1f	Ttn	3149	VPSEM				1.01	0.95	0.05	0.00	0.00	0.00	0.00	1.00		0.00	0.00	0.00	0.00	0.00	5.00
Pure jadeitite	MCB1f	Ttn	3150	VPSEM				1.00	0.92	0.10	0.00	0.00	0.00	0.00	1.00		0.00	0.00	0.00	0.00	0.00	5.00

Rock type	Sample	Phase	Point	serie	Px type	Px type	Jd mole%	Si	Ti	Al	Fe3+	Fe2+	Mn	Mg	Ca	Ba	Na	K	F	Cl	H	O
Pure jadeitite	MCB1f	Ttn	3161	VPSEM				1.02	0.92	0.08	0.00	0.00	0.00	0.00	1.00		0.00	0.00	0.00	0.00	0.00	5.00
Pure jadeitite	MCB1f	Ttn	3162	VPSEM				1.02	0.92	0.08	0.01	0.00	0.00	0.00	0.99		0.00	0.00	0.00	0.00	0.00	5.00
Pure jadeitite	MCB1f	Ttn	3188	VPSEM				1.00	0.87	0.16	0.00	0.00	0.00	0.00	1.03		0.00	0.00	0.00	0.00	0.00	5.00
Pure jadeitite	MCB1f	Ttn	3189	VPSEM				1.00	0.96	0.05	0.01	0.00	0.00	0.00	0.98		0.00	0.00	0.00	0.00	0.00	5.00
Pure jadeitite	MCB1f	Ttn	3190	VPSEM				1.03	0.85	0.14	0.00	0.00	0.00	0.00	1.04		0.00	0.00	0.00	0.00	0.00	5.00
Pure jadeitite	MCB1f	Ttn	3191	VPSEM				1.00	0.93	0.07	0.00	0.00	0.00	0.00	1.02		0.00	0.00	0.00	0.00	0.00	5.00
Pure jadeitite	MCB1f	Ttn	3195	VPSEM				1.01	0.93	0.07	0.00	0.00	0.00	0.00	1.01		0.00	0.00	0.00	0.00	0.00	5.00
Pure jadeitite	MCB1f	Ttn	3218	VPSEM				1.01	0.96	0.04	0.00	0.00	0.00	0.00	1.01		0.00	0.00	0.00	0.00	0.00	5.00
Pure jadeitite	MCB1f	Ttn	3219	VPSEM				1.01	0.91	0.10	0.00	0.00	0.00	0.00	1.02		0.00	0.00	0.30	0.00	0.00	4.85
Pure jadeitite	MCB2d	Ttn	3237	VPSEM				1.01	0.96	0.04	0.00	0.00	0.00	0.00	1.00		0.00	0.00	0.00		0.00	5.00
Pure jadeitite	MCB2d	Ttn	3248	VPSEM				1.00	0.96	0.03	0.00	0.00	0.00	0.00	1.02		0.00	0.00	0.00		0.00	5.00
Pure jadeitite	MCB2d	Ttn	3251	VPSEM				1.03	0.94	0.05	0.01	0.00	0.00	0.00	0.97		0.04	0.00	0.00		0.00	5.00
Pure jadeitite	MCB2e	Ttn	3277	VPSEM				1.05	0.91	0.07					0.97						0.00	5.00
Pure jadeitite	MCB3h	Ttn	388	EPMA				1.00	0.96	0.05	0.00	0.00	0.00	0.00	0.99		0.00	0.00	0.03	0.00	0.00	4.99
Pure jadeitite	MCB3h	Ttn	3508	VPSEM				1.01	0.96	0.04					1.00						0.00	5.00
Pure jadeitite	MCB3h	Ttn	3547	VPSEM				1.05	0.91	0.08					0.95						0.00	5.00
Pure jadeitite	MCB3h	Ttn	3572	VPSEM				1.00	0.96	0.05					1.01						0.00	5.00
Pure jadeitite	MCB3h	Ttn	3574	VPSEM				1.00	0.97	0.04					0.99						0.00	5.00
Pure jadeitite	MCB3h	Ttn	3579	VPSEM				1.01	0.96	0.04					1.00						0.00	5.00
Pure jadeitite	MCB3h	Ttn	3583	VPSEM				1.00	0.98	0.05					0.98						0.00	5.00
Pure jadeitite	MCB3h	Ttn	3601	VPSEM				0.99	0.97	0.04					1.02						0.00	5.00
Pure jadeitite	MCB3h	Ttn	3608	VPSEM				1.00	0.95	0.05					1.02						0.00	5.00
Pure jadeitite	MCB3h	Ttn	3611	VPSEM				1.02	0.89	0.11					1.03						0.00	5.00
Pure jadeitite	MCB3h	Ttn	3612	VPSEM				1.02	0.95	0.04					1.01						0.00	5.00
Pure Jdt/Ab-Ep rock/Chloritite	09SC8a3	Ttn	2392	VPSEM				1.00	0.95	0.05	0.01	0.00			1.02						0.00	5.00
Pure Jdt/Ab-Ep rock/Chloritite	09SC8a3	Ttn	2393	VPSEM				1.00	0.95	0.06	0.01	0.00			1.00						0.00	5.00
Pure Jdt/Ab-Ep rock/Chloritite	09SC8a3	Ttn	2396	VPSEM				1.00	0.94	0.06	0.01	0.00			1.01						0.00	5.00
Pure Jdt/Ab-Ep rock/Chloritite	09SC8a3	Ttn	2397	VPSEM				1.00	0.94	0.06	0.01	0.00			1.01						0.00	5.00
Pure Jdt/Ab-Ep rock/Chloritite	09SC8a3	Ttn	2398	VPSEM				0.99	0.94	0.04	0.01	0.00			1.03						0.00	5.00
Pure Jdt/Ab-Ep rock/Chloritite	09SC8a3	Ttn	2400	VPSEM				1.00	0.96	0.05					1.01						0.00	5.00
Pure Jdt/Ab-Ep rock/Chloritite	09SC8a3	Ttn	2409	VPSEM				1.00	0.96	0.05					1.01						0.00	5.00
Pure Jdt/Ab-Ep rock/Chloritite	09SC8a3	Ttn	2416	VPSEM				1.01	0.96	0.03	0.01	0.00			0.98						0.00	5.00
Pure Jdt/Ab-Ep rock/Chloritite	09SC8a3	Ttn	2417	VPSEM				1.00	0.96	0.04	0.01	0.00			1.01						0.00	5.00
Pure Jdt/Ab-Ep rock/Chloritite	09SC8a3	Ttn	2418	VPSEM				1.01	0.94	0.05	0.01	0.00			1.00						0.00	5.00
Pure Jdt/Ab-Ep rock/Chloritite	09SC8a3	Ttn	2425	VPSEM				1.00	0.97	0.03					1.00						0.00	5.00
Pure Jdt/Ab-Ep rock/Chloritite	09SC8a3	Ttn	2426	VPSEM				1.00	0.95	0.04	0.01	0.00			1.02						0.00	5.00
Pure Jdt/Ab-Ep rock/Chloritite	09SC8a3	Ttn	2451	VPSEM				1.02	0.97	0.02	0.01	0.00			0.99						0.00	5.00
Pure Jdt/Ab-Ep rock/Chloritite	09SC8a3	Ttn	2466	VPSEM				1.02	0.92	0.07	0.01	0.00		0.01	0.98						0.00	5.00
Pure Jdt/Ab-Ep rock/Chloritite	09SC8a3	Ttn	2470	VPSEM				1.01	0.93	0.07	0.01	0.00			1.00						0.00	5.00
Pure Jdt/Ab-Ep rock/Chloritite	09SC8a3	Ttn	2474	VPSEM				1.00	0.96	0.05					1.01						0.00	5.00
Pure Jdt/Ab-Ep rock/Chloritite	09SC8a3	Ttn	2478	VPSEM				1.02	0.94	0.05					1.00						0.00	5.00
Pure Jdt/Chloritite	MCB3f	Ttn	3412	VPSEM				1.00	0.96	0.04	0.01	0.00	0.00	0.00	1.00		0.00	0.00		0.00	0.00	5.00
Pure Jdt/Chloritite	MCB3f	Ttn	3413	VPSEM				1.00	0.96	0.04	0.00	0.00	0.00	0.00	1.01		0.00	0.00		0.00	0.00	5.00
Pure Jdt/Chloritite	MCB3f	Ttn	3444	VPSEM				1.01	0.97	0.03	0.00	0.00	0.00	0.00	1.01		0.00	0.00		0.00	0.00	5.00

Rock type	Sample	Phase	Point	serie	Px type	Px type	Jd mole%	Si	Ti	Al	Fe3+	Fe2+	Mn	Mg	Ca	Ba	Na	K	F	Cl	H	O
Pure Jdt/Chloritite	MCB3f	Ttn	3462	VPSEM				1.00	0.95	0.07	0.00	0.00	0.00	0.00	1.00		0.00	0.00		0.00	0.00	5.00
Pure Jdt/Chloritite	MCB3f	Ttn	3476	VPSEM				1.01	0.94	0.06	0.00	0.00	0.00	0.00	1.01		0.00	0.00		0.00	0.00	5.00
Pure Jdt/Chloritite	MCB3f	Ttn	3496	VPSEM				1.04	0.89	0.09	0.00	0.00	0.00	0.00	0.99		0.02	0.00		0.00	0.00	5.00
Pure Jdt/Chloritite	MCB3f	Ttn	3497	VPSEM				1.02	0.94	0.05	0.00	0.00	0.00	0.00	1.00		0.00	0.00		0.00	0.00	5.00

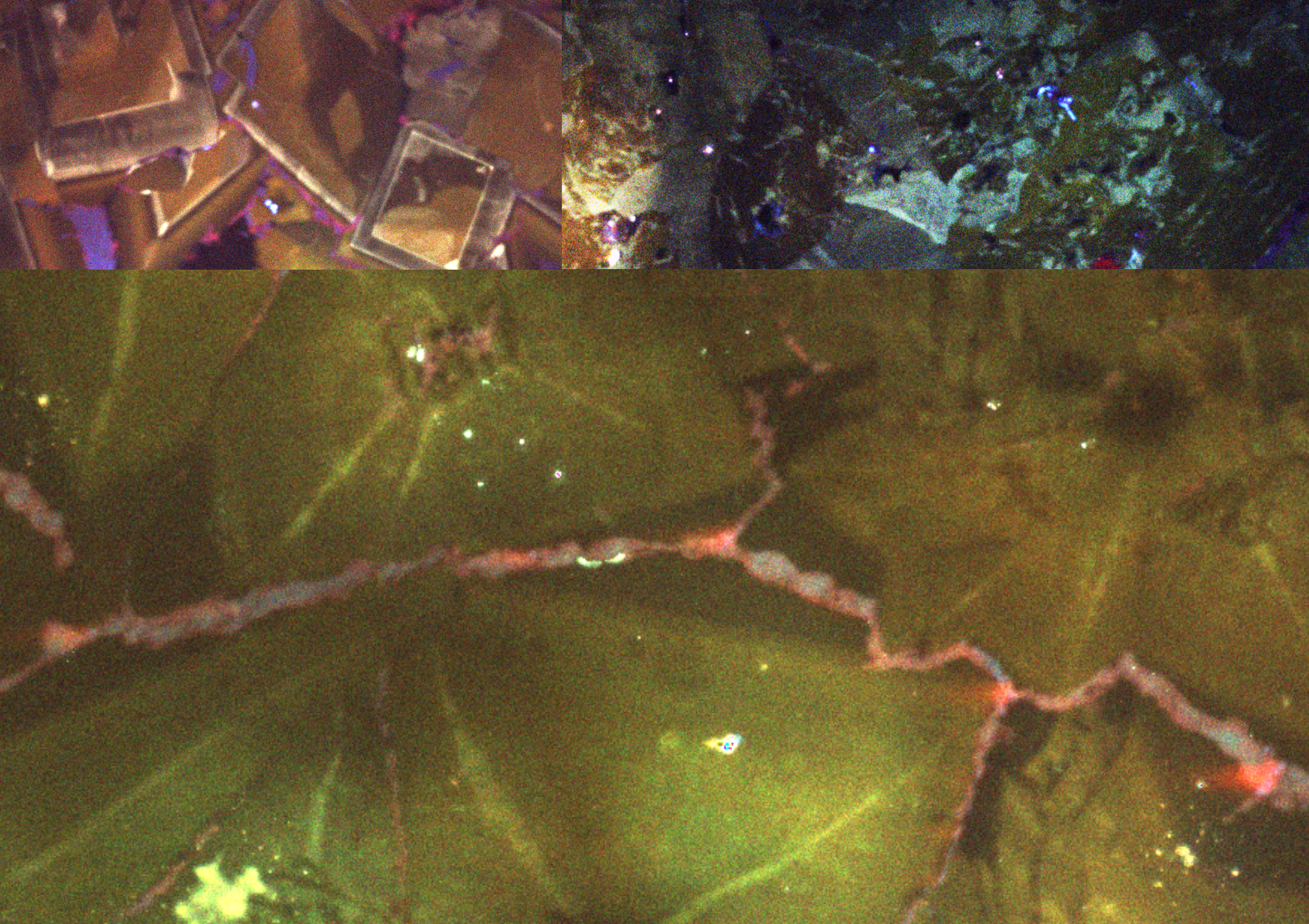

Mineralogy, geochemistry and petrogenesis of a new jade deposit, Sierra del Convento Mélange, E. Cuba D. JUAN CÁRDENAS PÁRRAGA